

NATIONAL COOPERATIVE HIGHWAY RESEARCH PROGRAM

US6 RDA12
93 P256
Davis

UNIVERSITY OF WATERLOO



31187 020 725 436

NCHRP Report 356

Anchorage Zone Reinforcement for Post-Tensioned Concrete Girders

Transportation Research Board
National Research Council

@Seismicisolation

TRANSPORTATION RESEARCH BOARD EXECUTIVE COMMITTEE 1994

OFFICERS

Chairman: A. Ray Chamberlain, Executive Director, Colorado Department of Transportation

Vice Chairman: Joseph M. Sussman, JR East Professor and Professor of Engineering, Massachusetts Institute of Technology

Executive Director: Thomas B. Deen, Transportation Research Board

MEMBERS

KIRK BROWN, Secretary, Illinois Department of Transportation

DAVID BURWELL, President, Rails-to-Trails Conservancy

L. GARY BYRD, Consulting Engineer, Alexandria, Virginia

L. STANLEY CRANE, former Chairman and CEO of CONRAIL

RICHARD K. DAVIDSON, Chairman and CEO, Union Pacific Railroad

JAMES C. DELONG, Director of Aviation, Stapleton International Airport, Denver, Colorado

JERRY L. DEPOY, former Vice President, Properties & Facilities, USAir

DON C. KELLY, Secretary and Commissioner of Highways, Transportation Cabinet, Kentucky

ROBERT KOCHANOWSKI, Executive Director, Southwestern Pennsylvania Regional Planning Commission

LESTER P. LAMM, President, Highway Users Federation

LILLIAN C. LIBURDI, Director, Port Department, The Port Authority of New York and New Jersey

ADOLF D. MAY, JR., Professor and Vice Chairman, Institute of Transportation Studies, University of California, Berkeley

WILLIAM W. MILLAR, Executive Director, Port Authority of Allegheny County, Pennsylvania (Past Chairman, 1992)

CHARLES P. O'LEARY, JR., Commissioner, New Hampshire Department of Transportation

JUDE W. P. PATIN, Secretary, Louisiana Department of Transportation and Development

NEIL PETERSON, Executive Director, Los Angeles County Transportation Commission

DARREL RENSINK, Director, Iowa Department of Transportation

DELLA M. ROY, Professor of Materials Science, Pennsylvania State University

JAMES W. VAN LOBEN SELS, Director, California Department of Transportation

C. MICHAEL WALTON, Ernest H. Cockrell Centennial Chair in Engineering and Chairman, Civil Engineering Department, University of Texas at Austin
(Past Chairman, 1991)

FRANKLIN E. WHITE, CEO, Los Angeles Co. Metropolitan Transportation Authority

JULIAN WOLPERT, Henry G. Bryant Professor of Geography, Public Affairs and Urban Planning, Woodrow Wilson School of Public and International Affairs, Princeton University

HOWARD YERUSALIM, Secretary of Transportation, Pennsylvania Department of Transportation

ROBERT A. YOUNG III, President, ABF Freight Systems, Inc.

MICHAEL ACOTT, President, National Asphalt Pavement Association (ex officio)

ROY A. ALLEN, Vice President, Research and Test Department, Association of American Railroads (ex officio)

ANDREW H. CARD, President and CEO, American Automobile Manufacturers Association

THOMAS J. DONOHUE, President and CEO, American Trucking Associations (ex officio)

FRANCIS B. FRANCOIS, Executive Director, American Association of State Highway and Transportation Officials (ex officio)

JACK R. GILSTRAP, Executive Vice President, American Public Transit Association (ex officio)

ALBERT J. HERBERGER, Maritime Administrator, U.S. Department of Transportation (ex officio)

DAVID R. HINSON, Federal Aviation Administrator, U.S. Department of Transportation (ex officio)

GORDON J. LINTON, Federal Transit Administrator, U.S. Department of Transportation (ex officio)

ROSE A. McMURRAY, Research and Special Programs Administrator, U.S. Department of Transportation (ex officio)

JOLENE M. MOLITORIS, Federal Railroad Administrator, U.S. Department of Transportation (ex officio)

RODNEY E. SLATER, Federal Highway Administrator, U.S. Department of Transportation (ex officio)

HOWARD M. SMOLKIN, National Highway Traffic Safety Administrator, U.S. Department of Transportation (ex officio)

ARTHUR E. WILLIAMS, Chief of Engineers and Commander, U.S. Army Corps of Engineers (ex officio)

NATIONAL COOPERATIVE HIGHWAY RESEARCH PROGRAM

Transportation Research Board Executive Committee Subcommittee for NCHRP

A. RAY CHAMBERLAIN, Colorado Department of Transportation (Chairman)

FRANCIS B. FRANCOIS, American Association of State Highway and Transportation Officials

WILLIAM W. MILLAR, Port Authority of Allegheny County

JOSEPH M. SUSSMAN, Massachusetts Institute of Technology

C. MICHAEL WALTON, University of Texas at Austin

L. GARY BYRD, Consulting Engineer

THOMAS B. DEEN, Transportation Research Board

Field of Materials and Construction

Area of Specifications, Procedures, and Practices

Project Panel D-10-29

GEORGE MARKICH, Olympia, Washington (Chair)

J. A. McKEE, California Department of Transportation

JAMES HOBLITZELL, Federal Highway Administration

JULIO RAMIREZ, Purdue University, Lafayette, IN

THOMAS T.C. HSU, University of Houston, Texas

FRIEDER SEIBLE, University of California, San Diego

E. GENE McCOLLOM, Poe & Associates, Inc., Oklahoma City, OK

SUSAN N. LANE, FHWA Liaison Representative

ALAN B. MATEJOWSKY, Texan Department of Transportation

D. WM. DEARASAUGH, JR., TRB Liaison Representative

Program Staff

ROBERT J. REILLY, Director, Cooperative Research Programs

KENNETH S. OPIELA, Senior Program Officer

CRAWFORD F. JENCKS, NCHRP Manager

DAN A. ROSEN, Senior Program Officer

LOUIS M. MACGREGOR, Administrative Officer

SCOTT SABOL, Program Officer

STEPHEN E. BLAKE, Senior Program Officer

EILEEN P. DELANEY, Editor

AMIR N. HANNA, Senior Program Officer

KAMI CABRAL, Editorial Assistant

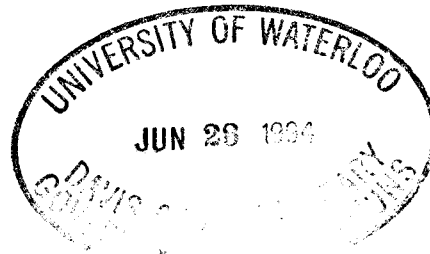
FRANK R. McCULLAGH, Senior Program Officer

@Seismicisolation

Report 356

Anchorage Zone Reinforcement for Post-Tensioned Concrete Girders

J.E. BREEN, O. BURDET, C. ROBERTS, D. SANDERS, and G. WOLLMANN
Phil M. Ferguson Structural Engineering Laboratory
Department of Civil Engineering
The University of Texas at Austin



Subject Areas

Maintenance
Public Transit
Rail

Research Sponsored by the American Association of State
Highway and Transportation Officials in Cooperation with the
Federal Highway Administration

TRANSPORTATION RESEARCH BOARD
NATIONAL RESEARCH COUNCIL

@Seismicisolation
NATIONAL ACADEMY PRESS
Washington, D.C. 1994

NATIONAL COOPERATIVE HIGHWAY RESEARCH PROGRAM

Systematic, well-designed research provides the most effective approach to the solution of many problems facing highway administrators and engineers. Often, highway problems are of local interest and can best be studied by highway departments individually or in cooperation with their state universities and others. However, the accelerating growth of highway transportation develops increasingly complex problems of wide interest to highway authorities. These problems are best studied through a coordinated program of cooperative research.

In recognition of these needs, the highway administrators of the American Association of State Highway and Transportation Officials initiated in 1962 an objective national highway research program employing modern scientific techniques. This program is supported on a continuing basis by funds from participating member states of the Association and it receives the full cooperation and support of the Federal Highway Administration, United States Department of Transportation.

The Transportation Research Board of the National Research Council was requested by the Association to administer the research program because of the Board's recognized objectivity and understanding of modern research practices. The Board is uniquely suited for this purpose as: it maintains an extensive committee structure from which authorities on any highway transportation subject may be drawn; it possesses avenues of communications and cooperation with federal, state and local governmental agencies, universities, and industry; its relationship to the National Research Council is an insurance of objectivity; it maintains a full-time research correlation staff of specialists in highway transportation matters to bring the findings of research directly to those who are in a position to use them.

The program is developed on the basis of research needs identified by chief administrators of the highway and transportation departments and by committees of AASHTO. Each year, specific areas of research needs to be included in the program are proposed to the National Research Council and the Board by the American Association of State Highway and Transportation Officials. Research projects to fulfill these needs are defined by the Board, and qualified research agencies are selected from those that have submitted proposals. Administration and surveillance of research contracts are the responsibilities of the National Research Council and the Transportation Research Board.

The needs for highway research are many, and the National Cooperative Highway Research Program can make significant contributions to the solution of highway transportation problems of mutual concern to many responsible groups. The program, however, is intended to complement rather than to substitute for or duplicate other highway research programs.

Note: The Transportation Research Board, the National Research Council, the Federal Highway Administration, the American Association of State Highway and Transportation Officials, and the individual states participating in the National Cooperative Highway Research Program do not endorse products or manufacturers. Trade or manufacturers names appear herein solely because they are considered essential to the object of this report.

NCHRP REPORT 356

Project 10-29 FY'86

ISSN 0077-5614

ISBN 0-309-05354-4

L. C. Catalog Card No. 93-060637

Price \$41.00

NOTICE

The project that is the subject of this report was a part of the National Cooperative Highway Research Program conducted by the Transportation Research Board with the approval of the Governing Board of the National Research Council. Such approval reflects the Governing Board's judgment that the program concerned is of national importance and appropriate with respect to both the purposes and resources of the National Research Council.

The members of the technical committee selected to monitor this project and to review this report were chosen for recognized scholarly competence and with due consideration for the balance of disciplines appropriate to the project. The opinions and conclusions expressed or implied are those of the research agency that performed the research, and, while they have been accepted as appropriate by the technical committee, they are not necessarily those of the Transportation Research Board, the National Research Council, the American Association of State Highway and Transportation officials, or the Federal Highway Administration, U.S. Department of Transportation.

Each report is reviewed and accepted for publication by the technical committee according to procedures established and monitored by the Transportation Research Board Executive Committee and the Governing Board of the National Research Council.

Published reports of the

NATIONAL COOPERATIVE HIGHWAY RESEARCH PROGRAM
are available from:

Transportation Research Board
National Research Council
2101 Constitution Avenue, N.W.
Washington, D.C. 20418

Printed in the United States of America

FOREWORD

By Staff
Transportation Research
Board

This report contains the findings of a study that was performed to provide guidance for designing reinforcement for tendon anchorage zones of post-tensioned concrete bridge girders. The study included both analytical and experimental investigations, including 137 physical tests of anchorage applications. Both existing literature and the results of research conducted for this study were examined in an attempt to develop design and construction procedures for end and intermediate anchorage zones for post-tensioned concrete girders. The report provides a comprehensive description of the research, including a discussion of the state of the art, the finite element analyses performed, the physical experiments undertaken, and recommended revisions to the AASHTO *Standard Specifications for Highway Bridges*. The proposed revisions are intended to provide information on the safe and efficient design of reinforcement for tendon anchorage zones, and were adopted by the AASHTO Highway Subcommittee on Bridges and Structures in 1993. The contents of this report will be of immediate interest and use to bridge engineers, concrete bridge constructors, post-tensioning-system suppliers, specification-writing bodies, researchers, and others concerned with the design and construction of post-tensioned concrete bridge elements.

Some current designs for anchorage zone reinforcement for post-tensioned concrete bridge girders have resulted in excessive cracking or congested reinforcing details. A perceived lack of adequate guidance in the AASHTO *Standard Specifications for Highway Bridges* has resulted in inconsistent design practices for some structural elements. Thus, it is important that engineers be provided with sufficient direction to ensure structural integrity and efficiency in design. Additionally, proper placing techniques for anchorage devices, reinforcement, and concrete must be followed, and an acceptable division of responsibilities among engineer, supplier, and constructor should be delineated.

NCHRP Project 10-29, "Anchorage Zone Reinforcement for Post-Tensioned Concrete Girders," was initiated in response to the need for improvements in design and construction guidance for anchorage zone reinforcement for post-tensioned girders. The researchers evaluated existing literature and data, and performed analytical studies and laboratory tests to develop new information. This report documents the work performed under Project 10-29 and discusses the testing procedures used and the finite element analyses performed in the preparation of the proposed specifications.

The recommended specifications represent a comprehensive revision to the existing AASHTO provisions. Detailed procedures are included for predicting first cracking load and ultimate load in post-tensioned concrete girder anchorage zones, and the overall recommendations are based on a limit state approach. A load factor for the maximum post-tensioning load is proposed, as well as a strength-reduction factor for anchorage zone calculations. In addition to these and other design (Division I) provisions, recommendations

for construction (Division II) also are presented, including a section on a special anchorage-device acceptance test that replaces Sections 10.3.1.4.3 through 10.3.1.4.5 of the current specifications. The recommended specifications provide for efficient and conservative design, and they were adopted by the AASHTO Highway Subcommittee on Bridges and Structures in 1993.

CONTENTS

1	SUMMARY
4	CHAPTER ONE Introduction and Research Approach
	Introduction, 4
	Problem Statement and Research Objectives, 4
	Research Approach, 5
	Scope of Study, 6
7	CHAPTER TWO Findings
	State-of-the-Art Summary, 7
	Background Information, 7
	Literature Review, 8
	Code Provisions, 11
	User Survey, 11
	Damages and Failures, 12
	Regulatory Framework, 13
	Local Zone, 14
	Important Parameters and Definitions, 14
	Rigid Bearing Plates, 16
	Present Code Provisions for Local Zones, 17
	Experimental Program, 17
	Cracking Load Predictions, 31
	Ultimate Load Predictions, 32
	General Zone Analysis Procedures, 34
	Introduction, 34
	Finite Element Analysis, 37
	Strut-and-Tie Models, 40
	Comparison of Finite Element Analysis and Strut-and-Tie Models, 46
	General Zone End Anchorage Tests, 75
	Anchorage Zones with Single Straight Concentric Tendons, 75
	Anchorage with Single Straight Eccentric Tendons, 86
	Anchorage Zones with Multiple Straight Tendons, 93
	Anchorage Zones with Inclined and Curved Tendons, 104
	Summary of Results, 110
	Slab Edge Anchorage Tests, 118
	Failure Patterns, 120
	Test Results, 123
	Findings of Test Results, 127
	Evaluation of Strut-and-Tie Model Predictions, 132
	Results of the End Reaction Tests, 132
	Behavior, 133
	Evaluation of Test Results, 135
	Results of the Intermediate Anchorage Tests, 137
	Behavior, 138
	Evaluation of Test Results, 141
	Results of Diaphragm Tests, 143
	Behavior, 143
	Evaluation of Test Results, 145
	Overall Findings from the Experimental Program, 147

150	CHAPTER THREE Interpretation, Appraisal and Application Approach for Design and Construction Regulations, 150
	Responsibilities, 150
	Limit States Judgements, 150
	General Zone Design Procedures, 153
	Local Zone Design Procedures, 155
	Recommended Provisions for AASHTO Bridge Specifications, 157
158	CHAPTER FOUR Conclusions and Recommendations
	Conclusions, 158
	General, 158
	Local Zone, 158
	General Zone, 159
	Recommendations for Future Research, 161
163	REFERENCES
166	APPENDIX A Literature Review
166	APPENDIX B User Survey and Assessment
166	APPENDIX C Details of Physical Test Specimens
167	APPENDIX D Design Examples
179	APPENDIX E Proposed Post-Tensioned Anchorage Zone Provisions

ACKNOWLEDGMENTS

The research reported herein was performed under NCHRP Project 10-29 by the Ferguson Structural Engineering Laboratory, Department of Civil Engineering, The University of Texas at Austin.

John E. Breen, holder of the Nasser I. Al-Rashid Chair in Civil Engineering, was the principal investigator. Gregory L. Fenves, formerly Assistant Professor of Civil Engineering at Texas and now Associate Professor of Civil Engineering at the University of California, Berkley, was a co-principal investigator for Phase A. John L. Tassoulas, Associate Professor of Civil Engineering, was co-principal investigator for Phase B.

The other authors of this report are Olivier L. Burdet, formerly Assistant Research Engineer at Texas, now Research Engineer, Swiss Federal Institute of Technology, Lausanne; Brian A. Falconer, Assistant Research Engineer; Carin L. Roberts, Assistant Research Engineer; David H. Sanders, formerly Assistant Research Engineer at Texas, now Assistant Professor of Civil Engineering, The University of Nevada at Reno; and Gregor P. Wollmann, Assistant Research Engineer.

The work was done under the general supervision of Dr. Breen. The authors would like to acknowledge the contributions of Drs. Fenves and Tassoulas to the analytical studies. Roy Duncan, Assistant Research Engineer, made substantial contributions to the slab anchorage tests while Dimitrios Koutsoukas, Assistant Research Engineer, investigated the application of nonlinear finite element analysis.

Throughout the study, the investigators were assisted by a wide range of professional associates and industrial interests who provided advice, shared knowledge and contributed materials. In particular, the authors would like to recognize the following:

- a) The Project 10-29 NCHRP Advisory Panel, George Markich, Chairman.
- b) The project consultant panel who helped formulate the overall approach. Members included Clifford L. Freyermuth (PTI and ASBI); T.Y. Lin (T.Y. Lin International); Robert F. Mast (ABAM Engineers); John Corven (Figg & Muller Engineers); and Earl Cutter (Cutter & Gallaway Services).
- c) The post-tensioners who provided equipments and devices: DSi International (Khaleel Shawef); Freyssinet International; Prescon Corporation; and VSL (David Swanson, Hans R. Ganz, Peter Marti, David Rogowsky).
- d) Florida Wire and Cable who provided strand.
- e) FIP Commission Liaison through Walter L. Podolny (FHWA) and Peter Matt (Switzerland).

Special thanks are expressed to Clifford L. Freyermuth who arranged widespread distribution of early drafts of the specification proposal, which resulted in substantial comment, and to all those potential users who took time to send us their valuable input.

ANCHORAGE ZONE REINFORCEMENT FOR POST-TENSIONED CONCRETE GIRDERS

SUMMARY

This study evolved from a widely perceived lack of guidance in the AASHTO *Standard Specifications for Highway Bridges* (henceforth referred to as the AASHTO Bridge Specifications) for the design and the approval of reinforcement for post-tensioned tendon anchorage zones. A comprehensive review of the current state of the art confirmed this perception and indicated that worldwide variations in the applications of current design approaches resulted in tensile force and reinforcement quantities which could literally differ by an order of magnitude (1000 percent).

The overall study encompassed a comprehensive literature review and an extensive state-of-the-art survey; comprehensive elastic finite element analyses, broad usage of strut-and-tie models, and 137 physical tests of anchorage applications. The tests included not only the traditional tests of concentric anchors in prisms, but also a wide variety of applications including concentric, eccentric, single, multiple, straight, inclined, curved, laterally post-tensioned, intermediate pocket, blister, rib, diaphragm, and slab anchors. It culminated in a comprehensive proposal for a complete revision in the AASHTO Bridge Specifications provisions for post-tensioned anchorage zones.

A major result is the proposed division of the anchorage zone into a local zone and a general zone. The local zone consists of the prism of concrete surrounding and immediately ahead of the anchorage device and its confining reinforcement. Its behavior is strongly influenced by the anchor device characteristics and the confining reinforcement. The local zone behavior is influenced very little by the geometry and loading of the overall structure. The general zone consists of the large volume of concrete through which the concentrated post-tensioning force spreads transversely until there is a more linear stress distribution across the entire member cross section. The importance of this division of the anchorage zone is that it allowed a corresponding logical arrangement of design criteria and acceptance testing. It was especially significant in that it facilitated a logical and equitable division of responsibility. The anchorage device supplier is responsible for furnishing a proper device as well as documented recommendations for local zone cover, spacing, confining reinforcement and supplementary reinforcement. Specific guidance is given for two types of anchorage devices. Basic anchorage devices can be accepted on the basis of calculations if they meet specified bearing stress and stiffness requirements. Detailed acceptance test requirements are given for special anchorage devices. Acceptance criteria are based on

crack width limitations at service levels, crack stability, and ultimate strength levels. The engineer-of-record is responsible for final approval of the local zone details.

The engineer-of-record has primary responsibility for design of the general zone. The constructor is responsible for correctly placing the device, specified reinforcement, well-compacted concrete, and for carrying out the stressing operations as specified. The local zone criteria become the lower bound criteria for the main nodes in the general zone. Additionally, general zone reinforcement must be provided for substantial tensile bursting stresses normal to the tendon axis, compatibility induced spalling tensile stresses along the loaded edge, equilibrium induced spalling tensile stresses between widely spaced multiple anchors, and longitudinal edge tensile stresses when anchor loads are applied outside the kern. It was shown that final failure often depends on the compression strut (or stress field) capacity ahead of the local zone node. Detailed evaluation of the test program results indicated that the general zone design could be based conservatively and expeditiously on strut-and-tie models using general principles outlined in the proposed Specification revision. Alternatively, the general zone design could be based on elastic analysis results although proportioning of reinforcement is somewhat more difficult. For many simplified, although widely used applications, a much simpler approximate procedure was presented which gives the magnitude and centroid of the bursting force, as well as an estimate of the maximum compressive stress at a critical section ahead of the anchorage. This approximate procedure was developed from parametric studies using the more accurate strut-and-tie models and finite element analysis. They produce equivalent results for a wide range of practical cases.

Detailed procedures are presented for first cracking load prediction and ultimate load prediction. The overall recommendations are based on a limit state approach. Serviceability is ensured by crack width limits at normal stressing levels in the local zone anchorage device acceptance tests. It was shown conclusively that these are acceptable lower bounds to behavior of the device in the general zone. Robustness at ultimate is ensured by proper choice of load factors and resistance factors. A load factor of 1.2 is proposed for application to the maximum post-tensioning load. A Φ factor of 0.85 is proposed for all anchorage zone calculations. Maximum compressive stress in the unconfined concrete of the general zone is limited to $0.75f'_c$. Use of these limits will produce robust, conservatively designed anchorage zones with realistic safety levels.

Comparison of the test results with the calculation procedures indicated that the proposal is safe and has substantial conservatism in many cases. This is primarily due to two factors. One is the neglect of the concrete tensile capacity which can be substantial but also unreliable. The second factor is the plastic redistribution of the forces at the far end of the anchorage zone. Both the basic strut-and-tie model and the elastic finite element analyses assume forces are distributed elastically at the end of the anchorage zone. Test results indicated that substantial redistribution and higher capacity are possible but are not totally dependable at this stage of knowledge. Further studies are necessary in this area.

Specimens that had reinforcement significantly different from that indicated by elastic analysis had additional cracking and sometimes reduced strength. Therefore, it is recommended that only the reinforcement placed within a distance of 1.5 times the section width from the loading surface be considered in bursting calculations and the centroid of that reinforcement should be located somewhat close to the pattern suggested by elastic analysis. Good engineering judgment should be exercised in detailing so that overly large plastic redistribution is not required. In detailing, it is extremely important that the designer be sensitive to the requirements of constructability. Reinforcement tolerances and bending requirements, as well as the need for adequate paths for concrete placement and vibration, must be provided.

The extensive and detailed recommendations for revision to the AASHTO Bridge Specifications regarding post-tensioned anchorage zones should result in clearer, more consistent and more rational design, detailing and approvals. By relating technical issues with division of responsibility, the overall framework for anchorage design and construction is significantly advanced and the potential for unfair claims and accidents is diminished.

CHAPTER 1

INTRODUCTION AND RESEARCH APPROACH

INTRODUCTION

The performance of concrete structures can be dramatically improved by imposing a self-equilibrating state of stress that partially offsets the stresses due to external loads. This "pre-stressing" of the structure permits the construction of longer, more slender girders, allows better control of deflections, and delays cracking of the concrete. Because of these advantages, prestressed concrete has become a very popular construction material throughout the world.

Prestressing of concrete requires the introduction of large, concentrated tendon forces into the member. The dispersion of this tendon force induces tensile stresses over some distance ahead of and behind the anchorage. The region affected by the introduction of the tendon force is called the "anchorage zone." In pretensioned concrete structures the transfer of forces from the tendon onto the concrete occurs through bond stresses over the transfer length of the prestressing steel and is gradual. In post-tensioned concrete, anchorage hardware is used and the transfer of the tendon force is localized, causing high compressive stresses immediately ahead of the anchorage device and substantial tensile stresses normal to the tendon axis. Frequently, proprietary anchorage devices are used for anchorage of post-tensioning tendons that employ local confinement reinforcement to achieve higher bearing pressures than normally accepted for concrete. Use of such anchorage devices should be based on acceptance tests that have to prove that such high bearing pressures do not cause serviceability problems and that the anchor is capable of developing the full tendon force.

Pretensioned concrete has been used extensively in North America. Because of the repetitive, industrialized production of pretensioned concrete components, manufacturers are very experienced with this type of structure. In contrast, the use of post-tensioned concrete puts high demands on designer, anchorage device supplier, and constructor because of its greater versatility and the more concentrated stresses in the anchorage zone. Yet, there is a lack of general guidelines for the design of anchorage zones in post-tensioned concrete structures. Considerable confusion exists about the responsibilities of the designer, the anchorage device supplier, and the constructor. This has led to a wide range of problems. At one extreme is the total absence of anchorage zone reinforcement, because of ignorance of the necessity for anchorage zone design or because of reliance on the other parties involved. At the other extreme are highly congested anchorage zone details resulting in poor concrete placement and compaction around the anchorage devices. These problems have resulted in a number of actual failures and substantial delays and litigation (1).

A large number of studies of anchorage zone behavior and design have been conducted for more than 70 years; yet, this abundance of information seems to have contributed more to the confusion rather than to the alleviation of it. While research has focused on a narrow range of special and often very idealized problems, the versatility of post-tensioned concrete requires a general and systematic procedure for anchorage zone design. Current U.S. code provisions were developed with a very special application in mind and are not adequate to cover the wide range of anchorage zone problems encountered in modern post-tensioned concrete construction.

PROBLEM STATEMENT AND RESEARCH OBJECTIVES

NCHRP Project 10-29, "Anchorage Zone Reinforcement for Post-Tensioned Concrete Girders," was initiated with the objective to develop design procedures for end and intermediate anchorage zones for post-tensioned concrete girders and slabs. The NCHRP research problem statement for this project stated:

The AASHTO *Standard Specifications for Highway Bridges* do not provide adequate guidance for designing reinforcement for tendon anchorage zones of post-tensioned concrete girders and slabs. Current designs can result in excessive cracking or congested reinforcing details. The wide variation of design practices currently in use suggests the need for research in this area.

Recent investigations at The University of Texas at Austin have developed design procedures for single tendons anchored in the webs of girders. However, additional information is needed for multiple tendons and other problems such as: influence of additional shear in support regions, bearing stresses for different types of anchorage systems, and the influence of diaphragms. Design criteria are needed for reinforcement details for inclined, sharply curved, and/or highly eccentric tendons, and for intermediate anchorages and coupling joints of tendons. [Post-tensioning couplers and looped anchors were later deleted from the scope.]

From the detailed tasks formulated by NCHRP in its original request for proposals, it was obvious that the major concerns leading to the study were the almost complete absence of guidance and regulations in the AASHTO Bridge Specifications regarding post-tensioned anchorage zones. In post-tensioning, it is necessary to transfer the often appreciable forces in the post-tensioning tendon to the concrete structure through a highly concentrated mechanical device called a post-tensioning anchorage device. Extremely high local bearing stresses can be applied by these devices. Often proprietary hardware devices are used with substantial confining reinforcement. At the start of this study, the AASHTO Bridge Specifications had very limited ways to check allowable bearing stresses and no procedures to check

confinement requirements or adequacy. Design procedures for other reinforcement required in the anchorage zones were rudimentary and, in fact, there was not a clear definition of the anchorage zone extent. Growing numbers of applications with eccentric tendons, inclined tendons, curved tendons, multiple tendons, external tendons, intermediate anchorages, and diaphragm anchorages had far exceeded the limitations of simplified design procedures suggested in American texts. In addition to the technical uncertainties, a considerable number of problems were occurring in which the question of responsibility for contract matters as well as failures was vague and unassigned. Designers, anchorage device suppliers, constructors, and owners were not clear as to their responsibilities. AASHTO sponsored this study, which was conducted within the NCHRP, with the objective of developing specific specification recommendations that AASHTO could consider for adoption to minimize both the technical and the responsibility problems.

RESEARCH APPROACH

The general approach to this problem consisted of a series of highly interactive tasks: (1) determination of the state-of-the-art, (2) analytical investigations, (3) experimental investigations, and (4) design criteria development. Substantial detail on each of these tasks will be given in subsequent sections of this report. In this section a very brief description is given to explain the overall approach followed.

The current approach and existing knowledge concerning the design and performance of post-tensioning anchorages were determined by comprehensive reviews of technical literature, of catalog material and descriptions of commercially available anchor systems provided by manufacturers and the Post-Tensioning Institute, and of reports including substantial application details and summaries of problems. The latter were provided by respondents to a comprehensive questionnaire sent to all state and provincial transportation departments and a wide range of design firms.

The state-of-the-art results indicated that while a wide range of analytical and experimental investigations had been carried out, and while a number of design approaches had been suggested or adopted, there was not a recognized coherent, logical framework for anchorage zone design. Study of the material submitted indicated substantial conflict in design approach and criteria, as well as no clear division of responsibility between anchorage system suppliers, designers, and bridge constructors.

It was concluded from these initial studies that the most feasible approach to the development of possible AASHTO criteria lies in adoption of a limit states approach with a clear division of responsibilities. It was envisioned that the criteria would address the serviceability limit state by establishing procedures for assessing the onset of surface cracking at realistic tendon stressing levels in typical applications, and providing guidelines for proportioning anchorages to avoid cracking or to provide effective reinforcement to control such cracking to acceptable limits. This would require experimental verification of cracking loads and crack widths, as well as a heavy reliance on analytical determination of tensile stress distributions in the uncracked state. The ultimate limit state at maximum probable tendon force levels would be addressed by establishing procedures to determine the effective contribution of various reinforcement tech-

niques using the strut-and-tie models similar to those detailed by Schlaich et al. (2). Practical implementation of such an approach required the availability of elastic or plastic stress trajectories to assist in the development of realistic strut-and-tie models for a wide range of applications. The analytical and experimental phases of this project were primarily aimed at the development of such techniques, as well as a comprehensive verification of the adequacy of such strut-and-tie models in accurately predicting anchorage zone capacity. The analytical studies would also indicate where modern analytical techniques like finite element analysis (FEA) would be used, if desired, and comparison with the experimental results would provide guidance on proper use of such analyses. In addition, it was hoped that the analytical studies would indicate where simpler approximate equations could be safely used for anchorage zone design.

The range of applications to be examined were determined from the survey of user groups such as the AASHTO Bridge Committee membership. The large number of applications tend to fall into a few generic classes, as outlined later in this report. These generic classes provided the basis for the various test and analysis series of the detailed working programs.

The reexamination of the anchorage zone problem indicated that substantial clarity is introduced if the anchorage zone is subdivided, as shown in Figure 1, into two areas that reflect some difference in responsibilities. The first, or local, zone is that region which closely surrounds the specific hardware device. In this region the manufacturer or supplier often has a proprietary product and is basically interested in the local behavior. Such questions as effective bearing area and local confinement immediately around the anchor fall into this classification. While the manufacturer or supplier has the prime responsibility, there is a need for AASHTO criteria to establish performance requirements or provide checking procedures even for this local problem. The second or general region is the portion of the anchorage zone more remote from the immediate anchorage hardware device. These are the areas subject to spalling or bursting stresses, where the designer and the constructor must ensure that proper reinforcement is provided to prevent premature failure or unwanted cracking. There is an obvious need for better AASHTO criteria for these general cases.

In order to properly develop the final design and construction criteria, the analytical and experimental investigations were organized to first explore local zone criteria and spot check the adequacy of possible local zone criteria for several widely used types of anchorage devices. The study then explored the general zone behavior and analysis for the most frequently reported anchorage zone configurations, assuming that local zone behavior could be appropriately controlled by the criteria resulting from the local zone investigations. In the general zone studies, the approach basically consisted of using a linear elastic analysis to indicate the general distribution of stress fields. Appropriate strut-and-tie models were then developed for use in the proportioning of the general zone reinforcement. This reinforcement was instrumented in test specimens to provide confirmation or evaluation of the reinforcement patterns used. Specimens were tested to failure with cracking development, force distributions patterns, and ultimate loads being monitored. The results were checked against the design assumptions and the final criteria developed in such a fashion that designers should be able to implement the procedures for design without requiring complex analysis except for the most unusual cases. It is emphasized

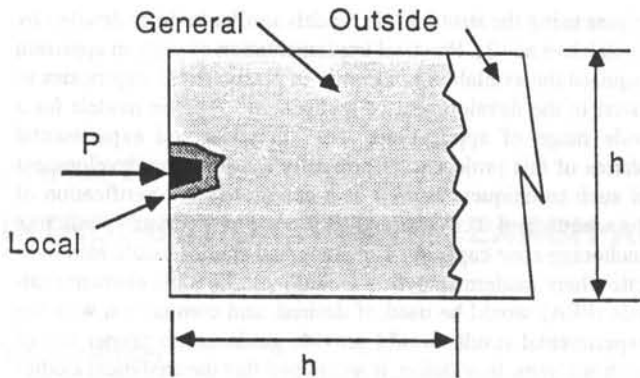


Figure 1. Subdivision of anchorage zone.

that the physical tests were used in verification of the largely equilibrium analysis of the strut-and-tie models and finite element analyses. The tests were not used to develop empirical expressions. This allowed a wide ranging scope of tests with few replications and seemed to be the best use of the limited resources.

SCOPE OF STUDY

The objective and scope of the project was the development of a definitive proposal for a revision of the AASHTO Bridge Specifications that would provide a safe, economical, and technically correct approach to the design and construction of post-tensioned concrete anchorage zones.

The overall approach to achieve the project objective was accomplished as follows.

The analytical and design model approaches investigated included: (1) linear elastic analysis using finite element models (FEA); (2) strut-and-tie models (STM) based on linear elastic force paths at the end of the anchorage zone; (3) approximate equations to represent in a convenient way the effect of variables that were principally based on the results of the finite element analysis parameter studies; (4) an exploratory study of nonlinear finite element models; and (5) modified strut-and-tie models based on nonlinear force distributions at the end of the anchorage zone.

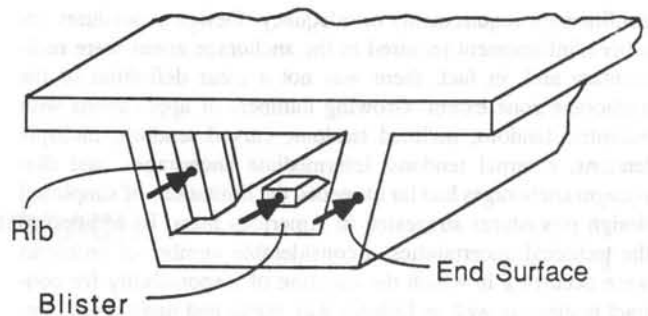


Figure 2. Anchorage location types.

The applications studied included: (1) local zone series (relationship between local and general zones (see Figure 1), studies of cover, reinforcement, and device geometry relationships to develop local zone criteria, and verification of local zone performance test criteria); (2) end anchors, end surface in Figure 2 (single anchorage in beam ends, multiple anchorages in beam ends, concentric anchorages, eccentric anchorages, anchorage inclination, tendon curvature, effects of transverse post-tensioning on single and multiple anchorages in beam ends, effect of variations in reinforcement distributions in the general zone, and effect of local applied loads or end reactions); (3) multiple anchorages along slab edges (effect of anchor plate type, effect of varied spacing and grouping of tendons on anchorage zones, and effect of stressing sequence); (4) end anchorages in diaphragm type applications; (5) intermediate anchorages, blister or rib in Figure 2 (intermediate anchorage post-tensioning load distribution reinforcement requirements (especially behind the anchorage zone), pocket anchorages, slab or flange blisters, corner blisters, and ribs).

Criteria and design procedures to be developed included: (1) limit state post-tensioning load levels with appropriate load and resistance factors; (2) performance criteria and test procedures for local zone hardware acceptance; (3) analysis methods and proportioning criteria for single and multiple anchors in beam ends; (4) analysis and proportioning criteria for anchorages in diaphragms and for the effects of local concentrated loads and reactions; (5) analysis and proportioning criteria for distribution of load transfer reinforcement in front of and behind intermediate anchorages; and (6) analysis and proportioning criteria for intermediate anchorage zones such as slab, flange, and corner blisters including out-of-plane deviation effects.

CHAPTER 2

FINDINGS

STATE-OF-THE-ART SUMMARY

Throughout the duration of this project, an appreciable effort was made to maintain direct contact with a wide range of individuals and organizations active in the application of post-tensioning to bridge structures. Early in the study a survey document was developed and approximately 150 surveys were sent to all bridge division members of AASHTO, a number of post-tensioning suppliers, a group of design firms and active research contributors. Approximately 70 responses were received and tabulated. The overall scope and approach of the study was reviewed and refined in cooperation with both the NCHRP project panel and the project advisory panel developed from outstanding practitioners in the field. Interim recommendations were published and distributed by the Post-Tensioning Institute (PTI) and the American Segmental Bridge Institute (ASBI) for industry-wide comment. Meetings were held with representatives of major post-tensioning systems who provided substantial test reports and background information. A comprehensive design seminar and workshop were presented at the ASBI annual meeting in Miami in December 1990, and a presentation was made to the AASHTO Prestressed Concrete Structures Committee in San Francisco in May 1991. On each of these occasions, substantial comments and suggestions were received that were introduced into the study and helped to shape the recommendations.

Background Information

The concentrated prestressing force is transferred through anchorage hardware from the tendon onto the concrete, and then spreads out to reach a more linear stress distribution over the cross section of the member at some distance from the anchor. Figure 3(a) illustrates this flow of forces for the case of a concen-

tric end anchor. As the compressive stresses spread out, they have to deviate from the direction parallel to the load. This induces lateral compressive stresses immediately ahead of the anchor and, then, lateral tensile stresses that eventually diminish (b in Figure 3). The lateral tensile stresses are usually referred to as "bursting stresses." The interaction between the deviation of the longitudinal compressive stresses and the lateral stresses can be readily visualized by the strut-and-tie model (STM) shown in Figure 3(c).

Figure 4 shows contour plots for the principal tensile and compressive stresses for the same anchorage zone problem. Three critical regions can be identified: (1) the region immediately ahead of the load is subject to large bearing and compressive stresses; (2) the bursting zone extends over some distance ahead of the anchorage and is subject to lateral tensile stresses; and (3) local tensile stress concentrations exist along the loaded edge of the member. The tensile stresses along the loaded edge have become known as "spalling stresses," despite the fact that they do not cause any spalling of the concrete.

At some distance from the anchor, the stresses on the cross section can be determined from ordinary bending theory. Within this distance bending theory is not valid, because the ordinarily assumed linear strain distribution is disturbed by the introduction of the concentrated anchorage force. The region affected by this disturbance is the "anchorage zone."

The extent of the anchorage zone can be estimated using the principle of Saint Venant. This principle states that, if a load on a structure is replaced by a set of statically equivalent loads, the state of stress in the structure is changed only in the vicinity of the load application. At a distance approximately equal to the distance between the statically equivalent applied loads both statically equivalent load cases cause the same state of stress. For example, a concentric axial force at the end of a beam might

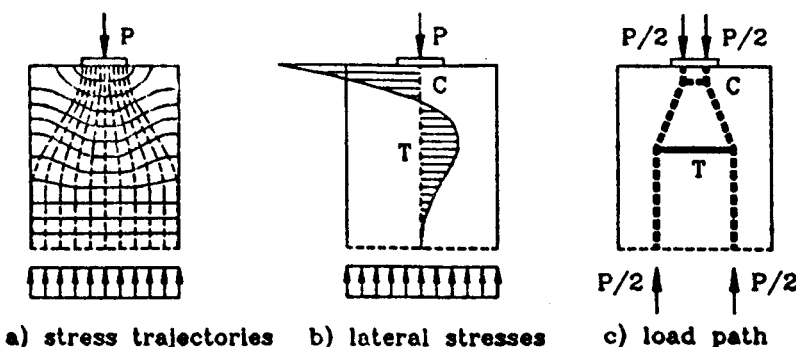


Figure 3. Flow of forces in concentrically loaded anchorage zone.

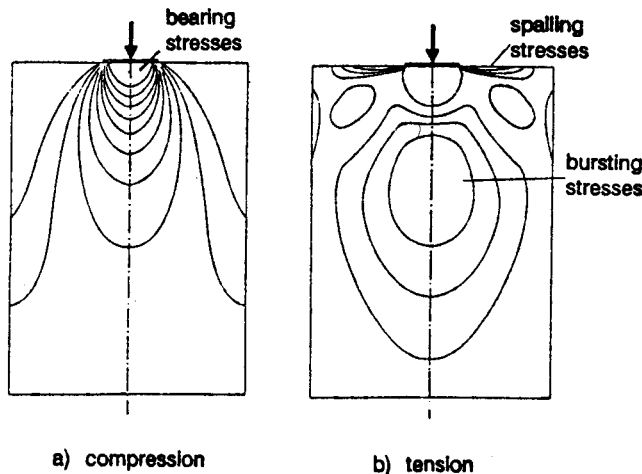


Figure 4. Stress contours for concentrically loaded anchorage zone.

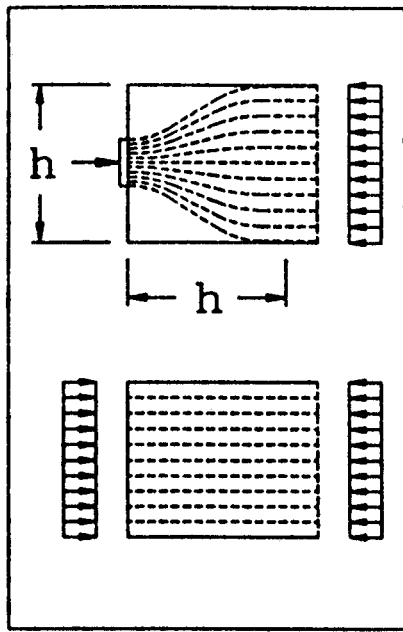


Figure 5. Principle of Saint Venant.

be replaced by an equivalent uniform load over the full height of the member (Figure 5). Of course, this will change in the state of stress near the end of the beam. However, at a distance equal to the extent of the uniform load, in this example one beam height, the state of stress in the structure is not affected by the change of loading.

As indicated in Figure 4(a), the magnitude of the compressive stresses is highest immediately ahead of the anchor, but decreases rapidly as the compression stresses spread out into the structure. For this reason, proprietary special anchorage devices are frequently used. They enhance the local compressive strength by some form of confinement and reduce the bearing pressure by distributing the anchorage force over a series of bearing plates

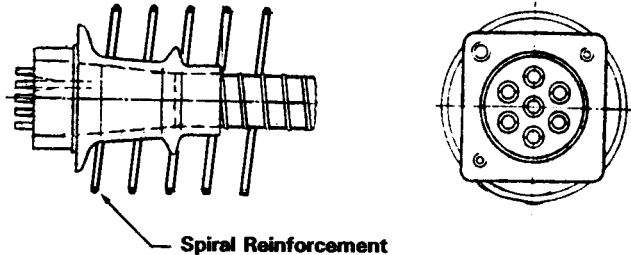


Figure 6. Special anchorage device (from Ref. 60).

or ribs (Figure 6). In many European countries the acceptance of such special anchorage devices is based on standardized acceptance tests (3,4).

In the early stages of the project, Sanders (1) conducted a very comprehensive review of the state of the art of anchorage zone design, which included a review of technical literature, product information and current code provisions. A detailed discussion is given in Appendix A. In addition, an industry-wide user survey was conducted and details of this survey are contained in Appendix B. Only brief summaries of these reviews will be given in the main text of this report.

Literature Review

The problems associated with the introduction of concentrated loads into a structure have been studied for almost 70 years. In 1924 Mörsch introduced an equilibrium-based model to visualize the load path in concentrically loaded members (Figure 7) (5). Since then a large number of studies on anchorage zone problems have been conducted. They include linear elastic studies, such as theory of elasticity, finite element analyses, photoelastic investigations, nonlinear analyses, and experimental studies. A comprehensive review of many of these past studies is included in Appendix A. Only highlights are given here.

A classic solution based on the theory of elasticity was presented by Guyon in 1953 and is still widely used today (6). He determined the bursting stress distribution ahead of a concentric end anchor for different ratios of plate width to member width (Figure 8). Figure 9 shows the magnitude of the integrated bursting stresses and a comparison to the bursting force obtained from Mörsch's simple truss solution. The agreement is remarkably good and many codes use some variation of Mörsch's equation even today. Guyon extended the application of his solution to eccentrically loaded anchorage zones by introducing the "symmetrical prism" approach (Figure 10).

A large number of linear elastic studies were conducted, all of which essentially confirm Guyon's solution, including the symmetrical prism approach. But they also revealed some of its limitations. For example, spalling stresses, which occur along the loaded edge in concentrically and eccentrically loaded anchorage zones and between multiple anchors, are not predicted. Also, Guyon's solution is only valid for members with rectangular cross section. The bursting stresses in I-sections, as an example, are larger than those in beams with rectangular cross section.

Adeghe and Collins conducted a nonlinear finite element study and pointed out that a significant redistribution of stresses takes place after cracks have developed in the anchorage zone (7).

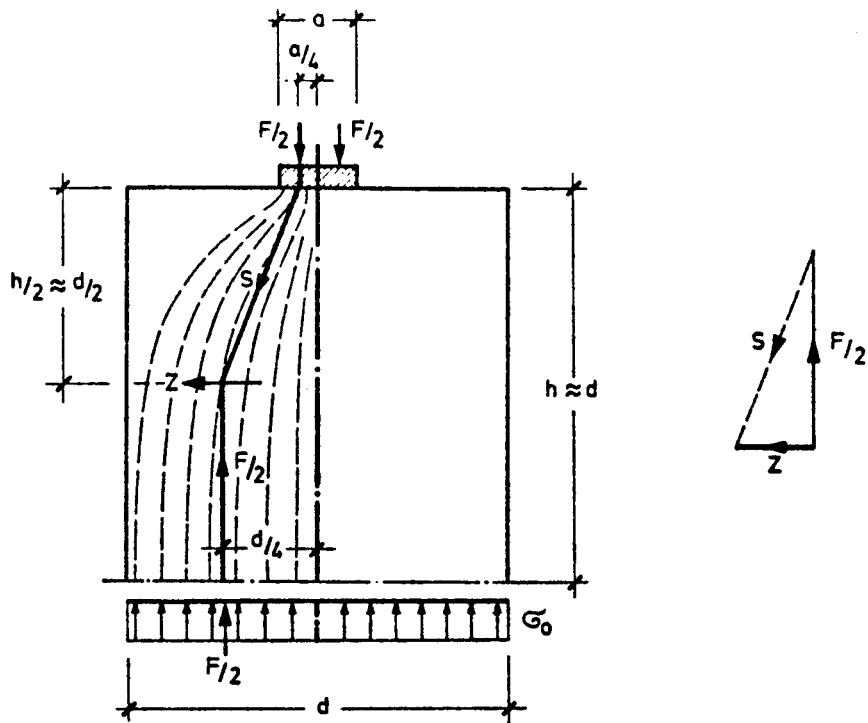


Figure 7. Mörsch's load path model (from Ref. 21).

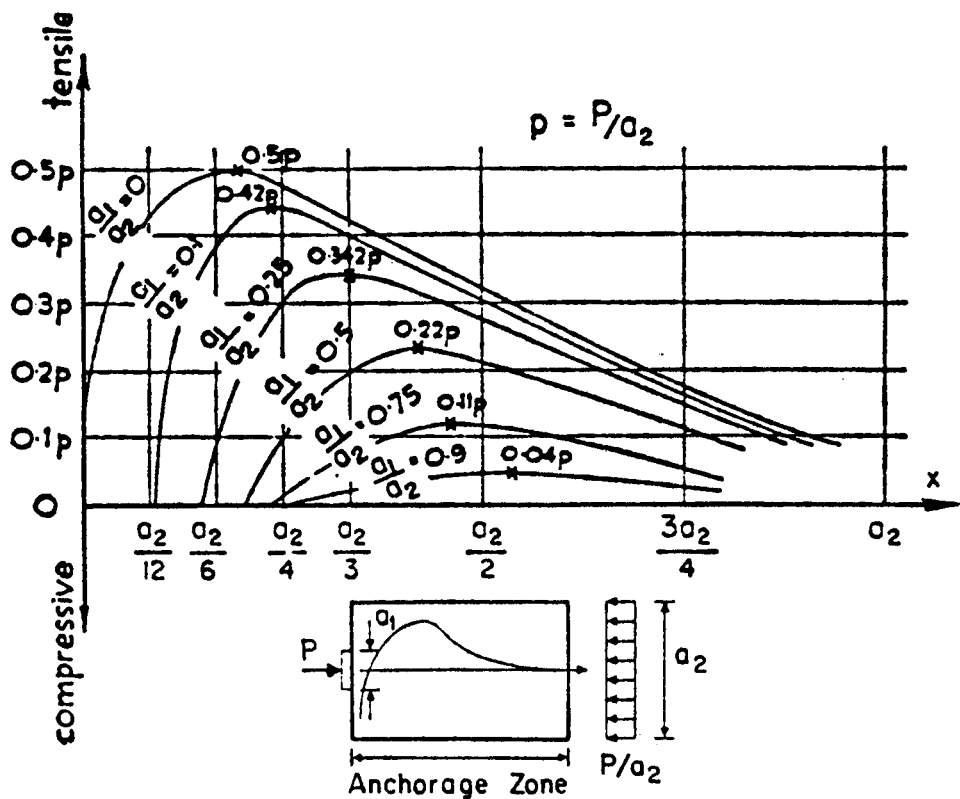


Figure 8. Guyon's solution for the bursting stresses in concentrically loaded anchorage zones (from Ref. 6).

@Seismicisolation

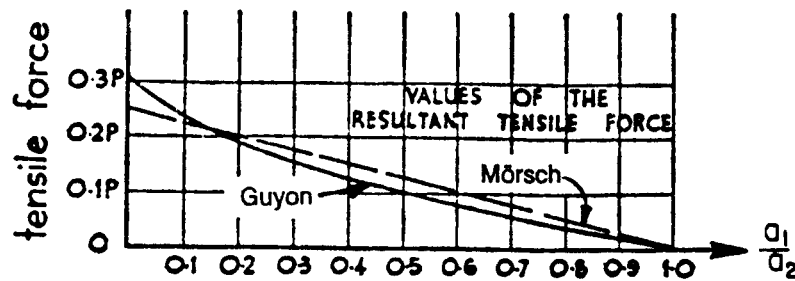


Figure 9. Magnitude of bursting force (adapted from Ref. 6).

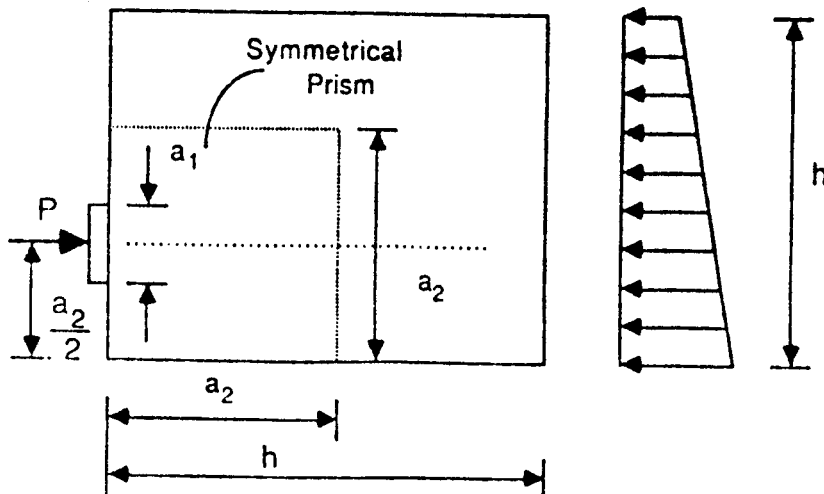


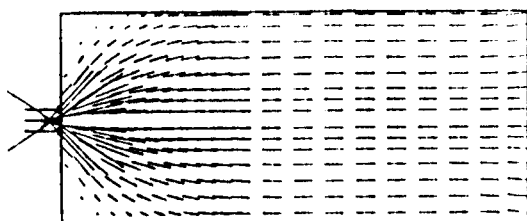
Figure 10. Guyon's symmetrical prism (from Ref. 25).

This redistribution causes the compressive stresses in the anchorage zone to spread out at a steeper angle (Figure 11). Fenwick and Lee made the same observation in an experimental study and pointed out that the redistribution of stresses tends to reduce the bursting force (8). They also confirm the increase of the bursting force in members with I-sections.

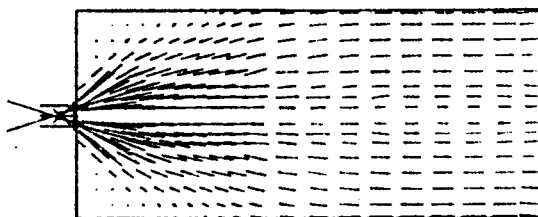
Other experimental studies dealt with the effect of increasing tendon inclination and eccentricity, which tend to increase the tensile force along the loaded edge of the member. Guyon's symmetrical prism approach is found to be useful and safe for the determination of the bursting force within its range of applicability in many of these investigations.

Stone and Breen conducted a comprehensive experimental and analytical study of single anchorages in thin web members, which is frequently quoted by users and researchers (9,10). They developed empirical equations for cracking and ultimate load predictions, which take into account type of anchor, tendon eccentricity, tendon inclination, anchor plate size, section thickness, concrete strength, and type and amount of supplemental reinforcement (spiral, orthogonal reinforcement, lateral post-tensioning). The major difficulty with their recommendations appears to be that they are very conservative and are limited to anchorage zone problems not too different from those of their study.

A number of experimental studies were concerned with the bearing strength of concrete. The equations generally used today assume the bearing strength of concrete to be proportional to



(a) compressive stress flow, linear elastic analysis



(b) Compressive stress flow, nonlinear analysis

Figure 11. Redistribution of stresses after cracking (from Ref. 7).

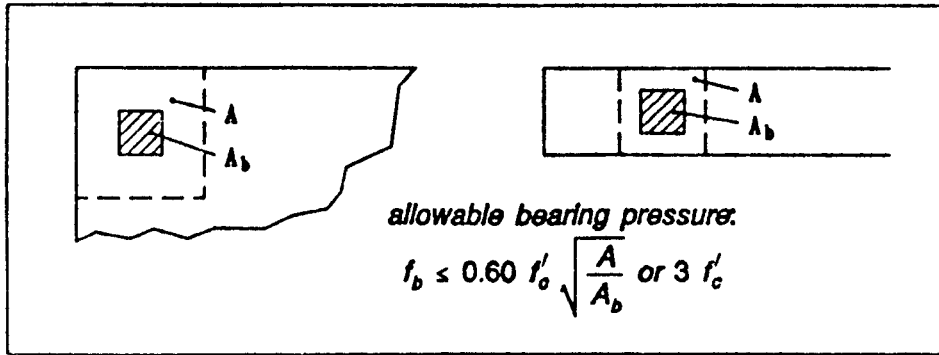


Figure 12. Middendorf's bearing pressure equation (adapted from Ref. 4).

the cylinder strength, and to the square root of the ratio of the supported area to the loaded area, where the supported area is geometrically similar to and concentric with the loaded area. The square root relationship was proposed by Komendant (11) in 1952 and again by Middendorf (12) in 1960. They based their recommendations on a large number of tests on unreinforced concrete blocks and cylinders (4). Figure 12 illustrates the definition of the supported area and shows Middendorf's proposal for the allowable bearing pressure.

Hawkins (13,14,15) conducted a study on the influence of the stiffness of the bearing plate. Increase in thickness of the bearing plate increased the capacity of his specimens. However, beyond a certain thickness the bearing plate acted as a rigid plate and further increase in thickness was not effective.

Code Provisions

A detailed survey of U.S. and foreign code provisions is included in Appendix A. Current code provisions generally are concerned with limiting the bearing stress ahead of the anchorage, with the determination of the bursting force, and with arrangement of the bursting reinforcement. Some codes include provisions for spalling forces (1).

Limits on the bearing pressure generally are very similar to the equation recommended by Middendorf, with some variation on the multiplication factor and the maximum allowable bearing strength. One exception is the AASHTO code (16), which prescribes a flat bearing stress limit of $0.9f'_c$, but not more than 3000 psi after seating of the tendon. In the segmental bridge guide specifications proposed by the Post-Tensioning Institute the following allowable bearing pressure limitations are recommended (17):

$$\text{at stressing } f_b \leq 0.8 f'_c \sqrt{A/A_b} - 0.2 \text{ or } 1.25 f'_c \quad (1a)$$

$$\text{after seating } f_b \leq 0.6 f'_c \sqrt{A/A_b} \text{ or } 1.25 f'_c \quad (1b)$$

These equations were adopted in the 1991 AASHTO interim specifications (18). In Europe many codes include provisions for special anchorage devices that are not subject to bearing pressure limitations, but have to pass a standardized acceptance test.

Determination of the bursting force is generally based on some variation of Mörsch's expression or Guyon's solution for the

concentrically loaded anchorage zone. Usually, provisions for arrangement of the bursting reinforcement are also included. AASHTO does not give any recommendations on the determination of the bursting force, but requires a grid of horizontal and vertical reinforcement placed less than $1\frac{1}{2}$ in. from the anchor bearing plate "to resist bursting stresses" (16). The effectiveness of this reinforcement arrangement for the purpose of resisting bursting stresses must be questioned. Bursting stresses usually are critical significantly further ahead of the anchorage device than $1\frac{1}{2}$ in. Probably this grid is intended to enhance the bearing strength of the concrete immediately ahead of the anchor. However, for this purpose, spiral confinement reinforcement is more effective. This is reflected by the design codes used in Florida and North Carolina, which require the use of spirals and explicitly exclude the use of grids (1).

User Survey

Sanders (1) conducted an industry-wide survey to obtain information on commonly used anchorage zone configurations and reinforcing details, problems encountered in design or checking of anchorage zones, analysis procedures and references used, and specific failures or severe distress.

A questionnaire was sent out to researchers, designers, and to all bridge division members of AASHTO. The questionnaire and a more detailed summary of the responses are given in Appendix B. Some of the conclusions of the survey results follow (1):

1. The reference and design methods most frequently used include the PTI recommendations (19), Guyon's symmetrical stress block (20), and recommendations by Leonhardt (21).
2. The empirical equations by Stone and Breen often are very conservative and require too much reinforcement and a very high concrete strength before stressing. This leads to congestion of the anchorage zone and slows down casting cycles.
3. The AASHTO provisions are either overconservative or nonexistent. The grid of horizontal and vertical reinforcement close to the anchors is not effective, but leads to congestion and concrete consolidation problems.
4. A spiral is much more effective than the orthogonal reinforcement grid required by AASHTO. The spiral should be large enough to enclose the entire anchor bearing plate and its length should be at least one and one-half times the diameter of the

spiral or twice the width of the bearing plate. One responder reported problems with concrete placement and consolidation with the typical spiral pitch of 1 in. to 1½ in. and recommended a spiral pitch of 2½ in. to 3½ in.

5. Congestion of reinforcement is a serious problem. Poor concrete consolidation due to congestion was the direct reason for a number of anchorage zone failures.

Damages and Failures

Problems with objectionally wide cracking in anchorage zones have occurred in the past. A precast bridge in Texas (22), a cast in-place box-girder bridge described by Dilger and Ghali (23), the Olympic Stadium in Montreal (24), and a major light weight concrete bridge in California (22) have all developed cracks in the anchorage zone that were of concern to designers or owners. Breen et al. (25) conducted a survey of designers and contractors who are involved in post-tensioned concrete design and construction to get their input on various aspects of the anchor zone. The survey asked if failures or excessive cracking had been experienced in any structure of which the respondent was aware. Many respondents, particularly engineers with various states' departments of transportation, reported problems in anchorage zones. These problems ranged from small hairline cracks in the end blocks of post-tensioned girders to explosive failures in transversely post-tensioned bridge decks. Many other incidents of cracking in structures attributed to a lack of proper confinement reinforcing around the anchor have also been reported. In many of these cases the cracking which occurred was partially controlled by supplementary reinforcement and there was no appreciable reduction in member strength. The cracks could be detrimental in that they provide a path for the penetration of moisture and salts that can potentially cause corrosion and frost damage. The formation of these wide cracks negates one of the major factors leading to the choice of prestressed concrete, the minimization of cracking at service loads.

Most damages to anchorage zones in post-tensioned concrete structures occur during construction, when large tendon stressing forces are applied to usually immature concrete. However, Libby describes an anchorage zone failure of a post-tensioned roof slab after 5 years of service (26). He attributed the failure to the combined effect of anchorage zone stresses and cyclic flexural tensile stresses at a slab-column joint in close proximity to the anchorage.

Reinforcement congestion in the anchorage zone is a frequent cause for poor concrete consolidation, resulting in failures caused by crushing of the concrete ahead of the anchor (27). Congested anchorage zone details also complicate placing of the reinforcement. A respondent to Sanders' survey pointed out that special attention must be paid to placing confining spiral reinforcement coaxially with the tendon.

Another frequent problem in anchorage zones is cracking of the concrete, particularly along the tendon path. However, such cracking does not necessarily imply a structural deficiency. In fact, because of the presence of tensile stresses in the anchorage zone, a limited amount of cracking should be expected. That makes it all the more necessary to provide well-detailed anchorage zone reinforcement to control cracking and to inhibit potential corrosion problems. A popular detail for anchorage zones in slabs does not provide any bursting reinforcement in the slab

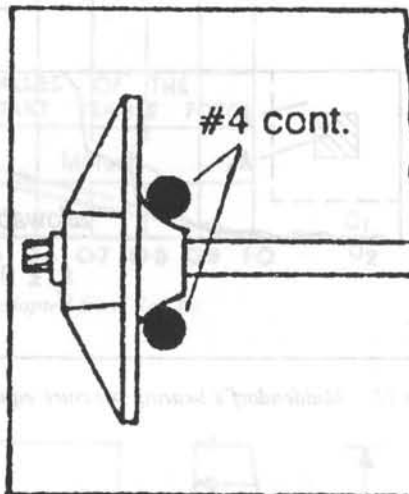


Figure 13. Typical slab anchorage detail.

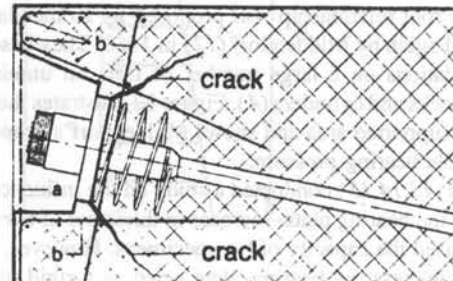


Figure 14. Unstressed corner cracking (from Ref. 58).

thickness direction and, therefore, relies completely on the concrete tensile strength (Figure 13). This may be acceptable for single, widely spaced strands in thin slabs, but problems are common for closely spaced anchors and anchors close to the side edge of the slab. Macchi describes explosive failures due to splitting of the slab, where closely spaced tendons caused large bursting stresses and at the same time created a weak plane in the slab (28).

Figure 14 shows how "unstressed corners" are susceptible to severe cracking or even spalling. This does not affect the introduction of the tendon force into the structure, but certainly is unsightly and may also lead to corrosion problems. Other anchorage zone problems due to the effects of tendon curvature were reported, particularly where kinked tendons cause a concentrated deviation force (29,30).

Unclear Responsibilities

In U.S. practice, contract drawings frequently do not include complete post-tensioning details. Rather, the contractor is expected to determine size, number, and location of the anchorage devices and to provide details for the anchorage zone (26). The contractor, in turn, relies heavily on the anchorage device supplier to furnish the necessary information. This procedure has led to considerable confusion about the responsibilities of the engineer-

of-record, the anchorage device supplier, and the contractor. This is not limited to the design of the anchorage zone, but also includes confusion about who should furnish and pay for the anchorage zone reinforcement.

Another problem arising as a consequence of this method of practice is pointed out by Libby (26). The contract drawings do not show anchorage zone details, while the shop drawings for the anchorage zone prepared by the contractor show anchorage details only, but none of the other reinforcement in the same region. This practice leaves congestion of the anchorage zone undetected, as well as physical conflicts between ordinary reinforcement, anchorage zone reinforcement, and tendon hardware. Often field changes are required to make reinforcement placement possible. Congestion of the anchorage zone is one of the major reasons for poor concrete consolidation and subsequent failures.

Lack of Knowledge

A wide range of technical literature on behavior and design of anchorage zones has been published. However, available information is limited to special applications and apparently lacks the generality required to address the wide variety of anchorage zone problems encountered in innovative post-tensioned concrete applications. Current AASHTO provisions were obviously developed with I-girders in mind and are vague. The little specific guidance given in AASHTO seems to have done more harm than good.

Another problem is the fact that education in the United States has not kept up with the dramatic increase in the use of prestressed concrete. Breen (31) points out that many U.S. universities do not offer prestressed concrete courses or limit access to graduate students, despite the fact that 75 percent of new concrete bridges and 75 percent of new parking structures are built with prestressed concrete.

The current confusion and lack of knowledge is not restricted to the United States. A survey conducted by the Comité Euro-International du Bréton (CEB) (32) asked engineers to design, according to their own national code or handbook, a beam having six anchorages applying a total force of 2700 kN (607 kips). The engineers were asked to calculate the bursting force (the force caused by the spreading of the applied concentrated force), the length of the bursting zone, and the cross-sectional area of reinforcement necessary to carry the bursting force. The range in responses was rather striking. For the bursting force, the average was 192.5 kN (43.3 kips) with a range from 49.5 kN (11.1 kips) to 440 kN (98.9 kips). The same wide range of values was seen for the length of the bursting zone and reinforcement area. The distribution length for the bursting force ranged from 170 mm (6.69 in.) to 850 mm (33.5 in.) with an average of 508 mm (20.0 in.). The required reinforcement ranged from 207 mm² (0.32 in.²) to 2000 mm² (3.10 in.²) with an average of 790 mm² (1.22 in.²). The survey makes it clear that progress in the current state of the art in design of anchorage zones is not a matter of refining 5 or 10 percent, but rather is at the point of reducing differences that can range from 50 to 500 percent.

REGULATORY FRAMEWORK

The literature review, responses from the state-of-the-art survey, and evaluation of current codes and standards convinced

the project staff early in the course of the project that a fundamental need was a coherent framework for regulatory standards for post-tensioned anchorage zones. No such coherent framework had been found.

Examination of technical issues pointed out that there were two almost distinct sets of concerns in post-tensioned anchorage zones. These were:

1. The anchorage device and its ability to transfer the load from the tendon to the concrete. This included concerns about the anchorage device strength and stiffness, bearing pressure on the concrete and confinement required around the device to increase bearing strength.

2. The proper configuration and reinforcement of the much larger zone in which the concentrated tendon force spreads into the overall structure. This includes the determination of the flow of forces outward from the anchor devices, the design of adequate reinforcement to resist tensile forces in the anchorage zone and to control cracking, and the check of compressive stresses at critical places in the overall anchorage zone.

Examination of normal engineering practice, legal responsibilities, and traditional commercial practices with respect to post-tensioning anchorages indicated that a major amount of confusion and differences existed regarding responsibilities and usage; yet, several distinct trends were noted. These were the following:

1. The engineer-of-record has clear responsibilities for life safety issues under most state professional registration laws. These can only be transferred to another qualified registered engineer with the express consent of that individual (33).

2. The manufacturers and suppliers of anchorage devices were usually engaged in extensive testing of their devices, but in isolated prisms similar to those specified by FIP (3). Availability of test documentation and design recommendations for confining reinforcement to the engineer-of-record was limited and variable.

3. In some cases the manufacturer of the anchorage devices did review the application plans for the devices. In many cases the manufacturers did not review working drawings, particularly for smaller tendon size anchors.

4. In some cases the engineer-of-record relied totally on the post-tensioner to provide adequate reinforcement for the entire anchorage zone to ensure safe transfer of the tendon force into the overall structure. In some states provisions of any supplementary reinforcement required to control bursting or spalling due to post-tensioning anywhere in the structure was assumed to be the responsibility of the post-tensioner, and payment for such reinforcement (even though not indicated on the plans) was assumed to be part of the bid item for post-tensioning anchorage device.

5. The absence of explicit limit state guidelines resulted in uneven expectations regarding anchorage zone performance. When coupled with the traditional "overselling" of prestressed concrete as a "crack-free" material, some engineers regarded the appearances of *any* crack in the anchorage zone as a serious problem and possible reason for nonacceptance or repairs.

6. Everyone consulted (from post-tensioning supplier, to contractor, to designer, to owner) indicated that fairly apportioning the responsibilities of the parties was as important as solving the technical problems.

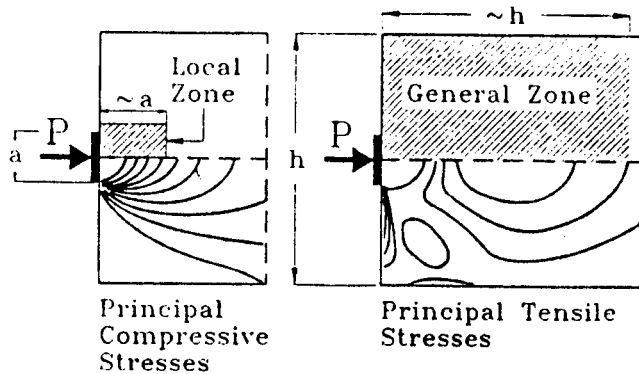


Figure 15. Local zone and general zone.

Studies of these broad concerns and consideration of the technical issues outlined earlier suggested to the project staff that there was a certain parallelism between the technical issues and the responsibility issues. In the 1987 interim report of this project (25), it was proposed to consider the anchorage zone as composed of two regions (Figure 15). The region of very high compressive stresses immediately ahead of the anchorage device is the *local zone*, and the region subjected to tensile stresses due to spreading of the concentrated tendon force into the structure is the *general zone*.

This approach allows one to clearly delineate the responsibilities for the design of the anchorage zone. The main considerations in local zone design are the effects of the high bearing pressure and the adequacy of any confinement reinforcement provided to increase the bearing strength. Design of this region should be the primary concern of the anchorage device supplier. On the other hand, the main consideration in general zone design is to determine and provide for the flow of forces as the concentrated tendon force spreads into the structure. This includes the design of adequate reinforcement to resist tensile forces in the anchorage zone and to control cracking, and the check of compressive stresses at the interface with the local zone and at loading or geometry discontinuities. Design of the general zone should be the primary responsibility of the engineer-of-record.

The division of the anchorage zone into a local zone and a general zone is a very useful concept to identify the different concerns in anchorage zone design. In order to develop code-language specifications it is essential to provide rather precise definitions. For this purpose it is more convenient to define local zone and general zone geometrically rather than by stress levels.

In the proposed anchorage zone provisions given in Chapter 3, the geometric extent of the general zone is defined as being identical to that of the overall anchorage zone including the local zone. This implies that the responsibility for the overall anchorage design, and particularly the integration of local zone details into the overall anchorage zone, remains with the engineer-of-record who is the designer of the general zone. The proposal includes definitions for the extent of the anchorage zone for end anchors, intermediate anchors, and multiple slab anchors (Figure 16). These definitions are based on the principle of Saint Venant (Figure 5). The definitions of the local zone were developed by Roberts and are based on the geometry of the anchorage devices including any confining reinforcement, required concrete cover over reinforcement or anchorage hardware,

and manufacturer's recommendations on anchorage edge distance or spacing, if available (Figure 17).

The concept of "general zone" and "local zone" received broad acceptance in the industry well before this current study was completed. NCHRP Project 20-7 (Task 32), carried out by the Post-Tensioning Institute, incorporated the concept in their design specifications for segmental bridges (17). This was accepted by AASHTO as an interim standard in 1990. NCHRP Project 12-33, carried out under the supervision of Modjeski and Masters, has incorporated the concept in the proposed total revision of the AASHTO Bridge Specifications. The large international post-tensioner VSL has recently published a comprehensive design guide entitled "Detailing for Post-Tensioning" and subtitled "General Principles—Local Zone Design, General Zone Design, Examples from Practice" (34).

The final part of the regulatory framework is the overall limit states approach. In view of the state of post-tensioned concrete design practice in the United States today, as well as the current extension of the traditional Load Factor-Resistance Factor procedures used in concrete design to all materials, it was felt that the most appropriate limit state philosophy would be, as follows:

1. Service load level control of crack width in the local zone would be governed by specifying crack width limitations in anchorage device tests.
2. Service load level control of crack widths in the remainder of the general zone would be governed by applying sufficient load factors and resistance factors along with general detailing rules.
3. Ultimate load level performance in the local zone would be governed by regulating bearing stresses to acceptable levels for simple, stiff devices. These would be termed *basic* anchorage devices.
4. Ultimate load level performance in the local zone would be governed by specifying acceptance test criteria for more complex devices not meeting the bearing stress or stiffness requirements. These would be termed *special* anchorage devices.
5. Ultimate load level performance in the general zone would be governed by specifying load factors, resistance factors, acceptable design procedures, and minimum required detailing practices.

Implementation of this overall approach was a major goal that greatly influenced the analytical studies and the physical tests in the overall program.

LOCAL ZONE

Roberts conducted a detailed study of behavior and design of the local zone as part of this overall study. Detailed information on her test specimens, results and analyses are contained in Ref. 4., a copy of which has been put on file at NCHRP. That study included a review of the current test procedures for anchorage device acceptance tests, a comprehensive evaluation of previous local zone studies, and 31 physical tests. The variables investigated included edge distance, spiral parameters, supplementary reinforcement, type of anchorage device, concrete strength, loading history, and interaction with the general zone.

Important Parameters and Definitions

The behavior of the anchorage zone is dependent on many parameters directly related to the geometry of the zone. The ratio

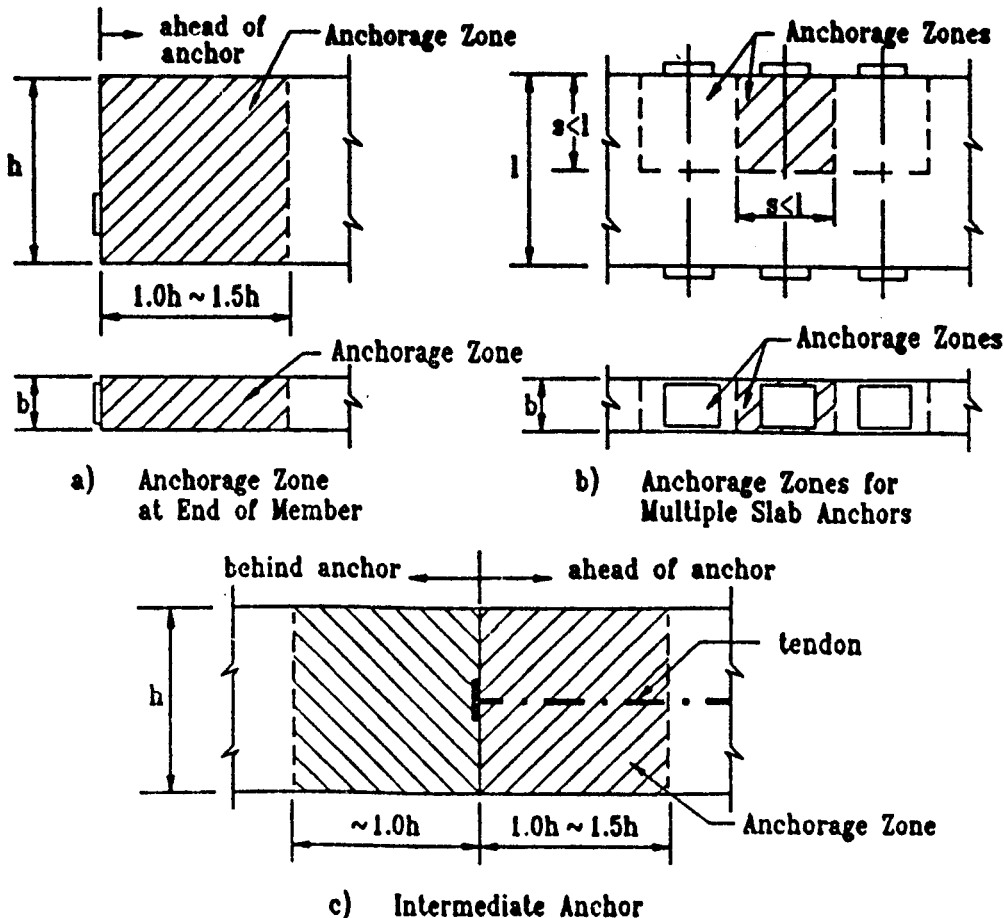


Figure 16. Anchorage zone dimensions.

of the length of the side of the anchorage device to the width of the block into which the force is transferred is one critical parameter (see Figure 18) and will be referred to as the a/h ratio. Another important ratio is the net area of the concrete supporting the plate to the net area of the bearing plate, which will be referred to as the A/A_b ratio, A is the maximum area of the portion of the supporting surface that is similar to the loaded area and concentric with it. A_g is the gross area of sufficiently rigid bearing plates (defined subsequently) or, for less rigid bearing plates, the area geometrically similar to the wedge plate with dimensions increased by twice the bearing plate thickness. A_b is the effective net area of the bearing plate calculated as the area A_g minus the area of openings in the bearing plate.

Other parameters involved in the local zone are shown in Figure 19. Edge distance is the distance from the center of the anchorage device to the nearest edge of concrete. Confinement cover is the depth of concrete over the outermost confining reinforcement, and anchor cover is the depth of concrete over the anchorage device. Spacing is the distance from the center of one anchor to the center of the next.

Parameters related to the confining steel are illustrated in Figure 20. For spiral reinforcing, the diameter of the spiral is measured from outside to outside of the steel bars, and the spiral size refers to the diameter of the reinforcing bar or rod from which the spiral is made. The pitch refers to the distance in the

direction normal to the spiral diameter that is measured from the center of the bar to the center of the bar 360 deg. away. For orthogonal ties, the side length, spacing, and bar size are also illustrated in Figure 20.

In the local zone, confining reinforcing is defined as the reinforcing closely surrounding the anchorage device and providing the primary confinement. Supplementary reinforcement is reinforcing present in addition to the primary confinement reinforcing, usually added for crack control purposes (see Figure 21). Such supplementary reinforcement is often present in actual girders and is often added in anchorage device acceptance test specimens.

In order to develop a consistent design philosophy, a precise definition of the local zone is required. As illustrated in Figure 17, the local zone is defined as a rectangular prism whose transverse dimensions in each direction are: (1) when independently verified manufacturers recommendations for cover, edge distance, and spacing are not available, the larger of the plate size plus twice the minimum concrete cover required over the embedded plate for the particular application and environment, or the outer dimension of any required confining reinforcing plus the required concrete cover over the confining reinforcing steel for the particular application and environment; or (2) when independently verified manufacturers recommendations are available, the smaller

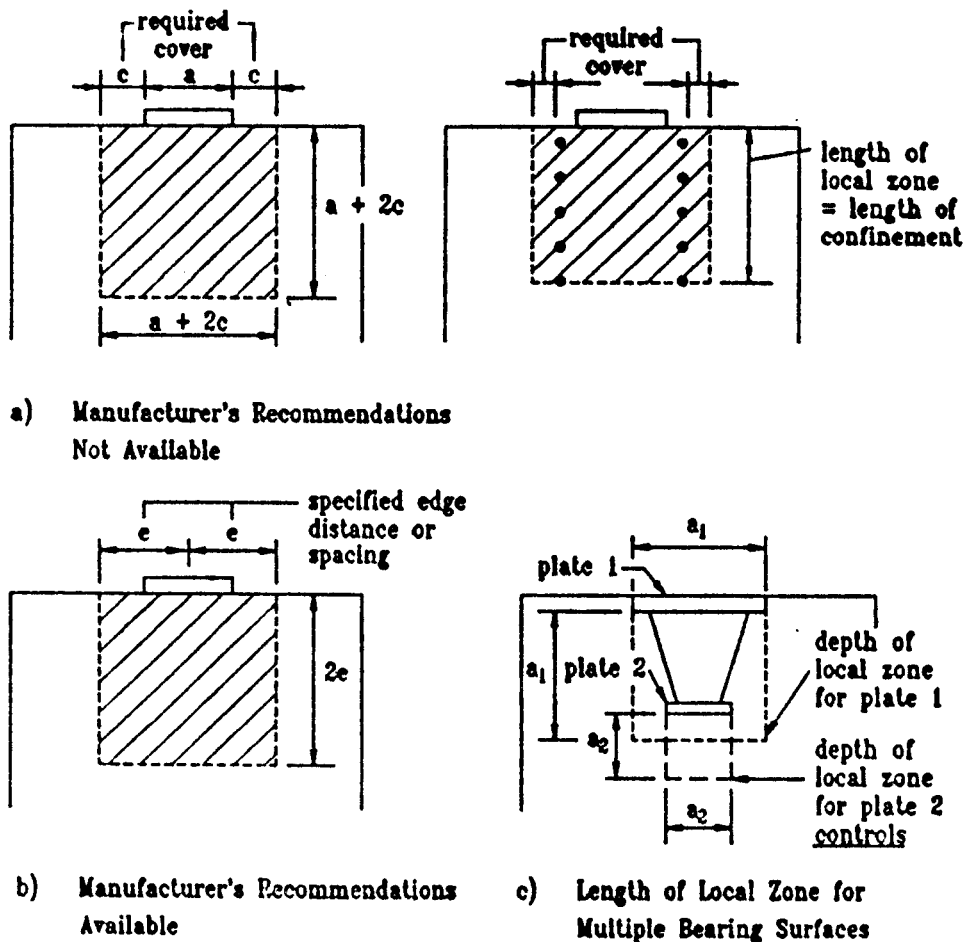


Figure 17. Local zone dimensions.

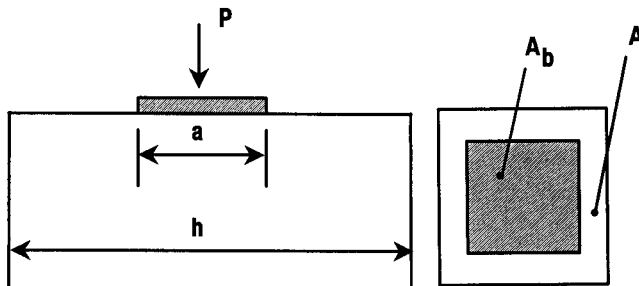


Figure 18. Definition of a/h and A/A_b ratios.

of twice the supplier's recommended edge distance, or the recommended center-to-center spacing.

The length of the local zone is defined as the greatest of the following (see Figure 17): (1) the maximum width of the local zone; (2) the length of the confining reinforcing, but no greater than 1.5 times the maximum width of the local zone; or (3) for anchorage devices with multiple bearing surfaces, distance from the loaded concrete surface to the farthest face of each bearing surface plus the maximum dimension of that bearing surface (see Figure 17c).

Rigid Bearing Plates

Based on extensive work by Hawkins (13,14,15), Niyogi (35,36), Williams (37), and Wurm and Daschner (38,39), as well as the AISC (40) expression for the required thickness of a bearing plate, Roberts (4) concluded that there were two important conditions which must be satisfied to consider a bearing plate as rigid. The first is that a flexural check indicate that the plate material does not yield. The second is that the plate be sufficiently stiff. The most complete study of the effect of stiffness of bearing plates on concrete was the work reported by Hawkins. However, all of his specimens had height to width ratios less than 1.5. Williams (37) and Niyogi (35,36) have shown that this parameter has a substantial influence and should be varied. Hawkins also used square punches (wedge plates) while most post-tensioning wedge plates are circular. Based on a reexamination of Hawkins data, Roberts found a consistent relationship between the load achieved by specimens and the calculated deflections of the edges of the plate. "Rigid" plates tended to have ratios of edge deflection to length of less than about 0.0005. Nonpublished data submitted by several post-tensioners for bearing type anchorage devices, which have been widely used without problems in the United States, indicated that ratios of edge deflection to length of about 0.00075 were actually acceptable. This can be satisfied if

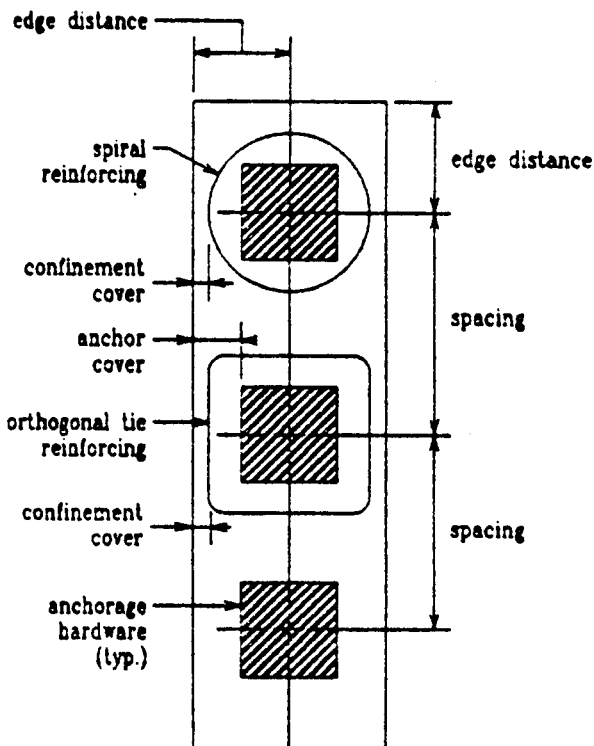


Figure 19. Parameter definitions.

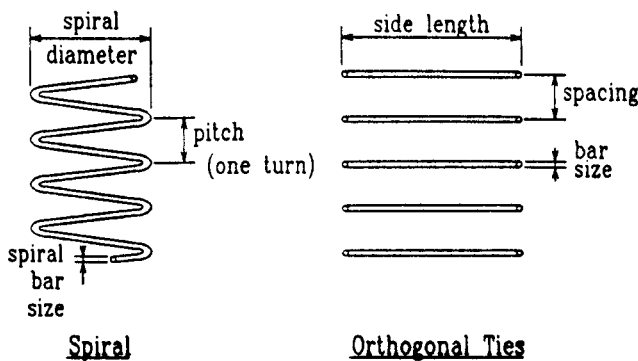


Figure 20. Confining reinforcing steel parameters.

$$n/t \geq 0.08 \sqrt[3]{E_b/f_b} \quad (2)$$

where n is the largest distance from the outer edge of the wedge plate to the outer edge of the bearing plate, t is the average thickness of the bearing plate, E_b is the modulus of elasticity of the bearing plate material, and f_b is the maximum factored tendon load, P_u , divided by the effective bearing area A_b .

Present Code Provisions for Local Zones

In many building and bridge design standards, references to allowable or ultimate bearing stresses under post-tensioning anchorage devices are vague, conservative, and not particularly

uniform. Most give formulas based on some allowable fraction of the concrete's characteristic strength and some are also a function of the A/A_b ratio.

Figure 22 indicates the wide scatter of a number of these current standards for a concentrically loaded square prism.

While most researchers have developed qualitative conclusions that agree well with one another, the quantitative conclusions are confusing, difficult to apply, and inconsistent with one another. The wide variety of bearing stresses allowed by the codes is also a source of frustration to designers. Although an increase in bearing strength due to confinement by reinforcing has been proven in many experimental programs, no code allows an increase in bearing pressure based on the amount of confining steel present. There is still much room for refinement and improvement of design guides and code provisions. In particular, specific provisions need to be included to reflect modern multiplane anchors and the effects of confining reinforcement.

Experimental Program

In this study a series of 31 test specimens were used to evaluate the behavior, test criteria, and design procedures for the local zone. Complete details are provided by Roberts (4). A summary of specimen details is included in Appendix C. The local zone experimental program was divided into three main categories: (1) tests to evaluate current acceptance testing procedures and develop new acceptance test procedures; (2) parametric studies; and (3) local zone-general zone interaction tests. Variables investigated included edge distance, spiral parameters, supplementary reinforcement, type of anchorage device, concrete strength, interaction with the general zone, and loading history.

Test Specimens and Methods

The majority of the specimens were very similar rectangular concrete prisms. The construction and testing procedures were almost identical. Specimen details are given in Appendix C. All specimens were cast horizontally. Tolerance on the concrete dimensions was $\pm\frac{1}{8}$ in. All reinforcing steel was bent in the laboratory using CRSI standard bends and hooks. Stirrups were bent from Grade 60 deformed bars and spirals were fabricated from smooth Grade 60 bars. All reinforcing dimensions were kept within a $\frac{1}{4}$ -in. tolerance. Strain gages were affixed to selected reinforcing bars, as shown in Figure 23. Demec locating discs for mechanical extensometer measurement of concrete surface strains were placed on two faces of every specimen as illustrated in Figure 24. All specimens were concentrically loaded through spherical heads onto wedge plates in either a 600-kip or a 1200-kip testing apparatus. The bases were uniformly supported on teflon pads. Loading was applied incrementally with careful observation of first cracking, crack development, and ultimate load. Steel strains were monitored by an automated data logger.

Tests to Evaluate Acceptance Testing Procedures— Multiple Plane Anchors

Two different recommended testing procedures were evaluated in this study. The first is the test described in the FIP Recommen-

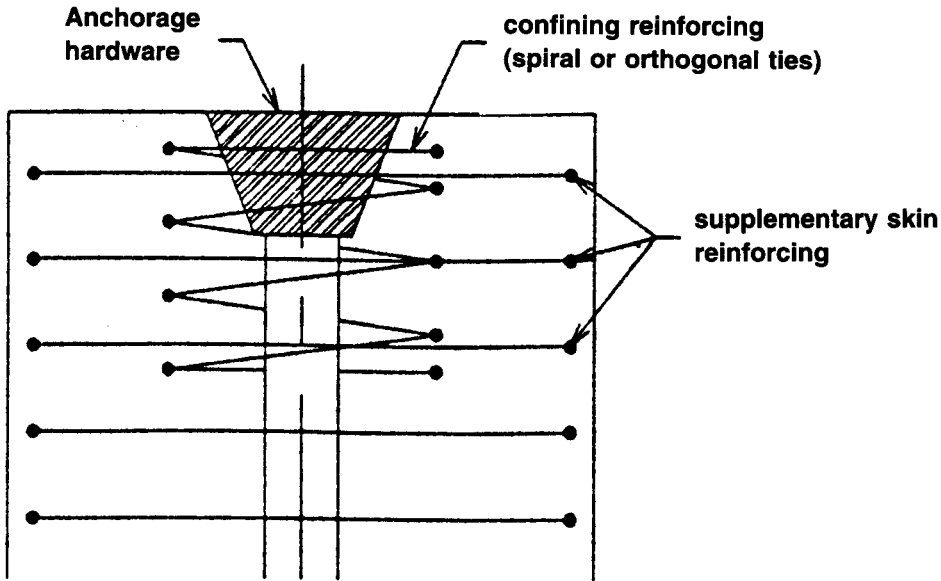


Figure 21. Definition of supplementary reinforcement.

Comparison of Allowable Bearing Stresses

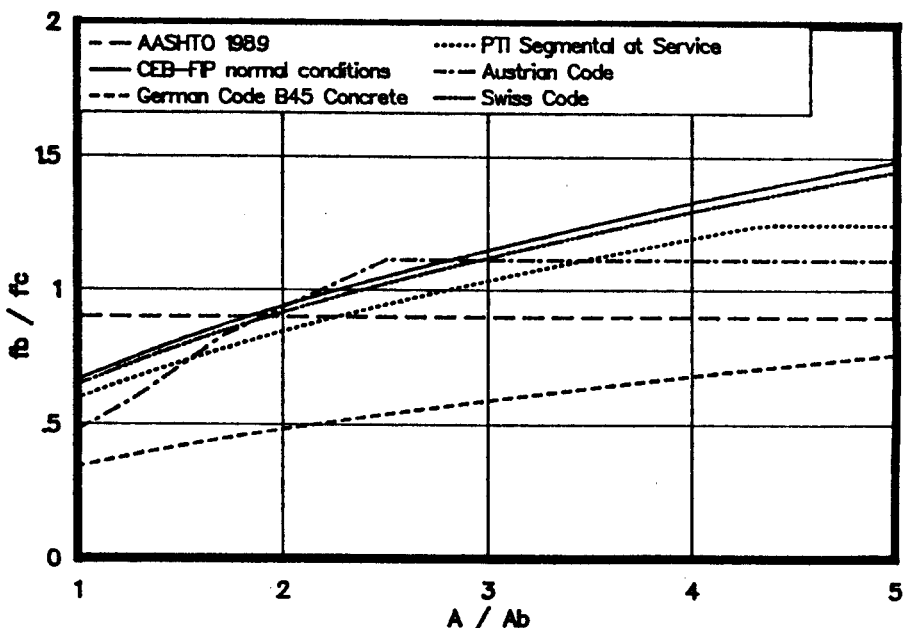


Figure 22. Comparison of code equations for bearing stresses.

dations for the Acceptance Application of Post-Tensioning Systems (3). The FIP outlines a test block (see Figure 25), test procedure, and criteria for evaluation. Side lengths, m and n , perpendicular to the tendon shall be taken as twice the permissible minimum distance from the center of the anchorage to the edge of concrete structure as recommended by the manufacturer (supplier). The height of the prism shall be twice the longer dimension, m or n , measured from the end of the device farthest from

the load application. The test should be started when the concrete has reached approximately 85 percent of its characteristic strength (28-day cube strength), and strength gain should be limited so the characteristic strength is not exceeded during the course of the test. They recommend a cyclic or sustained loading procedure (see Figure 26) and ultimate limit state evaluation criteria.

Regardless of the test method chosen, the test must prove that

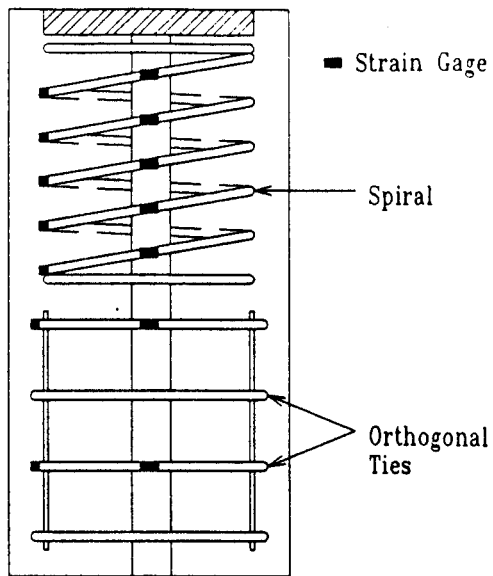


Figure 23. Typical strain gage layout.

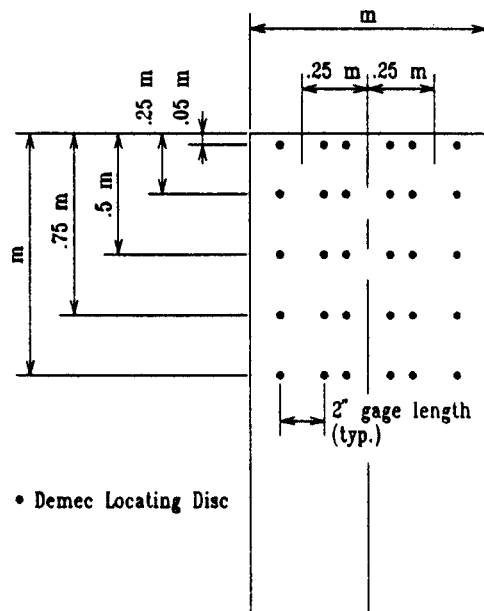


Figure 24. Typical Demec locating disc layout.

the anchorage zone is capable of transferring forces to the concrete without premature failure of the concrete or the bursting reinforcement. It must be designed in such a way that the maximum prestressing force is carried with an adequate factor of safety against failure. FIP also requires that the possible formation of small cracks in the anchorage zone not impair the permanent efficiency of the anchorage. The only other stipulation that FIP puts forth is that the minimum spacing of anchorages and minimum edge distance be determined in such a manner that the reinforcement can be easily placed, and that adequate compaction of the concrete is possible.

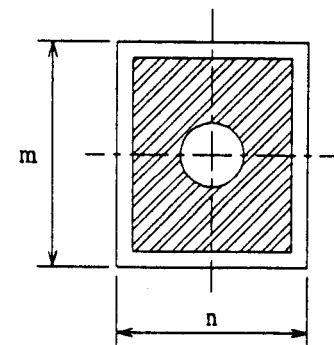
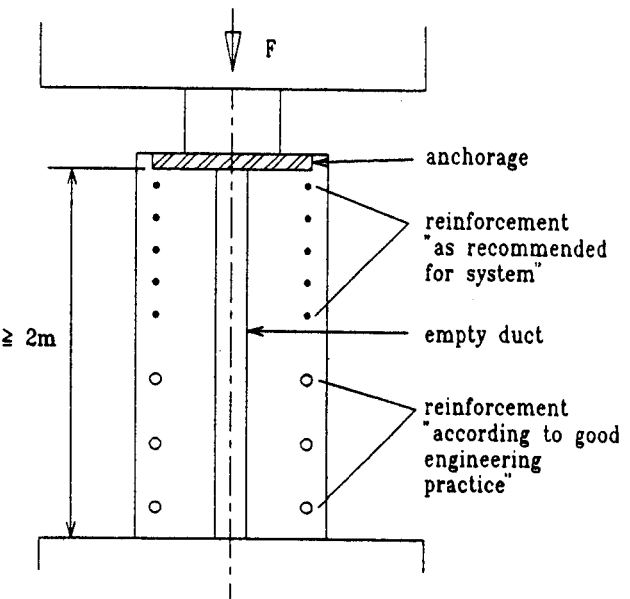


Figure 25. FIP test specimen.

The second test is described in the PTI specifications for segmental post-tensioned box girders (17), and is a significantly different acceptance test. The dimensions of the test block are somewhat different, the loading is monotonic, and serviceability (specific crack width), as well as ultimate criteria, are used for evaluation. PTI specifies a concrete prism with a cross-section dimension twice the minimum distance from the centerline of the tendon to the face of concrete in the actual structure in one direction, and equal to the minimum spacing of the anchorages plus 3 in. in the other direction (see Figure 27). The length of the test block is to be at least 1.5 times the largest cross-sectional dimension.

The specification further requires that the reinforcement in the anchor zone ahead of the anchorage, for a distance equal to the largest of the two cross-sectional dimensions of the specimen, shall simulate the actual reinforcement used in the structure. For the remaining length of the test block, the reinforcement may be increased as required to prevent failure in that portion. The strength of the concrete in the test block at the time of test must not exceed the minimum concrete strength at the time of post-tensioning.

The ultimate load criterion which must be satisfied is that the anchorage be capable of developing 95 percent of the guaranteed

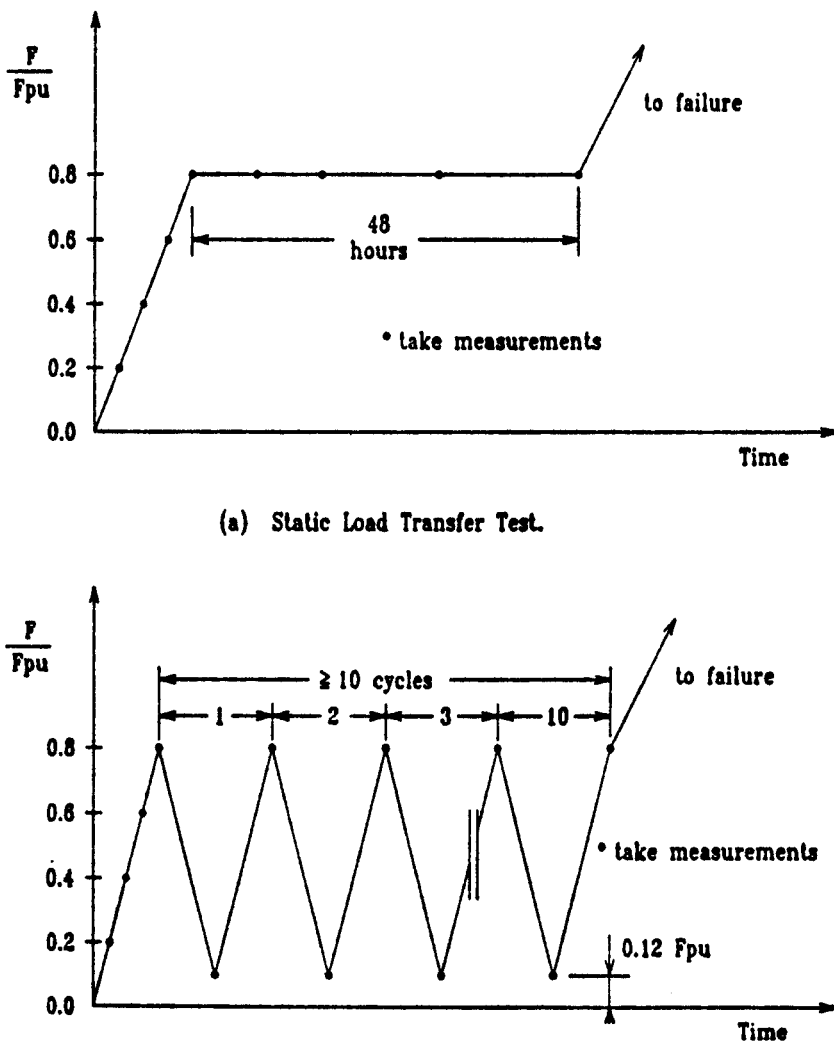


Figure 26. FIP loading procedure.

ultimate tensile strength of the maximum size tendon for which the anchor is rated, without measurable permanent distortion of the anchorage and without concrete failure. Measurable permanent distortion is defined as a distortion of 0.01 in. or more across the anchor face of the assembly measured from the original plane after the load has been released.

PTI also defines serviceability criteria. The test block must have no concrete cracks at a load of 40 percent F_{pu} , and concrete cracks at 70 percent F_{pu} must not exceed 0.005 in. After loading to 95 percent F_{pu} and releasing the load, concrete crack widths must not exceed 0.015 in.

These different procedures were evaluated by several series of tests. In test series MP (Multiple Plane Anchors), six test specimens were built following the general outlines of the FIP procedures, but were loaded monotonically to failure. All specimens used a multiplane anchorage with a rated capacity of 12-0.6-in. diameter, 270-ksi strands. Manufacturer's literature required a minimum concrete strength of 3000 psi. MP-A had reinforcing details conforming to the manufacturers' European literature and allegedly proven in FIP tests. MP-B incorporated the spiral that is welded to the anchor when sold in the United

States. MP-C and MP-E had details similar to MP-B but substantially higher concrete strengths. MP-D and MP-F were the same as MP-C and MP-E except three additional #4 supplementary ties were added to improve crack control. The rated capacity, F_{pu} , of the 12-0.6-in. strand anchor at a guaranteed ultimate tensile strength (GUTS) of 270 ksi is 700 kips.

Test results for the MP series are given in Table 1 along with a summary of the confining and supplementary reinforcing provided. The specimens incorporating the manufacturer's suggested configurations (MP-A and MP-B) failed to develop the rated ultimate capacity by substantial margins. At failure all of the anchorages had visibly depressed into the specimen's top bearing surface from $\frac{1}{4}$ to $\frac{1}{2}$ in. (see Figure 28). The concrete confined within the spiral confinement moved along with the anchor as it depressed into the concrete, as can be seen from Figure 29, taken when the spalled concrete was removed. The presence of supplementary skin reinforcement did little to improve the cracking load, which is substantially below the 0.80 F_{pu} temporary stressing level allowed by AASHTO. It appears futile to think of "uncracked" anchorage zones. The supplementary reinforcement did help in controlling crack widths, and a

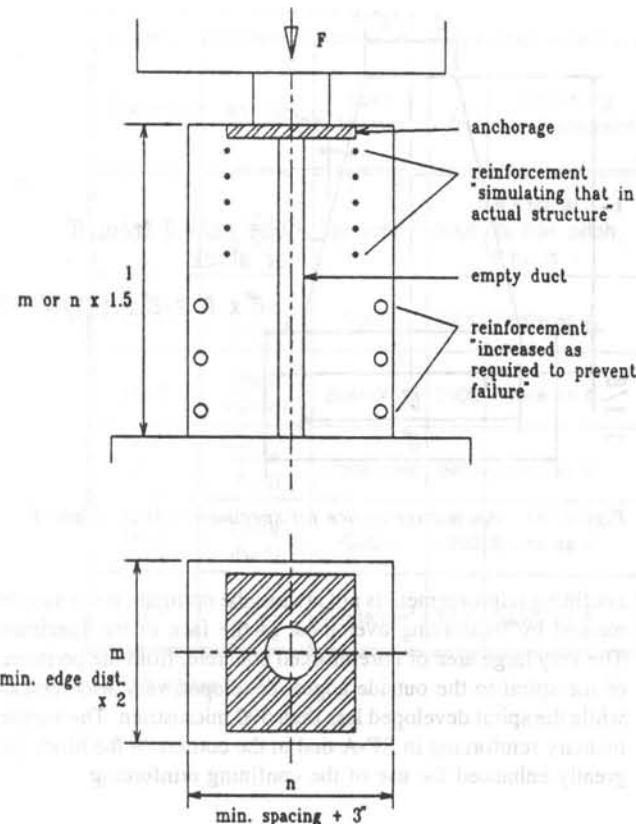


Figure 27. PTI test specimen.



Figure 28. Specimen MP-B anchorhead at failure.

comparison of MP-A and MP-B shows that the supplementary reinforcement can combine with the primary confining reinforcement to increase the ultimate capacity of the anchorage. Specimens MP-B, MP-C, and MP-E were identical in all details except for concrete compressive strength. Interestingly, first cracking was highest for the lowest concrete strength specimen. Ultimate loads increased at only about 90 percent of the increase in concrete strength.

Tests to Evaluate Acceptance Testing Procedures— Rectangular Plate Anchors

A similar investigation was carried out in the RP (Rectangular Plate Anchor) series. Two specimens each with a 4-0.6-in. dia-

Table 1. Multiplane anchor test series

Specimen	f'_c psi ¹	Confining Reinforcing	Supplementary Reinforcing	Cracking Load	Ultimate Load
MP-A	3200	#4 spiral, 2-1/8 in. pitch, 5 turns	5 ea. #3 ties at 1-3/8 in.	0.46	0.81
MP-B	3200	#5 spiral, 2 in. pitch, 6 turns	None	0.46	0.63
MP-C	6400	Same as B	None	0.35	1.13
MP-D	6400	Same as B	3 ea. #4 ties at 4-1/2 in.	0.35	1.30
MP-E	4200	Same as B	None	0.30	0.80
MP-F	4200	Same as B	Same as D	0.30	1.05

¹ Manufacturer required: 3000

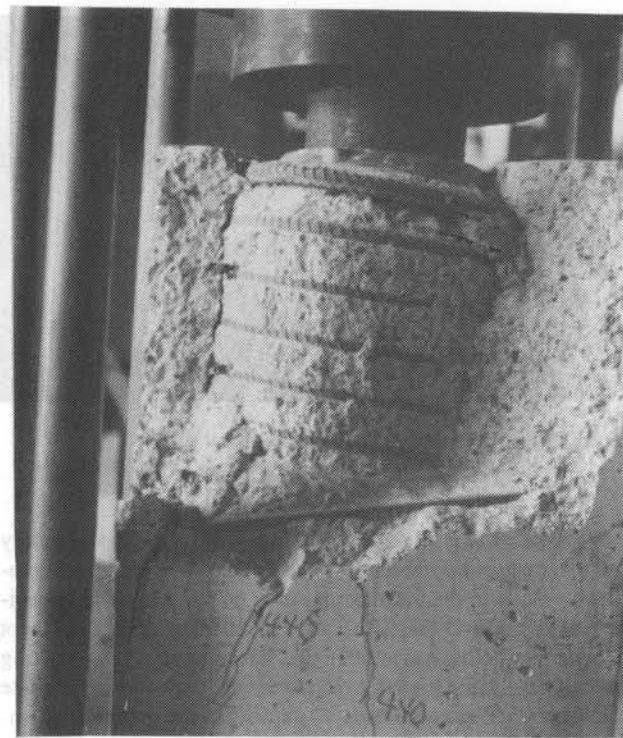


Figure 29. Specimen MP-B after failure.

ter, 270-ksi strand rectangular plate anchor ($F_{pu} = 232$ k) were tested. Specimen RP-A had the manufacturers' recommended reinforcing details consisting of five #4 closed stirrups at $2\frac{3}{8}$ -in. centers over the specimen cross section with three smaller additional #3 closed stirrups at $2\frac{3}{8}$ -in. centers as additional confining reinforcement. Specimen RP-B had a $6\frac{1}{2}$ -in. diameter #3 spiral with $1\frac{1}{4}$ -in. pitch and nine turns. The spiral was sized to provide adequate confinement to the cone to develop F_{pu} using Richart's (41) approach. No other supplementary reinforcement was provided so that there was substantial concrete area without reinforcement. Test results are shown in Table 2. The rectangular specimen, RP-B, clearly indicated that a spiral arrangement of

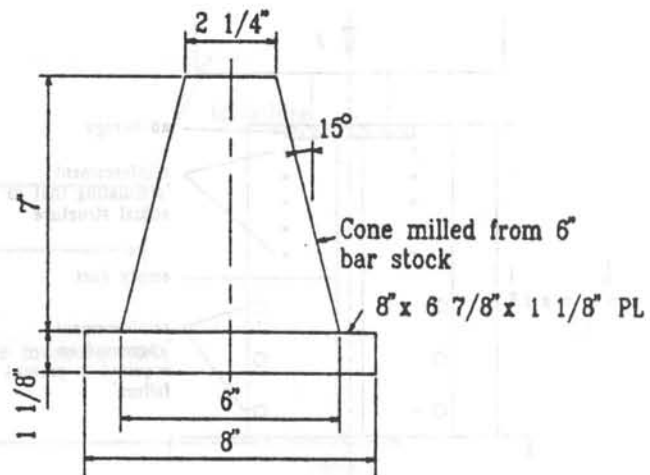


Figure 30. Anchorage device for specimens LH-D, E and F.

confining reinforcement is not always the optimum if not supplemented by reinforcing over most of the face of the specimen. The very large area of unreinforced concrete, from the perimeter of the spiral to the outside edges, developed very wide cracks, while the spiral developed less than 500 microstrain. The supplementary reinforcing in RP-A tied in the corners of the block and greatly enhanced the use of the confining reinforcing.

Test to Evaluate Acceptance Testing Procedures—Load History

The influence of Load History was specifically investigated in the LH series. Loading histories included monotonic, cyclic, and 48-hour static load transfer tests. Two sets of specimens were used. In the first set (LH-A, LH-B, and LH-C) a "good" commercially available 4-0.6-in. strand rectangular flat plate anchor ($6\frac{1}{8}$ -in. by 8-in.) was used with a confining spiral. In the second set a purposefully designed "bad" anchor was used to see if the test procedure would discriminate between "good" and "bad" anchors. This anchor was the same rectangular plate but had a heavy milled cone (see Figure 30) welded onto the

Table 2. Rectangular plate anchor test series

Specimen	f'_c psi	Confining Reinforcing	Supplementary Reinforcing	% F_{pu} (232 k)	
				Cracking Load	Ultimate Load
RP-A	3370	3 - #3 stir- rups at $2\frac{3}{8}$ in.	5, #4 stirrups at $2\frac{3}{8}$ in.	0.64	0.97
RP-B	3370	#3 spiral, $1\frac{1}{4}$ in. pitch, 9 turns	None	0.43	0.82

Table 3. Load history test series

Specimen	Anchor	Load History	f'_c	Confining Reinforcement	Supplementary Reinforcement	Max. Crack Width at 0.80 F_{pu}	% F_{pu} (232 k)	
							Cracking Load	Ultimate Load
LH-A	Plate (good)	Monotonic	3900	#3 spiral, @ 2-in. pitch, 5 turns	None	0.005 in.	0.55	1.00
LH-B	Plate (good)	Cyclic	3900	Same as A	None	0.013 in. 0.125 in. ¹	0.50	0.96
LH-C	Plate (good)	Sustained	3900	Same as A	None	0.011 in. 0.017 in. ²	0.55	1.12
LH-D	Cone (bad)	Monotonic	3900	Same as A	None	0.003 in.	0.45	1.15
LH-E	Cone (bad)	Cyclic	3900	Same as A	None	0.005 in. 0.125 in. ¹	0.45	1.15
LH-F	Cone (bad)	Sustained	3900	Same as A	None	0.009 in. 0.188 in. ²	0.55	1.27

¹ 10 cycles² 48 hr.

plate. The design of the anchor was based on the design of an anchor no longer being sold, which was known to have caused problems, such as excessive local zone cracking, in several structures. Test results are given in Table 3).

One of the basic conclusions, which can be drawn from this series, is that the ultimate failure load is not greatly affected by the loading history. Therefore, if ultimate load criteria are the only measure of performance, a simple monotonic testing procedure would be adequate. The level of distress, that is, the number and widths of cracks, is however greatly influenced by the method of test. The cyclic and sustained load tests showed the greatest amount of distress, while the monotonically loaded specimens showed the least. If serviceability criteria, such as crack widths, were to be considered in the evaluation of the test specimens, the sustained or slow cycle load transfer tests would better represent the conditions that would be present in a real structure.

From a testing standpoint, however, the sustained load transfer test is tedious and expensive. It is not always possible to tie up an expensive piece of testing equipment for the 48 hours required for this test. The slow cycle transfer test solves this problem very nicely. The levels of distress at the end of the sustained load and the cyclic loads were very similar. The cyclic test, therefore, is a viable replacement for the 48-hour sustained load test.

In terms of the "bad" anchor tests, it was interesting to note that the specimens with the stiff cones cracked earlier, but actually achieved higher ultimate loads than the identical anchors with flexible plastic transition cones. The difference in strength is attributable to the additional bearing area provided by the stiff cone. The cone increased the net bearing area by 19 percent and the average ultimate load increased by 15 percent, while the average cracking load decreased by 10 percent.

Tests to Evaluate Acceptance Testing Procedures— Multiple Bearing Plane Anchors

The final series for evaluation of test methods was the MB (Multiple Bearing Plane) series. Four identical specimens using a commercially available 7-0.5-in. 270-ksi strand anchor device were constructed with edge distance, spacing, and reinforcing details given by the manufacturer. The PTI test recommendations were used, resulting in a specimen 9 in. by 12 in. with a 24-in. height. The rated F_{pu} of the four specimens was 289 kips. MB-A and MB-B were unloaded, as specified by PTI, at 0.95 F_{pu} . They were subsequently loaded to failure. Specimens MB-C and MB-D were loaded continuously to failure. The specimens were tested at f'_c of 4100 psi.

Test results are given in Table 4. This was a very interesting series of specimens. There were basically two modes of failure illustrated in the four specimens and two distinct levels of ultimate load. MB-A and MB-C both failed very one-sided, with large diagonal cracks developing on only one side of the specimen. They failed at similar loads as well. MB-B and MB-D exhibited more symmetrical failures with the centerline cracks opening to greater widths and additional longitudinal, rather than diagonal, cracks developing.

What caused the difference in the failure mode is unknown. All four specimens were cast and tested identically. Small variations in positioning of the reinforcing steel or placement of the specimen in the loading machine could have been enough to make a difference. Once the slightly weaker path was found the one-sided failure occurred. The dimensioning of the specimen and the absence of auxiliary reinforcing tying in the corners seem to make the blocks very susceptible to the lopsided failure mode. The PTI specification forces a rectangular test specimen

Table 4. Multiple bearing plane anchor test series

Specimen	f'_c	Loading	Crack Width 0.70 F_{pu}	Confining Reinforcement	Supplementary Reinforcement	Residual Crack Width	% F_{pu} (289 k)	
							Cracking Load	Ultimate Load
MB-A	4100	Unloaded at 0.95 F_{pu}	0.005 in.	#4 spiral, 2 in. pitch, 5 turns	None	0.25 in.	0.55	0.96
MB-B	4100	Unloaded at 0.95 F_{pu}	0.005 in.	Same	None	0.10 in.	0.45	1.13
MB-C	4100	Continuous	0.010 in.	Same	None	0.25 in. ¹	0.45	1.00
MB-D	4100	Continuous	0.005 in.	Same	None	0.10 in ¹	0.45	1.08
Average							0.48	1.04
σ							0.04	0.07

¹ Actual (not residual)

for most anchors, which are square and have equal edge distances and spacings in each direction. Because most anchors are spirally reinforced, the specimen that results has more than 2 in. of extra unreinforced concrete in one direction. As seen in specimens MB-A and MB-C, when cracks open in this unreinforced area, they propagate and widen quickly. As a result, the specimen tends to fail at a lower load than one which fails more symmetrically.

This is the only series of this test program in which multiple specimens were constructed with identical details and tested with similar procedures. This presents the opportunity to examine the variability in first cracking and ultimate loads, which are inherent in the specimens because of the variable nature of reinforced concrete. Cracking loads were repeatable as were ultimate loads. Standard deviations were only 4 percent and 7 percent, respectively, which is very acceptable for any type of structural concrete test.

Tests for Parameter Studies

Many aspects of the local zone test specimens might have a significant effect on the behavior of the specimen and the outcome of the test. Effects of type of confining reinforcement and compressive strength of the concrete seemed to have been well explored in the literature. However, because of a shortage of documented test information, three areas were chosen for further study: edge distance, confining spiral parameters, and supplementary reinforcement.

Tests for Parameter Studies—Edge Distance

Test series ED (Edge Distance) used four specimens to isolate the effects of changing edge distance. Two used a 7-0.5-in. strand

flat plate anchor and two used a 7-0.5-in. strand multiplane anchor device with an F_{pu} of 289 kips. All specimens were constructed using the manufacturer's recommended spiral parameters for B45 concrete, which corresponds to 6500 psi 28-day cylinder strength. The manufacturer's literature gave information for the reinforcing steel parameters for all of its anchors in a wide variety of concrete strengths. It then stated that for all cases the minimum edge distance is equal to one-half of the spiral diameter plus the cover according to local standards. According to AASHTO specifications for prestressed concrete the minimum cover over reinforcing steel is 1 in. for the bottom of slabs or over stirrups and ties. The maximum cover required is 2 in. for reinforcing on the top of slabs where de-icers may be used.

Using this information, for each anchor one specimen was built with transverse dimensions equal to the spiral diameter plus 2 in. and the other specimen had transverse dimensions equal to the spiral diameter plus 4 in. The specimens were dimensioned following the FIP recommendations and were loaded monotonically.

Test results are given in Table 5. As edge cover increases, the ratio A/A_b increases. It can be seen that with both types of anchors, this increase in edge cover increased the cracking load 20 percent. It increased the ultimate load 32 percent for multiplane anchors and 12 percent for flat plate anchors, and greatly reduced crack widths at both 70 percent and 95 percent F_{pu} . Thus, the edge cover used in an acceptance test is a critical decision and should be carefully chosen to be representative of applications.

Figure 31 shows load-deformation comparisons of the ED series specimens. These curves are typical of spirally confined local zone specimens and indicate reasonable ductility. They also indicate, as found by Wurm and Daschner (38), that the stiffness is only 7 percent to 15 percent of the expected stiffness based on the concrete elasticity modulus. Most of the deformation

Table 5. Edge distance test series

Specimen	Anchor	f'_c	A/A _b Ratio	Confining Reinforcement	Supplementary Reinforcement	Edge Cover	Crack Width (in.)		% F_{pu} (289 k)		
							70% F_{pu}	95% F_{pu}	Cracking Load	% F_{pu} Spiral Yield	Ultimate Load
ED-A	Multi-plane	5150	2.31	#4 spiral, 2 in. pitch, 4 turns	None	1 in.	0.005	0.188	0.50	1.08	1.10
ED-B	Multi-plane	5150	3.33	Same	None	2 in.	0.002	0.010	0.60	1.17	1.45
ED-C	Flat Plate	5150	1.54	Same	None	1 in.	0.004	0.015	0.50	1.18	1.24
ED-D	Flat Plate	5150	2.20	Same	None	2 in.	0.002	0.007	0.60	1.33	1.39

results from punching of the large, confined concrete plug into the prismatic specimen. Internal strain gages mounted on the spirals indicated that the spiral strains were well below yield at 0.95 F_{pu} (see Figure 32) for all specimens. As shown in Table 5, final failure occurred shortly after spiral yield for all specimens, except ED-B which had substantial extra load above spiral yield. This specimen had the largest A/A_b ratio and suggests that the extra confining concrete can enhance the effectiveness of the spiral confinement.

A very different level of strains is measured as longitudinal strain on the external face of the specimens. As shown in Figure 33, external strains dropped off fairly rapidly beyond a distance from the loaded face of 0.5 widths. Strains for specimen ED-A are not shown because they were so great they could not be measured with the Demec gage. They were approximately double the values shown for ED-B. With both types of anchors, the lower edge covers resulted in substantially greater external strains.

Figure 34 shows the development of splitting crack width with increasing load. The large diamonds shown on the figure are the PTI crack width criteria:

0.40 F_{pu} —no cracks

0.70 F_{pu} —crack widths less than 0.005 in.

0.95 F_{pu} —crack widths less than 0.015 in. after release of load

All specimens met all crack width criteria with the possible exception of ED-A at the 0.95 F_{pu} level. Load was not released, therefore, this could not be checked. However, in view of the very wide crack under load, it is unlikely that satisfactory recovery would occur.

Tests for Parameter Studies—Confining Spiral

In the SP (Confining Spiral) series, the parameters of spiral pitch and diameter were altered while the spiral bar size and other specimen physical dimensions remained the same. In order

to minimize the number of specimens, a previously tested specimen, ED-D, was chosen as the first specimen of this series. Three new specimens were constructed with the same anchor, a 7-0.5-in. strand flat plate anchor, concrete dimensions, base area reinforcing and approximate concrete strength. The only variable was the spiral. The first specimen, SP-A, had no spiral at all. The increased capacities of the three other specimens in the series above the failure load of SP-A could then be attributed entirely to the confinement provided by the spiral. Specimen SP-B had the same volumetric ratio of confining reinforcing steel to confined concrete as specimen ED-D, but the spiral diameter was increased from 8.25 in. to 10.25 in. Specimen SP-C had the same cross-sectional area of reinforcing steel in the spiral as ED-D, but an increased diameter. Test results are given in Table 6.

The provision of the spirals had a dramatic effect on the performance of the specimens. Specimens SP-C and SP-B, with 10.25-in. diameter spirals, had first cracking loads 45 percent higher than the unreinforced specimen, SP-A. Increased diameter of the spirals also helped somewhat since their cracking load was 9 percent higher than specimen ED-D. The spirals greatly controlled crack width. The provision of the spirals and especially the increase in spiral diameter also had a profound effect on the ultimate load.

Tests for Parameter Studies—Supplementary Reinforcing

Some of the manufacturers whose reinforcing details were studied during the course of this research recommended provision of supplementary (auxiliary) tie reinforcing in addition to the use of a spiral for primary confinement. Specimens in the MP series were tested with and without supplementary reinforcing. It was apparent that supplementary reinforcing significantly enhanced the ultimate strength of the specimen and also made the failure somewhat more ductile.

Series AR (Auxiliary Reinforcing) was designed to observe the effects of varying the amount of supplementary reinforcing

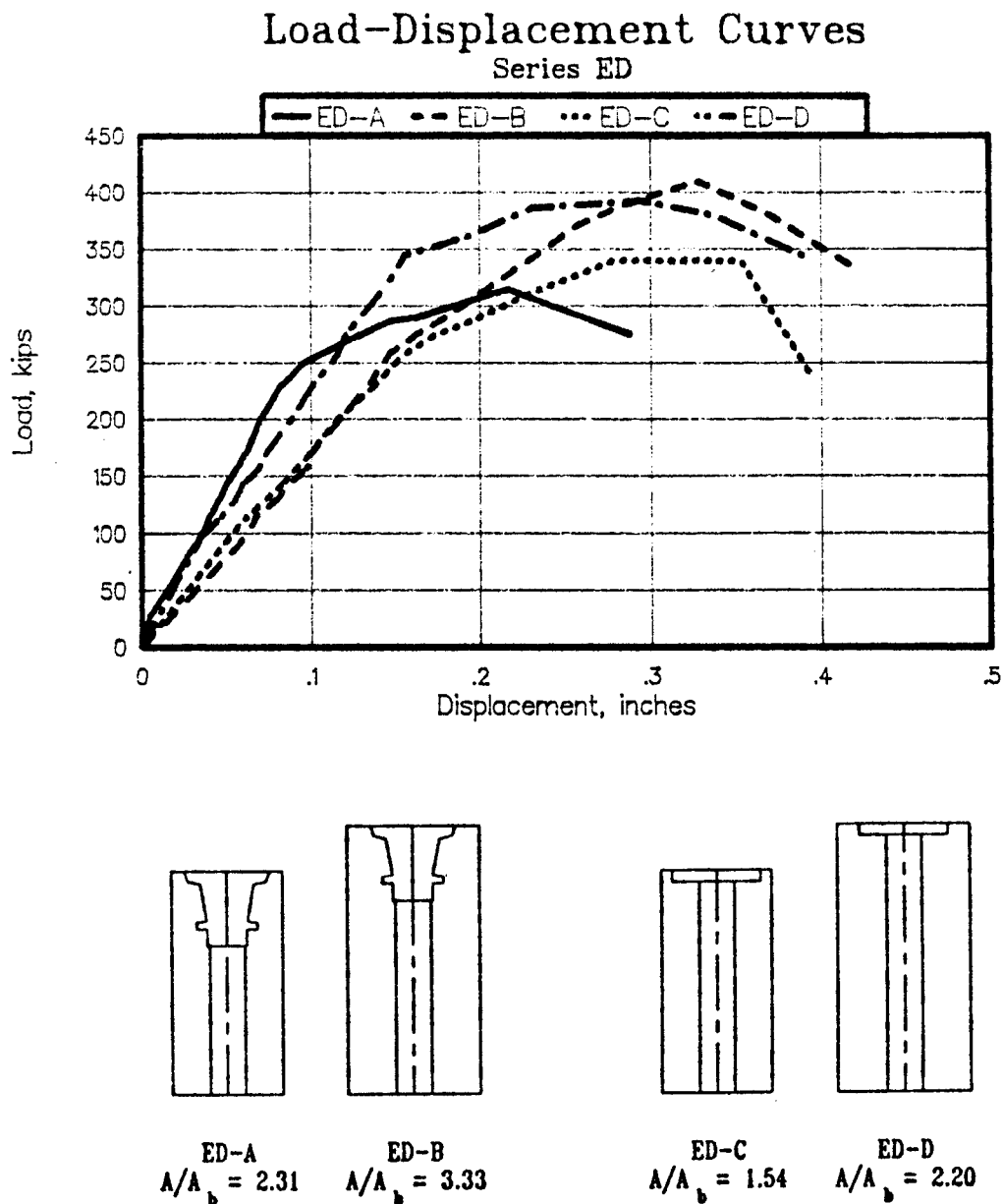


Figure 31. Load-deformation response for ED series.

in otherwise identical specimens. Specimen ED-A was chosen as the specimen whose basic parameters would be used for this series. The three new specimens were constructed with the same 7-0.5-in. strand multiplane anchor, same spiral and base area reinforcing, same concrete dimensions and approximate concrete strength as ED-A.

The AASHTO Bridge Specifications (16) gives a guideline for stirrups to be provided at the ends of prestressed beams in order to resist the splitting forces created by the transfer of the strand forces to the concrete. AASHTO recommends stirrups acting at a unit stress of 20 ksi to resist at least 4 percent of the total prestressing force. This guideline was used as the basis for the design of the specimens of this series. A 7-0.5-in. strand anchor has a capacity of 289 kips. Four percent of this is 11.6 kips. The cross-sectional area of steel required to carry 11.6 kips at a unit stress of 20 ksi is 0.578 in².

Specimen AR-A was designed with three #2 ties surrounding the spiral. This provided 0.30 in.² of cross-sectional area, which was one-half of the AASHTO recommendation. Specimen AR-B had three #3 ties. This provided 0.66 in.², which is just slightly greater than the AASHTO recommendation. The third specimen of the series, AR-C, had no local zone reinforcing. Test results are given in Table 7 and shown in Figure 35.

The first comparisons to be made are between the totally unreinforced local zone specimen, AR-C, and the specimen with only spiral confining reinforcing ED-A. The presence of spiral reinforcing dramatically improves the performance of the local zone specimen in terms of both ultimate load and crack width criteria, although the cracking load is less affected. Unlike the reinforced specimens that exhibit very wide cracking before failure, the unreinforced specimen failed quickly once the concrete began to crack. Table 7 shows that the first cracking load of

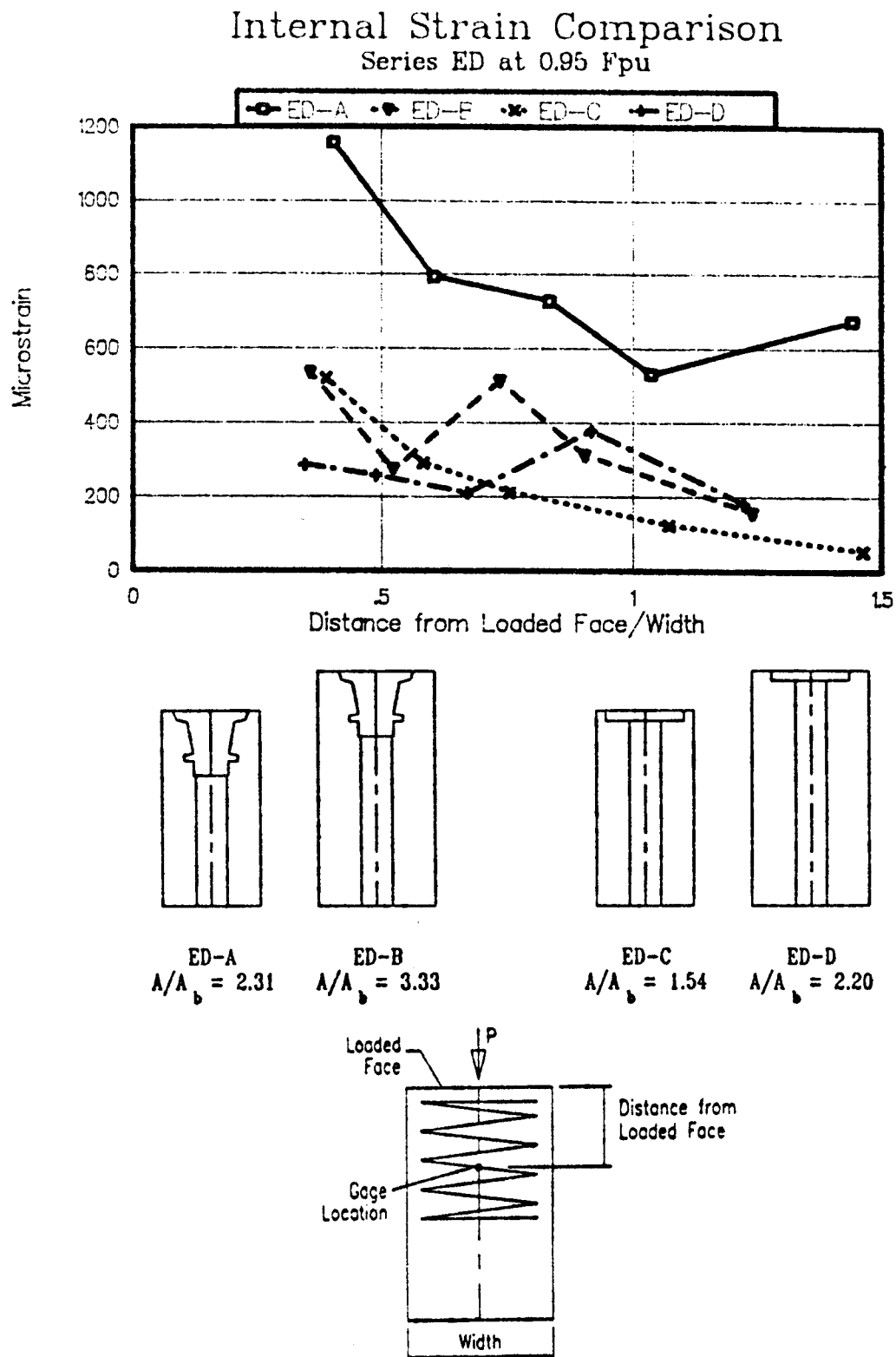


Figure 32. Spiral strains for ED series.

specimens with supplementary reinforcing was not significantly affected when compared with ED-A. However, the supplementary reinforcing did somewhat improve the ultimate load and substantially reduce the crack widths at high load levels.

Although supplementary reinforcement was clearly of substantial value in these acceptance test specimens, the final questions are whether the supplementary reinforcing needed for the anchor to pass the test requirement must be included in exactly the

External Strain Comparison

Series ED at 0.95 Fpu

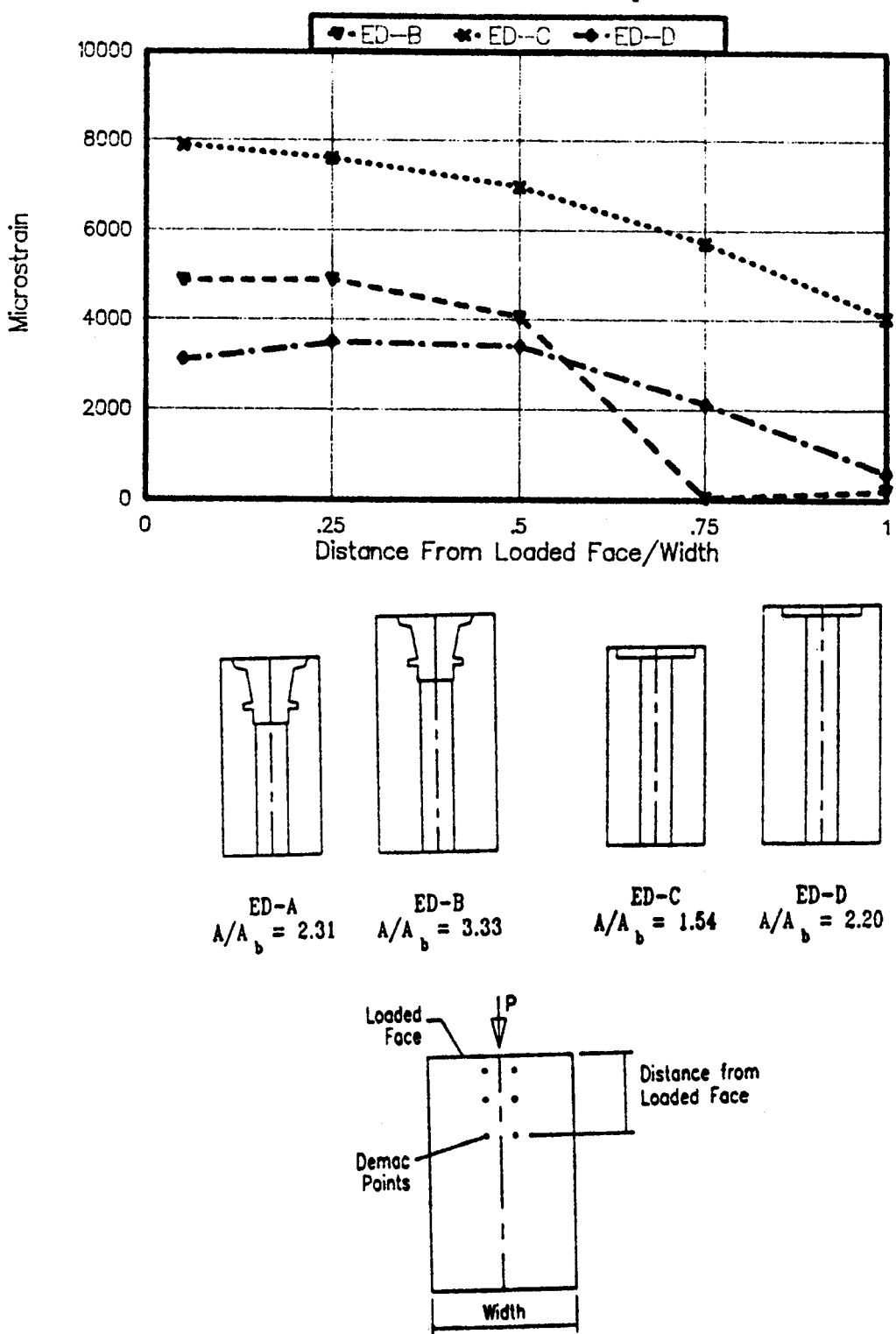


Figure 33. External strains for ED series.

Crack Widths vs. Load Series ED

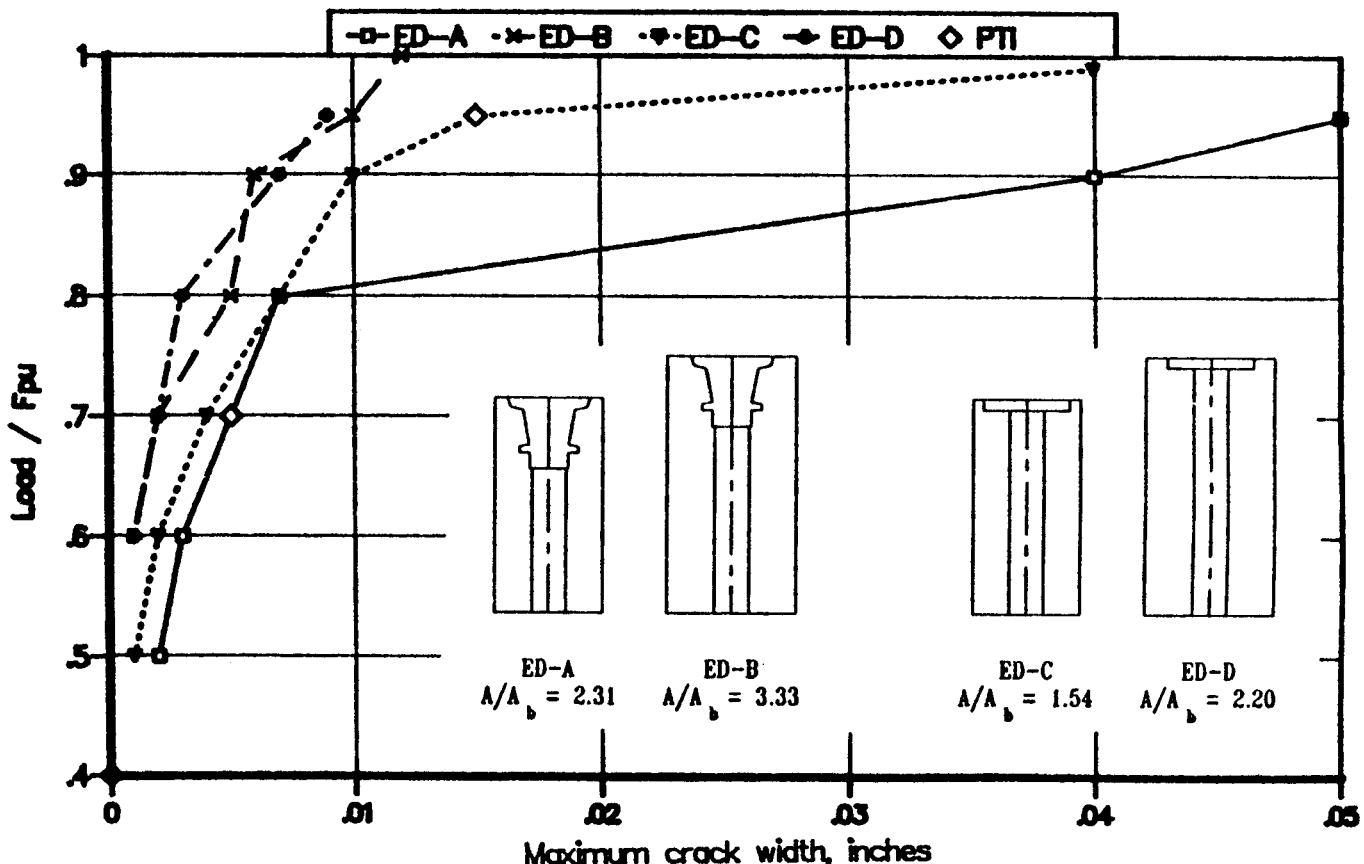


Figure 34. Crack width comparison for ED series.

Table 6. Series SP performance comparison

Specimen	f'_c	Spiral Parameters					Test Results			
		Bar Size	Diameter (in.)	Pitch (in.)	No. Turns	Volumetric Ratio	1st Crack	Ultimate	Crack Width @ 70% F_{pu} (in.)	Crack Width @ 95% F_{pu} (in.)
ED-D	5150	#4	8.25	2	5-1/2	0.0540	0.60	1.39	0.002	0.007
SP-A	4800	N.A.	—	—	—	0.0	0.45	1.10	0.007	0.016
SP-B	4800	#4	10.25	1-1/2	7	0.0570	0.65	2.10	0.001	0.004
SP-C	4800	#4	10.25	2	5-1/2	0.0430	0.65	1.89	0.001	0.007

same form in a real structure or whether the function of this supplementary reinforcing could be performed by other reinforcing present in the local zone for other purposes, such as shear resistance or shrinkage control.

Local Zone-General Zone Interaction Tests

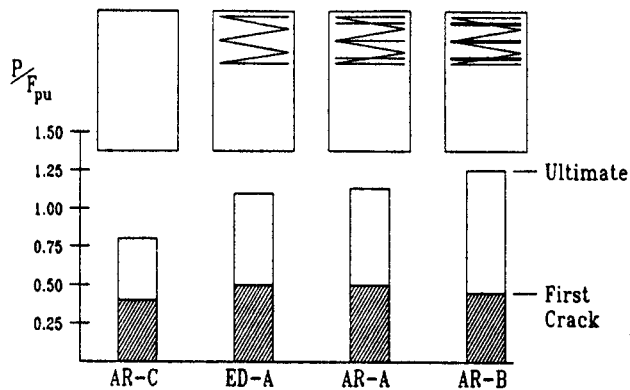
A fundamental assumption in the envisioned overall design strategy for post-tensioned anchorage zones is that the perform-

Table 7. Series AR performance comparison

Specimen	t_c'	Confining Reinforcing Details	Auxiliary Reinforcing Details				Test Results			
			Bar Size	Side Length (in.)	Spacing (in.)	No. Ties	1st Crack	Ultimate	Crack Width at 70 % F_{pu} (in.)	Crack Width at 95 % F_{pu} (in.)
AR-C*	5880	None	N.A.	—	—	—	0.40	0.80	0.007	N.A.
ED-A	5150	#4 spiral, 2 in. pitch, 4 turns	N.A.	—	—	—	0.50	1.10	0.005	0.188
AR-A	4825	Same	#2	7-7/8	2	3	0.50	1.13	0.002	0.030
AR-B	4825	Same	#3	7-7/8	2	3	0.45	1.25	0.003	0.007

* AR-C had no confining spiral

First Cracking and Ultimate Load Comparison



by a limited analysis or acceptance test program without new verification having to be made for each new structural application.

The final series of specimens in the local zone program was the LG (Local Zone-General Zone) Series. Three specimens were designed and constructed using the same local zone details as used in specimen ED-A with a 7-0.5-in. strand multiplane anchor with a #4 spiral and with 1-in. cover over the spiral. As shown in Table 7, it had first cracking load of 0.5 F_{pu} and very wide cracking (0.188 in.) at 95 percent F_{pu} , and it failed at 1.10 F_{pu} . In specimen LG-A, the anchor and the same confining spiral were placed in a concentric general zone situation; in LG-B they were placed in an eccentric situation and in LG-C they were placed in a multi-anchor specimen (specimen details are in Appendix C).

Specimen LG-A was designed using a simple strut-and-tie model. Bursting reinforcement was distributed over a zone extending from 0.19 h to 1.12 h . The bursting reinforcement bar sizes were proportioned to ensure that the general zone capacity would exceed the known capacity of the local zone test specimen, ED-A, which failed at 316 kips. Demec gages were placed on all the general zone specimens in the same pattern used in the local zone specimen.

Specimen LG-B was constructed with a single anchor placed eccentrically at the quarter point of the specimen. Spalling and bursting reinforcement were based on a successful specimen from the general zone test program, with the general zone reinforcing steel increased slightly to ensure that the general zone would not fail at a load lower than the known capacity of the local zone test specimen.

Specimen LG-C was a twin anchor concentrically loaded specimen with each anchor at the eighth point from the centerline. Details were based on previously tested general zone specimen.

In the comparison of results, data for specimen AR-B are also included. It had supplementary local zone reinforcement quite comparable to the portion of the general zone reinforcing which

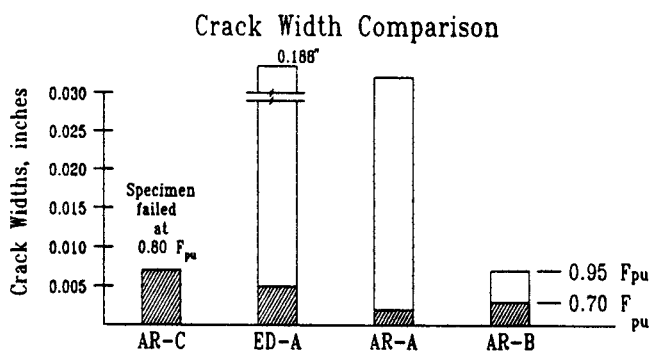


Figure 35. Series AR comparison.

ance of an anchorage device in a local zone test specimen will be a safe lower bound of its actual performance in the general zone of a more realistic bridge application. In this way, the acceptance criteria for the anchorage device could be satisfied

Table 8. Series LG performance comparison

Specimen	f'_c	Specimen Configuration	Confining Reinforcing Details	Supplementary Reinforcing Area in Local Zone (sq)	Test Results			
					% F_{pu}		Crack Width at 70% F_{pu} (in.)	Crack Width at 95% F_{pu} (in.)
					1st Crack	Ultimate		
ED-A	5150	Local Zone Test Prism	#4 spiral, 2 in. pitch, 4 turns	None	0.50	1.09	0.005	0.188
AR-B	4825	Local Zone Test Prism	Same	0.66	0.45	1.25	0.003	0.007
LG-A	4800	Concentric General Zone	Same	0.44	0.50	1.38	0.003	0.010
LG-B	4800	Eccentric General Zone	Same	0.44	0.50	1.40	0.003	0.009
LG-C	4800	Multi-Anchor Specimen	Two of Same	0.62	0.70	1.20	0.001	0.003

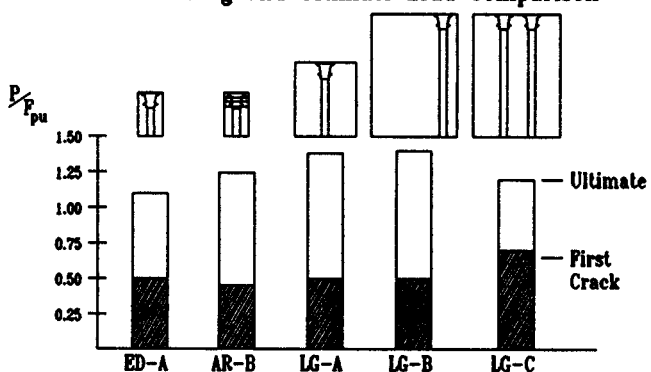
* $F_{pu} = 289$ k except for LG-C, which has two anchors so $F_{pu} = 578$ k

passed through the local zone in the general zone test specimens. Test results are given in Table 8 and shown in Figures 36 and 37. They clearly indicate that the detail used in local zone specimen ED-A performed far better in the general zone specimens than in the local zone specimen. Furthermore, the general zone test specimens had equal or greater ultimate load capacities and comparable crack width control than the local zone specimen AR-B, even though there was less reinforcing in the local zone portions of the general zone specimens. This fulfills the requirement that the local zone test present a harsher environment for the anchorage than any it would experience in a real world application. It is interesting to note that specimen ED-A would have failed the PTI crack width criteria; yet, the detail performed quite adequately in the three general zone situations. This suggests that the local zone criteria may be unduly harsh for some anchors, if supplementary reinforcement is not used in the local zone test specimen as with AR-B.

Cracking Load Predictions

Historically, the first cracking load has been of interest to the designer, particularly when serviceability criteria are important. PTI (17), in its test specification, for example, requires that a specimen have no cracks prior to 40 percent F_{pu} . As pointed out previously, such criteria have little practical value in actual applications because in the United States design specifications permit temporary loading during stressing to 0.80 F_{pu} . A reliable method for prediction of first cracking might be used to screen

First Cracking and Ultimate Load Comparison



Crack Width Comparison

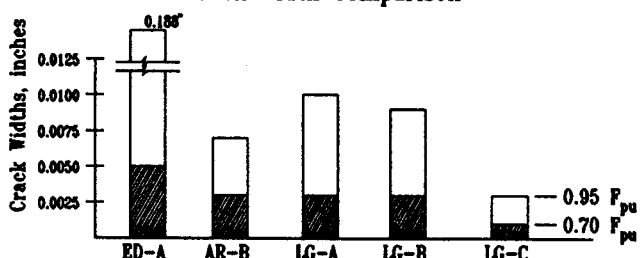


Figure 36. Series LG comparison.

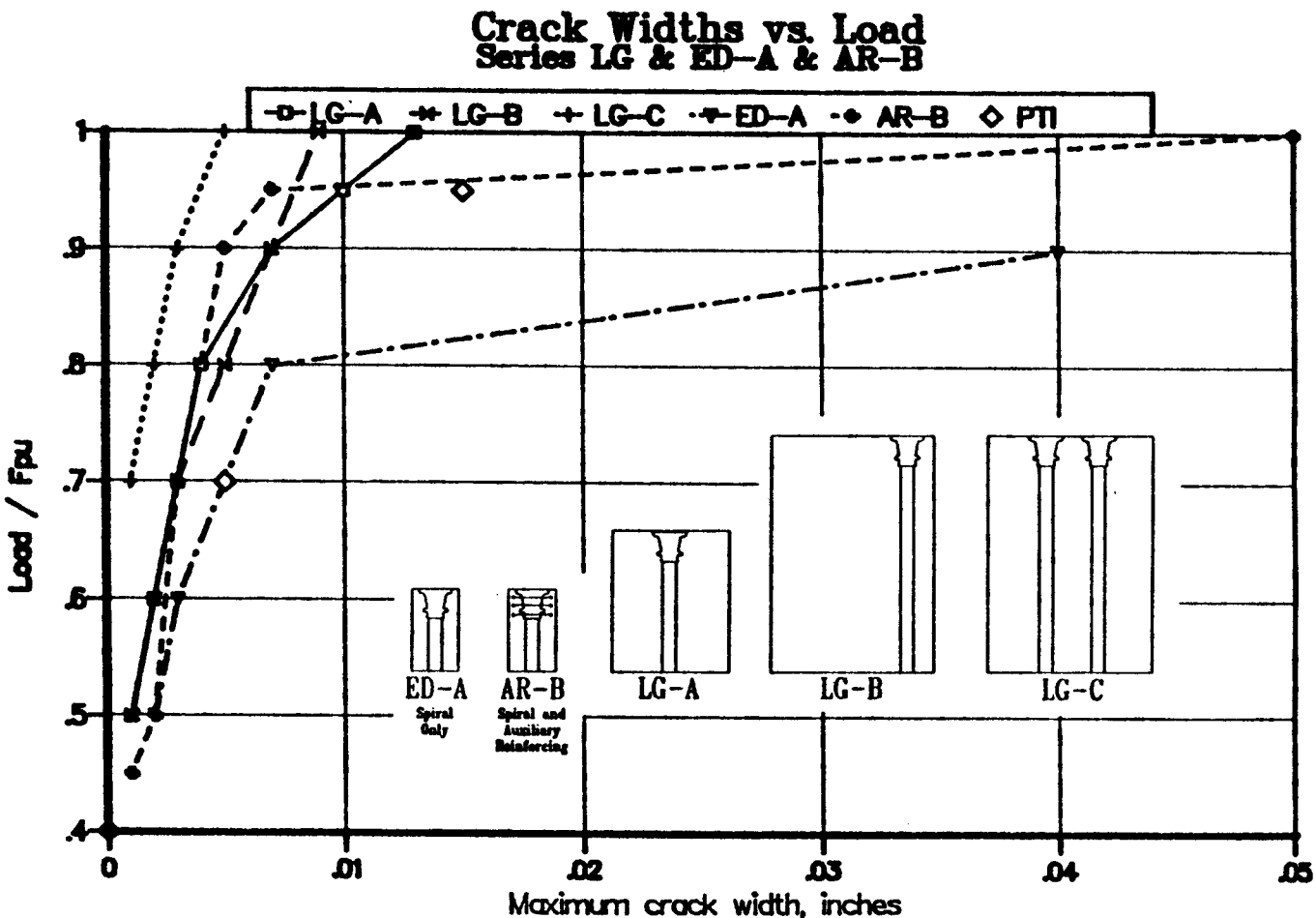


Figure 37. Crack width comparison for LG series.

anchorage proposed for use. Three widely reported crack prediction methods were evaluated as possible tools for estimating first cracking loads: (1) Guyon's (6) two-dimensional elasticity studies, (2) Yettram and Robbins (42) three-dimensional finite element (FEA) studies, and (3) Zielinski and Rowe's (43) experimental studies.

Roberts (4) pointed out that in past tests and theoretical analyses, the investigators used or assumed bearing plates over the entire specimen width and loaded by extremely stiff loading heads. The commercial anchorage devices in this study were loaded through smaller wedge plates as in actual usage. This changes the distribution of bearing stresses, as shown in Figure 38. Effective bearing areas were calculated, as shown in Figure 39, considering the effective bearing plate as circular and using the widely accepted principle of similar geometries to determine the effective area, A . These methods are not precise, but they do give a better estimation of the critical parameters, A_b , A , and a , for use in existing formulas.

Studies showed that critical tensile stress was best based on Ottosen's (44) three-dimensional failure criteria for concrete because of the high compressive stresses present under the plates. It was assumed that, at first cracking load, the maximum tensile stress predicted by the analysis procedure would equal the tensile capacity of the concrete, which was based on the previously

measured split cylinder results adjusted by the Ottosen theory for the difference in stress state in a split cylinder specimen and in a local zone specimen (4).

The computed values are compared to the existing theories in Figure 40. Yettram and Robbins' three-dimensional FEA method is the most reasonable predictor for the local zone specimen with an average of 0.95 and a standard deviation of 0.19. Overall, it seems safe to say that an actual first cracking load will be well below Guyon's prediction and, quite probably, it will be above Zielinski and Rowe's conservative prediction.

Ultimate Load Predictions

There are two factors that have been proven in the past to have a great effect on the bearing capacity of concrete: (1) the A/A_b ratio and (2) the confinement by reinforcing steel.

Each of these variables was first studied independently by Roberts (4). However, she showed that the two work together in influencing the ultimate capacity of the local zone since the ultimate capacity is influenced by confinement provided by both the concrete and the reinforcing steel. Application of the bearing pressure formulas proposed by Hawkins (13), Billig (45), Kondamat (11), and Williams (37) to the local zone specimens

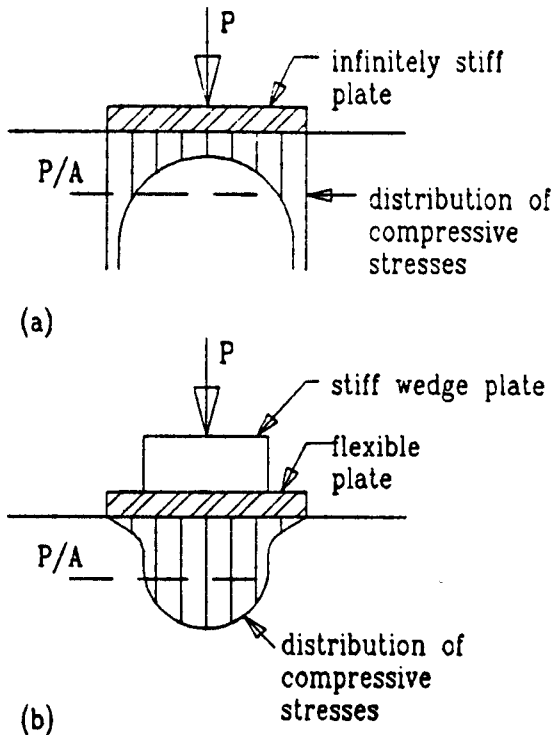


Figure 38. Stress distribution under bearing plates (from Roark, Ref. 62; Hawkins, Ref. 14).

of this investigation indicated conservative predictions, as shown in Figure 41. This is not surprising because all of the test specimens except two (SP-A and AR-C) had reinforcing in the local zone, while the bearing stress formulas were developed from tests on unreinforced concrete. However, it does indicate that present local zone approaches based on concrete bearing stress alone are not sufficient, because most commercial applications of anchorage devices for multiple strand tendons have confining reinforcement.

The effect of confinement on the ultimate capacity of the local zone specimens was also studied extensively by Roberts (4). The classic work by Richart et al. (41) was modified by Roberts to reflect the fact that the size and pitch of spirals typically used with anchorage devices do not produce the uniform confinement of the lateral oil pressure used by Richart. Roberts introduced a reduced confining pressure for square or rectangular ties that are often used in place of spirals (see Figure 42). She suggested that there will be arching of the confined concrete between spiral turns (see Figure 42c), so that a reduced area of compressive core should be considered. This area can be expressed as $A_{core}(1 - s/D)^2$. With this modification, the basic Richart equation would become

$$P_{ult} = A_{core} (f'_c + 4.1 f_{lat}) (1 - s/D)^2 \quad (3)$$

This expression was used to compute the capacity of all the local zone tests. The ratio of test result to predicted capacity was a slightly unconservative 0.94 with a standard deviation of 0.21.

Further examination of the extensive work of Niyogi (35,36) and of Schlaich and Shäfer (46) indicated that the most effective

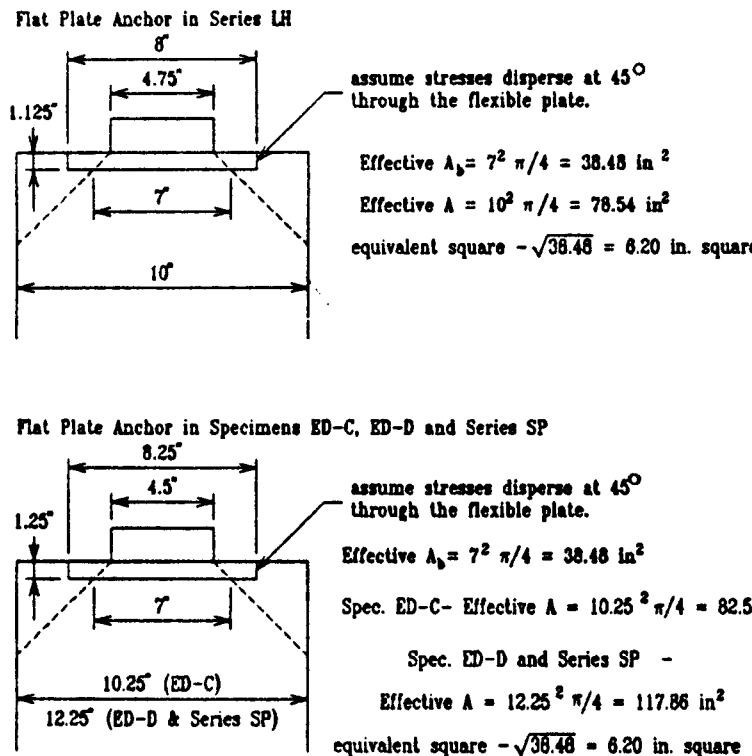


Figure 39. Calculation of effective bearing areas.

A Comparison of First Cracking Predictions with Ottosen Criteria

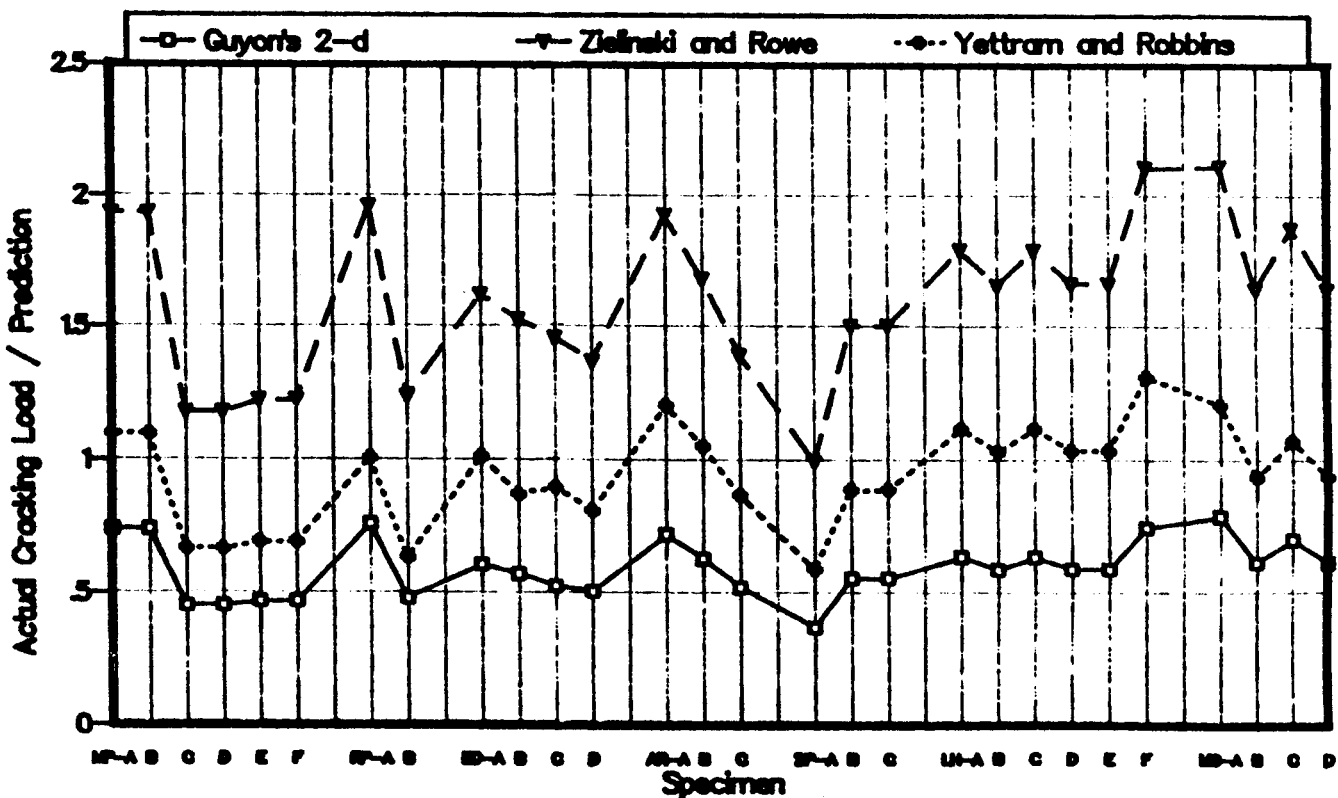


Figure 40. Comparison of first cracking predictions modified by Ottosen's criteria.

expression would be one which incorporated both the confinement of surrounding concrete (the A/A_b ratio effect) and the confinement provided by reinforcing (the f_{lat} effect). Wurm and Daschner (39) had found that there is an upper limit on the effectiveness of confining reinforcement (see Figure 43). Roberts suggested that since this limit seemed to be at $2A_s f_y/D_s = 1.2$, as shown in Figure 43, the corresponding limit on effective f_{lat} should be 1.20 ksi.

Roberts proposed that the ultimate load of local zones be computed as

$$F_{ult} = 0.80 f'_c \sqrt{A/A_b} (A_b) + 4.1 f_{lat} A_{core} (1 - s/D)^2 \quad (4)$$

This predictive equation was compared to the local zone specimens of this study, the 27 reinforced specimens of Wurm and Daschner (39), and the 39 specimens of Niyogi (35,36) (see Table 9). The prediction was very good with an average of test/predicted of 1.03 and a coefficient of variation of 15 percent.

GENERAL ZONE ANALYSIS PROCEDURES

Introduction

Typical anchorage zones, as shown in Figure 44, are extremely complex. In this case there are four local zones, one around each

anchorage device. The overall anchorage zone, or general zone as shown in Figure 15, would extend along the member for a distance equal to about the depth of the member, around 8 ft. Even the simplest possible geometry for an anchorage zone, a rectangular cross section loaded by a straight concentric tendon, is more complicated than it appears. The tendon duct causes a void in the structure, the reinforcement causes discontinuities in the material, and typical anchorage devices have a sophisticated geometry. Therefore, it is desirable to develop a general methodology for the analysis and the design of anchorage zones, rather than to attempt to define empirical expressions to solve the entire problem. Such expressions may be useful for certain cases within carefully defined limits.

At this stage of development of analysis procedures, the most likely candidates are: (1) linear elastic analysis (the older theory of elasticity approaches having been replaced by the much more versatile finite element analysis, FEA), (2) equilibrium based solutions (strut-and-tie models, STM), and (3) approximate equations.

Some studies using nonlinear finite element analysis have been published (7). As part of this project, such studies were also explored. At this stage of development they show some promise in explaining test phenomena, but they are not directly useful in design so they will not be treated explicitly in this report.

Frequently, anchorage zones are designed on the basis of a linear elastic analysis, such as Guyon's solution or finite element

Comparison of Data to Bearing Formulas

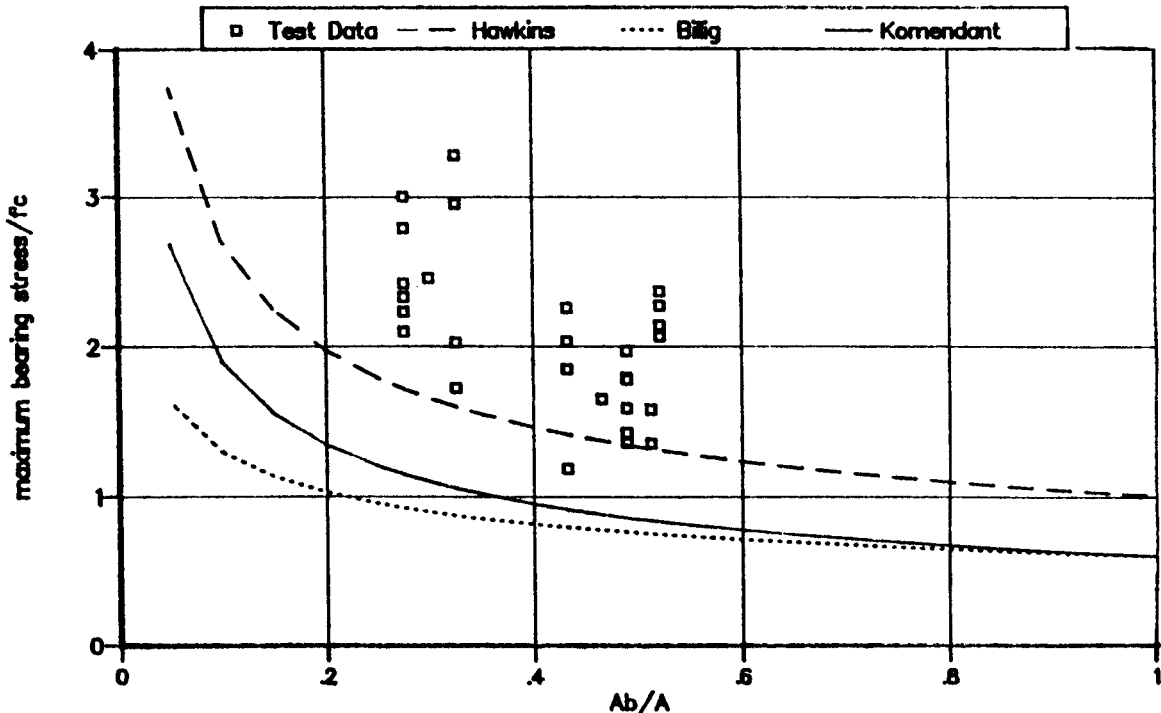


Figure 41. Comparison of bearing stress equations.

results, by integrating the transverse tensile stresses along the tendon path. However, the applicability of Guyon's solution is limited, and finite element analyses are involved and difficult to translate into reinforcement arrangements. Linear elastic finite element computer programs are widely available today, but their application to the analysis of cracked concrete is not entirely satisfactory. One of their main benefits is to indicate elastic force paths through plots of results as stress contours or stress vectors. In this way engineers can develop better understanding of the flow of forces for unfamiliar applications. For practical design applications, simple equilibrium-based solutions are very appealing to the design engineer (Figure 45). Such methods have become known as strut-and-tie models and have received wide attention lately.

Material Properties

As previously shown in Figure 15, the concrete is stressed over a large range, from extremely high compression in the vicinity of the anchorage to tension and possibly cracking in the general zone. Reinforcing steel is provided to confine the concrete surrounding the anchorage and to resist the tension forces that are released upon cracking of the concrete. Thus, the material properties of concrete and reinforcing steel must be carefully considered.

Although the concrete of the general anchorage zone is reinforced, the concrete in the general zone can generally be considered as unconfined except for the local zone. The absence of general zone confinement is not usually a major problem because,

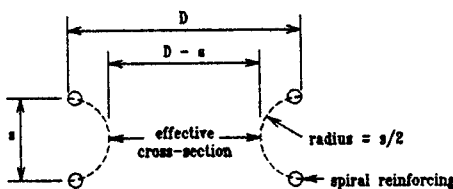
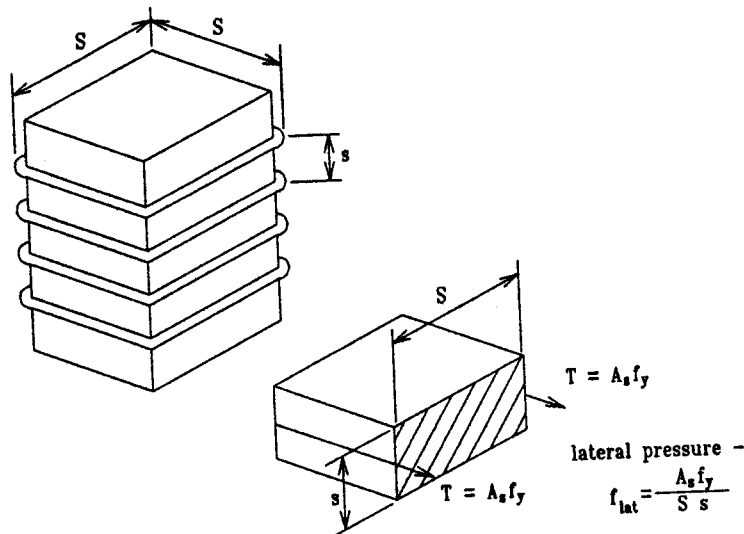
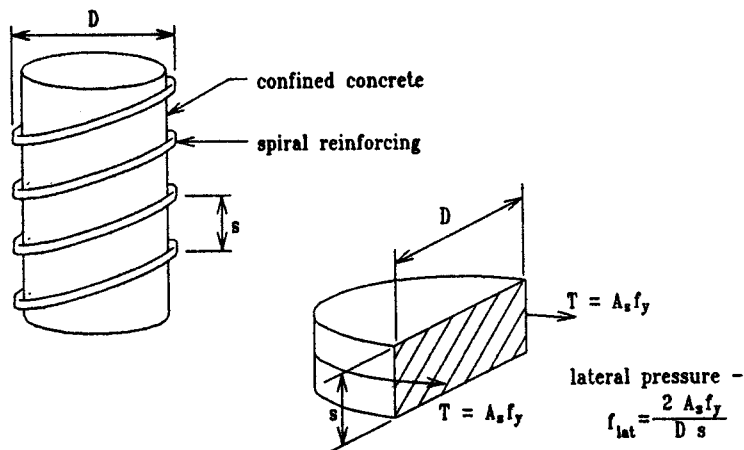
as shown in Figure 15, the compressive stresses decrease very rapidly with increased distance from the anchor. Because the concrete of the general zone is subjected to relatively low compressive stresses, in finite element analysis it is generally considered as a linear elastic material.

Unconfined concrete can resist compressive stresses in the vicinity of its uniaxial compressive strength f'_c . In beam bending, the limit value is $0.85 f'_c$. For anchorage zones, where the state of stresses is more complex, the maximum value should be lower. The higher compressive strength of confined concrete was used in Eq. 4 in the discussion of the local zone.

Material models that assume perfect plasticity are commonly used in soil mechanics applications and efforts have been made to extend plastic analysis to structural concrete. The stress-strain curve of a perfectly plastic material exhibits an unlimited horizontal yield plateau, so that arbitrarily large strains without change of stress are possible after yielding (Figure 46). Collapse of a structure made of perfectly plastic material is characterized by the formation of a kinematic mechanism that allows unlimited deformations under constant stress. This collapse load or limit load can be bracketed by applying the lower bound theorem and the upper bound theorem, respectively. These limit theorems (48) say:

Lower bound theorem: If an equilibrium distribution of stress can be found which balances the applied loads and is everywhere below yield or at yield, the structure will not collapse or will just be at the point of collapse.

Upper bound theorem: The structure will collapse if there is any compatible pattern of plastic deformation for which the rate of work of the external loads exceeds the rate of internal dissipation.



(c) Reduced spiral area

Figure 42. Calculation of lateral confining pressures.

The assumption of perfect plasticity is not particularly good for the description of the behavior of plain concrete because of the falling branch of its stress-strain curve and because of the limited ultimate strains. This is especially true for higher strength concrete. However, for reinforced concrete, and particularly for

flexure of underreinforced members, plastic analysis works very well. The strip design method for slabs is an example for the application of the lower bound theorem, while yield line analysis is based on the upper bound theorem. But even if the concrete strength has a stronger influence on the limit load, good correla-

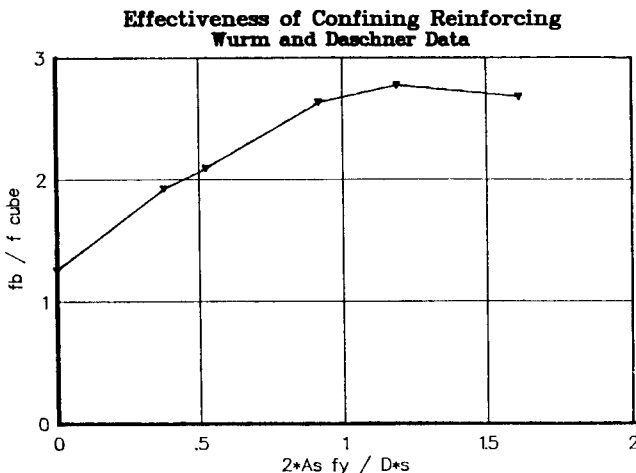


Figure 43. Effectiveness of confining reinforcing.

tion with test results can be achieved when a reduced "effective concrete strength" is taken into account. The reduction factor depends on a wide range of variables, such as concrete strength, tensile strains perpendicular to the compressive stresses, cracking, and geometry of the structure. Therefore, it has to be determined experimentally or estimated conservatively.

As shown in Figure 15, a large part of the anchorage zone is subjected to tensile stresses. Thus, the concrete of the general zone will be subjected to appreciable tensions. If the strains in the concrete reach the cracking strain, a crack opens and the tensile forces are transferred to the reinforcing steel. The tensile capacity of the concrete is generally neglected in design of an anchorage zone, because the concrete may crack during the lifetime of the structure due to other influences such as temperature or differential settlement. However, as will be demonstrated in the discussion of test results, this concrete tensile capacity can contribute substantially to anchorage zone strength.

In most cases, the reinforcement of the anchorage zone is provided by rolled deformed reinforcing bars of Grade 60. The confining reinforcement, if it is in the form of a spiral, is sometimes made of smooth bars of Grade 40 steel. Before cracking of the concrete, the strains in the reinforcing steel are very small, and most of the tensile forces are resisted by the tensile capacity of the stiffer concrete section. After cracking occurs, the forces that were carried by the concrete are transferred to the reinforcing steel. When the reinforcing steel reaches its yield strength, the force in the bars ceases to increase. Only when the strains in the reinforcement become significantly larger will the steel strain harden. In most cases, the extensive cracking and the large deformations required to reach strain hardening of the reinforcement are not attained before another mode of failure takes place, or before ductility of the anchorage zone is exhausted. For the study of anchorage zones, the reinforcing steel therefore, can be considered as a bilinear material exhibiting a perfectly elastic behavior up to its yield point, and a perfectly plastic behavior beyond that point.

Three-Dimensional Effects

All structures are three-dimensional. However, in many instances they can be represented using a simpler geometric model,

such as a linear member for a beam. In anchorage zones, the concentrated force introduced by an anchorage device must be distributed to the entire cross section of the member, requiring a three-dimensional spreading of the forces. As a simplification, it is often sufficient to consider the spreading of the forces in two principal planes perpendicular to each other. In the simplest case of the distribution of a tendon force over a rectangular cross section, the spreading of the post-tensioning force can be considered separately in the main plane of the structure (largest dimension) and over the thickness.

In many cases in which post-tensioning is used, the cross section of the member is not a simple rectangle. Rather, it can be described as an assemblage of elements, each of which can be approximated as a thin rectangular cross section. Even though the overall problem is three-dimensional, the state of stresses in each component of the structure is essentially planar, with the exception of the local zone and the interfaces between the various components.

As an example, Figure 47 shows the case of the box-girder bridge. The top and bottom flanges, as well as the webs, can be considered as rectangular components of the cross section and the spreading of the tendon force can independently be investigated on each of the components of the cross section. This method of breaking down the section into planar elements was proposed by Schlaich et al. (2) and was successfully used in this project.

Finite Element Analysis

The finite element method has become increasingly popular for calculating the detailed state of stresses in structures of arbitrary shape. Modern computer programs allow the user to model arbitrary structures and to define sophisticated material laws for the model. Figure 48 shows an example of a finite element mesh, showing the subdivision of the anchorage zone into quadrilateral elements. Burdet (48) has reported in detail on proper modeling of anchorage zones including information on convergence, accuracy, and variability as influenced by mesh size, number of nodes, and assumptions as to bonding between the anchorage device and the concrete.

Application of the finite element method is often limited by the lack of appropriate models for the behavior of the materials. This is especially true of the modeling of cracks in concrete. Cracks are usually not modeled as discrete discontinuities that extend as the load increases. Instead, the crack is considered as smeared over the considered elements, accordingly decreasing their stiffness (49). While this hypothesis may be acceptable for large structures with a uniform distribution of reinforcement, it is much less accurate for small regions of reinforced concrete structures where the stresses in the reinforcing steel vary sharply at the cracks, as is the case for anchorage zones. Finite element modeling of structural concrete is very much a field of research and rapid development at the present time (50). For this research, the Finite Element Program ABAQUS (51) was used to perform the stress analysis. The generation of the finite element models was performed using PATRAN (52), a general purpose preprocessor for finite element analysis.

The vast majority of analyses performed during this phase of the project were linear elastic. This choice was made to simplify the individual analyses, allowing a wider range of geometries

Table 9. Comparison of prediction equations with test data

Roberts (4) Specimen	Test/Eq.	Wurm & Daschner (38) Specimen	Test/Eq.	Niyogi (34, 35) Specimen	Test/Eq.
MP-A	0.70	13	1.14	B11	0.98
MP-B	0.69	19	1.03	B12	1.00
MP-C	0.82	25	1.14	B13	0.95
MP-D	0.94	14	0.92	B14	0.97
MP-E	0.75	20	0.94	B15	0.98
MP-F	0.96	26	0.96	B16	1.00
RP-A	0.64	15	1.14	B17	1.13
RP-B	0.75	21	1.19	B18	1.11
ED-A	0.93	27	1.31	B21	0.72
				B22	0.76
ED-B	1.10	16	1.16	B23	0.80
ED-C	0.93	22	1.13	B24	0.86
ED-D	0.94	28	1.12	B25	0.94
AR-A	0.99	18	1.08	B26	1.02
AR-B	1.10	24	1.08	B27	1.18
AR-C	0.97	30	1.05	B28	1.09
SP-A	1.23	36	1.17	B31	0.64
SP-B	1.10	37	1.12	B32	0.76
SP-C	1.05	38	1.20	B33	0.77
LH-A	0.74	35	1.14	B34	0.85
LH-B	0.71	39	1.09	B35	0.91
LH-C	0.83	40	1.13	B36	1.07
LH-D	0.90	33	1.33	B41	0.82
LH-E	0.90	34	1.31	B42	1.12
LH-F	0.99	41	1.30	B43	1.01
MB-A	0.97	31	0.95	B44	1.22
MB-B	1.12	32	0.92	B45	1.29
MB-C	1.00	42	0.93	B46	1.44
MB-D	1.07			B47	1.48
				B48	1.78
				S11	1.10
				S12	0.99
				S13	0.84
				S21	0.93
				S22	1.01
				S23	0.90
				S24	1.00
				S25	0.91
				S26	1.09
Average	0.92	Average	1.11	Average	1.01
Max.	1.23	Max.	1.33	Max.	1.78
Min.	0.64	Min.	0.92	Min.	0.64
Std. Dev.	0.15	Std. Dev.	0.12	Std. Dev.	0.22
Coef. Var.	0.163	Coef. Var.	0.107	Coef. Var.	0.215

and load configurations to be investigated analytically. An exploratory study of nonlinear finite element analysis was used to more closely investigate some specific configurations.

Simplifying hypotheses are necessary for the analysis of the very complex behavior of anchorage zones. The simplest model is to assume the material to be linear elastic. Because the stresses in the concrete and the reinforcing steel are generally small up to the cracking of the concrete, a linear model is quite accurate to describe the behavior of the general zone of a specimen up to cracking. Reasonable estimates of the cracking load of the general zone, therefore, can be obtained from a linear elastic stress analysis. The accuracy of the cracking load predictions

could be influenced by the very large compressive stresses in the local zone. However, the presence of confining reinforcement is presumed to minimize this effect.

As will be shown, the results of a linear elastic finite element analysis can also be successfully used to determine the required amount of tensile reinforcement and to estimate the maximum compressive force that can be applied on an anchorage zone. Regardless of the method used to obtain the required amount of reinforcement, it is often desirable for effective crack control to pattern the tensile reinforcement somewhat according to the elastic stress distribution.

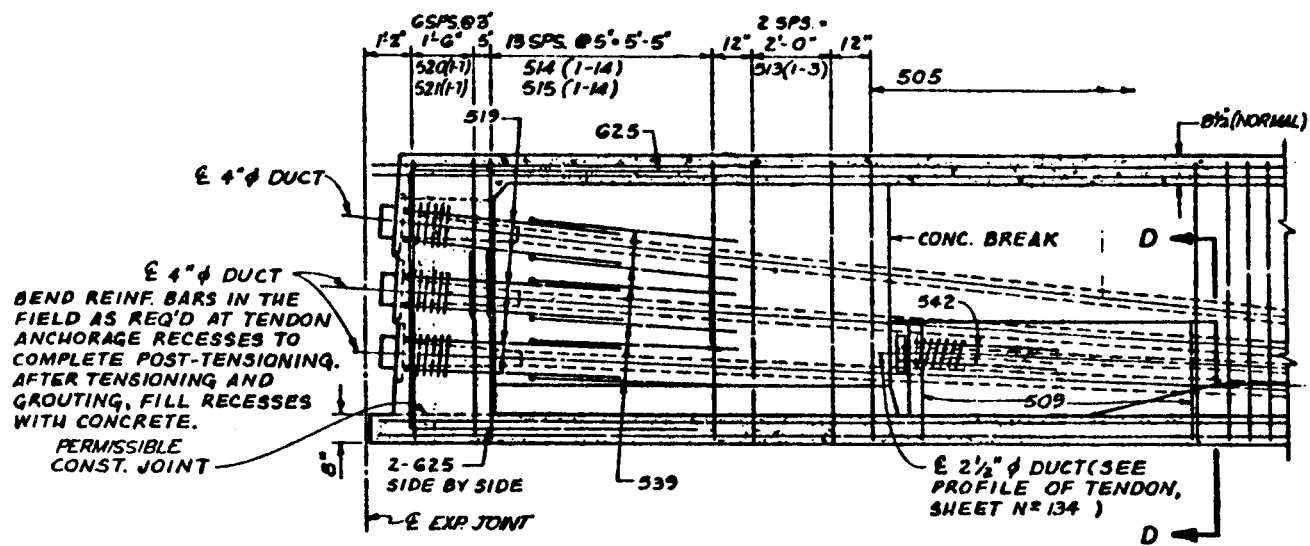


Figure 44. Typical anchorage zone with four tendons.

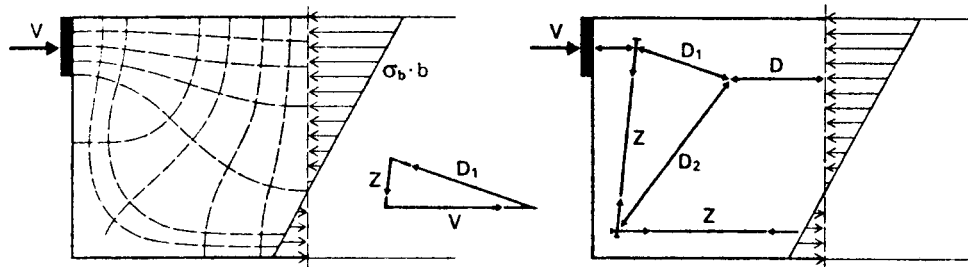


Figure 45. Flow of forces in anchorage zone.

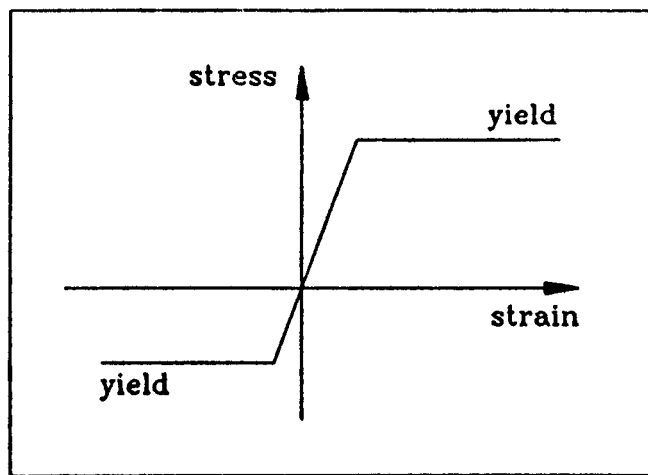


Figure 46. Elastic-plastic stress-strain curve.

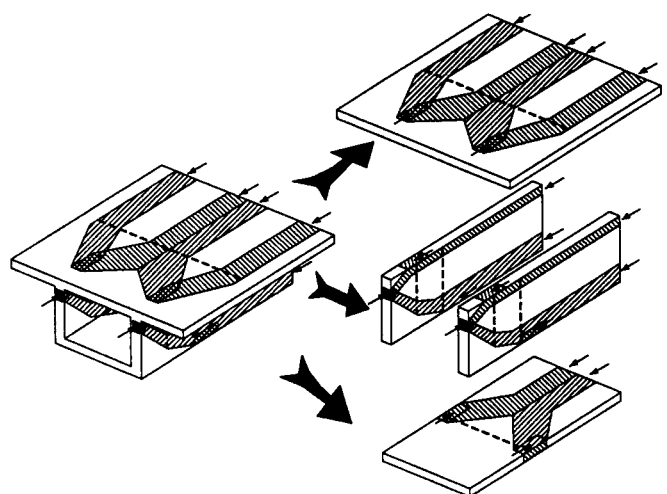


Figure 47. Principle of decomposition of a complex cross section into principal planes.

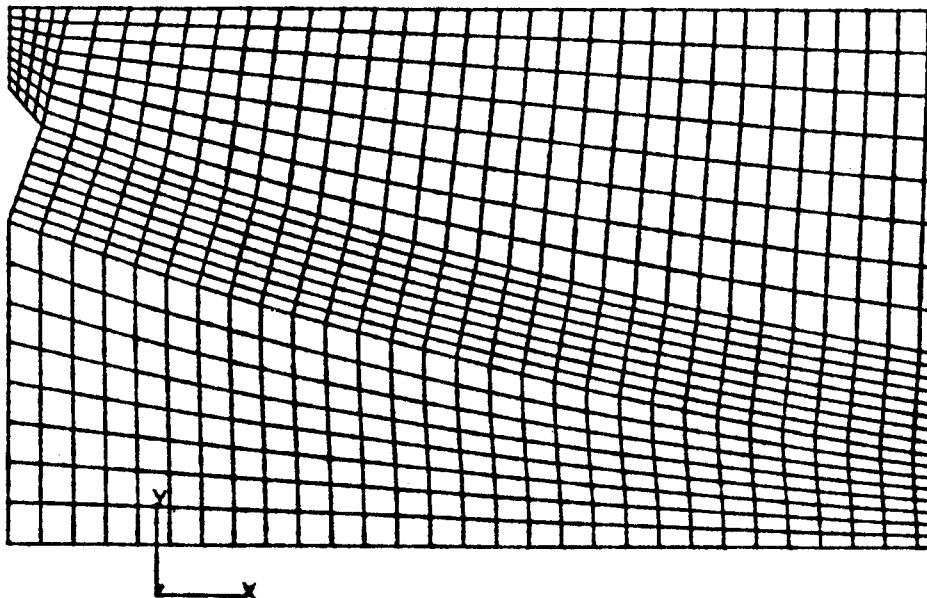


Figure 48. Example of two-dimensional finite element mesh of an anchorage zone.

Once a finite element analysis has been performed, it is best to represent the stress distribution in graphical form. Several representations exist. Because stress is a second-rank tensor, it seems best to combine several representations to present the results for evaluation.

A contour plot, as shown in Figure 49, is a plot of lines of equal stresses. However, because a stress function has several components, contour plots of one component give an incomplete picture of the state of stresses. In plane stress analysis, for example, a total of three contour plots is necessary to represent the three components of stresses in the plane. Despite their limitations, contour plots are helpful, especially for simple configurations. One single plot of the stresses normal to the tendon path can yield sufficient information to design the bursting reinforcement for the general anchorage zone. Both ABAQUS and PATRAN offer facilities to generate contour plots of the stresses.

An X-Y plot, such as the one shown in Figure 50, can be used to show the stresses perpendicular to the axis of the tendon. A comparison is made between the results of the three-dimensional analysis and the plane stress analysis. They are seen to be practically identical.

Isostatic lines, as shown in Figure 51, are lines that are at all points tangent to the direction of the principal stresses. They are similar to the equipotential lines of a flow net plot for underground fluid flow. Isostatic lines correspond to the intuitive idea of "spreading of forces" through a body. As a matter of fact, it is relatively easy to "guess" and draw isostatic lines for a simple configuration.

The tensorial nature of the stress function, in contrast to the scalar potential in fluid flow, renders an automated computation of isostatic lines complicated. However, a plot representing a field of principal stress vectors, as shown in Figure 51, gives a visual idea that is very close to isostatic lines. The generation of principal stress vector plots can easily be automatized. If isostatic lines are desired, they can be drawn tangent to the corresponding vectors. If the vectors are scaled so that their

lengths represent the magnitude of the stresses, plots of principal stress vectors also give indications of the relative magnitude of the stresses.

A program to process the results of the finite element analysis and to display the principal stress vectors and X-Y plots was developed by Burdet (48) on a microcomputer. This program allows a quick and easy interpretation of the results of a finite element analysis and can export the results in several common file formats for further treatment. Because the program is based on a microcomputer and is user friendly, it was extensively used in the design of specimens to evaluate the various design options.

The results of a linear elastic analysis of the anchorage zone can be used for the design of the reinforcement in the general zone. Placing an amount of reinforcement, corresponding to the calculated elastic tensile forces, in the locations where the stresses in the concrete exceed the tensile strength, allows an immediate load transfer when cracking occurs. The method of systematically placing reinforcement to resist any tensile stress in the model has often been used and is generally conservative. Furthermore, because the reinforcement is located exactly where it will be needed, it is expected that such a procedure will limit the extent of cracking. The knowledge of the elastic state of stresses in an anchorage zone is, therefore, a good starting point for design of reinforcement.

The compressive capacity of the anchorage zone can be estimated by computing the level of compressive stresses in the concrete under the factored tendon force. Because the confining reinforcement of the local zone generally extends for a length approximately equal to the lateral dimension of the anchorage device, the present study limits the stresses in the concrete at that location ahead of the anchorage device to $0.70 f'_c$.

Strut-and-Tie Models

Today's strut-and-tie model procedures have evolved from the truss model for shear design. Although the truss model was

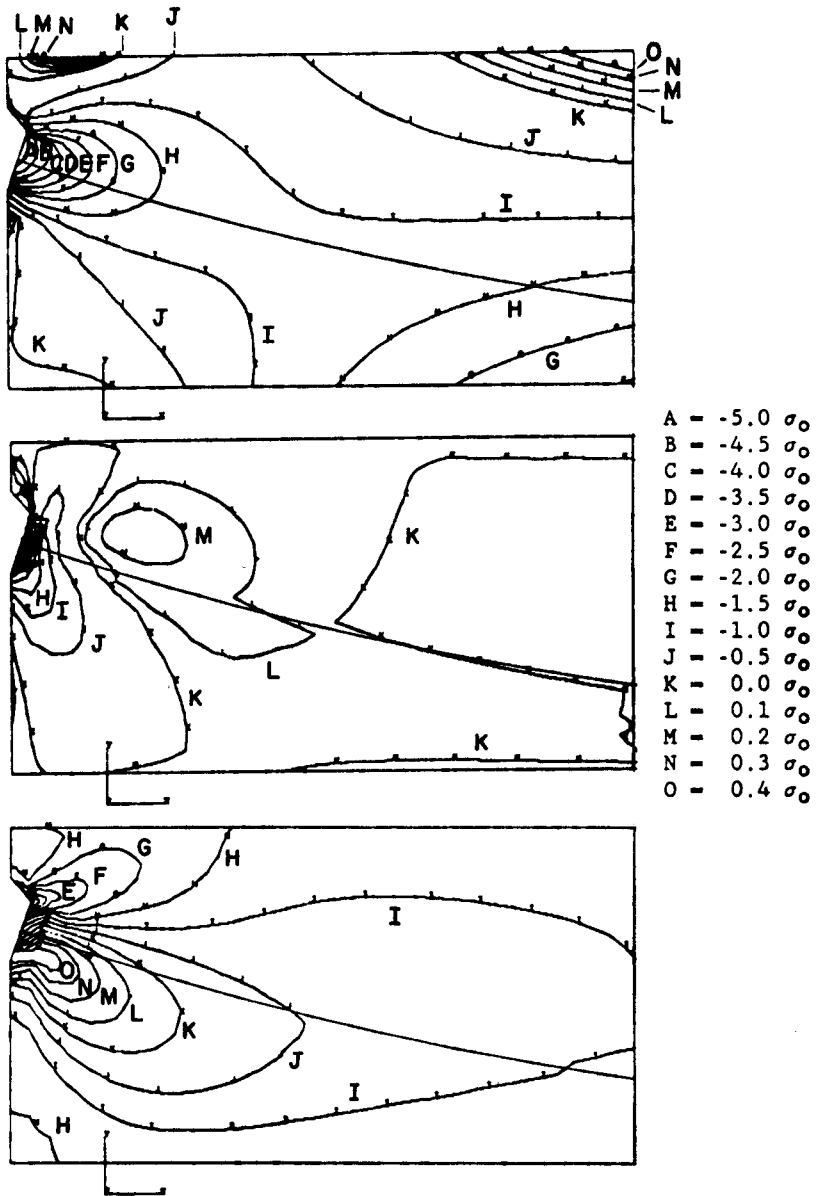


Figure 49. Contour plot of the normal stresses σ_{xx} and σ_{yy} , and of the shearing stress τ_{xy} in an anchorage zone.

developed at the turn of this century, it is still a powerful concept and is the basis for the code provisions for shear design in many countries (Figure 52). Schlaich, et al. (2) proposed to generalize the truss model and to use it in the form of strut-and-tie models for the design of the disturbed regions of a structure in the vicinity of static or geometric discontinuities.

In strut-and-tie models the flow of forces in a structure is approximated by a two-force member system formed of compression members, the struts, tension members, the ties and nodes where the members intersect. The forces in the members are determined from equilibrium conditions, and can then be used to evaluate compressive stresses in the concrete and to proportion the reinforcement. Besides being an approximation to the state of stress in a structure, the strut-and-tie model can also be inter-

preted as a lower bound solution to a plastic limit load in the context of theory of plasticity.

Schlaich proposes to divide a structure into B-regions and D-regions (2). In B-regions beam theory applies and traditional design and analysis methods may be used. D-regions are the disturbed regions in the vicinity of static or geometric discontinuities. The extent of these D-regions may be estimated using the principle of Saint Venant (Figure 5). The forces acting on a D-region are the external loads and the internal forces at the boundaries between the D-region and adjacent B-regions. The internal forces can be determined from flexural theory.

In a next step the flow of forces in the D-region is approximated by a series of compression struts and tension ties that are connected at nodes. This strut-and-tie model must establish a load

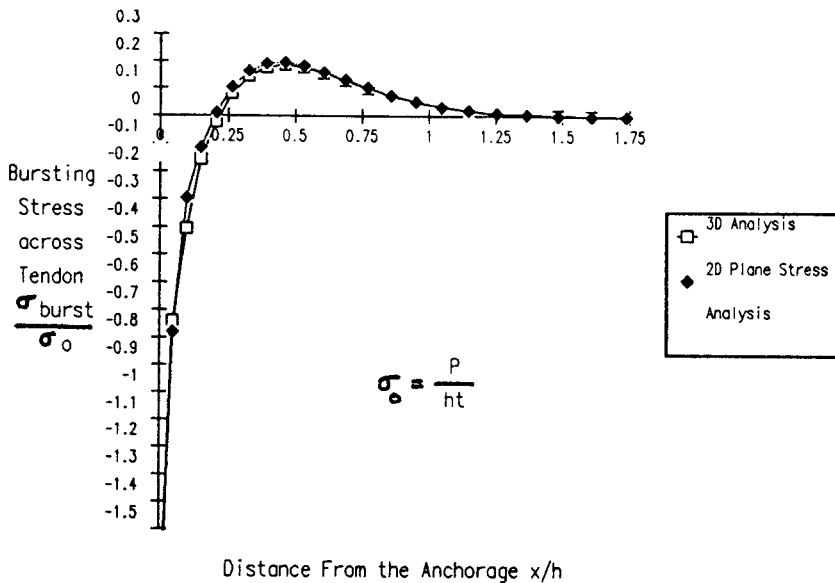


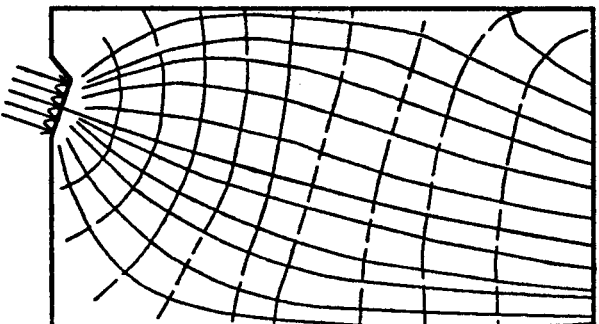
Figure 50. X-Y plot of the stresses perpendicular to the axis of the tendon σ_{xx} represented along the axis.

path between the external and internal loads acting on the D-region, and must satisfy equilibrium conditions. The ties represent the reinforcement in the structure. The struts represent compression stress fields.

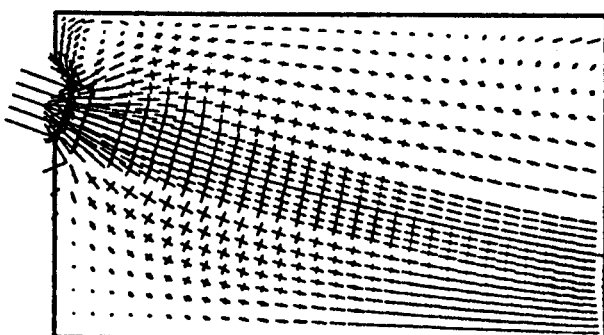
Finally, reinforcement is proportioned based on the tie forces obtained from the strut-and-tie model. Compressive stresses may be checked by assigning a width to the struts. The strut widths are controlled by the dimensions of bearing plates, the dimensions of the overall D-region, and the reinforcement arrangement.

Figure 53 shows a strut-and-tie model for an eccentrically loaded anchorage zone. Reinforcement is visualized as being anchored through bearing plates. The strut widths were selected such that all struts are stressed equally. This causes a hydrostatic state of stress in the nodes and is characterized by the node boundaries perpendicular to the struts. A nonhydrostatic state of stress in the nodes is acceptable if the ratio of stresses on adjacent edges of a node is not less than 0.5 or no more than two (2).

The state of stress in the struts is assumed as uniaxial and uniform over the strut width. The stresses are critical at nodal points where bottle necks in the compression fields occur. Schlaich recommends the following values for the nominal concrete strength, $f_c = v_e f'_c$, for struts: $v_e = 0.85 f'_c$ for an undisturbed uniaxial state of stress; $v_e = 0.68 f'_c$ if moderate cracking parallel to the strut may occur or in regions where reinforcement is anchored; $v_e = 0.51 f'_c$ for skew cracking or skew reinforcement; and $v_e = 0.34 f'_c$ for skew cracking with large crack widths.



a) Isostatic Lines



b) Principal Stress Vectors

Figure 51. Isostatic lines and principal stress vectors in an anchorage zone.

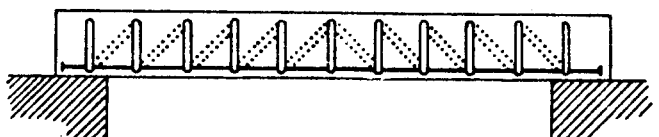


Figure 52. Ritter's truss model.

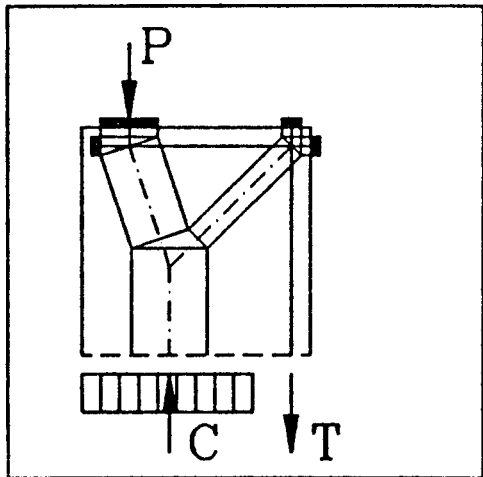


Figure 53. Strut-and-tie model for eccentrically loaded anchorage zone.

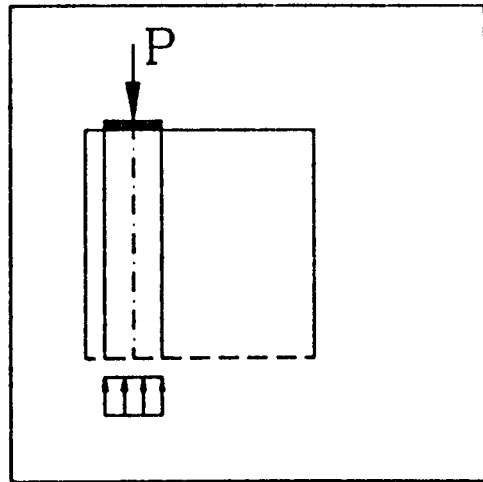


Figure 54. Direct load path in eccentrically loaded anchorage zone.

There is no unique strut-and-tie model solution for a given problem. Rather, any strut-and-tie model that satisfies equilibrium and for which the effective concrete strength and the yield strength of the reinforcement are nowhere exceeded is a lower bound to the plastic limit load. Figure 54 shows an alternative load path for the eccentrically loaded anchorage zone discussed above. This model consists of a single strut that connects the applied load to a uniform stress distribution that extends only over a portion of the end of the anchorage zone. This is a perfectly acceptable lower bound solution, provided the concrete stresses in the strut do not exceed the effective concrete strength. However, this load path does not provide much guidance as to the reinforcement requirements and should not be used.

This example illustrates that equilibrium conditions and material strength limitations alone are not sufficient to develop reasonable strut-and-tie models. Additional rules are needed to eliminate unsatisfactory solutions. The most important rule was

already discussed—the internal forces at the boundaries of the D-region should be determined from flexural theory. This requirement provides substantial additional information for the development of a strut-and-tie model, as can be seen by comparing Figure 54 to Figure 53. The enforcement of a flexural theory stress distribution is equivalent to reintroducing compatibility conditions along the interface of the D-region and the adjacent B-region.

There is still considerable freedom in the selection of the strut-and-tie model geometry, even with the restriction discussed above. Schlaich, et al., recommend the orientation of the strut-and-tie model according to the elastic stress trajectories with deviations up to 15 deg. as acceptable (2). But even if results of an elastic stress analysis are not available, the flow of the stress trajectories generally can be estimated using engineering judgment with sufficient accuracy for the development of a strut-and-tie model (Figure 45).

Obviously, the approximation of the state of stress in a structure by strut-and-tie models is highly idealized. Such models, therefore, are not particularly useful as research models, where usually more accurate predictions are desired. However, strut-and-tie models are an excellent tool for ultimate load design. The designer is led to visualize a clear load path in the structure and attention is directed to global equilibrium. Furthermore, tie forces can be translated directly into reinforcement requirements and the importance of well-anchored reinforcement is emphasized by the nodal concept.

Strut-and-tie models have only a limited capability to detect compatibility and constraint induced stresses. However, such stresses disappear upon cracking of the concrete and reinforcement is required for crack control, but not for structural safety. This is well established for the case of compatibility torsion, for example. Consequently, crack control reinforcement should supplement the primary reinforcement determined from a strut-and-tie model. The regions where such crack control reinforcement are required can be determined from linear elastic analysis, experience, and common sense. As long as adequate reinforcement is provided for the primary load path, the amount of supplementary crack control reinforcement is not critical in terms of ultimate capacity.

For the designer inexperienced in the use of strut-and-tie models, most likely the biggest problem is the nonuniqueness of the solution. In fact, to a certain degree, a reinforced concrete structure can and will adjust to the load path envisioned by the designer. This adjustment does not even require a perfectly plastic material, but is induced by the change of stiffness and by the stress redistributions that come with cracking of the concrete.

Verification of Strut-and-Tie Models

Part of this project was an experimental study to evaluate the use of strut-and-tie models as a tool for the design of the general zone (1). Sanders conducted 36 tests of general anchorage zone specimens. Results will be reported later in this chapter. In the tests the local zone was adequately confined to preclude failure in this region. Tendon configurations included concentric, eccentric, multiple, and curved and inclined tendons. Other variables were reinforcement distribution, presence of lateral post-tensioning, and concrete strength. All specimens had a rectangular cross section except one which had a T-section.

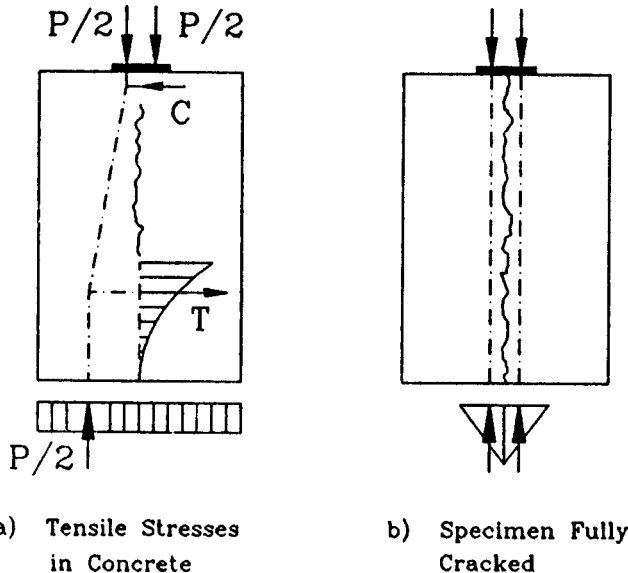


Figure 55. Effect of bursting crack.

The primary conclusion of Sanders' study is that strut-and-tie models oriented on the elastic solution and neglecting concrete tensile strength are quite conservative. This is because of two reasons. Before the bursting crack extends all the way to the base of the specimen, there is a considerable contribution of the concrete tensile strength of the remaining uncracked portion of the specimen. As the crack extends, the compression struts become steeper, which makes the concrete tensile contribution more effective (Figure 55a). After the bursting crack has reached the base of the specimen, a dramatic redistribution of stresses takes place. This can be well visualized by considering the limiting case of an unreinforced block (Figure 55b). The bursting crack splits the block into two separate eccentrically loaded portions. Because no tensile stresses can be transferred across the base of the specimen or across the bursting crack, the stress distribution at the base of each of the portions must be approximately triangular with the resultant force balancing the corresponding portion of the applied load. This, in fact, is the load path shown in Figure 54 that was so rashly discarded as unreasonable.

If bursting reinforcement is present, some spreading of the compressive stresses in the anchorage zone will take place. The stresses in the reinforcement depend on the lateral stiffness provided by that reinforcement and are not easily calculated. However, even after the bursting reinforcement has reached its yield strength, further increase of the applied load is possible. This causes the compression struts to become progressively steeper until a compression failure occurs (Figure 56). In Sanders' tests this compression failure usually was located immediately ahead of the confined concrete of the local zone.

Sanders confirmed the redistribution of stresses after full cracking of the specimen by an analytical model, where the separated portions of the cracked specimens were analyzed as beam columns on elastic foundation. He also developed modified strut-and-tie models, which allowed deviation from the elastic stress distribution at the base of the specimens and, thus, was able to improve the ultimate load predictions for his tests significantly,

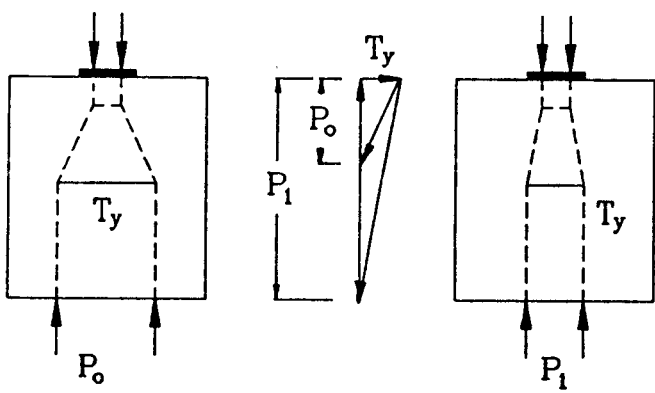


Figure 56. Increase of load after yielding of bursting reinforcement.

The important conclusion of Sanders' study is that, while strut-and-tie models oriented on the elastic solution are quite conservative, stress redistributions after development of bursting cracks reduce the stresses in the bursting reinforcement but increase the compressive stresses in the anchorage zone. For design, the basic strut-and-tie model approximating the elastic stress distribution is recommended.

Use of the Strut-and-Tie Model in Design of Anchorage Zones

Once the geometry of the strut-and-tie model has been defined, the resulting truss structure can be analyzed. If the truss is statically determinate, the equilibrium equations can be solved in a manner similar to the analysis of truss structures. It frequently occurs that the resulting structure is kinematic; it is stable only for a specific loading. As a consequence, the model will need to be adapted for various loadings. If an analysis program is used to calculate the forces and deformations, additional members or boundary conditions must be added to make it stable.

Sometimes, the strut-and-tie model is statically indeterminate. One possible solution is to assign reasonable values of forces to some members. By attributing to the force in a tension tie the strength of a given reinforcing bar, the corresponding unknown can be replaced by a known applied force. This procedure can be repeated until the structure becomes determinate (54). It is also possible to perform a normal linear truss analysis of the indeterminate structure. Material properties and cross-sectional areas are attributed to the struts and ties based on an assumed geometry of the members. Some iterations may be required before a satisfactory solution is reached.

The ultimate load predicted by the strut-and-tie model is controlled by the failure of any one of the components, strut, tie or node.

As indicated previously, it is frequently assumed that the concrete in the node can resist a biaxial, hydrostatic compression with a pressure equal to the nominal concrete strength f'_c . Although there is little experimental evidence about this hypothesis, it seems to be well accepted. The main problem in applying this philosophy is the design of nodes that involve tension ties. Schlaich et al. (2) present a model to explain the load transfer between the tension ties and the compression struts.

With the exception of failures in the local zone, no failure of the nodes was observed in the tests of anchorage zones. This is most likely because all nodes involved in strut-and-tie models of anchorage zones, with again the exception of the local zone, are smeared nodes. In all test specimens, however, the reinforcing steel of the ties was carefully detailed in order to be fully developed within or before the nodes. Failure of the anchorage zone in the local zone has been observed several times during the tests. Such failures would be prevented if the recommendations for design of local zones given in Chapter 4 had been available and followed.

In the general zone, stresses in the unconfined concrete are largest at the interface of the strut with the concrete of the local zone node, which is generally confined. The critical section for the compression struts is generally located at the bottom of the confining reinforcement of the local zone. Its exact location varies because of the lateral spreading of stresses, which causes unconfined concrete to interact with confined concrete. In this study, a critical section located at the end of the confining reinforcement, or at one times the lateral dimension of the anchorage device, ahead of the device is proposed. As indicated previously, several values have been proposed for the maximum effective compressive stress in the concrete of compression struts. Most of these values were based on judgment or on tests that were basically on members with bending or shear, with no local introduction of large forces. The values proposed range from $1.0 f'_c$ to $0.3 f'_c$, depending on the state of stresses in the considered area and on the expected cracking pattern. For anchorage zones, the value of $0.7 f'_c$ was found to be appropriate.

A tension tie is considered as failed when all bars contributing to it have yielded. If the structure becomes a mechanism at this point, failure of the anchorage zone is assumed to occur. Failure of the steel ties in tension is the desired mode of failure because the yielding of steel is ductile. In the case of anchorage zones, this ductile behavior is not really observed because there are high compressive forces and, also, because the contribution of uncracked concrete in tension is present until very late in the loading history.

Strut-and-tie models that rely explicitly on the tensile capacity of a concrete tie can fail if a concrete tension tie cracks and the crack propagates, releasing the tension force. Schlaich et al. (2) emphasize that concrete ties should be relied upon only where no progressive collapse is expected. Because the anchorage zone is a critical part of the structure, it is undesirable to rely on any tensile capacity of the concrete for the design. However, it was obvious when observing the behavior of laboratory test specimens that uncracked concrete has an appreciable contribution to the behavior of the anchorage zone even after crack has occurred. Figure 57 shows the load-deflection curve of the loading head of the testing machine for one specimen. The onset of cracking at a load of 345 kips has no obvious influence on the stiffness of the test specimen.

Serviceability Considerations

The purpose of a serviceability analysis is to ensure that the anchorage zone will perform satisfactorily under normal loading conditions. The performance is sufficient when the deformations of the anchorage zone are small, and the extent and opening of cracks is limited. Uncracked anchorage zones are very stiff

members because of the massive section of concrete. As shown in Figure 57, the presence of cracks does not dramatically reduce the stiffness of the anchorage zone. Even if the contribution of concrete in tension is neglected for the strength design of the anchorage zone, it will be present at service loads.

It is unrealistic to expect that concrete will not crack at all in the anchorage zone of a member resisting service loads. The presence of post-tensioning forces in a structure will limit the opening of concrete cracks, but only in the direction of the prestressing force. Transverse stresses caused by the tendon force in the anchorage zone, unaccounted external effects caused by differential settlements or impact loads, and internal effects caused by shrinkage or temperature may well cause the concrete to crack anyway. It is therefore preferable to assume that the concrete will crack and to provide reinforcement that will both prevent the failure and limit the cracking. The main cracks in the general zone are caused by bursting stresses.

If the tensile stresses in the concrete are necessary for the equilibrium of the structure, as in the case of bursting stresses, the crack will extend until a new state of equilibrium is reached. For a given loading, the crack will stop propagating when the force in the reinforcing steel that crosses it replaces the tensile force resisted by the concrete before cracking. In order to limit the opening of cracks, reinforcement must cross the crack close to the location where a crack is forming. The location of the reinforcement relative to a developing crack has a considerable influence on the growth of the crack. A reinforcement layout that follows relatively closely the elastic distribution of stresses will be most able to efficiently limit cracking. The tensile cracks in the concrete extend in the direction of the principal compressive stress and open perpendicular to it. Because the tendon path is a line of principal compressive stress, the bursting reinforcement should be placed perpendicular to it.

Spalling stresses and stress concentrations in reentrant corners are primarily caused by the condition of compatibility. In these cases, the magnitude of the tensile stress is very large (theoretically infinite for a reentrant corner with an angle of 90 deg.), and cracking should, therefore, be observed first at these locations. However, examinations made during the experimental testing of specimens did not reveal an observable cracking of these areas before other areas cracked. Cracks in reentrant corners were only observed in the final stages of the loading. Some cracking, other than cracking along the axis of the tendon (caused by bursting stresses), was observed during the testing of eccentrically loaded specimens with a large eccentricity, thus following the prediction of the elastic stress analysis.

Because of the large freedom given to the designer in the choice of the geometry of a strut-and-tie model, it is necessary to define criteria such as minimum potential energy by which, in the absence of physical test results, various strut-and-tie model configurations can be compared and evaluated. At the same time, it should be recognized that in plastic design there is generally no unique solution to a given problem. Instead, the goal of the designer should be to obtain a safe, constructible design that performs satisfactorily under service loads and under ultimate loads.

The most important consideration in the development of a serviceable strut-and-tie model for an anchorage zone is to locate the centroid of the tensile reinforcement (tension tie of the strut-and-tie model) close to the elastic centroid of the tensile stresses. The specimens designed with strut-and-tie models in which the

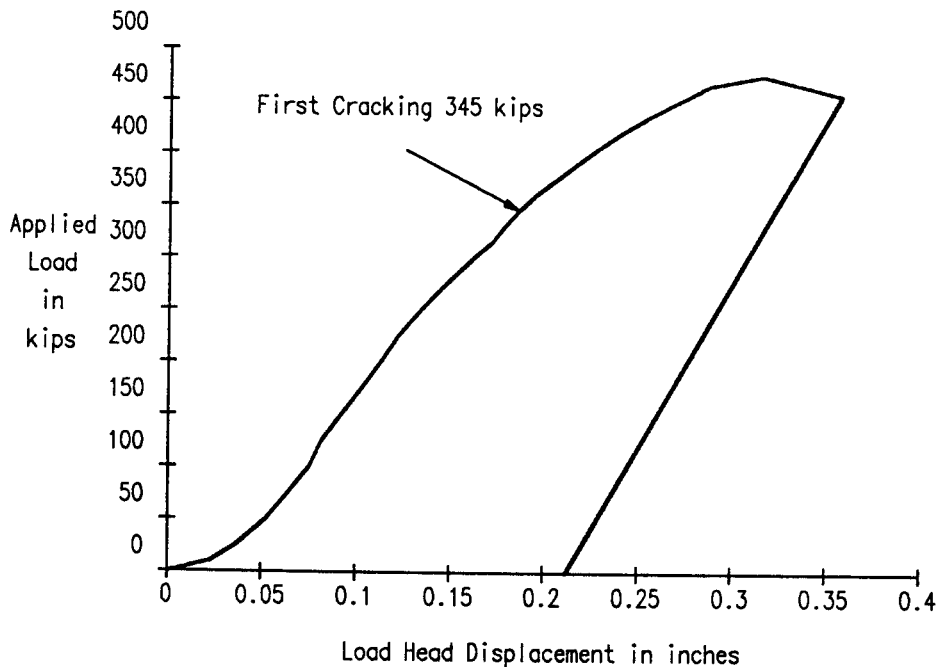


Figure 57. Load deflection curve measured at the loading head for specimen E1.

reinforcing patterns followed the elastic stress distribution performed better in the experimental tests than the specimens with reinforcement departing more strongly from it.

Comparison of Finite Element Analysis and Strut-and-Tie Models

In the extensive study of anchorage zones using finite element analysis conducted as part of this project, and reported by Burdet (48), a number of typical anchorage zone configurations were studied.

Comparison of Finite Element Analysis with Published Results

Because of their relative simplicity, many studies focus on the analysis of concentric configurations with straight tendons. In Figure 58, adapted from the paper by Lenschow and Sozen (54), the bursting stresses obtained from the present series of finite element analyses show a good agreement with the magnitude of the maximum bursting stress with the other solutions. The stress distribution is slightly different from the other solutions, particularly Magnel and Lenschow and Sozen, and is closest to the elastic solution obtained by Guyon using closed form solutions and Fourier series (6). For a wide range of bearing plate depths, a , to member depth, h , the bursting force, T_{burst} , can vary significantly. As shown in Figure 59, the finite element solution corresponds fairly closely to the theoretical solution of Guyon. Also shown in Figure 59 are two lines showing two linear approximations proposed by Guyon and described by Eq. 5

The factor K in Eq. 5 is proposed as 0.3 by Guyon, which leads to a solution that is conservative over the entire range of values for a/h . By taking $K = 0.25$, a better fit of the results is obtained, but the values are smaller than predicted by the elastic analysis for plate sizes smaller than approximately $0.15h$.

The forces obtained from the finite element analysis are slightly larger than the forces obtained by Guyon, except for very small plates. Because of numerical problems for the case of $a/h = 0.0$, it is assumed that Guyon's closed form elasticity solution is closer to the true elastic solution for $a/h = 0.0$. Guyon's approximate formula gives a good approximation of the bursting force.

Guyon (6) is one of the few authors to address the case of spalling stresses. Even though he reports some calculated values for the spalling forces, he does not indicate a precise value as a function of the plate size, as in the case of bursting stresses. His recommendations are mostly of a practical matter, such as a constant value of 4 percent of the applied load recommended as a design value.

Figure 60 shows the value of the spalling force obtained from the finite element analysis compared with the integrated values reported by Guyon and the constant value that he proposes for design purposes. Based on the results of the elastic finite element analysis, it appears that Guyon's solution is quite conservative.

Stone (55) places a large emphasis on spalling stresses. He mentions a decrease in the confining pressure of the local zone caused by spalling stresses as a possible cause for the initiation of the failure mechanism in the anchorage zone. It seems more likely that the very high level of bearing stresses, combined with the reduction in confinement caused by the spalling stresses, seems to be the cause of failure. In this case, the initiation of cracking will most likely be quickly followed by the failure of the anchorage zone.

$$T_{burst} = K \cdot P(1 - a/h) \quad (5)$$

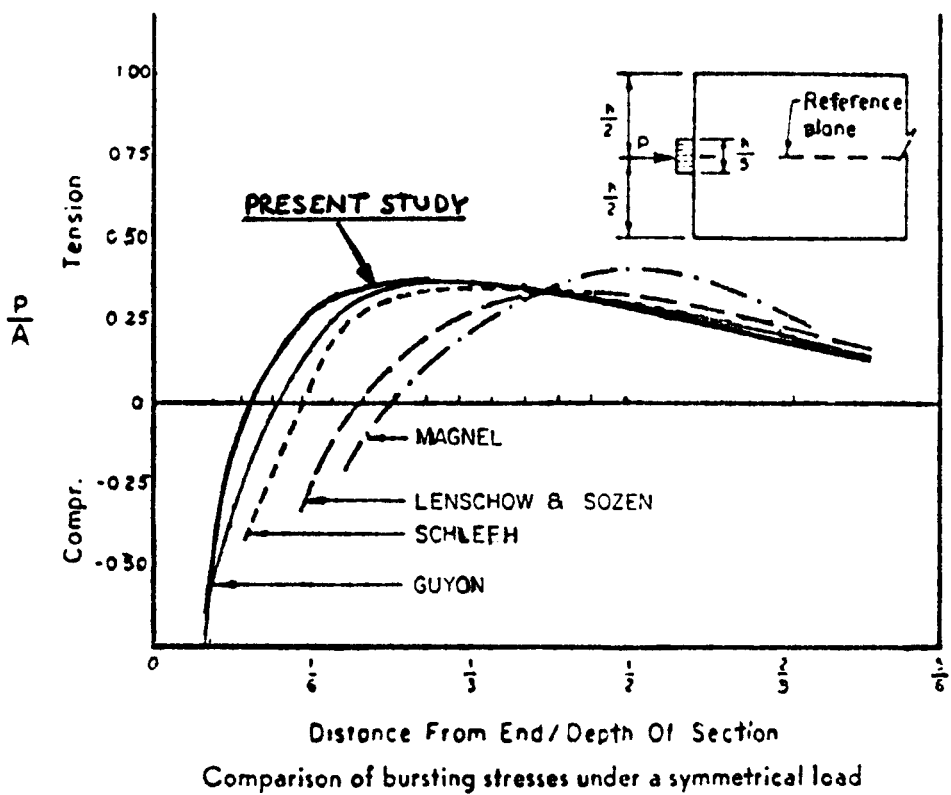


Figure 58. Comparison of present study with previous publications.

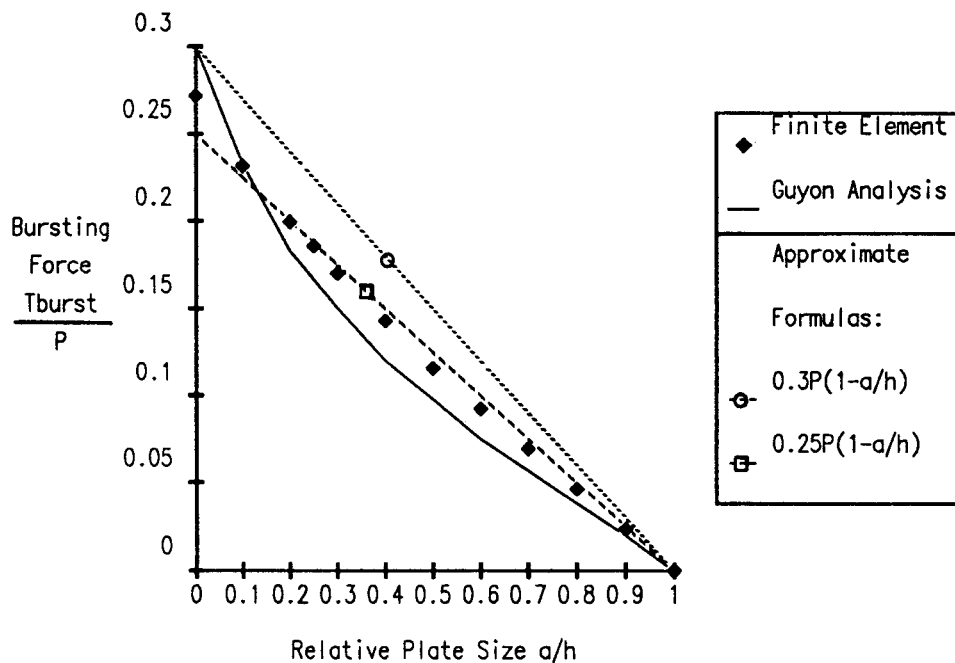


Figure 59. Comparison of finite element analysis with published results: bursting force.

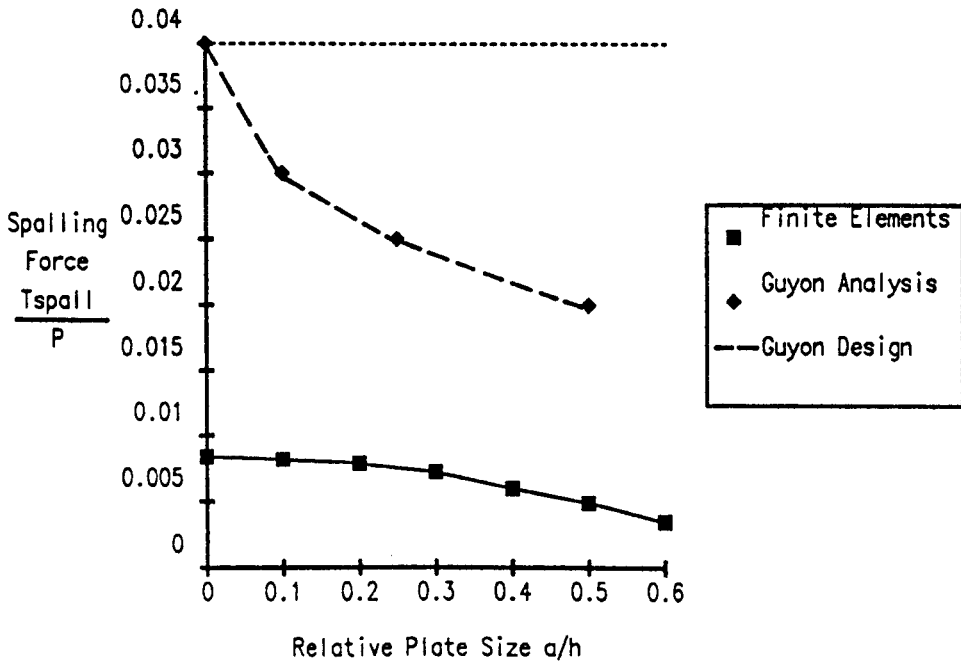


Figure 60. Comparison of finite element results with published results from Guyon: spalling force.

Construction of Strut-and-Tie Models

The finite element analytical results for the concentric application can be readily compared to the more convenient strut-and-tie model results. Because of unfamiliarity of many engineers in the United States with strut-and-tie model techniques, development of this specific example is given in very detailed fashion.

When the strut-and-tie model method has been described (2,57) it is often assumed that the geometry of the model is a given or that it will be "chosen" by an engineer trained in the application of the strut-and-tie model. While this is usually true, it is necessary to add some specificity to the definition of the model geometry. In the most frequent case, when no finite element analysis is available for the design of the anchorage zone, the engineer will "choose" a strut-and-tie model based only on the geometry of the anchorage zone and on some calculations of equilibrium.

The first step to model the general anchorage zone is to cut the structure at the end of the discontinuity zone, which is approximately 1.5 times the depth of the girder for rectangular cross sections, and draw the forces and reactions on the free body. Because the cut is made at a reasonably large distance from the anchor itself, a simplified analysis, such as simple beam theory, can be used to determine the reactions (Figure 61a).

The reactions at the extremity of the anchorage zone are then lumped into a series (at least two) of concentrated reactions. In most cases (except for tendons with a large curvature or inclination) it is recommended to separate the reactions that are "on one side" of the tendon from the reactions that are "on the other side." The tendon load on the anchor will also be represented by several components. However, it seems unnecessary to use more than two nodes to represent the local zone around the anchor, because this gives an unjustified sense of accuracy to the modeling (Figure 61b). In this example, the nodes modeling

the anchor plate are located at the interface between the anchorage device and the concrete. This assumption has little influence on the results if the relative plate size is small.

At this stage, it is likely that a limited number of main reactions (two to four) will approximately sum up to the totality of the applied tendon load (at least 80 percent of it). Based on the knowledge of the location and magnitude of the main reactions, the engineer draws force paths from the anchor to the main reactions (Figure 61c). Schlaich et al. recommend that the initial forces considered should exactly sum up to the tendon forces. Then, in a second step, the engineer should introduce the additional forces that result from eccentricities or other sources. Although this requirement is helpful, it does not seem to be absolutely necessary to develop reasonable strut-and-tie models for either concentric or eccentric cases.

The compression struts follow the force paths. For best control of cracking, the angle between the axis of the tendon and the struts should be limited to between 20 and 35 deg. If more than two struts are used, or if a multiple level or a thrust-line model is used, larger angles may be allowed. The struts are to align exactly with the reactions at the extremity of the anchorage zone (Figure 61d).

The tension ties balance the deviation of the forces in the struts. The ties can be oriented in the desired direction for the reinforcement. If necessary, the geometry of the struts may have to be adjusted for the possible locations of the ties. The forces in the ties can be closely estimated because the forces in the struts and the deviation angles are known. Because the strut-and-tie model obtained so far includes only the main forces, every node may not be in equilibrium. It is therefore possible that two or more values are obtained for a given tie. At this point, it is conservative to choose the largest value (Figure 61e).

Notice that the forces obtained up to this point resist the majority of the tendon force (80 percent or more), so that none

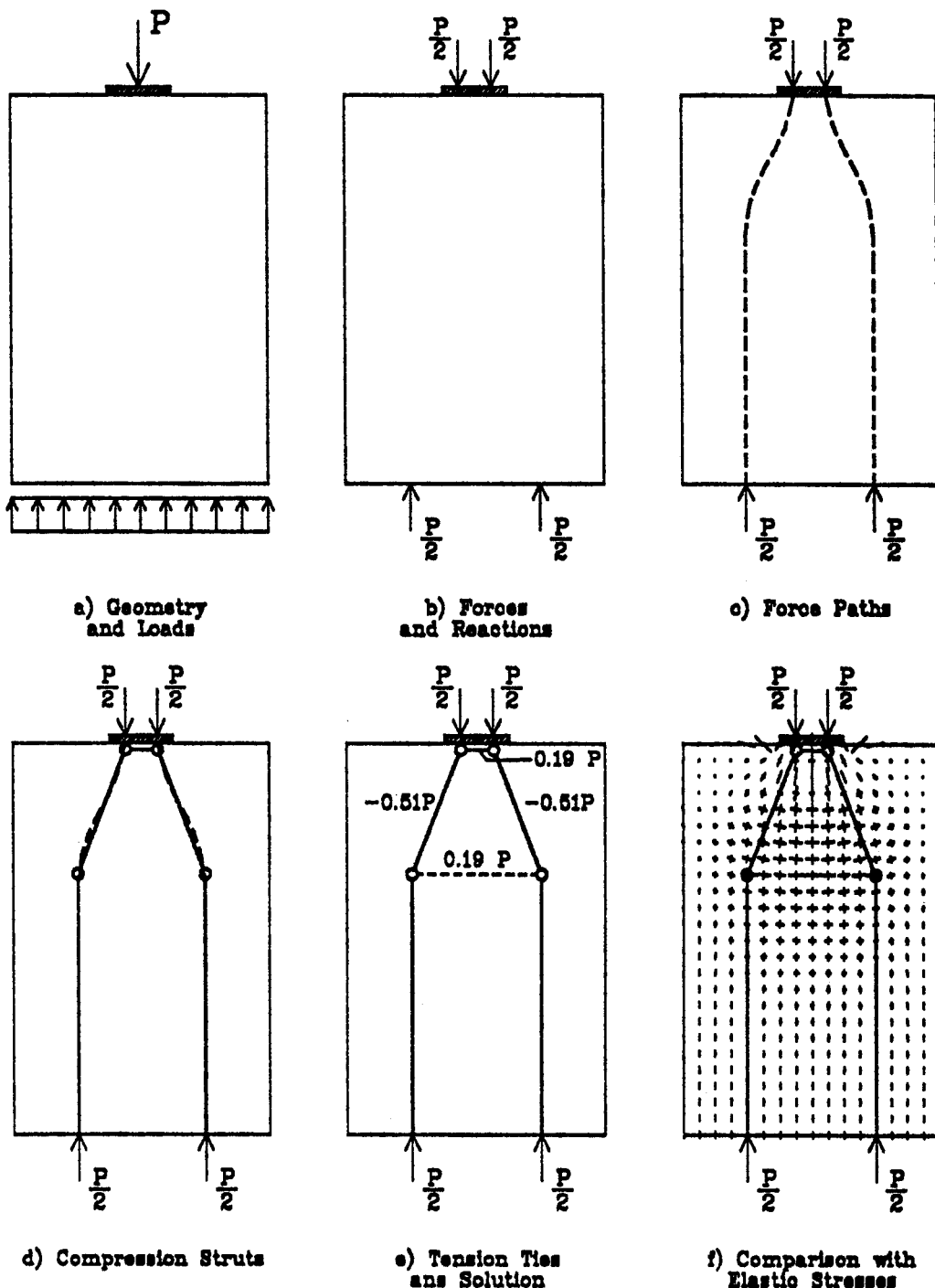


Figure 61. Steps for the development of a strut-and-tie model.

of the remaining strut or tie forces is likely to dramatically change the load carrying mechanism of the model. However, these forces are necessary to satisfy the overall equilibrium conditions of the strut-and-tie model. Note, also, that in the case of a concentric anchorage, there is no tension tie close to the anchorage at the surface, which would correspond to the effect of spalling forces. This is because spalling forces are compatibility induced and are not required for the overall equilibrium of concentric configurations.

At this stage, force paths are drawn for the remaining reaction forces and the corresponding struts and ties are incorporated in the strut-and-tie model. In the case of the concentric anchor example, all forces were considered as main forces, so that no additional forces are required to satisfy equilibrium.

If the results of a finite element analysis are available, the principal stress vectors can be used to help draw the force paths of Figure 61(c). The location of the tension ties can be adjusted to coincide with the centroid of the tensile stresses.

If no additional information is available, such as the results of a finite element analysis, it is sometimes difficult to assess the adequacy of a strut-and-tie model. The designer should evaluate the sensitivity of the strut-and-tie model to changes in the geometry. For example, larger angles between the tendon axis and the compression struts can be used. This gives larger tension forces in the ties and a larger compression force in the struts. There seems to be no reason, however, to use angles larger than 45 deg., because they will lead to overconservative forces. The value of 45 deg. is often quoted in relationship to the diffusion of stresses in the concrete. If the stresses are diffusing at angles between 0 and 45 deg., the average diffusion angle is 22.5 deg., which is the angle of the compression strut. Taking the inclination of the strut as 45 deg. corresponds to taking the angle of diffusion of the stresses as 90 deg.

If the stress trajectories (or principal stress vectors) are available for the anchorage zone, the adequacy of a strut-and-tie model can be assessed by comparing the layout of the struts and ties with the elastic flow of stresses (Figure 61f). In order for the structure to be well behaved at service state, it is desirable that the struts and ties follow the elastic flow paths closely (with a deviation of at most 15 deg. from the elastic principal stresses, according to Schlaich et al. (2)). Although it is difficult to apply quantitatively, this requirement is especially important for the main members that carry a significant portion of the load. For the other members that carry only a small portion of the load, a larger deviation is permissible. This implicitly takes into account the fact that in areas of low stresses, the concrete will remain essentially uncracked and will therefore be able to transfer elastically a portion of these stresses.

While there are no unique strut-and-tie models for a given application, some are clearly easier to formulate or more efficient. Figure 62 shows four different types of models that can be formulated for the concentric anchor application. The basic model originally introduced by Mörsch in the 1920's is shown in Figure 62(a). The load is assumed to be applied as two loads of magnitude $P/2$ at the quarter points of the anchorage plate. This tension force Z results from the spreading of the compression struts toward the quarter points of the concrete section and is assumed to act at a depth of $d/2$.

The tension force can be simply calculated by equilibrium as:

$$Z = 0.25 \cdot P \cdot (1 - a/d) \quad (6a)$$

The ultimate load capacity for a given strength of the tension tie, Z , is

$$P_u = 4 \cdot Z/(1 - a/d) \quad (6b)$$

Equation 6a is identical to the simplified formula proposed by Guyon (see Figure 59). This formula is used, for example, in the CEB code (57) and in recent PTI recommendations (17) (both use the more conservative coefficient of 0.3 instead of 0.25 in the formula). The simple and powerful solution of this basic configuration illustrates the powerful tool offered by the strut-and-tie model to solve anchorage zone problems.

A more refined model for the same configuration is shown in Figure 62(b). In this multiple level strut-and-tie model, the applied force is transmitted through a series of compression struts directly to the individual reinforcing bars.

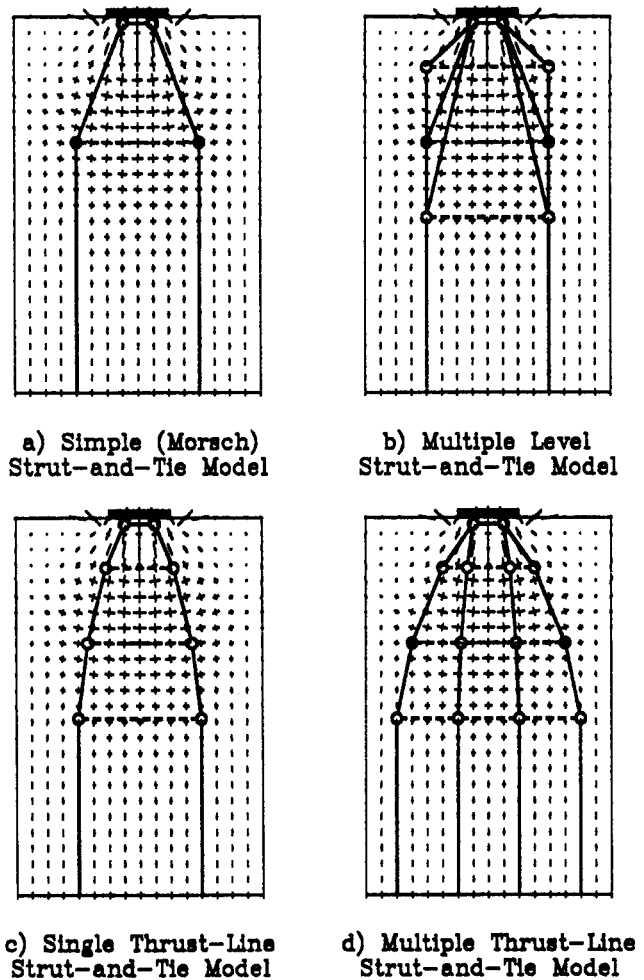


Figure 62. Comparison of the various strut-and-tie models with principal stress vectors.

Figure 62(c) shows still another strut-and-tie model for the same configuration. In this thrust line model, the compression force coming from the anchor is deflected each time it crosses a reinforcing bar, until it aligns exactly with the reactions at the end of the zone of introduction of forces.

The multiple thrust-line model of Figure 62(d) is an extension of the single thrust line model. It has the advantage of more closely following the flow of stresses in the concrete. Using these models and the equations of equilibrium one finds the same answer for the ultimate load P_u . The assumption of complete yielding of the reinforcing steel at ultimate makes the problem determinate.

Figure 62 shows the four strut-and-tie models superimposed on the principal stress vectors obtained from a finite element analysis. The simplest strut-and-tie model of Figure 62(a) is very easy to establish, and may be used to crudely estimate the stresses in the concrete. However, it does not follow very closely the stress distribution. The multiple level strut-and-tie model of Figure 62(b) is clearly inadequate in describing the state of stresses in the concrete and, therefore, should be avoided. The problems related to the computation of concrete stresses in strut-and-tie models involving overlapping or crossing struts are difficult to

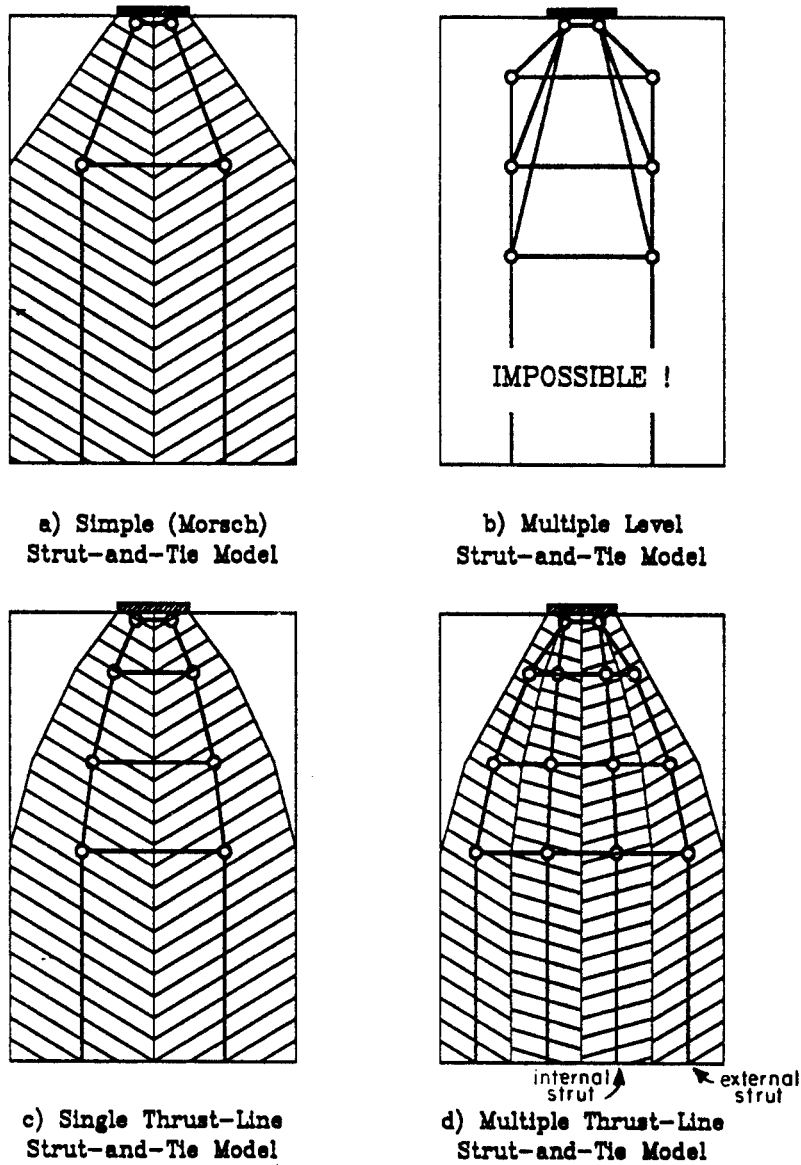


Figure 63. Geometric definition of the concrete struts.

solve. The thrust line strut-and-tie models of Figures 62(c) and 62(d) approximate more closely the elastic flow of stresses.

Figure 63 shows as hatched zones the various concrete struts as they were used to compute the concrete stresses. Figure 64 shows the stresses in the concrete struts as approximated by the thrust-line strut-and-tie models compared with the stresses along the axis of the tendon (where the compressive stresses are maximum) obtained by an elastic analysis. Because of the inclination of the concrete struts, the stresses in the concrete are overestimated in the vicinity of the plate. The stresses are fairly well approximated by the internal strut and the single strut. The simple thrust-line strut-and-tie model of Figure 63(c) actually gives better results than the more elaborate multiple thrust-line strut-and-tie model of Figure 63(d). All four struts carry the same portion of the tendon force ($P/4$), but in order for the external struts that have a larger inclination to carry that force, a larger

resultant is needed ($P/4 \cos(\alpha)$). Therefore, contrary to common sense and to the results of the theory of elasticity, the stresses in the external struts are larger than the stresses in the internal struts. This inaccuracy is compounded by the fact that only two nodes were used to represent the local zone.

According to Schlaich et al. (2), the best strut-and-tie model is the configuration that minimizes the strain energy in the ties. Because the struts are assumed to be extremely rigid, the strain energy of the system will be concentrated in the ties. Minimizing the strain energy in the ties is, therefore, equivalent to applying the principle of minimum strain energy to the system. In this example, the thrust-line strut-and-tie model of Figure 62(c) has the lowest strain energy (see Table 10), and is therefore the best of the three models. The multiple level strut-and-tie model is clearly the worst solution because of the large plastic strains in the bars that are caused by incremental yielding of the individual

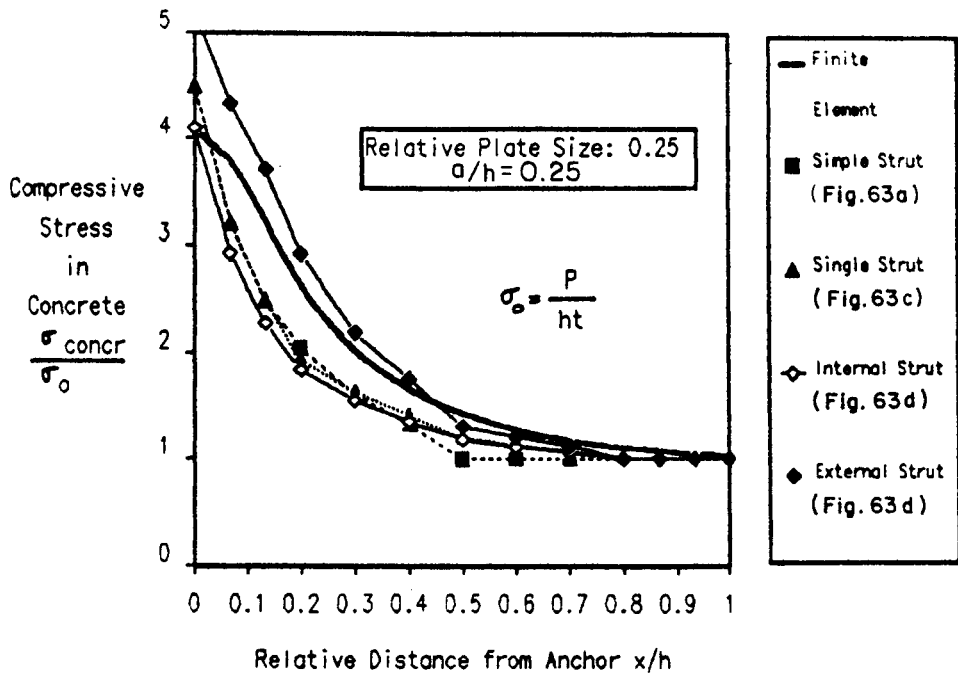


Figure 64. Stresses in the concrete struts for the various strut-and-tie models compared with the stresses from the finite element analysis.

Table 10. Strain energy at failure for the various strut-and-tie models

Strut-and-Tie Model (STM)	Strain Energy at Failure
Simple STM	$0.75 h \cdot A_s \cdot f_y \cdot \epsilon_y$
Multiple Level STM	$2.0 h \cdot A_s \cdot f_y \cdot \epsilon_y$
Thrust-Line STM	$0.6 h \cdot A_s \cdot f_y \cdot \epsilon_y$
Multiple Thrust-Line STM	$0.7 h \cdot A_s \cdot f_y \cdot \epsilon_y$

bars before the ultimate load is reached. In contrast, the other three models have all their bars simultaneously reaching the yield strength, thus minimizing the strain energy in the bars at ultimate. The small differences between these three models are due to the slightly different lengths of the tension ties and to the fact that some parts of the reinforcement are not at yield in the multiple thrust-line strut-and-tie model.

Analytical Results for Concentric Tendons

Figure 59 shows that the finite element analysis results for tensile bursting force agree well with Guyon's equation as does

the strut-and-tie model results. Figure 64 shows good correspondence between FEA and STM for compressive stresses. Considering the accuracy required for a satisfactory design, either method gives acceptable results.

Analytical Results for Eccentric Tendons

Anchorage zones with eccentric anchorages are very common in practice. If the eccentricity, e , of the post-tensioning force is small (within the kern), the state of stress in the anchorage zone is generally similar to that previously observed for concentric anchorages, as shown in Figure 65(a).

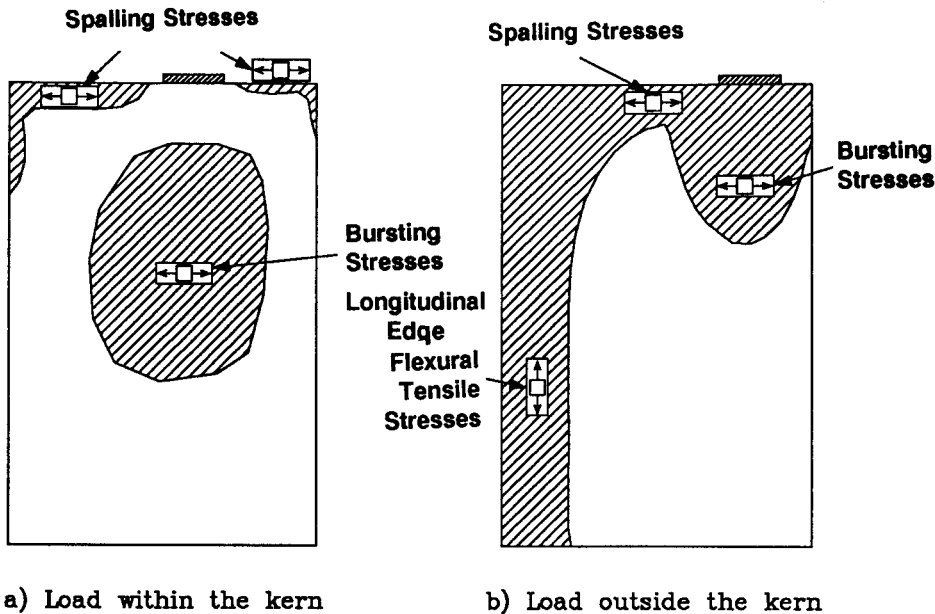


Figure 65. Areas of bursting, spalling, and flexural tensile stresses for eccentrically loaded anchorage zones.

If, however, the load is applied outside of the kern, the state of stress in the anchorage zone is more complex. An additional area of tension parallel to the tendon path appears on the side face farthest from the anchorage device because of the bending moment. The corresponding tensile stresses are called flexural tensile stresses and the resulting force is referred to as the *longitudinal edge tension force* (Figure 65b). The spalling stresses and force increase considerably as the region subjected to spalling stresses becomes connected to the region subjected to flexural tensile stresses.

Finite element analysis for eccentric configurations does not require special techniques. Meshes were virtually identical in general arrangement to those used for concentric tendons, with allowance made for the shift in point of load application. Resulting vector plots of maximum principal stress (tension) and minimum principal stress (compression) are shown in Figure 66. It is obvious from Figure 66(b) that there is a direct connection between the longitudinal edge tensile stresses induced by the overall bending of the section and the top surface spalling stresses. In this case the spalling stresses not only are induced by compatibility, but are necessary for equilibrium. This had also been recognized by Guyon who, in later editions of his textbook (20), expanded his recommendations for spalling force by adding a term that was dependent on the eccentricity of the load to the original constant 4 percent term. This enhanced expression of Guyon's is plotted in Figure 67, along with the results of the finite element analyses and the tensile bending force obtained from simple beam theory. With the additional term, the improved Guyon formula is generally conservative, but it clearly overestimates the spalling forces for loads within the kern.

While the simple concentric strut-and-tie model of Mörsch was proposed in the first quarter of this century, strut-and-tie models involving more complex configurations have only been proposed in relatively recent times (2,46,59).

Figure 68 shows the steps of the procedure to develop the strut-and-tie model for an eccentric load case. The forces and reactions acting on the anchorage zone are first determined using simple beam theory (Figure 68a), then lumped into discrete forces. The forces acting on one side of the post-tensioning cable are lumped separately from the forces acting on the other side; tension and compression forces are lumped separately (Figure 68b).

Force paths for at least 80 percent of the total force are drawn. Based on the force paths, corresponding struts and ties are drawn, and the forces in the members are calculated (Figures 68c and 68d). Finally, the struts and ties corresponding to the remaining forces are introduced in the strut-and-tie model (Figure 68e). It is often necessary to slightly modify the geometry in order for the model to be stable, or at least kinematic; that is, stable for the given load case. These adjustments have usually only a small influence on the main forces.

As in the case of concentric tendons, simple equilibrium considerations would allow the determination of the ultimate load knowing the magnitude and the location of the tie force T_1 , but the determination of the other tie forces, most notably T_3 , would not be so evident. More elaborate strut-and-tie models, including thrust-lines, can also be used with eccentric configurations. However, it is best to focus the use of thrust-lines on the limited number of struts that carry the majority of the load.

Parametric studies were performed by Burdet (48) using finite element analysis and a strut-and-tie model with the geometry shown in Figure 69. The depth, d_1 , at which the bursting force acts was defined as $[(h/2) - e]$, corresponding to a diffusion angle of about 26 deg.

Figure 70 shows the geometry as it evolves with increased eccentricity for a constant $a/h = 0.2$. Figure 71 shows the forces in the struts and the ties of Figure 69 as a function of the eccentricity.

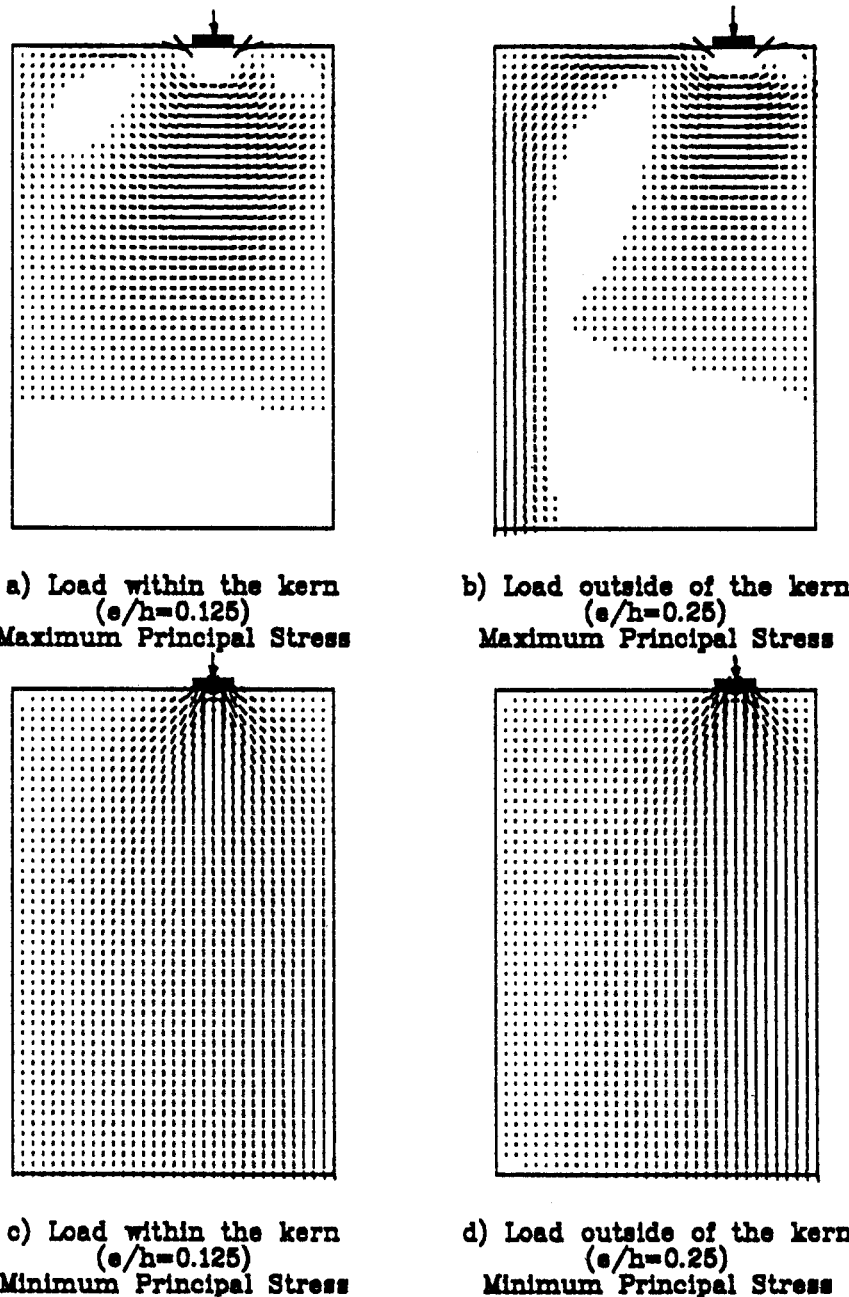


Figure 66. Vector plots of the principal stresses for eccentric cases with load acting within and outside the kern.

Figure 72 shows the tension forces in the ties T_1 and T_2 as a function of the eccentricity, compared with the integrated bursting forces obtained from the finite element analysis. The correlation between the bursting force and T_1 is good, taking into account the relative simplicity of the model used. The magnitude of T_2 , about one-half of the bursting force T_1 for most eccentricities, indicates the necessity of extending the reinforcement laterally well outside of the region defined by the Guyon "symmetrical prism." Figure 73 shows the flexural tensile force (T_4) and the spalling force (T_3) from the strut-and-tie model compared to the results of the finite element analyses and Guyon's enhanced

formula for spalling forces. The flexural tensile force obtained by the finite element method is not shown in the figure because it is identical to the value obtained by the strut-and-tie model, and is defined by simple combined axial and flexural action theory. Here again, the correlation is good.

Analytical Results for Inclined Tendons

In most cases, post-tensioning tendons have some inclination in the anchorage zone. In typical girder applications, this inclination is less than 20 deg.

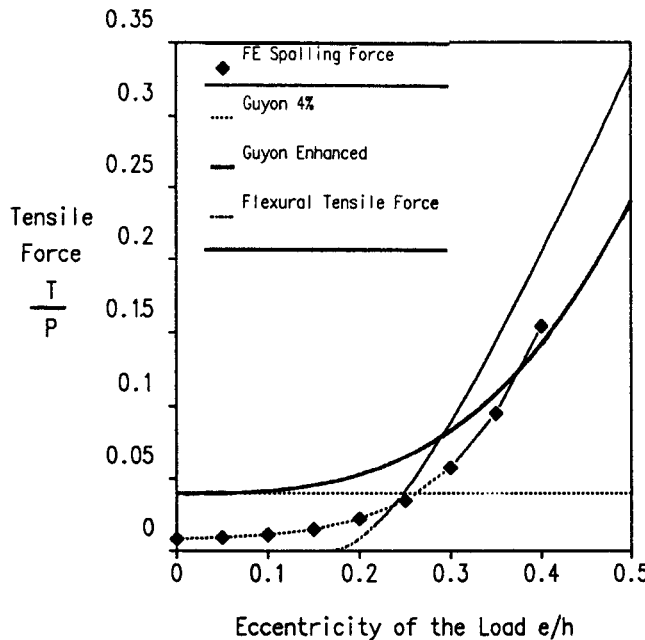


Figure 67. Spalling force according to Guyon compared with finite elements results and bending force.

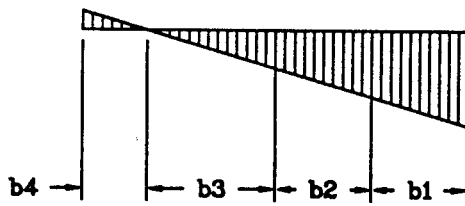
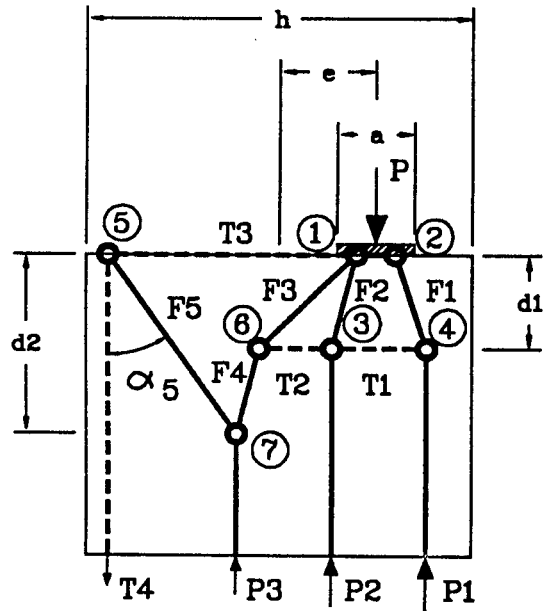


Figure 69. Geometric definition of the strut-and-tie model used for the parametric study of eccentric configurations.

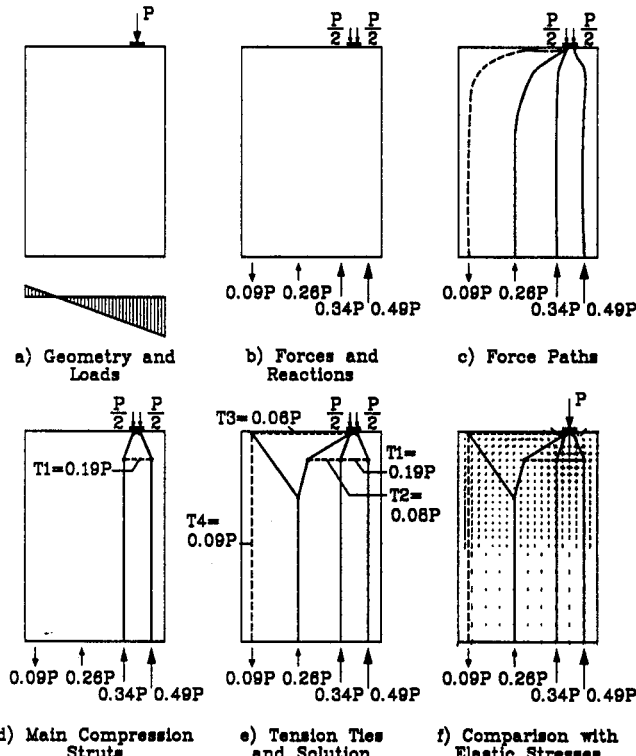


Figure 68. Steps for the development of a strut-and-tie model for eccentric configurations.

A series of finite element analyses for inclined tendons was performed. To limit the number of variables, the size of the anchor was kept constant at $a = 0.125h$. The angles of inclination α investigated were 10 and 20 deg. Angles larger than 20 deg. would require that the tendon be curved in the anchorage zone.

The principal stress vector plots of Figures 74 and 75 show that the stress distribution due to tendons with a small inclination is similar to the stress distribution observed in concentric and eccentric configurations, with a zone of bursting stresses along the axis of the tendon and zones of spalling stresses on either side of the anchorage. However, the inclination of the tendon changes the orientation of the principal stresses, which are more or less perpendicular to the axis of the tendon, depending on the angle of inclination. Figure 76 shows the variation of the transverse force as a function of the inclination of the tendon for various eccentricities. This force was obtained by integrating the stresses perpendicular to a line going from the middle of the anchor to a point located in a section at a distance $h/\cos \alpha$ from the anchor. In general the transverse force, which is a combination of bursting force and shearing force, increases with increased inclination of the tendon. The figure also shows the values given by a conservative proposed simplified formula, Eq. 7, in which the effect of the inclination of the tendon on the transverse (bursting) force is estimated as one-half the transverse component of the post-tensioning force.

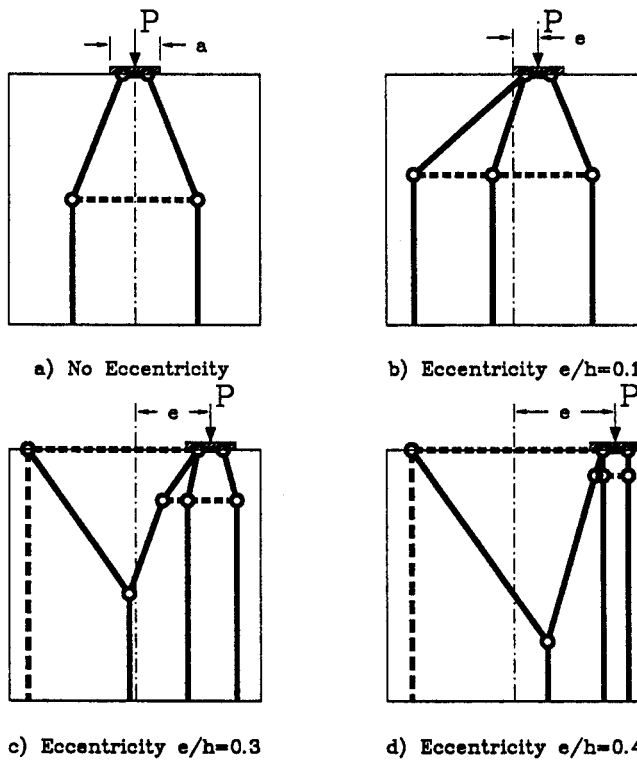


Figure 70. Geometry of the strut-and-tie model used in the parametric study for various eccentricities for $a/h = 0.2$.

$$T_{burst} = 0.25 \cdot P \cdot (1 - a/h) + 0.5 \cdot P \cdot \sin(\alpha) \quad (7)$$

Burdet (48) studied the effect of the assumed distribution of the transverse force between the compression struts in strut-and-tie models of the inclined tendon anchorage zones.

Figure 77 shows three series of strut-and-tie models for two values of eccentricity and inclination. Each series is based on a different assumption for the distribution of the transverse force. The strut-and-tie models are superimposed on the stress trajectories from the theory of elasticity. In Figures 77(a) and 77(b), because the transverse forces are not proportional to the axial forces, there are different inclinations of the struts at the end of the general zone. Because all the strut-and-tie models shown fulfill the conditions of equilibrium, they can all be considered valid plastic solutions.

Figure 78 shows the transverse force predicted on the basis of a parabolic distribution of the transverse reaction (Figure 77a) as a function of the inclination of the tendon for various eccentricities of the anchor. The correlation with the results of the finite element analyses is good. The tendencies observed in the finite element solution are well represented by the strut-and-tie model. At the largest eccentricity, the values obtained are less than the elastic values from the finite element analysis. Similar studies (48) for the transverse force distributions assumed with Figures 77(b) and 77(c) showed substantially poorer agreement. Other studies (48) showed that STM, based on bursting reinforcement perpendicular to the section axis rather than to the inclined tendon, also gave good results.

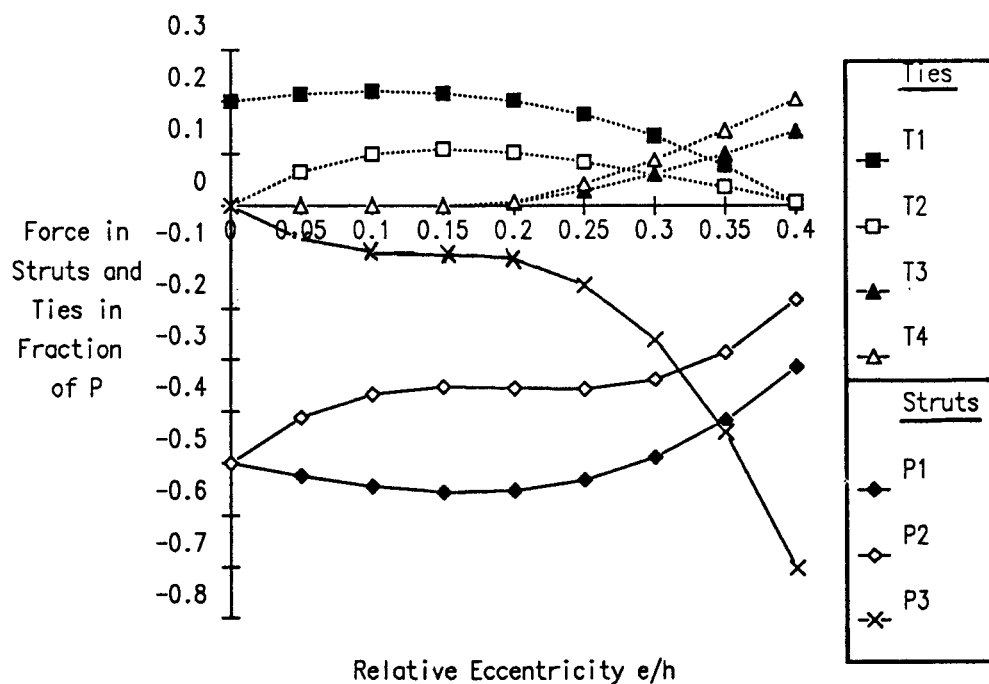


Figure 71. Forces in the struts and ties of Figure 69 as a function of the eccentricity of the load for $a/h = 0.2$.

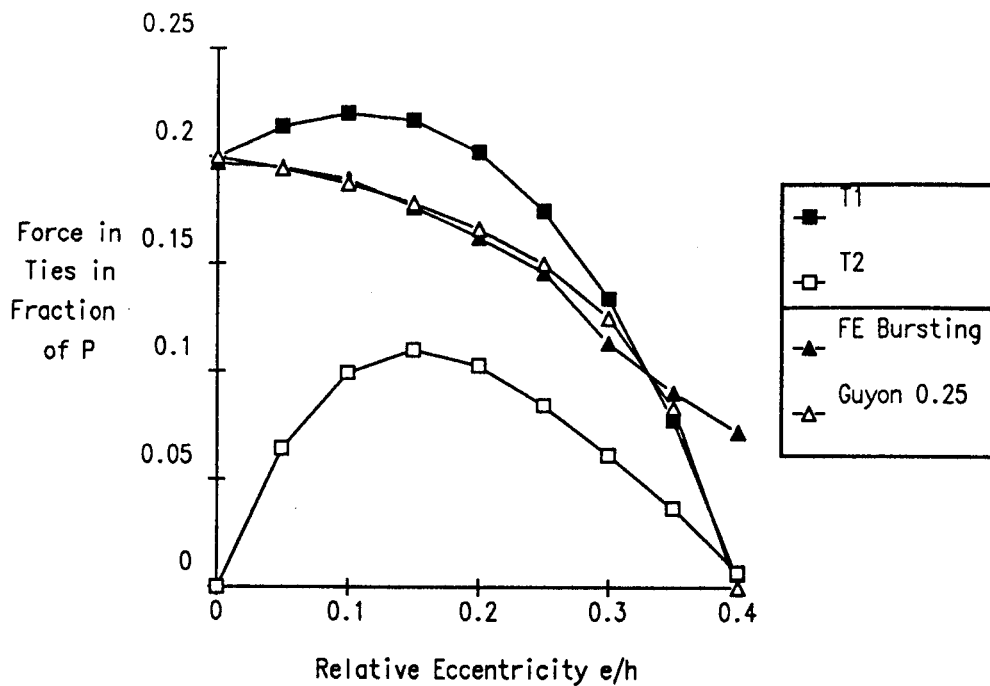


Figure 72. Tie forces in the bursting region compared with finite element results and Guyon's linearized formula.

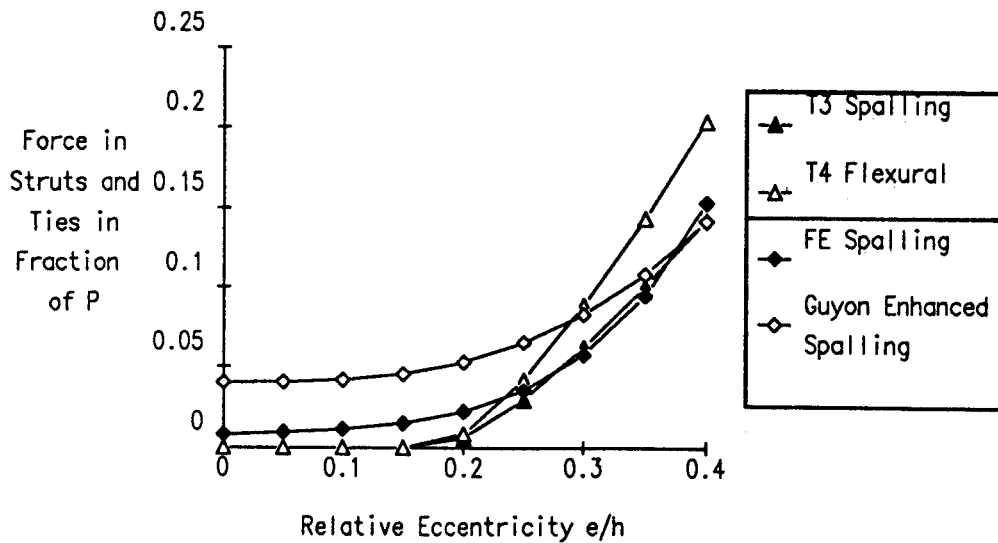


Figure 73. Tie forces in the spalling and flexural region compared with finite element results and Guyon's enhanced formula.

Analytical Results for Curved Tendons

In general, anchorage zones that involve curved tendons also involve an inclination of the tendon at the anchorage. Stone and Breen (9,10) describe applications of post-tensioning in segmental box-girder bridges with inclinations of the cables at the anchorage up to 45 deg. Applications with such an extreme inclination are rather rare, but cases with inclinations of up to 30 deg. are more common in practice.

The presence of the deviation forces due to the curvature of the cable complicates the state of stresses by introducing discontinuities in the stress field near the tendon. Before cracking, the part of the structure located on the inside of the tendon is subjected to compressive stresses acting in the radial direction that are induced by the curvature of the tendon. These stresses decrease the tensile transverse stresses caused by the lateral spreading of the concentrated tendon force and by the inclination of the tendon. On the other hand, assuming that no cracking has

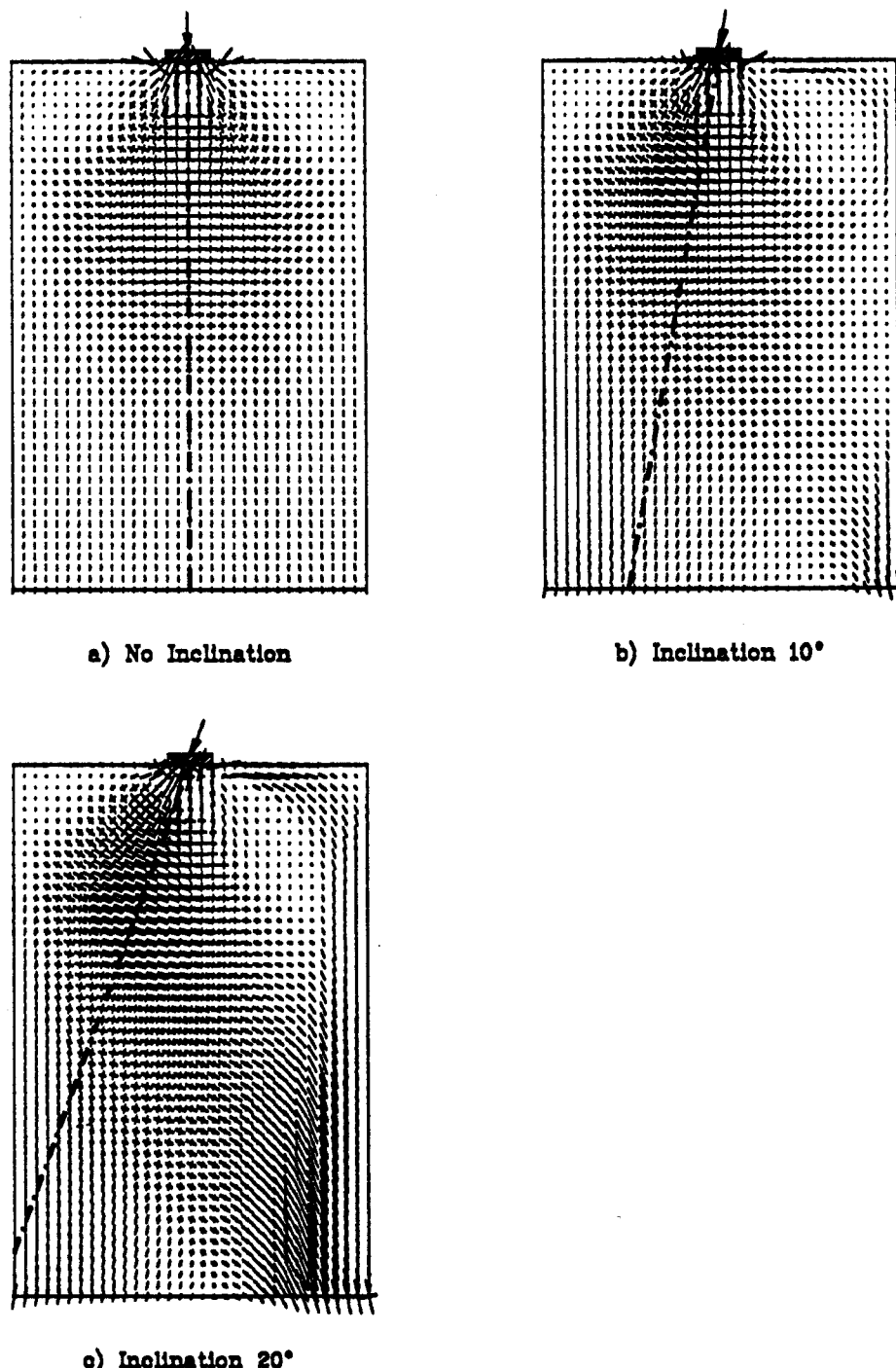


Figure 74. Vector plots of the maximum principal stress for $e/h = 0.0$ and inclinations of 0, 10, and 20 deg.

occurred, the part of the structure located on the outside of the tendon sees an increase in the tensile transverse stresses due to the radial tensile force caused by the curvature of the tendon.

In an elastic body, like the ones studied using the elastic finite element method, the deviation force is transmitted, in part as a compression force to the inside of the tendon and in part as a tension force to the outside of the tendon, in proportion to the

relative stiffness of both sides. In a real concrete structure, especially in thin sections like girder webs, a crack is likely to form along the axis of the tendon because the largest transverse tensile stresses are observed perpendicular to the tendon.

Once a crack forms along the tendon axis, the distribution of the deviation force from the tendon depends exclusively on the reinforcement that crosses the tendon axis. Thus, in addition to

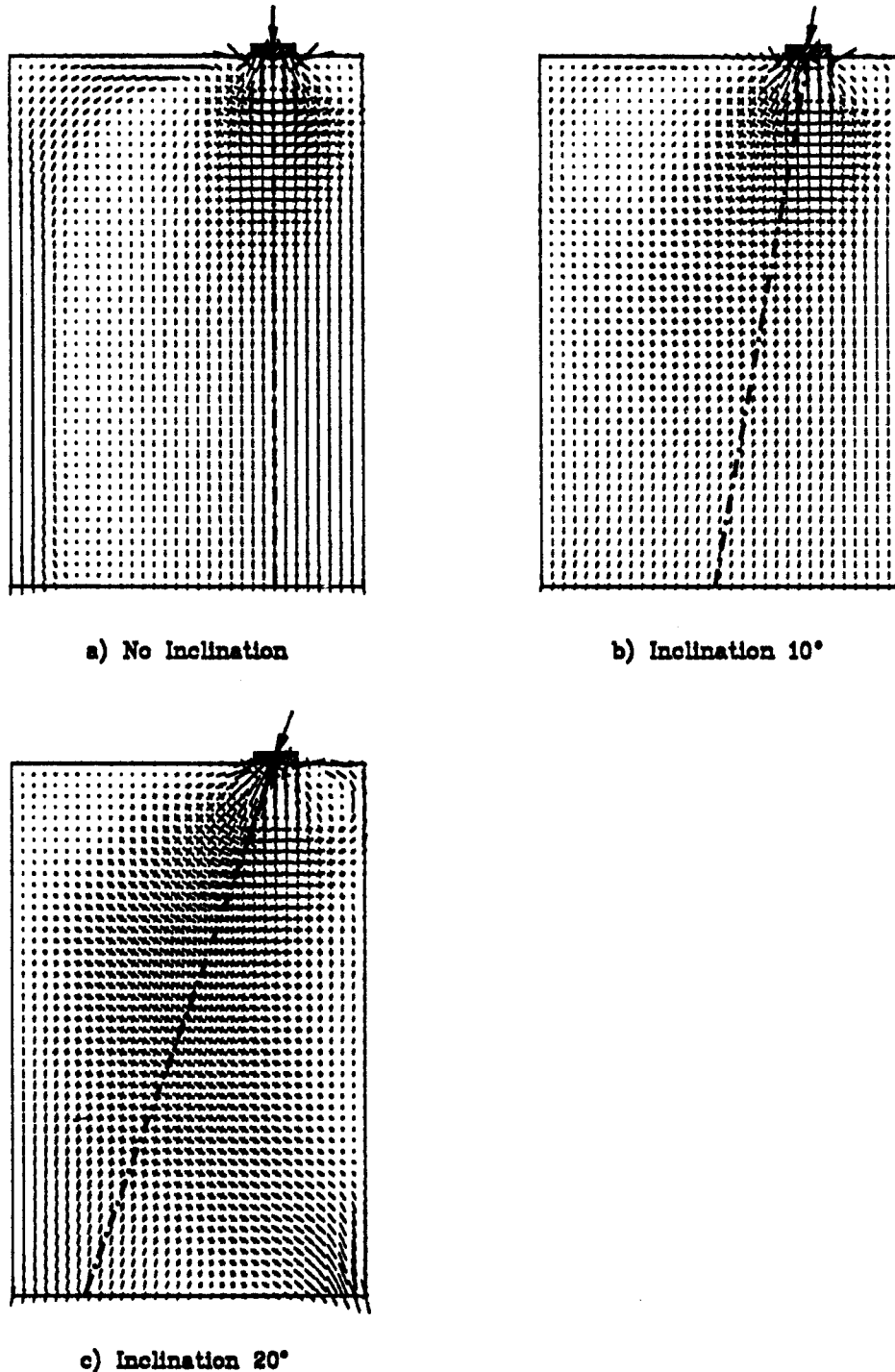


Figure 75. Vector plots of the maximum principal stress for $e/h = 0.25$ and inclinations of 0, 10, and 20 deg.

resisting the lateral spreading of forces, the transverse reinforcement has to tie part of the deviation force of the tendon back across the crack. In practice, it is possible to use two different sets of reinforcing bars to fulfill the two functions, using one set of bars to provide the tie-back reinforcement and another set of bars to provide the spreading reinforcement, or to simply design the transverse reinforcement to resist both components.

The influence of the curvature of the cable was investigated by finite element analysis assuming an uncracked section. Various combinations of inclination, curvature, and eccentricities were investigated. Figures 79 and 80 show typical results in the form of stress vectors. As can be seen, the maximum transverse stress increases with increased inclination and curvature of the tendon, and its location tends to move slightly closer to the anchorage

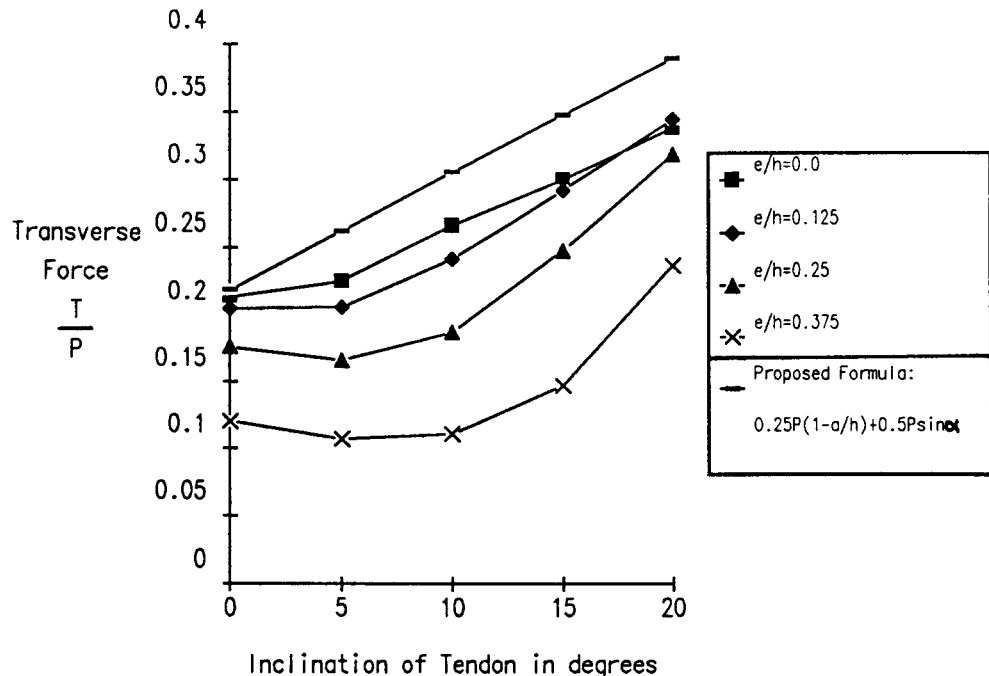


Figure 76. Transverse force as a function of the inclination of the tendon for various eccentricities of the anchor and proposed simplified formula.

device. The length over which tensile stresses are acting tends to remain the same with increased initial inclination of the tendon. Note that the vectors representing tension stresses on the outside of the tendon are much larger.

In anchorage zones with curved tendons, deviation forces caused by the curvature of the tendon are present in addition to the tendon load applied at the anchorage. Figure 81 shows free bodies of an anchorage zone with a curved tendon. Under the assumption of no tensile concrete contribution across the tendon axis (as it is likely a crack will form at that location), and if no separate tie-back reinforcement is provided to anchor all or part of the deviation force, the tendon deviation forces will be distributed only to the part of the anchorage zone located inside of the tendon (Figure 81a). The struts located inside of the tendon are curved because of the deviation forces, while the struts located outside of the tendon are straight between the reinforcing bars (Figure 81c). The transverse reinforcement obtained by solving the strut-and-tie model based on this hypothesis will resist the combination of both the lateral spreading of the concentrated anchorage load and the deviation forces.

If dedicated reinforcement is provided to anchor back part or all of the deviation forces induced by the curvature of the tendon force, as shown schematically in Figure 81(b), the deviation forces will be distributed to the struts located both inside and outside of the tendon, in proportion to the amount of force that is anchored back. Because of these deviation forces, the compression struts are curved between the transverse reinforcing bars (Figure 81d). The transverse reinforcement obtained from the strut-and-tie model based on this hypothesis will only resist the lateral spreading of forces; the provision of additional tie-back reinforcement is required to resist the deviation forces.

For a meaningful comparison between the various possibilities, it is necessary to add both lateral spreading and tie-back of the

deviation forces when comparing the forces obtained by the strut-and-tie model.

The influence of the tie-back reinforcement was investigated on the basis of strut-and-tie models. The variable used to quantify the amount of tie-back reinforcement provided is defined as the ratio F of the available tie-back force to the deviation force produced by the curvature of the post-tensioning tendon. If no tie-back reinforcement is provided, the tie-back ratio $F = 0$. For the parametric studies, the value of the tie-back ratio F was defined geometrically. The tie-back ratio is given by the average part of the section that is located outside of the tendon relative to the overall depth of the section, with a limit of one half of the deviation force induced by the tendon.

The presence of deviation forces and the hypotheses on the distribution of the deviation forces have a significant influence on the geometry of the strut-and-tie model. Only thrust-line strut-and-tie models were considered because of their flexibility in handling complex loading conditions. Starting at the end of the anchorage zone, two resultants are determined for the forces to the left and to the right of the tendon. Then, working toward the anchor, the deviation forces and the effect of transverse reinforcement are introduced in the compression struts at given locations in the general zone, according to the tie-back ratio. A satisfactory strut-and-tie model is obtained when the thrust-lines converge to the quarter points of the plate. The process is iterative, but can be stopped as soon as the thrust-lines actually cross each other before reaching the plate. A conservative (if not optimal) design is then obtained. For a precise analysis of the ultimate load capacity of a given configuration, several iterations are required.

Figure 82 shows two examples of strut-and-tie models for curved tendons with an initial eccentricity of $0.25 h$ and an initial inclination of the tendon of 20 deg. The strut-and-tie model in

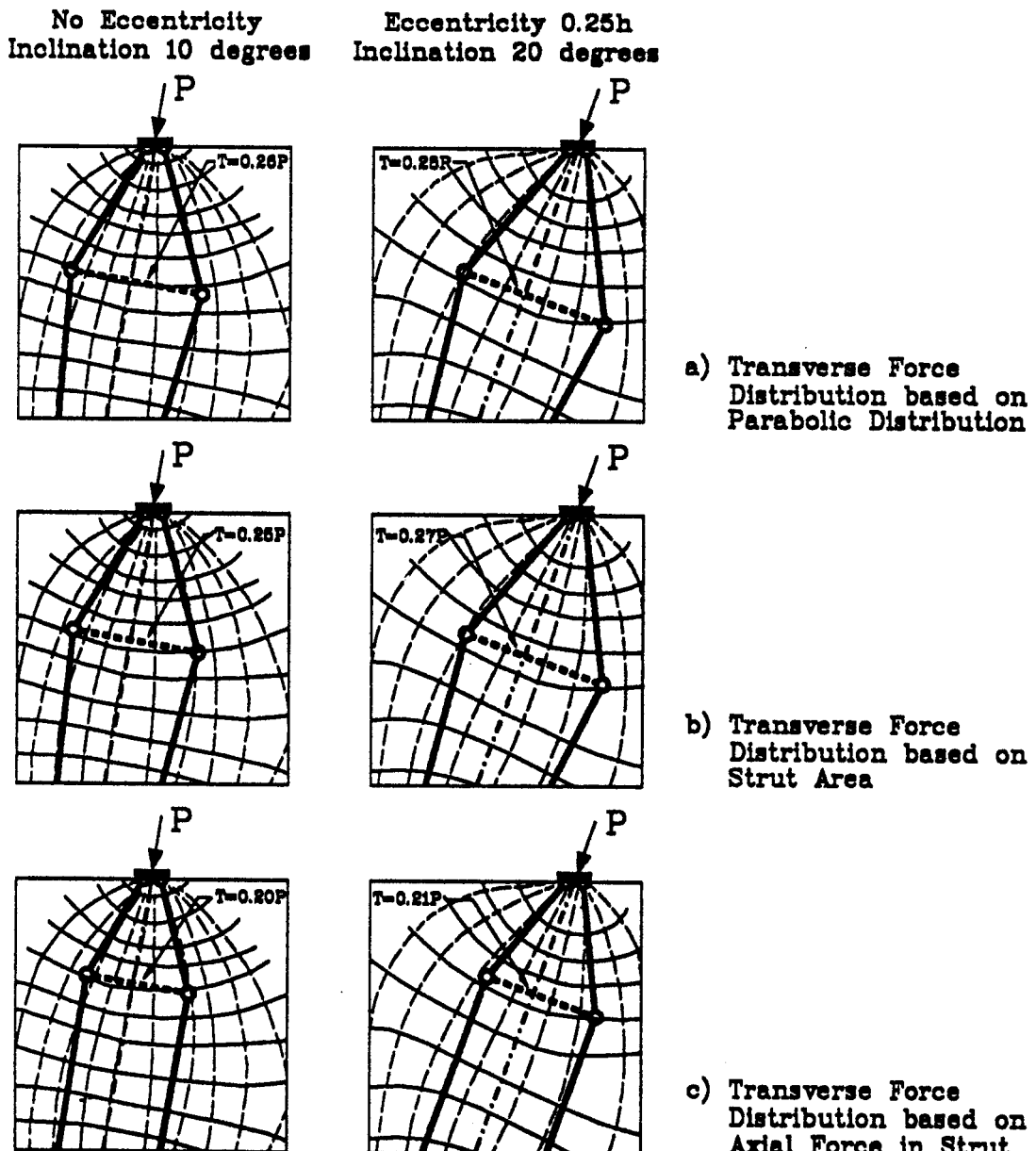


Figure 77. Elastic principal stress trajectories and strut-and-tie models based on the various assumptions on the distribution of the transverse reaction two initial eccentricities and inclinations.

Figure 82(a) assumes that no tie-back reinforcement is available, while the strut-and-tie model in Figure 82(b) has a tie-back reinforcement to resist half the deviation forces. When the contributions of all the reinforcement that crosses the axis of the axis of the tendon are summed, the strut-and-tie model with no tie-back reinforcement requires 37 percent of the tendon load, while the strut-and-tie model with tie-back reinforcement requires a total of 38 percent of the tendon load, showing how close the results of the two methods are.

A parametric study (48) was performed on the influence of initial inclination and curvature of the tendon using thrust-line strut-and-tie models. Figures 81(c) and 81(d) show the geometry used for this study. In order to simplify the model, the reinforce-

ment was assumed to be located in one layer perpendicular to the axis of the member. Because reinforcement is usually detailed perpendicular to the axis of the member, this does not appear to be restrictive.

Figures 83 and 84 present the transverse force obtained from the strut-and-tie model as a function of the initial inclination of the tendon, for the two hypotheses for the tie-back reinforcement [$F = 0$ and $F = F(e)$] and for two eccentricities. In addition, they show the integrated forces obtained from the finite element analyses and the results of the approximate formula (Eq. 7).

The results obtained by both strut-and-tie models are very close if the tie-back reinforcement is included in the total transverse force. There is a satisfactory correlation between the force

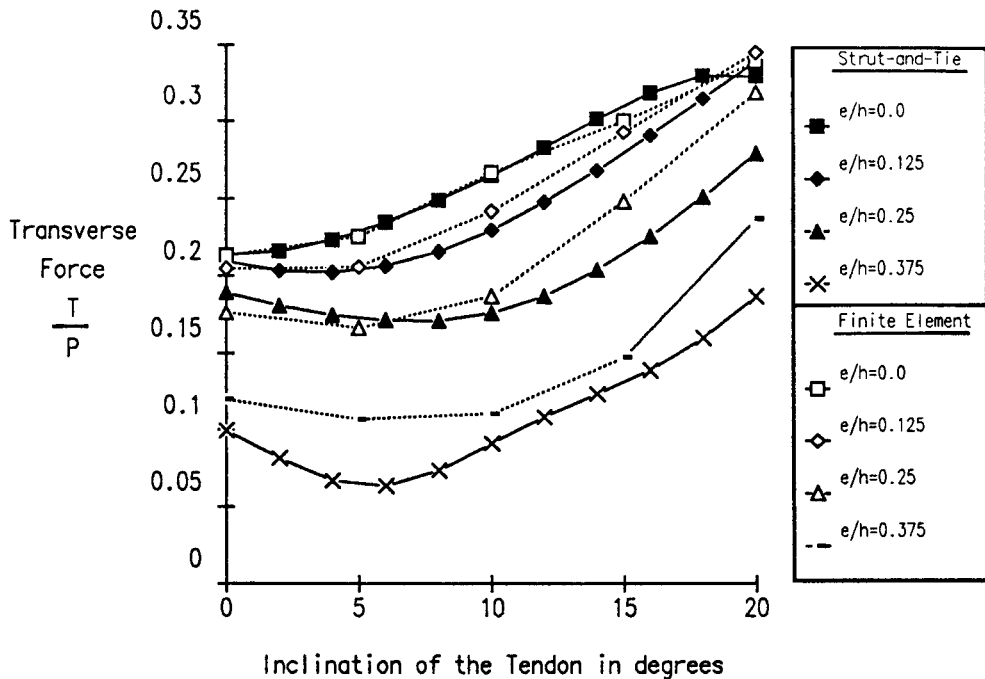


Figure 78. Tie force as a function of inclination and eccentricity for a parabolic distribution of the transverse reaction.

obtained by the strut-and-tie model and the force obtained by integrating the elastic stresses. Both methods predict a sharp increase in the required transverse reinforcement as the initial inclination of the tendon increases (and the radius of curvature decreases).

Analytical Results for Multiple Tendons

Multiple anchorages are generally used to provide a post-tensioning force that is not readily achieved with a single tendon, or to introduce a distributed post-tensioning force as in the case of transverse deck post-tensioning. This section focuses on configurations involving two anchors. Configurations involving more than two tendons (or two groups of tendons) tend to be less critical from the standpoint of the general zone, because the forces are already partially distributed over the cross section, inducing less transverse spreading of forces in the general zone. The case of uniform transverse deck post-tensioning will be treated later.

A parametric study of the influence of the distance between the two anchors in a concentric configuration was performed (48) using the finite element method. The size of each anchorage plate was held constant at $0.167 h$. Some additional cases with an eccentric resultant were also investigated.

Figure 85 shows the stress vector plots for two spacings $2 s$ of the plates in configurations where the resultant of the tendon forces is concentric. For cases where the two anchorages are close (up to one plate size between the plates), as for example Figure 85(a), the stress distribution in the bursting region is similar to the stress distribution observed for a single concentric anchorage. As the half spacing between the tendon axes increases

beyond one plate size, two clearly separated areas of bursting stresses appear, one ahead of each anchorage device, along the axis of the tendon (see Figure 85b). The bursting stresses along the tendon axis in configurations with two concentric tendons acting outside the quarter points are comparable to the bursting stresses induced by a single eccentric tendon load.

When the distance between the plates increases beyond approximately the size of the plate, substantial spalling stresses develop between the two plates. As the distance further increases, the area subjected to tensile bursting stresses decreases while the area subjected to spalling stresses increases. When the point of application of the forces moves outside the quarter points of the section, the spalling forces are combined with flexural tensile forces in unsymmetrical loading cases.

Anchorage devices located within a short distance from one another may be considered as one single plate for the purpose of analysis. It is, of course, necessary to consider the actual stressing sequence in determining the amount of reinforcement. By choosing an appropriate stressing sequence, the cracking of the general zone can be minimized, as well as the amount of reinforcement necessary in the general zone.

The basic principles used to develop strut-and-tie models for single anchor configurations were used to develop strut-and-tie models for multiple anchor configurations. The reactions at the end of the general zone are obtained by dividing the cross section into struts separated by the axes of the tendons and by the centroid of the section. Figure 86 shows the geometry for configurations with two tendons with a concentric resultant. Figure 86(a) shows the geometry of the strut-and-tie model when the tendon loads act within the quarter points. Figure 86(b) shows the geometry of the strut-and-tie model when the tendon loads act outside the quarter points.

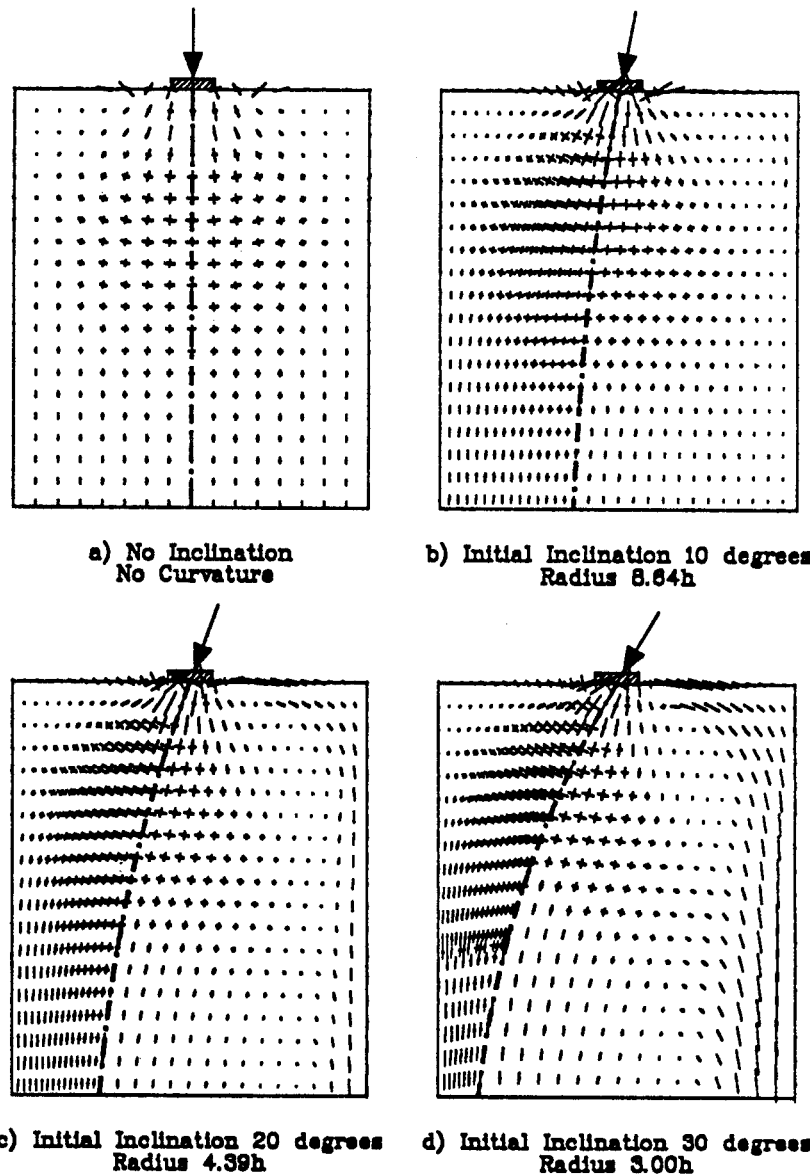


Figure 79. Vector plots of the principal stresses for tendon inclinations of 0, 10, 20, and 30 deg. and no initial eccentricity.

Figures 86(c) and 86(d) show how the location of the transverse ties is determined. For the load within the quarter points, as shown in Figures 86(a) and 86(c), the two internal struts (BE and CF) converge until they reach the line of action of their respective resultants (JE and KF), at which points they are deviated by the same amount, creating a compression strut (EF) between the two internal struts. The internal struts do not require a tension tie for equilibrium. The two external struts are balanced by a tension tie (GH) crossing the internal struts. The horizontal equilibrium of the anchorage requires a compression strut (BC) between the two plates. In the configuration with the load outside the quarter points, shown in Figures 86(b) and 86(d), the two external struts (AE and DH) extend to the line of action of their resultants (KE and NH) from the end of the general zone, and are balanced by tension ties (EF and GH) anchored back into

the corresponding internal struts (BFI and CGJ). The horizontal equilibrium of the nodes at the anchorage device requires a horizontal tendon tie (AD) between the anchors close to the surface of the concrete. This tie corresponds to the transverse flexural tension stress previously observed in the results of the finite element analysis.

A parametric study (48) was performed based on the geometry defined in the previous section. The size of the plates used for this parametric study was $a = 0.167 h$, the same value used for the finite element analyses.

Figure 87 shows the horizontal forces in the tension ties obtained from the parametric study performed using the strut-and-tie model described, as well as the results from the finite element analyses. Overall, there is a fair agreement between the two methods, with a good prediction of the bursting force for the

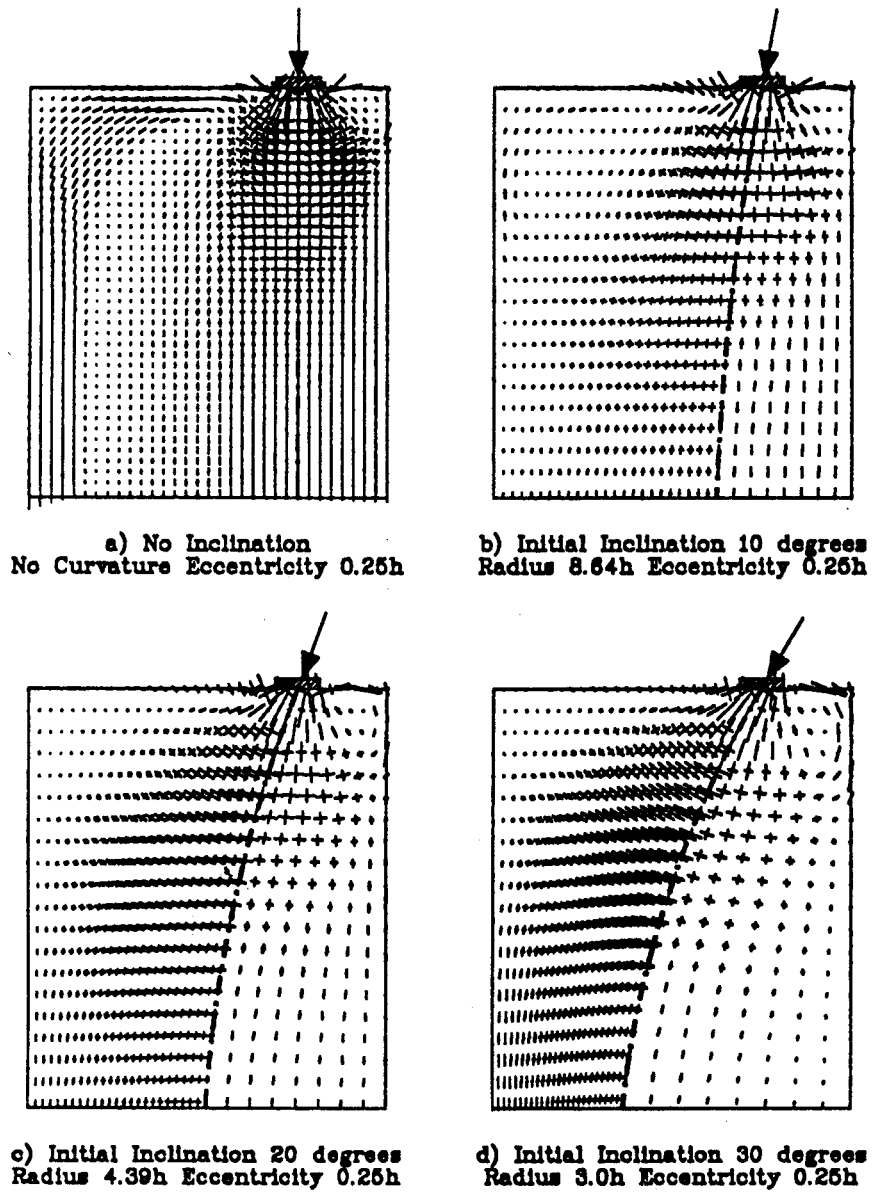


Figure 80. Vector plots of the principal stresses for tendon inclinations of 0, 10, 20, and 30 deg. and initial eccentricity $e = 0.25 h$.

case with small spacing between the plates and a good prediction of the flexural tensile force for the larger spacings. When the loads are located outside the quarter points, that is for half spacings larger than $0.25 h$, the bursting force predicted by the strut-and-tie model is less than the value obtained by the finite element method, probably because the strut-and-tie model does not consider the fact that the spalling and flexural forces tend to merge with the bursting force at large eccentricities. However, this difference is probably not a serious concern because the reinforcement, provided for the flexural tensile force and the spalling force, would most likely extend all the way through the bursting region and be anchored on the edge of the section. In such a case, it is most likely that the reinforcement would be designed on the basis of the larger of the two forces.

Because they are induced by the condition of compatibility, the strut-and-tie model does not predict any tensile forces at the surface of the concrete between the anchorage plates for cases where the anchorages are located within the quarter points. Furthermore, the strut-and-tie model tends to underestimate the magnitude of the tensile force in cases where the anchorages are located just outside of the quarter points. No test data are available for two anchorages with a half spacing of about $0.25 h$, so it is not possible to determine if these forces actually develop. Data available for smaller spacings show that, even though the calculated elastic tensile stresses at the surface of the concrete between the anchorages are very high, no early cracking of the concrete was observed in this area. This indicates that these compatibility induced stresses may be released by microcracking.

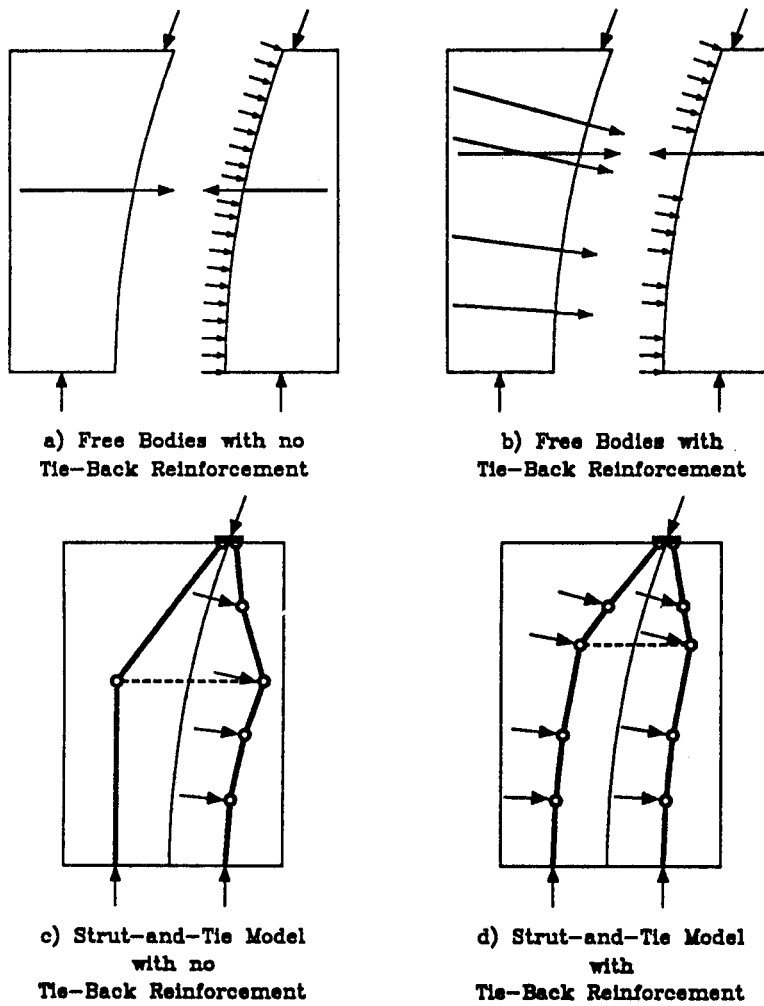


Figure 81. Free bodies and strut-and-tie models for curved tendons with and without tie-back reinforcement.

and not develop to the level predicted by elastic theory. In all cases, it appears prudent to at least provide some reinforcement to distribute and limit the opening of possible cracks in this region of the anchorage zone.

Analytical Results for Lateral Post-Tensioning

One of the major advantages of post-tensioned concrete is the reduction, and *ideally* the suppression of cracks in the concrete under service loads. Unfortunately, the local introduction of post-tensioning forces in the anchorage zone produces transverse tensile stresses that can lead to cracking of the concrete. The main post-tensioning of the structure cannot suppress this effect because it produces stresses that act perpendicular to it. Nonprestressed reinforcement is only effective in controlling cracking. In cases where cracking is highly undesirable, one solution is to add secondary lateral (or transverse) post-tensioning.

A series of finite element analyses were performed (48) for concentric single anchor configurations to investigate the effects of the amount of transverse post-tensioning and the distance d

of its centroid relative to the location of the main anchor. Figure 88(a) shows a vector plot of the maximum principal stresses caused by lateral post-tensioning alone with a magnitude of $P_{lat} = 0.2 P$. Figure 88(b) shows the vector plot resulting from the combination of the main tendon load P and the lateral post-tensioning $P_{lat} = 0.2 P$. The almost complete control of tensile bursting stresses is evident.

Figure 89 shows the distribution of transverse stresses along the tendon axis caused by a lateral post-tensioning load. The distribution of transverse tensile stresses along the tension axis, caused by a tendon load applied on a plate with size $a = 0.36 h$, is also shown in the figure. It is apparent that the most efficient location for the transverse post-tensioning is a location at about $0.5 h$ from the main anchor. This location corresponds, more or less, to the location of the centroid of the tensile bursting stresses caused by the main post-tensioning. For depths of the lateral post-tensioning greater than approximately $0.2 h$, the maximum compressive stress becomes constant.

Previous studies by Stone and Breen (24,55,59) recommended location of the lateral post-tensioning as close as possible to the main anchorage device. Stone's specimens were generally

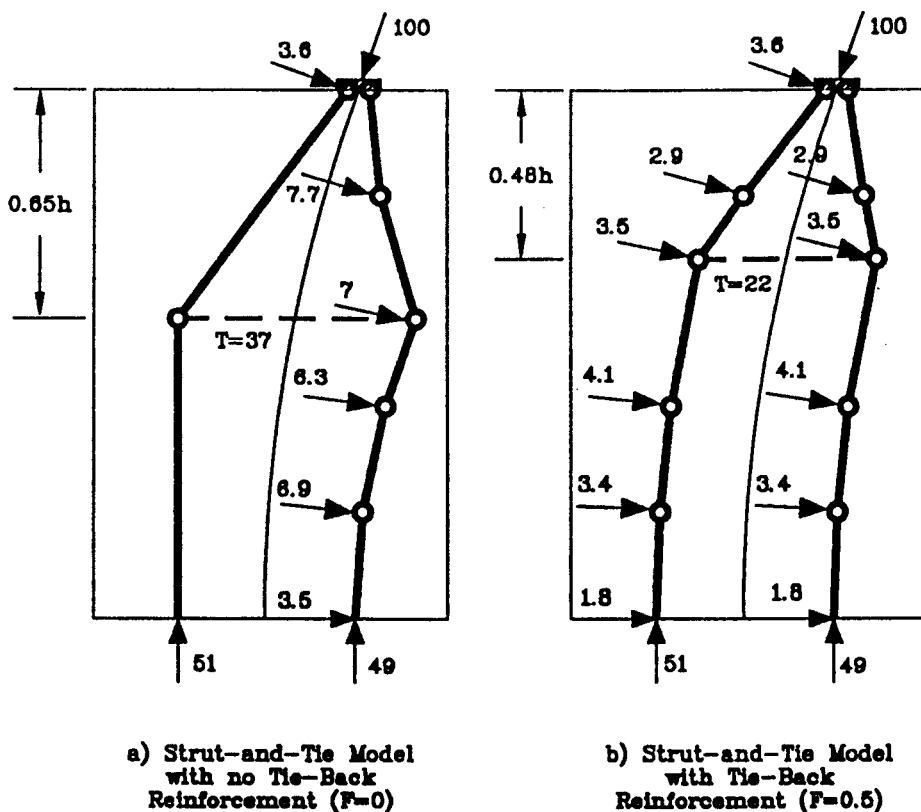


Figure 82. Strut-and-tie models of anchorage zone with a curved tendon of initial inclination 20 deg. and initial eccentricity $0.25 h$, for tie-back ratios $F = 0$ and $F = 0.5$.

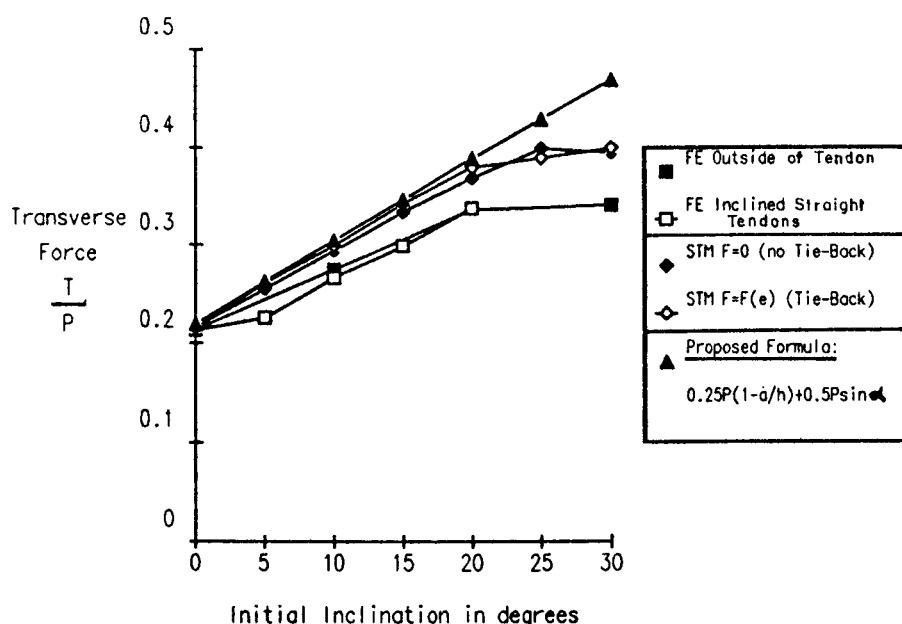


Figure 83. Transverse force obtained from the strut-and-tie model as a function of the initial inclination for various ratios of the tie-back reinforcement with no initial eccentricity.

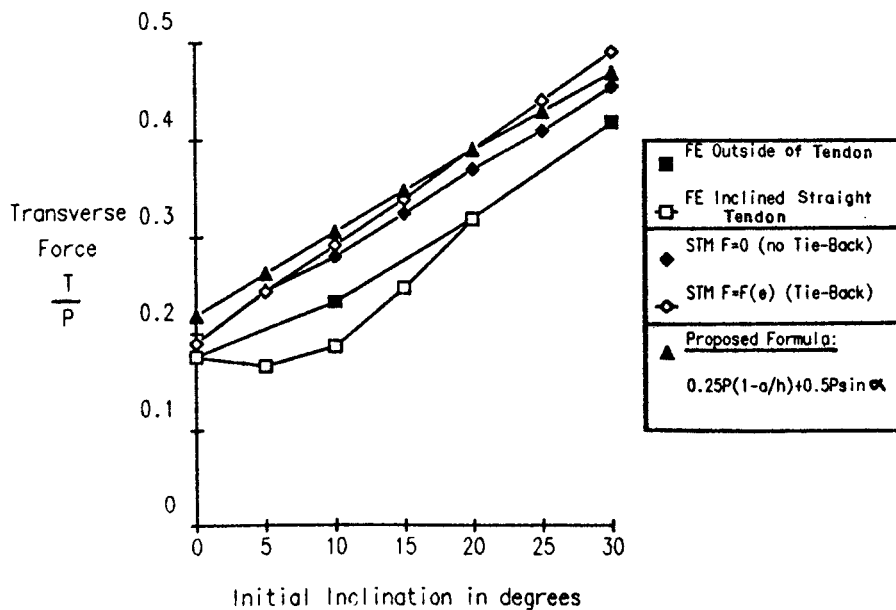


Figure 84. Transverse force obtained from the strut-and-tie model as a function of the initial inclination for various ratios of the tie-back reinforcement with an initial eccentricity $e = 0.25 h$.

overreinforced in the general anchorage zone, forcing the failure to occur in the local zone, or at the interface between the local zone and the general zone, close to the anchorage device. Their conclusion is logical under those circumstances. A transverse compressive force will confine and, hence, increase the capacity of the local zone. In addition, the large inclination of the main tendons at the location of the anchorage in Stone's specimens induced high spalling stresses that were greatly reduced by the lateral post-tensioning. Under more typical circumstances, however, the local zone should be sufficiently reinforced to transmit the tendon force to the general anchorage zone and the level of stress in the concrete struts at the interface between the local zone and the general zone should not be excessive. If these hypotheses are met, the best location for the transverse post-tensioning would be at a distance of about $0.4 h$ from the main anchor for anchorage zones with a small to moderate inclination of the tendon (up to 25 deg.).

Figure 90(a) shows the principle of the strut-and-tie model for use with lateral post-tensioning, which is considered as an external force acting on the anchorage zone and deviating the flow of forces coming from the anchorage device. This strut-and-tie model also incorporates a layer of nonprestressed reinforcement that will contribute to the ultimate strength. Figure 90(b) shows an analogous two-level thrust-line strut-and-tie model with two layers of nonprestressed reinforcement.

The top layer has the same capacity as the force introduced by the lateral post-tensioning. Notice that, with the exception of the compression strut coming from the anchorage devices for the lateral post-tensioning, both strut-and-tie models are identical. This means that the methods previously developed for anchorage zones using conventional, nonprestressed reinforcement can be directly applied to anchorage zones using lateral post-tensioning. It appears prudent to base the capacity of this tie on

the effective post-tensioning force and not on the yield value, as for conventional nonprestressed reinforcement.

Analytical Results for Nonrectangular Sections

In most applications of post-tensioning, especially for bridge girders, the cross section over which the post-tensioning acts is not rectangular. In typical bridge applications, the post-tensioning forces are applied to the webs and distribute over the entire cross section. Figure 91 illustrates how two tendon forces acting on the webs of a box-girder section are distributed first to the web, and then to the top and bottom flanges. The top and bottom flanges are only indirectly subjected to the tendon forces that are introduced in a distributed fashion over a longer length further from the anchors. This is not as severe as in members that are directly subjected to the post-tensioning force.

Figure 92 shows a strut-and-tie model of the same box-girder cross section. The struts and nodes actually are distributed over areas larger than suggested by this representation. It is advantageous, whenever possible, to analyze separately the individual components instead of solving the complex three-dimension strut-and-tie model. The principles for developing strut-and-tie models for cross sections involving several components are the same as for the rectangular cross sections presented previously. Starting at the end of the general zone, the stresses can be determined based on simple beam theory. The resultant forces on the various components on the cross section are computed as resultants of these stresses. It has been found practical to have at least two struts corresponding to each anchorage device, with the tendon axis acting as a line of separation between the two. A path for the post-tensioning force from the anchorage device to the end of the general anchorage zone can then be drawn.

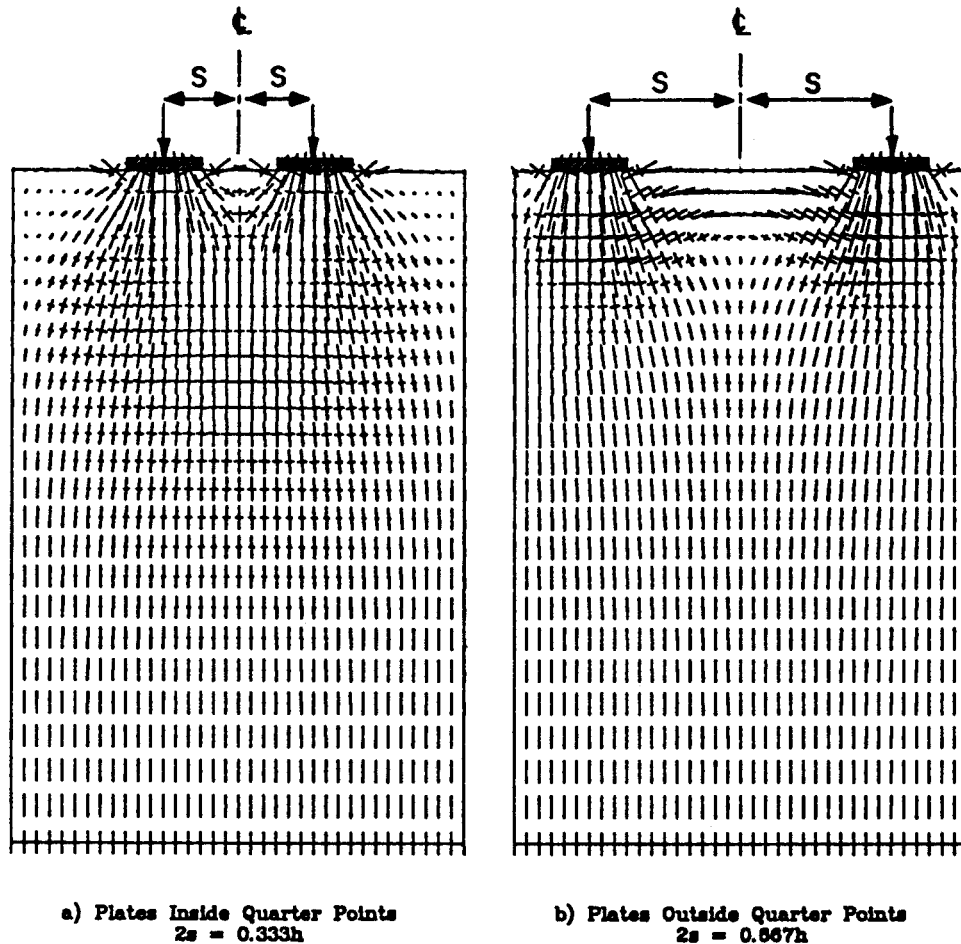


Figure 85. Principal stress vector plot of multiple anchor configuration with $2s = 0.33 h$ and $2s = 0.667 h$.

Once the magnitude and point of application of the forces acting on each component on the section are known, each component can be analyzed and designed independently using the methods presented for rectangular cross sections. The interaction of the planar models must be considered and the planar model loadings and results must be consistent. Alternatively, a single, three-dimensional strut-and-tie model can be developed.

A series of finite element analyses (48) were performed on flanged T-sections to investigate the influence of the presence of the flange on the overall state of stresses.

Figure 93 shows the vector plot of the principal stresses for a configuration with two anchorage plates of size $0.19 h$, located at $0.65 h$ and $0.88 h$ from the bottom of the cross section. The state of stresses in the web is similar to the state of stresses in an eccentrically loaded rectangular cross section, while the top flange presents similarities with a concentrically loaded rectangular cross section. The strut-and-tie model shown in Figure 94 was developed based on one of Sanders' (1) experimental specimens. The same specimen was modeled with the finite element analysis program. The angle used for the diffusion of the compressive forces was 26 deg., as in the previous models. Minor adjustments were made to simplify the geometry. Figure 94 shows the strut-and-tie model with the forces in the main mem-

bers. The total transverse force in the web is $0.11 P$, compared with $0.085 P$ from the finite element solution, and the total transverse force in the flange is $0.105 P$, compared with $0.082 P$ from the finite element analysis. Considering the number of assumptions necessary to obtain a strut-and-tie model of this level of complexity, the results of the strut-and-tie model are fairly close to the elastic value obtained from the finite element analysis and are on the conservative side.

Analytical Results for Influence of a Reaction Force in the Anchorage Zone

Wollmann (60) conducted linear elastic, two-dimensional finite element analyses for a beam with a rectangular cross section subjected to a concentric tendon force, P , and a single vertical load, V (Figure 95). Variables were the shear span and the magnitude of the load V . V was selected such that the maximum bending moment in the beam was the same and equal to $Ph/3$ for all shear spans investigated. Poisson's ratio was taken as 0.16.

The maximum bursting stresses do not occur along the tendon path but are located along the main strut that is inclined because of the effect of the reaction force in the anchorage zone. This

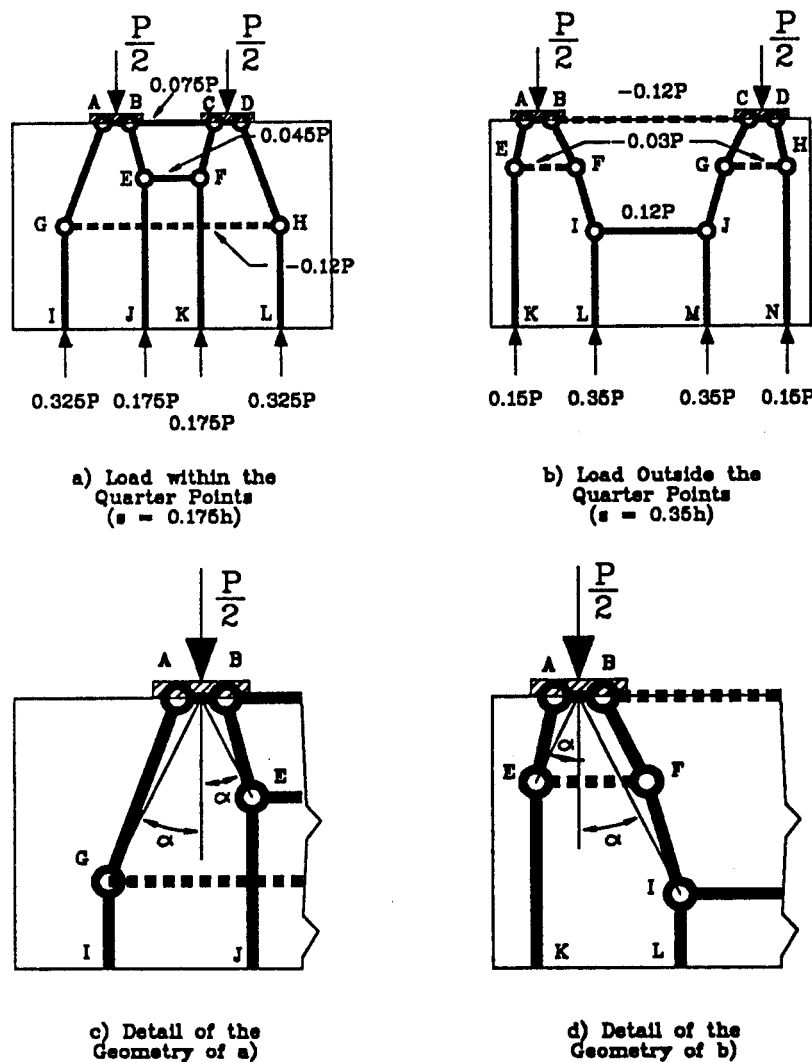


Figure 86. Definition of the geometry of the strut-and-tie models for anchorage zones with two tendons.

main strut approximately follows a line from the center of the anchor plate to the centroid of the flexural compression force at the maximum moment section (Figure 96a).

Figure 96(b) shows the relative tensile stresses perpendicular to the main strut for V/P ratios of 0, 0.078, and 0.148, respectively. These relative stresses were obtained by dividing the actual stresses by the average stress at the end of the anchorage zone. The relative magnitude and relative location of the resulting bursting forces are given in Table 11. A reaction force in the anchorage zone tends to reduce the maximum bursting stress, but the effect on the resultant bursting force is very small. The beneficial effect on the maximum bursting stress is largely independent of the magnitude of the reaction force for the range of variables investigated. The magnitude of the bursting force is close to Guyon's solution for a concentrically loaded rectangular member in all cases. With $a/h = 0.25$, Guyon found a bursting force equal to about 17 percent of the anchor force Figure 97.

Figure 98 shows a possible strut-and-tie model solution for a beam subjected to a concentric tendon force and a reaction force.

equal to 10 percent of the tendon force. The disturbed region where simple beam theory is not valid extends for a distance equal to one beam height measured from the end of the support bearing plate. At the end of the D-region, flexural stresses and shear stresses may be determined based on simple beam theory. These stresses are then integrated to find magnitude and location of the resultant forces at the end of the D-region.

The location of the bursting tie is selected to coincide approximately with the centroid of the bursting stresses from the finite element analysis (Table 11, Figure 98). The distance to the center of the local zone nodes from the anchor bearing plate depends on the state of stress at that node. It may be approximated as being equal to one-fourth of the anchor plate width.

With these assumptions and satisfying equilibrium conditions, the geometry of the strut-and-tie model is fully defined and the member forces can be determined. The bursting force T_{burst} is about 15 percent of the applied tendon force. For comparison, Guyon's solution for an a/h ratio of 0.4 is $T_{burst} = 0.13 P$ (Figure 97). The strut-and-tie model prediction is within 15 percent of

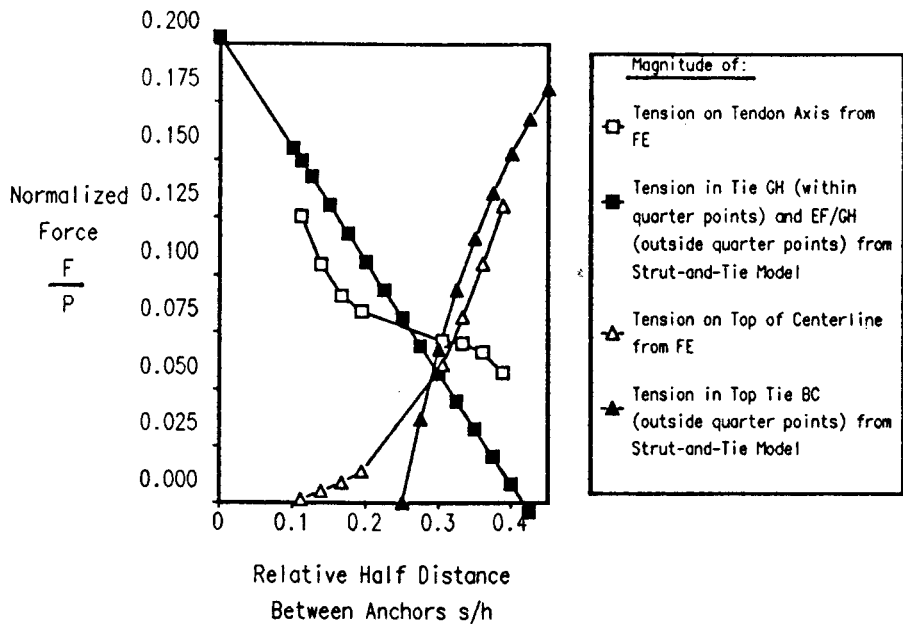


Figure 87. Tension forces obtained from the strut-and-tie model for an anchorage zone with two concentric tendons compared with the results from the finite element analyses.

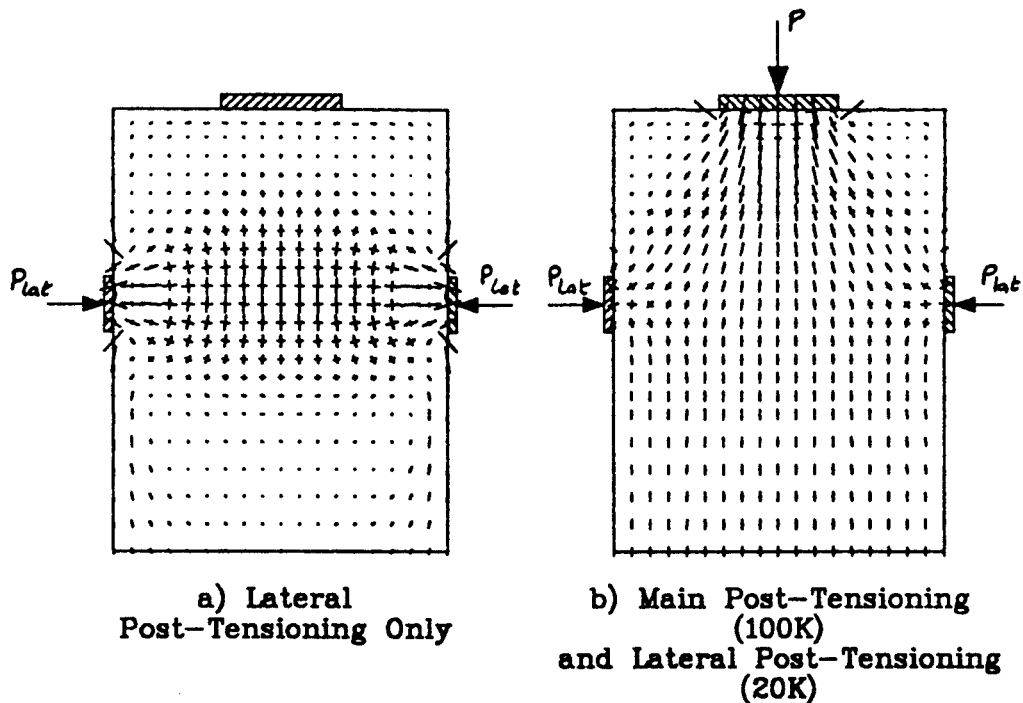


Figure 88. Vector plot of the principal stresses for lateral post-tensioning only and for main post-tensioning and lateral post-tensioning ($P_{lat} = 0.2 P$).

this solution and is conservative. Even better agreement could be achieved by fine tuning the distance of the local zone nodes and of the bursting tie from the anchor plate.

Analytical Results for Intermediate Anchorages

Figure 99 shows the results of a linear-elastic finite element analysis of a plane slab with a concentrated intermediate anchor-

age force (60). The distribution of the bursting stresses ahead of the anchor is very similar to the stress distribution for end anchors. However, the magnitude of the peak tensile stress, and of the resulting bursting force, is smaller. Additional tensile stresses exist locally behind the anchor both parallel and perpendicular to the tendon. These stresses become larger with increasing ratio of slab width to bearing plate width. For ratios larger

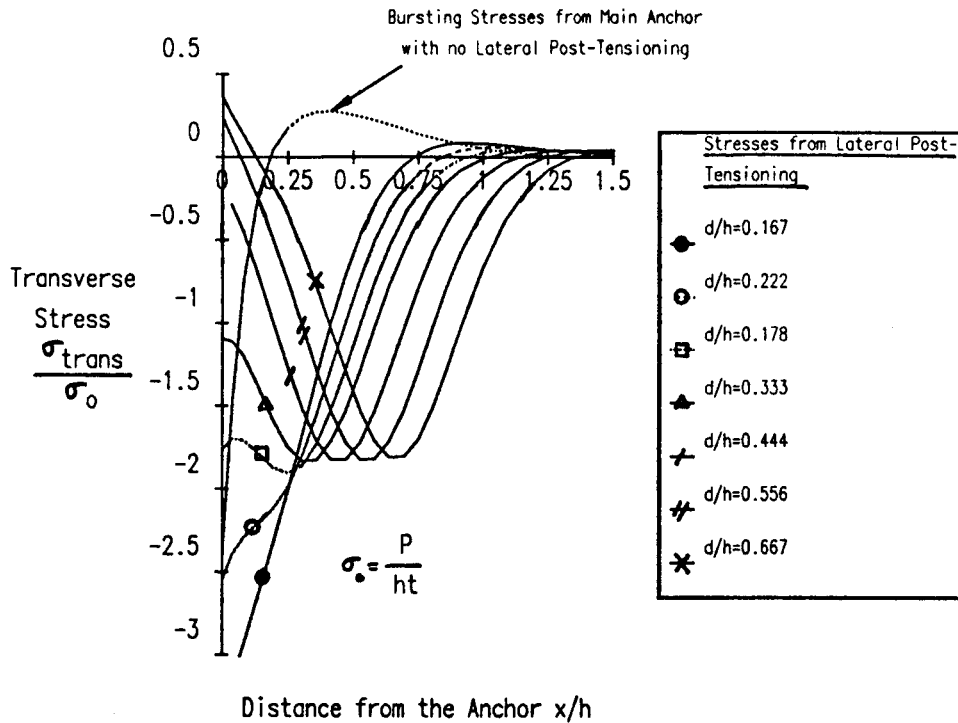


Figure 89. Distribution of stresses perpendicular to the tendon axis caused by various locations of the lateral post-tensioning force.

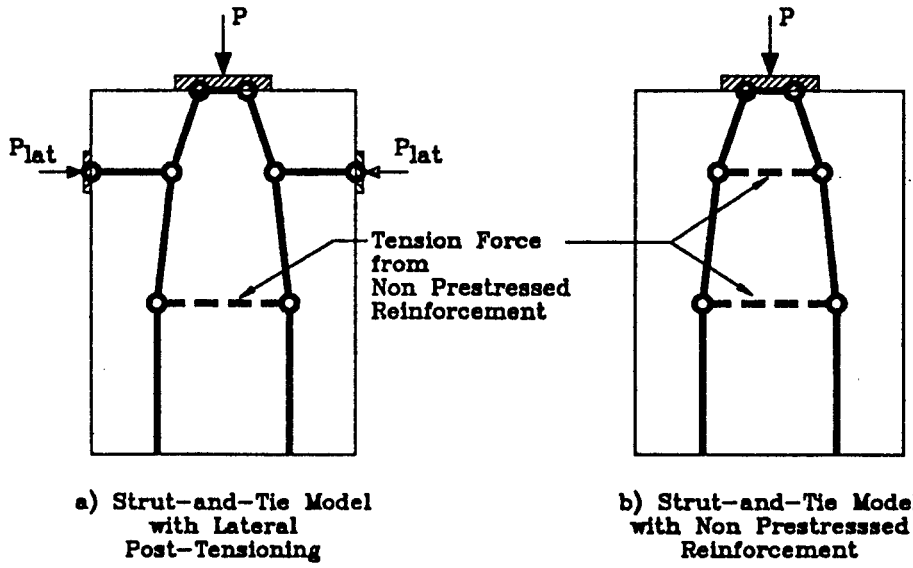


Figure 90. Strut-and-tie model for an anchorage zone with lateral post-tensioning compared with an anchorage zone with nonprestressed reinforcement only.

than 5, 40 to 50 percent of the anchor force is carried in tension behind the anchor.

Frequently, for intermediate anchorages, the tendon is deviated out of the plane of the slab and is anchored in a blister or rib. Figure 100 shows a three-dimensional finite element mesh for such a blister. The stress contours for the principal tensile stresses

in the center plane of this blister are plotted in Figure 101. Critical regions subjected to large tensile stresses occur behind the anchor, particularly at the reentrant corner, and at the toe of the blister where the tendon is curved to enter the blister. Smaller tensile stresses exist close to the bottom of the slab because of the eccentricity of the tendon.

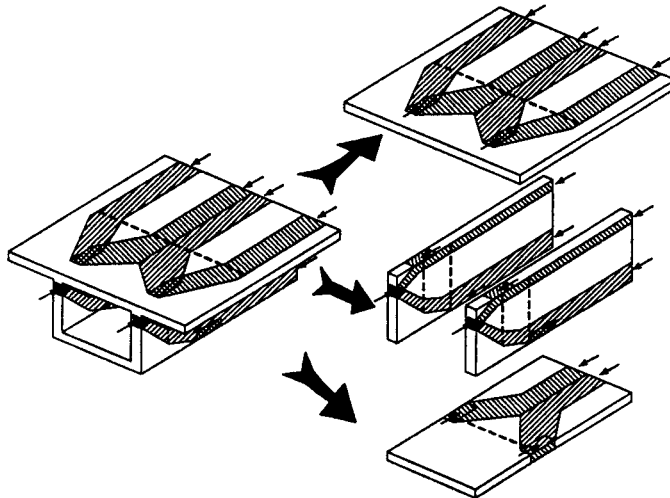


Figure 91. Flow of forces in the anchorage zone of a box-girder cross section.

The magnitude of the tensile stresses behind the anchor is significantly larger than that for the plane slab case because of the stress concentrations at the reentrant corner. However, the gradual transfer of the anchor force from the blister into the slab reduces the resulting tensile force behind the anchor. Figure 102 shows a strut-and-tie model that closely approximates the stress trajectories of the elastic solution for the intermediate anchorage in a plane slab. For these simple cases it is relatively easy to select the geometry of the strut-and-tie model such that the member forces match the corresponding resultant forces of the finite element solution exactly. However, in practice such close agreement is not necessary.

In the linear-elastic finite element analysis the same material stiffness is used for tension and compression. In reality, large tensile stresses will cause early cracking behind the anchor plate, which greatly reduces the stiffness of this load path. Hence, only a small portion of the anchor load is carried in tension behind the anchor. A pragmatic, practical approach would be to ignore this load path in the development of the strut-and-tie model but to provide nominal reinforcement for crack control. The bursting force ahead of the anchor is determined from the same strut-and-tie model procedures as used for end anchors.

For analysis and design of the blister problem three-dimensional analysis is required. This introduces considerable complexity, and makes it more difficult to find a precise match of the finite element solution and the strut-and-tie model solution. However, strut-and-tie models can be found which capture all essential characteristics of the load path in blisters. Design of the reinforcement, based on such load paths, is actually easier than using finite element analysis results because the interpretation of a three-dimensional stress distribution, and its translation into reinforcement requirements, is quite difficult.

Figure 103 shows a strut-and-tie model for a tendon anchorage in a blister. Tensile forces behind the anchor were neglected in this model for the reasons discussed above. The model correctly identifies the blister bursting force ahead of the anchor, an inclined tensile force due to corbel action, and a horizontal tensile force along the bottom of the slab. Tie-back reinforcement has to be provided in the region of tendon curvature to resist the deviation forces (Figure 103c). Figure 103(b) shows a model for spreading of the compressive stresses in the plane of the slab.

Analytical Results for Anchorage of External Tendons in Diaphragms

Figure 104 shows dimensions and loading conditions of a specimen representing a diaphragm used as abutment for the

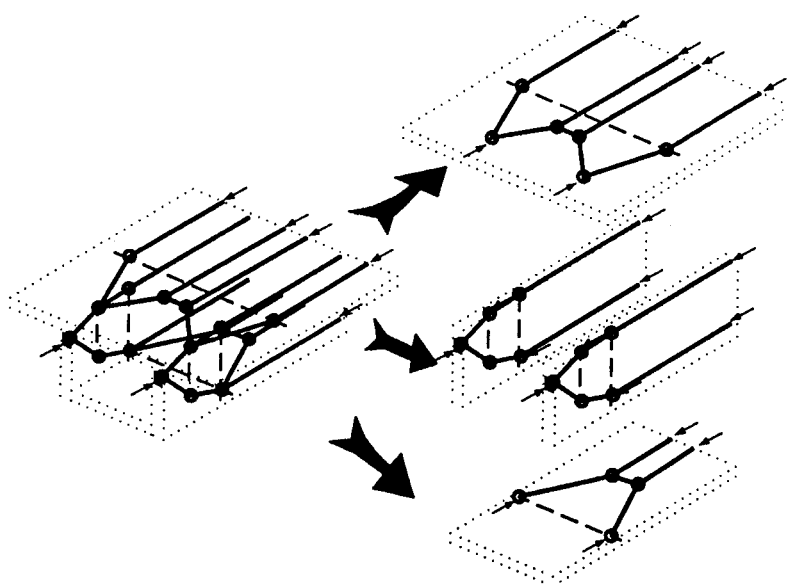


Figure 92. Three-dimensional strut-and-tie model of the anchorage zone of a box-girder cross section.

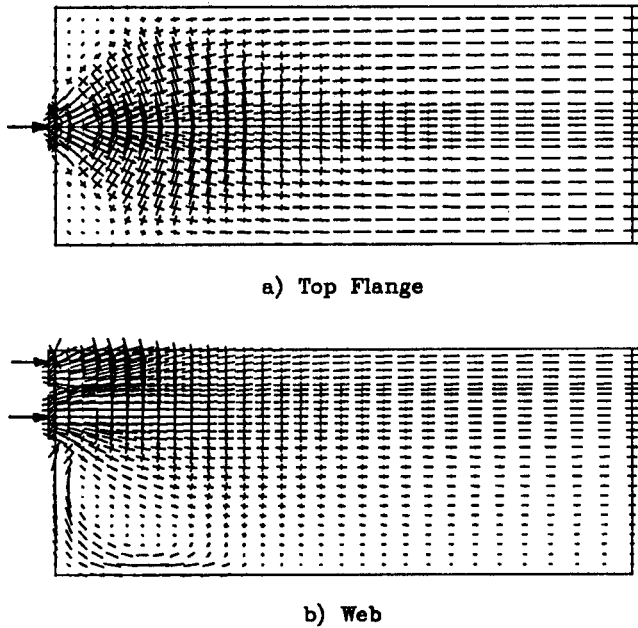


Figure 93. Vector plot of the principal stresses in the anchorage zone of a flanged cross section.

anchorage of external tendons in a box-girder bridge (60). The wings of the top flange of the cross section were clipped so that advantage of symmetry about plane X-X could be taken.

The stress distributions shown in Figure 105 clearly indicate that the diaphragm acts similarly to a deep beam. In addition, bursting stresses occur in the web. Figure 106 shows the principal tensile stress contours in plane X-X, further illustrating the stresses due to diaphragm bending and web bursting. Location and magnitude of the resulting vertical tensile forces in the diaphragm and web can be found by integrating the tensile stresses perpendicular to plane X-X. The results are shown in Figure 107.

Figure 108 shows a three-dimensional, yet fairly simple, strut-and-tie model for the diaphragm problem. Two-dimensional models are not satisfactory to model the flow of forces in diaphragms. The anchor forces are carried by inclined struts to the web and flanges of the cross section. Tensile forces are generated at the end of the diaphragm because of deviation of these struts.

Linear-elastic finite element results and strut-and-tie model results for the vertical tensile forces in the web and diaphragm are given in Table 12. The total tensile force compares very favorably, with the strut-and-tie model solution being about 15 percent higher. The location and distribution of web and diaphragm forces are somewhat different. Closer agreement could be achieved by refining the strut-and-tie model and by adjusting its geometry. However, this would be at the expense of the simplicity of the model and is not necessary for practical purposes.

Analytical Results for Closely Spaced Slab Anchors

Falconer (61) examined the effect of post-tensioning loads on bridge deck edge anchors using both the ABAQUS finite element code (51) and strut-and-tie models. In order to correlate results

with half-scale test specimens, all analyses were done assuming 35 kips on the anchors, which represents the scaled force on a typical four-strand deck anchor. Typical slab horizontal plane stress vector results are shown in Figures 109 and 110 for various loading configurations and stressing sequences.

Compressive stresses extend directly from the anchor and flow down to the base of the slab. The tensile stresses wrap around the anchors before extending away from them. Bursting stresses are ahead of loaded anchors, and spalling stresses are along the slab's top edge beside or between loaded anchors, and sometimes extend down the slab's side.

From Figures 109(a) and 109(b), it is obvious that the anchorage zone bursting stresses are confined to a smaller region for the exterior anchor than for the interior anchor. The spalling stresses are much larger and extend over a much greater area for the exterior anchor. Figures 109(c) and 109(d) demonstrate the two loaded anchors that are close to one another (two plate widths apart center-to-center) have one larger combined anchorage zone, but otherwise follow the general patterns of the single anchors.

In Figure 110(a), two distant anchors are loaded (eight plate widths apart center-to-center). In this case the anchors develop individual anchorage zones, although substantial tension stresses develop between anchors. However, when an anchor midway between them is loaded (Figure 110b), the spacing becomes four plate widths and the three anchorage zones show substantial interaction. Bursting stresses become larger and move further ahead of the bearing plate and spalling stresses are concentrated closer to the edge. Figure 110(c) shows that subsequent stressing of a fourth exterior anchor, with an edge distance of one plate width, causes all of the previous three anchors to develop more distinct individual anchorage zones. Figure 110(d) shows the pattern when all eight anchors are loaded on the slab edge. The spacing of two plate widths resembles a uniformly loaded edge in between the two exterior anchors. Substantial horizontal bursting stresses are present only ahead of exterior anchors.

The smaller of the exterior anchor edge distance or the anchor spacing determines if the anchors will behave as one large anchor or as separate anchors. If twice the smallest edge distance is greater than the center-to-center spacing, the anchors act as one edge load. If twice the smallest edge distance is equal to or less than the center-to-center spacing, the anchors act as individual anchors on the slab edge.

Slab vertical plane stresses (Figure 111) are a localized effect. The computer model only represented the section of the slab directly ahead of the anchor. Therefore, effects of sequenced stressing or adjacent anchor loading were not considered in the vertical plane analysis. All of the vertical plane stresses were conservatively assumed to be dispersed directly ahead of the anchor across its 6-in. width. The calculated stresses are across the tendon path and are due to maximum tendon jacking force ($0.8 F_{pu}$) on the anchor.

Figure 111 shows both the principal stress vectors in the cross section and the bursting stress distribution across the center of the cross section. The vertical plane bursting stresses were concentrated very close to the anchor. The maximum vertical plane bursting stress under service loads was predicted to be 249 psi, over twice the magnitude of the highest bursting stress in the horizontal plane created from loading any or all of the anchors.

Falconer (61) explored various strut-and-tie models for slab anchors. For slab horizontal plane action, the more complex

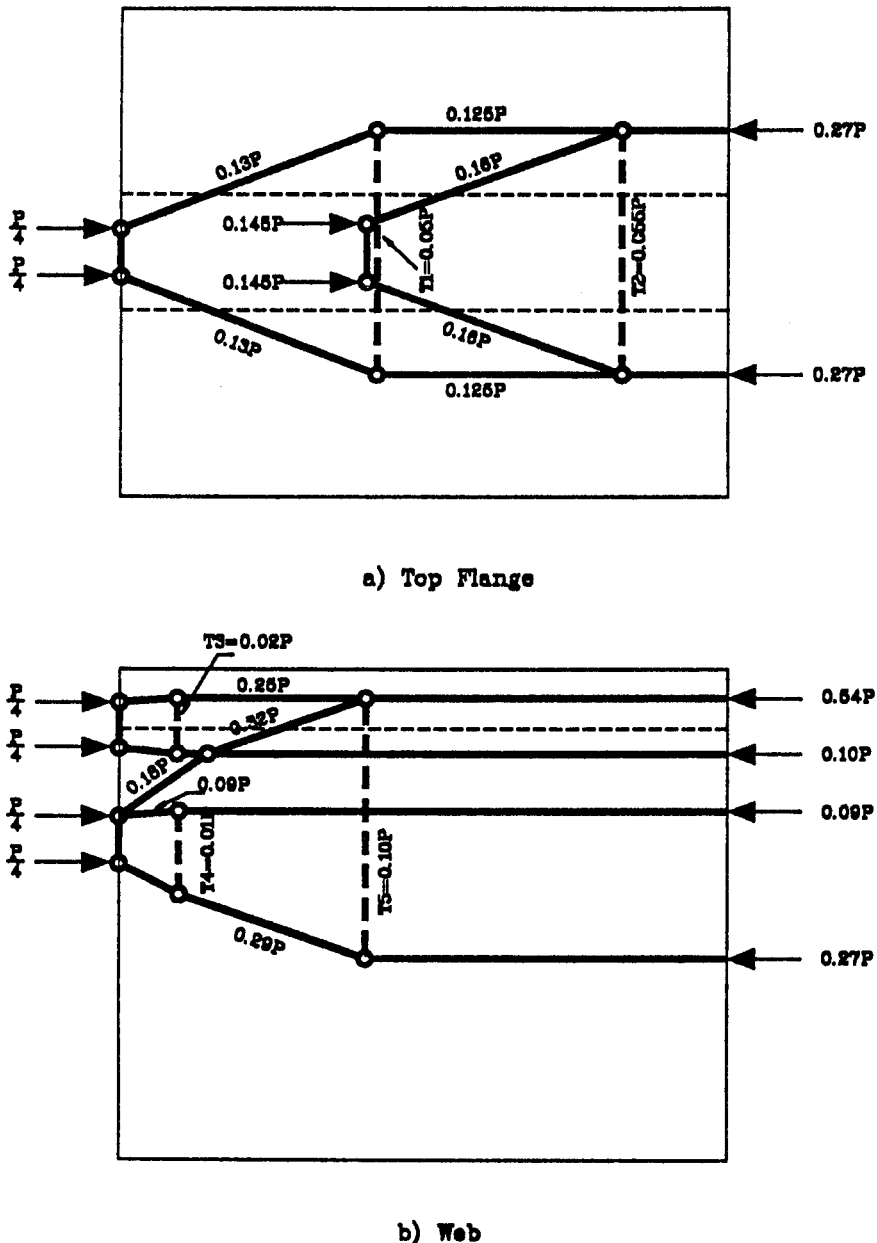


Figure 94. Strut-and-tie model of anchorage zone in flanged cross section.

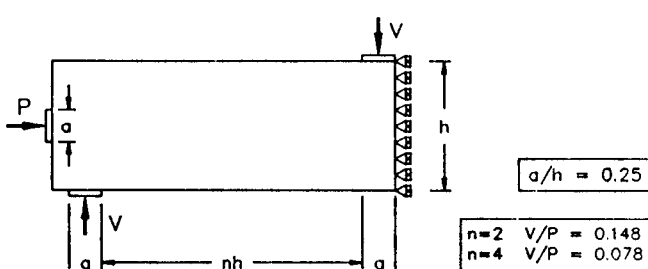


Figure 95. Parameters for finite element analysis.

model of Figure 112 indicates that edge spalling stresses can be incorporated into STM, but their very low magnitude indicates that they can be ignored or treated prescriptively with the STM greatly simplified as shown in Figure 113. Note that the difference in bursting tie force is less than 10 percent.

A strut-and-tie model based on the FEA indications of Figure 109(b) for a loaded exterior anchor is shown in Figure 114. Spalling stresses are caused by continuity strains and are not usually critical because they are often dispersed through micro-cracking. However, with a highly eccentric anchor, tensile stresses can be set up on the far face and some reinforcement is required if concrete tensile strength is not to be depended upon. The bursting stress ahead of the exterior anchor is critical

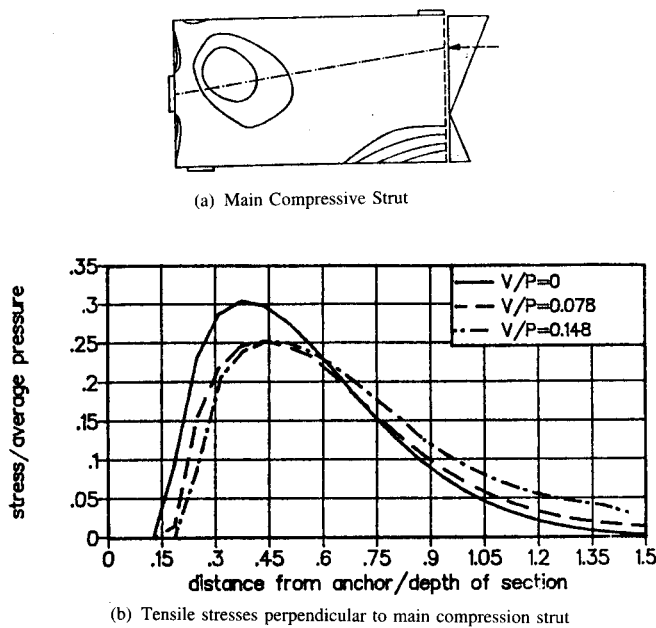


Figure 96. Results from finite element analysis.

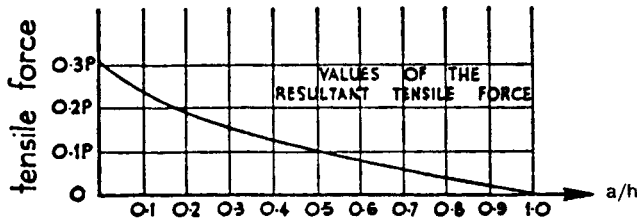


Figure 97. Guyon's solution for magnitude of bursting force (from Ref. 6).

because the region is small and, in an actual slab reinforcing, will need to be concentrated in the region of this tensile tie.

In Figure 115, the strut-and-tie model for loaded alternate anchors has four separate bursting regions that are similar to the four separate bursting regions indicated by the finite element stress distribution. As in the exterior anchor model, a bursting tie is placed close to the exterior anchor.

Figure 116 shows a strut-and-tie model with all the anchors loaded (two plate widths center-to-center). The finite element analysis showed that loading close adjacent anchors reduces or

negates bursting stresses immediately ahead of anchors. Notice that loading all the anchors is assumed to produce *struts* between anchors rather than *ties* below them as the finite element analysis indicates. The exterior anchors, however, require their own bursting stress ties, and half the load of the exterior anchor is applied to that separate exterior anchor strut-and-tie model.

In Figure 117, the slab vertical plane bursting forces are illustrated with the transverse strut-and-tie model. The magnitude of this force (5.3 kips/35-kip anchor load) is not unusually large compared to the horizontal plane forces, but it is centered at only 3 in. from the slab's edge. In this confined region it is difficult to place sufficient reinforcement to develop a tie.

GENERAL ZONE END ANCHORAGE TESTS

In one of the experimental phases of this project, Sanders (1) explored the general zone behavior for the most frequently reported girder end anchorage zone configurations. The approach for the design of all test specimens was to select the appropriate strut-and-tie models and proportion the general zone reinforcement. Details of each specimen are given in Appendix C. In addition, a linear elastic analysis was performed to verify the general distribution of stress fields (48). The critical reinforcement in each test specimen was instrumented to provide confirmation or evaluation of the design model used. Specimens were tested to failure with crack development, force distribution patterns, and ultimate loads being monitored. Complete loading and behavior details for each specimen are included in Ref. 1. The results were checked against the design assumptions and the evaluated results were used to develop the design criteria of Chapter 4. The final criteria were developed in such a fashion that designers should be able to implement procedures for design without requiring complex analysis, except in the most unusual cases. It is emphasized that the physical tests were being used to verify the strut-and-tie models and not to develop empirical expressions. This allowed a wide ranging scope of tests with few replications, and made the best use of the limited resources.

Reporting of the experimental test program herein is limited to a brief summary highlighting the important observations. Subsections report on the different variables. These include 17 concentric single-anchorage specimens, 6 eccentric single-anchorage specimens, 8 multiple-anchorage specimens, 5 specimens with tendon curvatures and inclined anchorages, and 3 specimens with transverse loads and reactions.

Anchorage Zones with Single Straight Concentric Tendons

In post-tensioned concrete, the most basic anchorage zone configuration includes the anchorage device located on the geo-

Table 11. Magnitude and location of bursting force in beam

V/P	T _{burst} /P	d _{burst} /h
0	0.173	0.56
0.078	0.159	0.62
0.148	0.169	0.68

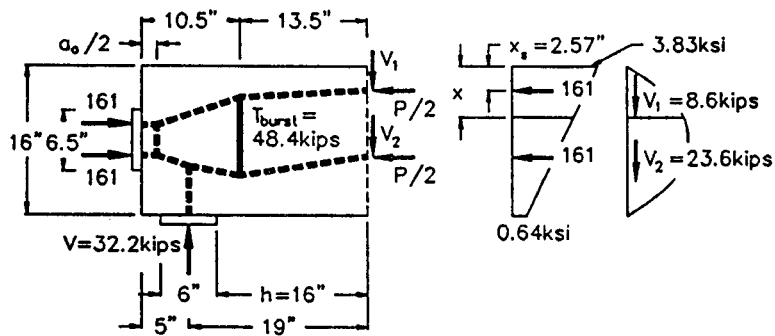


Figure 98. Strut-and-tie model for beam.

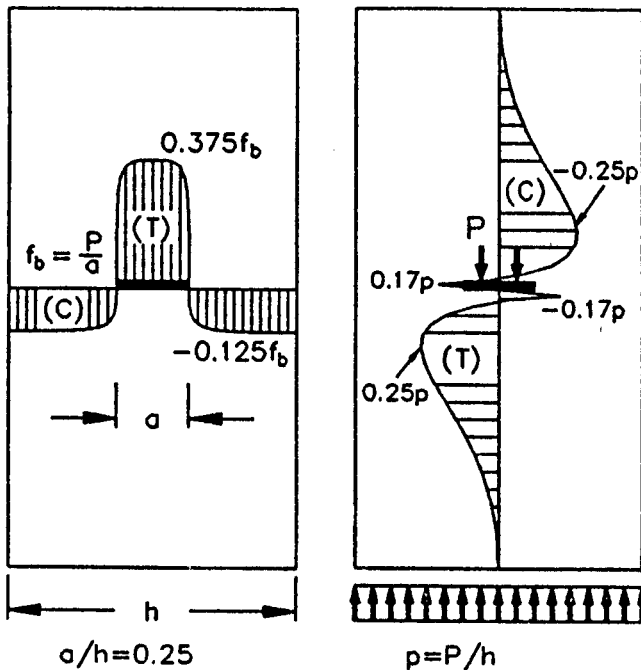


Figure 99. Longitudinal and transverse stresses at an intermediate anchorage.

metric centroid of the concrete cross section. Thirteen specimens were used to investigate concentric anchorage variables including reinforcement distribution, the ratio of the anchorage device width, a , to the section depth, h , and the effect of lateral post-tensioning.

All of the concentric specimens were loaded monotonically through a spherical loading head in a universal testing machine and were supported on sheets of teflon to reduce base friction. Concrete surface cracks were located by careful visual observation and the monitoring of strain gage data placed on the key reinforcement. For each test, concrete compression strength and tensile strength were determined by averaging at least three standard compression or split cylinder tests. All specimens were cast horizontally. Reinforcing bars were tested for their yield strength and modulus of elasticity, and were ductile in behavior. Yield points were 81 ksi for #3, 67 ksi for #4, and 60 ksi for #5 bars.

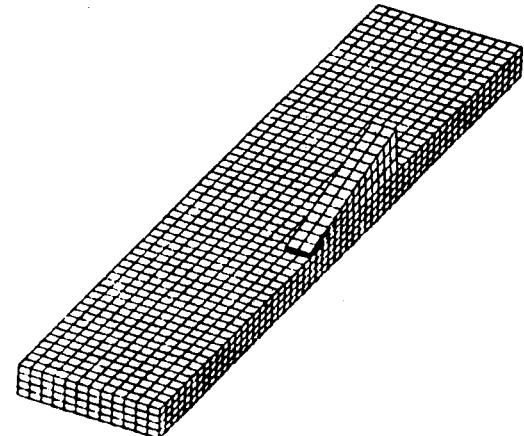


Figure 100. Finite element mesh for blister analysis.

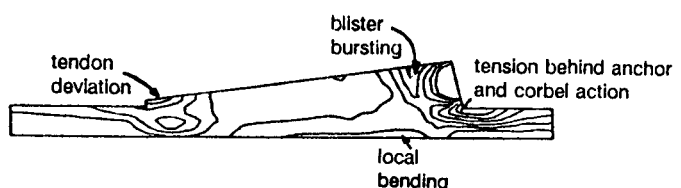


Figure 101. Principal tensile stresses in blister.

Tests with Rectangular Bearing Plates Having Little Confinement

Series "A" consisted of four rectangular prism specimens. Details are given in Table 13. All four specimens were identical except that the centroid and size of the bursting reinforcement varied. The specimens were loaded over the full thickness so that the specimen would behave as two-dimensional as possible. Bearing plate anchors (6-in. by 12-in. plate) for a nominal 7½-in. strand tendon ($F_{pu} = 289$ k) were used.

These tests were run very early in the program. The only confining reinforcement in the local zones of the specimens

intermediate anchor

strut and tie model
elastic stresses

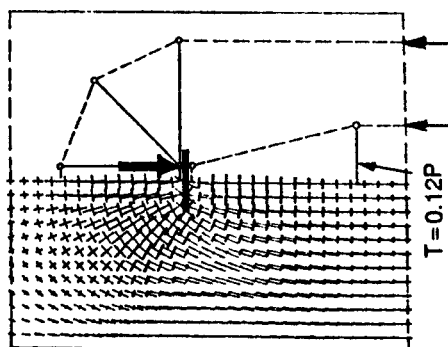


Figure 102. Stress trajectories and strut-and-tie model for intermediate anchor in plane slab.

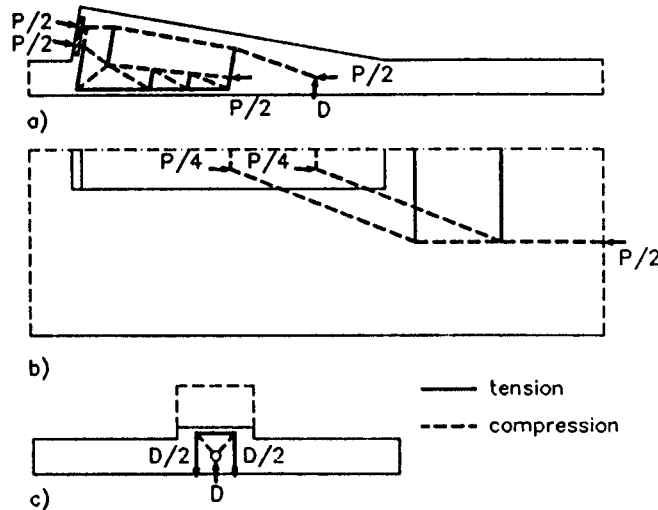


Figure 103. Strut-and-tie model for blister.

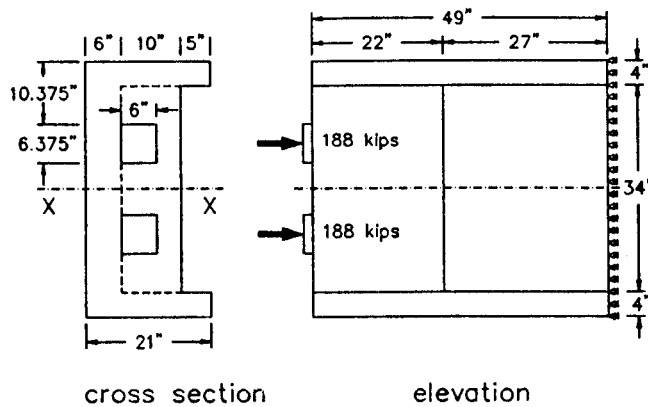


Figure 104. Geometry and loading of diaphragm specimen.

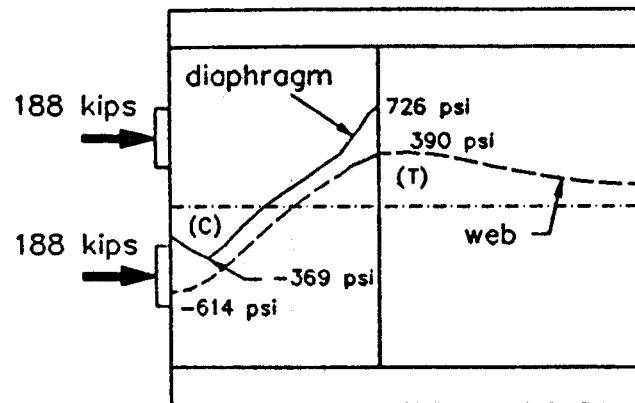


Figure 105. Vertical stresses in diaphragm and web.

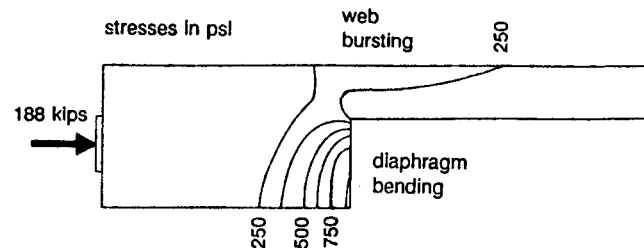


Figure 106. Diaphragm bending and web bursting stresses.

consisted of very light orthogonal grids as called for by Guyon and AASHTO and reported in Table 13. Test results are summarized in Table 13. None of the bursting reinforcement in specimens A1 or A3 yielded before failure and only one gage yielded in A2, virtually at failure. Typically, failures were bulging of the concrete immediately ahead of the anchor and a typical sign of local zone failure. Bearing stresses at failure were about 50 percent higher than values allowed under the local zone criteria proposed in this study. These specimens clearly indicate the importance of local zone confinement. Ultimate loads for these three unconfined specimens are identical or only marginally above cracking loads. Specimen A4 was given extra local zone confinement by lateral post-tensioning equivalent to $0.17 F_{pu}$, applied by plates over the upper 4 in. of the local zone. This extra confinement was of substantial benefit, and the specimen developed over 50 percent more load than the unconfined specimens.

In A4 it was apparent that a small percentage of the bursting force was carried by the reinforcement before the first crack occurred. After the first cracking load, the total bursting force being carried by the bursting reinforcement increased substantially and had a distribution similar to that predicted by the elastic analysis. As the load approached ultimate, the stress level in the bursting reinforcement deeper in the section began to increase, and the force distribution became more uniform. Typical cracking patterns and bulging are shown in Figure 118.

Tests with Rectangular Bearing Plates Having Substantial Confinement

Series "B" consisted of eight 9-in. by 16-in. by 24-in. prism specimens designed with highly conservative local zone rein-

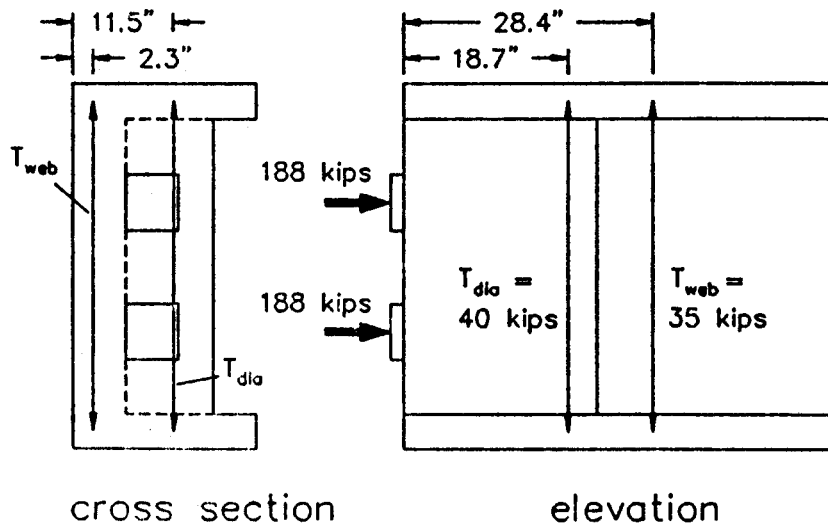


Figure 107. Resultant vertical tensile forces in diaphragm and web.

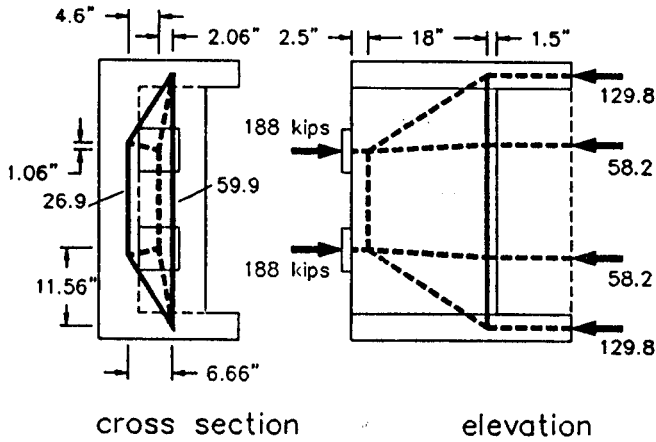


Figure 108. Strut-and-tie model for diaphragm.

forcement to prevent any local zone failure. As in series "A", a determination of the effect of reinforcement distribution was the major objective (specimens B1 to B4). Other specimens investigated the effect of zero general zone bursting reinforcement (B5), zero local zone reinforcement (B6), the void caused by a post-tensioning duct (B7), and partial loading of the bearing plate (B8). The dimensions, material properties, and reinforcing details for series "B" specimens are given in Appendix C and summarized in Table 14. The general zone reinforcement consisted of #2 bars with 45 ksi yield, #3 bars with 67 ksi yield, or #4 bars with 64 ksi yield. The spiral used for local zone reinforcement (except in B6) consisted of a #4 smooth bar with a yield strength of 80 ksi. All eight specimens had a $6\frac{1}{2}$ -in. by $6\frac{1}{2}$ -in. by 1-in. loading plate, patterned after a nominal 3-0.6-in. strand anchor. All specimens had electronic strain gages along with specimen centerline on a majority of the bursting reinforcement.

The major variable in the "B" series was the amount and distribution of bursting zone reinforcement. With the exception of B5, which purposely had no general zone reinforcement, all

Table 12. Magnitude and location of vertical tensile forces in diaphragm and web

force (kips)	finite element solution	strut-and-tie model solution
diaphragm	40.0	59.9
web	35.0	26.9
total	75.0	86.8
distance from anchor (in.)	finite element solution	strut-and-tie model solution
diaphragm	18.7	20.5
web	28.4	20.5

general zone reinforcement was proportioned using strut-and-tie models for the same nominal loading. As shown in Figure 119, the general zone reinforcement was distributed in various patterns ranging from a close match of the elastic distribution of bursting stresses (B4, B6, B7, B8) to extreme mismatches (B1, B2). Cracking, first yielding of the general zone reinforcement and ultimate loads are given in Table 14 as a function of the anchor nominal tendon ultimate load, $F_{pu} = 174$ kips. In these specimens, longitudinal splitting cracks tended to form and propagate along the specimen centerlines, with secondary longitudinal cracking towards the edges. Near failure, spalling cracks around the plates and substantial displacement of the plates into the concrete surface were obvious. Spiral local zone confining reinforcement indicated definite strains but the strains were usually short of yield at failure. Axial load and plate displacement curves tended to exhibit limited ductility, as shown in Figure 120. The exception was specimen B6 which had no local zone confinement and had a very brittle failure. Even bursting reinforcement distributions, with arrangements substantially different from the elastic distribution, tended to yield at failure (see Figure 121). The only bars that did not yield at failure tended to be bars very close to the spiral confinement where, in fact, excessive reinforcement makes yielding difficult. This series showed conclusively that general zone specimens, designed by radically different strut-and-tie

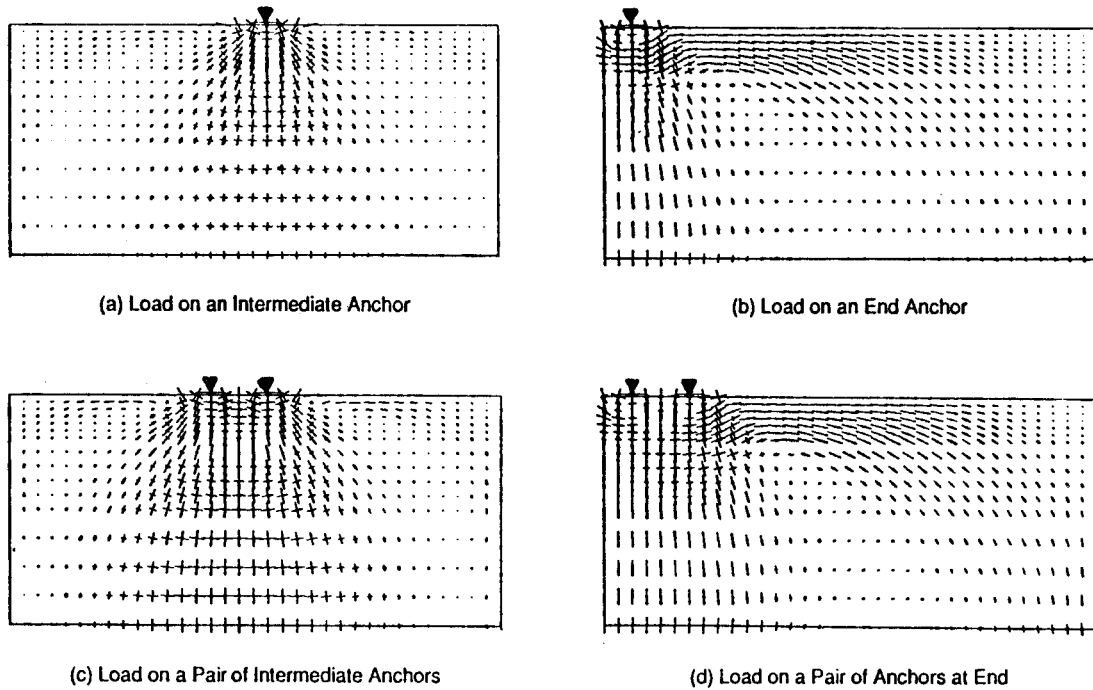


Figure 109. Horizontal plane principal stresses under varied loading configurations.

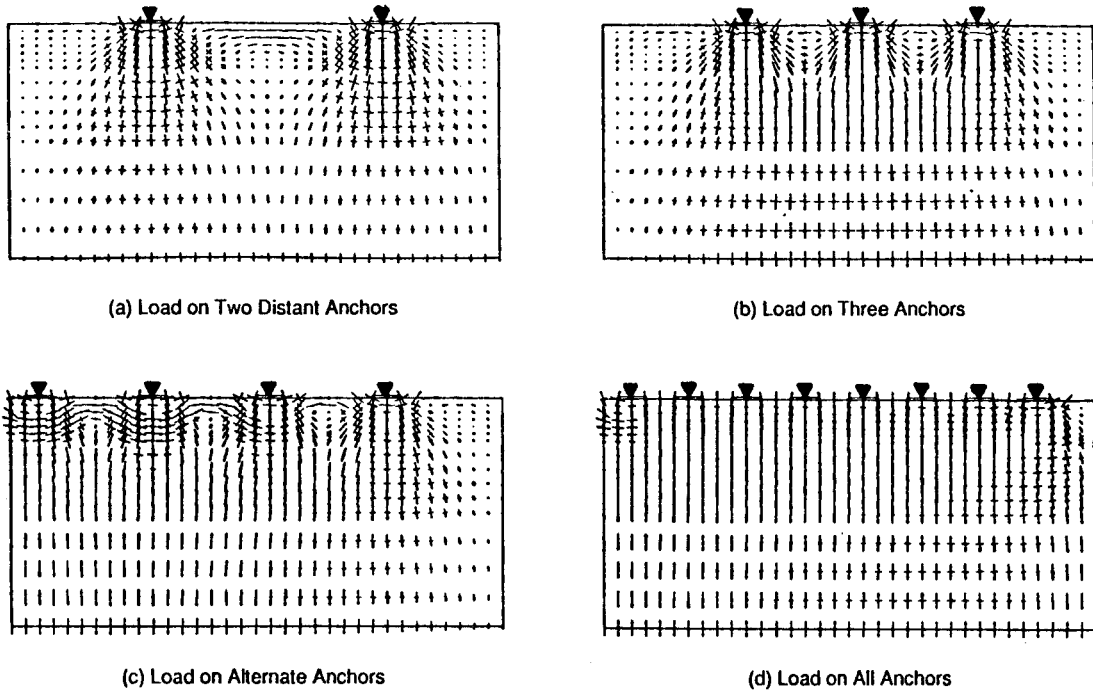


Figure 110. Horizontal plane principal stresses during stressing sequence.

models, could perform very well and had sufficient plasticity to allow very different reinforcement distributions to work effectively. The tensile contribution of the concrete prior to cracking was extremely significant. The maximum stressing load allowed under AASHTO or ACI rules would be approximately 80 to 81

percent F_{pu} . Note from Table 14 that actual cracking loads for all specimens are above these values. The local or general zone reinforcement has little influence on the cracking load. Surprisingly, the presence of the duct hole in specimen B7 did not seem to affect the cracking load significantly, even though the loss in

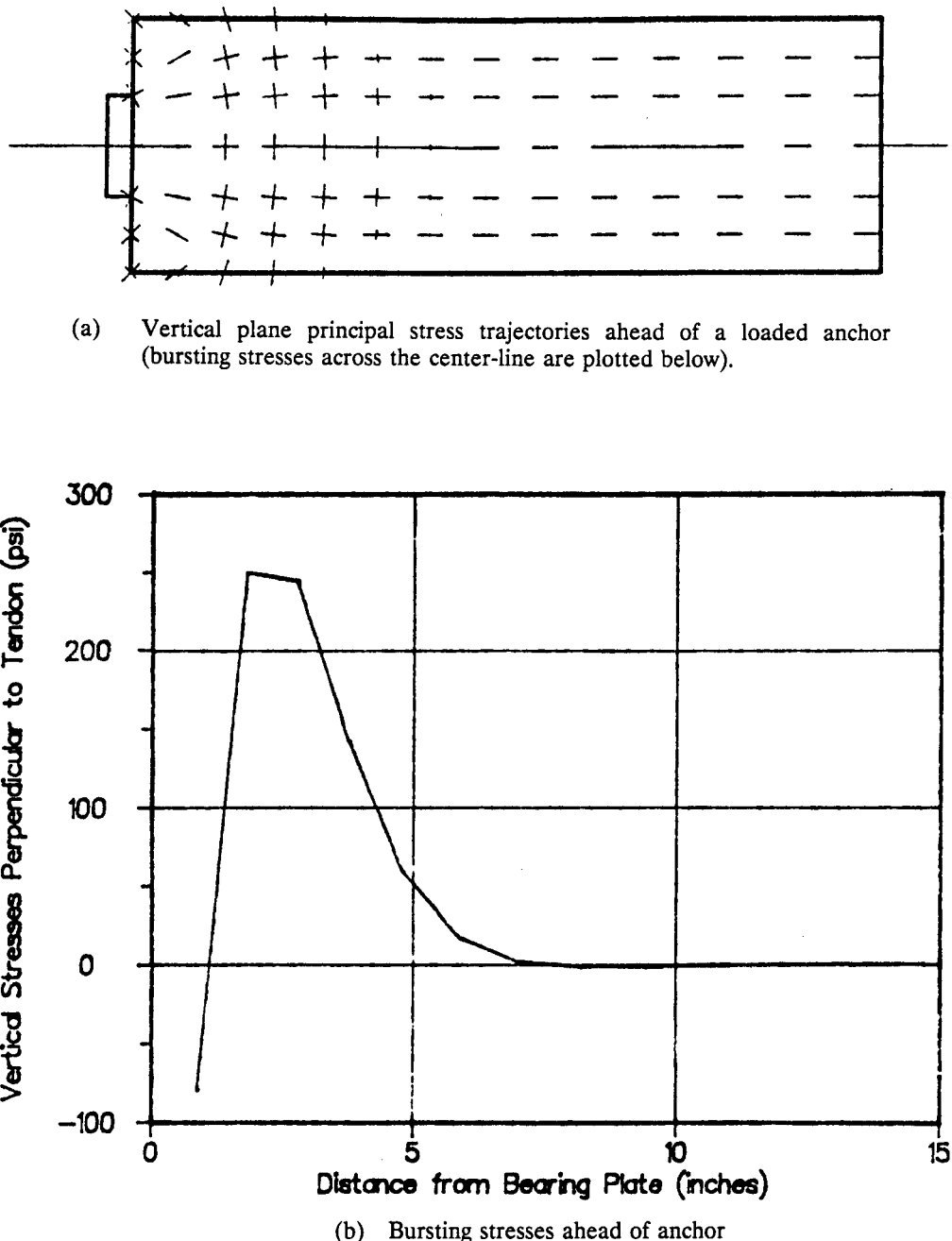


Figure 111. Vertical plane bursting stresses.

net area across the plane amounts to 23 percent. This is a surprising result considering that the first crack started along the path of the tendon duct. This contradictory result may be caused by the large scatter normally exhibited by the tensile strength of concrete, and by the strength provided by the corrugated steel duct itself.

It is apparent from the considerably lower ultimate load of specimen B5 that the general zone reinforcement is crucial. If no general zone reinforcement is provided, the ultimate load is

only 23 percent more than the cracking load. In all other cases, the ultimate load was 50 to 80 percent larger than the cracking load.

Specimen B6 did not have any local zone reinforcement, but nonetheless reached 88 percent of the load of B4. The nominal bearing stress under the anchor plate was $1.3 f_c'$ at failure. This confirms the necessity of including local zone reinforcement in order to avoid a local zone failure and to develop the full strength predicted by the strut-and-tie model.

Specimen B7 had exactly the same reinforcement as B4, but

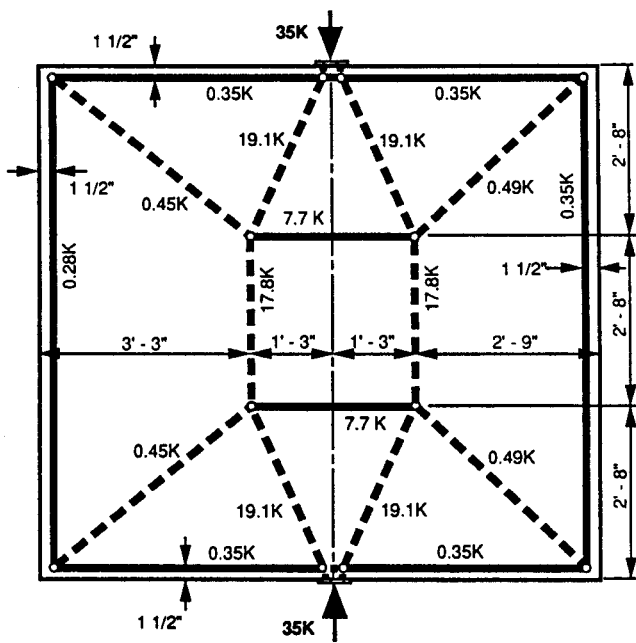


Figure 112. Horizontal plane strut-and-tie model 1 for load on an interior anchor (based on principal stress distribution at cross sections).

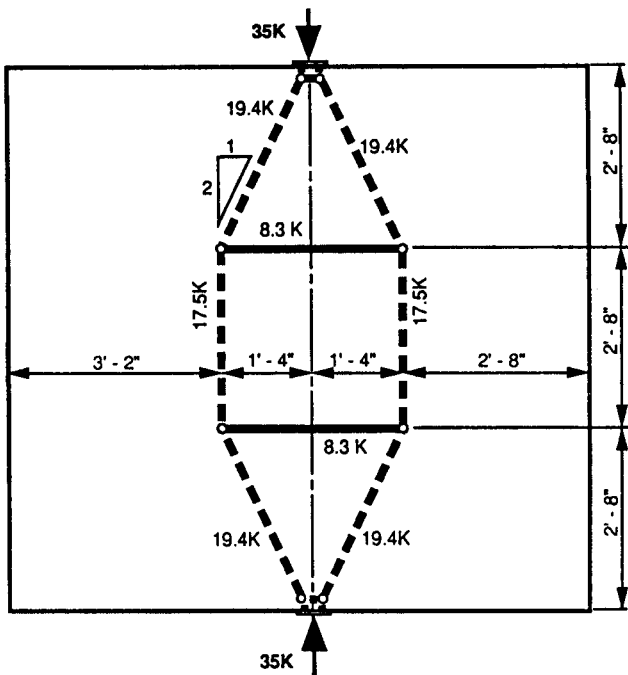


Figure 113. Horizontal plane strut-and-tie model 3 for load on an interior anchor (struts maintain 2:1 slope with two bursting ties at one-third points).

included a tendon duct. The ultimate load was 87 percent of the load of B4. The difference in ultimate strength may be caused by the high level of bearing stresses under these plates ($1.48 f'_c$ for B4 and $1.43 f'_c$ for B7), perhaps indicating a contributory failure of the local zone.

Specimen B8 is identical to specimen B7, except for having been loaded through a smaller wedge plate. Specimen B8 reached a lower ultimate load than B7, presumably because the flexibility of the anchorage plate made the stress distribution under the plate nonuniform. To take into account the flexibility of the plate, it is possible to consider a plate smaller than it is in reality. Assuming a diffusion angle of the stresses of 45 deg. through the steel plate, the effective diameter of the loading plate would only be 6 in. Using this value, the predicted ultimate load from the strut-and-tie model is 315 kips. The ratio of the predicted ultimate load to the actual value is 0.88, which is very close to the result obtained for specimen B7 (0.89). This example shows that it may be possible to take the flexibility of the anchorage device into account by considering a reduced anchorage size in the design.

Tests with Multiplane Anchors

The "C" series consisted of a simple $8\frac{1}{2}$ -in. by 36-in. by 72-in. specimen with a $7\frac{1}{2}$ -in. strand multiplane anchor and a substantially reduced a/h ratio of 0.18. Material properties and test results are given in Table 15. Details are in Appendix C.

In general, this specimen behaved much like the concentric bearing plate specimens of series "B", except for substantially lowered cracking and ultimate load ratios, probably because of the greatly reduced a/h ratio and the much higher localization of the force application with the small anchor device. All bursting reinforcement yielded, and gages mounted across some of the bursting reinforcement bars showed the importance of extending the bars across the full width of the anchorage zone and providing full development of the bars. Crack width was fairly well controlled until 350 kips when yielding of the bursting reinforcement occurred, and the centerline crack propagated to the specimen base. Gages on the transverse spiral indicated relatively low strains.

Tests with Lateral Post-Tensioning

Test series "TPT" consisted of four 10-in. by 18-in. by 42-in. specimens with the same multiplane anchors as C1, and with identical geometry and nonprestressed reinforcement. The only variables were the position and the amount of lateral post-tensioning (see Table 16). All lateral post-tensioning was carefully controlled to monitor and minimize losses. The applied lateral post-tensioning force was unbonded, and increased only 10 to 15 percent at ultimate due to specimen splitting. The effects of lateral post-tensioning calculated by Burdet (48) using a finite element analysis are shown in Figure 122. The post-tensioning force curves are additive to the concentric load curve. Figure 123 shows the predicted resultant for specimen TPT4, with and without lateral post-tensioning at the actual cracking load. It can be seen that there is a very large decrease in the maximum tensile stress (about 40 percent). The actual test results showed marked decreases in cracking loads due to lateral post-tensioning, but considerably less than the analysis predicts. In addition, the crack width data given in Table 17 shows that the lateral post-tensioning in TPT2, TPT3, and TPT4 were effective in substantially reducing crack widths when compared to TPT1, which had

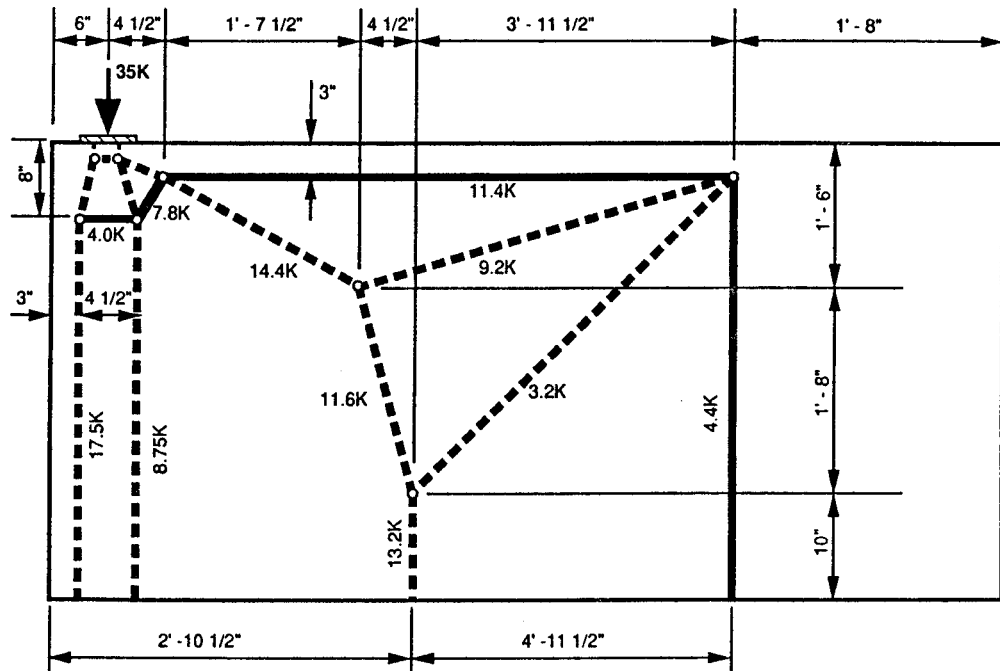


Figure 114. Horizontal plane strut-and-tie model for load on an end anchor.

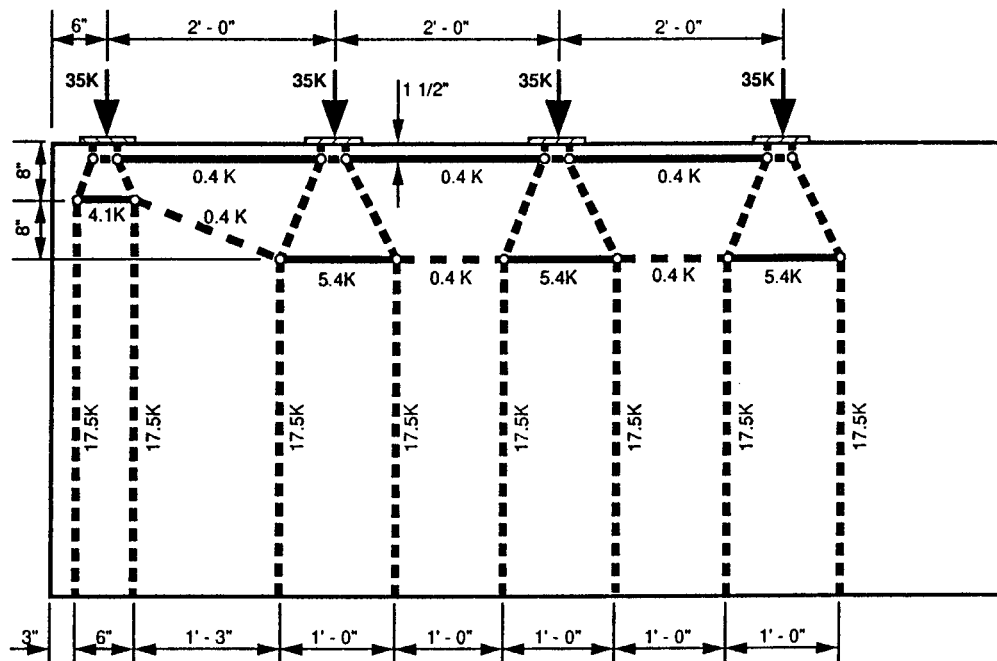


Figure 115. Horizontal plane strut-and-tie model for load on an alternate anchor.

no lateral post-tensioning. At levels close to $F_{pu} = 289$ kips, the higher level of post-tensioning in TPT3 and TPT4 was more effective. In addition to the longitudinal bursting crack on the wide face from the main anchor, a vertical crack was also found on the narrow face as the load increased (see Figure 124). Anchor load-displacement curves again showed some limited ductility, with the maximum load level being able to be sustained for

greater axial deformation in the laterally post-tensioned specimens.

Prediction of First Cracking Load

The prediction of the first cracking load may be important in some special applications of post-tensioned construction. There

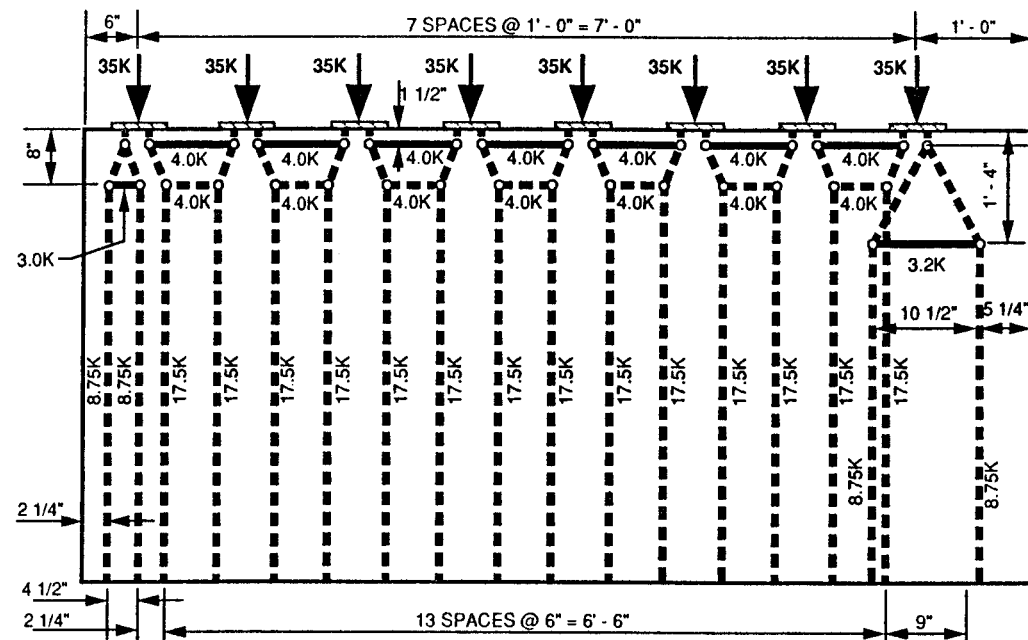


Figure 116. Horizontal plane strut-and-tie model for loads on all anchors.

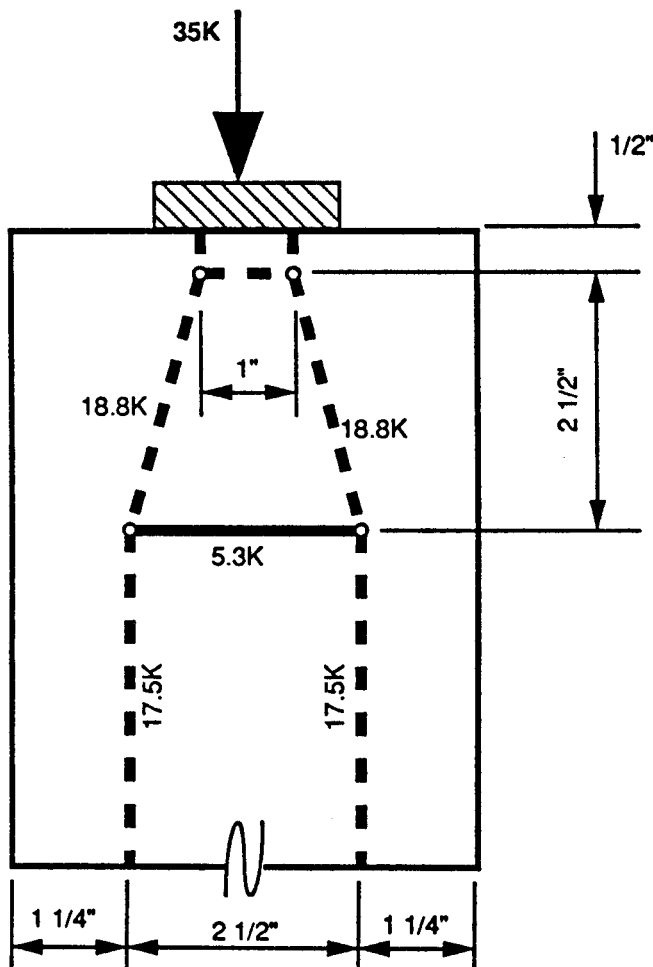


Figure 117. Transverse slab plane strut-and-tie model.

are instances when post-tensioned concrete is used in highly corrosive environments and it is important that it stay uncracked. It is usually acceptable to have very well controlled and very narrow cracks. In those applications where it is important for the anchorage zone to remain uncracked, it is desirable to have a crack predictive method.

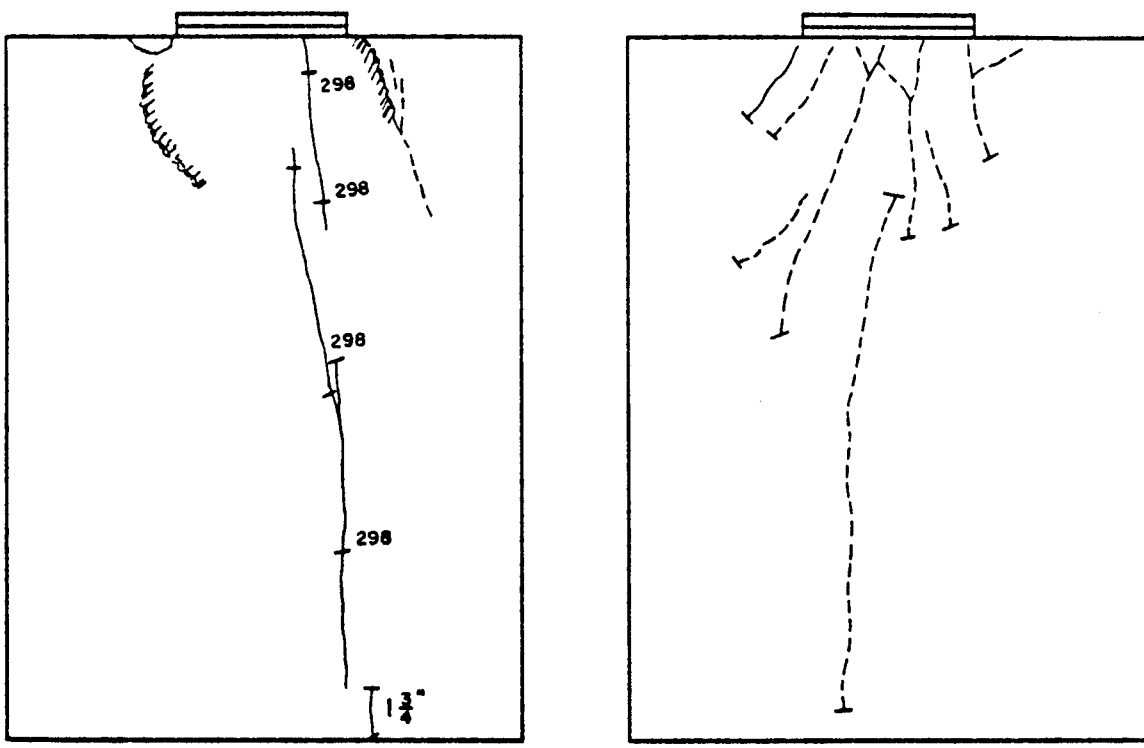
Sanders (1) emphasizes that it is difficult to determine the actual cracking load, even in well-controlled experiments. Even measured internal strains were not reliable indicators. In this study, cracking loads are first visual observations of cracking. Initial crack widths are of the 0.001-in. magnitude and hard to detect. Tensile strengths are based on measured split cylinder test values. The test specimens are unrestrained; in actual structures, restraint effects due to shrinkage, temperature, and creep, as well as construction imperfections, could substantially lower cracking loads. Effects of discontinuities like ducts are neglected.

In a comprehensive evaluation of first cracking predictions models, Sanders (1) showed that the greatest accuracy was obtained by matching the elastic peak bursting stress predicted by a finite element analysis to the effective tensile strength of the concrete, as measured by the split cylinder strength and corrected by the triaxial stress criterion of Ottosen (44). The latter connection is necessary because the level of orthogonal compressive stress in the standard split cylinder test is well below the level of compressive stress in the critical region of the anchorage zone. As shown in Table 18 under the heading "Accurate Procedure", this results in an average ratio of Test/Predicted of 1.05 and a standard deviation of 0.21.

A much simpler and more conservative approach is to modify the finite element analysis results by using a transformed section calculation to account for duct holes and duct material, but then to base the tensile capacity of the concrete on a nominal $4.2 \sqrt{f'_c}$ which represents a rough reduction to allow for the triaxial effect. Results of these calculations are given in Table 18 under the heading "Lower Bound Procedure". The average for this procedure is a more conservative 1.26, but the standard deviation

Table 13. Information for specimens A1 to A4

Specimen	Concrete		Anchor	Local Zone Confining Reinforcement	General Zone Bursting Reinforcement	% F_p (289k)		
	f_{sp} (psi)	f_c' (psi)				1st Cracking Load	Yield Load	Ultimate Load
A1	308	3360	2PL 6" X 12" X 1"	2-2" x 4" grid #3 bars @ 2" centers, 1 @ 1", 1 @ 1-3/4" from anchor	4 - #5 bars 2 @ 10", 14"	1.03	None	1.03
A2	308	3360	Same	Same	12 - #3 bars, 2 @ 6", 11", 16", 21", 26", 31"	0.78	0.95	0.95
A3	314	3480	Same	Same	6 - #4 bars, 2 @ 7; 11; 15"	0.87	None	0.92
A4	330	3840	Same	Same plus local transverse PT	12 - #3 bar, 2 @ 6", 10", 14", 19", 25", 31"	1.04	1.51	1.51



(a) Left side

(b) Right side

Figure 118. Crack patterns, specimen A1.

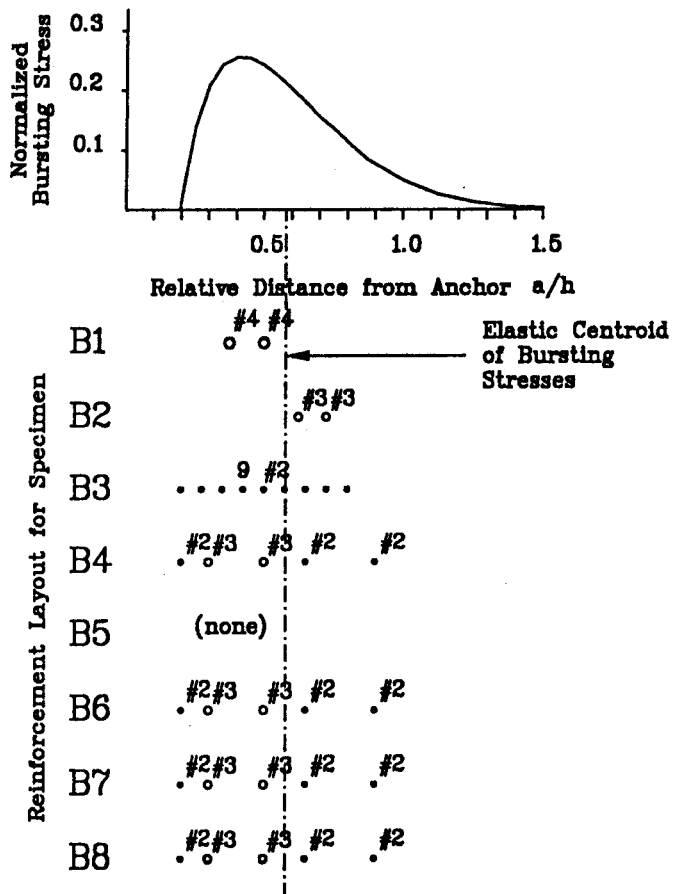


Figure 119. Bursting stress and distribution of general zone reinforcement for specimens B1 to B8.

is slightly reduced to 0.18. Most importantly, not one of the cracking loads is underestimated by more than 1 percent. Such a procedure may be useful in those infrequent cases where no cracking is desired.

Prediction of Ultimate Load

Currently used procedures for anchorage zone analysis basically use simplified expressions, such as Guyon's (Eq. 5), to predict maximum bursting capacity coupled with a check of bearing stresses. Current design practice does not check compressive stresses except the bearing stresses immediately ahead of the bearing plate. It was shown previously that Guyon's equation and the strut-and-tie model results for tension controlled capacity are virtually identical. Table 19 gives the capacities of all concentric tendon specimens as computed by current procedures, and compares them to test results. In Table 19 and similar tables, the lowest predicted value for the possible failure modes of each specimen is underlined and should be considered as the governing predicted load. The average is a respectable 1.15 and the standard deviation is 0.28. The only seriously unconservative specimens are the "A" series which failed in the compressive zones ahead of inadequate local zones. Several of these specimens have unacceptably low values.

The basic strut-and-tie model, developed earlier in the section on analysis, assumes that the internal load distribution at the end of the anchorage zone will be essentially that indicated by elastic analysis. Computations can then be made of anchor load capacity as governed by the tensile ties, the compression struts, the discrete local zone nodes, and the critical sections where the compressive struts and the nodes intersect. Detailed calculations for the capacities are based on yield forces in the tensile ties, local zone node capacity as recommended by Roberts (4) and expressed by Eq. 7, and unconfined compressive strut capacity based on an assumed effective compressive stress capacity of $v_e f'_c = 0.7 f'_c$. The value of v_e of 0.7 was chosen as appropriate for the generally uncracked compression struts of an anchorage zone at time of stressing. These detailed calculations by Sanders (1) are also based on the assumption of local zone subnodes or secondary local zone nodes at the anchor plate quarter points, as shown in Figure 125.

Based on failure observations, the shape of the node was assumed to be a pyramid. In this and several previous studies (4,9,13), a pyramid or cone was observed under the loading plate when a bearing failure occurred. The depth of the pyramid can be determined from the width of the anchorage device in each of the principal directions. The height of the triangle is taken to be half of the plate width in the direction under consideration. In a concentric anchorage zone, the forces in both the elastic state and the plastic state divide evenly on either side of the specimen centerline. Therefore, the node is symmetrical.

The struts in the anchorage zone are excellent examples of Schlaich's (2) bottle struts shown in Figure 126(a). The struts will continue to increase in width as the compressive forces move away from the anchorage device until they reach a uniform stress distribution. An approximation of this spreading is shown in Figure 126(b). The width of the compression strut is assumed to be equal to twice the distance from the section centerline to the centerline of the strut as measured normal to the strut axis. However, the struts cannot overlap or extend outside the section.

Four checks were made to verify the strength of the nodes and compressive struts: (1) local zone bearing capacity ahead of the loading surface including confinement effects; (2) nodal compression capacity perpendicular to the tendon path; (3) compressive strut capacity at the node-strut interface; and (4) strut compressive capacity as the strut leaves the confined local zone and/or when the section thickness changes.

Table 20 is a summary of the predicted loads for all the failure modes for the concentric anchorage specimens. The minimum or governing load predicted for each specimen is underlined. The tension tie was predicted as the controlling failure mode for all of the tests except specimens A1, A2, A3, A4, B5, and B6. Specimen B5 is shown as a compression failure, because the theoretical STM tie failure (0 kips) is not reasonable because of the large concrete tension contribution. Specimen B6 had all of the tension tie reinforcement yield prior to failure, but did show considerably less post-maximum load ductility than specimen B4. Note that the test-to-predicted ratio for this specimen is the highest of all of the series "B" specimens. The compression failure predictions for the "A" series specimen are confirmed by the experimental results. The maximum bursting reinforcement strains measured in specimens A1, A2, and A3 were below 70 percent of their yield value. The strut-and-tie model is supposedly a *lower bound* model. It predicts a conservative load for all the tests except specimens B2 and B5, which are respectively only 1 and 3 percent unconservative. On the average, the model is

Table 14. Information for specimens B1 to B8

Specimen	Concrete		Anchor	Local Zone Confining Reinforcement	General Zone Bursting Reinforcement	1st Cracking Load % F_{pu} (289k)	Yield Load % F_{pu}	Ultimate Load % F_{pu}
	f_{sp} (psi)	f'_c (psi)						
B1	464	5380	6-1/2" x 61/2" x 1"	#4 spiral, 7: diam., 1-1/4 pitch, 7 turns	4 - #4 bars 2 @ 7-3/8", 9-7/8"	1.15	2.10	2.10
B2	464	5380	Same	Same	4 - #3 bars 2 @ 12-1/2", 14-5/8"	1.07	1.61	1.67
B3	464	5380	Same	Same	18 - #2 bars 2 @ 4, 5-3/4, 7-1/2, 9, 10=1/2, 12, 13-1/2, 16-1/4, 18	1.25	1.32	1.90
B4	464	5380	Same	Same	6 - #2 and #4 bars #2 - 2 @ 4-1/8, 13- 1/8, 18-1/2 #3 - 2 @ 6, 10-3/8	1.15	1.32	1.94
B5	420	5320	Same	Same	None	0.98	N/A	1.21
B6	420	5320	Same	None	6 - #2 and 4 - #3 #2 - 2 @ 4, 13, 18 #3 - 2 @ 6, 10	0.98	1.06	1.71
B7	420	5320	Same w/ 2-1/8" diam. hole	Same	Same as B6	0.98	1.20	1.70
B8	420	5320	Same w/2-1/9" diam hole loaded through 4" diam. PL	Same	Same as B6	0.90	1.15	1.59

32 percent conservative with a coefficient of variation of 19 percent. This is quite acceptable for this type of application for a design model.

Sanders (1) also explored, in depth, reasons for the very conservative prediction when using the basic strut-and-tie model. Using a beam-column theory, he showed that the centroid of forces at the end of the anchorage zone can shift appreciably from the elastic theory locations assumed in the basic STM. He developed a modified STM, which allowed the strut locations to move inward until tension failure capacity balanced compression failure capacity. This reduced the overall average of test-to-predicted for the concentric anchors to 0.98 with a standard deviation of 0.26. However, unconservative results as low as 0.68 occurred. He observed that this seemed to be in specimens with long spirals, and suggested that confinement effectiveness may diminish with length. When the depth of confined concrete was assumed as no more than the plate width for longer spirals, the agreement was a more conservative average of 1.12 with a standard deviation of 0.17. This improvement indicates that further application of plasticity can refine STM.

The overall conservatism of the STM is also due to the deliberate neglect of concrete tensile capacity. Such capacity definitely contributed to specimen strength and, in many practical applications, could further increase capacities.

On the basis of the extensive tests of this program as well as checks with other investigators' specimens, the strut-and-tie model approach for the general zone was found to be a conservative and sensitive way of estimating the ultimate strength of the specimens. Since it had been shown in Figures 60 and 65 that results of STM and FEA showed good agreement for concentric anchors, the same general conservatism could be obtained with elastic analyses with similar tensile and compression limits.

Anchorage with Single Straight Eccentric Tendons

Eccentric anchorage zones can be divided into two groups: those located inside the section kern and those located outside the section kern. As shown in Figure 65, very different stress patterns result.

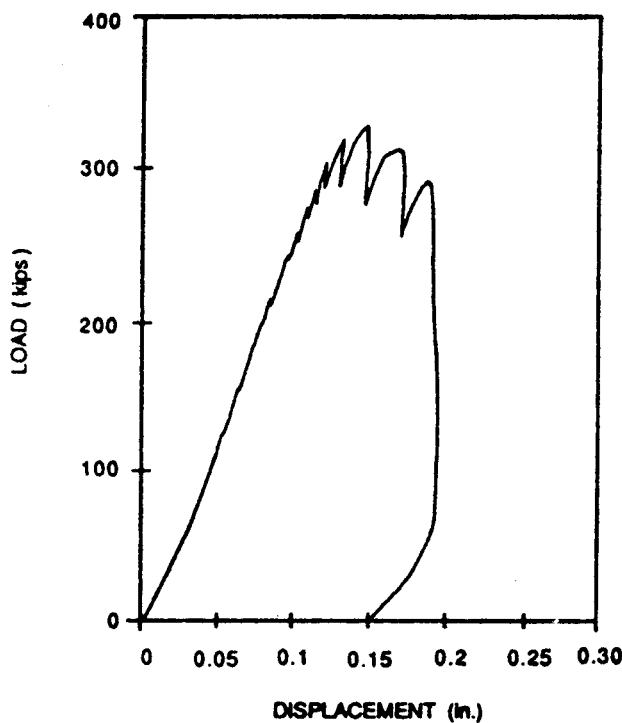


Figure 120. Load-displacement curve, specimen B3.

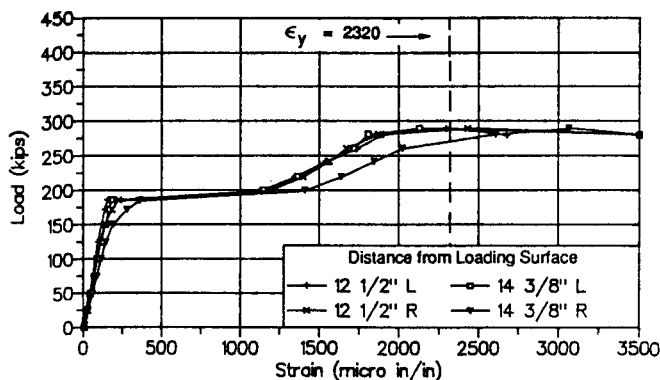


Figure 121. Bursting strain data, specimen B2.

Seven eccentric specimens were tested. Two had the anchor located at the kern, while five had the anchor axis outside the kern. The test procedures for the eccentric anchorage specimen series were generally identical to the concentric anchorage test series.

Tests with Anchors at the Kern

Two specimens had anchors at the kern (E1: 11 in. by 36 in. by 72 in.; E5: 8.5 in. by 35 in. by 72 in.). Both were loaded through spherical loading heads, after being leveled at the base with metal shims and set in hydrostone. Table 21 gives the basic information for specimens E1 and E5.

Specimen E1 was heavily reinforced with 16 #3 Grade 60 reinforcing bar ties ($f_y = 67$ ksi) and an 80 ksi spiral. If all the reinforcement along the tendon axis was effective, the total tension bursting resistance force would be 235 kips with a centroid of 25 in. measured from the loading surface. Its flat plate anchor was designed for four 0.6-in. diameter strands. Cross ties, #2 bar ($f_y = 72$ ksi), were included to carry any bursting forces caused by the transverse spreading of the forces.

Specimen E5 had a thinner section and much less bursting reinforcement than specimen E1. The total bursting reinforcement tension capacity was 73.4 kips with a centroid 10.8 in. from the anchorage plate, neglecting reinforcement well outside the general zone at 58 in. and 70 in. Number three cross ties were furnished on each side of the spiral to a depth of 15 in. ahead of the anchor, which was a plate anchor for four 0.5 strands. In E1, the bursting reinforcement deeper in the specimen was just approaching yield at failure, while it appeared that bursting reinforcement within about $1\frac{1}{2}$ plate width depth had yielded. In E5, fully plastic behavior was exhibited by the bursting reinforcement, with the bursting force almost evenly distributed between the four reinforcement layers. Both specimens showed some ductility, with maximum displacement of the anchors about 50 percent greater than the displacement at peak load. Table 21 indicates both specimens had high cracking and ultimate loads for the rated capacity, F_{pu} , of the anchor plates.

Tests with Anchors Outside the Kern

Four single tendon specimens and one double tendon specimen (M5) were loaded through a spherical head with the load axis

Table 15. Information for specimen C1

Specimen	Concrete		Anchor	Local Zone Confining Reinforcement	General Zone Bursting Reinforcement	% F_{pu} (289 k)		
	f_s (psi)	f'_c (psi)				1st Cracking Load	Yield Load	Ultimate Load
C1	379	5190	6-1/2" x 6-1/2" multiplane	#4 spiral, 1-3/4 in. pitch, 7 in. diam., 6 turns	8-#3 bars 2 @ 7-1/2, 12-1/2, 17-1/2, 22-1/2	0.78	1.21	1.28

Table 16. Information for TPT series

Specimen	Concrete		Anchor	Local Zone Confining Reinforcement	General Zone Bursting Reinforcement	Lateral Post Tensioning		Yield Load % F_{pu}	Ultimate Load % F_{pu}
	f'_c (psi)	f'_s (psi)				Force (kips)	Location (in.)		
TPT1	326	4950	6-1/2" x 6-1/2" multiplane	#4 spiral, 1-3/4 pitch, 8" diam., 5 turns	8 - #2 bars: 2 @ 5-1/2, 9-1/2, 13-1/2, 17-1/2	0	-	0.69	1.04
TPT2	326	4950	Same	Same	Same	10.2	10.5	0.78	1.07
TPT3	409	5150	Same	Same	Same	28.9	5	0.93	1.28
TPT4	326	4950	Same	Same	Same	20.3	5	0.83	1.14
									1.15

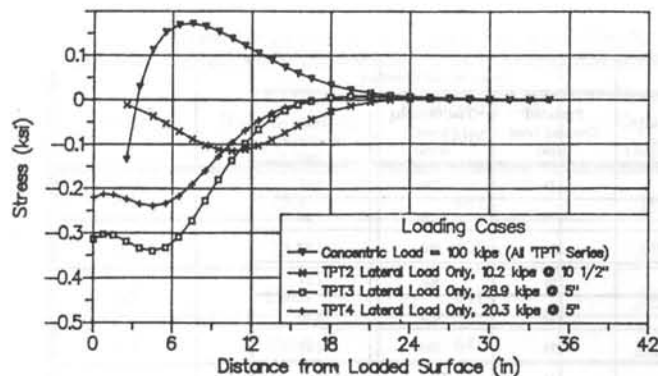


Figure 122. Lateral post-tensioning stress results.

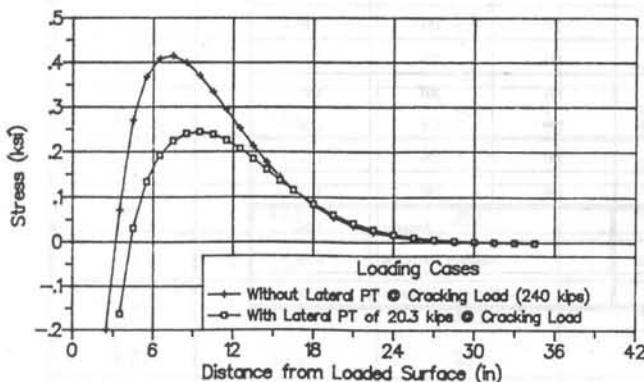


Figure 123. Effect of lateral post-tensioning on bursting stress distribution, specimen TPT4.

Table 17. Crack summary for TPT series

Specimen	Maximum Bursting Crack Width (in.)		
	275 kips	300 kips	Ultimate
TPT1	0.010	0.025	0.055
TPT2	0.006	0.016	0.030
TPT3	No Crack	0.001	0.038
TPT4	0.002	0.005	0.033

outside the kern. Three specimens (E2, E3, E4) were 11 in. by 36 in. by 72 in. and had plate anchors for 4-0.6 in. strands. The other specimen (E6) was 10 in. by 36 in. by 72 in. and had a multiplane anchor for 7-0.5 in. strands. Key information is given in Table 21. Specimens E2, E3, and E4 were used to examine the effects of longitudinal edge tension stresses and spalling stresses shown in Figure 65. Specimen E2 was the control specimen (details in Appendix C). The specimen was heavily reinforced with #3 and #4 Grade 60 ($f_y = 67$ ksi) reinforcing bars. The total tension bursting capacity was 248 kips with a centroid of 23.0 in. from the loading surface. The total tension capacity of the spalling reinforcement and the longitudinal edge tension reinforcement was 68.5 kips. Transverse bursting forces were carried by #2 cross ties.

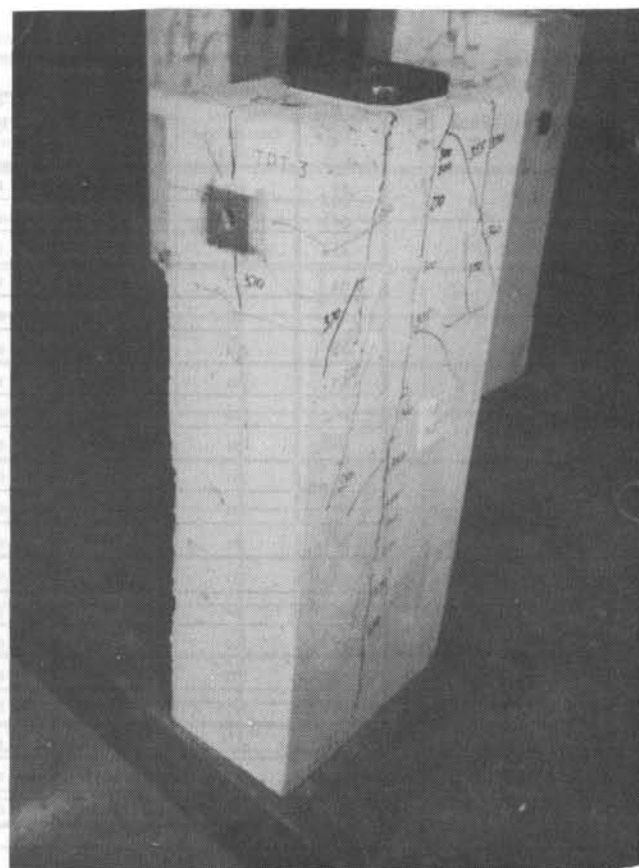


Figure 124. Specimen TPT3 crack pattern on transverse face.

The cracking patterns were extensive in specimen E2 with cracking occurring on all of the exposed concrete surfaces. Figure 127 shows the southeast corner of the specimen underneath the loading plate. Because the anchorage plate was only 6 in. from the south surface, the concrete capacity was not enough to carry the transverse bursting force. The transverse spreading of forces caused vertical and diagonal cracking on the south face. Cracking also occurred in the spalling region (see Figure 128). The first crack on the loaded surface occurred at 360 kips ($1.55 F_{pu}$). The cracks extended over the full thickness of the section but only extended 2 in. into the specimen. The strain gages indicated the maximum spalling force was 12.9 kips at an applied load of 500 kips (2.6 percent). A crack formed at 250 kips ($1.08 F_{pu}$) on the longitudinal edge tension face (north face, see Figure 129). Longitudinal edge tension cracks extended onto the west and east faces for a maximum of 10 in. The elastic analysis indicated that the longitudinal edge tension force should be 12.5 percent of the axial load. The maximum longitudinal edge tension force determined from the reinforcement strains was 10.5 kips at an axial load of 500 kips (2.1 percent). This was well below the 12.5 percent that was calculated.

During reapplication at the ultimate load, most of the concrete outside the reinforcing bars and immediately ahead of the anchor spalled off (see Figure 130) showing the crushed cone of confined concrete under the anchor. While first cracking was lower than E1, yield and ultimate load levels were similar and slightly higher. This specimen indicated that elastically determined

Table 18. First crack prediction

Specimen	Accurate Procedure			Lower Bound Procedure		
	Predicted Cracking Load (kips)	Test Cracking Load (kips)	Test/Predicted	Predicted Cracking Load (kips)	Test Cracking Load (kips)	Test/Predicted
A1	189	298	1.57	179	298	1.67
A2	189	226	1.19	179	226	1.26
A3	194	250	1.29	182	250	1.37
A4	207	300	1.45	191	300	1.57
B1	201	200	0.99	173	200	1.15
B2	201	186	0.92	173	186	1.07
B3	201	217	1.08	173	217	1.25
B4	201	200	0.99	173	200	1.15
B5	191	170	0.89	172	170	0.99
B6	191	171	0.90	172	171	0.99
B7	191	170	0.89	135	170	1.26
B8	181	156	0.86	120	156	1.30
C1	271	225	0.83	181	225	1.24
TPT1	184	200	1.08	131	200	1.53
TPT2	230	225	0.98	179	225	1.26
TPT3	272	270	0.99	230	270	1.18
TPT4	261	240	0.92	216	240	1.11
		Average	1.05			Average
		Standard Deviation	0.21			Standard Deviation
		Coefficient of Variance	0.20			Coefficient of Variance
						0.15

amounts of spalling and edge tension reinforcement were over-conservative, possibly because of significant tensile concrete contributions.

Specimen E3 had the same reinforcement as specimen E2, but differed in that thin plastic sheets were placed in the concrete in the regions of longitudinal edge tension and spalling to eliminate any tension concrete contribution. The first cracking load on the bursting faces occurred at a somewhat higher load level than for E2 (see Table 21). The cracking patterns were very similar to those of specimen E2. On the loaded surface and the longitudinal edge tension surface, the cracks were initially restricted to the location of the crack formers. On the loaded surface, a crack eventually opened between the crack former and the edge of the plate. On the longitudinal edge tension surface, additional cracks opened both above and below the crack former. The strain data from the spalling region and from the longitudinal edge tension force region showed significant strain increases from the beginning of the test. This indicates that the reinforcement was carrying most of the load and that there was negligible concrete tension contribution.

Neither spalling nor edge tension reinforcement strains exceeded 50 percent of yield strain at failure. Both strains were very close together but showed these forces to be about 4.5 percent of the axial load at failure, rather than the 12.5 percent predicted by combined stress analysis. Bursting reinforcement within 12 in. of the loaded surface yielded before failure. At ultimate, the concrete ahead of the anchorage plate bulged out and could be removed by hand.

Specimen E4 had essentially the same bursting steel as specimens E2 and E3, but only 22 percent of the spalling and edge

tension reinforcement. The first cracks in specimen E4 occurred on the spalling stress surface and the longitudinal edge tension surface at 225 kips (0.97 F_{pu}). The first bursting crack occurred at lower loads than in E2 and E3. The cracking patterns were similar to those of specimens E2 and E3 except that the cracks in the loaded surface and longitudinal edge tension regions were much longer. The ultimate load and failure mode were about the same as that for E2 and E3.

The bursting steel strain data showed that, although bars within 11 in. of the loaded surface yielded, most of the deeper bursting reinforcement was not well used. Even though the total areas of longitudinal edge tension and spalling reinforcement in specimen E4 were greatly reduced from those in specimens E2 and E3, they were well below yield. Clearly, elastically determined spalling and edge tension stresses are very conservative and this specimen, with substantially less reinforcement for spalling and edge tension, developed the same ultimate load levels as E2 and E3.

The first cracking load was significantly reduced in comparison to the bearing plate anchor specimens. This reduction was both in absolute load terms as well as percentage of rated ultimate. The ultimate load was significantly reduced, reflecting the greatly reduced amount of bursting reinforcement. All bursting reinforcement within 12 in. of the anchor surface yielded, but spalling reinforcement only reached 50 percent of yield.

Specimen E6 had a decreased eccentricity, e/h , of $\frac{1}{4}$ and a multiplane anchor. The specimen was 9 percent thinner than specimens E2, E3, and E4 and had significantly less bursting steel. The total tension capacity of the bursting steel was 36.7 kips at a centroid of 13.9 in. from the loading surface. The

Table 19. Current design procedure ultimate load prediction for concentric specimens

Specimen	Bursting Reinforcement $A_f y$ (kips)	Predicted Load (kips)	Bearing Capacity (kips)	Controlling Load (kips)	Ultimate Load (kips)	Peak/Predicted
A1	73.9	443	<u>340</u>	340	298	0.88
A2	79.8	479	<u>340</u>	340	275	0.81
A3	106.8	641	<u>340</u>	340	265	0.78
A4	106.8	641	<u>544</u>	544	437	0.80
B1	50.8	<u>342</u>	639	342	366	1.07
B2	29.4	<u>198</u>	639	198	290	1.46
B3	39.6	<u>267</u>	639	27	331	1.24
B4	42.6	<u>287</u>	639	287	337	1.17
B5	0	<u>0</u>	636	0	212	*
B6	42.6	<u>287</u>	<u>218</u>	218	297	1.36
B7	42.6	<u>287</u>	636	287	296	1.03
B8	42.6	<u>261</u>	464	261	276	1.06
C1	52.8	<u>258</u>	450	258	370	1.44
TPT1	26.2	<u>164</u>	462	164	310	1.89
TPT2	38.1	<u>239</u>	462	239	300	1.26
TPT3	55.1	<u>345</u>	471	345	370	1.07
TPT4	49.8	<u>312</u>	462	312	332	1.06

NOTE: Underlined values show which load case controls

* Theoretically infinity and disregarded in average

Average	1.15
Standard Deviation	0.28
Coefficient of Variance	0.25

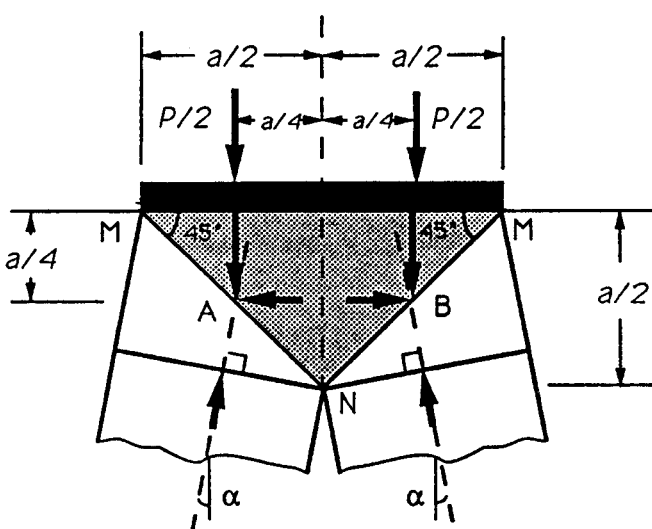


Figure 125. Idealized concentric local zone node

specimen had the same greatly reduced longitudinal edge tension reinforcement as E4, but 10 percent less spalling reinforcement.

Specimen M5 was a rectangular prism 17 in. by 32 in. by 60 in. with an e/h of $\frac{1}{4}$ and had two $7\frac{1}{2}$ -in. strand multiplane anchorage devices located at the same eccentricity. The bursting steel consisted of six #2 ties with a total tensile capacity of 39.4 kips (6.8 percent F_{pu}), and a centroid located 15.25 in. from the loading surface. The spalling and longitudinal edge tension reinforcement tensile capacity was 3.5 percent F_{pu} . The local zone was designed as two separate anchors, and then they were tied together with additional reinforcement. This specimen was similar to E6 in anchor type and eccentricity. First cracking occurred at the same load level when F_{pu} and concrete tensile strength are considered. Failure loads are almost identical in terms of F_{pu} (see Table 21). All of the bursting steel yielded but spalling reinforcement was well below yield. The maximum spalling steel force was only 0.8 percent of the axial load. No spalling cracks were seen during the test. No longitudinal edge tension cracks were observed. At failure, both anchors were still tied together, effectively acting as one larger anchor. This series confirmed the importance of bursting reinforcement, as well

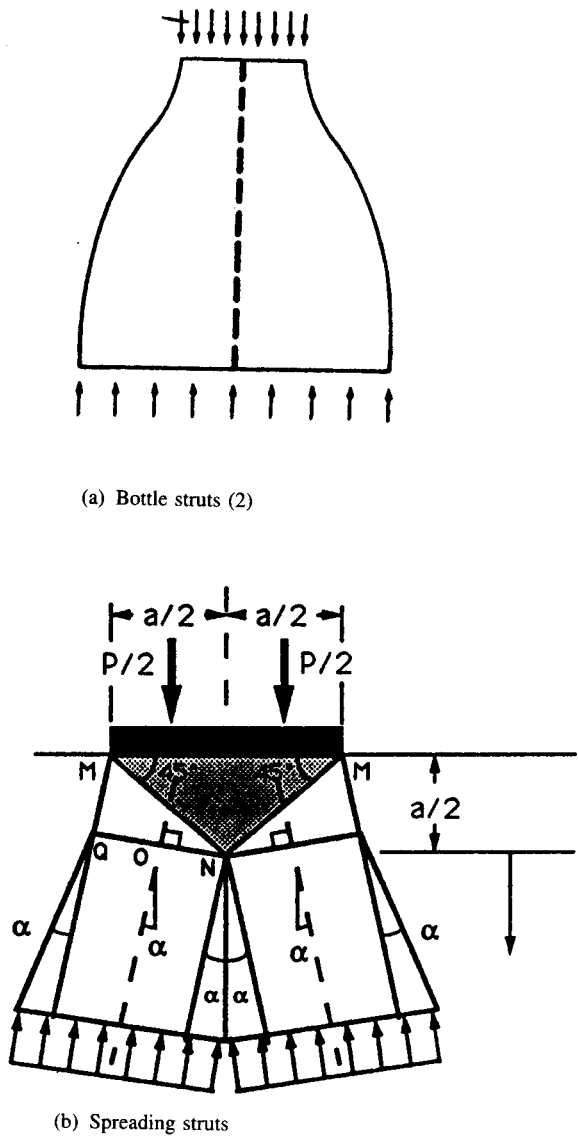


Figure 126. Strut development.

as the ability to vary the failure load by varying the bursting reinforcement. It showed that elastically determined amounts of spalling and edge tension reinforcement were very conservative. Significant reductions of these reinforcements did not seem to affect ultimate load levels very much.

Prediction of First Cracking Load

In eccentric anchorage zones, there are three regions (see Figure 65b) where cracking can occur: bursting, spalling, and longitudinal edge tension. The cracking load in each of these regions was determined by Sanders (1) by matching the best estimate of the actual concrete tensile strength with the elastically computed maximum tensile stress.

The first longitudinal edge tension cracking load was calculated as that which causes a tensile stress on the outer fiber equal to the split cylinder strength. The results were conservative in all applicable cases, with a mean of 1.22 and a standard deviation of 0.12.

The tensile spalling stresses near the loading surface are difficult to determine because of the high stress gradient and the high computed stresses near the edge. They were computed using a finite element analysis by Burdet (48).

Two peak values were compared. The first was the normalized maximum tensile stress on the loaded surface, while the second was stress at a depth of $1\frac{1}{2}$ in. below the loaded surface. Using the stress on the loaded surface had a very conservative average of 2.18 with a standard deviation of 0.77, while utilizing the stresses slightly below the surface yields an average value of 1.04 with a standard deviation of 0.38 and some very unconservative values. This calculation must be termed as relatively unsatisfactory. Fortunately, it is of little importance in actual design.

The methods used to determine the first bursting crack load along the tendon axis for eccentric specimens are the same as those for the concentric specimens. The peak tension stress value was determined from an elastic analysis modified to consider duct hole and duct (48,63). The concrete tensile strength was determined from a split cylinder test and modified to consider the lateral compression stress effects.

Table 22 indicates that the more "accurate" procedures considering the Ottosen triaxial stress criteria result in a quite good prediction of cracking load (average 1.02 and standard deviation of 0.13). The "lower bound procedure" based on an estimated tensile strength of $4.2 \sqrt{f_c'}$ was conservative with an average of 1.39 and a standard deviation of 0.15. Sanders (1) showed a similar level of accuracy to that of the "lower bound procedure" if the tensile stress was determined from Guyon's symmetrical prism theory.

Prediction of Ultimate Load

Currently used procedures for anchorage zone analysis for eccentric anchorages use Guyon's symmetrical prism method (20) to predict maximum bursting capacity coupled with a check of bearing stress. Table 23 gives the capacities of all eccentric tendon specimens, as computed by current procedures, and compares them to test results. All results are essentially conservative, and the two specimens controlled by the symmetrical prism tension tie (E6 and M5) are extremely conservative. The average ratio of test/prediction of 1.89 and standard deviation of 1.21 show that current criteria are overconservative and unrealistic.

The basic strut-and-tie model results using an effective concrete compressive strength of $v_e f_c' = 0.7 f_c'$, and Roberts' confined local zone node capacity, were computed by Sanders (1) and are given in Table 24. All possible failure nodes were checked and the critical ones are underlined. Not shown in this table are the associated STM values for spalling and edge tension. Computations (1) showed that E4 would be governed by edge tension, whereas E6 would be governed by spalling at very low load levels. In fact, as discussed previously, the "inadequate" reinforcements for edge tension and spalling in these specimens did not come close to yielding and the forces obviously redistribute after cracking. Because of this, spalling and edge tension results were not included in Table 24.

Table 20. Basic STM prediction summary for specimens A1 to A4, B1 to B8, C1, and TPT1 to TPT4

Specimen	Tension Tie (kips)	Bearing (kips)	Node-Strut Interface (kips)	L.Z.-G.Z. Interface (kips)	Controlling Load (kips)	Ultimate Test (kips)	Test/Predicted
A1	222	340	<u>195</u>	—	195	298	1.52
A2	213	340	<u>190</u>	—	190	275	1.45
A3	552	340	<u>204</u>	—	204	265	1.30
A4	516	544	<u>306</u>	321	306	437	1.43
B1	<u>299</u>	602	646	533	299	366	1.22
B2	<u>292</u>	602	636	425	292	290	0.99
B3	<u>296</u>	602	642	482	296	331	1.12
B4	<u>277</u>	602	645	511	277	337	1.22
B5	—	599	599	<u>218</u>	218	212	0.97
B6	269	<u>218</u>	261	—	218	297	1.36
B7	<u>269</u>	599	642	511	269	296	1.10
B8	<u>252</u>	567	605	<u>507</u>	252	276	1.09
C1	<u>192</u>	439	528	565	192	370	1.93
TPT1	<u>180</u>	484	550	436	180	310	1.72
TPT2	<u>253</u>	484	550	434	253	300	1.19
TPT3	<u>347</u>	492	564	524	247	370	1.50
TPT4	<u>235</u>	484	554	485	235	332	1.41

NOTE: Underlined values show which load case controls

Average	1.32
Standard Deviation	0.25
Coefficient of Variance	0.19

The use of the basic STM is a conservative but reasonable way to design eccentric anchorage zones. The average of the test to the predicted capacity of the seven eccentric tests was 1.29 with a standard deviation of 0.19. It is important to check all the components of the STM: compression strut stresses, node stresses, and tie strengths. Caution should be exercised when counting on bursting reinforcement at depths where the slope of the strut boundary, between the secondary local zone node and the furthest effective layer of reinforcement, is less than 6 deg. The furthest bar in specimen M5 had an angle of 6.1 deg., and the specimen performed well. However, when reinforcement is placed deep in the section, the local cracking in the section closest to the loading surface may be excessive and the reinforcement may not be fully developed. All of the specimens eventually failed in compression because the force paths were able to adjust to allow higher axial capacity than that predicted by the yielding of the bursting ties. Therefore, the most critical check of the actual failure becomes the compression checks.

Anchorage Zones with Multiple Straight Tendons

To develop the necessary level of post-tensioning force in a girder, it is often essential to use multiple anchorages. Beams with multiple anchorages can have the resultant of the forces either along the centroidal axis of the specimen or eccentric to it. Five multiple anchorage specimens were tested with their resultant force axis along the centroidal axis, while three had the resultant eccentric to the centroidal axis. The objectives of testing multiple anchorage specimens were to determine if the behavior varied from that of single anchors and to verify if models developed for single anchorages would apply.

The test results for each of the multiple anchorage specimens are described in detail in the following discussion. The specimen descriptions are divided into two groups: specimens with concentric force axis and specimens with eccentric force axis. A crack history is given for typical specimens along with strain gage data from the tension reinforcement. The test procedure was identical to that of the concentric test series, but the testing machine and the support conditions varied and will be discussed.

Tests with Concentric Load Axis

The resultant load axis was concentric because the anchorages were symmetrical about the specimen centerline and were loaded simultaneously. Four 8.5-in. by 36-in. by 72-in. specimens examined the effect of spacing between the anchors (M1 to M4), and one 17-in. by 32-in. by 60-in. specimen (M6) studied the effects of tightly grouping four anchorages. Specimen details appear in Appendix C and are summarized in Table 25. Specimens M1 to M4 used 6-in. by 6-in. flat plate anchors for 4-0.6-in. strands. Specimen M6 used 6.5-in. by 6.5-in. multiplane anchors for 7-0.5-in. strands. The elastic stress trajectories for closely spaced anchors in specimen M1 were very similar to those of a single concentric anchorage. The elastic stress trajectories of one plate with clear spacing for specimens M2 and M4 indicated large bursting tension stresses along the centerline of the section, as in the concentric specimens, but the independent behavior of the anchorages became somewhat more pronounced. The stress patterns for specimen M3 (with very wide anchor spacing) were completely different, with a large spalling tension force along the loading face between the anchorages, in addition to two independent bursting tension regions ahead of the anchors.

Table 21. Information for eccentrically loaded specimens

Specimen	Concrete f'_c (psi)	Concrete f'_c (psi)	Anchor	Eccentricity e/h	Local Zone Confining Reinforcement	General Zone Bursting Reinforcement	F_{pu} (k)	1st Bursting Cracking Load $\% F_{pu}$	1st Yield Load $\% F_{pu}$	Ultimate Load $\% F_{pu}$
E1	428	5450	8" x 7" x 1" Plate with 3-1/2" dia. hole		#4 spiral, 2-1/2" pitch, 7-1/4" dia., 5 turns	16 - #3 ties: 1 @ 1, 9 @ 2-1/2, 3 @ 5, 3 @ 10	232	1.49	2.02	2.05
E5	459	5710	6" x 6" x 1" Plate with 2" dia. hole		#4 spiral, 2" pitch, 6-1/2" dia., 3 turns	7 - #3 ties 1 @ 2, 1 @ 5, 3 @ 7, 1 @ 39, 1 @ 12	165	1.30	1.97	2.01
E2	460	5950	Same as E1	1/3	Same as E1	16 - #3 ties 1 @ 1, 6 @ 2, 5 @ 4, 1 @ 5-1/2	232	1.14	2.13	2.16
E3	492	6130	Same as E1	1/3	Same as E1	Same as E2	232	1.29	2.02	2.25
E4	475	5690	Same as E1	1/3	Same as E1	15 - #3 ties 1 @ 3, 5 @ 2, 5 @ 4, 1 @ 5, 3 @ 10	232	1.08	2.11	2.16
E6	443	5650	6-1/2" x 6-1/2" multiplane	1/4	#3 spiral, 2" pitch, 8; dia., 4 turns	5 - #2 ties 1 @ 2, 1 @ 11, 3 @ 7 1 - #3 tie @ 6	289	0.78	1.18	1.20
M5	393	4670	2 - 6-1/2" x 6- 1/2" multiplane	1/4	(each anchor) #4 spiral, 2" pitch, 7" dia., 4 turns	6 - #2 ties 1 @ 1-1/2, 5 @ 5-1/2	578	0.69	1.13	1.17

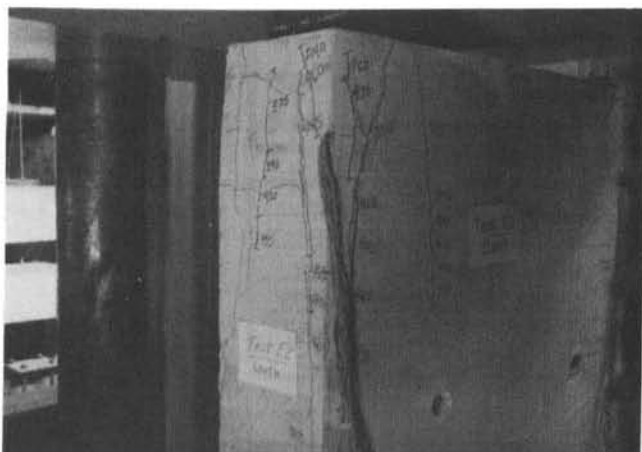


Figure 127. Bursting crack patterns, specimen E2.



Figure 128. Spalling cracks, specimen E2.

Specimen M1 had a bursting resisting force centroid at 29.7 in. with a total tension capacity of 92.4 kips. Specimens M1 and M4 had plastic crack formers along the tops of the tendon ducts. Specimens M2, M3, and M4 had slots formed and bursting zone reinforcement cut below the general zone. The effect of the crack formers was to hasten the development of tensile strains in the bursting reinforcement compared to the single anchorage specimens. In M1 almost all bursting reinforcement along the tendon axis yielded at failure, and some of the bars also yielded along the specimen centerline, although the concrete was mostly uncracked there. Spiral strains were low.

In the specimens with one plate width clear spacing (M2, M4) a small spalling crack was evident between the plates at a load of $1.67 F_{pu}$. In M2 bursting reinforcement in the lower part of the specimen was cut, leaving an effective bursting tension capacity of 79.2 kips at a centroid 19 in. from the loading surface. All of the bursting reinforcement above or at this level yielded before failure. Specimen M4 had a reduced bursting tension capacity of 52.8 kips at a 13.8-in. centroidal distance. At failure most of the bursting reinforcement had yielded. Final failure

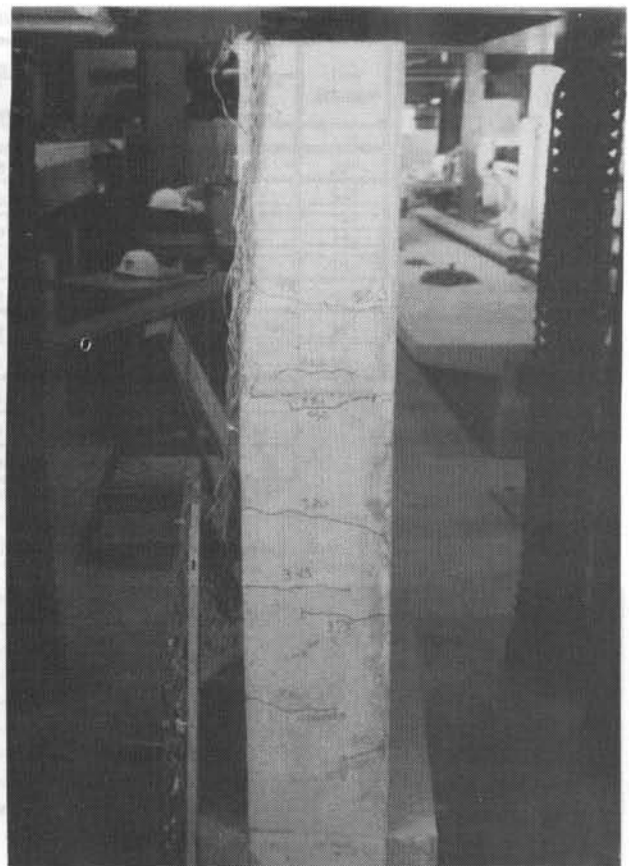


Figure 129. Longitudinal edge tension cracks.

was due to compression failure at the local zone-general zone interface region, as shown in Figure 131.

Specimen M3 had anchors placed symmetrically about the specimen centerline but outside the quarter points of the specimen. Because the anchors were outside the quarter points, it was necessary to place four #4 bars between the anchors as a tension tie to carry the spalling tension force along the loading surface. The crack caused by the spalling tension force midway between anchors was first seen at $0.45 F_{pu}$ and, by $1.82 F_{pu}$, had extended into the lateral surface for 6 in.

Figure 132 shows the final crack pattern. The spalling crack on the loaded surface propagated 10 in. into the specimen. The large interior bursting diagonal cracks propagated 20 in. from the loading surface and to within 10 in. of each other. On the transverse faces, extensive cracking occurred because of the closeness of the anchorages to the transverse surface. The final failure was a compression failure, with concrete spalling and bulging ahead of the anchorage plate. The bursting strain measurements along the load axis indicated that all the bars within 15 in. of the loading surface yielded. Strain measurements along the specimen centerline indicated that reinforcement at 2 in. and 5 in. from the loading surface was highly effective in controlling the spalling force.

Specimen M6 was similar to specimen M1 with a very small lateral spacing, 1.5 in., between the anchorage plates, but the section thickness was increased to permit four anchorages. The bursting reinforcement had a total tension capacity of 50.0 kips

Table 22. First bursting crack load prediction for specimens E1 to E6 and M5

Specimen	Accurate Procedure			Lower Bound Procedure		
	Predicted Cracking Load (kips)	First Cracking Load (kips)	Test/Predicted	Predicted Cracking Load (kips)	Cracking Load (kips)	Test/Predicted
E1	359	345	0.96	256	345	1.35
E5	242	215	0.89	175	215	1.23
E2	268	265	0.99	195	265	1.36
E3	284	300	1.05	198	300	1.52
E4	272	250	0.92	190	250	1.31
E6	229	225	0.98	176	225	1.28
M5	303	400	1.32	238	400	1.68
	Average	1.02		Average	1.39	
	Standard Deviation	0.13		Standard Deviation	0.15	
	Coefficient of Variance	0.13		Coefficient of Variance	0.11	



Figure 130. Specimen E2 at ultimate.

and a centroid of 19.9 in. from the loading surface. A combination of "U" bars and spirals was used for the local zone reinforcement. "U" bars (#2 and #3) were used to join the four individual local zones by tying the four anchors together, as well as providing auxiliary reinforcement because of the closeness of the anchorages to the surface.

First cracking in this specimen with four multiplane anchors was at $0.84 F_{pu}$, which is almost identical to the comparable single multiplane anchor specimen C1 which first cracked at $0.78 F_{pu}$. However, both first yield and ultimate were only about three-quarters of the single anchor specimen strength which had about 10 percent higher concrete compressive strength. The specimen exploded at failure (see Figure 133) with concrete spalled near the anchorage plates, along the tendon axes, and at the specimen base. By failure all except the topmost two bursting bars had yielded but spiral strains were low.

Tests with Eccentric Load Axis

Three multiple anchorage specimens were tested that did not have the resultant load axis along the centroidal axis of the specimen. Specimen M5, which had two anchors at the same e/h ratio, was discussed previously. Specimen ME1 (details in Appendix C) was a 10-in. by 36-in. by 60-in. rectangular specimen with one anchorage "A" located at -4 in. from the specimen centerline and the other anchorage "B" located at +12 in. Because the anchorages were loaded simultaneously, this placed the specimen resultant load axis at +4 in. During the casting process, the duct at -4 in. floated upward $\frac{7}{8}$ in. in the section, at $5\frac{1}{2}$ in. below the load surface, which is just below the anchorage device. A drill bit was used to widen the passage to allow the tendon to pass through the duct. It was necessary to widen the duct down to 18 in. below the loading surface. The effect of this widening was to reduce the effective concrete width from $7\frac{3}{8}$ in. to $6\frac{1}{2}$ in., and to reduce the duct cover on one side of the specimen from $3\frac{11}{16}$ in. to $2\frac{13}{16}$ in. at the end of the anchorage device. The second specimen, specimen F1, was a "T" section with two anchors (details in Appendix C). It had a 4.25-in. by 34-in. by 90-in. flange and 8-in. by $29\frac{3}{4}$ -in. by 34-in. web. The centroid of the section was at 21.3 in. from the bottom of the web, while the resultant load axis was at 26 in. The two anchors were loaded simultaneously and located at 22 in., anchorage A, and 30 in., anchorage B, from the bottom of the web. Bursting regions exist in both the web and the flange. Table 25 gives important information for specimens ME1 and F1. Both speci-

Table 23. Current design procedure ultimate load prediction for eccentric specimens

Specimen	Bursting Tension using the Symmetrical Prism	a (in.)	h' (in.)	Tension Tie Prediction (kips)	Bearing Prediction (kips)	Controlling Load (kips)	Test Ultimate (kips)	Test/Prediction
E1	146.80	7.00	24.00	829	<u>369</u>	369	475	1.29
E5	73.40	6.00	24.00	391	<u>343</u>	343	332	0.97
E2	100.80	7.00	12.00	968	<u>391</u>	391	500	1.28
E3	100.80	7.00	12.00	968	<u>399</u>	399	522	1.31
E4	73.40	7.00	12.00	705	<u>380</u>	380	500	1.32
E6	23.48	6.50	18.00	<u>147</u>	339	147	348	2.37
M5	21.42	6.50	16.00	<u>144</u>	657	144	677	4.69

NOTE: Underlined values show which load case controls	Average	1.89
	Standard Deviation	1.21
	Coefficient of Variance	0.64

Table 24. Basic STM prediction summary for specimens E1 to E6 and M5

Specimen	Tension Tie	Bearing Spiral Only	Bearing Ties Included	Node-Strut Interface		L.Z.-G.Z. Interface		Controlling Load	Ultimate Load	Test/Prediction
				Short	Long	Short	Long			
E1	884	369	<u>404</u>	479	505	772	1002	404	475	1.17
E5	<u>238</u>	343	343	400	413	<u>485</u>	591	238	332	1.39
E2	4240	391	<u>445</u>	477	500	517	695	445	500	1.12
E3	4240	399	<u>453</u>	487	511	532	716	453	522	1.15
E4	4240	380	<u>434</u>	461	484	494	665	434	500	1.15
E6	<u>259</u>	339	339	418	436	527	647	259	348	1.34
M5	403	657	657	771	795	631	799	403	677	1.68

NOTE: Underlined values show which load case controls	Average	1.29
	Standard Deviation	0.19
	Coefficient of Variance	0.15

mens had two 6½-in. by 6½-in. multiplane anchors for 7½-in. strands. Ahead of anchorage A in specimen ME1, the total bursting reinforcement capacity was 35.7 kips with a centroid of 14.1 in. from the loading surface. Ahead of anchorage B, the total bursting reinforcement capacity was 21.4 kips with a centroid of 10.0 in. The first crack noted was a spalling crack along the loading surface between the anchors and ahead of anchorage A at 0.60 F_{pu} . Table 25 summarizes the first bursting cracking loads, first yielding, and the ultimate loads for specimens ME1 and F1. Cracks ahead of anchorage A propagated to the base at 1.21 F_{pu} , whereas the cracks near anchorage B were still small. While marking the cracks at ultimate, an internal cracking of concrete could be heard. The failure of the specimen occurred at 1.21 F_{pu} with massive spalling of concrete ahead of anchorage A (see Figure 134).

At the ultimate load, most of the bursting reinforcement was very close to yielding. After the specimen cracked to the base, all the reinforcement along the anchorage A tendon axis had yielded. Strains along the anchorage B tendon axis were smaller and, at the ultimate load, none of the reinforcement had yielded. The spalling force at failure was slightly less than 1 percent of the total load. Spiral strains were small.

Because there was still reserve capacity in anchorage B after the failure, it was decided to retest anchorage B without load on anchorage A. The load was then increased on anchorage B until it failed at 1.21 F_{pu} of a single tendon. When the bursting crack ahead of anchorage B shot to the base at 350 kips, the bursting reinforcement yielded and the specimen below anchorage B ex-

ploded (see Figure 135). This demonstrates the importance of distributing reinforcement along the entire length of the general zone to prevent catastrophic failures.

Specimen F1 was the only specimen tested that did not have a rectangular cross section. Both anchors were loaded simultaneously. According to elastic analysis, 54 percent of the total load would be resisted by the flange. Closed reinforcing ties were used in the web, and single tie bars with 180-deg. hooks were used in the flange. The flange bursting reinforcement had a tension capacity of 25.0 kips and a centroid of 24 in. from the loading surface. The web bursting reinforcement had a tension capacity of 28.6 kips and a centroid of 19.0 in. from the loading surface. The first three ties in the web were closed hoops that extended into the flange. The last two ties were open ended in the flange and anchored with 135-deg. hooks. In addition to gages on the bursting reinforcement along each tendon path, concrete gates were placed on the surface of the flange to study the compressive stress distribution.

The first flange crack occurred at the flange-web interface at 0.50 F_{pu} . As measurements were being taken at 0.86 F_{pu} an internal cracking of concrete could be heard. The concrete near the anchorage plane then exploded (see Figure 136) with two distinct explosions. The flange crack propagated to the far end of the specimen, and a compression failure occurred ahead of anchorage B, which was quickly followed by a compression failure ahead of anchorage A (see Figure 137). No bursting cracks had been seen in front of anchorage B before the failure load. Extensive cracking was observed in the flange near the

Table 25. Information for multiple tendon specimens

Specimen	Concrete f'_c	Concrete f_{tp}	Anchor	a/c Spacing	Eccentricity	Local Zone Confining Reinforcement	General Zone Bursting Reinforcement	F_{pu} (kips)	1st Bursting Crack Load	$\% F_{pu}$
M1	5940	441	2 - 6-in. x 6-in. plate	8-in.	0	2 - #4 spiral, 6" dia., 1.5" pitch, 4 turns	8 - #3 ties: 1 @ 2, 3 @ 6, 2 @ 3, 1 @ 29, 1 @ 12	330	(Crack Formers)	1.84
M2	5730	500	2 - 6-in. x 6-in. plate	12-in.	0	Same	10 - #3 ties: 1 @ 2, 1 @ 5, 3 @ 4, 2 @ 8, 1 @ 11, 2 @ 12	330	1.29	1.82
M3	5730	500	2 - 6-in. x 6-in. plate	25-in.	0	Same	4 - #4 @ 2-in. 4 - #2 ties; 1 @ 3, 3 @ 2 8 - #3 ties; 1 @ 15, 1 @ 6, 6 @ 8	330	0.68	2.43
M4	6620	511	2 - 6-in. x 6-in. plate	12-in.	0	Same	7 - #3 ties: 1 @ 2, 2 @ 5, 2 @ 4, 1 @ 18, 1 @ 12	330	1.70	2.21
M6	4750	415	4 - 6.5 in. x 6.5- in. multiplane	8-in.	0	4 - #4 spiral, 7-in. dia., 2-in. pitch, 4 turns	9 - #2 ties; 1 @ 1.5, 1 @ 5.5, 1 @ 5, 5 @ 4, 1 @ 3.5	1156	(Crack Formers)	0.84
ME1	6210	571	2 - 6.5-in. x 6.5- in. multiplane	16-in.	4-in.	2 - #4 spiral, 8-in. dia., 2-in. pitch, 4 turns	1 - #3 ties @ 1.5-in. 5 - #2 tie: 1 @ 6, 3 @ 4, 1 @ 4.5	578	0.60A*	1.21
F1	4540	316	2 - 6.5-in. x 6.5- in. multiplane	8-in.	4.7-in.	2 - #4 spiral, 7-in. dia., 2-in. pitch, 4 turns	Web: #2 ties: 1 @ 1.5, 4 @ 7 Flange: 7 - #2: 1 @ 9, 6 @ 5	578	0.50A*	1.21

* The A designates that first cracking was ahead of Anchorage A.

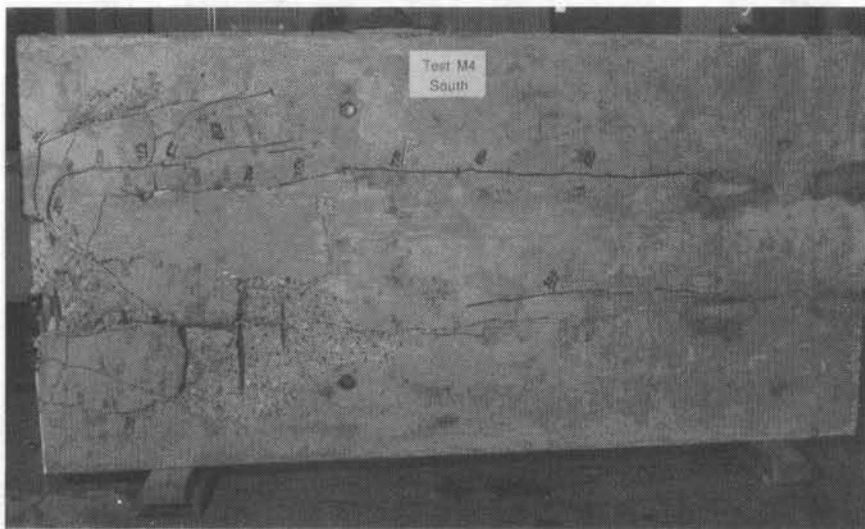


Figure 131. Crack pattern at ultimate, specimen M4.

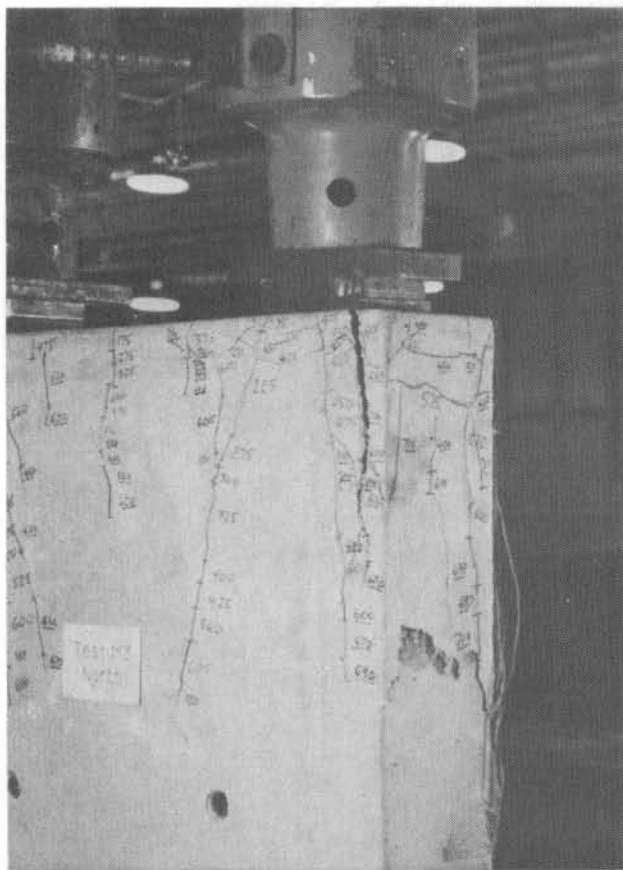


Figure 132. Cracking pattern at ultimate, specimen M3.

outside edge of the flange and perpendicular to the tendon path (Figure 137). Flange bursting reinforcement strains were near yield as the flange crack propagated to the far end when the strains increased significantly. Web strains near the upper anchor A were much lower than near lower anchor B until failure.

Bursting reinforcement strains ahead of anchor B increased more rapidly after the flange-web cracks occurred. Flange concrete gages showed a strong concentration of compressive stress above the webs until flange cracking. Spiral strains around upper anchor B were much higher than around lower anchor A, but still well below yield.

Prediction of First Cracking Load

In multiple anchorage sections, anchorage zone cracking can occur in three areas: the bursting zone, the spalling zone, and the longitudinal edge tension zone (when the resultant is outside the kern). Eight multiple anchorage specimens with straight tendons were tested. Specimen M5 was examined previously with the single anchorage eccentric specimens. Of the seven remaining specimens, five provided bursting crack information, while all provided spalling crack information. Specimens M1 and M4 were precracked by using crack formers with the expectation of reducing the ultimate load. Specimens M1 to M6 vary the spacing between anchorages, but their resultant force was along the centerline of the specimen. ME1 had two anchorages placed so that the resultant force was at an e/h of 0.11. Specimen F1 investigated the three-dimensional effects of a flange with two anchorages and an e/h of 0.14.

Because none of the multiple anchorage specimens had the resultant of the tendon force outside the kern, longitudinal edge tension cracking did not occur until extensive cracking had formed in the bursting region and the specimen was near its ultimate load.

Spalling cracks were observed on M2, M3, and ME1. However, the spalling tension stresses that induce the spalling cracking are difficult to determine because of the high stress gradients and the high stresses predicted near the loading surface. Attempts to correlate observed cracking with results of the finite element analysis by Burdet (48) gave poor agreement—extremely conservative at the surface and unconservative at the first node line.

In the experimental program it was found that the spalling crack width remained small as long as reinforcement was placed

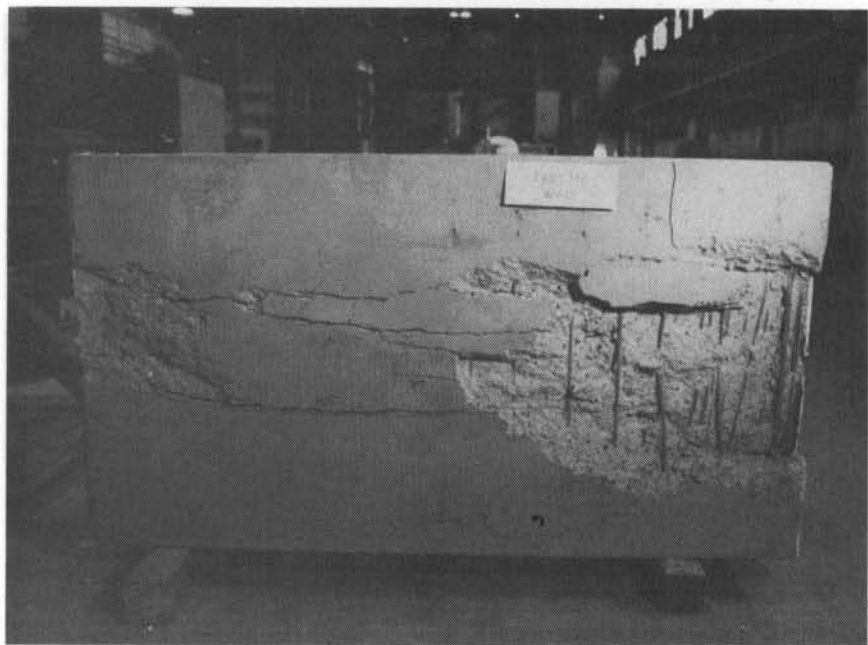


Figure 133. Cracking pattern at ultimate, west side, specimen M6.

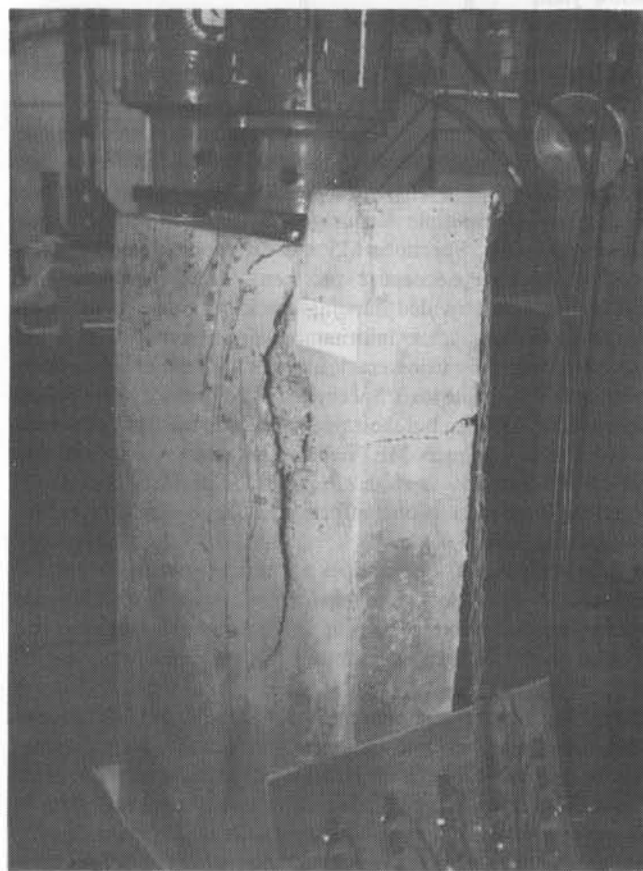


Figure 134. Spalling ahead of anchorage "A", specimen ME1.

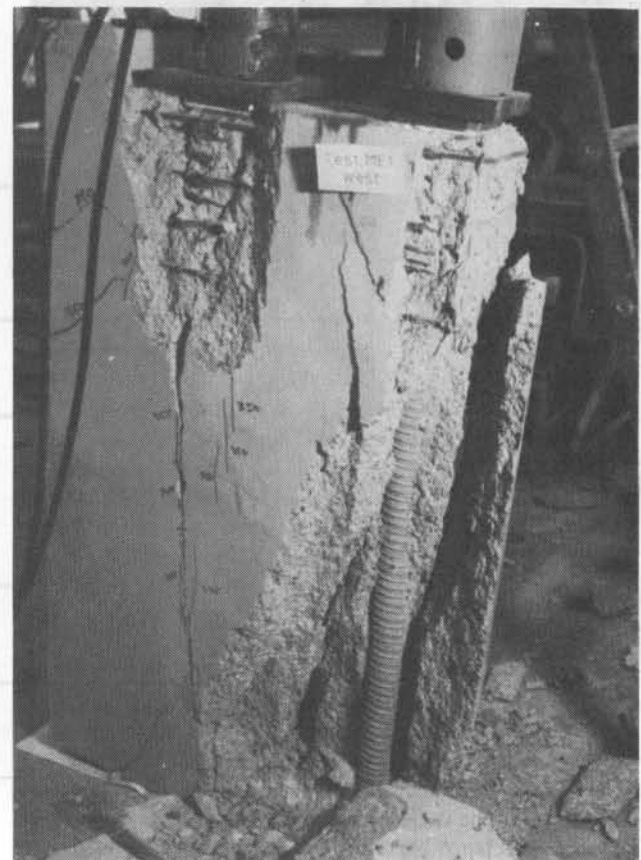


Figure 135. Cracking pattern at ultimate load of test 2, specimen ME1 (only anchorage "B" loaded).

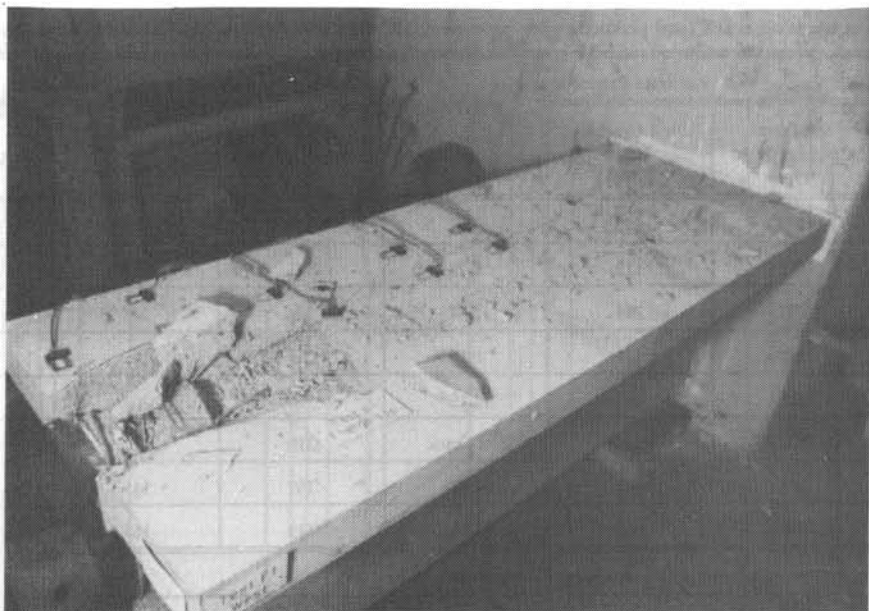


Figure 136. Top of flange after specimen failure, specimen F1.

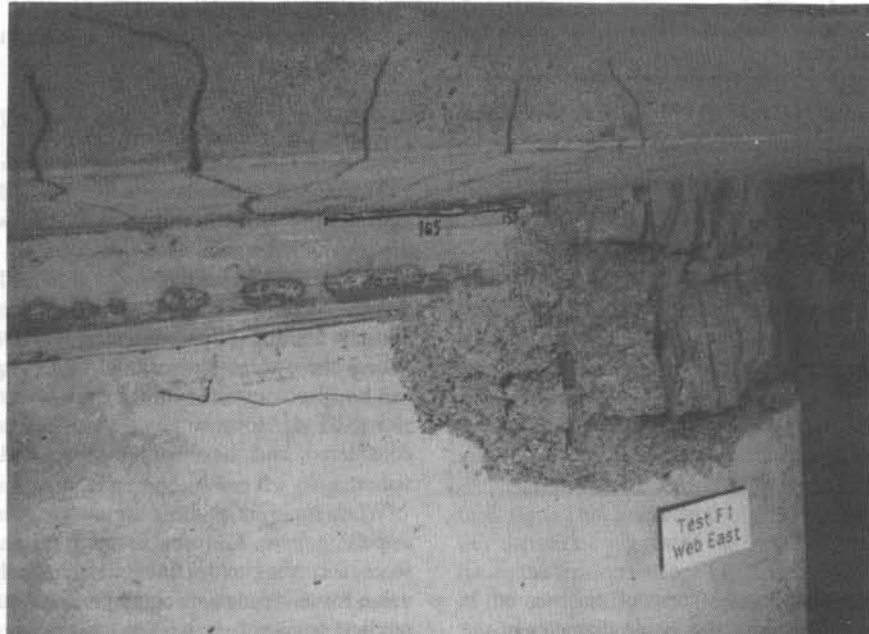


Figure 137. Anchorage "A" failure and flange bottom face cracking, specimen F1.

The first bursting crack load is typically the crack prediction of most interest to the designer. The same analytical models as used in previous sections were used to predict bursting cracks. Results are given in Table 26.

The first crack analysis shown in Table 26 reduces the concrete thickness by the outside diameter of the duct, and it reduces the concrete tensile strength from the split cylinder strength to in-

clude the triaxial stress effects. The overall model is conservative, but there are still three specimens that are unconservative. In the "accurate procedure" using the transformed thickness of the section and the triaxial stress state (see Table 26), the average of the test-to-predicted ratios is one but the coefficient of variance is very large. Several very unconservative values occur, possibly because the thin cover over the duct may not be sufficient to smooth out stress concentrations.

Table 26 also gives the results of the lower bound prediction

Table 26. First bursting crack load prediction for specimens M2, M3, M6, ME1A, ME1B, F1A, F1Bw, and F1Bf

Specimen	Accurate Procedure			Lower Bound Procedure		
	Predicted Cracking Load (kips)	First Cracking Load (kips)	Test/Predicted	Predicted Cracking Load (kips)	Cracking Load (kips)	Test/Predicted
M2	297	213	0.71	214	213	0.99
M3	154	113	0.73	101	113	1.12
M6	178	244	1.37	134	244	1.82
ME1A	342	175	0.15	259	175	0.68
ME1B	225	260	1.16	166	260	1.57
F1A	210	None	No Crack	210	None	No Crack
F1Bw	177	145	0.82	169	145	0.86
F1Bf	136	165	1.22	119	165	1.39
			Average	1.00	Average	1.29
			Standard Deviation	0.26	Standard Deviation	0.33
			Coefficient of Variance	0.26	Coefficient of Variance	0.26

Table 27. Bursting crack prediction using symmetrical prism for same specimens as in Table 26

Specimen	Predicted Cracking Load (kips)	Cracking Load (kips)	Test/Predicted
M2	106	213	2.00
M3	108	113	1.04
M6	164	244	1.49
ME1A	153	175	1.15*
ME1B	148	260	1.75
F1A	147	None	No Crack
F1Bw	147	145	0.99
F1Bf	75	165	2.21
*Duct shifted	Average		1.58
	Standard Deviation		0.46
	Coefficient of Variance		0.29

method developed previously. The thickness of the concrete is equal to the section thickness minus the inside diameter of the duct. The tensile strength of the concrete is reduced to $4.2 \sqrt{f_c'}$ from $6 \sqrt{f_c'}$, to approximately include the tensile capacity reduction due to triaxial stress state effects. The model is still unconservative for several specimens. As the complexity of the anchorage zone increases, a large safety factor must be used in order to ensure that no cracking occurs.

If the anchorage zone is in an area where the other forces besides the post-tensioning force are small, Guyon's symmetrical prism method for determining the maximum bursting stress can be used.

Cracking loads determined from a conservative tensile stress ($4.2 \sqrt{f_c'}$) and the conventional symmetrical prism compared to the test results are shown in Table 27. The analysis is conservative but with a very high standard deviation. Therefore, if cracking

is critical, it is very important to use a high factor of safety to avoid cracking.

Prediction of Ultimate Load

The particular details for using the STM for multiple anchorages are discussed in this section only where differences from the previous methods used occur.

In Figures 138 and 139, the basic STM's for multiple and flanged sections are shown. When a structure is not planar or of constant width, the three-dimensional effects must be considered. Where these three-dimensional effects appear significant, they can be approximated with the use of a two or more two-dimensional STM. However, the interaction of the models must be considered, and the model loadings and results must be consistent.

When multiple anchors are widely spaced (see Figure 138b) a spalling force, T_3 , forms between the anchorages. The spalling force, according to the finite element analysis (48) has a tension value for anchorage spacings greater than $0.2 h$. The STM only predicts tension forces when the spacing of the anchorages exceeds $0.5 h$ because it does not include the compatibility effects. In order to provide some reinforcement for the localized tension, it is recommended that minimum spalling force reinforcement be provided to resist a force equal to 2 percent of the loads applied to each anchor when the STM requires less than that amount.

For the concentric and eccentric anchorage specimens investigated previously, the load applied to each anchorage was divided into two almost evenly divided compression struts. Figure 140(a) shows a local zone node when the magnitudes of the compression struts are close to being equal. Since the division line of the struts in the node and the tendon path are very close together, the difference may be ignored. In the STM's shown and discussed so far, the division of compression strut forces was based on the

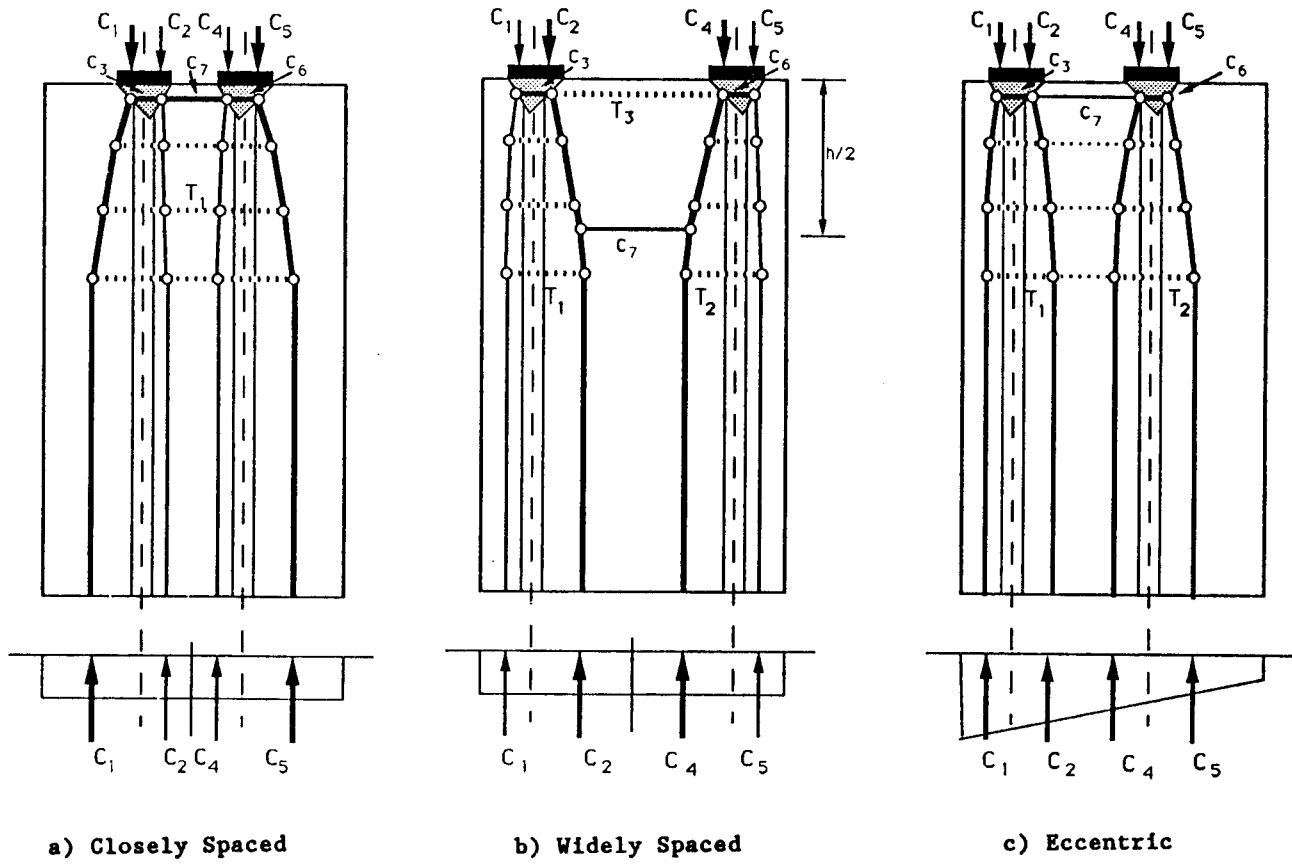


Figure 138. Strut-and-tie models for multiple anchorage sections.

location of the forces on each side of the tendon path. If the anchorages are symmetrical about the centerline of the specimen, the other compression forces are then divided into forces on each side of the specimen centerline (see struts C_2 and C_4 in Figures 138a and 138b). Equilibrium determines the location and magnitude of the compression struts at the end of the general zone. It is usually based on the elastic stress distribution.

Figure 140(b) shows a local zone node when the magnitudes of the compression struts are very different, 25 percent to 75 percent. A large discrepancy between the strut magnitudes becomes much more common in multiple anchorages. In fact, it can affect the results. When the difference between the two struts is more than 10 percent of the axial load, the division line for determining the resultant forces should be shifted from the tendon axis to the location where the division line of the node and the division line for the strut are identical. Using the basic strut-and-tie model principles, Sanders (1) computed in detail the capacities of all multiple straight tendon specimens.

All specimens were checked for tie capacity (spalling, bursting, and longitudinal edge); local zone bearing capacity; node compression capacity; compression strut capacity at the node-strut interface; and compression strut capacity at the local zone-general zone interface.

As shown in Table 28, all specimens but specimen M2 are controlled by the tension ties. At the ultimate load, all of the specimens were extensively cracked in and around the local zones. This indicates that the compression capacities of the local

zone-general zone and/or the node-strut interface were also close to their maximum. The low tension tie capacity predictions are causing the high degree of conservatism in the results. If the tension tie results are neglected, the test-to-predicted ratio average drops to 1.01 with a coefficient of variance of 0.14, and all the specimens are controlled by the local zone-general zone interface capacity except specimen ME1, which is controlled by the bearing. The tension tie capacity limit should *not* be neglected in design. This interaction of the compression strut and tension ties capacities suggested exploration of a modified STM to enhance the tension tie capacity, based on a more plastic distribution of the compressive stresses and the compression strut capacity. Sanders (1) developed such a procedure but it is not yet practical for design reliance.

In current design practice, the symmetrical prism method is often used in conjunction with a bearing stress check to determine the capacity of the sections with multiple anchorages. A comparison of these procedures with test results is given in Table 29. The results are conservative for all the specimens except specimen M1 which, interestingly, was the only specimen in which bearing stress was predicted to have controlled. The current design method, though not as rational as the STM, produces results that are, overall, more accurate for these test results than the basic STM, but unfortunately are quite unconservative in isolated cases.

The use of the basic STM is a conservative method for the design of multiple anchorage zones. The conservatism of the

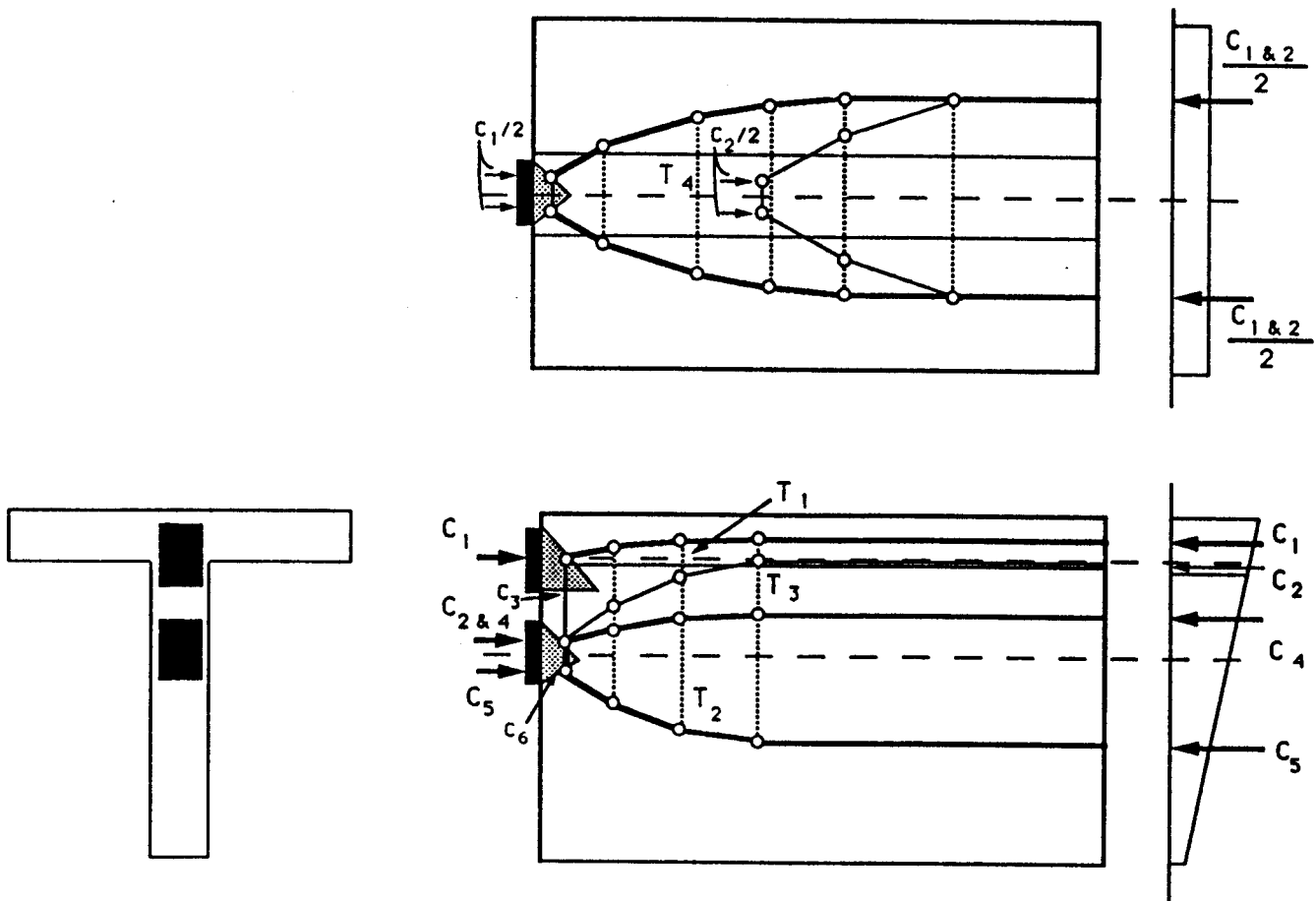


Figure 139. Multiple anchorage section with a flange.

method is due mainly to the low tension tie capacity prediction because the location of the compression struts is assumed to be at the centroid of the linear stress profile. The average of the test-to-predicted ratios was 1.81. It is important to check both tension tie capacity and compression strut capacity. When determining the dimensions of the local zone node, it is important that the division line of the node struts and the general zone be the same in the cases where the difference between the struts is more than 10 percent.

All of the specimens eventually failed in compression because the force paths were able to adjust to allow a higher axial capacity than that predicted when the compression struts were assumed to be located according to the elastic combined stress distribution at a depth of section, h , away from the loading surface.

Anchorage Zones with Inclined and Curved Tendons

In order to economically resist the forces induced by dead load and live load on a girder or other post-tensioned structures, curved tendons that result in inclined anchorages are often used. By using an initial inclination in the tendon, a large transverse force is induced at the end of the girder. If the tendon is curved, the external shear is reduced by the "load balancing" because of the deviation of the tendon.

Five specimens were tested with anchorage inclination and tendon curvature. Details are given in Appendix C. Table 30 shows the variables investigated and the basic material properties for the five specimens. All specimens used 7½-in. strand multiplane anchors. Specimens I1 and I3 were loaded along the centroidal axis of the section ($e = 0$ in.). Specimens I2, I4, and ME2 had eccentricities other than zero. Specimens I2 and I4 investigated the effect of different amounts of tie-back reinforcement. The anchorage for these two specimens was placed at an e/h of $\frac{1}{4}$. Tie-back reinforcement is the reinforcement placed around the duct so that, when a crack forms along the tendon path, a portion of the radial compression force due to the tendon curvature can be resisted by tension on the opposite side of the tendon. Specimen ME2 was a multiple anchorage specimen with anchorages at +12 in. and -4 in. from the specimen centerline.

All of the curved tendon specimens were tested using tendons, hydraulic rams, and the tunnel slab as shown in Figure 141. All of the tendons were designed to be perpendicular to the specimen base, at the top of the tunnel slab, in order for there to be no base shear. In addition, each specimen had a straight portion of tendon extending from the loading surface of the anchorage device for the initial 12 in. All the specimens used multiple plane 7½-in.-strand anchorages that were loaded with 12½-in. strands. The excess number of strands permitted an ultimate load testing of the anchorages. All of the specimens were mounted on teflon

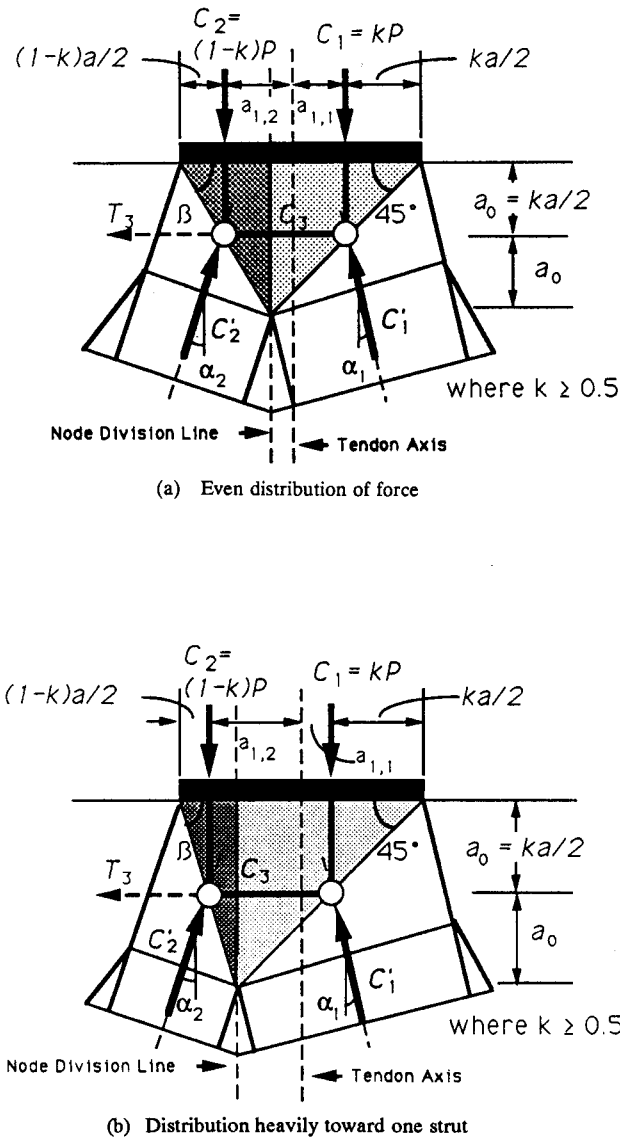


Figure 140. Multiple anchorage node.

sheets laid on top of the test slab. The specimens were not tested in numerical order. Therefore, the specimens will be described in the order in which they were tested: I4, I2, I3, I1, and ME2.

Specimen I4 was an eccentric anchorage specimen with an anchorage inclination of 20 deg. The specimen had no tie-back reinforcement along the tendon path, but did have bursting tie reinforcement with a centroid located 14.5 in. from the loading surface and a total tension capacity of 52.8 kips. The first crack was detected at $1.21 F_{pu}$ on both sides of the specimen. The load was increased to $1.45 F_{pu}$, the safe capacity of the loading system, and cycled twice to that level.

Strains in the bursting reinforcement increased slightly but not enough to cause failure. The higher than expected capacity was attributed to the transverse force contribution of the reinforcement that crossed the tendon duct at the base of the specimen. These bars were cut and the specimen was reloaded. When the load reached $1.45 F_{pu}$ again, the rate of internal cracking

began to accelerate. No additional load was added. The main tendon crack grew for about 4 minutes, until the specimen exploded and split into two parts. The bearing plate was pushed into the specimen approximately 1 in. At failure, the spiral yielded as did all the bursting reinforcement.

Specimen I2 had the same geometry as specimen I4, but the amount of bursting reinforcement was reduced to a total tension capacity of 35.7 kips with a centroid located at 14 in. ahead of the loading surface. The initial behavior of specimen I2 was very similar to that of specimen I4. The first crack occurred at $1.12 F_{pu}$. The cracks were long, extending from the loading surface to a depth of 35 in. from the loading surface. Failure had not occurred when strand capacity was reached. Therefore, as with specimen I4, the load was reduced and the reinforcement at the base of the specimen was removed.

On reloading, the specimen momentarily reached $1.51 F_{pu}$ when transverse cracks opened on the transverse face nearest the anchorage device. The load immediately decreased. While being reloaded, the specimen exploded at $1.47 F_{pu}$. The tie-back reinforcement closest to the base of the specimen had yielded by the conclusion of the test, although tie-back reinforcement nearest the anchorage device had not yielded. Spiral strains showed yielding post failure.

Specimen I3 was the most basic of the inclined tendon specimens. The anchorage device was located on the centerline of the specimen. The tendon exits the base of the specimen within the kern. Specimen I3 had the smallest angle of inclination, 10 deg., and the largest radius of curvature, 239 in. The specimen had six closed ties extending across the full width of the specimen, with a total bursting tension capacity of 35.7 kips and a centroid of 14 in. from the loading surface. The supplementary tie-back reinforcement consisted of five #2 ties at a 9-in. spacing. The base reinforcement was not extended over the duct to prevent any of the problems experienced in specimens I2 and I4.

The first bursting crack occurred at $0.86 F_{pu}$ on the east side. At $1.30 F_{pu}$ the specimen failed dramatically (see Figure 142). The strains showed all bursting reinforcement and the tie-back reinforcement near the anchor yielded. Spiral strains were high toward the top of the spiral. The top portion of the spiral in the transverse direction yielded.

Specimen I1 had the anchorage device located on the section centerline, as in specimen I3. Specimen I1 had a larger anchorage inclination, 20 deg., and smaller radius of curvature, 131 in., than specimen I3. The radius of curvature and anchorage inclination are the same as those used in specimens I2 and I4. Because of the large initial angle, the tendon exits the specimen outside the kern of the main section but inside the kern of the extended base. The closed ties anchored fully across the specimen had a total bursting tension capacity of 35.7 kips with a centroid of 14 in. Supplementary tie-back reinforcement consisted of five #2 ties spaced at 8 in. apart. Because the bottom of the specimen has a resultant force outside of the kern, longitudinal edge tension reinforcement was needed along the surface farthest away from the tendon axis. This reinforcement consisted of four #4 bars.

The first bursting crack along the tendon duct occurred at $0.86 F_{pu}$. It was extremely straight and followed the initial projection of the load to a point 32 in. ahead of the loading surface. The bursting strains increased steadily until failure at $1.46 F_{pu}$. At the ultimate load, horizontal cracks formed on the transverse face at 10 in. below the centroid of the loading surface. The concrete on the lateral face bulged out from the anchor. The

Table 28. STM prediction summary

Specimen	Tension Tie (kips)	Bearing (kips)	Node-Strut Interface		L.Z.-G.Z. Interface		Controlling Load (kips)	Ultimate Test (kips)	Test/Predicted
			Exterior (kips)	Interior (kips)	Exterior (kips)	Interior (kips)			
M1	<u>189</u>	418	496	368	319	369	189	304	1.61
M2	<u>393</u>	411	479	455	<u>322</u>	342	322	401	1.25
M3	<u>290</u>	411	464	471	382	330	290	364	1.26
M4	<u>180</u>	440	522	519	409	464	180	411	2.28
M6	<u>104</u>	331	401	366	277	294	104	300	2.88
ME1A	<u>226</u>	473	583	553	701	550	226	350	1.55
ME1B	<u>228</u>	473	550	551	503	520	228	350	1.54*
F1A	<u>141</u>	324	380	369	344	276	141	248	1.76*
F1Bw	<u>133</u>	324	368	N/A	268	N/A	133	248	1.86
F1Bf	<u>141</u>	324	285	277	257	257	141	248	1.76*
Note: Node compression was found to not control. Loads are per anchor. *Other anchor for specimen controls. NOTE: Underlined values show which load case controls									

Table 30. Information for inclined and curved tendon specimens

Specime n	Concrete f'_c	Anchor	Eccentricity θ degree s	Radius in.	Percent Tieback Reinforce- ment	General Zone Bursting Reinforce- ment	F_{pu} k	1st Bursting Crack F_{pu}	1st Yield F_{pu}	Ultimate Load f_{pu}
I1	5720	358	6.5-in. x 6.5-in. multiplane	0	20	131	24	See C34	289	0.86
I2	6410	423	Same	9	20	131	35	See C35	289	1.12
I3	4510	348	Same	0	10.3	239	53	See C36	289	0.86
I4	6170	393	Same	9	20	131	0	See C37	289	1.21
ME2	6730	491	Two of Same					See C38	578	
Tendon A			-4	15	170	29			0.83	1.21
Tendon B			+12	30	131	36			0.83	1.21
										1.27

Confining Reinforcement - All Tendons

#4 spiral, 8-in. dia., 2-in. pitch, 9.5-in. long

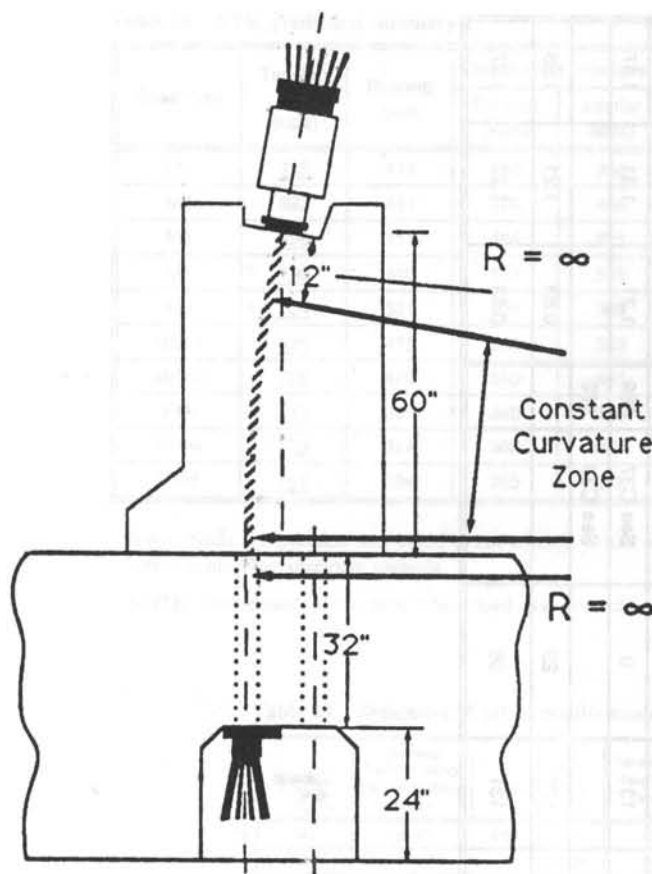


Figure 141. Schematic of test setup, "I" series.

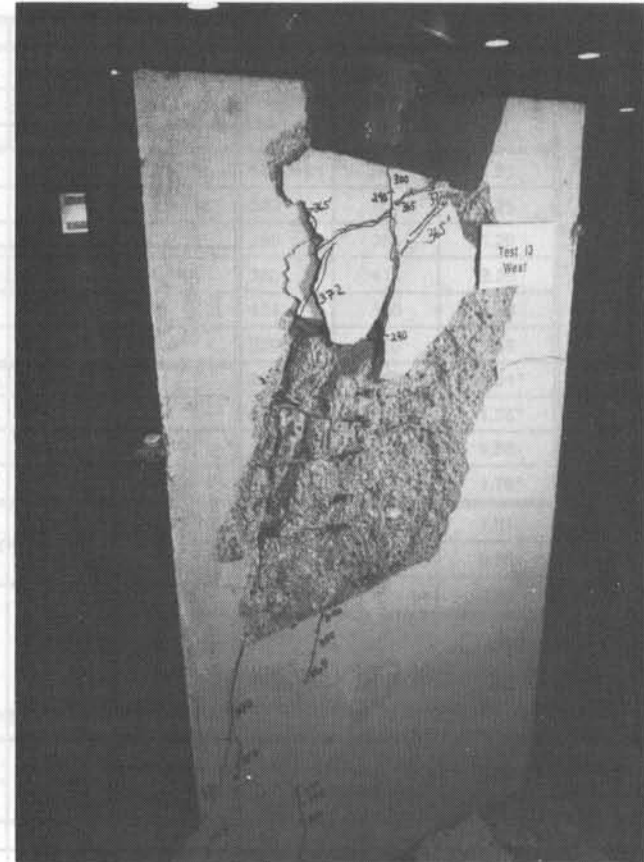


Figure 142. Crack pattern at ultimate, specimen I3.

analysis conducted by Burdet (48). Figure 144(a) shows the tension principal stresses. The circles represent the magnitude of the two-dimensional principal stress while the lines represent the direction. The maximum circle represents a tensile stress of 1.5 ksi for a 100-kip load. Figure 144(b) shows the compression principal stresses. The maximum circle represents a compression stress of 3 ksi for a 100-kip load. For straight tendon specimens, bursting stress fields were essentially similar on either side of the tendon axis. Because of the lateral force component caused by the inclined anchorage, the bursting region has higher tension stresses to the right of the tendon path very close to the anchorage. The tendon curvature begins 12 in. ahead of the loading surface. The radial tension stresses increase to the left of the tendon path, and decrease to the right, because of the radial forces caused by the tendon curvature. The only cracking observed at the service loads in the inclined tendon series were bursting cracks ahead of the anchorage device. The first bursting crack loads can be predicted by matching the peak stress (determined from the elastic finite element analysis (48)) to an estimate of the tensile strength of the concrete.

Table 31 shows the results from the "accurate" and "lower bound" procedures used previously. By incorporating the transformed thickness and the triaxial effects, the average of the test-to-predicted ratios is very close to one. However, it is slightly unconservative, especially for specimen ME2. Table 31 also shows the cruder first bursting crack analysis. All the first crack

predictions on this basis are conservative, except the bursting crack ahead of anchorage B in specimen ME2.

Because it is inconvenient in many applications to use a finite element analysis, a correlation was attempted between the cracking loads, determined from Guyon's symmetrical prism and the test results. Table 32 shows these results. The model has a very high coefficient of variance but is conservative for all specimens.

Prediction of Ultimate Load

The use of a tendon with curvature adds another component to the STM—radial forces along the tendon path. These radial forces can be assumed to act as a distributed load, perpendicular to the tendon path. They have a value at any point along the curved portion of the tendon that is equal to the tendon load divided by the radius of curvature of the tendon at that point. Because the multistrand tendon in a curved duct is pushing against the sides of the post-tensioning duct, transverse forces are also generated. Figure 145(a) shows the location of the strands within the duct when they are not stressed, and Figure 145(b) shows the stressed state. The component of the force in the "y" direction is radial force. The components of the force in the positive and negative "x" directions are the transverse forces. The magnitude of these transverse forces is dependent on the configuration of the tendons within the duct. The tendon duct used in this series had an inside diameter of $2\frac{1}{2}$ in. When $12\frac{1}{2}$ -

in. strands were placed in the duct, their total area was 41 percent of the available duct area. Therefore, when the tendon force was applied, the tendon was assumed to occupy half of the duct. According to the report, "Design and Construction Specifications

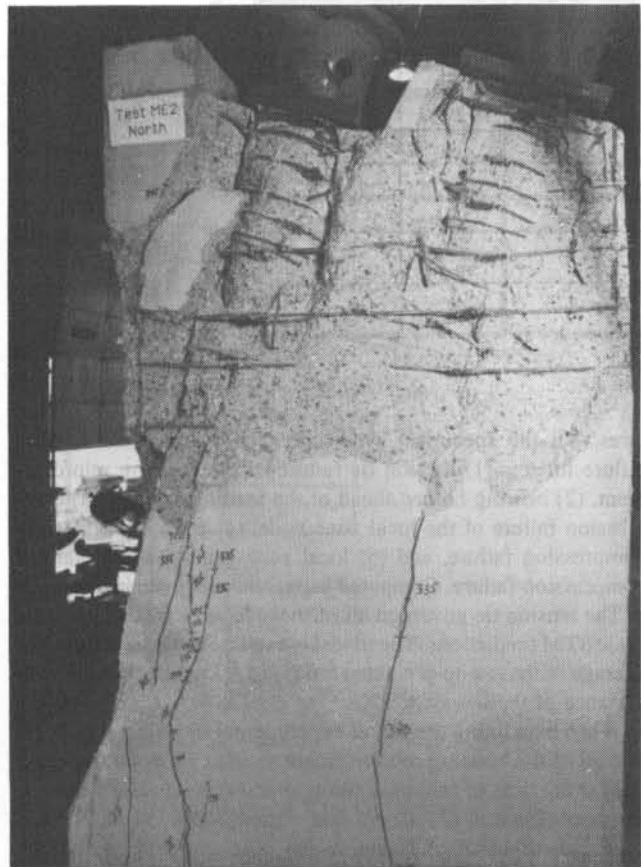


Figure 143. Local zone close-up at failure, specimen ME2.

for Segmental Concrete Bridges" (17), reinforcement must be provided for this transverse force if the value of the shear stress along the transverse plane is greater than $2\sqrt{f_c}$.

In addition to providing confining reinforcement in the areas of curved tendon to counter the transverse force, reinforcement must be provided to tie-back or equilibrate the radial forces. According to the elastic analysis, a portion of the radial force is resisted by the compression in the concrete ahead of the duct, while the remaining portion of the radial force is resisted by the concrete in tension behind the duct. In actuality, the concrete is very weak in tension and cannot be relied upon to resist high tensile force levels. Cracks will form in zones of high concrete tension. Reinforcement must be provided to carry a large portion of the radial force in tension in order to provide for proper resistance if a crack forms along the tendon path. This reinforcement is in addition to the bursting reinforcement necessary to handle the spreading of the axial force applied to the anchorage device.

Figure 146(a) shows a STM including the radial forces. The STM uses the tendon path at the end of the general zone to divide the compression force between struts C_1 and C_2 . The radial forces are modeled as forces being applied to the compression struts. The assumed division of the radial force between the compression and tension resistances has a great effect on the resulting STM. Figure 146(b) illustrates a resulting STM, where tie-back reinforcement is furnished to provide tension resistance for the radial forces. Figure 146(c) is a resulting STM when zero tie-back reinforcement is provided.

Table 33 gives the calculated percentage of the radial force carried in tension for each specimen with respect to the radial force component of the ultimate load. The magnitude of the radial forces carried in tension is computed by using the full yielding strength of the radial reinforcement. In the tests, all the instrumented radial reinforcement yielded except one tie-back hoop in specimen I3, which was 52 in. from the loaded surface at the base of the specimen. Also given in the table is the capacity of the bursting force reinforcement provided, its capacity as a

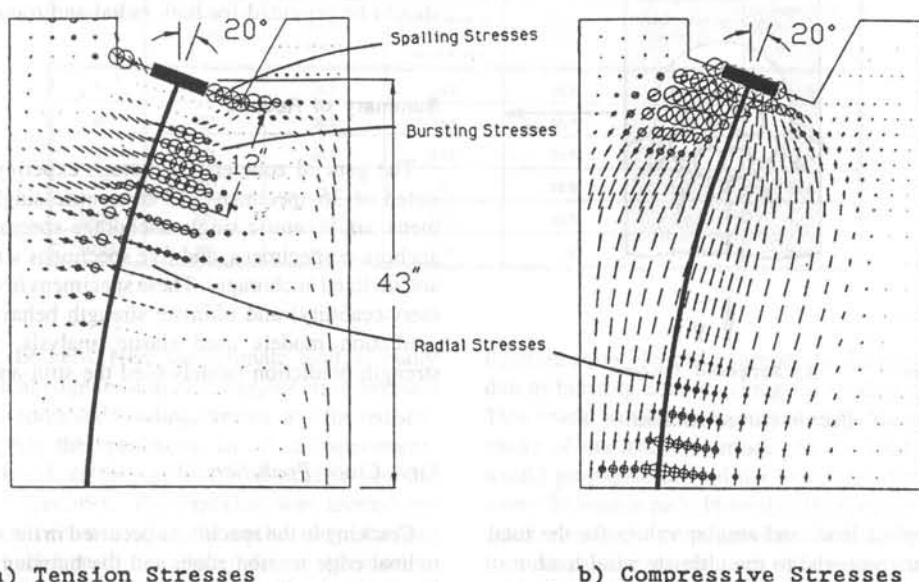


Figure 144. Elastic stress distribution for specimen II.

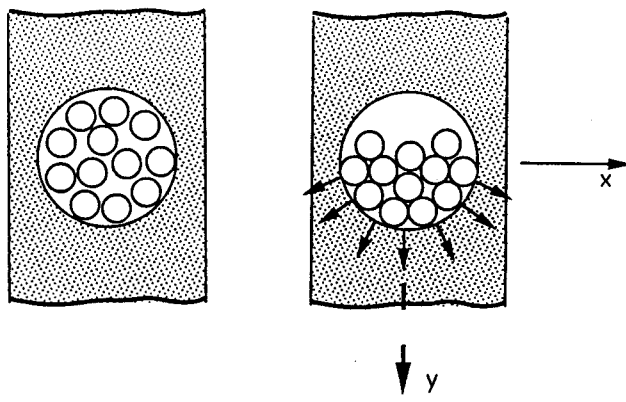
@Seismicisolation

Table 31. First bursting crack load prediction for specimens I1 to I4, ME2A, and ME2B

Specimen	First Cracking Load (kips)	Accurate Procedure		Lower Bound Procedure	
		Predicted Cracking Load (kips)	Test/Predicted	Predicted Cracking Load (kips)	Test/Predicted
I1	250	205	1.22	179	1.39
I2	325	347	0.94	288	1.13
I3	250	233	1.07	196	1.27
I4	350	325	1.08	282	1.24
ME2A	240	275	0.87	196	1.23
ME2B	240	342	0.70	266	0.90
		Average	0.98	Average	1.19
		Standard Deviation	0.17	Standard Deviation	0.15
		Coefficient of Variance	0.17	Coefficient of Variance	0.13

Table 32. First bursting crack prediction using Guyon's symmetrical prism for same specimens as in Table 31

Specimen	First Cracking Load (kips)	Predicted Cracking Load (kips)	Test/Predicted
I1	250	238	1.05
I2	325	163	1.99
I3	250	211	1.18
I4	350	160	2.19
ME2A	240	159	1.51
ME2B	240	154	1.55
		Average	1.58
		Standard Deviation	0.40
		Coefficient of Variance	0.26

**Figure 145.** Multistrand effect in curved tendons.

percentage of the applied load, and similar values for the total tension reinforcement compared to the ultimate axial load.

Sanders (1) reports the calculations necessary for using the STM for specimens with inclined anchorages and tendon curva-

tures. All the specimens were checked against the following failure modes: (1) tension tie failure of the bursting reinforcement, (2) bearing failure ahead of the loading surface, (3) compression failure of the local zone node, (4) node-strut interface compression failure, and (5) local zone-general zone interface compression failure. Computed capacities are given in Table 34.

The tension tie governed all of these failures according to the basic STM predictions. The model is extremely conservative. The average of the test-to-predicted ratios is 1.93 with a coefficient of variance of 0.38.

When examining the actual experimental results, it was noted that all of the bursting reinforcement yielded prior to failure and that, at the time of failure, a compression type of failure seemed to occur. Sanders (1) shows that a modified STM based on a plastic distribution of forces at the base gives more accurate results.

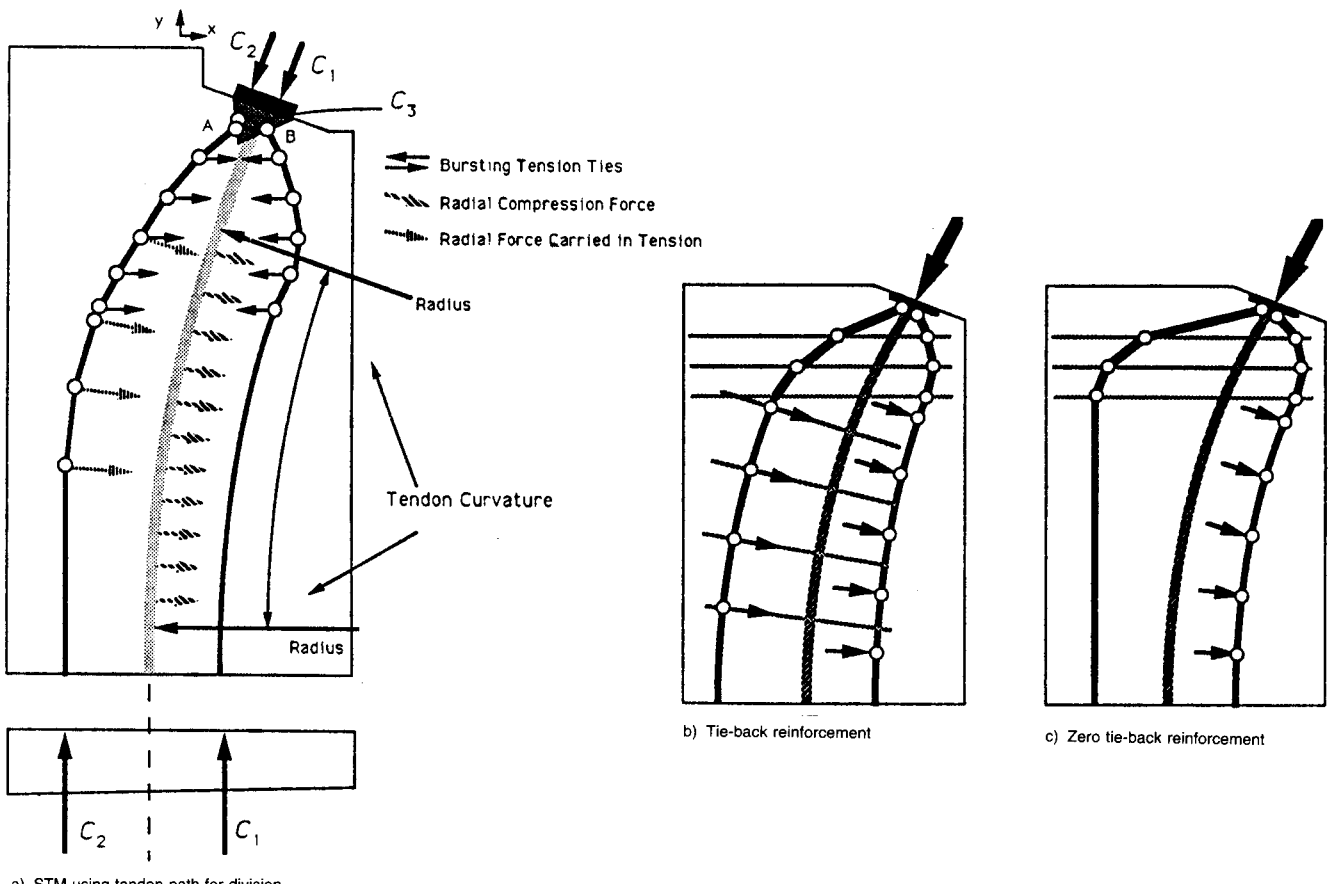
One of the most important observations from this series was that tie-back reinforcement along the tendon path is necessary to prevent large cracks and explosive failures. Reinforcement should be provided for both radial and transverse forces.

Summary of Results

The general zone end anchorage experimental program consisted of 36 specimens: 17 concentric single anchorage specimens, six eccentric single anchorage specimens, eight multiple anchorage specimens, and five specimens with tendon curvature and inclined anchorages. These specimens investigated first crack (serviceability) and ultimate strength behavior. The first crack prediction models used elastic analysis, while the ultimate strength prediction models used the strut-and-tie model.

First Crack Prediction

Cracking in the specimens occurred in the spalling zone, longitudinal edge tension zone, and the bursting zone. Spalling and longitudinal edge tension cracking at service stress levels occurred only in specimens with anchorages that had a resultant



a) STM using tendon path for division of compression struts

Figure 146. Effect of tie-back reinforcement on STM.

Table 33. Percentage of load carried in tension

Specimen	Ultimate Test Load (kips)	Radial Tension		Bursting Tension		Total Tension Capacity as Percentage of Ultimate
		Force (kips)	Percentage of Ultimate Radial Force	Force (kips)	Percentage of Ultimate Load	
I1	423	35.7	24.2	35.7	8.4	16.9
I2	437	52.8	34.6	35.7	8.2	20.3
I3	375	35.7	53.0	35.7	9.5	19.0
I4	420	0	0	52.8	12.6	12.6
ME2A	370	28.6	29.3	35.7	9.6	17.4
ME2B	366	46.2	36.1	42.8	11.7	24.3

eccentricity outside the kern. Near the ultimate load of many specimens, longitudinal edge tension cracking occurred because of the combined axial force and bending stresses, and the redistribution of forces within the specimens. In all the specimens, spalling cracks occurred as the applied load approached the ultimate load of the specimen. The cracking was around the anchorage device, and occurred when the anchor displacement became nonlinear in relation to the applied force. Attempts to accurately predict spalling cracking were futile. The major focus of the cracking investigation was the first cracking within the

bursting zone. For most specimens, the first observed crack was due to bursting stresses along the tendon path or the load axis. This crack would start approximately one to two plate widths ahead of the loading surface. As the load increased, the crack would propagate toward the loading surface, as well as farther along the tendon path. In most of the specimens, the main bursting crack eventually propagated to the specimen base. Cracks also formed parallel to the axis of the compression struts. These cracks would start near the loading surface, then propagate out away from the loading surface.

Table 34. Basic STM capacity summary

Specimen	Tension Tie (kips)	Bearing (kips)	Node-Strut Interface		L.Z.-G.Z. Interface		Controlling Load (kips)	Ultimate Test (kips)	Test/Predicted
			1 (kips)	2 (kips)	1 (kips)	2 (kips)			
I1	281	454	541	519	507	441	281	423	1.51
I2	223	481	576	574	649	834	223	437	1.96
I3	262	406	469	478	425	558	262	375	1.43
I4 - Thrust	126	472	809	535	1326	554	126	420	3.33
ME2A	261	494	575	591	531	638	261	370	1.42
ME2B	267	494	613	578	749	584	267	366	1.26*
								Average	1.93
								Standard Deviation	0.73
								Coefficient of Variance	0.38

Note: Node Compression was found to not control. Loads are per anchor

* Other anchor for that specimen controls.

Accurately predicting the first bursting crack load proved to be difficult. Variables included concrete surface conditions, the prediction of peak elastic bursting stresses, and an accurate determination of the concrete tensile strength of the specimen. Finite element analysis by Burdet (48) determined the peak bursting stress of the specimens. These were mostly two-dimensional elastic analyses. The analyses for specimens M5 and M6 were three-dimensional finite element analyses. The finite element analysis for specimen F1 used shell elements for the web and flange. To include the effects of a post-tensioning duct, the peak stress from the two-dimensional analysis was divided by an effective section thickness. The effective section width that yielded the best results was a transformed section. After the peak bursting stress was determined, it was matched to the concrete tensile strength to find the cracking load.

The split cylinder test was used to experimentally estimate the concrete tensile strength of the specimens. Because of the high compressive stresses in the anchorage zone, the relationships for the biaxial and the triaxial stress effects, developed by Ottosen (43), were used to adjust the measured split cylinder strength in order to represent more "accurately" the tensile strength of the concrete in the critical regions of the specimen. This was an involved process; therefore, a simplified formula was developed to conservatively estimate the concrete tensile strength. The "lower bound estimate" of the concrete tensile strength was taken to be $4.2 \sqrt{f_c}$.

The methods for determining the first cracking load were visual observation and the monitoring of strain gage results. Most first cracks occurred when the strain readings from strain gages located on the nearby bursting reinforcement were approximately 250 microstrain. Most cracks had a width of approximately 0.001 in. when they were first noticed. The rough surface conditions could have prevented earlier observation of some of the cracks.

To determine if serviceability would have been a problem for these specimens, the first cracking load can be compared with the nominal peak stressing load of the specimen anchors. The peak stressing load is specified by AASHTO to be 0.9 times the yield strength of the tendon. For stress-relieved strands, the yield

strength is approximately $0.85 F_{pu}$, where F_{pu} is the maximum tensile strength of the tendon. For low-relaxation strands, the yield strength is approximately $0.9 F_{pu}$. The maximum tensile force of a tendon for a particular anchor is often called "GUTS". ACI 318-89 limits the nominal maximum force to a comparable 0.8 times "GUTS". The most commonly used prestressing steel has an F_{pu} equal to 270 ksi. Table 35 shows the relationship between the first surface crack load and the peak nominal stressing load for the particular anchors used in each specimen. Seventy-five percent of the specimens did not crack until above the peak nominal stressing load. When cracks did initially form, they were very narrow, typically 0.001 to 0.002 in. Therefore, most of these anchorage configurations should not present any serviceability problem because of the anchorage zone stresses alone. It is important to note that the specimens tested provide cracking data for only isolated anchorages. Anchorages located in areas where other forces are influencing the stress distribution, or where there is restraint or shrinkage cracking, could have significantly different behavior.

Several specimens need additional explanation before discussing the first crack models. Specimens M1 and M4 did not provide first bursting crack data because crack formers existed along the tendon ducts. Anchorage A in specimen ME1 is not included in the statistical analyses because the post-tensioning duct ahead of that anchorage shifted during casting. This is believed to have caused a premature cracking of the specimen. Specimen F1 is included in analyses, but the finite element analysis that modeled the specimen had a crude mesh, especially in the area around the web flange interface. Therefore, the peak stress estimate for specimen F1 may not be as accurate as those for the other specimens.

Table 36, Figure 147, and Figure 148 show the results of a refined crack prediction model compared with the experimental tests. This prediction model uses the Ottosen (44) triaxial stress law to determine the appropriate tensile strength from measured split cylinder strength data, and uses the transformed section to modify the finite element analysis to account for the three-dimensional effects of the duct opening and sheath. The average of the test-to-predicted ratios is close to one and is slightly

Table 35. First crack load versus the maximum stressing load

Specimen	Test First Crack Load (kips)	Anchorage 0.81 x Guts Load (kips)	Test First Crack / 0.81 x Guts	Specimen	Test First Crack Load (kips)	Anchorage 0.81 x Guts Load (kips)	Test First Crack / 0.81 x Guts
A1	298	234	1.27	M1	Cr. Formers	134	
A2	226	234	0.96	M2	213	134	1.59
A3	250	234	1.07	M3	113	134	0.84
A4	300	234	1.28	M4	Cr. Formers	134	
				M5	200	234	0.85
B1	200	141	1.42	M6	244	234	1.04
B2	186	141	1.32				
B3	217	141	1.54	ME1A	175	234	0.76*
B4	200	141	1.42	ME1B	260	234	1.11
B5	170	141	1.21	ME2A	240	234	1.02
B6	171	141	1.21	ME2B	240	234	1.02
B7	170	141	1.21				
B8	156	141	1.11	F1A	No Crack	234	
				F1Bw	145	234	0.62
C1	225	234	0.96	F1Bf	165	234	0.70
TPT1	200	234	0.85	I1	250	234	1.07
TPT2	225	234	0.96	I2	325	234	1.39
TPT3	270	234	1.15	I3	250	234	1.07
TPT4	240	234	1.02	I4	350	234	1.49
E1	345	188	1.83		Average for both columns		1.19
E2	265	188	1.41				
E3	300	188	1.60				
E4	250	188	1.33				
E5	215	134	1.61				
E6	225	188	1.20				

*Duct shifted during casting

conservative. The coefficient of variance is large, but reasonable, for cracking load prediction. Figures 147 and 148 are graphical representations of the results given in Table 36. Of the 36 measurements of first cracking, 17 of the predictions were unconservative, while 19 were conservative. The model determines an adequate average value but would not be appropriate for design because of the large percentage of low values.

Table 37, Figure 149, and Figure 150 show the results for the simpler prediction model that uses a lower bound approximation, $4.2\sqrt{f'_c}$, for the concrete tensile strength, and uses the section thickness minus the inside diameter of the post-tensioning duct for the effective thickness in adjusting the finite element analysis stresses. The average value of the model is conservative by 28 percent, and the coefficient of variance is even slightly lower than in the Ottosen model discussed previously. Only five of the specimens are unconservative and three of these barely so.

The tests also showed a large amount of post cracking strength. Figure 151 shows the relationship between the ultimate load and first cracking load. The average for all the specimens was 1.57. Therefore, the observation of cracking does not necessarily indi-

cate an immediate failure. There were only five specimens (15 percent) that had ratios of ultimate to first crack of less than 1.25. Three of these specimens were from the "A" series where compression stresses were very high at the ultimate and first crack loads, and local zone failures predominated.

Ultimate Capacity Prediction

The strut-and-tie model (STM) was effective in predicting the ultimate capacity of the specimens. Five ultimate capacities within the STM must be checked. They are tension tie capacity, bearing compression capacity, node compression capacity, node-strut interface compression capacity, and local zone-general zone interface compression capacity.

The basic STM assumes an elastic stress distribution at the end of the general zone, assumed to be located a depth of the section away from the loading surface. Other basic assumptions include: the confining spiral does not contribute to the tension tie capacity; the strut width is equal to twice the distance from

Table 36. First crack prediction summary for triaxial model

Specimen	Predicted First Crack (kips)	Test First Crack (kips)	Test/Prediction	Specimen	Predicted First Crack (kips)	Test First Crack (kips)	Test/Prediction
A1	189	298	1.67	M1	Crack	Formers	
A2	189	226	1.19	M2	297	213	0.71
A3	194	250	1.29	M3	154	113	0.73
A4	207	300	1.45	M4	Crack	Formers	
				M5	152	200	1.32
B1	201	200	0.99	M6	178	244	1.37
B2	201	186	0.92				
B3	201	217	1.08	ME1A	342	175	0.51*
B4	201	200	0.99	ME1B	225	260	1.16
B5	191	170	0.89	ME2A	275	240	0.87
B6	191	171	0.90	ME2B	342	240	0.70
B7	169	170	1.01				
B8	158	156	0.99	F1A	210	No Crack	No Crack
				F1Bw	177	145	0.82
C1	221	225	1.02	F1Bf	136	165	1.22
TPT1	157	200	1.28	I1	205	250	1.22
TPT2	197	225	1.14	I2	347	325	0.94
TPT3	237	270	1.14	I3	233	250	1.07
TPT4	227	240	1.06	I4	325	350	1.08
E1	359	345	0.96			Average	1.05
E2	268	265	0.99			Standard Deviation	0.20
E3	284	300	1.05			Coefficient of Variance	0.19
E4	272	250	0.92				
E5	242	215	0.89				
E6	229	225	0.98				

* Duct shifted during casting

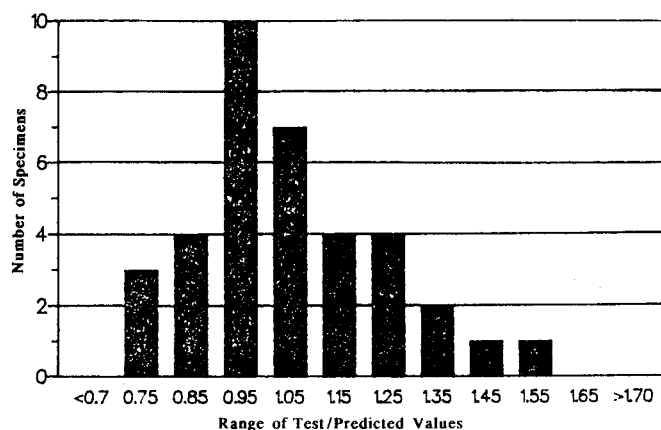


Figure 147. Frequency of occurrence for triaxial first crack model.

the tendon axis to the line of action of the strut; the concrete tension capacity does not contribute to the tension tie capacity; the anchorage zone has sufficient ductility to mobilize the necessary anchorage zone reinforcement; and the node compression capacity can be estimated using the equation developed by Roberts (4). Table 38, Figure 152, and Figure 153 give a comparison between the ultimate test loads and the predicted values for the basic STM.

The basic STM is very conservative, with a test-to-predicted ratio equal to 1.50 with a coefficient of variance of 0.33. The STM is a lower bound model based on the theory of plasticity. It should be a conservative estimate of the ultimate strength of the specimens. The degree of conservatism and coefficient of variance are very reasonable when examined from the perspective of the CEB survey, which showed a range of responses of current design procedures that differed by an order of magnitude of ten. Figure 153 shows that only two specimens (specimens B5 and B2) were unconservative, and those were barely so. They were both within 3 percent of the ultimate load. Specimen B5 was reinforced with zero bursting reinforcement. Therefore, the tension tie capacity was zero. The specimen reached its ultimate load because of its concrete tension capacity, which the prediction

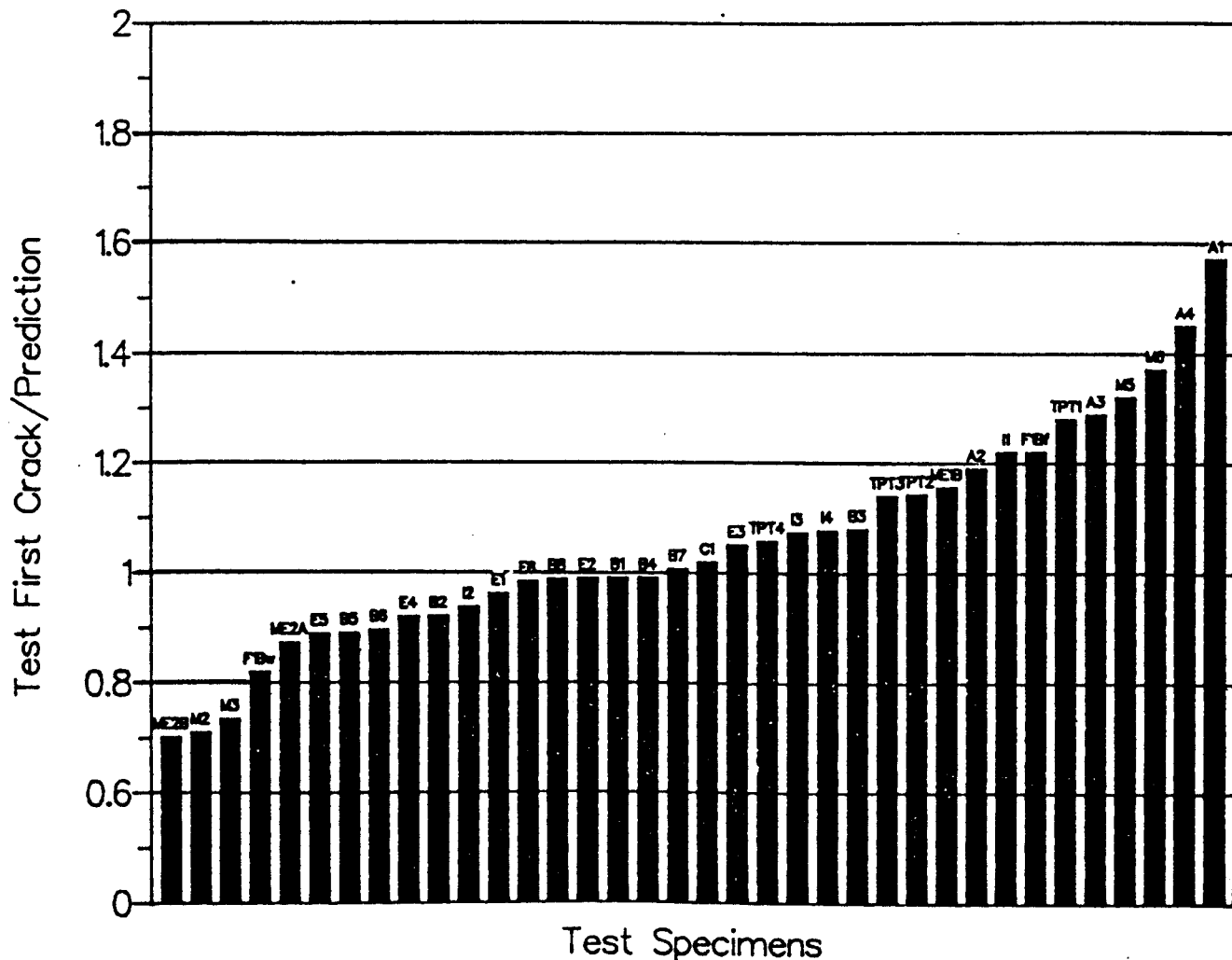


Figure 148. Distribution of results for triaxial first crack prediction.

models neglected. The analysis and design of specimen B5 using the basic STM would have had an ultimate capacity prediction of zero. Using this, of course, the results would have been extremely conservative. Specimen B2 was probably unconservative because of the distance of the bursting reinforcement centroid from the loading surface ($d_{centroid}/h = 0.84$). Care should be taken not to place reinforcement that is to be considered to be effective too far from the anchorage devices or at locations significantly different from the elastic distribution. The use of reinforcement far from the loading surface requires greater ductility in the anchorage zone in order to permit complete redistribution of paths. It is recommended that all reinforcement should be placed within 1.5 times the width (not thickness) of the section to be considered effective, and that it should have a centroid at approximately 0.5 times the width from the loaded surface to prevent the need for large plastic deformations. If the section is very wide, all reinforcement considered effective should be placed closer than one times the section width.

The specimen concrete compressive strength at testing ranged from 3360 psi to 6730 psi. Existing literature, summarized in Ref. 59, indicates a reduction in the efficiency of concrete compressive

struts with increasing concrete compressive strength. With the increased use of very high strength concretes, and especially in the cases where fully cured concrete is being post-tensioned, designers may desire to use compressive strength at time of stressing significantly higher than the 7000 psi range for which this study is adequate. Therefore, additional research is recommended for design of anchorage zones with concrete compressive strengths at the time of stressing greater than 7000 psi.

The basic STM indicated that most specimens would be controlled by the bursting tension tie failure. This agreed with the experimental results in that the tests showed most of the bursting reinforcement to be at or above its yield value at the time of specimen failure. The spalling tension tie between the anchors controlled the design in specimen M3, although the spalling crack propagated farther into the specimen to mobilize additional reinforcement. Many of the specimens also suggest a large amount of force redistribution by displaying significant cracking in and around the local zone, and horizontal cracking on the extreme longitudinal fiber. In a design process, specimen E4 would have been controlled by the longitudinal edge and spalling tension capacities. These controlling capacities were not included

Table 37. First crack prediction summary for approximate model

Specimen	Predicted First Crack (kips)	Test First Crack (kips)	Test/Prediction	Specimen	Predicted First Crack (kips)	Test First Crack (kips)	Test/Prediction
A1	179	298	1.67	M1	Crack	Formers	
A2	179	226	1.26	M2	214	213	1.00
A3	182	250	1.37	M3	101	113	1.12
A4	191	300	1.57	M4	Crack	Formers	
				M5	119	200	1.68
B1	173	200	1.15	M6	134	244	1.82
B2	173	186	1.07				
B3	173	217	1.25	ME1A	259	175	0.68*
B4	173	200	1.15	ME1B	166	260	1.57
B5	172	170	0.99	ME2A	196	240	1.23
B6	172	171	0.99	ME2B	266	240	0.90
B7	135	170	1.26				
B8	120	156	1.30	F1A	210	No Crack	No Crack
				F1Bw	169	145	0.86
C1	181	225	1.24	F1Bf	119	165	1.39
TPT1	131	200	1.53	I1	179	250	1.39
TPT2	179	225	1.26	I2	288	325	1.13
TPT3	230	270	1.18	I3	196	250	1.27
TPT4	216	240	1.11	I4	282	350	1.24
E1	256	345	1.35			Average	1.28
E2	195	265	1.36			Standard Deviation	0.22
E3	198	300	1.52			Coefficient of Variance	0.17
E4	190	250	1.31				
E5	175	215	1.23				
E6	176	225	1.28				

* Duct shifted during casting

because they would have been artificially low. Specimen E4 had small amounts of longitudinal edge and spalling tension reinforcement. In all of the eccentric specimens with resultant eccentricities outside the kern, the longitudinal edge tension and the subsequent spalling forces along the loading surface were much lower than expected, as shown by the strain gage results on the corresponding reinforcement. This is attributed to the concrete tensile capacity, a redistribution of forces, and possibly to the specimen configuration. Potentially, a full development of these forces was not possible because the specimen base did not provide tension capacity. Therefore, although the prediction capacities for the longitudinal edge and spalling tension would have controlled the design of specimen E4, they did not control the failure.

The significant amounts of increased cracking, force redistribution, and high compression stresses observed and calculated for the specimens led to the development by Sanders (1) of a modified STM. The stress distribution was modified at the far end of the general zone to include more plastic behavior of the specimens. Such behavior was observed in the tests by the lengthening of the anchorage zone through increased cracking.

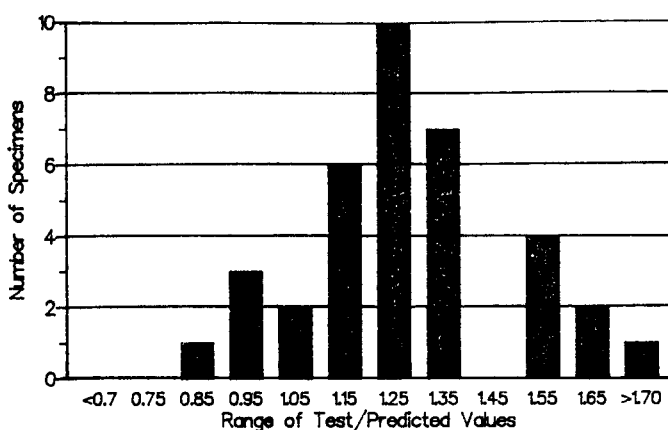


Figure 149. Frequency of occurrence for approximate first crack model.

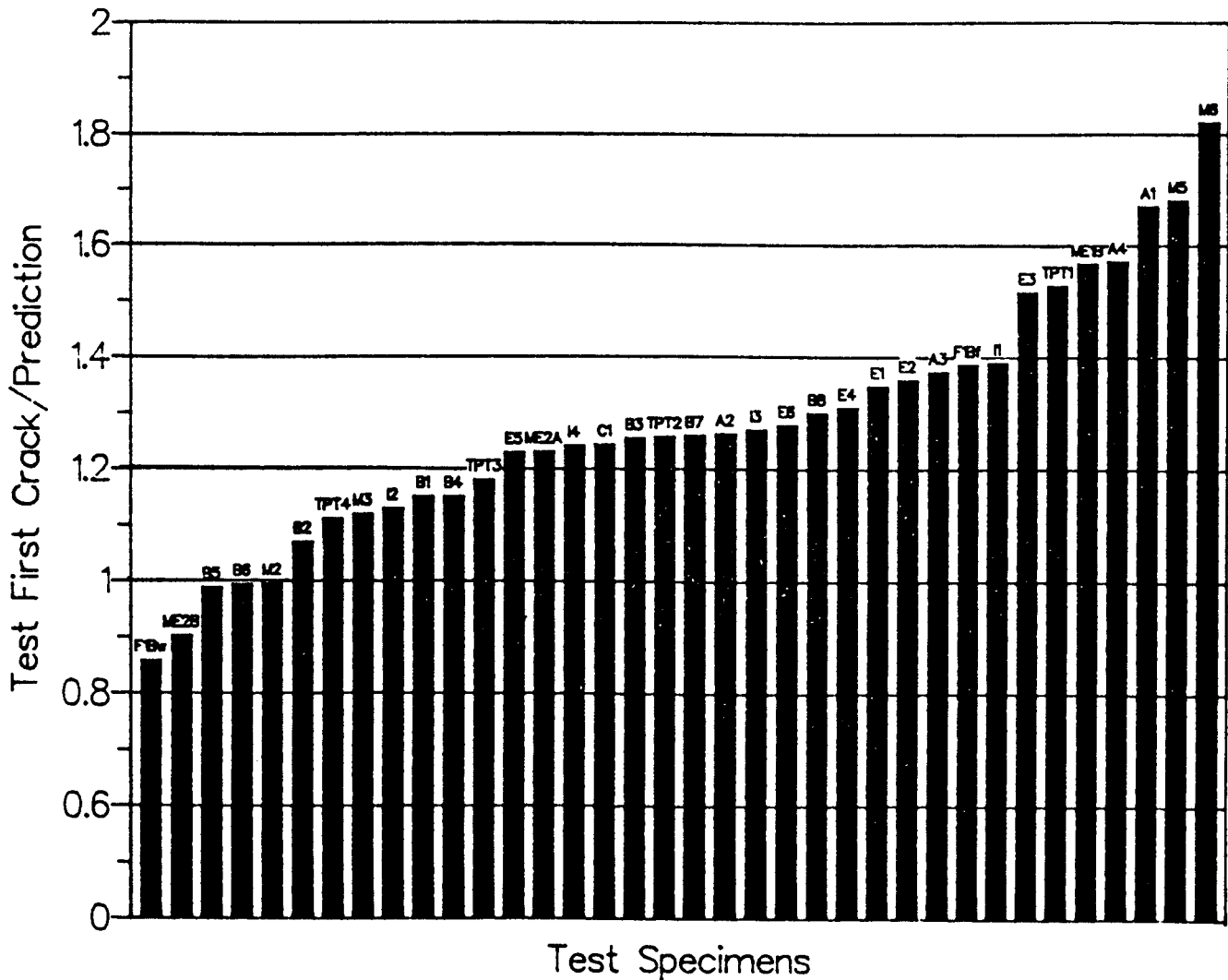


Figure 150. Distribution of results for approximate first crack prediction.

The modified STM ultimate load predictions were in better agreement, on the average, than the basic STM. However, it was unconservative for many specimens and is not suggested as a design model at this time.

It is also important to realize that, while the anchorage zone failure tends to be compressive in nature with much shattering of the concrete, there is some limited ductility in that the bursting reinforcement usually yields prior to failure. Table 39 and Figure 154 show that the ratio of ultimate load to first yielding load had an average of 1.14 and that only the "A" series, with generally deficient local zones, had specimens in which the bursting reinforcement did not yield. Crack levels associated with yielding of the reinforcement should provide reasonable warning of distress.

Post-tensioning anchorages cannot develop a force greater than "GUTS", the guaranteed ultimate tensile strength of the tendon, unless higher strength material is furnished or more strands are furnished than called for on the plans. In either of these cases, extra safety is present. It is interesting to note from Figure 155 that in all except three specimens, the ultimate load was above 1.0 GUTS. All three of the lower level specimens exceeded the AASHTO stressing limit of 0.81 GUTS.

Lastly, the current methods for estimating ultimate capacity can be seen to be inadequate. The most common method for currently estimating ultimate capacity as determined from the extensive state-of-art survey is a combination of checking the bearing capacity by relatively crude equations and verifying the tension tie capacity using equations based on Guyon's symmetrical prism method. Table 40, Figure 156, and Figure 157 show the results of this type of analysis. The specimens with inclined anchorages and tendon curvatures were not included because the survey results did not indicate a simple current method to design or analyze these types of sections. Most engineers indicated they would use finite element analysis or existing experience to design anchorage zones with tendon curvature or inclined anchorages. Using Guyon's symmetrical prism method, coupled with a bearing capacity check, is often a conservative method, but six of the specimens (20 percent) were unconservative. However, five of these six specimens had bearing failures. Local zone design rules should preclude such failures in practice. When using the STM model, four of the unconservative specimens failed at the node-strut interface, which is not checked with current methods. The method has an unacceptably large coefficient of variance

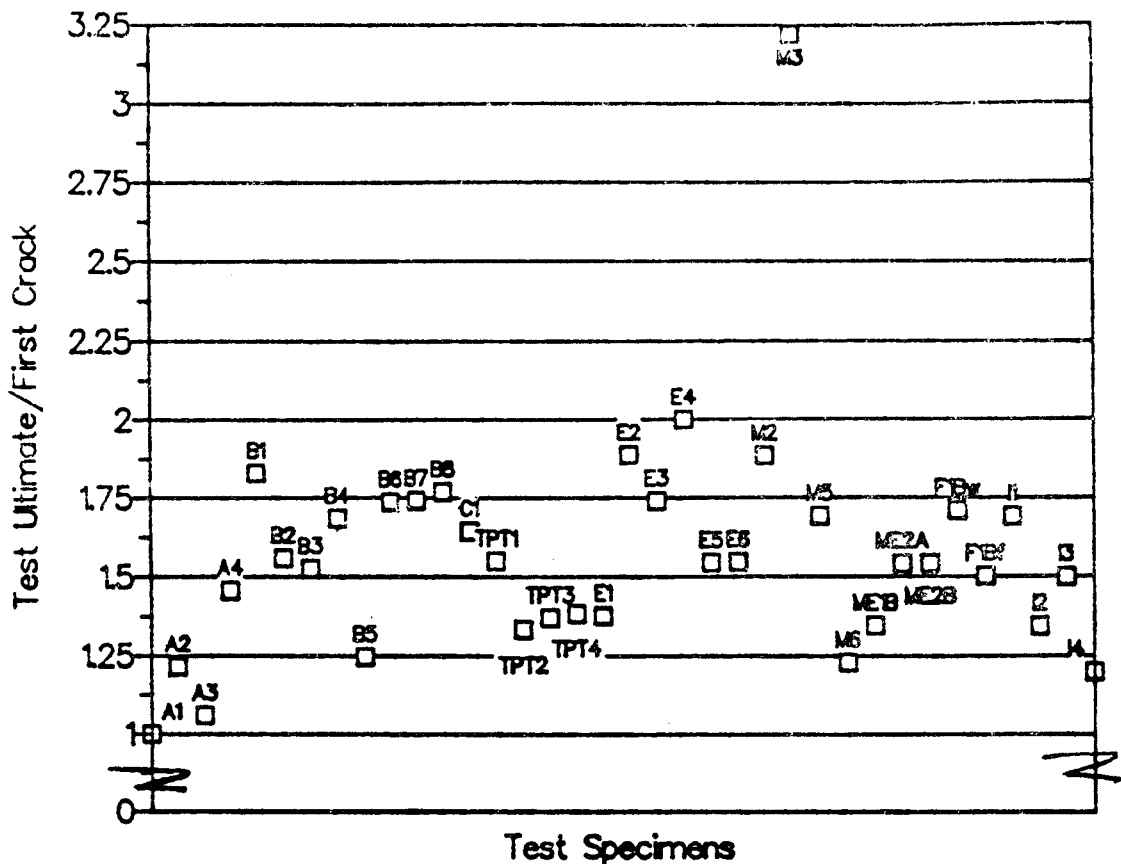


Figure 151. Ultimate-first crack summary.

(0.52). Table 40 shows that several specimens were more than 200 percent conservative, while two specimens were more than 20 percent unconservative. Clearly, a better method is desirable.

SLAB EDGE ANCHORAGE TESTS

Post-tensioning of bridge decks is increasing for structural efficiency, crack control, and durability. Generally, bridge deck tendons are multiple strand for 4-0.5 in. or 0.6-in. strands, or monostrand for single unbonded tendons. Typical deck anchors are shown in Figures 158 and 159. Usual applications are as a series of fairly closely and uniformly spaced tendons running from one edge to the other, either longitudinal or transverse. There have been a limited number of studies published in this area, as summarized in Appendix A.

The experimental program examined the effects of multiple edge anchor loading on anchorage zone strains, and the effects of adjacent anchor loading and exterior anchor edge distance on failure. Anchor types, anchor spacings, reinforcement layouts, and tendon inclination were also varied to examine their effects on anchor failure. In order to evaluate the effects of stressing sequence, anchor spacing, and edge distance on post-tensioning anchorage zones in bridge decks, six slabs with a total of 56 anchor pairs were tested. The anchorage zones incorporated monostrand and four-strand anchors, different edge distances and spacings, and a variety of reinforcing details. Anchorage

zones were to be loaded to standard post-tensioning loads and ultimately to failure. Figure 160 shows a slab during testing. Six slabs were constructed modeling 10-in.-thick bridge decks. The first five slabs were built at half scale and the sixth slab was built at full scale. The slabs incorporated various geometric properties and reinforcing details that are outlined in Table 41. For detailed plans of each slab's geometry and reinforcement, refer to Appendix C.

Three sizes of rectangular post-tensioning anchor plates were used at two orientations—horizontal and vertical. Anchor spacings and end anchor edge distances were varied (Figure 161). Eight of the 56 anchorage zones tested had vertically oriented plates. Anchors were spaced at two plate or four plate widths center-to-center distance, and the edge distance varied from one-half an anchor width to two anchor widths.

Steel plates of 2 in. by 6 in. by 0.5 in. and 2 in. by 5 in. by 0.5 in. were used to model commercial anchors. Those dimensions represent both four-strand rectangular anchors at half scale and monostrand anchors at full scale. Forty-eight pairs of the anchorage zones were half-scale four-strand anchor models, and eight pairs were monostrand full-scale anchorage zones. The vertically oriented anchors modeled four-strand anchors.

All horizontally oriented anchors were spaced at two plate widths center-to-center. The vertically oriented plates were placed at four anchor widths center-to-center. Of the 12 end anchors, two had an edge distance of two plate widths, and one

Table 38. Basic STM results summary

Specimen	Failure Mode	Predicted Capacity (kips)	Test Ultimate (kips)	Test/Prediction
A1	Node-Strut Interface	195	298	1.52
A2	Node-Strut Interface	190	275	1.45
A3	Node-Strut Interface	204	265	1.30
A4	Node-Strut Interface	306	437	1.43
B1	Tension Tie	299	366	1.22
B2	Tension Tie	292	290	0.99
B3	Tension Tie	296	331	1.12
B4	Tension Tie	277	337	1.22
B5*	L.Z.-G.Z. Interface	218	212	0.97
B6	Bearing	218	297	1.36
B7	Tension Tie	269	296	1.10
B8	Tension Tie	252	276	1.09
C1	Tension Tie	192	370	1.93
TPT1	Tension Tie	180	310	1.72
TPT2	Tension Tie	253	300	1.19
TPT3	Tension Tie	247	370	1.50
TPT4	Tension Tie	235	332	1.41
E1	Bearing	404	475	1.17
E2	Bearing	445	500	1.12
E3	Bearing	453	522	1.15
E4**	Bearing	434	500	1.15
E5	Tension Tie	238	332	1.39
E6	Tension Tie	259	348	1.34
M1	Tension Tie	189	304	1.61
M2	L.Z.-G.Z. Interface	322	401	1.25
M3	Tension Tie	290	364	1.26
M4	Tension Tie	180	411	2.28
M5	Tension Tie	202	339	1.68
M6	Tension Tie	104	300	2.88
ME1	Tension Tie	226	350	1.55
ME2	Tension Tie	261	370	1.42
F1	Tension Tie	133	248	1.86
I1	Tension Tie	281	423	1.51
I2	Tension Tie	223	437	1.96
I3	Tension Tie	262	375	1.43
I4	Tension Tie	126	420	3.33
				Average
				1.50
				Standard Deviation
				0.49
				Coefficient of Variance
				0.33

*Tension tie capacity ignored

**Longitudinal edge tension and spalling capacity ignored.

had an edge distance of one-half a plate width. The other nine end anchors had an edge distance of one plate width. In the second slab constructed, crack formers were placed ahead of three anchors to negate the effects of concrete tensile strength in the horizontal plane during sequenced stressing.

The most standard bridge slab reinforcement is horizontal steel (longitudinal and transverse in the plane of the slab) for serviceability, temperature, and distribution of loads (Figure 162). In this study, the term horizontal steel will be used to refer to reinforcement in the plane of the slab and normal to the axis of the tendon. Four horizontal reinforcing ratios were used—

unreinforced, temperature reinforcement, 64 percent of temperature reinforcement, and double temperature reinforcement. Most slabs contained the minimum horizontal temperature reinforcement required by AASHTO (16) which is 0.25 in.² per foot of slab per face in each direction (#2 bars at 9-in. on center for half scale and #3 bars at 9-in. on center for full scale).

A variety of anchorage zone reinforcing details were used in fabrication of the slabs (Figure 163). The details were picked because they were either common or easily constructed. Some details, such as back-up bars, hairpins, and spirals, were considered standard anchorage zone reinforcement. Details, such as

cross ties or a pair of hairpins tied into a hoop, were considered easy to construct and efficient anchorage zone reinforcement. Unreinforced anchorage zones were used as a control group for evaluation of anchorage zone reinforcement in general.

Concrete strains, reinforcing steel strains, cracking loads, and failure loads were recorded during slab testing. Loading was achieved by tensioning threaded post-tensioning bars or steel strands that were passed through each duct and anchored against each duct's plates. Hydraulic rams tensioned the bars individually, emulating jacking forces and seating forces upon each bar's

corresponding anchors. The anchors were loaded one by one in stressing sequences to produce large horizontal plane stresses in slabs 1 through 3. After all anchors were loaded to a standard post-tensioning load of 30 kips ($0.70 F_{pu}$), each pair of anchors was loaded until anchorage zone failure occurred. Full details of loading, instrumentation, and observations have been reported by Falconer (61).

Concrete compressive, split cylinder and elastic modulus tests were run for each slab. Values are given in Table 42. Tensile tests indicated deformed #2 bars had f_y of 61 ksi, #3 bars had f_y of 59 ksi, and #2 bars in welded wire fabric had f_y of 86 ksi.

All prestressing strands were a nominal 270 ksi. The 4-strand post-tensioning anchor would have an $F_{pu} = 4 \times 0.153$ in.² \times 270 ksi = 165.2 kips. If modeled at $\frac{1}{2}$ scale, it would be modeled by $\frac{1}{4}$ this force, or 41.3 kips. For low relaxation strand, AASHTO would limit temporary overstressing before seating to 0.81 of this value, or 33.5 kips. For simplicity in the test program, this was taken as 35 kips. The same value would be used for full-scale monostrand tests. Anchors were set at 30 kips to model the 0.70 F_{pu} limit after initial setting. No anchors were loaded to failure until all of the slab's anchors had been locked off at 30 kips.

Failure Patterns

Failures typically burst a semicircular piece of concrete from either the top, bottom, or top and bottom of the slab at the

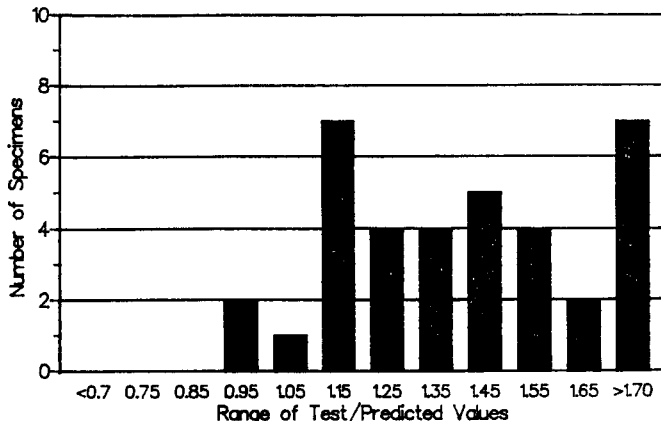


Figure 152. Frequency of occurrence for basic STM.

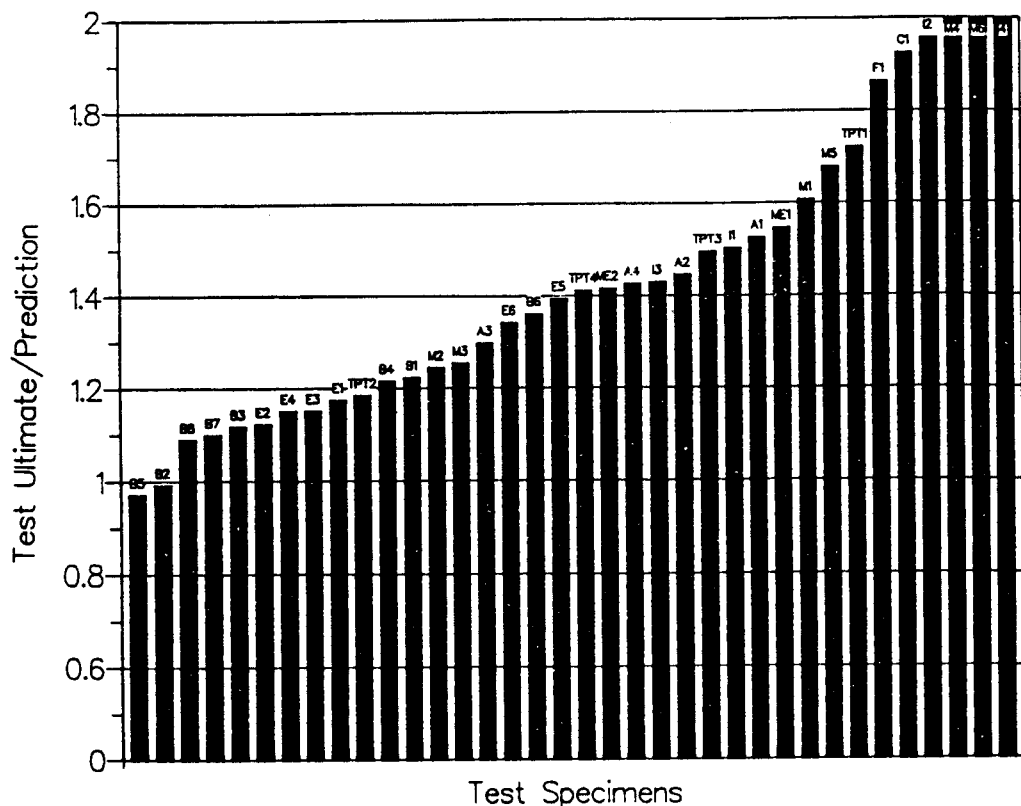


Figure 153. Distribution of results for basic STM.

Table 39. Comparison between ultimate load and first yielding load

Specimen	Test Ultimate Load (kips)	First Yield Load (kips)	Ultimate / First Yield
A1	298	Reinforcement did not yield	-
A2	275	275	1.00
A3	265	Reinforcement did not yield	-
A4	437	437	1.00
B1	366	366	1.00
B2	290	275	1.05
B3	331	240	1.38
B4	337	240	1.40
B5	212	No bursting reinforcement	-
B6	297	175	1.70
B7	296	220	1.35
B8	276	210	1.31
C1	370	350	1.06
TPT1	310	300	1.03
TPT2	300	280	1.07
TPT3	370	370	1.00
TPT4	332	330	1.01
E1	475	470	1.01
E2	500	495	1.01
E3	522	475	1.10
E4	500	490	1.02
E5	332	325	1.02
E6	348	340	1.02
M1	304	304	1.00
M2	401	300	1.34
M3	364	280	1.30
M4	411	390	1.05
M5	339	325	1.04
M6	300	250	1.20
ME1	350	350	1.00
ME2	370	350	1.06
F1	248	248	1.00
I1	423	310	1.36
I2	437	290	1.51
I3	375	375	1.00
I4	420	380	1.11
Average			1.14

failed anchor (Figure 164). These failures often split the slab transversely, and they also revealed that a shear cone had developed ahead of the anchor plate during failure (Figure 165). For end anchors, bursting cracks were often able to penetrate either the slab's side, or top and bottom (Figure 166). For interior anchors, vertical splitting along the tendon occurred infrequently and never before failure. Prefailure cracking typically extended from the corners of the slab similar to the elevations in Figure 167 demonstrating anchor failure.

The first two slabs concentrated primarily on the effects of

stressing sequence on strains in horizontal and vertical planes, and the final four slabs concentrated primarily on failure testing of anchorage zones. In slabs 3 through 6, on each anchorage pair, a heavily reinforced anchorage was positioned opposite from an anchorage zone reinforcing detail that was under investigation. This enabled the slab's anchor failures to be alternated from side to side, and prevented an anchorage zone from being damaged by adjacent failures before it was tested. However, in some cases, the heavily reinforced anchorage failed and the

maximum load of the detail being tested was not reached. Failure

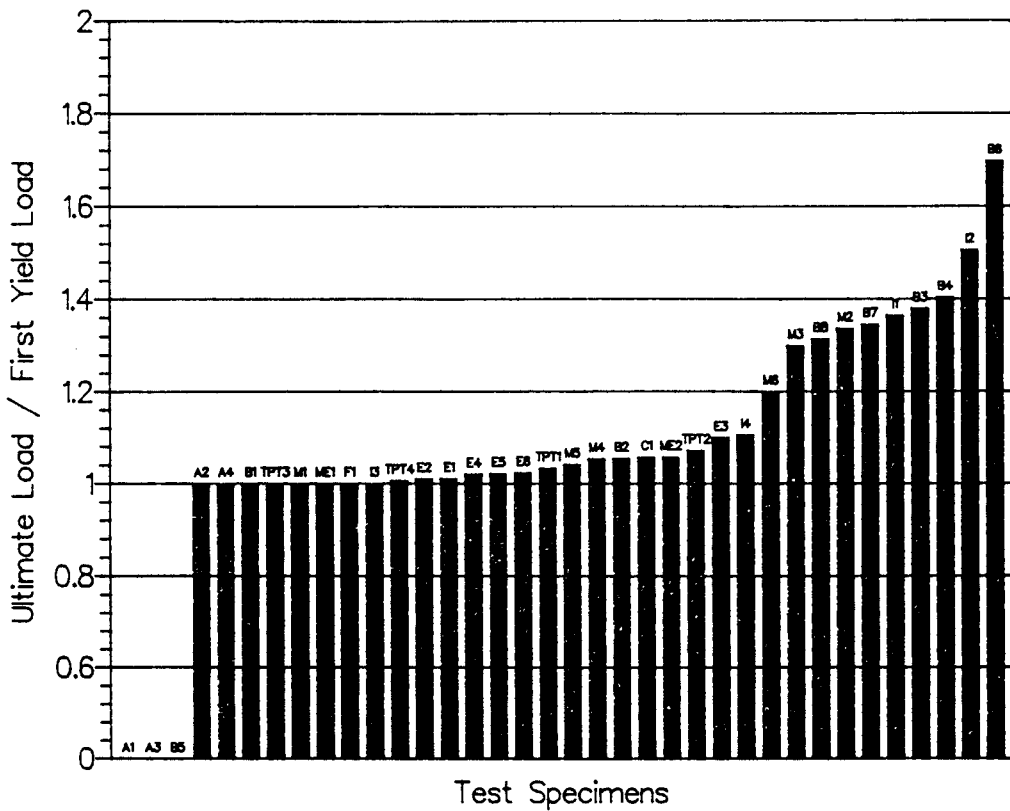


Figure 154. Graphical comparison between ultimate and first yielding load.

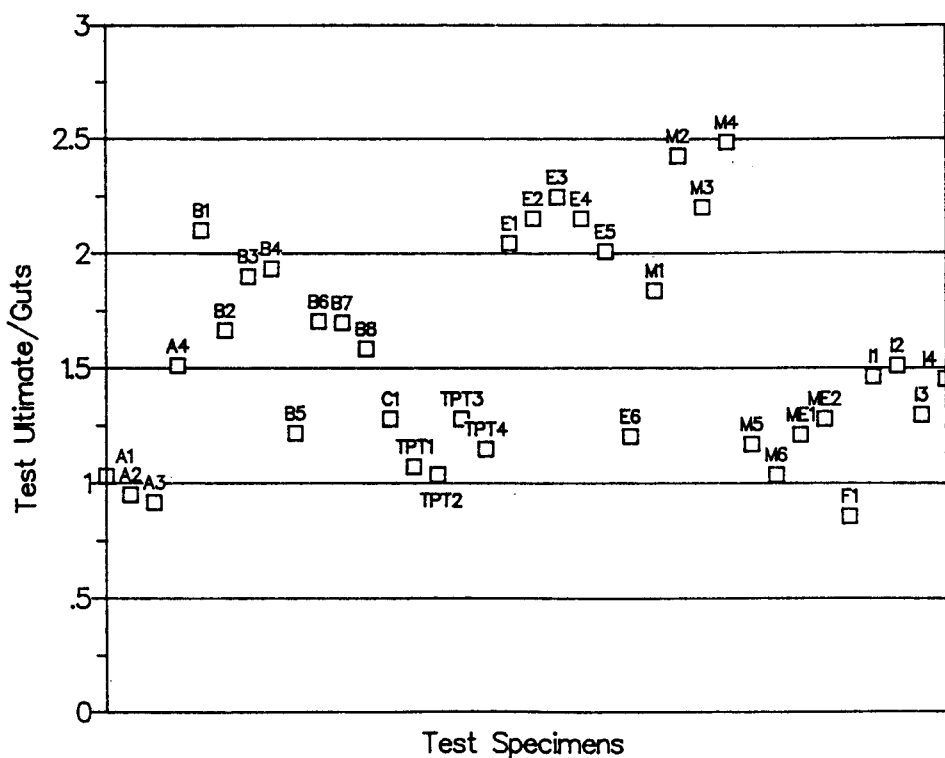


Figure 155. Test ultimate versus "GUTS".

Table 40. Current ultimate prediction method results

Specimen	Failure Mode	Predicted Capacity (kips)	Test Ultimate	Test/Prediction
A1	Bearing	340	298	0.88
A2	Bearing	340	275	0.81
A3	Bearing	340	265	0.78
A4	Bearing	544	437	0.80
B1	Bursting Tension Tie	342	366	1.07
B2	Bursting Tension Tie	198	290	1.46
B3	Bursting Tension Tie	267	331	1.24
B4	Bursting Tension Tie	287	337	1.17
B5	Bursting Tension Tie	0	212	—
B6	Bearing	218	297	1.36
B7	Bursting Tension Tie	287	296	1.03
B8	Bursting Tension Tie	261	276	1.06
C1	Bursting Tension Tie	258	370	1.44
TPT1	Bursting Tension Tie	164	310	1.89
TPT2	Bursting Tension Tie	239	300	1.26
TPT3	Bursting Tension Tie	345	370	1.07
TPT4	Bursting Tension Tie	312	332	1.06
E1	Bearing	369	475	1.29
E2	Bearing	391	500	1.28
E3	Bearing	399	522	1.31
E4*	Bearing	380	500	1.32
E5	Bearing	343	332	0.97
E6	Bursting Tension Tie	147	348	2.37
M1	Bearing	418	304	0.73
M2	Bursting Tension Tie	317	401	1.27
M3	Bursting Tension Tie	314	364	1.16
M4	Bursting Tension Tie	317	411	1.30
M5	Bursting Tension Tie	72	339	4.69
M6	Bursting Tension Tie	152	300	1.97
ME1	Bursting Tension Tie	240	350	1.46
ME2	Not Available		370	
F1	Bursting Tension Tie	177	248	1.40
I1	Not Available		423	
I2	Not Available		437	
I3	Not Available		375	
I4	Not Available		420	
*Longitudinal edge tension and spalling capacity ignored		Average	1.36	
		Standard Deviation	0.71	
		Coefficient of Variance	0.52	

of the heavily reinforced anchorage was typically effected by damage caused to the anchorage zone by previous adjacent anchorage failure.

Test Results

Horizontal Orientation of Half-Scale Four-Strand Anchors

Slabs 1 through 4 contained half-scale rectangular four-strand anchors with horizontal orientation. Tendon locations and alpha-

betical designations are given in Figures C39, C40, C42, C44, C46, and C48 in Appendix C. Anchors are designated by these alphabetical designations, i.e., anchor C. These slabs were used to evaluate both the effects of stressing sequences on vertical plane and horizontal plane stresses and the efficiency of anchorage zone reinforcement in post-tensioned bridge decks.

A stressing sequence, identical to the one analyzed using finite elements, was used to load the anchor pairs up to the permissible jacking force of $0.8 F_{pu}$ (35 kips). This sequence included loaded

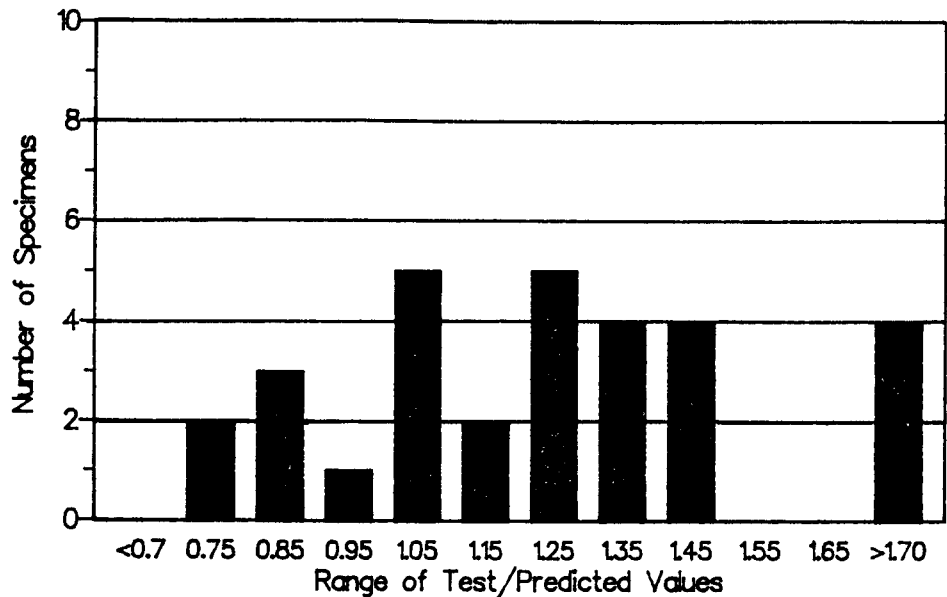


Figure 156. Frequency of occurrence for current ultimate capacity method.

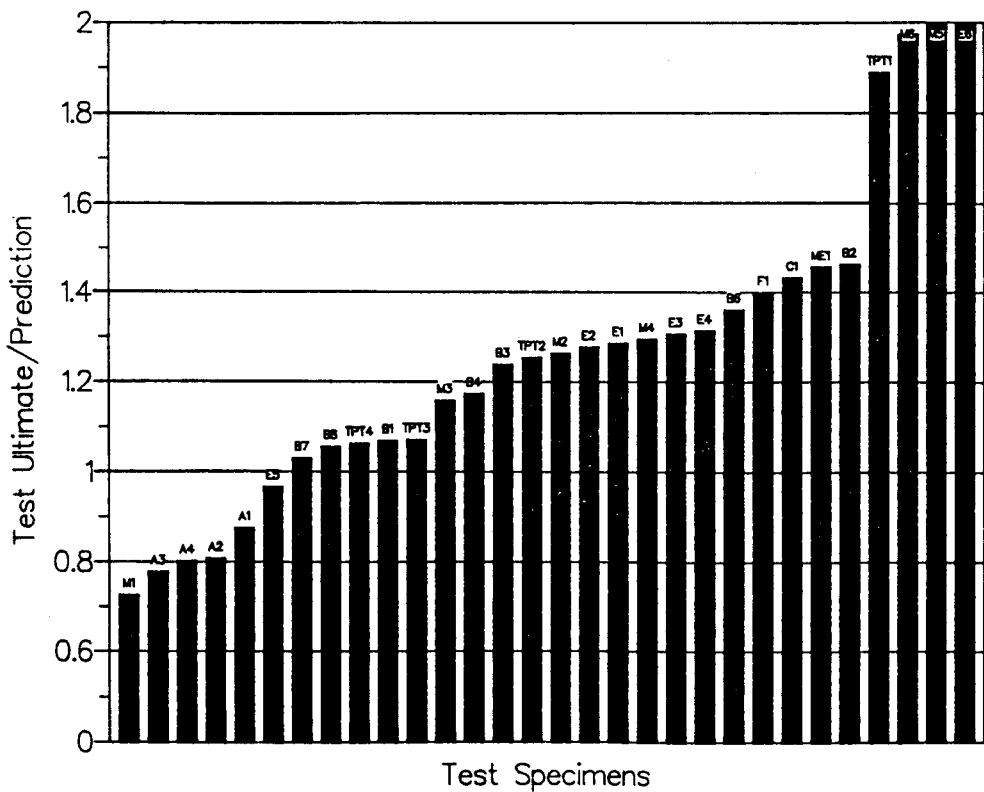


Figure 157. Distribution of results for current ultimate capacity method.

anchors at spacings of eight plate widths, four plate widths, and two plate widths, and loaded anchor edge distances of five, four, three, two and one plate widths. While loading the unreinforced slab 1 with the initial service loads, cracks extended diagonally

from the corners of some anchors (Figure 167). After sequenced loading, anchors were loaded to failure.

During sequenced stressing of the slabs, bursting and spalling stresses were developed in the horizontal plane, and bursting

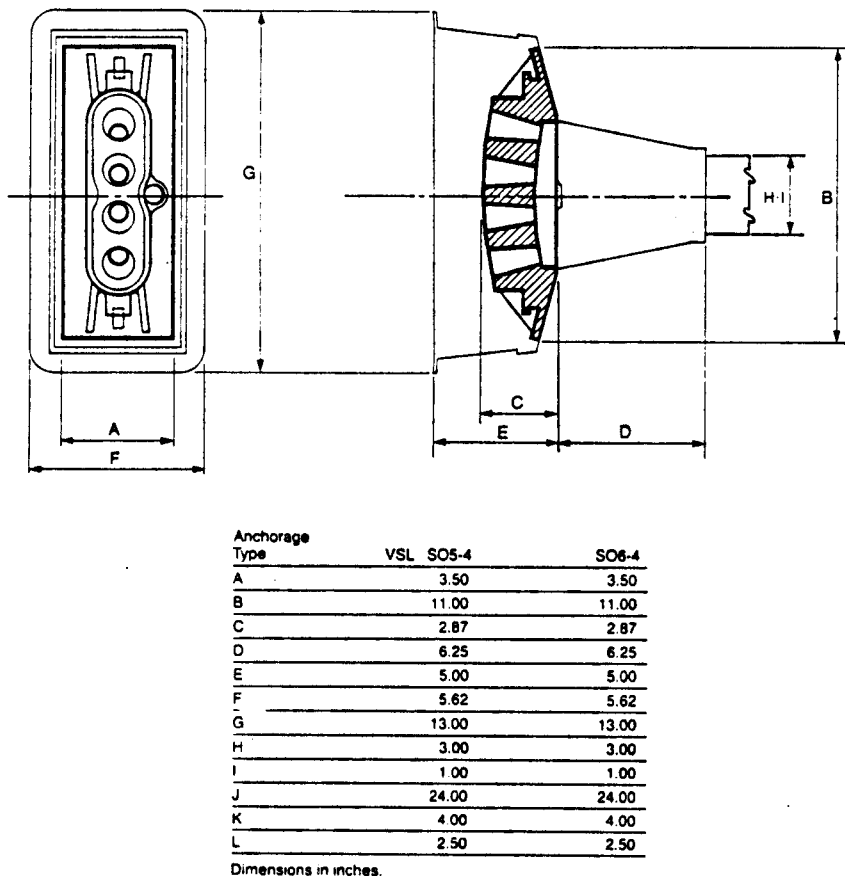


Figure 158. Four-strand post-tensioning anchorage (from VSL catalog).

stresses were developed in the vertical plane. Two stressing sequences were used on slab 1 and slab 2. One stressing sequence loaded every fourth anchor, then every other anchor, and finally all anchors. The other stressing sequence stressed the end anchor with the smallest edge distance first, and then adjacent anchors all the way across the slab. Horizontal bursting stresses were highest when every other anchor was loaded, including the end anchor with the one-plate-width edge distance. Loading the exterior anchor also modified the anchorage zone of anchor C, the third from the edge. The horizontal plane bursting stresses ahead of anchor C became higher and concentrated closer to the anchor. Anchor spacing and stressing sequence had little effect on vertical strains and failure load for anchors spaced at a distance larger than two plate widths. Stressing of every second anchor caused the highest stresses in the horizontal bursting reinforcement. However, these stresses were not critical.

As shown in the details in Appendix C, these slabs contained unreinforced anchors, back-up bars, hairpins with backup bars, cross ties, spirals with backup bars, hoops with backup bars, and hairpin hoops with backup bars. Backup bars never gained high stresses before anchorage failure occurred for horizontally oriented four-strand anchors. The average failure loads of these anchorage zones are shown in Figure 168, and f_b/f'_c ratios are shown in Figure 169. All values are given in Table 43. The failure loads of anchorage zones reinforced with backup bars, exclusively, did not appear to be higher than unreinforced anchor-

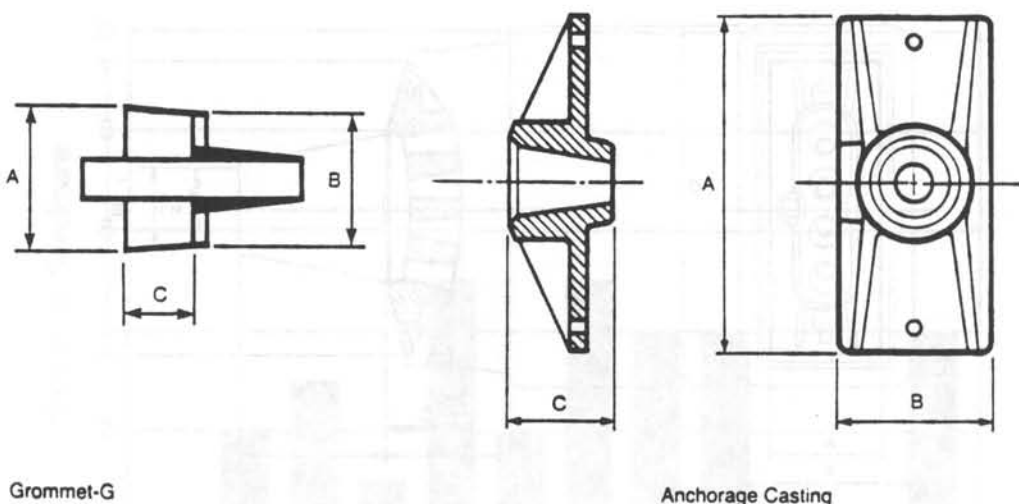
age zones. The anchorage zones with hoop or spiral reinforcing reached the highest f_b/f'_c ratios. All specimens developed the nominal GUTS ($1.0 F_{pu}$) of the tendons.

Vertical Orientation of Half-Scale Four-Strand Anchors

Slab 4 had eight vertically oriented four-strand anchor pairs spaced four plate widths apart center-to-center. At failure they tended to show a semicircular bursting region that was much more confined for the vertically oriented anchor than for the horizontally oriented anchor. The failure loads and f_b/f'_c ratios for these anchors are shown in Figures 170 and 171, respectively, and in Table 44. Unlike the horizontally oriented anchor specimens, the vertically oriented anchor specimens demonstrated high stresses in the backup bars because of anchor loadings. The hairpins and the spirals were the most effective reinforcement. The average failure loads for both reinforcement types were 92.5 kips ($2.25 F_{pu}$) and the average f_b/f'_c ratio was 1.90.

Half-Scale Four-Strand Anchors with Inclined Tendons

Inclined tendons, at an angle of approximately 17 deg., were placed in slab 5 with eight half-scale horizontally oriented four-



Component	Length or Diameter	Width or Diameter	Depth or Thickness	Bearing Area (in ²)	Conc. Strength at Stressing* (lb/in ²)
	A	B	C	—	—
SSN	5.00	2.25	1.50	11.25	2050
SSNW1	5.25	2.88	1.50	15.09	1500
SSNW2	4.00	3.50	1.50	14.00	1700
S8N	4.63	3.50	1.63	16.19	2100
S8NW	6.00	3.50	1.63	21.00	1600
G5	2.25	2.00	1.25/2.25	—	—
G6	2.50	2.13	1.25/2.25	—	—

Dimensions in inches.

*Values are based on ACI formula $l_e = 0.8 l'_e \sqrt{A_y/A} - 0.2 \leq 1.25 l'_e$ with edge distance of 1" for hardrock concrete.

Figure 159. Monostrand post-tensioning anchorage (from VSL catalog).



Figure 160. Slab 3 during testing.

strand anchor pairs. In general, these anchors carried higher loads relative to tendon ultimate and their concrete compressive strength. Figures 172 and 173 and Table 45 show the failure loads and f_b/f'_c ratios of the eight anchor pairs. During all failures, the extended ridge of the inclined anchorage zone was separated from the slab (Figure 174).

Backup bars were not used in this specimen because they could not be placed ahead of the anchors along the slab's jagged edge. The slab horizontal reinforcement was placed as close to the anchors as possible, while still maintaining a $\frac{3}{4}$ -in. concrete cover. It was highly effective as anchorage reinforcement, although it did not reach over 20 ksi at failure.

Full-Scale Monostrand Anchors

Slab 6 had eight horizontally oriented monostrand anchor pairs, spaced four plate widths apart center-to-center. The failures of these anchorages were used to evaluate the effects of monostrand anchors on failure geometry and anchorage zone reinforcing efficiency. Figure 175 shows the failed anchor B, which occurred under a 145 kip load; this is 4.14 times the maximum

Table 41. Physical properties of the experimental program

<u>Scales</u>	
Half-scale	(5 slabs)
Full-scale	(1 slab)
<u>Anchor Types Modeled</u>	
4-in. x 12-in. four-strand anchor	(40 anchor pairs)
4-in. x 10-in. four-strand anchor	(8 anchor pairs)
2-in. x 5-in. monostrand anchor	(8 anchor pairs)
<u>Anchor Orientations</u>	
Horizontal	(48 anchor pairs)
Vertical	(8 anchor pairs)
<u>Edge Distance</u>	
1/2 plate width	(1 anchor pair)
1 plate width	(9 anchor pairs)
2 plate width	(2 anchor pairs)
<u>Tendon Orientation</u>	
Perpendicular	(48 anchor pairs)
Inclined	(8 anchor pairs)
<u>Slab Condition</u>	
Concrete initial uncracked	(5 slabs)
Cracks in anchorage zone before loading	(1 slab - 3 anchor pairs)
<u>Reinforcing Details</u>	
Unreinforced	(20 anchors)
Horizontal reinforcing	(12 anchors)
Anchorage zone reinforcement	
Back-up bars	(6 anchors)
Hairpins	(8 anchors)
Cross ties	(14 anchors)
Spiral	(8 anchors)
Hoops	(2 anchors)
Hairpins ties into a hoop	(2 anchors)
Control detail	(40 anchors)

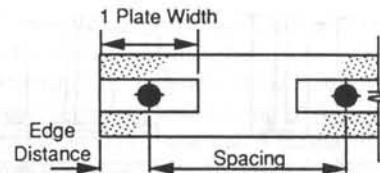
jacking force ($0.8 F_{pu}$) that would ordinarily be applied to a monostrand anchor for a $\frac{1}{2}$ -in. strand ($f_b/f'_c = 3.96$). For this failure, the horizontal crack is not localized. The failure loads and f_b/f'_c ratios for all of the anchors are shown in Figures 176 and 177, respectively, and in Table 46. The anchorage zones reinforced with a spiral could not be failed with the maximum capacity of the loading equipment, 150 kips. The control detail failed along two tendons where the anchorage zone had been damaged by prior adjacent anchor failures. When alone, the backup bars did not attain more than 6 ksi of stress prior to failure. When combined with cross ties or spirals, the backup bars picked up substantial force and, in some cases, yielded.

Summary of Test Results

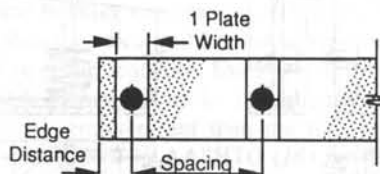
On the basis of the measured test results, bridge deck post-tensioning anchorage zones examined were generally strong enough to safely withstand the tendon jacking force ($0.8 F_{pu}$) of typical monostrand and multistrand slab anchorage devices, with the exception of exterior anchors with small edge distances.

Exterior Anchors and Edge Distance

Twelve exterior anchors were tested in the six slabs. Comparing anchorage zones in the same slab with the same anchor type,



(a) Horizontally Oriented Rectangular Anchorage Plate with 1/2 Plate Width Edge Distance for End Anchor and 2 Plate Width Center-to-Center Spacing



(b) Vertically Oriented Rectangular Anchorage Plate with 1 Plate Width Edge Distance for End Anchor and 4 Plate Width Center-to-Center Spacing

Figure 161. Anchor orientation, edge distance and spacing.

orientation, center-to-center spacing, and reinforcing, exterior anchors failed at an average of 88 percent of the failure loads of interior anchors (see Figure 178). Exterior anchors with small edge distances failed at significantly lower loads. Four anchors, with edge distances that were less than the slab thickness, failed at an average of 58 percent of the failure loads of similar interior anchors.

In interior anchors the failure mode was generally concrete crushing or spalling. In exterior anchors the failure mode changed to horizontal or vertical splitting of the slab, clearly requiring general zone reinforcement in both transverse planes.

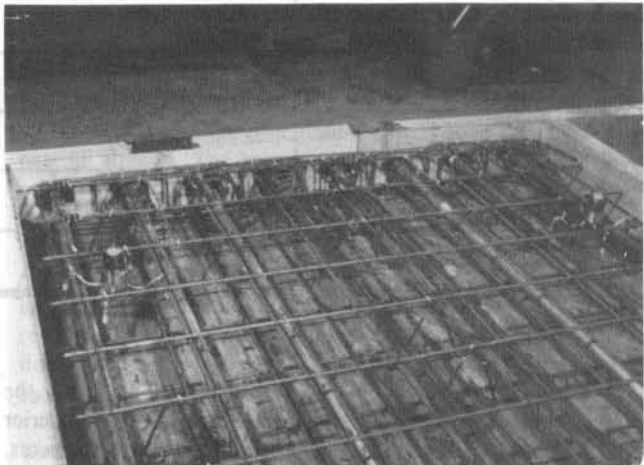


Figure 162. Horizontal steel in slab 6.

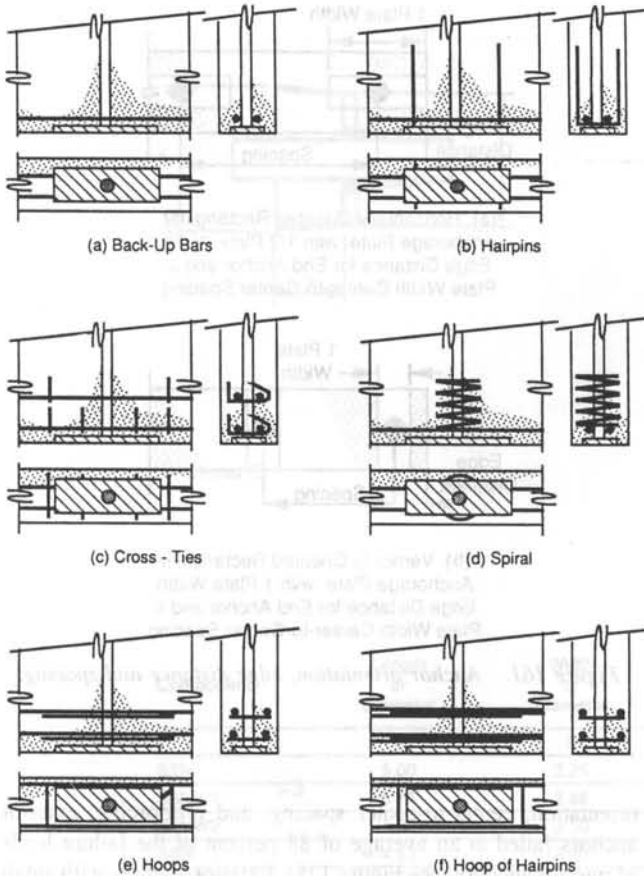


Figure 163. Anchorage zone reinforcing details.

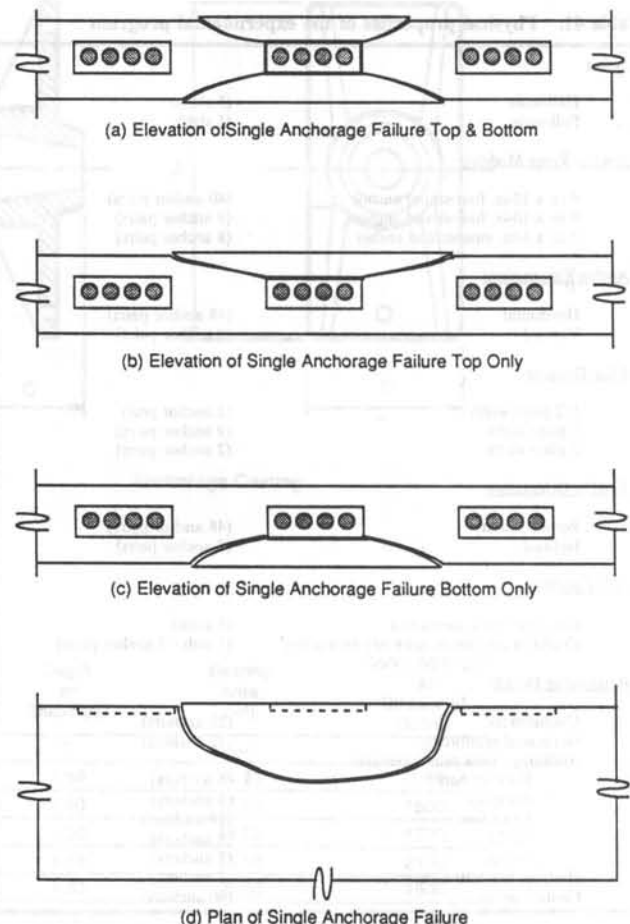


Figure 164. Single edge anchorage failures.

Table 42. Concrete strengths of slabs

Slab #	f'_c (psi)	f'_{sp} (psi)	E_c (psi)
1	3106	361	3,177,000
2	4635	363	3,881,000
3	4363	325	3,765,000
4	3797	319	3,512,000
5	4555	414	3,847,000
6	4448	386	3,802,000

Overall, it is apparent that edge distances of less than the slab thickness significantly reduce the strength of the exterior anchorage zone. For these anchorages, confining reinforcements, such as spirals and hoops, are effective in strengthening the anchorage zone.

Anchor Spacing and Stressing Sequence

The effects of anchor spacing and stressing sequence are slight on horizontal plane strains but, as shown by Sanders, Breen and

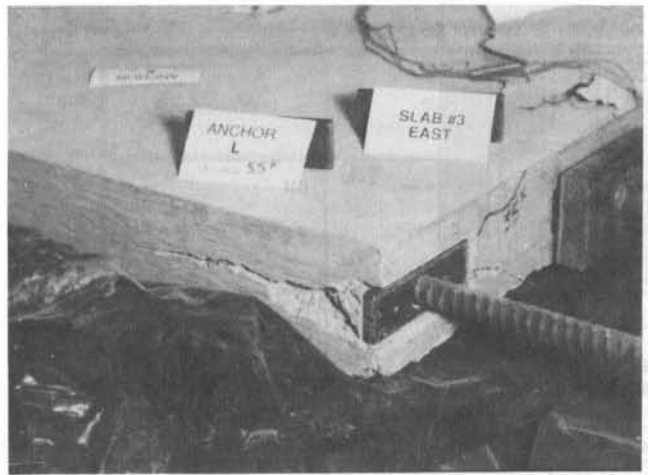


Figure 165. Shear cone ahead of anchor slab 3 at failed anchor L (back-up bars).



Figure 166. Slab 3 at failed anchor A (unreinforced).



Figure 167. First cracking at anchor E of slab 1.

Duncan (62), the reduced effective area of closely spaced anchors can reduce the anchorage zone strength of individual anchors.

In the experimental program, horizontal and vertical plane stresses in plain concrete were calculated from gage strain readings acquired from slab 1 and slab 3 during sequenced loading of the anchors to service loads. Horizontal and vertical reinforcement stresses were calculated from gage readings acquired from slab 2 during sequenced anchor loading. The finite element generated principal stress distributions were similar to the concrete and reinforcement strain distributions measured during sequenced tendon stressing. All of these cases indicate that the calculated vertical plane bursting stresses, due to loading a single anchor, are higher than the calculated horizontal plane bursting stresses due to any stressing sequence. Even in slab 2, which was reinforced across preformed cracks in the anchorage zones with less horizontal reinforcement than the minimum temperature reinforcement allowed by AASHTO (16) for bridge decks, the light horizontal reinforcement reached only one-third of its yield strength. Therefore, the AASHTO minimum reinforcement placed in bridge decks is sufficient to carry horizontal plane bursting forces in edge anchorage zones.

Figure 179 shows the ratios of interior anchor failure loads, without service level stressing loads on adjacent anchors, to the failure loads of interior anchors with adjacent loads. It is obvious that this is not an important variable for interior anchors.

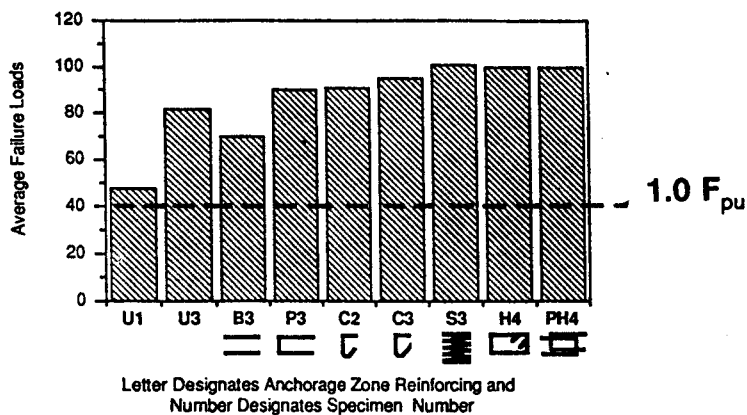
Evaluation of Anchorage Zone Reinforcing Details

All of the anchors, even unreinforced, withstood loads in excess of their expected maximum field stressing loads, which was 33 kips for tendon force transfer loading ($0.8 F_{pu}$) for all the tested anchors considering scale effects. The weakest anchorage group was the vertically oriented four-strand anchors, which failed at an average of 81.6 kips (2.3 times the realistic maximum load of a half-scale four-strand anchorage). Vertical reinforcing generally reached high stresses ahead of horizontally oriented anchors, and horizontal reinforcing generally reached high stresses ahead of vertically oriented anchors. However, only a few failures produced anchorage zone splitting, which indicate critical tensile forces. Exterior anchors and the monostrand anchors produced splitting.

Figure 180 shows the average f_b/f'_c ratios of interior anchors by group and reinforcement. Spiral anchorage reinforcement was consistently effective in sustaining high loads without reaching high steel stresses. The consistently low level of steel stresses indicates that the spiral acts as a confining reinforcement, which stiffens the anchorage zone until the local zone fails because of bearing stresses. The hairpin, cross tie, hoop and hairpin hoop reinforcement ahead of horizontal anchorages all reached high stresses, and most yielded during loading of the anchorage.

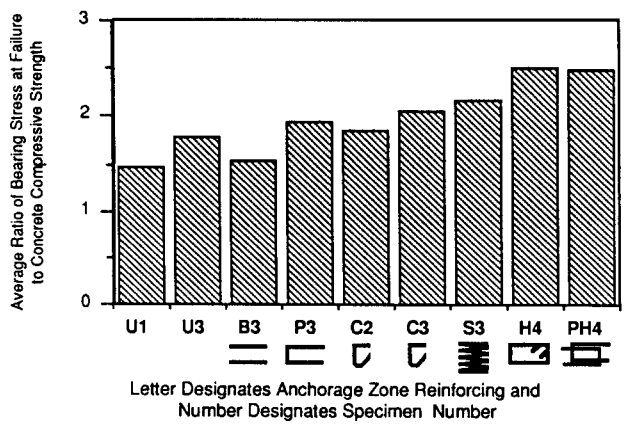
Spirals, hoops, and hairpin hoops had the highest average f_b/f'_c ratios ahead of horizontal four-strand anchors. However, unlike the spiral, the hoop and hairpin hoop reinforcement reached high stresses approaching failure, which indicates a reaction to vertical plane stresses rather than just confinement of the local zone.

The vertical interior anchor with only backup bars was much weaker than the vertical interior anchors containing vertical reinforcement. These anchors exhibited bearing failures, and apparently benefited from the anchorage zone confinement provided



- U - Unreinforced Anchors
- B - Back-up Bars
- P - Hairpins w/Back-up Bars
- C - Cross Ties
- S - Spiral w/Back-up Bars
- H - Hoops w/Back-up Bars
- HP - Hairpin Hoops w/Back-up Bars

Figure 168. Average failure loads of four-strand horizontally oriented anchors at half scale.



- U - Unreinforced Anchors
- B - Back-up Bars
- P - Hairpins w/Back-up Bars
- C - Cross Ties
- S - Spiral w/Back-up Bars
- H - Hoops w/Back-up Bars
- HP - Hairpin Hoops w/Back-up Bars

Figure 169. Average ratio of bearing stress at failure to concrete compressive strength for four-strand horizontally oriented anchors at half scale.

by the vertical reinforcement. The hairpin, cross tie, and spiral reinforced vertical interior anchors had an average f_b/f'_c ratio of 2.73, and the backup bar reinforced interior anchor's ratio was 2.13.

In contrast to the interior anchor failures, the exterior vertical anchor failure produced primarily horizontal plane splitting and failed with an f_b/f'_c ratio of 1.37. Although the backup bars reached high stresses ahead of all of the vertical anchorages,

they spanned the crack that caused the failure in this case and play an obvious role in resisting the failure. For the case of the vertical exterior anchor with a small edge distance, the horizontal plane bursting stresses are critical and the horizontal reinforcement should also be critical.

The inclined tendon anchorage zones produced similar failure loads regardless of reinforcement ranging from 95 kips to 110 kips. It should be noted, however, that the spiral reinforced anchorage zones withstood 110-kip loads without failure (f_b/f'_c ratio was 2.297), then failed at lower anchor loads because of what was considered to be eccentric loading. The average f_b/f'_c ratio for the other six anchors was 2.15. The strength of the anchorage zones in this specimen was apparently unaffected by most reinforcing. The concrete tensile strength may have been sufficient to carry loads that were beyond the capacity of all but the spiral reinforcement.

The full scale, spirally reinforced monostrand anchorage zones withstood a 150-kip load and an f_b/f'_c ratio of up to 3.90. A monostrand anchor is typically loaded with 35 kips at transfer loading (0.8 F_{pu}) with a $\frac{1}{2}$ -in. strand. The anchorages reinforced with cross ties both failed at a load of 150 kips. The tendon with the back-up bar reinforced monostrand interior anchorage failed at the control detail, and the interior anchorage zone reinforced with hairpins and back-up bars failed at 145 kips. Therefore, hairpins and back-up bars as monostrand anchorage zone reinforcement are not conclusively worse than cross ties, even though they failed in this test at lower loads. The horizontal monostrand failures produced vertical splitting ahead of the anchors, which indicates critical vertical stresses, but the failure loads of five of the monostrand anchors exceeded four times the expected anchor loading of a monostrand anchor.

Evaluation of Finite Element Analysis Predictions

The linear-elastic finite element analysis of the four-strand horizontally oriented anchors estimated that a 249 psi of vertical

Table 43. Failure of four-strand horizontally oriented anchors at half scale

Reinforcement	Slab	Anchor	Failure (kips)	f_b / f'_c (ksi/ksi)
Unreinforced	#1	A	56	1.715
		D	42*	1.286
		H	45*	1.378
		Average	47.7	1.460
Unreinforced	#3	A	75	1.635
		B	80	1.744
		C	80	1.744
		D	90	1.962
		Average	81.25	1.771
Backup	#3	K	85	1.853
		L	55	1.199
		Average	70	1.526
Hairpins	#3	E	85	1.853
		F	95	2.071
		Average	90	1.962
Cross Ties	#2	A	75	1.539
		D	102	2.093
		H	95	1.949
		Average	90.7	1.860
Cross Ties	#3	G	90	1.962
		H	100	2.108
		Average	95	1.949
Spiral	#3	I	95	2.071
		J	107	2.332
		Average	101	2.202
Hoops	#4	A	90**	2.254
		B	100	2.505
		Average	100	2.505
Hairpin Hoops	#4	C	100	2.505
		D	100	2.505
		Average	100	2.505

* Eccentricities in loading system

** Control detail failed

plane bursting stress and a 1404 psi local-general zone bearing stress are ahead of a half-scale horizontal four-strand anchor with a load of 35 kips applied to the anchor. The splitting tensile strength and compressive cylinder strength of the concrete were measured for each slab. The first cracking load was calculated as the load which would create an estimated vertical plane bursting stress equal to the slab's concrete splitting tensile strength. However, prefailure visible cracking loads were infrequent for edge anchors, and the first cracking loads predicted by the finite element analysis were, in general, much lower than the anchorage failure loads.

The failure loads of anchorages were compared to predictions made from the finite element analysis based on the calculated bearing stress at the interface between the local zone and the

general zone. The calculated bearing stress at the interface was limited to 75 percent of the concrete's compressive strength ($0.75f'_c$). The vertical finite element model calculated the highest stresses, and the depth of the local zone was chosen to be 2 in. (the plate width) for unreinforced and back-up bar reinforced anchorages, 4 in. for anchorages with one layer of vertical reinforcement ahead of the anchor, and 6 in. for anchorages with local zones confined with spirals or two layers of vertical reinforcement ahead of the anchor.

Figure 181 shows the ratio of actual failure loads to finite element predicted failure loads for horizontally oriented four-strand anchors with and without inclined tendons. The predictions were fairly accurate and always conservative. The average ratio of actual to predicted failure load was 137 percent. The least

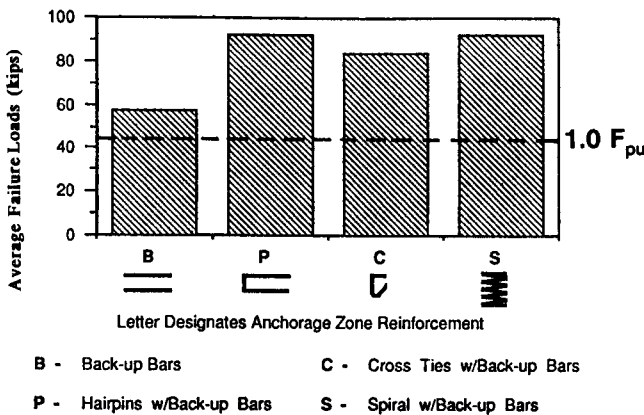


Figure 170. Average failure loads for four-strand vertically oriented anchors at half scale.

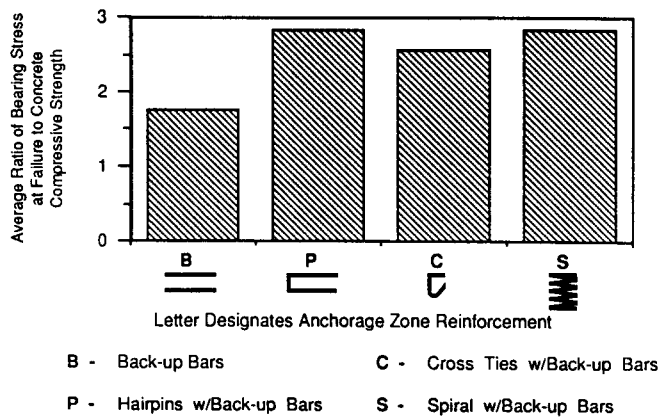


Figure 171. Average ratio of bearing stress at failure to concrete compressive strength for four-strand vertically oriented anchors at half scale.

accurate predictions were for the anchors lacking vertical reinforcement. This inaccuracy is probably related to the inaccuracy in picking the depth of the local zone.

Evaluation of Strut-and-Tie Model Predictions

The strut-and-tie model predicts failures by comparing the model's strut, tie, and node strength to the forces that each component will be subjected to during loading. The vertical plane strut-and-tie model controlled all of the horizontally oriented anchor failure predictions, and the horizontal plane strut-and-tie model controlled the vertically oriented anchor predictions. Tension forces carried by the plain concrete caused the accuracy of tie failure predictions to be very inconsistent, particularly for hairpin, back-up bar reinforced, or unreinforced, anchorages that are assumed to have little or no tie load capacity. Predictions of node and strut failure should provide more consistent results in cases where node or strut failure controls. Failures were very localized and often seemed to involve concrete crushing directly ahead of the anchor, which would indicate that the strut-and-tie

model failed at the node-strut connection or node-anchor plate connection directly ahead of the anchor plate. Those failures could be considered local zone failures. The vertically oriented exterior anchor failure and the monostrand anchors produced slab splitting which extended ahead of the anchor across assumed tie locations. This suggests that failure was due to bursting tie forces, rather than concrete crushing at the anchor-node-strut interface, and these failure could be considered a general zone failure.

Table 47 and Figure 182 show the actual failure loads and the predicted component strut-and-tie anchorage failure loads for the tested anchorage group. The model is conservative whenever the actual failure load level is higher than the lowest predicted component failure load level. For anchorages with horizontally oriented anchors with no vertical reinforcement or hairpins, tie failure predictions were excluded because concrete tensile strength withstood tie forces that allowed the anchor to carry 10 or more times the predicted tie failure anchor loads.

In general, the strut-and-tie models' failure load predictions were most accurate for the horizontally oriented four-strand anchors with and without inclined tendons. Tie failure predictions were most accurate overall because the strut and node failure loads were conservative for the vertically oriented anchors and the monostrand anchors. However, the failure geometry of the interior vertical anchors does not indicate that the anchorage zone failure included tie component failure.

For every anchor tested in this investigation, the actual failure level was higher than the predicted failure level. The strut-and-tie model proved to be a consistently conservative procedure for predicting anchorage zone failure load levels in bridge decks. Bridge deck post-tensioning anchors usually fail in their local zone. This makes analysis of the local zone the primary concern. Node failure, strut failure, vertical plane tie failure ahead of all anchors and horizontal plane tie failures ahead of exterior anchors should be analyzed with the strut-and-tie model. The disregard of concrete tensile strength in this application results in considerable overconservatism for splitting in the plane of the slab, but not for edge and closely spaced anchors.

RESULTS OF THE END REACTION TESTS

The experimental program investigating the effect of reaction forces on the behavior of post-tensioned anchorage zones was conducted by Wollmann (60). It included three 9-in. by 16-in. by 108-in. beam specimens, labeled beam 1, beam 2, and beam 3. These specimens were patterned after Sanders' specimen B3. Dimensions and details are provided in Appendix C. Specimen beam 1 was subjected to a concentrated tendon force only. Specimens beam 2 and beam 3 were designed to investigate the effect of a reaction force in the anchorage zone. Therefore, in addition to the tendon force a vertical concentrated load was applied at midspan and the beams were supported on 6-in.-wide steel plates centered 4 in. ahead of the end face of the anchor bearing plate. All anchors were 6.5 in. by 6.5 in. by 2 in. The shear span for these beams was 48 in. or three times the depth of the cross section (Figure 183).

Table 48 includes information on the concrete cylinder compressive strengths at the day of testing and on the anchorage zone reinforcement. Specimen beam 3 was added to the experimental program after specimen beam 2 developed an excessively high

Table 44. Failure of four-strand vertically oriented anchors at half scale in slab 4

Reinforcement	Anchor	Failure (kips)	f_b/f_c' (ksi/ksi)
Backup	K	70	2.131
	L	45*	1.368
	Average	57.5	1.750
Hairpins	E	90	2.740
	F	95**	2.892
	Average	92.5	2.815
Cross Ties	G	78	2.375
	H	90	2.740
	Average	84	2.560
Spiral	I	90	2.740
	J	95	2.892
	Average	92.5	2.815

* Exterior anchor with small edge distance

** Control detail failed

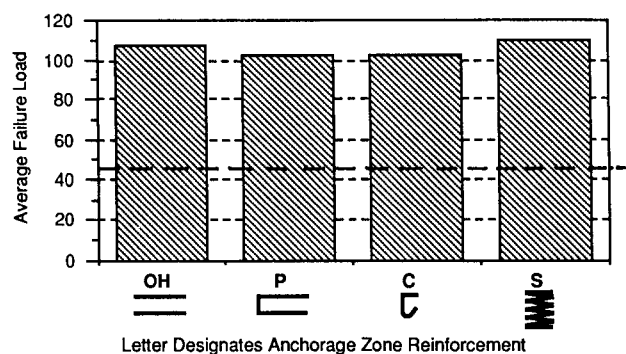


Figure 172. Average failure loads for horizontal anchors with inclined tendons.

concrete strength. Reinforcement sizes 3 and larger were standard ASTM A615 GR60 steel. Instead of #2 bars, Swedish reinforcement bars with 6-mm diameter, an area of 0.44 in.² and a yield strength of 72 ksi were used.

The design prestressing load, F_{pu} , was 284 kips for all specimens. This load is approximately equal to the breaking strength of a 7½-in. strand tendon. The design vertical load for specimens beam 2 and beam 3 was 56.8 kips, which results in a reaction force equal to 10 percent of the axial load at each support. Specimen beam 2 was initially loaded at a V/P ratio between 0.05 and 0.06, where V is the reaction force or half the applied vertical load and P is the tendon force. After V reached approximately 15 kips the specimen was unloaded. In a second loading step, the V/P ratio was kept between 0.10 and 0.12 until V reached its final load of 28.4 kips. The vertical load was then held constant while the tendon load was increased to failure. This procedure

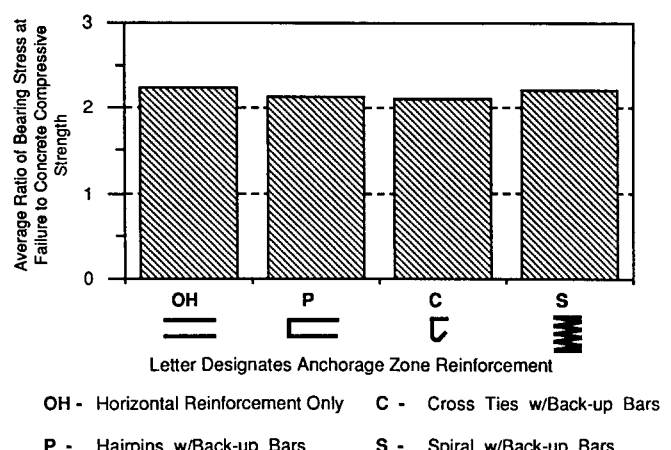


Figure 173. Average ratio of bearing stress at failure to concrete compressive strength for horizontal anchors with inclined tendons.

was chosen to avoid an axial-flexural failure in midspan and to ensure an anchorage zone failure. The test procedure for specimen beam 3 was identical except for the omission of the first load step with V/P = 0.05 to 0.06.

Behavior

Table 48 shows first cracking, first yield, and ultimate loads of the beam specimens. Values for both live end and dead end are given where appropriate. The loads are expressed as a ratio of the design load, F_{pu}/F_{pd} . F_{pd} is approximately equal to the breaking strength of a tendon composed of 7½-in. strands. Crack pattern and failure mode were very similar for all three specimens. The

Table 45. Failure of four-strand anchors with inclined tendons at half scale in slab 5

Reinforcement	Anchor	Failure (kips)	f_b / f_c' (ksi/ksi)
Horizontal	G	105	2.192
	H	110	2.297
	Average	107.5	2.245
Hairpins	A	95	1.983
	B	110	2.297
	Average	102.5	2.140
Cross ties	C	100	2.088
	D	105	2.192
	Average	102.5	2.140
Spiral	E	110	2.297
	F	105*	2.192
	Average	110	2.297

* Control detail failed

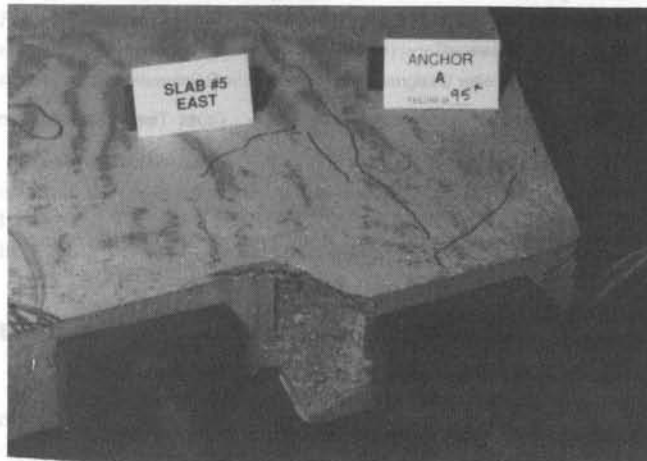


Figure 174. Failed anchor A in slab 5.

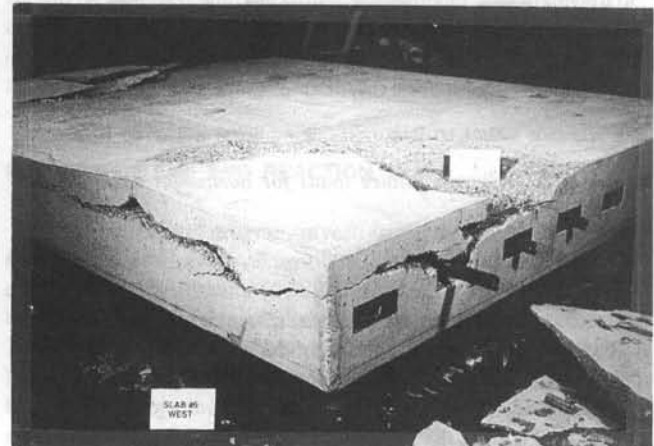


Figure 175. Failed anchor B in slab 6.

test results for specimen beam 2 are influenced by its significantly higher concrete strength, but comparison of the results for beam 1 and beam 3 indicates a beneficial effect of a reaction force in the anchorage zone.

Figure 184 shows crack development and final crack pattern for specimen beam 3, which is typical for all three specimens.

Anchorage zone cracking initiated at some distance ahead of the anchor plate and propagated in both directions towards and away from the anchor plate. First cracking loads are given in Table 48. Numbers shown on the crack sketches are the load level in kips when that extension of the cracking was noted. The bursting cracks extended as far as 26 in. or approximately one and one-

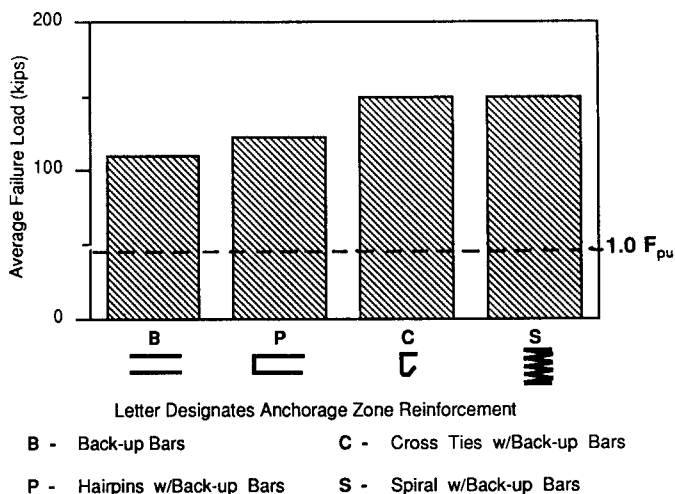


Figure 176. Average failure loads for monostrand anchors.

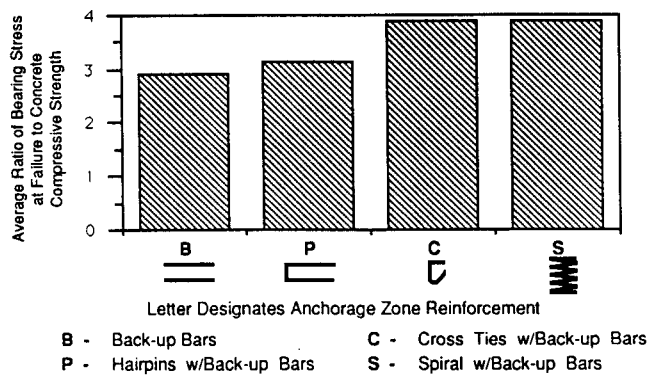


Figure 177. Average ratio of bearing stress at failure to concrete compressive strength for monostrand anchors.

half times the height of the beam ahead of the anchor plate prior to failure. Maximum crack widths remained below 0.03 in.

Figure 185 shows the vertical tie strains in specimen beam 1 at various load stages. The strain distribution is very similar for the other specimens of the test series. The region affected by the introduction of the tendon force extends for about 16 in. or a distance equal to one beam height for specimen beam 1. This distance was 24 in. or one and one-half beam heights for specimens beam 2 and beam 3, where a reaction force was present in the anchorage zone. First yielding of the bursting ties occurred at 85 to 95 percent of the failure load (Table 48). Associated crack widths were 0.01 in. to 0.015 in. Peak strains were measured 4 in. to 8 in. ahead of the bearing plates and diminished rapidly with the distance from the anchor. Only one or two bursting ties in the anchorage zone yielded.

Specimens beam 1 and beam 3 failed at the live end, while specimen beam 2 failed at the dead end. The ultimate tendon loads relative to F_{pu} are given in Table 48. In specimens beam 2 and beam 3 a vertical load of approximately 60 kips acted simultaneously with the tendon load at failure. The failure mode was identical for all three specimens. The concrete outside of the ties and of the spiral in the anchorage zone spalled off and

the concrete ahead of the spiral was crushed completely. The concrete confined by the spiral formed a plug that punched into the beam along its axis up to 2 in. at failure. The plug completely separated from the surrounding material and a thin layer of pulverized concrete was noticed on the skin of this plug. Removal of all loose concrete revealed a cone ahead of the spiral, typical for compression failures of unconfined concrete. The concrete within the plug was in good condition, and plug and cone could be removed easily from the specimen. Failures occurred with little warning and were explosive, particularly for specimen beam 2 with its high concrete strength. Prior to failure the bearing plates had punched into the beam less than $\frac{1}{10}$ of 1 in.

Evaluation of Test Results

Finite Element Analysis Predictions

Table 49 compares the actual failure loads to the predictions of the finite element analysis. The 2.5-in. dia. tendon duct was ignored in the analysis. The predictions are controlled either by the limit on the compressive stresses at the critical section, according to sections 9.21.3.2, 9.21.3.4, and 9.21.5 of the proposed anchorage zone specifications (Appendix E), or by the capacity of the bursting reinforcement, neglecting the tensile strength of the concrete. The governing prediction is underlined. The critical section for the compression check ahead of anchors with local confinement reinforcement is located at a distance equal to one plate width ahead of the anchor. The compressive stresses at this section must not exceed $\phi(0.7f'_{ci})$. ϕ was taken as 1.0 for laboratory conditions. While the prediction for specimen beam 1 is slightly unconservative, the overall agreement is good.

Strut-and-Tie Model Predictions

Table 50 compares the actual failure loads to the strut-and-tie model predictions. Predictions based on the capacity of the local zone, of the local zone-general zone interface, and of the bursting reinforcement are included. The capacity of the local zone is calculated from Eq. 7 (4). The other predictions are based on the strut-and-tie model procedures outlined in section 9.21.4 of the proposed anchorage zone specifications (Appendix E). Figure 98 shows a possible strut-and-tie model solution for the beam specimens with a reaction force in the anchorage zone. A nominal concrete strength of $0.7f'_{ci}$ and a ϕ -factor of 1.0 was used. Again, the prediction for beam 1 is slightly unconservative.

Conclusions

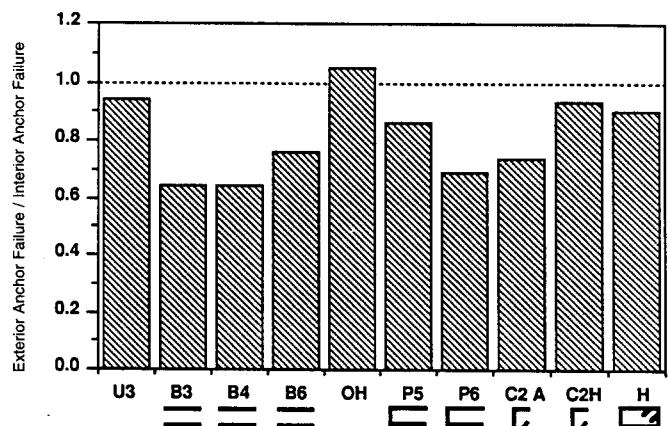
Both finite element analysis and strut-and-tie model predictions are within 10 percent of the actual failure load in most cases. However, it should be noted that the strut-and-tie model predicts a failure of the bursting tie in two cases as does the finite element method in one case, whereas the actual failure mode was always in compression. This is because the concrete tensile strength and possible stress redistributions after cracking are not included in the prediction models. However, for design such models are safe and useful, as evidenced by the test results.

Table 46. Failure of monostrand anchors at full scale in slab 6

Reinforcement	Anchor	Failure (kips)	f_b / f_c (ksi/ksi)
Backup	G	125*	3.300
	H	95	2.508
	Average	110	2.904
Hairpins	A	100	2.460
	B	145**	3.828
	Average	122.5	3.144
Cross Ties	C	150	3.960
	D	150	3.960
	Average	150	3.960
Spiral	I	> 150 **	> 3.960
	J	> 150 **	> 3.960
	Average	> 150	> 3.960

* Control detail failed

** Anchors E and F could not be failed with the 150-kips capacity loading system



First Letter Designates Anchorage Zone Reinforcing, Number Indicates Specimen Number, and Second Letter Indicates Anchor When Necessary

U - Unreinforced Anchors

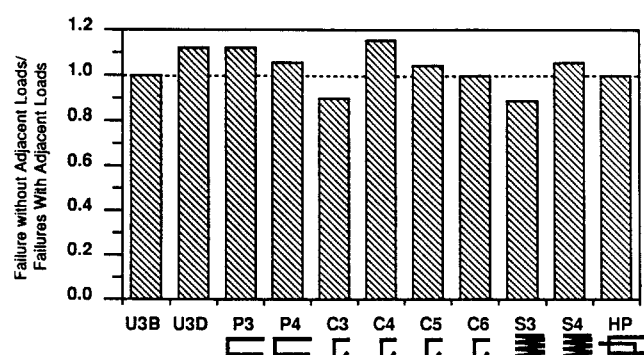
P - Hairpins w/Back-up Bars

B - Back-up Bars

C - Cross Ties

OH - Horizontal Reinforcing Only

H - Hoops w/Back-up Bars



First Letter Designates Anchorage Zone Reinforcing, Numbers Designate Specimen Number, and Second Letter Designates Anchor When Necessary

U - Unreinforced Anchors

S - Spiral w/Back-up Bars

P - Hairpins w/Back-up Bars

HP - Hairpin Hoops w/Back-up Bars

C - Cross Ties w/Back-up Bars

Figure 178. Ratio of exterior anchor failure loads to similar reinforced interior anchor failure loads.

Figure 179. Ratio of failure loads of anchors without adjacent anchor loads to failure loads of anchors with adjacent anchor loads.

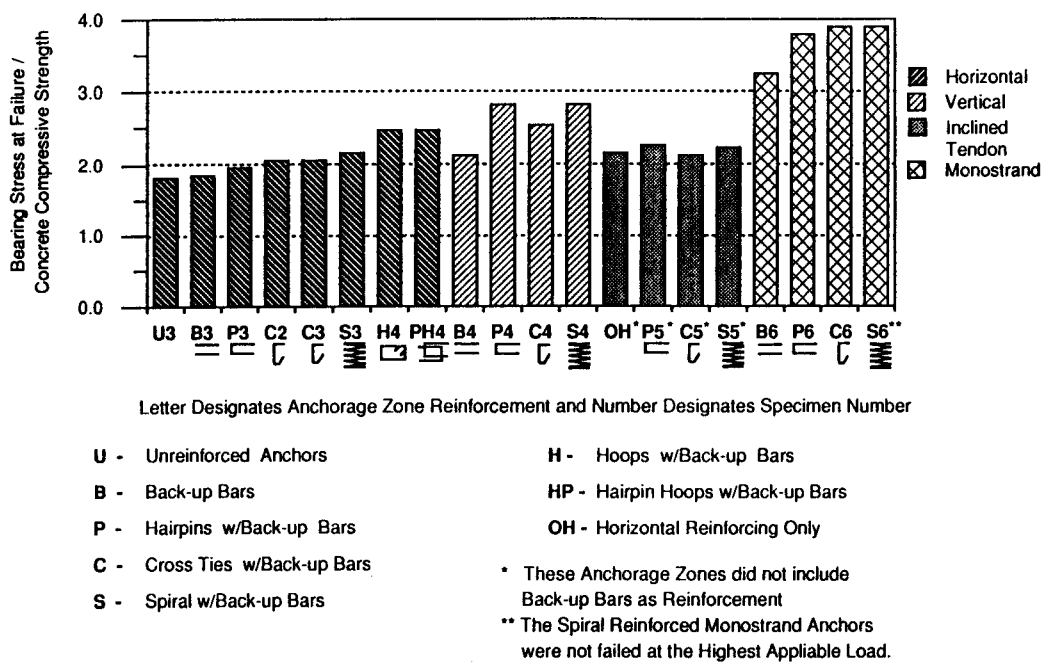


Figure 180. Ratio of bearing stress to concrete compressive strength for horizontal four-strand, vertical four-strand, horizontal four-strand with inclined tendons, and monostrand anchors.

Table 47. Average strut-and-tie predicted anchor failure loads for various anchors

Anchor Description	Strut-and-Tie Predicted Component Failures (kips)			Actual Failure (kips)
	Strut	Tie*	Node	
Horizontal Four-Strand	85	58*	74	89
Vertical Four-Strand	64	96	34	82
Horizontal Four-Strand Inclined	77	72*	77	105
Horizontal Monostrand	122	124*	73	133**

* Tie strengths which were far less than actual failure loads (10 percent or less) were excluded from these averages because no method was used to estimate concrete-tie strength. These cases were typically backup bars and hairpins.

** The spiral reinforced monostrand anchorage zones were never failed. This number is a lower bound.

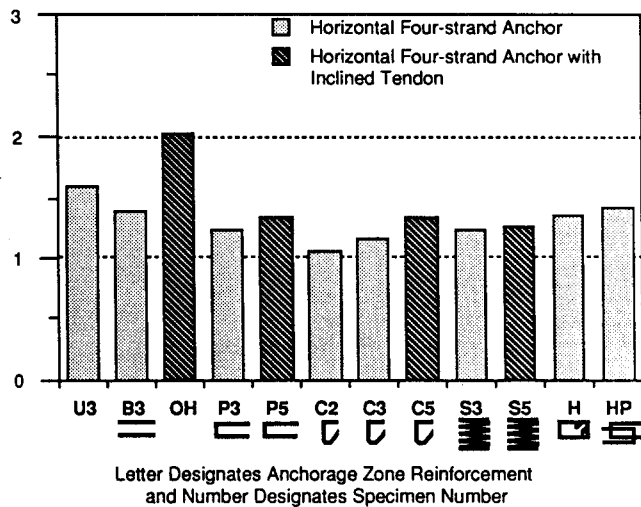


Figure 181. Ratio of actual average anchor failure loads to predicted failure loads from finite element analysis.

RESULTS OF THE INTERMEDIATE ANCHORAGE TESTS

The intermediate anchorage series comprised eight half-scale specimens (60). Details for all specimens are shown in Appendix C. Specimens blister 1 and blister 2 modeled isolated, concentric

slab blisters with a single anchor (Figure 186a), while specimen blister 3 had two anchors. Specimen blister 4 had a rib extending over the full slab width and anchored a single, concentric tendon (Figure 186b). Specimens corner 1, corner 21, and corner 22 modeled the anchorage of a single tendon in a blister located at the junction of web and flange of a box-girder bridge (Figure 186c). Specimen corner 3 represented a corner blister for an external tendon, which acts much like a corbel (Figure 186d).

Table 51 gives the concrete cylinder compressive strengths for all specimens at the time of testing and gives information on some of the local and general zone reinforcement. Number 2 bars were Swedish reinforcement steel with a yield strength of 72 ksi and a cross-sectional area of 0.44 in.²; more complete

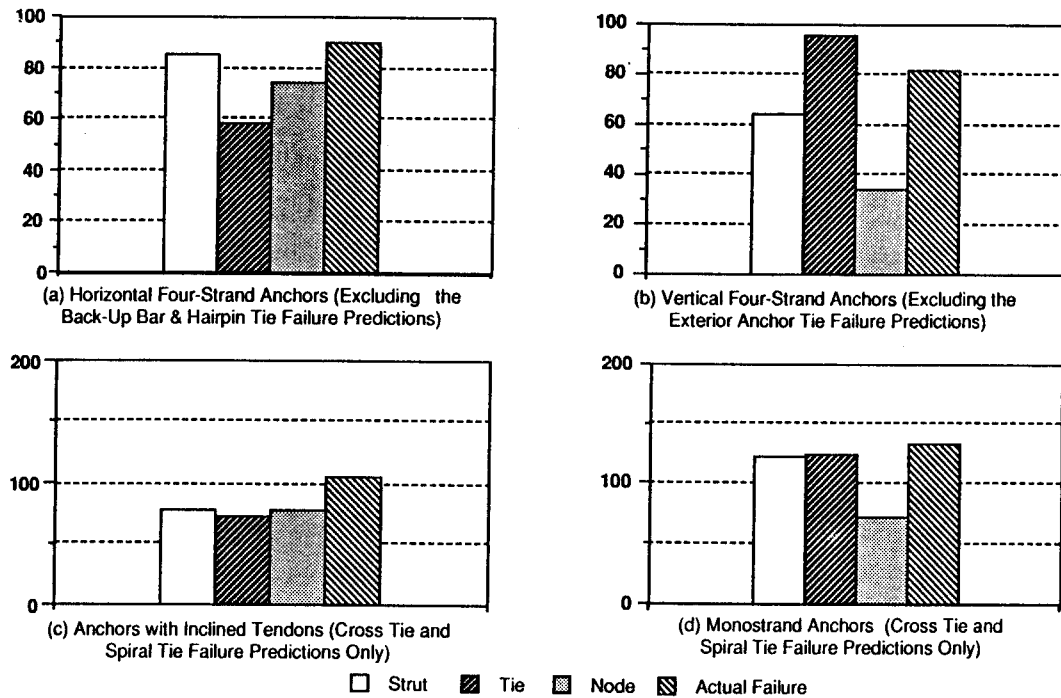


Figure 182. Predicted strut-and-tie component failure loads and actual failure loads for various anchor types, anchor orientations, and tendon inclination.

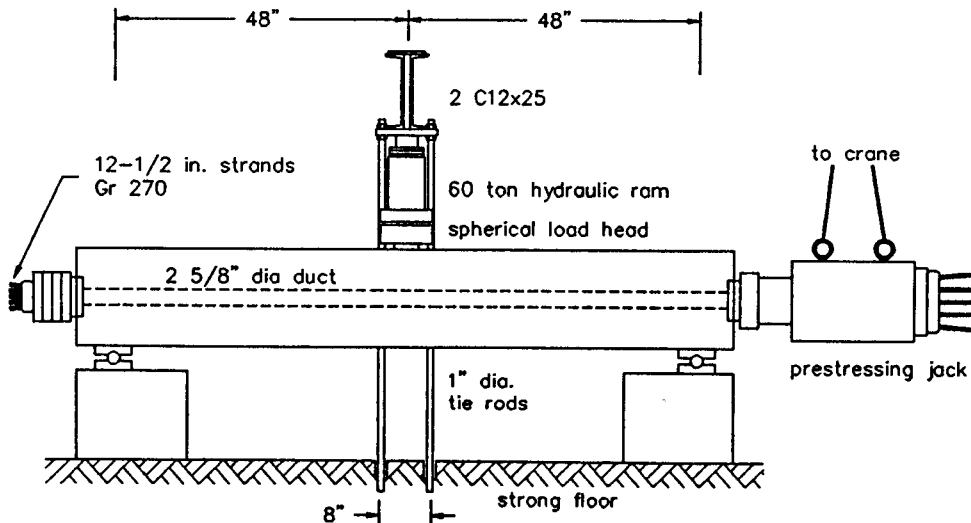


Figure 183. Test set-up for beam specimens.

details are shown in Appendix C. Specimen corner 22 is a duplicate of specimen corner 21, which became necessary after specimen corner 21 failed to reach the desired concrete strength.

The design load F_{pu} was 124 kips for specimens blisters 1 through blisters 4 and for specimen corner 3. This load corresponds to the breaking strength of a $12\frac{1}{2}$ -in. strand tendon, reduced by a factor of four for the half-scale model used. The remaining specimens were designed for a load F_{pu} of 196 kips, half-scale modeling of a $19\frac{1}{2}$ -in. strand tendon. All specimens were loaded by an oversized tendon.

Behavior

Despite the geometric differences the behavior of all specimens was quite similar. It was dominated by the behavior of the blisters close to the anchor and in the region of tendon curvature, where the tendon deviated from the slab into the blisters. Table 51 gives an overview of the test results in terms of the design load, F_{pu} .

Figure 187 shows the typical crack pattern for the isolated blister specimens. Crack pattern and crack development for the

Table 48. Materials and test data for beam specimens

Specimen	f'_d (psi)	Anchor	Local Zone Confining Reinforcement	General Zone Bursting Reinforcement (1)	1st Cracking Load % f_{pu} (289 kips)	1st Yield Load % f_{pu}	Ultimate Load % f_{pu}
Beam1 (LE)	5300	6.5" x 6.5" x 2" single plane	#3 spiral $D = 7"$, $s = 1.25"$	14 #2 @ 10.5"	0.88	1.04	1.11
Beam1 (DE)					0.88	---	---
Beam2 (LE)	7500	6.5" x 6.5" x 2" single plane	#3 spiral $D = 7"$, $s = 1.25"$	16 #2 @ 10.5"	1.13	1.57	---
Beam2 (DE)				14 #2 @ 12"	1.06	1.38	1.57
Beam3 (LE)	5100	6.5" x 6.5" x 2" single plane	#3 spiral $D + 7"$, $s = 1.25"$	16 #2 @ 10.5"	0.84	1.25	1.34
Beam 3 (DE)				14 #2 @ 12"	0.99	---	---

¹ distance is measured from anchor plate to centroid of bursting reinforcement

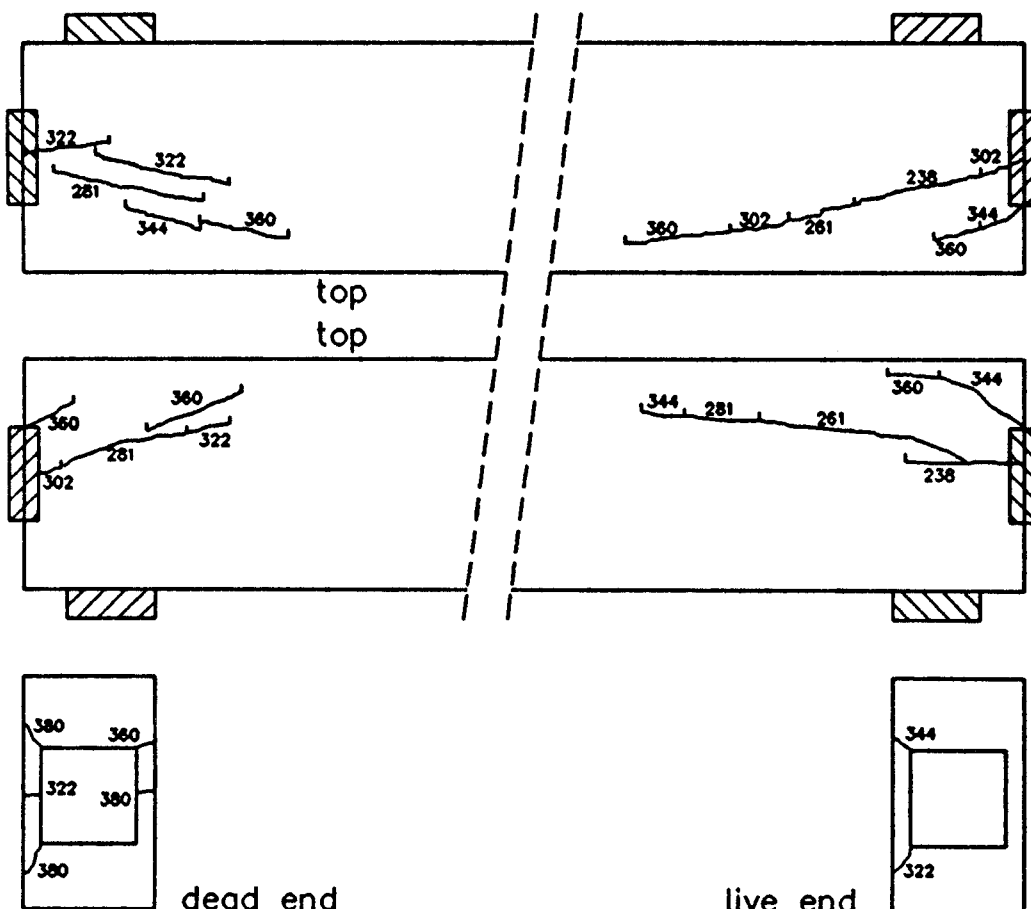


Figure 184. Crack patterns for specimen beam 3.
@Seismicisolation

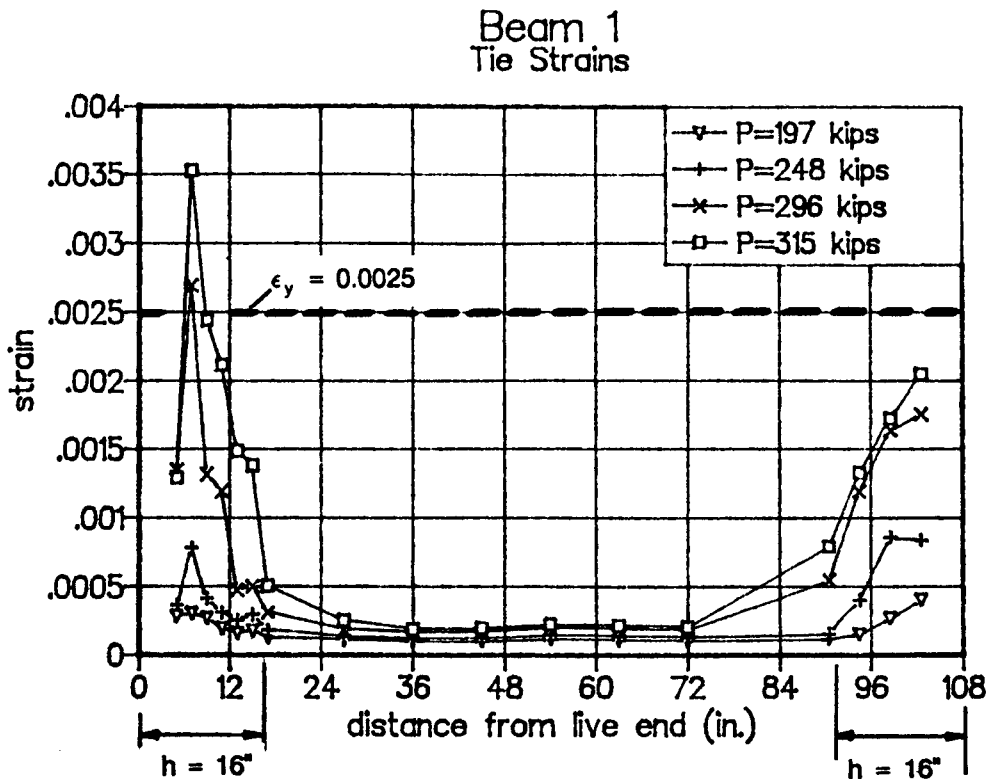


Figure 185. Tie strains in specimen beam 1.

Table 49. Finite element analysis predictions for beam specimens

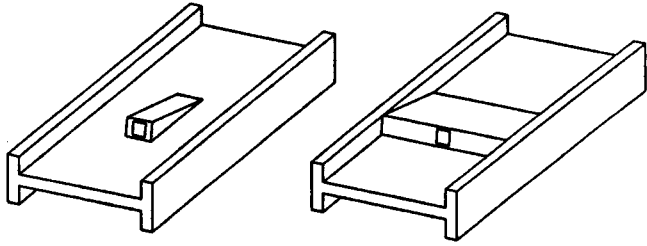
Specimen	P_{test} (kips)	FEM Predictions			$P_{\text{test}} / P_{\text{calc}}$
		Compression (kips)	Tension (kips)	P_{calc} (kips)	
Beam1	315	<u>334</u>	355	334	0.94
Beam2	447	473	<u>406</u>	406	1.10
Beam3	380	<u>321</u>	405	321	1.18
NOTE: Underlined values show which load case controls		Average			1.07
		Standard Deviation			0.10

other specimens were very similar. First cracking occurred at the reentrant corner behind the blister for all eight specimens (crack (1) in Figure 187). Subsequent cracking took place in the local zone region of the blister (cracks (2) in Figure 187) and at its toe, where stresses due to slab bursting and due to tendon deviation coincided (crack (3) in Figure 187). The crack widths behind the anchor never exceeded 0.008 in., even when no crack controlling reinforcement was present. The relative first cracking loads and the corresponding locations are given in Table 51.

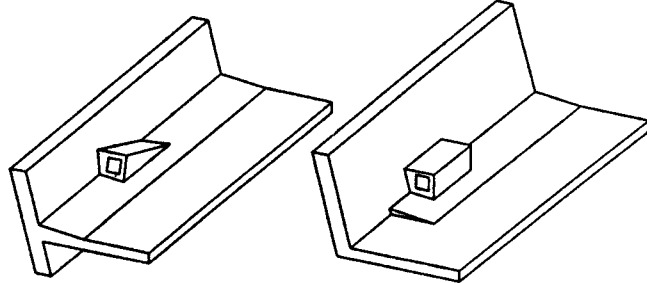
Peak strains occurred in the ties surrounding the local zone region and in the slab bursting reinforcement. Peak strains in the local zone region usually affected several ties, while peak strains in the slab bursting reinforcement usually were limited to one or two ties. Table 51 lists the tendon loads at first yielding for various regions of the specimens. Yielding of the ties surrounding the local zone consistently occurred at 85 percent to 95 percent of the ultimate load and was an excellent indicator of impending failure.

Table 50. Strut-and-tie model predictions for beam specimens

Specimen	P_{test} (kips)	Strut-and-Tie Predictions				$P_{\text{test}} / P_{\text{calc}}$
		Local Zone (kips)	Interface (kips)	Bursting (kips)	P_{calc} (kips)	
Beam1	315	379	365	<u>332</u>	332	0.95
Beam2	447	470	550	<u>363</u>	363	1.23
Beam3	380	370	<u>359</u>	373	359	1.06
NOTE: Underlined values show which load case controls		Average				1.08
		Standard Deviation				0.12

a) isolated slab blister
(Blister 1, Blister 2)

b) rib (Blister 4)

c) corner blister
(internal tendon)
(Corner 1, Corner 21, Corner 22)d) corner blister
(external tendon)
(Corner 3)**Figure 186.** Intermediate anchorage specimens.

The failure mode of all specimens involved crushing of the concrete ahead of the confining spiral in the local zone, similar to the failure mode observed for the beam specimens. Failure was explosive for specimens blister 1 through blister 4 which had little blister confinement reinforcement besides the local zone spiral. Failure was more ductile in specimens corner 1 through corner 3, which had closely spaced ties in the blister around and ahead of the local zone spiral. Table 51 gives the failure loads in terms of the design loads, F_{uw} .

Evaluation of Test Results

Finite Element Analysis Predictions

In Table 52 the finite element analysis and local zone predictions are compared to the actual failure loads. Analysis results are shown separately for the slab blisters and the corner blisters. Predictions based on the requirements for slab bursting and tendon deviation and on the check of the linear-elastic compressive stresses at the critical section located one plate width ahead of the anchor are included. Concrete tensile strength was ignored and the nominal concrete strength was taken as $0.7f'_{ci}$, as specified in the proposed anchorage zone provisions. The presence of the tendon duct was ignored in the predictions. The governing predictions are underlined. The predictions assuming slab bursting controls are inconsistent and do not reflect the actual failure mode. For these specimens, the predictions based on the blister compression check are conservative and much more reliable and reflect the actual failure mode.

Strut-and-Tie Model Predictions

In Table 53, two strut-and-tie model predictions are compared to the actual failure loads. Figure 103 shows a possible strut-and-tie model solution for the isolated slab blister specimens. The lowest load predictions are controlled by the capacity of the slab bursting reinforcement or of the tendon deviation reinforcement. The results indicate considerable conservatism for many specimens. If the limiting capacities of slab bursting and tendon deviation reinforcement are disregarded, the next lowest predictions are controlled by compression in the blister or by the local zone capacity (fifth and sixth columns in Table 53). These predictions are still conservative for all specimens, but the average is much closer to 1.0 and the standard deviation is significantly reduced.

Conclusions

Concrete tensile strength and stress redistributions reduce the reinforcement stresses substantially. Predictions based on the

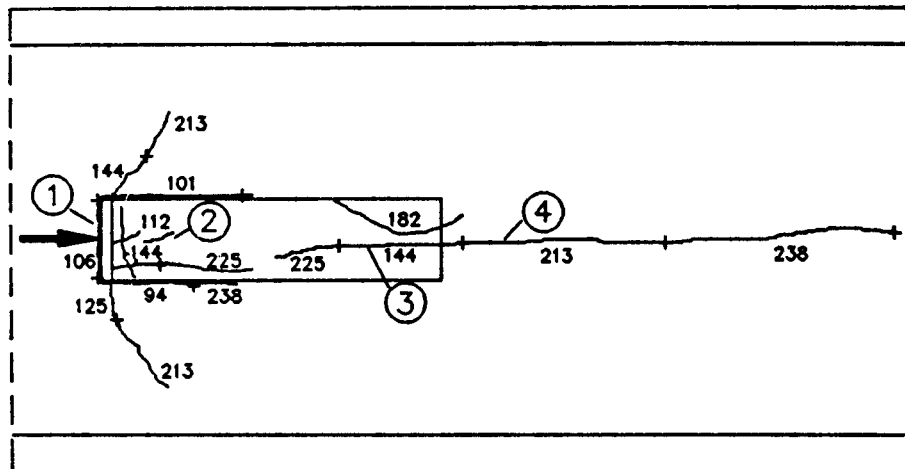
Table 51. Materials and test data for intermediate anchorage specimens

Specimen	f_a (psi)	Anchor	Local Zone Confinement/Bilster Bursting		Slab Bursting*	F_{pu} (kips)	1st Cracking Load ** (% F_{pu})	1st Yield Load *** (% F_{pu})	Ultimate Load (% F_{pu})
			Spiral	Ties*					
Blister1	4900	5"x5"x1" single plane	#3, D=5.75" s=1.75"	4 #3 @ 2"	9 #2 + 5 #3 @ 38.0"	124	0.85 (1) 1.16 (2, 3)	1.72 ² 1.92 2.04 ³	2.04
Blister2	4200	5"x5"x1" single plane	#3, D=5.75" s=1.75"	4 #3 @ 6"	9 #2 + 3 #3 @ 37.1"	124	0.73 (1) 0.97 (2, 3)	1.70 ² (1)	1.90
Blister3	4900	5"x5"x1" single plane (2x)	#3, D=5.75" s = 1.75"	20 #2 @ 5.3"	18 #2 @ 44.6"	124	0.77 (1)	1.81 ² (1)	1.91
Blister 4	4700	5"x5"x1" single plane	#4, d+6", s=1.75"	—	10 #2 + 4 #3 @ 32.3"	124	0.86 (1) 1.38 (2, 3)	1.68 ² 2.06 ³ (2)	2.22
Corner1	4600	5"x5"x1" single plane	#3, D=6", s=1.75"	8 #3 @ 4.6"	14 #2 21.0" (flange) 10 #2 28.0" (web)	196	0.51 (1) 0.91 (2, 3)	1.34 ² (1)	1.58
Corner21	2900	5"x5"x1" single plane	#3, D=6" s=1.75"	6 #2 @ 6.0"	12 #2 @ 46.0" (flange) 10 #2 @ 44.6" (web)	196	0.51 (1) 0.69 (2) 0.91 (3)	0.91 ^{2, 3} (1) (2) (3)	1.05
Corner 22	4600	5"x5"x1" single plane	#3, D=6" s=1.75"	6 #2 @ 6.0"	12 #2 @ 46.0" (flange) 10 #2 @ 44.8" (web)	196	0.44 (1) 0.89 (2, 3)	1.03 ^{2, 3} (1) (2)	1.17
Corner 3	4000	5"x5"x1" single plane	#3, D=5.75" s=1.75"	4 #3 + 4 #2 @ 4.0"	10 #2 @ 27.5" (flange) 8 #2 @ 27.5" (web)	124	0.91 (1) 1.01 (2) 1.58 (3)	1.69 ² (1) (2) (3)	2.06

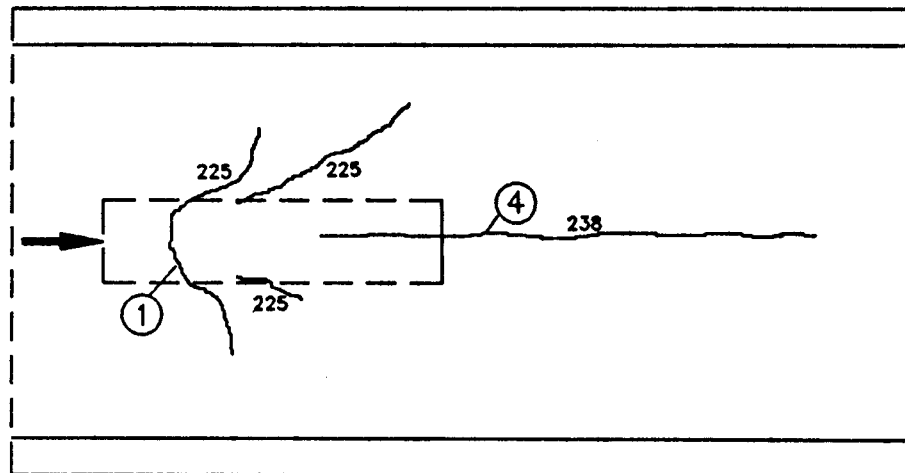
* distance is measured between anchor plate and centroid of reinforcement

1 longitudinal intermediate anchorage reinforcement
2 slab or rib bursting reinforcement
3 numbers in parentheses correspond to cracks as labeled in Figure 5

** numbers in parentheses correspond to bilster bursting/local zone ties



top side



bottom side

Figure 187. Typical crack pattern in isolated blister specimen (blister 1).

capacity of the reinforcement tend to be conservative and inconsistent and do not reflect the actual final failure mode. The predictions are significantly improved by considering compression failures in or ahead of the local zone only. For this case, both finite element analysis and strut-and-tie models are generally conservative and give predictions within 25 percent of the failure load for most specimens.

RESULTS OF DIAPHRAGM TESTS

Three half-scale specimens modeling a diaphragm for the anchorage of external tendons in a box-girder bridge were tested. Specimen details are given in Appendix C. Specimens Dia 1 and Dia 2 were designed for two loads of 196 kips each, representing at half-scale two $19\frac{1}{2}$ in. strand tendons. The design load for specimen Dia 3 was increased to 2×215 kips after the previous diaphragm specimens exhibited considerable capacity beyond their design load because of the tensile strength of the concrete.

Table 54 gives the concrete cylinder compressive strengths at time of testing. Specimen Dia 3 was added because of the excessively high concrete strength of specimen Dia 2. The table also includes information on some of the local and of the general zone reinforcement. More complete details are shown in Appendix C.

Behavior

The general behavior of all specimens was very similar. Table 54 gives an overview of first cracking, first yield, and ultimate loads in terms of the design load, F_{pu} . Specimen Dia 1 was loaded through a 600-kip testing machine. Problems with this machine limited the highest test load to 563 kips without achieving failure of the specimen. However, the degrading stiffness of the load-displacement curve indicated that failure was imminent and 563 kips is used as failure load for the comparisons in the following sections. The specimen subsequently did resist ten

Table 52. Finite element analysis predictions for intermediate anchorage specimens

a) Finite Element Analysis Predictions for Slab Blister Specimens

Specimen	P_{test} (kips)	Local Zone (kips)	Interface (kips)	Slab Bursting (kips)	P_{calc} (kips)	P_{test} / P_{calc}
Blister1	253	<u>210</u>	235	305	210	1.20
Blister2	235	<u>188</u>	201	235	188	1.25
Blister3	237 + 120	2 x 299	2 x 243	<u>2 x 190</u>	2 x 190	0.94
Blister4	275	240	258	<u>180</u>	180	1.53
Average						1.23
Standard Deviation						0.21

b) Finite Element Analysis Predictions for Corner Blister Specimens

Specimen	P_{test} (kips)	Local Zone (kips)	Interface (kips)	Slab Bursting (kips)	P_{calc} (kips)	P_{test} / P_{calc}
Corner1	310	<u>236</u>	265	(193)	236	1.31
Corner21	206	172	<u>167</u>	(165)	167	1.23
Corner22	230	<u>221</u>	265	(165)	221	1.04
Corner3	255	<u>226</u>	231	(211)	226	1.13
Average						1.18
Standard Deviation						0.10

NOTE: Underlined values show which load case controls

load cycles to approximately 425 kips before finally failing at a load of 385 kips. Specimens Dia 2 and Dia 3 were loaded through oversized tendons (Figure 188). Diaphragm specimen 3 could be failed under monotonic loading. Diaphragm specimen 2 had to be unloaded three times before reaching its peak load and failure during the fourth load cycle.

Figure 189 shows the typical crack pattern for the diaphragm specimens. Cracks at the diaphragm-flange interface (cracks (2) in Figure 189) and diagonal cracks progressing towards the bearing plates (cracks (1) in Figure 189) occurred first in all tests. Subsequent cracks included web-flange junction cracks (4) ahead of the diaphragm, diaphragm bending cracks (3), web bursting cracks (5), and corbel action cracks in the loaded face (6). Table 54 gives the loads at which these cracks occurred.

Cracks (1) became very large with approaching failure. At about 90 percent of the failure load their width was about 0.06 in. for diaphragm specimen 1 and approximately 0.02 in. for diaphragm specimens 2 and 3, where crack controlling reinforcement was present.

The highest strains were measured in the reinforcement crossing cracks (1) and (2), as shown in Figure 189. This reinforcement

is labeled "strut confinement reinforcement" and "diaphragm bending reinforcement", respectively, in Table 54. The strut confinement reinforcement reached first yield at 90 percent of the failure load in specimen Dia 2 and at 80 percent in specimen Dia 3. No strut confinement reinforcement was provided in specimen Dia 1. First yield of the reinforcement crossing crack (2) (diaphragm bending reinforcement) was registered at about 90 percent of the failure load in diaphragm specimens 2 and 3. Strain measurements for specimen Dia 1 were not available at this location. In none of the specimens did the diaphragm bending reinforcement reach yield at midspan. Strains were also critical in the flange reinforcement immediately ahead of the diaphragm and yielded prior to failure in specimens Dia 1 and Dia 3. Strains in the reinforcement provided for shear-friction transfer from the diaphragm into the web reached yield only for specimen Dia 1. However, for all specimens impending failure was announced by substantial flattening of the load-strain curve for this reinforcement (Figure 190). The transition from the initially very stiff response to the flexible response occurred at 75 percent to 90 percent of the failure load.

Table 53. Strut-and-tie model predictions for intermediate anchorage specimens

Specimen	P_{test} (kips)	Slab Bursting / Tendon deviation		Blister Compression / Local Zone	
		P_{calc} (kips)	P_{test} / P_{calc}	P_{calc} (kips)	P_{test} / P_{calc}
Blister1	253	249 ¹	1.02	210 ⁴	1.25
Blister2	235	161 ²	1.46	188 ³	1.25
Blister3	237	124 ¹	1.91	244 ⁴	1.03
Blister 4	275	148 ²	1.86	240 ³	1.15
Corner1	310	224 ¹	1.38	236 ³	1.31
Corner21	206	196 ¹	1.05	182 ⁴	1.13
Corner22	230	196 ¹	1.17	221 ³	1.04
Corner3	255	129 ¹	1.98	226 ³	1.13
Average		1.48		1.16	
Standard Deviation		0.37		0.09	

¹ Slab bursting controls³ Local zone capacity controls² Tendon deviation controls⁴ Blister compression controls

All specimens failed at the transition from the massive diaphragm to the thin flanges ahead of the diaphragm. Failure involved local crushing of the flange (specimen Dia 1) or was due to collapse of the shear transfer cross crack (2) (Figure 189) (specimens Dia 2 and Dia 3). However, this compression failure mode was preceded by yielding of the diaphragm bending reinforcement where it crossed crack (2) and of portions of the flange bursting reinforcement. Failure loads relative to the design loads are given in Table 54.

reinforcement, labeled "vertical tension" in Table 55. However, they tend to be very conservative and unreliable.

Strut-and-Tie Model Predictions

The strut-and-tie model predictions are given in Table 56. The predictions based on the vertical tension capacity are even more conservative than for the finite element predictions. This is because the finite element predictions are solely based on the reinforcement requirements in the plane of symmetry of the diaphragm specimen, whereas the strut-and-tie model predictions are based on the requirements for the overall load path and, also, are adjusted for the actual reinforcement arrangement.

The critical region for compression is located immediately ahead of the diaphragm, where inclined compression struts enter the thin flanges. Predictions based on this failure mode, using a nominal concrete strength of $0.7f'_{cp}$, are by far the best and while conservative are very consistent (Table 56). They also agree with the actual failure mode.

Conclusion

Both finite element analysis and strut-and-tie model predictions indicate that failure should be controlled by the capacity of the web bursting and of the diaphragm bending

Table 54. Materials and test data for diaphragm specimens

Specimen	f'_d (psi)	Anchor	Local Confinement Reinforcement	Diaphragm bending/ Web bursting reinforcement*	F_{pu} (kips)	% F_{pu}		
						1st Cracking Load**	1st Yield Load	Ultimate Load
Dia1	5900	7"x7" Multiplane (2x)	#4 spiral, D = 8" s = 2" (2x)	5 #5 + 4 #3 @ 18.75"	382	0.73 (1) 0.89 (2, 3, 4, 5) 1.28 (6)	1.38 ³ 1.44 ⁴	> 1.44
Dia2	8100	7"x7"x1" single plane (2x)	—	4 # 4 + 4 # 3 + 2-5/8" dia. PT bars @ 13.25"	392	1.03 (2, 3) 1.16 (1, 5) 1.26 (3, 4) 1.42 (6)	1.98 ² 2.04 ¹	2.20
Dia3	5200	7"x7"x1" single plane (2x)	—	3 #5 + 1 #4 + 2-5/8 dia. PT bars @ 15.2"	430	0.66 (2) 0.71 (1) 0.95 (5) 1.04 (3, 4) 1.14 (6)	1.14 ² 1.28 ¹ 1.43 ³	1.43

* distance measured from anchor plates to centroid of prestressed and non-prestressed reinforcement

** number in parentheses corresponds to cracks as labeled in Figure 7

1 diaphragm bending reinforcement

2 strut confinement reinforcement

3 flange bursting reinforcement

4 shear-friction reinforcement between diaphragm and web

the diaphragm bending and web bursting reinforcement (vertical tension reinforcement). These predictions are very conservative and inconsistent for several reasons. For one, the contribution of uncracked concrete in the massive diaphragm specimens is very significant. In addition, reinforcement distortions noticed in the specimens after completion of the tests indicated substantial

dowel action between diaphragm and flanges. Both contributions are difficult to assess and are not normally relied on in design.

OVERALL FINDINGS FROM THE EXPERIMENTAL PROGRAM

The results of the experimental program confirm that the proposed anchorage zone specifications provide a conservative design approach. Most specimens exhibited considerable reserve strength beyond the predictions based on the anchorage zone reinforcement capacity and failed in compression in or immediately ahead of the local zone region. The conservatism of the anchorage zone reinforcement design is a consequence of neglecting the concrete tensile strength and stress redistributions after cracking.

Future research should clarify when and to what extent the concrete tensile strength can be relied on and to what degree concrete plasticity should be recognized in the development of strut-and-tie models.

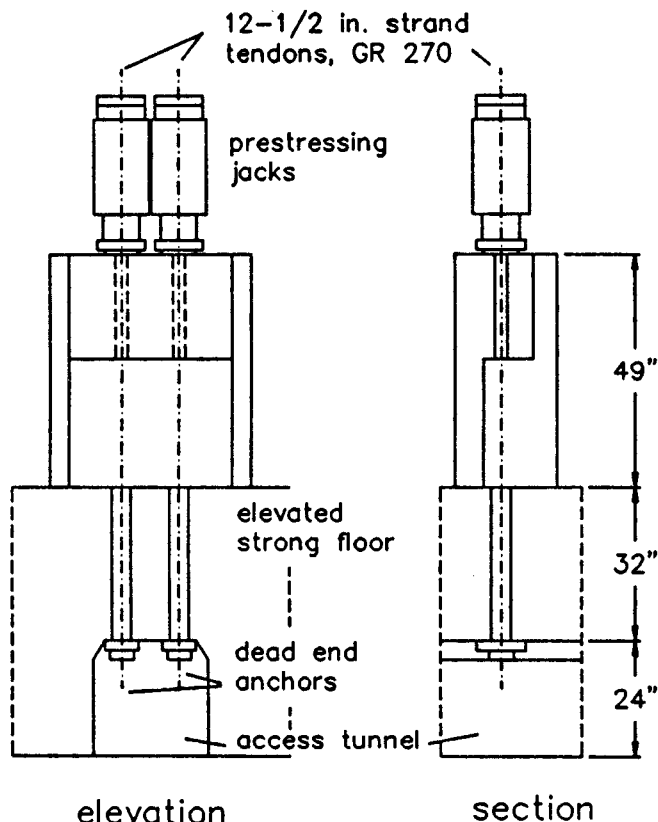


Figure 188. Test setup for diaphragm specimens 2 and 3.

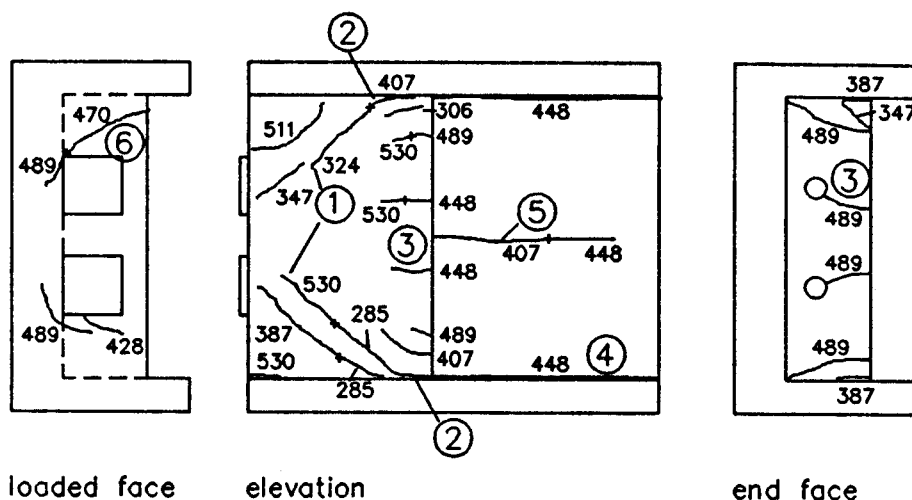


Figure 189. Typical crack pattern in diaphragm specimens (Dia. 3).

Diaphragm Comparisons Strains in Shear Friction Reinforcement

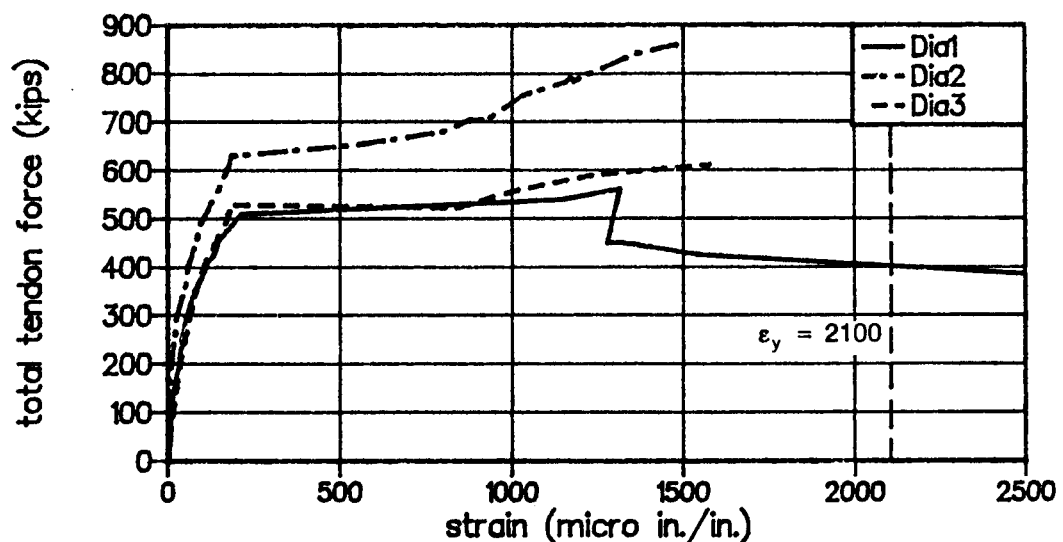


Figure 190. Strains in shear-friction reinforcement between diaphragm and web.

Table 55. Finite element analysis predictions for diaphragm specimens

Specimen	P_{test} (kips)	Base Compression		Vertical Tension	
		P_{calc} (kips)	$P_{\text{test}} / P_{\text{calc}}$	P_{calc} (kips)	$P_{\text{test}} / P_{\text{calc}}$
Dia1	563	813	0.69	472	1.19
Dia2	861	1116	0.77	352	2.45
Dia3	613	689	0.89	606	1.01
Average			0.78		1.55
Standard Deviation			0.08		0.64

Table 56. Strut-and-tie model predictions for diaphragm specimens

Specimen	P_{test} (kips)	Flange Compression		Vertical Tension	
		P_{calc} (kips)	$P_{\text{test}} / P_{\text{calc}}$	P_{calc} (kips)	$P_{\text{test}} / P_{\text{calc}}$
Dia1	563	459	1.230.69	360	1.56
Dia2	861	688	1.25	293	2.94
Dia3	613	494	1.24	362	1.69
Average			1.24		2.06
Standard Deviation			0.01		0.62

CHAPTER 3**INTERPRETATION, APPRAISAL AND APPLICATION**

The overall understanding gained from the survey of literature, the extensive state-of-the-art assessment, the analytical studies and the experimental studies regarding the influence of the major variables on the serviceability, strength and design approaches for post-tensioned concrete anchorages zones is summarized in the following sections.

APPROACH FOR DESIGN AND CONSTRUCTION REGULATIONS

One of the major contributions of the present study was the discovery, in the early stages of the project, that there was a certain parallel between technical areas and responsibility allocations that were plaguing the overall post-tensioned bridge industry. It became obvious, in discussions with owners, designers, material suppliers, and other researchers, that considerable progress could be made if a distinction could be made between the local, hardware-related behavior (local zone) and the more overall structure-related behavior (general zone).

Such a division, in spite of a few overlaps, could permit an orderly formulation of criteria for acceptance of post-tensioning anchorage devices, for design and proportioning of the more general concrete resistance and reinforcement required to control bursting, splitting and spalling throughout the anchorage zone, and for clear assignment of responsibilities in a logical and equitable manner.

The basic approach should provide for: (1) definitions of the general zone and local zone; (2) assignment of responsibilities to the engineer-of-record, anchorage device supplier, and constructor; (3) design procedures for the general zone allowing the engineer-of-record sufficient freedom to choose from several methods and to give guidance for proper detailing; (4) design procedures for the local zone which allow the engineer-of-record to determine the adequacy of relatively simple bearing plate anchorage devices (basic anchorage device) by analysis, or alternatively specify acceptance testing procedures and acceptance criteria for more complex anchorage devices (special anchorage device) (these criteria should require the device supplier to present full information on required confining reinforcement, supplementary reinforcement, edge distance, and center-to-center spacing along with independent evaluation reports to the engineer-of-record for final acceptance); (5) provisions to ensure that special confining or supplementary reinforcement used in special anchorage device acceptance tests is provided in similar or equal fashion in the actual structural application; and (6) consistency with an overall limit state approach considering serviceability, load factors, and resistance factors.

In the detailed provisions for post-tensioned anchorage zones proposed for inclusion in the AASHTO Bridge Specifications,

and provided in Appendix E in this report, very specific language is proposed to carry out these objectives. A complete commentary is included with the proposed specification provisions. Because of that commentary, discussion in the early portions of this chapter will be limited to avoid redundancy.

Responsibilities

One must try to separate legal responsibilities imposed by engineering practice regulatory standards for protection of public health and safety, from contractual responsibilities apportioned between the various parties of fiscal agreements. In this report, the assignment of responsibilities is based on the responsibility for protection of public health and safety traditional in building codes and professional registration laws. Responsibility for public health and safety aspects of engineered structures in most, if not all, states is assigned to a registered, chartered or professional engineer. This engineer is referred to herein as the engineer-of-record. This term is preferable to "owner", "designer", or "engineer." Responsibilities of the engineer-of-record can only be transferred to another party by mutual agreement, and then only if that party is legally qualified to assume such responsibilities. In that case, the second party becomes the "engineer-of-record" for that portion of the project. Because proper design of an anchorage zone requires knowledge of the flow of forces that depend on the tendons details, the engineer has the specific responsibility to indicate the location of the individual tendons and anchorage devices, and not simply the desired centroid of the tendon force. Should the engineer initially choose to indicate only total tendon force and eccentricity, the engineer retains the responsibility of approving the specific tendon layout submitted by a post-tensioning specialist or the constructor. The engineer is responsible for the proper design of general zone reinforcement required by the approved tendon layout. The engineer is responsible for approval of any anchorage devices and local zone confinement. The responsibility for the *adequacy* of the anchorage devices and for the suggestion of proper reinforcement of the local zone is assigned to the supplier of the hardware. It is expected that anchorage device suppliers will deliver specific product information indicating the required cover, edge distance, and concrete strength to the engineer in the form of manuals, in a manner similar to the current practice in some European countries. In addition, it is required that the supplier furnish to the engineer independent verification of the adequacy of those details. The constructor is responsible for the proper execution of the instructions of both the engineer-of-record and the anchorage device supplier.

Limit States Judgments

In quantifying design regulations, the modern approach in codes and design specifications is to consider various limit states. The *serviceability* limit state is concerned with the fitness for general use and considers such factors as visual appearance, durability, excessive deflections, and undesirable vibrations. The nature of a post-tensioned anchorage application is such that it generally would have no effect on deflections or vibrations. Thus, the main considerations are visual appearance and durability. Both of these are basically dependant on preventing excessive crack width from forming. Excessive crack widths can be visually unattractive and worrisome to users and the public. More importantly, excessive crack widths can allow the penetration of moisture through the cracks, lead to corrosion of the nonprestressed reinforcement, as well as the highly corrosion susceptible post-tensioned reinforcement, and accelerate the deterioration of the concrete. The *ultimate* limit state is concerned with the overall safety of the structure, structural element, or structural detail. It considers such factors as loss of equilibrium, rupture, and instability. Post-tensioning anchorage zones are key regions in structures. The post-tensioning tendons, which provide much of the structural load carrying capacity, must be well anchored at their ends. This is true for the life of the structure when unbonded tendons are used, and prior to grouting of the tendons when bonded tendons are used. Generally, it is most critical during the construction stages when the highest stressing loads are placed on the ungrouted and, hence, unbonded tendons and anchorages.

Serviceability Limit State

For post-tensioned anchorage zones, proper performance at the serviceability limit state means prevention or, more practically, effective control of cracking. As shown in Figure 66, substantial areas of an anchorage zone can be subject to tensile stresses. These tensile stresses can often be resisted by the tensile capacity of the concrete, if such tensile capacity can be relied on. Table 57 summarizes the first cracking behavior of the 32 specimens of the end anchorage series. The first noticeable cracking load (actual crack widths of only about 0.001-in. magnitude in general) is given as a ratio of the current AASHTO Bridge Design Specification maximum stressing load for the anchorage devices used. The ratio average is 1.20 with a standard deviation of 0.28. Statistically this would say that, if normally distributed, one might expect about 25 percent of the specimens to have cracked under normal stressing load. In fact, eight of the 32 specimens (25 percent) had cracked by that level. In these unrestrained specimens, built under laboratory conditions, cracking influences like shrinkage and temperature restraint are minimal. Only one specimen, ME1, was known to have a substantial flaw (a misaligned duct). Its cracking capacity was substantially reduced (over 25 percent) when compared to ME2. It is not judged prudent to rely on concrete tensile capacity for primary resistance to forces that are necessary for equilibrium. Thus, it is necessary to provide crack control reinforcement in every bursting zone, in widely spaced anchor spalling zones, and in longitudinal edge tension zones. Tensile stresses in spalling zones of closely spaced anchors are compatibility induced stresses that are dissipated upon first cracking. A minimum level of crack control reinforcement seems adequate for such regions.

In general zones, the design of such reinforcement can be based on a factored load and capacity resistance factor format. Choice of suitable load and resistance factors, coupled with good detailing and reinforcing steel development rules, will result in closely controlled cracking at service load levels. This was demonstrated by the specimens in the experimental series which were very well behaved at service load levels. In fact, cracking was hard to detect in most specimens at the $0.81 F_{pu}$ level. The exception is with some special anchorage devices where wedging effects tend to cause significant cracking (22). This can be controlled by imposing strict crack width limits for the test specimens in the special anchorage device acceptance tests. The ACI Building Code (63) has based its reinforcement distribution requirements on a maximum crack width of 0.013 in. for exterior exposure. AASHTO (16) implicitly uses a somewhat smaller limit, as does CEB (57). After considerable evaluation of the local zone specimens, the "no damage" limit state value of 0.008 in. suggested by Leonhardt (65) and the FIP draft value of 0.10 in. for their proposed criteria led to adoption of 0.010 in. for the maximum crack width at a test level comparable to maximum service load conditions.

Ultimate Limit State

For post-tensioned anchorage zones, proper performance at the ultimate limit state requires that

$$\text{Required Strength} \leq \text{Design Strength}$$

$$U \leq \phi R$$

where the "required strength", U , is determined from a structural analysis of the load effects of factored loads. Factored loads increase the ordinary or service loads to reflect the possibility of overloads or analysis limitations. " R " is the resistance and represents the best estimate of the idealized strength of the structural element, calculated in accordance with the requirements of the code or design specification. " R " is often termed the "nominal strength." The design strength, ϕR , represents a reduction in the nominal strength to reflect possible understrength or undesirable failure modes (lower ductility). ϕ is often termed a "strength reduction" or "resistance" factor and should be taken as less than one.

In order to apply this philosophy consistently to post-tensioned anchorage zones, both load factors and resistance factors must be selected. The post-tensioning load itself is a constructor imposed load. If construction proceeds correctly, it *will* occur. It does not have the uncertainty levels of many live loads that may or may not occur, and that may or may not be significantly exceeded. As previously stated, current AASHTO Bridge Specifications (16) impose limits on the maximum force that can be applied to a post-tensioning tendon during construction. Given the material characteristics, this effectively translates to about $0.81 F_{pu}$, in the worst case, where F_{pu} is the guaranteed ultimate strength of the tendons. In actuality, quality control on prestressing steel is very high and tendons do not usually significantly exceed F_{pu} in basic strength. Furthermore, the wedges used in most commercial prestressing anchorage systems cut into the strands and, hence, can develop only about 95 percent of the actual breaking strength of the tendons (This is recognized by the requirement of an efficiency test in section 9.26.1 of the present AASHTO specifications). Stressing is carried out under supervised conditions,

Table 57. Cracking load versus maximum stressing load

Specimen	Test 1st Cracking Load (kips)	Service 0.81 GUTS	Test Cracking 0.81 GUTS
A1	298	234	1.27
A2	226	234	0.97
A3	250	234	1.07
A4	300	234	1.28
B1	200	141	1.42
B2	186	141	1.32
B3	217	141	1.54
B4	200	141	1.42
B5	170	141	1.21
B6	171	141	1.21
B7	170	141	1.21
B8	156	141	1.11
C1	225	234	0.96
TPT1	200	234	0.85
TPT2	225	234	0.96
TPT3	270	234	1.15
TPT4	240	234	1.03
E1	345	168	1.84
E2	265	168	1.41
E3	300	168	1.60
E4	250	168	1.33
E5	215	134	1.60
E6	225	168	1.20
M1	FORMERS	134	—
M2	213	134	1.59
M3	113	134	0.84
M4	FORMERS	134	—
M5	200	234	1.04
M6	244	234	1.04
ME1	175	234	0.75
ME2	240	234	1.03
F1	145	234	0.62
I1	250	234	1.07
I2	325	234	1.39
I3	250	234	1.07
I4	350	234	1.50
*misaligned duct		Average	1.20
		Standard Deviation	0.28
		Coefficient of Variation	0.23

with calibrated equipment and, hopefully, trained personnel. Unless the wrong number or size of strands has been inserted into the tendon, it is virtually physically impossible to substantially exceed the efficiency factor (0.95) times F_{pu} . This suggests that a reasonable load factor for the controlled post-tensioning load is 1.2 (note that $1.2 \times 0.81 F_{pu} = 0.97 F_{pu} > 0.95 F_{pu}$ efficiency test requirement). This relatively low load factor is further justified by the nature and consequences of failure. The maximum load is applied to the tendon during construction. The structural element is generally supported by some other mechanism at this time.

Should failure occur during stressing, while it may be explosive, it is unlikely to be catastrophic because some other mechanism should support the structural element. Finally, every anchorage is in effect field tested. The full post-tensioning load is applied and the maximum load during stressing is essentially the maximum load that will ever be imposed on the anchorage. Tendon stresses drop off in seating and with further relaxation, creep, and shrinkage. If the tendon is unbonded, it is unlikely that the stress increase at structural failure of the bridge element will offset those losses. If the tendon is bonded, the higher stresses

at failure can be developed by bond transfer. Thus, while higher stresses may be developed, they will not be reflected in the anchor.

Based on all of these factors it is recommended that a load factor of 1.2 be applied to the maximum jacking force for design of post-tensioned anchorage zones.

The "strength reduction" or "resistance" factor ϕ must reflect possible understrength and undesirable failure modes. Consideration of all of the test results in this study show that the primary procedure (strut-and-tie model) recommended for design of anchorage zones was essentially conservative for all specimens (The alternate analysis procedures allowed are essentially equivalent.) Field construction conditions can reduce actual strength from the more ideal laboratory conditions. Anchorage zones tend to have a great deal of congestion so that concrete placement and consolidation are difficult. Failures can often be brittle and explosive. However, Figure 152 indicates that in almost all cases failure did not occur until at least 25 percent above cracking load. More importantly, Figure 156 indicates that before or at failure some reinforcement is yielding. Thus, wide cracking should give warning. Most general zone specimens experienced final failure by crushing and spalling of the concrete, but after some yielding of the reinforcement. Limited ductility was experienced with deformations at failure, about 50 percent more than deformations at first-yield. Thus, the ϕ factor selected should reflect some of the characteristics of a tied column ($\phi = 0.70$)—criticality, compression failure, limited ductility, sensitivity to placement, and compaction. On the other hand, the recommended design expressions used tend to be more of a lower bound than the expressions for tied columns. The brittleness is more like that of a shear failure ($\phi = 0.90$) than a flexural failure. The limited ductility is substantially below that of a flexural failure and, thus, the ϕ value should be substantially below that for flexure of a post-tensioned beam ($\phi = 0.95$). A final consideration is that the post-tensioning industry tends to be a world-wide industry. The combination of load factor and ϕ factor chosen must be reflected in the test loads required for acceptance testing of special anchorage devices. FIP is concurrently revising their criteria for post-tensioned anchorage acceptance tests. When compared to U.S. practice, implicit in their values is a ϕ of about 0.85. It is desirable to have the AASHTO and FIP standards in harmony so that expensive performance testing of special anchorage devices can be minimized.

Considering all of these complex factors, it is recommended that a resistance factor of 0.85 be applied to the nominal strength of normal concrete post-tensioned anchorage zones. This factor should be reduced to 0.70 for light-weight concrete.

GENERAL ZONE DESIGN PROCEDURES

Discussion of the test results in Chapter 2 and comparisons with computed capacities based on strut-and-tie models showed that the basic strut-and-tie model is a conservative and reasonably accurate procedure for computing the nominal resistance of post-tensioned anchorage zones. It is extremely useful in selecting reinforcement patterns and proportioning reinforcement. Its proper use warns designers of critical elements, such as the compression strut problems at the interface between confined nodes and unconfined struts and at sections where thicknesses change. It has the disadvantages that detailed calculations for

node and strut adequacy can be cumbersome, that it is unfamiliar for most American trained engineers, and that it requires some appropriate design aids, intuition or complex analysis to indicate basic force paths in unfamiliar applications. It is clearly a tool of great power and the primary method recommended for design of anchorage zones.

Because it has not been generally quantified in a design code or specification in the United States, a careful quantification for anchorage zone applications is given in the proposed specification. Some elements that would be useful for other applications, such as multiple values of effective concrete compressive stress, have not been included since the tests indicated a value of 0.7 f'_c was appropriate for unconfined concrete in the types of regions found in anchorage zones.

It was felt not only desirable but necessary to provide alternate design procedures. Some engineers expressed substantial discomfort with a procedure which basically requires use of structural intuition and judgment. Other engineers indicated that they preferred a procedure which could maximize electronic computation assistance such as finite element analysis. It was obvious that many simple applications could be treated with a more approximate, elementary approach.

Burdet's (48) analytical studies showed that a linear elastic finite element approach could be substituted for the strut-and-tie model. Details and assumptions for a satisfactory application of the finite element analysis are included in the proposed specifications. Examining the end anchorage specimens tested by Sanders (1), Burdet developed Figure 191 which shows the statistical distribution of the ratio of the actual ultimate load to the ultimate load predicted by the strut-and-tie model. The average ratio of actual to ultimate is 1.4 with a standard deviation of 0.44. In the figure, thick lines surround those test specimens for which the compressive capacity of the concrete struts controlled the design. Figure 192 shows the statistical distribution of the results obtained if the compressive capacity is estimated based on the elastic stresses obtained from the finite element analysis. The estimation of the ultimate load is slightly improved, with an average ratio of 1.32, but the standard deviation is essentially the same at 0.45. Because most of the designs are controlled by the capacity of the tensile ties, for which the results of the strut-and-tie model are used for both figures, the improvement obtained by using an improved model for the prediction of the compressive stresses is not substantial. However, the prediction of the ultimate load based on the results of the finite element analysis is substantially improved when the mode of failure is a compressive failure of the concrete at the interface between the local zone and the general zone. While the tensile stresses from a finite element analysis can be integrated to determine required tensile tie capacity, it is difficult to analyze a discrete tie with most linear analysis programs. Comparison of Figures 191 and 192 shows that the finite element analysis procedures recommended are certainly an equivalent procedure.

In order to extend the provisions to frequently occurring, relatively simple post-tensioning anchorage applications, Burdet (48) developed an approximate solution technique, based on his extensive finite element and strut-and-tie model parametric studies as well as earlier approaches such as Guyon (6,20) and Leonhardt (21). This procedure is detailed in the recommended provisions. Its use is limited to rectangular sections without discontinuities in or ahead of the anchorage zone. It cannot be used if tendons are too close to the edge or if multiple tendons

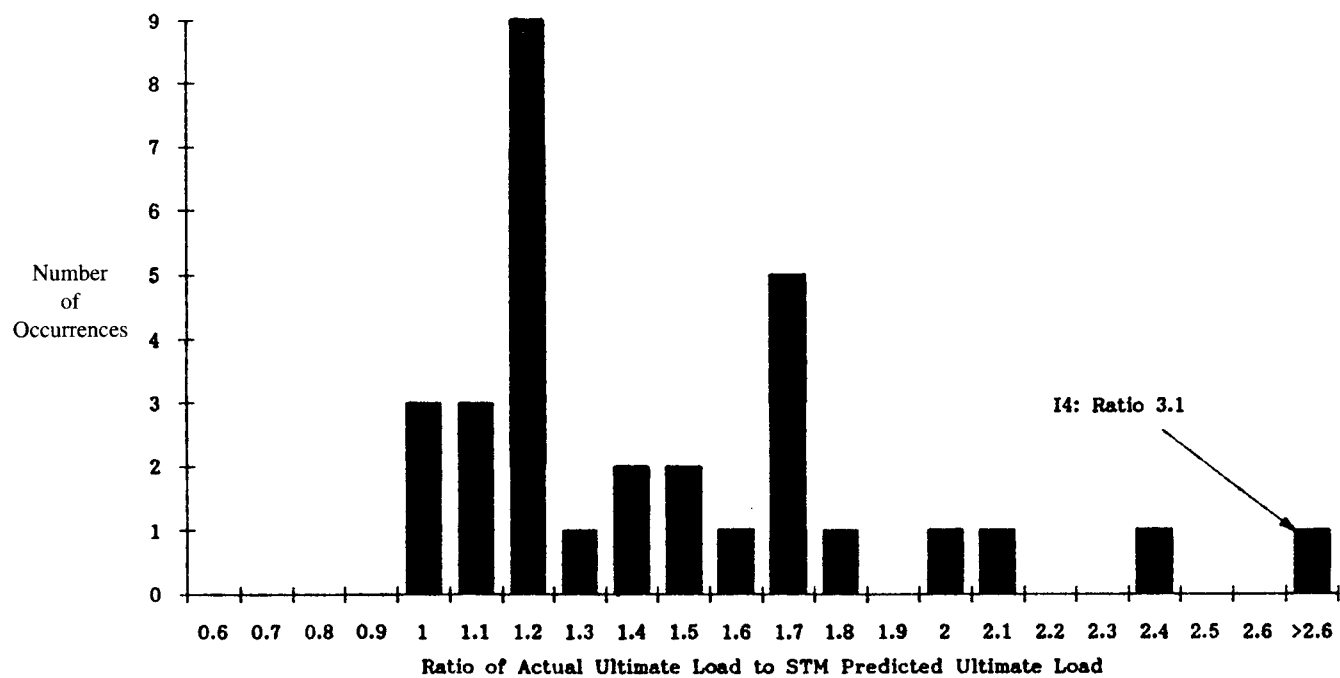


Figure 191. Statistical distribution of the ratio of the actual ultimate load to the ultimate load predicted by the strut-and-tie-model for end anchorage specimens.

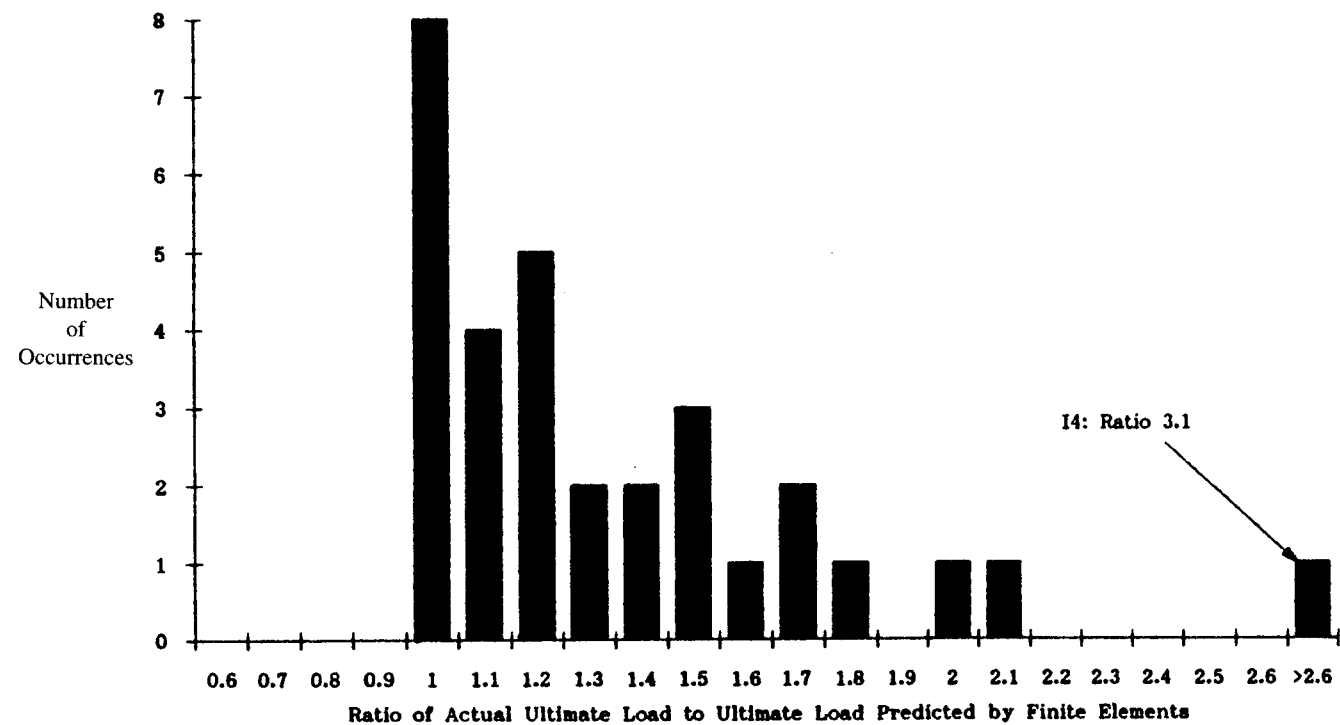


Figure 192. Statistical distribution of the ratio of the actual ultimate load to the ultimate load predicted based on the finite element results (compression capacity) for end anchorage specimens.

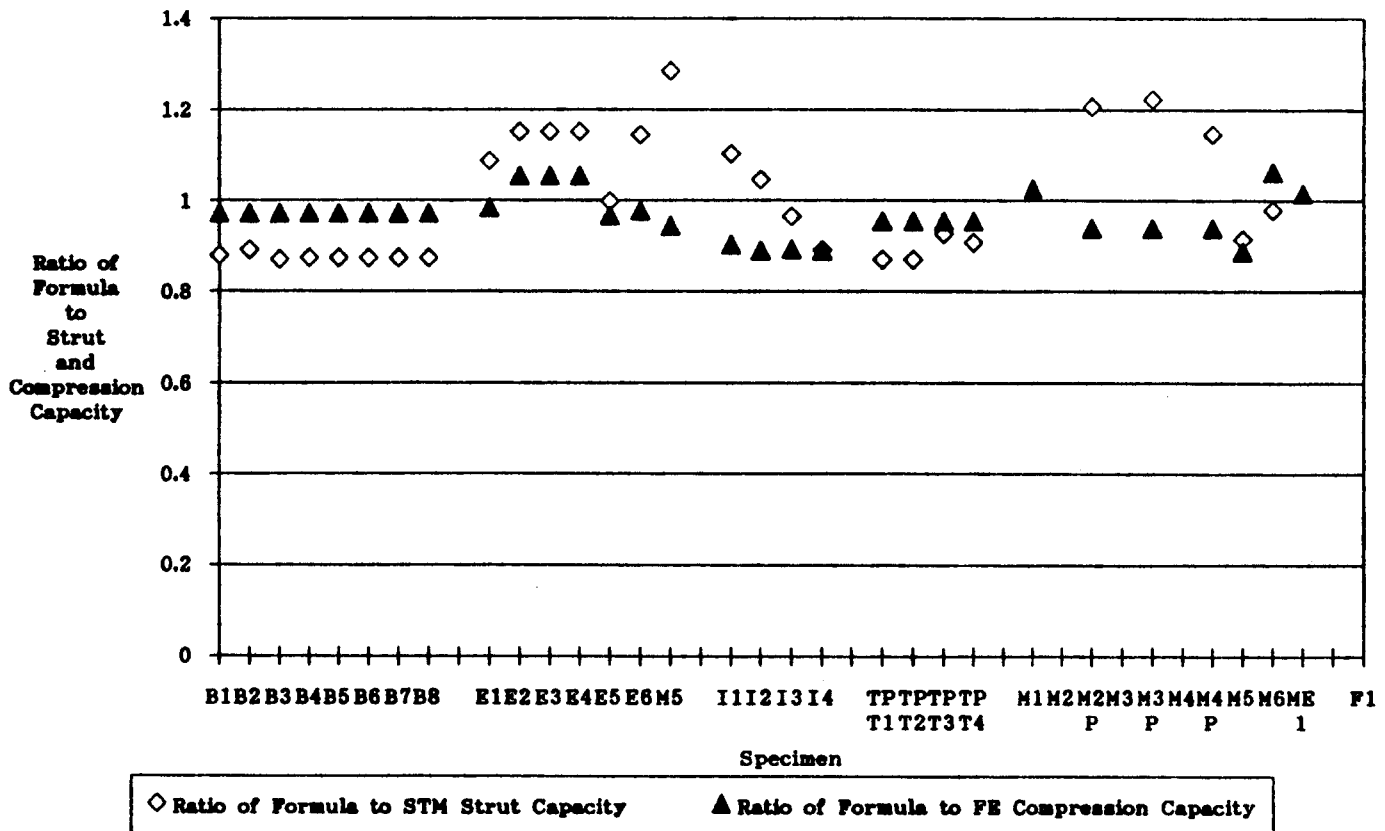


Figure 193. Ratio of the compressive capacity predicted by the code formula to the compressive capacity predicted by the finite element and the strut capacity predicted by the strut-and-tie model.

(other than a single closely spaced group) are used. The tendons must be straight within the anchor zone and inclined at less than 20 deg. Two equations are provided to approximate the compressive stresses at the interface of the general zone and local zones. They consider the actual spacing of anchors in closely grouped anchorages. Equations are also given for values of total bursting tension force and its centroidal location. These equations are based on the parametric studies and consider the relative anchor size, eccentricity, and inclination.

Figure 193 shows the ratio of the compressive capacity predicted by the approximate formula to the compressive capacity predicted by the finite element solution and the strut capacity predicted by the strut-and-tie model. The approximate formula gives results close to the values predicted by the finite element method. The formula approximates the strut capacity predicted by the strut-and-tie model with more scatter. As shown in Figure 194, the results are slightly unconservative for some cases in which compression controls the design (specimens E1 to E4 and M1) but are quite conservative for specimens controlled by tie capacity.

The guidelines for the determination of the bursting force, and for the disposition of bursting reinforcement, attempt to lead the designer toward reinforcement patterns that are relatively close to the elastic stress distribution. The experimental test results show that this leads to a satisfactory behavior under service loads by limiting the extent and opening of cracks and at ultimate by limiting the required amount of redistribution of forces in the anchorage zone.

The “edge tension forces” is the name given in the proposed specification to the forces often called spalling forces. They include spalling forces induced by the condition of compatibility, as well as the edge forces induced by eccentricity and wide spacing of multiple anchorages. The minimum edge tension force for the design is 2 percent of the total post-tensioning force. This value is smaller than the 4 percent proposed by Guyon, and reflects both analytical and experimental findings that show that Guyon’s values for spalling forces are high, that spalling cracks are very rarely observed in experimental tests, and that no direct evidence connects failures to spalling forces. In the case of eccentrically loaded anchorage zones, the edge tension force induced by the axial-flexural action can be simply computed by a combined axial load and flexure analysis. In the case of multiple anchorages, the tensile force between the anchors remains small as long as the distance between anchors is less than 0.4 times the lateral dimension of the member. In cases where the tendons are located further apart (not allowed in the approximate procedures), a strut-and-tie model can be used to compute the multiple anchors tensile forces.

LOCAL ZONE DESIGN PROCEDURES

The recommended specification provisions for local zone design and acceptance testing follow closely the recommendations of Roberts (4), adjusted for general compatibility with recent

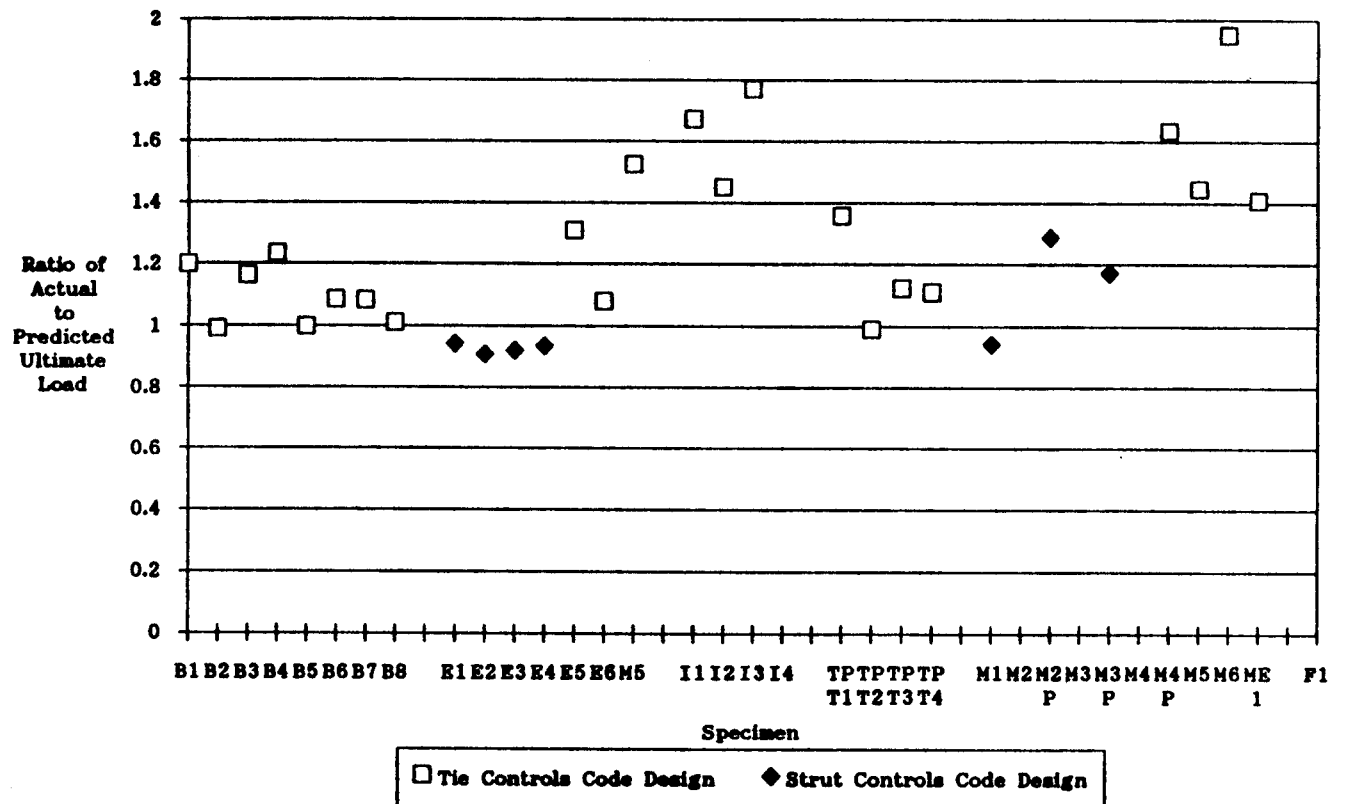


Figure 194. Ratio of the actual ultimate load to the ultimate load predicted using the approximate code formula.

proposed revisions of the international FIP anchorage acceptance test procedures.

Roberts showed conclusively that the primary parameters which affect the first cracking load of the local zone are the tensile capacity of the concrete and the a/h ratio. The presence of supplementary reinforcing, in addition to the primary confining reinforcing, does not elevate the first cracking load. Also, an increase in the spiral diameter does not increase the first cracking load. The presence of supplementary reinforcing, in addition to the primary confining reinforcing, does reduce crack widths compared to specimens with no supplementary reinforcing. Increasing the spiral diameter, without changing the dimensions of the block, does not significantly decrease crack widths. She also showed that increasing the edge distance (the a/h ratio and/or A/A_b ratio) increases the ultimate load. The presence of supplementary reinforcing, in addition to primary confining reinforcing, increases the ultimate load compared to specimens without supplementary reinforcing. Increases in spiral diameter, with no changes in block dimensions or increases in spiral pitch, increase the ultimate load. The configuration of the local zone reinforcing affects the magnitude of surface strains but not their distribution. A spirally reinforced specimen behaves better in all respects, including first cracking, than an unreinforced specimen. Increases in spiral diameter increase the ultimate deformation capacity of the specimen. The extensive tests by Roberts in this program, as well as the wide range of tests run by others and compared by Roberts, showed that one could reasonably make an accurate prediction of the ultimate capacity of a tendon anchorage

local zone by considering the bearing area, concrete strength, and confinement by surrounding concrete and confining reinforcement. An empirical equation developed in this study showed that the ultimate capacity of the specimen can be predicted to within ± 20 percent of the actual load. However, the prediction alone does not ensure that the specimen will behave adequately in terms of crack width criteria. A local zone test specimen, procedure, and criteria for acceptance have, therefore, been proposed to ensure proper local zone behavior.

The recommendations, if adopted, would cause anchorage device suppliers to either design large stiff anchors that would require no testing procedures (analytical expressions for bearing stress and stiffness are given), or to produce more compactly and innovatively designed anchors that would require the testing procedure to prove adequate performance.

The recommendations should also lead manufacturers to more uniform local zone designs. Tests to prove the adequacy of a particular anchor, situated in various classes of concrete with specific edge distances and reinforcing details, can be done relatively quickly and simply. The proven details can then be used in all post-tensioning applications safely and confidently. The guess work will disappear from local zone design. Manufacturers, designers, and contractors will be completely confident that an anchorage device, properly using its manufacturer's recommendations, will not cause problems in the structure.

The proposal for local zone tests, if adopted, could cause additional work and financial burdens for the manufacturers at the onset of the implementation of the requirements. However,

once the tests have been completed and the anchors and their details have been accepted, the manufacturer will have fewer problems. Local zone designs will be consistent, and manufacturers can be more confident that they would not be held responsible for causing structural damage or serviceability problems due to a faulty design.

In general, the testing procedure should simplify the anchorage zone design procedure, alleviate uncertainties, and improve local anchor zone behavior in all post-tensioned structures.

RECOMMENDED PROVISIONS FOR AASHTO BRIDGE SPECIFICATIONS

The proposed specification changes are the formal recommendations of NCHRP Project 10-29 staff at the Ferguson Structural Engineering Laboratory of the University of Texas at Austin. They represent a broad consensus of the staff, but in any areas of conflict final responsibility was taken by Principal Investigator John E. Breen. They have not been approved by NCHRP, any AASHTO Committee or formally accepted for the AASHTO Specifications. For clarity, the changes are submitted in the form of mandatory "Code" statements with accompanying background or explanation in "Commentary" statements (see Appendix E).

CHAPTER 4

CONCLUSIONS AND RECOMMENDATIONS

This study originated because of a strong feeling in the transportation bridge design community that the AASHTO *Standard Specifications for Highway Bridges* did not provide adequate guidance for designing or for checking and approving reinforcement for tendon anchorage zones of post-tensioned concrete girders and slabs. It was felt that current designs can result in excessive cracking or congested reinforcing details. The wide variation of current design practices suggested the need for research in this area. In addition, it was felt that design criteria were needed for reinforcement details for inclined, sharply curved and highly eccentric tendons, and for intermediate anchorages.

This study encompassed a comprehensive literature review; a state-of-the-art survey with good responses from transportation officials, consultants, hardware suppliers and researchers; comprehensive linear elastic finite element analysis studies; exploratory nonlinear, inelastic finite element analysis studies; two- and three-dimension strut-and-tie modeling; and a broad physical testing program. Physical tests included 28 local zone specimens; three local zone-general zone interaction specimens, 36 end anchorage specimens including concentric, eccentric, single, multiple, straight, inclined, curved, and laterally post-tensioned tendons in various combinations; three end reaction specimens; eight intermediate anchorage specimens including pockets, blisters and ribs; three diaphragm specimens; and 56 deck tendons in six slab specimens with various combinations of deck reinforcement, anchor orientation, bursting and spalling reinforcement and stressing sequence. It culminated in a comprehensive proposal for a complete revision in the AASHTO *Standard Specifications for Highway Bridges* provisions for post-tensioned anchorage zones.

CONCLUSIONS

General

The major objective of this research was to develop a rational and systematic approach to anchorage zone design for post-tensioned structures. One of the first developments was the division of the anchorage zone into a local zone and a general zone. The local zone is defined as the prism of concrete surrounding and immediately ahead of the anchorage device and any integral confining reinforcement. The behavior of the local zone is strongly influenced by the specific characteristics of the anchorage device and its confining reinforcement, but it is less influenced by the geometry and loading of the overall structure. The general zone is defined as the volume of concrete through which the concentrated prestressing force at the anchorage device spreads transversely to a more linear stress distribution across

the entire cross section of the member (Saint Venant region). This division of the anchorage zone into local zone and general zone enabled a logical and equitable division of responsibility. Furnishing of a proper device and documented recommendations for cover, spacing and confining and supplementary reinforcement in the local zone is the primary responsibility of the anchorage device supplier. Design of the general zone and approval of local zone devices are primary responsibilities of the engineer-of-record. Responsibilities for proper placement of materials and proper stressing procedures are assigned to the constructor.

The concept of subdivision of the anchorage zone into the local zone and the general zone allows for more flexibility in the choice of the post-tensioning hardware and, at the same time, ensures that the selection of a specific, satisfactory anchorage device does not have a major influence on the design of the rest of the structure.

The general concept followed in the recommendations is to adopt a limit states approach in which attention is paid to serviceability at normal stressing levels through crack width limits in local zone anchorage device tests and to robustness at the ultimate state by proper selection of load and resistance factors. The specific AASHTO specification revisions proposed are lengthy because of the wide variety of uses of post-tensioning tendons in highway structures, the attempt to give flexibility, and the basic lack of current AASHTO provisions for modern concepts in structural concrete design such as strut-and-tie models (STM). It is believed that substantial progress has been made toward ensuring more reliability, more consistency and more clarity in the design process for anchorage zones of post-tensioning tendons.

Local Zone

The designation of the local zone permitted detailed exploration of the characteristics of anchorage devices in manageable, isolated specimens. It is clear that the local zone problem is one of essentially confining a node that is under high bearing stress. The local zone tests clearly showed the importance of confinement by concrete and by confining reinforcement.

The detailed local zone tests showed that it was possible to accurately and conservatively express the ultimate load capacity of an anchorage device by an expression such as Eq. 4:

$$F_{ult} = 0.80 f'_c \sqrt{A/A_b} (A_b) + 4.1 f_{lat} A_{core} (1 - s/D)^2$$

In development of this equation it was demonstrated that spiral confinement is twice as effective as orthogonal confinement. However, while this type of equation is useful for preliminary evaluation

of anchorage device capacity and for sizing confining reinforcement such as spirals, the formula is not presented for code use because it does not address the problem of serviceability. A good estimation of the ultimate capacity does not ensure satisfactory condition of the local zone at service loads. A strict limit on bearing stress and device stiffness, or a thorough testing procedure, which is included in the provisions, is necessary to confirm both ultimate capacity and adequate serviceability.

Anchors that satisfy a specified bearing stress condition under factored load, and those that meet a minimum specified stiffness, are termed "basic" anchorage devices. Such anchors can be designed by the engineer-of-record or accepted from a post-tensioning supplier without acceptance tests.

Any other anchors are termed "special" anchorage devices. Such anchors must be tested under the supervision of an independent "third party" evaluator acceptable to the engineer-of-record. A proposed test specimen and test procedure are recommended patterned after PTI and FIP recommendations. Because post-tensioning is an international industry, it is important that test procedures be in general harmony with international standards. The test specimen allows the anchorage device to have confining reinforcement as well as supplementary skin reinforcement in the test prism. However, the same confining reinforcement and equivalent supplementary reinforcement must be present in the actual structural application. Three different loading regimes are allowed: cyclic, short-term sustained, or monotonic. Cyclic and short-term-sustained loading were found to be about equivalent in assessment of anchorage device suitability. However, the criteria for monotonic loading had to be adjusted to require somewhat higher load levels than cyclic or sustained load to determine suitability. Acceptance criteria are based on crack width limitations at service levels, crack stability, and ultimate strength levels.

A major new feature for practice in the United States is that the supplier of special anchorage devices will have to present the engineer-of-record specific recommendations for minimum concrete strength at the time of stressing, edge distance, center-to-center spacing, minimum confining reinforcement, and required supplementary reinforcement.

The separation of local zone design, testing, and acceptance procedures is possible because the local zone-general zone test series reported herein showed that placing a local zone detail into a general zone resulted in the somewhat enhanced behavior of the local zone. Thus, the local zone criteria become in effect minimal or lower bound criteria for the node of the general zone.

General Zone

The analyses and experimental tests showed clearly that the major areas of concern in design of post-tensioned anchorage zones could be broken into three categories: (1) very high bearing stresses ahead of the anchorage device and the proper confinement required to prevent compressive failure of this region (this category is controlled by the local zone provisions discussed previously); (2) substantial tensile bursting stresses oriented normal to the tendon axis and some distance ahead of the anchorage device; and (3) very high compressive stresses in the compression struts (or stress fields) ahead of the local zone node.

In addition to these major concerns, there are several secondary areas of concern: (1) compatibility-induced spalling tensile stresses along the loaded face (these were shown to be secondary

in magnitude and essentially self-relieving, virtually disappearing upon the formation of local cracking); (2) equilibrium-induced spalling tensile stresses between widely spaced multiple anchors (these are easily determined and designed for by use of STM); and (3) longitudinal edge tensile stresses when anchor loads are placed outside the kern (again, these can be readily treated by STM).

The test program on end anchorages in girder applications using multiple strand tendons indicated that current commercial multiplane anchors and equivalent bearing plate anchors perform quite well. Cracking along the tendon axis at maximum stressing levels found in practice only occurred in 25 percent of the cases. For all practical purposes, the full ultimate strength of the tendons were developed in all but 10 percent of the test specimens. Only one of these deficient specimens had an adequate local zone design. When taken into context with the limited number of actual failures reported in the state-of-the-art survey, it is emphasized that the anchorage zone problem may be one of lack of clarity, lack of education and unclear assignment of responsibility, but is not one of critical deficiency in hardware devices or rampant unsafe practices.

First Crack Predictions

In almost all applications, fine well-controlled cracks in the anchorage zone are tolerable. In a few extreme cases it might be desirable to try to have a "crack-free" environment. Initial bursting cracking can be estimated by using computed tensile stresses from a linear elastic analysis (finite element analysis or Guyon's equations for simple cases) and matching the peak stresses with the effective tensile strength of the concrete. It was shown that the most accurate procedure is to adjust the computed tensile stress for the effect of duct opening and sheath by using transformed area concepts. The effective tensile strength should consider the effect on the anchorage zones tensile strength due to the triaxial stress state. Specifically, the very different stress states in the material test specimen (split cylinder) and in the highly compressed anchorage zone should be recognized. It was also found that Ottosen's triaxial criteria were most effective. It was shown that a simple and generally conservative approximation for this difference is to assume the effective tensile stress as equal to $4.2 \sqrt{f_c'}$. Poor agreement was found in trying to predict longitudinal edge tensile cracking loads or spalling cracking loads. The very high localized stresses computed for the latter in finite element analyses seem to be relieved by micro-cracking and do not produce significant visible cracking except in the case of widely spaced multiple anchors.

These elastic models help to give an engineer an estimate for the first cracking load. The models were verified only on specimens with isolated anchorage forces, without restrained thermal creep or shrinkage effects, and with no forces other than the post-tensioning force applied to the specimens. In an actual girder, many other forces may exist that could induce cracking. Unfortunately, no data are available for prediction of the effects of these cracking forces. Fortunately, the calculation of the first cracking load is rarely critical in a design situation.

Ultimate Capacity Predictions

The most versatile and consistent predictor of ultimate capacity of the general zone was the strut-and-tie model. However, the

basic strut-and-tie model, which is developed assuming that the force distribution at the far end of the anchorage zone (where the discontinuity region ends) will be that given by elastic analysis, was extremely conservative in many cases. It was obvious in the tests that substantial redistribution of forces was occurring after cracking not only in the general zone, but at the base of the test specimens. Sanders (1) proposed a modified strut-and-tie model approach recognizing this redistribution. It was not adopted for the AASHTO recommendations made in this report because a number of the test results showed it to be unconservative. However, the overall average of test to predicted results was much closer to 1.0.

Strut-and-tie models are based on the lower bound theorem of the theory of plasticity. The lower bound theorem of plasticity assumes that both internal and external equilibrium are satisfied and that stresses do not exceed the material yield conditions. The theory also assumes that the system has sufficient ductility to develop the yield conditions. The comprehensive test results reported herein show that while the ductility of anchorage zones is limited, and while they frequently experience explosive crushing failures, the bursting reinforcement usually yields by or at failure and there is sufficient ductility to develop the plastic behavior required for strut-and-tie modeling.

In recent times, a large emphasis has been placed on the use of the strut-and-tie models for the design of discontinuity regions in reinforced and prestressed concrete structures. However, little research had been done on the applicability of the strut-and-tie model to regions like anchorage zones where, because of local confinement, the stresses in the concrete can exceed the uniaxial compressive strength and very strong gradients of stresses are present. The distinction made between failure of the local zone and failure of the general zone made possible the application of normal strut-and-tie model techniques to the general zone, excluding the local zone from the strut-and-tie model and treating it as a separate problem.

While most applications of the strut-and-tie model in design practice try to prevent a failure of the concrete in compression, this is not readily possible for anchorage zones because the tensile strength of the concrete is much more significant than for cases involving bending or shear. In most cases, the ultimate load of the anchorage zone test specimens was less than two times the cracking load, which is a much smaller ratio than usually observed in flexural members. Only a few cracks typically develop before failure of the anchorage zone, leaving a large part of the concrete uncracked and able to resist substantial tensile forces. The presence of an important component of tensile stresses in the concrete makes the failure of an anchorage zone generally very brittle, and the ductility of an anchorage zone is relatively small. However, a series of tests showed that the distribution of the tensile bursting reinforcement in the bursting region can diverge substantially from the elastic stress distribution without substantial deterioration of the performance. For design, it appears desirable that the strut-and-tie models of anchorage zones be reasonably close to the elastic stress distribution. For that effect, the principal stress vectors and principal stress trajectories obtained from a linear elastic finite element analysis are helpful.

Comparisons between the results of parametric studies using the strut-and-tie model and parallel parametric studies using the finite element method show that the results of both methods can give very close agreement. The main geometric parameter needed

for the development of a strut-and-tie model is the location of the centroid of the tensile bursting force. This location can be determined by setting the diffusion angle of the compression forces to 26 deg. on either side of the tendon path, measured from the center of the anchorage device, or to a total of 52 deg. for cases with inclined or curved tendons. This is a very advantageous property because, although finite element programs tend to be more and more available to the designer, it does not appear desirable nor likely that a finite element analysis will or should be performed for each and every anchorage zone. The results of the strut-and-tie model are sufficient to safely design the reinforcement. The stresses in the concrete struts at the interface between the local zone and the general zone must be considered and can often control the design. The accuracy of the prediction of the compressive strength based on the strut-and-tie model decreases with increasing complexity of the specimens. For very complex configurations, it may be desirable to use the results of a numerical analysis.

The results of linear finite element analyses of anchorage zones can be used in various ways for the design of anchorage zones. Principal stress vector plots can be used in constructing and evaluating strut-and-tie models. These are more useful in proportioning and detailing tensile reinforcement than finite element analysis plots. As previously mentioned, the distribution of the elastic tensile stresses can be used to estimate the cracking load. The distribution of compressive stresses can be used to estimate the maximum compressive strength of the anchorage zones. Because of the great flexibility of the finite element method, a large number of parametric studies were performed, exploring more general configurations that could not be experimentally tested within the limits of the current research project.

By using the results of the finite element analyses, the maximum compressive force that can be applied on the anchorage zone can be estimated. Because of the presence of confining reinforcement in the local zone, the bearing stress under the anchorage device can be in excess of the ultimate compressive strength f_c' of the concrete. The concrete of the general zone, on the other hand, is unconfined and can resist only compressive stresses in the vicinity of $0.75f_c'$. The critical section for the compressive stresses is, therefore, generally located at the interface between confined and unconfined concrete. Because the length of the confining reinforcement is usually about equal to the lateral dimensions of the anchorage device, it was found that, by allowing the compressive stress in the concrete at a distance equal to the lateral dimension of the anchorage device ahead of the anchorage to be $0.75f_c'$, a reasonable prediction of the ultimate compressive strength of the anchorage zones was obtained, assuming that failure does not occur at a lower load for another reason such as local zone failure or tension tie failure.

An extensive series of parametric studies on the influence of the various geometric parameters of the anchorage zone confirmed the results of Guyon (20), and investigated the influence of additional parameters like the inclination and curvature of the tendon.

Specimens that had reinforcement significantly different from that determined from an elastic analysis had additional cracking and sometimes reduced strength. Therefore, it is recommended that only the reinforcement which is placed within a distance of 1.5 times the section width from the loading surface be considered as effective for the STM calculations. It is recommended that the centroid of that reinforcement be located close to the pattern

that would be indicated by an elastic analysis. This does not mean that an elastic analysis must be performed, but that good engineering judgment should be exercised when placing reinforcement so that overly large plastic redistribution of forces is not required.

It is important that in members with curved tendons sufficient tie-back reinforcement be provided. Tie-back reinforcement is modeled in the STM through the use of equivalent forces applied to the compression struts or tension ties. To prevent large cracks and explosive failures, the resulting STM and the portion of the radial forces that are resisted by reinforcement in tension should approximate the elastic stress distribution.

The compression struts were assumed to have a width equal to twice the distance from the load axis to the line of action of the strut. The local zone node was also very critical and must be checked if a certification test has not been performed. Most other nodes in the anchorage zone, except the local zone node, are nodes distributed over a large enough distance to prevent high stresses. All nodes should be examined to ensure that this assumption is correct.

It is critical to consider anchorage zone analysis and design as a three-dimensional problem. One T-beam section was tested, and the applicability of the STM was quite good. The three-dimensional effects can be considered by dividing the member into multiple two-dimensional planes. The interaction of models used on these planes must be considered, and the model loadings and results must be consistent.

Using methods based on Guyon's symmetrical prism to predict the ultimate capacity proved to be not as consistent as the STM and can yield unconservative results, especially for anchorage zones that are more complicated than a concentric anchorage zone.

Many applications of anchorage devices are relatively straightforward. The devices may be in the center of a massive end block and have minimal geometry constraints. The elaborate provisions for strut-and-tie models or finite element analyses may be an "over-kill" for many practical applications. A much simpler approximate procedure was developed which gives the magnitude and centroid of the tensile bursting force, as well as an estimate of the maximum compressive stress at a critical section about a plate width ahead of the anchor. These approximate procedures, developed from parametric studies with more accurate finite element and strut-and-tie model analyses, produce equivalent results for a wide range of practical cases.

Constructability

Throughout the state-of-the-art and the experimental phases of this study it was apparent that the most severe problems with anchorage zones are in narrow web members without substantial end blocks or diaphragms. Such applications are typical in precast segmental construction, but less likely in much cast-in-situ construction where tendons are more often anchored at the end of the structure and a larger diaphragm is provided. None of the design procedures, no matter how accurate or elegant, will produce a satisfactory anchorage zone unless the designer is sensitive to the requirements of constructability. Good detailing and quality workmanship are as essential for the satisfactory performance of the anchorage zone as are an accurate analysis and a proven anchorage device. The designer must consider the constraints

imposed by the tolerances and minimum dimensions for bending reinforcement and spirals, by the need for adequate paths for placement of concrete and consolidation of the concrete in highly congested zones, and by the need to prevent voids and honeycombing in the anchorage zone and, particularly, in and near the local zones. In the experimental studies the need to maintain workable details, especially spiral pitch, and the use of superplasticizers to facilitate concrete placement and consolidation were invaluable. There is an old adage that says, "It's better not to know so much, as to know so much that's not so." It can be paraphrased for anchorage zones as, "It's better not to call for so much steel as to call for so much that concrete cannot go." It was found helpful to the project staff to detail some congested zones at close to full scale with all hardware, confinement reinforcement, supplementary reinforcement, grout tubes, and so on, shown. It often resulted in undertaking a more practical redesign. In the early stages of the project it was obvious that methods and opinions regarding analysis of forces and proportioning of reinforcement differed by an order of magnitude (1000 percent). Hopefully, the more scientific aspects of this project greatly narrowed that scatter to approximately 20 percent. Unless the designer considers constructability from the inception, that gap can widen back to 200 percent.

RECOMMENDATIONS FOR FUTURE RESEARCH

Although the scope of this project was broad, the effort was substantial, the interest and cooperation of the bridge design and construction family were overwhelming, and the project team spent 5 years on the subject, there are still many unanswered questions and areas for further research.

Further experimental research should include a more comprehensive treatment of the state of stresses at the interface between the local zone and the general zone, including the possible use of additional confining reinforcement in the general zone. Long-term testing, as well as observation of actual structures, should assess the dependability of concrete tensile stresses, possibly leading to the introduction of a contribution of concrete in tension in the design equation.

Additional analytical research should expand on the limited pilot study for the use of nonlinear models for the behavior of anchorage zones. An analytical study of the influence of the tensile strength of the concrete on the behavior is highly desirable to allow comparison with experimental test results. Although it has mainly been used for stress fields with small gradients, the compression field theory offers promising possibilities for the modeling of concrete after cracking, including nonlinearities in tension as well as in compression.

One specific area of research that will be generated by the implementation of the proposed design guidelines is the many questions that will unavoidably be raised by special details that are not covered in the present study. It is expected that Highway Departments or other organizations will desire that special anchorage detailing procedure be closely investigated in order to ensure consistent and economical designs.

It was shown that the local zone tests were a safe indicator of local zone performance in the general zone. There are a number of local zone related areas that need further study. One area not thoroughly examined in this study was the effect of the design of the local zone on the behavior of the general zone. It

would be very interesting to create a series of specimens with identical general zone configurations and place within those specimens a variety of local zone details (same plate size with various confining steel amounts and arrangements). The results of this type of test series would give a good indication of the effect of the node design on the resultant strut-and-tie model results.

Another interesting area for further study might be the relationship between supplementary reinforcing in local zone specimens and steel present in general zone situations. The Austrian Code allows supplementary reinforcing to be present in the local zone test specimen which need not be present in the actual structure. From the brief series of tests that incorporated supplementary reinforcing, it was apparent that the specimens with the greatest amount of supplementary reinforcing behaved very much like the general zone specimens, especially in terms of serviceability criteria. It could be that a small amount of supplementary reinforcing could be allowed in the test procedures which would give a better representation of the behavior of the local zone in real world applications.

There are several details requiring further exploration in the general zone. These include a study of a systematic approach to

the distribution of radial forces between tension and compression when curved tendons are used. Also, a study should determine if long spirals are effective in confining concrete at more than a plate width from the loading surface and whether reinforcement can be effectively used to confine compression struts in the general zone.

Future research should continue to keep the problem in perspective. The major goal is to have safe anchorage zone designs. Though extremely vital to the safety of a post-tensioned structure, the economic cost of reinforcement placed in the anchorage zone is small relative to the total cost of the construction project. Thus, the major goals in the research were a better understanding of the anchorage zone and the development of designs that are consistent and safe. The intent was not necessarily to reduce the reinforcement amounts.

Two areas outside the range of this present study should be explored. The first is the design of anchorage zones with concrete compressive strength at the time of stressing greater than 7000 psi in view of possible reductions in ductility and/or efficiency of the concrete in carrying the compression struts. The other is long-term and fatigue testing of anchorage zones to investigate any adverse effects.

REFERENCES

1. SANDERS, D.H., "Design and Behavior of Anchorage Zones in Post-Tensioned Concrete Members." Ph.D. Dissertation, The University of Texas at Austin (Aug. 1990).
2. SCHLAICH, J., SCHAFER, K., and JENNEWINE, M., "Toward a Consistent Design of Reinforced and Prestressed Concrete Structures." *PCI Journal*, Vol. 32, No. 3 (May–June 1987) pp. 74–151.
3. *Recommendations for Acceptance and Application of Post-Tensioning Systems*. Federation Internationale de la Précontrainte (FIP) (Mar. 1981).
4. ROBERTS, C., "Behavior and Design of the Local Anchorage Zone in Post-Tensioned Concrete." M.S. Thesis, University of Texas at Austin (May 1990).
5. MÖRSCH, E., "Über die Berechnung der Gelenkquader." *Beton-und Eisen*, No. 12 (1924) pp. 156–161.
6. GUYON, Y., *Prestressed Concrete*. John Wiley and Sons, Inc., New York (1953).
7. ADEGHE, L.N., and COLLINS, M.P., *A Finite Element Model for Studying Reinforced Concrete Detailing Problems*. Department of Civil Engineering, University of Toronto, *Publ. No. 86-12* (Oct. 1986) pp. 66–74.
8. FENWICK, R.C., and LEE, S.C., "Anchorage Zones in Prestressed Concrete Members." *Magazine of Concrete Research*, Vol. 38, No. 135 (June 1986) pp. 77–89.
9. STONE, W.C., and BREEN, J.E., "Behavior of Post-Tensioned Girder Anchorage Zones." *PCI Journal*, Vol. 29, No. 1 (Jan.–Feb. 1984).
10. STONE, W.C., and BREEN, J.E., "Design of Post-Tensioned Girder Anchorage Zones." *PCI Journal*, Vol. 29, No. 2 (Mar.–Apr. 1984).
11. KOMENDANT, A.E., *Prestressed Concrete Structures*. McGraw-Hill (1952) pp. 172–173.
12. MIDDENDORF, K.H., "Anchorage Bearing Stresses in Post-Tensioned Concrete." *ACI Journal* (Nov. 1960) pp. 580–584.
13. HAWKINS, N.M., "The Bearing Strength of Concrete Loaded Through Rigid Plates." *Magazine of Concrete Research*, Vol. 20, No. 62 (Mar. 1968) pp. 31–40.
14. HAWKINS, N.M., "The Bearing Strength of Concrete Loaded Through Flexible Plates." *Magazine of Concrete Research*, Vol. 20, No. 63 (June 1968) pp. 95–102.
15. HAWKINS, N.M., "The Bearing Strength of Concrete for Strip Loadings." *Magazine of Concrete Research*. Vol. 22, No. 71 (June 1970).
16. AASHTO, *Standard Specifications for Highway Bridges*. Fourteenth Edition, American Association of State Highway and Transportation Officials, Washington, D.C. (1989).
17. "Design and Construction Specifications for Segmental Concrete Bridges." Post-Tensioning Institute (Feb. 1988).
18. AASHTO, "Interim Guide Specifications for Design and Construction of Segmental Concrete Bridges," American Association of State Highway and Transportation Officials, Washington, D.C. (1990).
19. *Post-Tensioning Manual*, Fourth Edition, Post-Tensioning Institute (1986).
20. GUYON, Y., "Limit-State Design of Prestressed Concrete." Vol. 2, *The Design of the Member*, John Wiley and Sons, New York (1974).
21. LEONHARDT, F., "Das Bewehren von Stahlbetontragwerken." *Beton-Kalender*, von Wilhelm e. & Sohn (1973).
22. BREEN, J.E., COOPER, R.L., and GALLAWAY, T.M., "Minimizing Construction Problems in Segmentally Precast Box Girder Bridges." *Research Report No. 121-6F*, Center for Highway Research, The University of Texas at Austin (Aug. 1975).
23. DILGER, W.H., and GHALI, A., "Remedial Measures for Cracked Webs of Prestressed Concrete Bridges." *Prestressed Concrete Institute (PCI) Journal*, Vol. 19, No. 4 (Jul.–Aug. 1974) pp. 76–85.
24. STONE, W.C., and BREEN, J.E., "Behavior of Post-Tensioned Girder Anchorage Zones." *Center for Transportation Research Report No. 208-2*, University of Texas at Austin (Jan. 1981).
25. BREEN, J.E., FENVES, G., SANDERS, D.H., and BURDET, O., "Anchorage Zone Reinforcement for Post-Tensioned Concrete Girders." *National Cooperative Highway Research Program Interim Report*, Proj. 10-29, The University of Texas at Austin (Aug. 1987).
26. LIBBY, J., "Critique of a Post-Tensioned Roof Slab Failure." *Concrete International*, Vol. 7, No. 10 (Oct. 1985) pp. 28–32.
27. LIBBY, J., "Segmental Box Girder Bridge Superstructure Design." *ACI Journal*, Vol. 73, No. 5 (May 1976) pp. 279–290.
28. MACCHI, A.J., "Roof Slab Failure." Letters to the Editor, *Concrete International*, Vol. 9, No. 1 (Jan. 1987) pp. 7–8.
29. PODOLNY, W., "The Cause of Cracking in Post-Tensioned Concrete Box Girder Bridges and Retrofit Procedures." *PCI Journal*, Vol. 30, No. 2, (Mar.–Apr. 1985) pp. 82–139.
30. WIUN, D., and BUYUKOZTURK, O., "Problems in Designing Prestressed Segmental Bridges." Massachusetts Institute of Technology (Mar. 1984).
31. Breen, J.E., "Why Structural Concrete," *IABSE Report*, Vol. 62., IABSE Colloquium, Stuttgart 91, pp. 15–26.
32. Comité Euro-International du Béton, *Anchorage Zones of Prestressed Concrete Members*. No. 181 (Apr. 1987).
33. DEUTSCH, J.B., Decision in Missouri Board for Architects, Professional Engineers and Land Surveyors vs. D.M. Duncan, J.D. Gillum and G.C.E. International, Case No. AR-84-0239, Administrative Hearing Commission, State of Missouri, Jefferson City, 15 November 1985, p. 180.
34. ROGOWSKY, D.M., and MARTI, P., "Detailing for Post-Tensioning." *VSL Report Series No. 3*, VSL International Ltd., Berne (Apr. 1991).
35. NIYOGI, S.K., "Bearing Strength of Reinforced Concrete Blocks." *ASCE Structural Division Journal*, Vol. 101, No. ST5 (May 1975).
36. NIYOGI, S.K., "Bearing Strength of Concrete-Geometric Variations." *ASCE Structural Division Journal*, Vol. 99, No. ST7 (Jul. 1973) pp. 1471–1490.
37. WILLIAMS, A., "The Bearing Capacity of Concrete Loaded Over a Limited Area." *Technical Report 526*, Cement and Concrete Association (1979).

38. WURM, P., and DASCHNER, F., "Teilflächenbelastung von Normalbeton Verusche an Bewehrten Scheiben." *Deutscher Ausschuß für Stahlbeton*, Heft 344, Berlin (1983) (German).
39. WURM, P., and DASCHNER, F., "Versucheuber Teiflachenbelastung von Normalbeton." *Deutscher Ausschuß für Stahlbeton*, Heft 286, Berlin (1977) (German).
40. AISC *Manual of Steel Construction*. Eighth Edition, American Institute of Steel Construction, Inc. (1980).
41. RICHART, F.E., BRANTZAEG, A., and BROWN, R.L., "A Study of the Failure of Concrete under Combined Compressive Stresses." *Research Bulletin No. 185*, University of Illinois Engineering Experimental Station (1928).
42. YETTRAM, A.L., and ROBBINS, K., "Anchorage Zone Stresses in Axially Post-Tensioned Members of Uniform Rectangular Section." *Magazine of Concrete Research*, Vol. 21, No. 67 (June 1969) pp. 103–112.
43. ZIELINSKI, J.L., and ROWE, R.E., "An Investigation of the Stress Distribution in the Anchorage Zones of Post-Tensioned Concrete Members." *Research Report No. 9*, Cement and Concrete Association, London (Sept. 1960).
44. OTTOSEN, N.S., "A Failure Criterion for Concrete." *ASCE Journal of Engineering Mechanics*, Vol. 104, No. EM4 (Aug. 1977) pp. 527–535.
45. BILLIG, K., *A Proposal for a Draft Code of Practice for Prestressed Concrete*. Cement and Concrete Association, London (1948).
46. SCHLAICH, J., and SCHÄFER, K., "Konstruiren in Stahlbetonbau." *Béton-Kalender*, Part 2 (1989) pp. 563–715 (German).
47. DRUCKER, D.C., "On Structural Concrete and the Theorems of Limit Analysis." *IABSE Proc.*, Vol. 21 (1961) pp. 49–59.
48. BURDET, O., "Analysis and Design of Post-Tensioned Anchorage Zones Concrete Bridges." Ph.D. Dissertation, University of Texas at Austin (May 1990).
49. DEBORST, R., "Computational Aspects of Smeared Crack Analysis." *Computational Modelling of Reinforced Concrete Structures*, Pineridge Press, Swansea (1986) pp. 44–83.
50. MEYER, C., and OKAMURA, H. (eds.), *Finite Element Analysis of Reinforced Concrete Structures*. ASCE (1986).
51. "ABAQUS Users Guide." Hibbit, Karlsson, and Sorenson, Providence, R.I.
52. PATRAN *Users Guide* (1986).
53. ROGOWSKY, D.M., and MACGREGOR, J.G., "Design of Reinforced Concrete Deep Beams." *Concrete International* (Aug. 1986) pp. 49–58.
54. LENSCHOW, R., and SOZEN, M.A., "Practical Analysis of the Anchorage Zone Problem in Prestressed Beams." *ACI Journal* (Nov. 1965) pp. 1421–1437.
55. STONE, W.C., and BREEN, J.E., "Analysis of Post-Tensioned Girder Anchorage Zones." *Center for Transportation Research Report No. 208-1*, University of Texas at Austin (Jan. 1981).
56. THÜRLIMANN, B., MARTI, P., ET AL., "Anwendung der Plastizitätstheorie auf Stahlbeton." Institut für Baustatik und Konstruktion, Zürich (1983) (German).
57. COMITÉ EURO-INTERNATIONAL DU BÉTON and the FEDERATION INTERNATIONALE DE LA PRÉCONTRAINTE (FIP), *Model Code for Concrete Structures*. English Translation (proposed 1990).
58. KAMMENHUBER, J., and SCHNEIDER, J., "Arbeitsunterlagen für die Berechnung vorgespannter Konstruktionen." *Stahlton*, Zürich (1974).
59. STONE, W.C., and BREEN, J.E., "Design of Post-Tensioned Girder Anchorage Zones." *Center for Transportation Research Report No. 208-3F*, University of Texas at Austin (Jan. 1981).
60. WOLLMANN, G., Ph.D. Dissertation, "Anchorage Zones in Post-Tensioned Concrete Structures." University of Texas at Austin, Department of Civil Engineering (May 1992).
61. FALCONER, B.A., "Post-Tensioning Anchorage Zones in Bridge Decks." M.S. Thesis, University of Texas at Austin (May 1990).
62. ROARK, R.J., and YOUNG, W.C., *Formulas for Stress and Strain*. Fifth Edition, McGraw-Hill, New York (1982).
63. SANDERS, D.H., BREEN, J.E., and DUNCAN, R.R., "Strength and Behavior of Closely Spaced Post-Tensioned Monostrand Anchorages." Ferguson Structural Engineering Laboratory, Bureau of Engineering Research, The University of Texas at Austin (Oct. 1987).
64. "Building Code Requirements for Reinforced Concrete." American Concrete Institute (ACI) 318-89, American Concrete Institute (1989).
65. LEONHARDT, F., "Cracks and Crack Control at Concrete Structures." *IABSE Proc.*, P-109/87, pp. 25–44.
66. COLLINS, M., and MITCHELL, D., "Shear and Torsion Design of Prestressed and Non-Prestressed Concrete Beams." *PCI Journal*, Vol. 25, No. 5 (Sept.–Oct. 1980) pp. 32–124.
67. GERGELY, P., and SOZEN, M.A., "Design of Anchorage-Zone Reinforcement in Prestressed Concrete Beams." *PCI Journal*, Vol. 12, No. 2 (Apr. 1967) pp. 63–75.
68. GERGELY, P., SOZEN, M.A., and SEISS, C.P., "The Effect of Reinforcement on Anchorage Zone Cracks in Prestressed Concrete Members." *Civil Engineering Structural Research Series, No. 271*, University of Illinois (Jul. 1963).
69. GESTNER, R.W., and ZIENKIEWICZ, O.C., "A Note on Anchorage Zone Stresses." *ACI Journal* (Jul. 1963) pp. 970–974.
70. IYENGAR, K.T.S.R., "Two-Dimensional Theories of Anchorage Zone Post-Tensioned Prestressed Beams." *ACI Journal*, Vol. 59, No. 10 (Oct. 1962) pp. 1443–1446.
71. SIEVERS, H., "Über den Spannungszustand im Bereich der Ankerplatten von Spanngliedernvorgespannter Stahlbetonkonstruktionen." *Bauingenieur*, Vol. 31 (Apr. 1956) pp. 134–135.
72. BLEICH, F., "Der Gerade Stab mit Rechteckquerschnitt als ebenes problem." *Der Bauingenieur*, Berlin, No. 9 (1923) pp. 225–259; No. 10 (1923) pp. 304–307.
73. IYENGAR, K.T.S.R., and YOGANANDA, C.V., "A Three-Dimensional Stress Distribution Problem in the Anchorage Zone of a Post-Tensioned Concrete Beam." *Magazine of Concrete Research*, Vol. 18, No. 55 (June 1966) pp. 75–84.
74. DOUGLAS, D.J., and TRAHAIR, N.S., "An Examination of the Stresses in the Anchorage Zone of a Post-Tensioned Prestressed Concrete Beam." *Magazine of Concrete Research*, Vol. 12, No. 34 (Mar. 1960) pp. 9–18.
75. SOM, P.K., and GHOSH, K., "Anchor Zone Stresses in Prestressed Concrete Beams." *ASCE Structural Division Journal*, Vol. 90, No. St4 (Aug. 1964) pp. 49–62.
76. MAGNEL, G., *Prestressed Concrete*. Third Edition, McGraw-Hill, New York (1954).
77. CHRISTODOULIDES, S.P., "A Two-Dimensional Investigation of the End Anchorages of Post-Tensioned Concrete Beams." *The Structural Engineer* (Apr. 1955) pp. 120–133.

78. CHRISTODOULIDES, S.P., "A Photoelastic Investigation of Pre-stressed Concrete Anchorages." *Civil Engineering and Public Works Review*, Vol. 51, No. 603 (Sept. 1956) pp. 994–997.
79. CHRISTODOULIDES, S.P., "The Distribution of Stresses Around the End Anchorages of Prestressed Concrete Beams. Comparison of Results Obtained Photoelastically with Strain Gauge Measurements and Theoretical Solutions." *IABSE Memoirs*, Vol. 16 (1956) pp. 55–70.
80. CHRISTODOULIDES, S.P., "Three-Dimensional Investigation of the Stresses in the End Anchorage Blocks of a Prestress Concrete Gantry Beam." *The Structural Engineer*, Vol. 35, No. 9 (Sept. 1957) pp. 349–356.
81. LEONHARDT, F., *Prestressed Concrete—Design and Construction*. Wilhelm Ernest and Son, Berlin (1964).
82. SARGIOUS, M., "Beitrag zu Ermittlung der Hauptzugsspannungen am Endauflager vorgespannter Betonbalken." Ph.D. Dissertation, Technische Hochschule, Stuttgart (Jul. 1960).
83. RASHEEDUZZAFAR, I.M.A., and AL-SAADOUN, S.S., "A Photoelastic Investigation of Anchorage Bearing Stresses." *Magazine of Concrete Research*, Vol. 36, No. 127 (June 1984) pp. 81–91.
84. VAUGHN, S.D., "An Exploratory Photoelastic Investigation of Post-Tensioned Concrete Anchorage Zone Bursting Stresses." M.S. Thesis, The University of Texas at Austin (Aug. 1977).
85. EGEBERG, J.L., "A Finite Element Investigation of the Anchorage Zones of Prestressed Concrete Beams." *Report No. 363*, Department of Civil Engineering, University of California, Berkeley (Aug. 1968).
86. YETTRAM, A.L., and ROBBINS, K., "Anchorage Zone Stresses in Post-Tensioned Uniform Members with Eccentric and Multiple Anchorages." *Magazine of Concrete Research*, Vol. 22, No. 73 (Dec. 1970) pp. 209–218.
87. YETTRAM, A.L., and ROBBINS, K., "Anchorage Zone Stresses in Axially Post-Tensioned I-Section Members with End Blocks." *Magazine of Concrete Research*, Vol. 23, No. 74 (Mar. 1971) pp. 37–42.
88. MARTI, P., "Basic Tools for Reinforced Concrete Beam Design." *ACI Journal* (Jan.–Feb. 1985) pp. 46–56.
89. MARTI, P., "Truss Models in Detailing." *Concrete International* (Dec. 1985) pp. 66–73.
90. COLLINS, M., and MITCHELL, D., *Prestressed Concrete Basics*. Chapter 9, "Design of Disturbed Regions," Canadian Prestressed Concrete Institute (1987) pp. 386–429.
91. BAIN, S., MUGURAMA, H., and OGAKI, Z., "Anchorage Zone Stress Distributions in Post-Tensioned Concrete Members." *Proc. World Conference on Prestressed Concrete*, University of California, San Francisco (1957) pp. 16:1–14.
92. LEE, S.C., "Bursting Stresses in the End Block of a Post-Tensioned Prestressed Beam." *Library School of Engineering, Report No. 321*, University of Auckland (Jan. 1983).
93. HUANG, T., "Stresses in End Blocks of a Post-Tensioned Prestressed Beam." *ACI Journal*, Vol. 61, No. 5 (May 1964) pp. 589–601.
94. TAYLOR, S.J., Discussion of the paper, "A Three-Dimensional Stress Distribution Problem in the Anchorage Zone of a Post-Tensioned Concrete Beam." *Magazine of Concrete Research*, Vol. 19, No. 58 (Mar. 1967) pp. 54–57.
95. TRINH, J., "Resistance du Béton aux forces concentrées première partie: cas du béton non armé." *Annales de l'Institut Technique du Batiment et des Travaux Publics*, No. 439 (Nov. 1985) (French).
96. VIRLOGEUX, M., "Analyse de quelques problèmes spécifiques au calcul des ponts par encorbellements successifs." *Annales de l'Institut Technique du Batiment et des Travaux Publics*, No. 391 (Feb. 1981) (French).
97. WELSCH, W.A., Jr., and SOZEN, M.A., "Investigation of Pre-stressed Reinforced Concrete Highway Bridges, Part 2, Analysis and Control of Anchorage Zone Cracking in Prestressed Concrete." *Engineering Experimental Station Bulletin No. 497*, University of Illinois, Urbana (1968).
98. ZIELINSKI, J.L., and ROWE, R.E., "The Stress Distribution Associated with Groups of Anchorages in Post-Tensioned Concrete Members." *Research Report No. 13*, Cement and Concrete Association, London (Oct. 1962).
99. YONG, Y.K., GADUGBEKA, C., and NAVY, E., "Anchorage Zone Stresses of Post-Tensioned Prestressed Beams Subjected to Shear Forces." *ASCE Structural Division Journal*, Vol. 113, No. 8 (Aug. 1987) pp. 1789–1805.
100. MIDDENDORF, K.H., "Practical Aspects of End Zone Bearing of Post-Tensioning Tendons." *PCI Journal*, Vol. 8, No. 4 (Aug. 1963) pp. 57–62.
101. "Austrian Code for Prestressed Concrete-Road Bridges, Design and Construction." *ÖNORM B 4252* (Dec. 1975) (German).
102. CONSTRUCTION INDUSTRY RESEARCH AND INFORMATION ASSOCIATION, *A Guide to the Design of Anchor Blocks for Post-Tensioned Prestressed Concrete Members*. CIRIA Guide 1, London (June 1976).
103. *Florida Department of Transportation Design Criteria*.
104. "German Building Code." *DIN 1045*, Sec. 17 (1988) (German).
105. *North Carolina Department of Transportation Design Criteria*.
106. *Ontario Highway Bridge Design Code* (1983).
107. "Swiss Code for Concrete." *Betonbauteile, SIA Code 162*.
108. LOSINGER, LTD BERN, "VSL End Block Design in Post-Tensioned Concrete." Bern (Nov. 1975).
109. BURGESS, J.A., BREEN, J.E., and POSTON, R.W., "Anchorage Zone Cracking of Post-Tensioned Bridge Decks with Closely Spaced Anchors." *American Concrete Institute SP-113, Cracking in Prestressed Concrete Structures* (1989) pp. 79–108.
110. VSL INTERNATIONAL CATALOG, "Post-Tensioning Systems." Berne (1990).
111. SCHLAICH, M., and ANAGNOSTOU, G., "Stress Fields for Nodes of Strut-and-Tie Models." *ASCE Structural Division Journal*, Vol. 116, No. 1 (Jan. 1990) pp. 13–23.

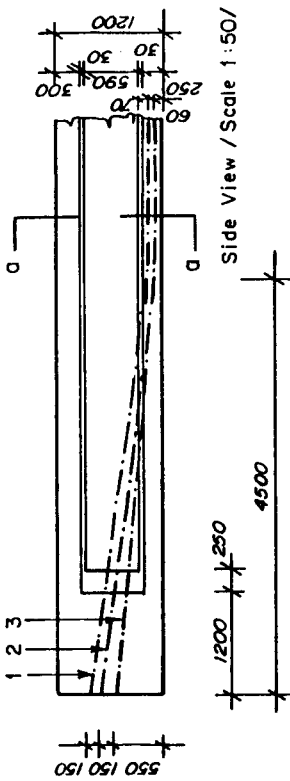
APPENDICES A, B, C

UNPUBLISHED MATERIAL

Appendices A, B, and C contained in the research agency's final report are not published herein, but complete copies of that report, entitled "Anchorage Zone Reinforcement for Post-Tensioned Concrete Girders," may be obtained on loan or may be purchased (\$25.00) by writing to the Transportation Research Board, Business Office, 2101 Constitution Avenue N.W., Washington, D.C. 20418. The available appendixes are titled as follows: Appendix A, "Literature Review"; Appendix B, "User Survey and Assessment"; Appendix C, "Details of Physical Test Specimens."

APPENDIX D

DESIGN EXAMPLES



D.1 Introduction

Figure D.1 shows an anchorage zone design problem which was sent out to European designers in a 1987 CEB survey [25]. This problem is used as a design

- example in this section. Figure D.2 shows the same problem with customary units.
- Some revisions and additional assumptions are necessary to make the design example workable:

- To avoid exceeding allowable extreme fiber concrete stresses some load has to be present on the girder in addition to its weight. Assuming that the tendons are draped at the 1/3 points of the girder, a uniform load of 2.23 kips/ft is needed.

- The girder is supported on 6 in. wide bearings with their center 6 inch

- As shown in Section D.2 the "anchorage steel rings" in the original problem statement (Figure D.1) do not qualify as basic anchorage devices, and special anchorage devices are needed.
 - The web of the I-section is too thin to accommodate two tendons in the same layer. However, this problem does not affect the procedures that are to be demonstrated with this design example and is ignored.



167

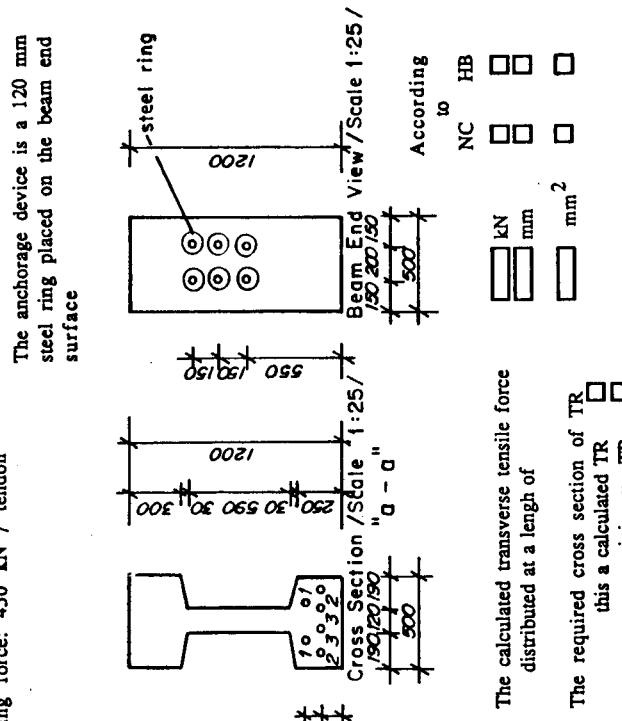


Figure D.1 CEB Survey Problem

A load factor of 1.2 and a ϕ -factor of 0.85 will be used, as specified in the proposed anchorage zone specifications. For convenience in calculations, the ϕ -factor is included on the load side. Hence the tendon force used in the design problem is $(1.2/0.85) \times 101 = 142.6$ kips per anchor or a total force of 855.5 kips. The uniform load and the reaction force tend to reduce the bursting force and a load factor of 1.0 is used for these loads.

D2 Local Zone Design

This section leads step by step through the design of the local zone.

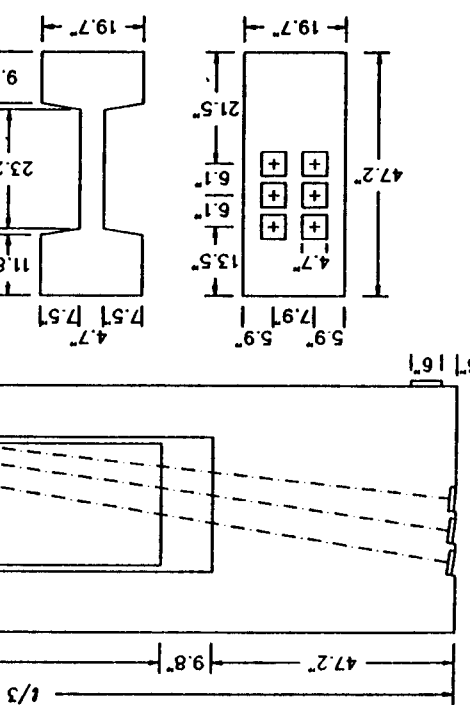


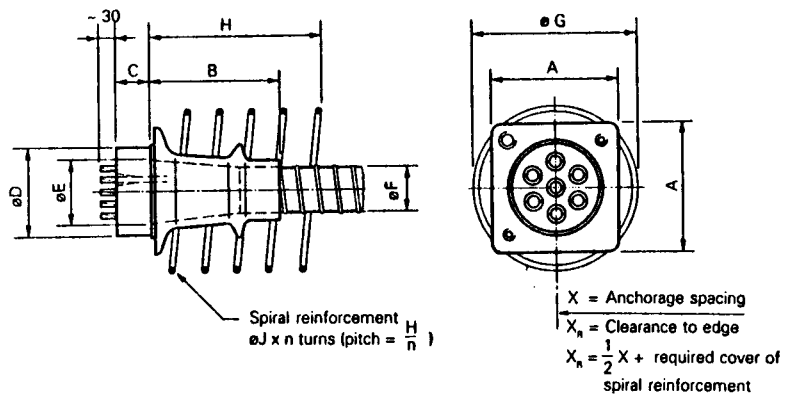
Figure D.2 Revised CEB Problem With Customary Units

$$f_b = 142.6 / 17.3 = 8.24 \text{ ksi}$$

The maximum bearing pressure to qualify as a basic anchorage device is (Code Eq. 9-39)

$$A_b = 4.7^2 \pi / 4 = 17.3 \text{ in}^2$$

and thus the bearing pressure is



Tendon unit	A	B	C	eD	eE	eF ⁿ internal/ external	eG	H	J	n	X ⁿ
5-3	120	130	50	90	50	40/45	130	150	10	3	155

Dimensions in mm

- 1) Standard diameter for corrugated steel duct. For polyethylene ducts PT-PLUS® see page 6
- 2) Anchorage spacings are in accordance with test requirements of CEB/FIP (Recommendations for acceptance and application of post-tensioning systems, March 1981). Modifications to these values may be possible.
- Dimensions are valid for Nominal concrete strength at 28 days: 35 MPa (cube), 28 MPa (cylinder).

Maximum prestressing force may be applied when concrete reaches 80 % of its nominal strength.

Max. prestressing force is 75 % of min. tendon breaking load (temporary overstressing to 80 %).

Dimensions for other concrete strengths on request.

Yield strength of spiral reinforcement: ≥ 420 MPa.

Spirals may be replaced by suitable orthogonal reinforcement.

$$f_{b,\max} = 0.7 f'_c \sqrt{A / A_b} = 0.7 \times 3.6 \times 5.9 / 4.7 = 3.16 \text{ ksi} < 8.24 \text{ ksi}$$

Hence the anchors do not qualify as basic anchorage device and special anchorage devices are needed. Information on required edge distance, minimum anchor spacing, confinement and auxiliary reinforcement, and concrete strength should be provided by the anchorage device supplier.

2. Select a special anchorage device.

In this example the VSL EC 5-3 anchor is used. This anchor can accommodate three $\frac{1}{2}$ in. strands, GR 270, with a maximum stressing force of 0.8 \times 0.153 in² \times 270 ksi \times 3 = 99 kips. This is close enough to the specified stressing force of 101 kips in the design problem.

Figure D.3 shows manufacturer's specifications for the anchorage device [109]. The EC 5-3 anchor is a square anchor with bearing plate widths of 120 mm (4.7 in.). The minimum spacing is 155 mm (6.1 in.). The minimum edge distance is one-half the spiral diameter plus required cover ($5.1/2 + 1.5 = 4.1$ in.). The anchor spacing in the original problem is 150 mm or 5.9 in. which has to be slightly increased to 6.1 in. to satisfy the manufacturers specifications.

Roberts' design equation for the capacity of the local zone (Equation (D.1)), Reference 4) is used to find a spiral equivalent to the spiral specified in the manufacturer's information.

Figure D.3 Manufacturer's Specifications for Special Anchorage Device (from [109])

$$P_n = 0.7f'_{ci} \sqrt{\frac{A}{A_s} A_b + 4 \frac{2A_{sp} f_y}{D_s} \left(1 - \frac{s}{D}\right)^2} A_{core} \quad (D.1)$$

The spiral specified by the manufacturer has a pitch, s , of $150/3 = 50$ mm (1.97 in.), an outside diameter, D , of 130 mm (5.1 in.), and a yield strength of 420 MPa (~ 60 ksi). The cross sectional area of the bar is $10^2\pi/4 = 78.5$ mm² or 0.12 in.². Hence the second term of Equation (D.1) divided by 4 A_{core} is

$$2 \times 0.12 \times 60/(5.1 \times 1.97) \times (1 - 1.97/5.1)^2 = 0.54 \text{ ksi.}$$

Try a #4 spiral, GR60, with a 2½ in. pitch as equivalent spiral:

$$2 \times 0.20 \times 60/(5.1 \times 2.25) \times (1 - 2.25/5.1)^2 = 0.65 \text{ ksi} > 0.54 \text{ ksi.}$$

∴ USE #4 Spiral, $s = 2\frac{1}{4}$ in., $D = 5\frac{1}{8}$ in.

Design the auxiliary reinforcement.

Ordinarily in the acceptance test of special anchorage devices auxiliary reinforcement is provided in addition to the local zone confinement reinforcement. Equivalent reinforcement should also be provided in the actual structure, according to the manufacturers specifications. Since no pertinent information is available in Figure D.3, Equation (D.1) is used for design of the auxiliary reinforcement.

The supporting area, A_s is 6.1^2 in², the gross bearing plate area, A_g is 4.7^2 in². The net bearing plate area is

$$A_b = 4.7^2 - 1.8^2\pi/4 = 19.6 \text{ in.}^2.$$

$$A_{core} = 5.1^2\pi/4 = 20.4 \text{ in.}^2. \quad \text{The area of the concrete core confined by the spiral is}$$

Thus the nominal capacity of the local zone is

$$\begin{aligned} P_n &= 0.7 \times 3.6 \times (6.1/4.7) \times 19.6 + 4 \times 0.65 \times 20.4 \\ &= 64.1 + 53.3 = 117.4 \text{ kips} < 142.6 \text{ kips.} \end{aligned}$$

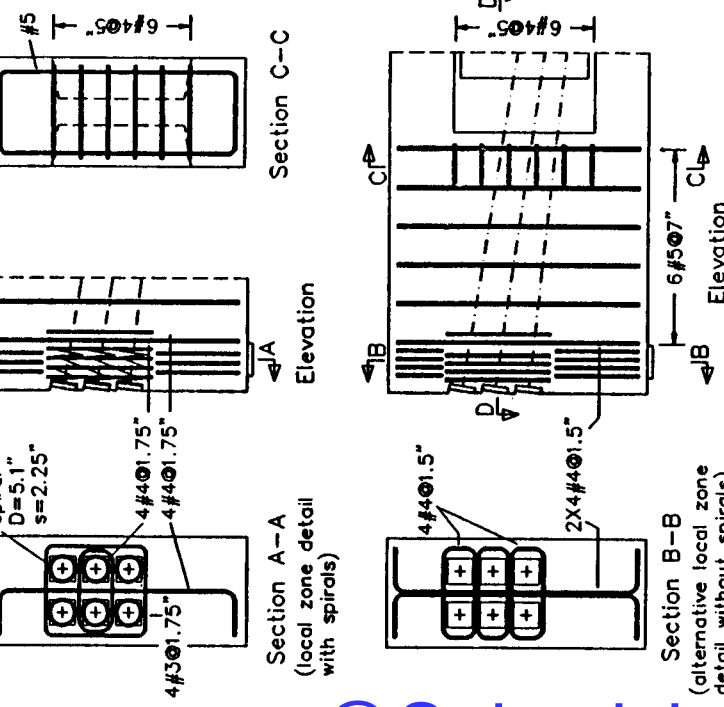
The difference to the required capacity of 142.6 kips has to be made up by the auxiliary tie reinforcement. With tie reinforcement, dimension D is the length of the legs of the ties.

Try #3 ties spaced at 1 in.:

$$\begin{aligned} P_n &= 117.4 + 4 \times (0.11 \times 60)/(6.1 \times 1.75) \times (1 - 1.75/6.1)^2 \times 20.4 \\ &= 117.4 + 25.7 = 143.1 \text{ kips} > 142.6 \text{ kips} \\ ∴ \text{USE } &\#3 \text{ ties @ 1 in.} \end{aligned}$$

Following Roberts' recommendations the tie reinforcement is considered to be only half as effective as spirals, and for A_{core} the area confined by the spiral is used if both spiral and ties are available for confinement of the local zone. This approach is quite conservative resulting in a somewhat crowded detail (Figure D.4). The spacing of the ties could be increased by increasing the concrete strength or by decreasing the pitch of the spiral. Ordinarily manufacturer's information should be available on the auxiliary reinforcement used in the acceptance test. This reinforcement should also be adequate for the actual application, and there would be no need to check Equation (D.1).

4. Investigate an alternative local zone detail.



Another method to reduce crowding of the local zone is to replace the spirals by closely spaced orthogonal ties. Such ties are roughly only half as effective as spirals, but the confined area, A_{core} , becomes larger if no spiral is used for confinement (D^2 versus $D^2\pi/4$).

Try #4 ties spaced at 1½ in.:

$$D = 6.1 - 0.5 = 5.6 \text{ in.}$$

$$P_n = 64.1 + 4 \times (0.20 \times 60) / (5.6 \times 1.5) \times (1 - 1.5/5.6)^2 \times 5.6^2 \\ = 64.1 + 96.1 = 160.2 \text{ kips} > 142.6 \text{ kips}$$

∴ USE #4 ties @ 1½ in. (alternative detail).

Section B-B in Figure D.4 shows this detail. The ties have to be bundled where they run adjacent to each other between the anchor plates. Alternatively, two overlapping #6 ties might be used. However, this is not a good detail, because the required center-to-center spacing of 1½ in. would violate the minimum clear spacing requirement of 1 in. and, more seriously, a solid wall of reinforcement would be created where the ties overlap.

D.3 General Zone Design

The approximate equations in the proposed anchorage zone specifications are limited to rectangular prismatic members and do not apply to the present

Figure D.4 Reinforcement Details for CEB Problem

problem. The following paragraphs lead step by step through the design of the general zone using strut-and-tie model procedures.

1. Determine the extent of the D-region.

There are several discontinuities in the end region of the girder which disturb the stress distribution based on simple beam theory. The concentrated post-tensioning force and the reaction force are loading discontinuities, and the transition from the end block to the regular I-section is a geometric discontinuity.

The region affected by these discontinuities extends approximately one girder height from the end of the reaction force bearing plate ($9 + 47.2 = 56.2$ in.) or one web width ahead of the end of the end block ($47.2 + 9.8 + 4.7 = 61.7$ in.). The second requirement controls and defines the end of the D-region.

2. Determine stress distribution and resultant forces at the end of the D-region.

Simple beam theory is employed to find the stress distribution at the end of the D-region (Figure D.5a). The resultant axial force in the web (346.8 kips) is determined by integrating the flexural stresses over the full girder height and the thickness of the web. The resultant forces in the flanges are determined by integrat-

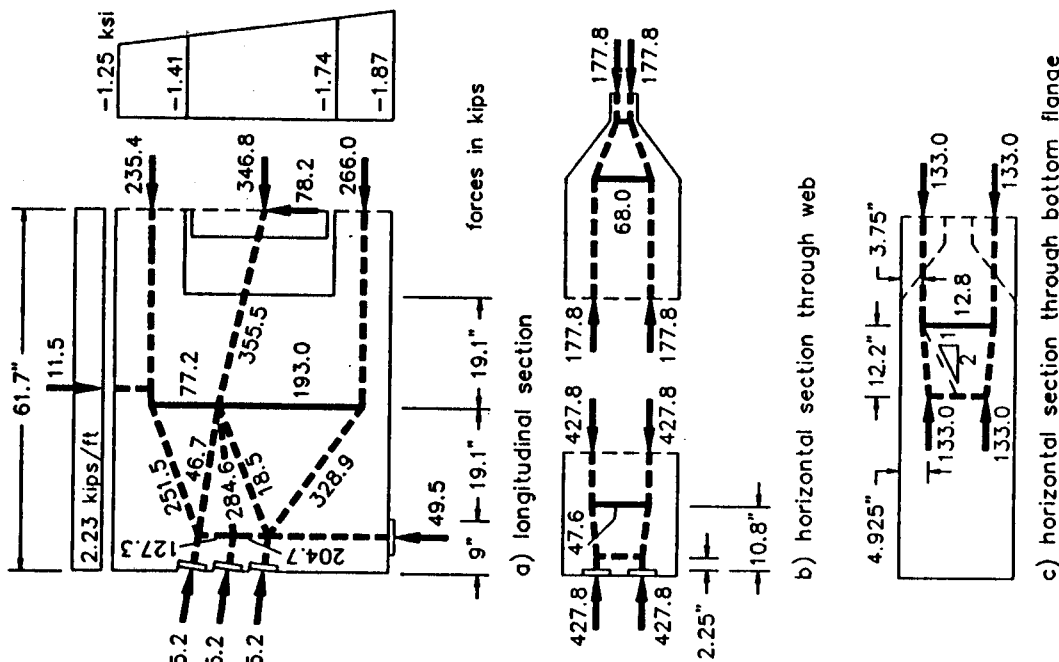


Figure D.5 Strut-and-Tie Model for CEB Problem

ing over the flange areas outside the web. Resultant shear forces could be assigned based on the shear stress distribution, but it is simpler and sufficiently accurate to assign all of the shear force to the web.

3. Select the location of the local zone nodes and of the bursting tie.

For simplicity the local zone nodes are selected 6 in. ahead of the anchor bearing plates, coinciding with the distance of the reaction force from the anchors. @ The closer to the anchors the local zone nodes are located, the smaller is the bursting force. However, the local zone nodes have to be far enough to accommodate the compression forces between the anchors.

For the bursting reinforcement a uniform arrangement of reinforcement between the end of the bearing plate for the reaction force and the beginning of the transition from the end block to the regular section is envisioned. This fixes the location of the bursting tie midway between these points. Thus the distance from the end face of the girder is $9 + 19.1 = 28.1$ in. or 60% of the girder height (Figure D.5a).

D.5a).

Draw the strut-and-tie model and determine the member forces.

With the information found in the previous steps the strut-and-tie model for a longitudinal section through the girder is defined (Figure D.5a). The member

forces can be determined with sufficient accuracy by graphic procedures. Figure D.6

shows a slightly different strut-and-tie model solution where force vector polygons for each node were used to construct the geometry of the strut-and-tie model and to determine the member forces graphically. Note that this is a kinematic model

which is stable only for this particular load configuration.

5. Develop strut-and-tie models in the thin direction of the girder.

Figure D.5b shows that tensile forces in the thin direction of the end block from the regular I-section. Small tensile forces are also found in the flanges of the I-section due to spreading of the compression stresses into the flanges (Figure D.5c). Additional tensile forces in the thin direction of the member are induced by horizontal curvature of the tendons. This curvature is necessary because the tendons have to flare out from the thin web of the I-section to their final position at the loaded face of the end block.

6. Check the compression stresses.

Compression stresses may be critical immediately ahead of the anchor plates (bearing pressure), immediately outside the locally confined region (local zone-

 Seismic Isolation

general zone interface), and at the transition from the end block to the thin web of the I-girder. Following Section 9.21.3.2.2 of the proposed specifications, the effective compression strength for unconfined concrete is taken as

$$f_c = 0.7 f_a = 0.7 \times 3.6 = 2.52 \text{ ksi.}$$

The adequacy of the confinement reinforcement to increase the bearing pressure sufficiently was already checked in Section D.2. The stresses immediately ahead of the transition from end block to I-section are less than 1.87 ksi, which is below the effective concrete strength (Figure D.5a).

The only remaining critical region is the local zone-general zone interface.

Two checks are necessary:

1. The distance of the local zone nodes from the anchor plates, d_o , must be large enough to accommodate the vertical compression force between the anchors (204.7 kips, Figure D.5a)
2. The compression stresses at the end of the confined region must be smaller than the effective concrete strength.

From the first requirement the minimum distance of the local zone nodes from the anchor plates is found to be

$$d_{o,\min} = \frac{1}{2} \times 204.7 \text{ kips} / (2 \times 4.7 \text{ in.} \times 2.52 \text{ ksi}) = 4.32 \text{ in.} < 6 \text{ in.}$$

In the calculation of $d_{o,\min}$ the strut area is taken as $(2 \times a) \times (2 \times d_{o,\min})$, where a is the side length of the anchor plates (4.7 in.). The minimum required distance is less than the actual distance, $d_o = 6$ in., and hence the first requirement is satisfied.

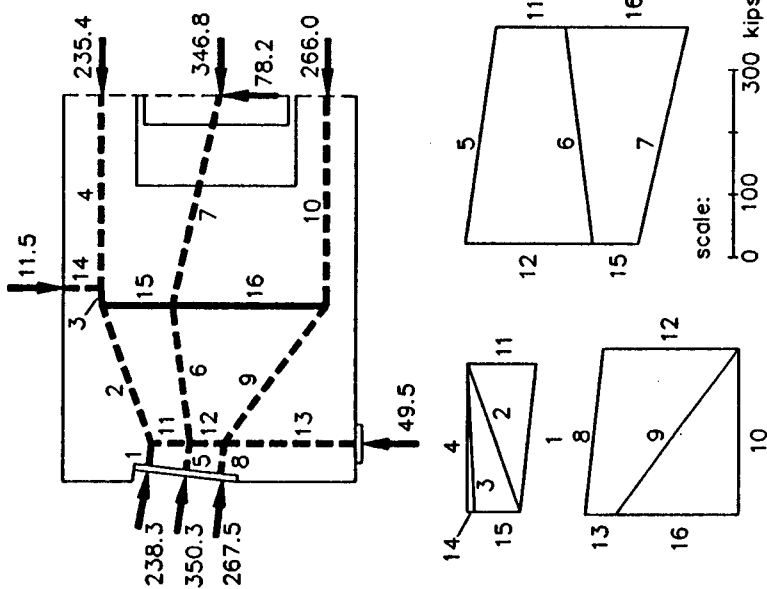


Figure D.6 Graphical Determination of Member Forces

The bursting force could be slightly reduced by moving the local zone nodes somewhat closer to the anchor plates.

For the second check information on the rate of spreading of the compression stresses is needed.

Burdet observed that in two-dimensional problems the linear-elastic peak compression stress at a distance equal to one plate width ahead of the anchor is approximately 60% of the bearing pressure immediately ahead of the anchor plate [47]. Figure D.7 shows that this relation is equivalent to

assuming spreading of the compression stresses at a 1:3 ratio.
The anchorage devices used in this problem have local confinement reinforcement extending for 5.9 in. However, in Section 3.4.5 of Ref. (59), it is recommended to check the concrete compressive stresses at a distance not more than 1.15 plate widths ahead of the anchors, which controls in this case (1.15 x 4.7 = 5.4"). Figure D.8 shows the effective concrete area ahead of the locally confined region, assuming a 1:3 spreading of compression stresses in all directions, as discussed above. This area has to resist the total anchor force, hence

$$f_{ca} = (6 \times 142.6) / (16.2 \times 20.5) = 2.58 \text{ ksi.}$$

The effective concrete strength is

$$f_c = 0.7 f_{ci} = 0.7 \times 3.6 = 2.52 \text{ ksi} - 2.58 \text{ ksi} :: \text{OK (2\% short).}$$

For practical purposes these two checks are sufficient to examine the local zone-general zone capacity. Figure D.9 shows the more rigorous strut-and-tie model procedure to check the compression stresses. All compression struts are drawn with their minimum width so that the effective concrete compressive strength is nowhere exceeded.

The effective concrete strength is $0.7 f_{ci}$, except immediately ahead of the bearing plates, where local zone confinement enhances the effective concrete strength. The full thickness of the end block (19.7 in.) may be used as effective thickness for the struts within the end block. The effective thickness in the I-region should be reduced to $19.7 - 4.7 = 15$ in. for the flange forces and to 4.7 in. for the web force (dashed strut portions in Figure D.9). For simplicity the same effective thickness is used in the entire model, since the stresses in the I-section immediately ahead of the end block do not exceed the effective concrete strength (Figure D.5a).

All nodes in the strut-and-tie model are hydrostatic nodes, except for the three nodes immediately ahead of the anchor plates. At hydrostatic nodes all struts are stressed to the same level and the boundaries of the nodes are perpendicular to the corresponding struts. Reference 110 includes an algorithm for the

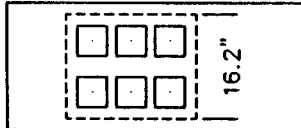
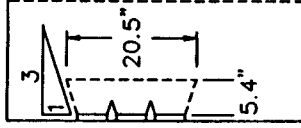
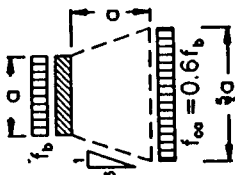


Figure D.7 Spreading of Compression Stresses
Figure D.8 Effective Concrete Area Ahead of Local Confinement Reinforcement



For the second check information on the rate of spreading of the compression stresses is needed.

Burdet observed that in two-dimensional problems the linear-elastic peak compression stress at a distance equal to one plate width ahead of the anchor is approximately 60% of the bearing pressure immediately ahead of the anchor plate [47]. Figure D.7 shows that this relation is equivalent to

assuming spreading of the compression stresses at a 1:3 ratio.
The anchorage devices used in this problem have local confinement reinforcement extending for 5.9 in. However, in Section 3.4.5 of Ref. (59), it is recommended to check the concrete compressive stresses at a distance not more than 1.15 plate widths ahead of the anchors, which controls in this case (1.15 x 4.7 = 5.4"). Figure D.8 shows the effective concrete area ahead of the locally confined region, assuming a 1:3 spreading of compression stresses in all directions, as discussed above. This area has to resist the total anchor force, hence

$$f_{ca} = (6 \times 142.6) / (16.2 \times 20.5) = 2.58 \text{ ksi.}$$

The effective concrete strength is

$$f_c = 0.7 f_{ci} = 0.7 \times 3.6 = 2.52 \text{ ksi} - 2.58 \text{ ksi} :: \text{OK (2\% short).}$$

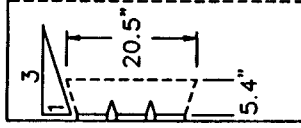


Figure D.7 Spreading of Compression Stresses
Figure D.8 Effective Concrete Area Ahead of Local Confinement Reinforcement

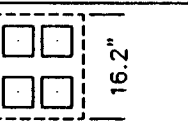


Figure D.7 Spreading of Compression Stresses
Figure D.8 Effective Concrete Area Ahead of Local Confinement Reinforcement

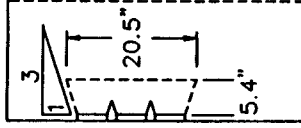


Figure D.7 Spreading of Compression Stresses
Figure D.8 Effective Concrete Area Ahead of Local Confinement Reinforcement

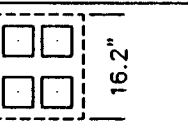
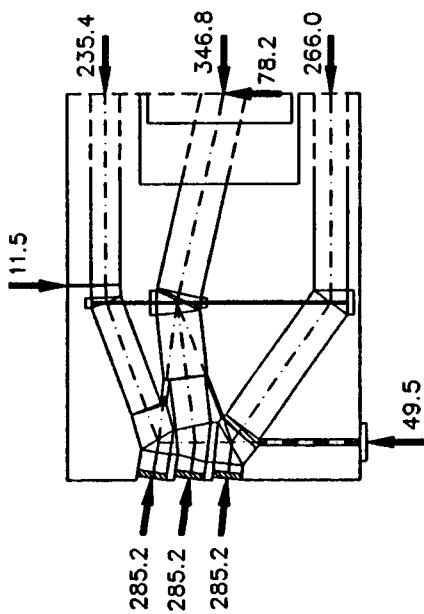
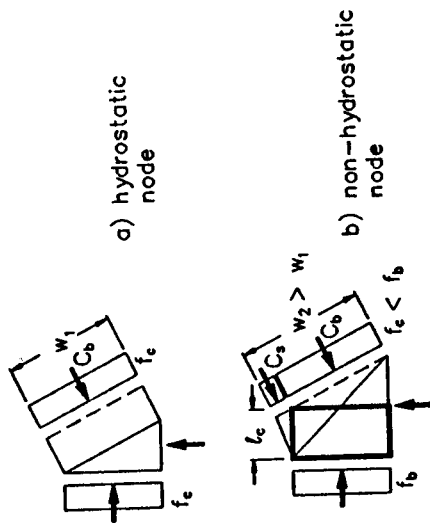


Figure D.7 Spreading of Compression Stresses
Figure D.8 Effective Concrete Area Ahead of Local Confinement Reinforcement



construction of hydrostatic nodes. The local zone node is the region within which the transition from the high bearing pressure to the lower effective concrete strength outside the confined region occurs. Hence hydrostatic nodes are not possible at the local zone, when special anchorage devices are used. This is illustrated in Figure D.10. The non-hydrostatic node in Figure D.10b allows the strut width to increase from width w_1 to width w_2 . Part of the anchor force is transferred in end bearing (force C_b) as for the hydrostatic node. Additional capacity comes from the inclined compression strut C_s along the skin of the confined region ("skin friction"). This concept is useful to estimate the required extent of the local zone confinement reinforcement (dimension ℓ_c in Figure D.10b).

The detail in Figure D.9 shows the local zone nodes for the example problem. The thick lines indicate the minimum extent of the local confinement reinforcement for each anchor. As seen in the figure, the local zone nodes could be moved about 1.3 in. closer to the anchor plates. With this adjustment the required length of confinement is controlled by the center anchor and is

$$l_c = 5.1 + 1.9 - 1.3 = 5.7 \text{ in.} < 5.9 \text{ in.} \therefore \text{OK.}$$

The bursting force is reduced by approximately the same ratio as the distance from the local zone nodes to the bursting tie increases:

$$T_{burst} = 193.0 \times (28.1 - 1.3)/28.1 = 184.7 \text{ kips.}$$

This is a 4% decrease and quite negligible.

Select the reinforcement.

Table D.1 lists the tensile forces in the anchorage zone, the corresponding reinforcement requirements, and the bars selected. Figure D.4 shows all local and general zone details for the design problem.

Number-five ties are selected for the bursting reinforcement for ease of construction. The spacing limitation of 12 in. (Code Section 9.21.3.4.5) would also allow the use of #6 ties. An extra closed tie close to the loaded face of the girder would be desirable but is not possible due to conflicts with the local zone reinforcement. Instead some of the bars provided for confinement of the local zone are extended over the full height of the girder (Figure D.4, Section A-A, Section

Although much attention was paid to proper detailing, it is very difficult to avoid congestion of the local zone for the given problem due to the presence of six

Table D.1 General Zone Reinforcement for Example Design Problem

action	force (kips)	required	reinforcement (in ²)	selected
transverse bursting	193.0	3.22	3.72 (12#5)	
bursting in thin direction	47.6	0.79	1.24 (4#3+4#4)*	
transition to I-section	68.0	1.13	1.20 (6#4)	
flange bursting	12.8	0.21	0.93 (3#5)**	

* partially provided by ties around local zone
** horizontal legs of transverse bursting reinforcement

B-B). The primary purpose of this reinforcement is to tie into the "unstressed corners" of the girder. At the same time it satisfies Section 9.21.3.4.8 in the proposed anchorage zone specifications, which requires spalling reinforcement for

2% of the anchor force:

$$0.02 \times 855.5/60 = 0.29 \text{ in}^2 < 0.40 \text{ in}^2 (2\#4).$$

The ties in the local zone are also effective to resist the bursting forces in the thin direction of the member. However, extra bursting reinforcement is added to achieve better agreement with the location of the tie used in the design model (Figure D.4, section D-D, and Figure D.5b).

Although much attention was paid to proper detailing, it is very difficult to avoid congestion of the local zone for the given problem due to the presence of six

closely spaced anchors. This problem could be eliminated by using larger tendons (for example three 6-½ in. strand tendons) and by distributing the anchors better over the height of the girder.

D.4 Discussion

The design example worked in this section is based on a design problem used in a 1987 CEB survey among European designers (Figure D.1). Designers were asked to calculate among other things the transverse tensile force in the anchorage zone and the required area of transverse reinforcement. Six responses were received. The range of solutions varied almost by a factor of ten, as shown in Table D.2 [25].

Table D.2 Range of Results for CEB Problem

	CEB survey results		example problem
	minimum	maximum	
bursting force (kips)	11	99	137
bursting reinforcement (in ²)	0.32	3.1	3.22

Table D.2 also includes the results found in the previous section. The bursting force of 193 kips (Figure D.5) includes load and ϕ -factors and was readjusted in the table ($193 \times 0.85/1.2 = 137$ kips). Bursting force and required bursting reinforcement are

slightly higher than the high-end responses to the CEB survey. It is noted that Guyon's solution (Figure 59) to a simplified version of this problem as a single concentric load gives a bursting force of

$$T_{\text{burst}} = \frac{1}{4}P(1-a/h) = (6 \times 101)/4 \times (1-16.9/47.2) = 97 \text{ kips.}$$

This is very close to the maximum bursting force found in the CEB survey. In fact, many code provisions for bursting reinforcement requirements are based on Guyon's solution. However, this solution is limited to rectangular, prismatic members, and hence does not apply to the I-girder in the CEB problem. In I-girders, the compression stresses have to spread out further, and consequently the bursting force should be larger. This is reflected by the results obtained in the design example.

APPENDIX E

PROPOSED POST-TENSIONED ANCHORAGE ZONE PROVISIONS for Inclusion in the AASHTO Bridge Specifications

These proposed specification changes (Code and Commentary) are the recommendations of NCHRP Project 10-29 staff at the Ferguson Structural Engineering Laboratory of The University of Texas at Austin. They have not been approved by NCHRP or any AASHTO Committee or formally accepted for the AASHTO Specifications. They are submitted for trial use and comment to engineers engaged in design of post-tensioned anchorage zones.

Please forward any comments to:

John E. Breen
Ferguson Structural Engineering Laboratory
Bldg 24, Balcones Research Center
The University of Texas at Austin
10100 Burnet Road
Austin, Texas 78758

CODE

DIVISION I - DESIGN

9.1.2 Notations [add to current Section 9.1.2]

F_{pu} = guaranteed ultimate strength of the preressing tendon, $A_s^* f_s'$
 P_u = factored tendon force

9.1.3 Definitions [add to current Section 9.1.3]

Anchorage Device - The hardware assembly used for transferring a post-tensioning force from the tendon wires, strands or bars to the concrete.

Anchorage Spacing - Center-to-center spacing of anchorage devices.

Anchorage Zone - The portion of the structure in which the concentrated prestressing force is transferred from the anchorage device onto the concrete (Local Zone), and then distributed more widely into the structure (General Zone)(Section 9.21.1).

Basic Anchorage Device - Anchorage device meeting the restricted bearing stress and minimum plate stiffness requirements of Sections 9.21.7.2.2 through 9.21.7.2.4; no acceptance test is required for Basic Anchorage Devices.

Diaphragm - Transverse stiffener in girders to maintain section geometry.

Edge Distance - Distance from the center of the anchorage device to the edge of the concrete member.

End Anchorage - Length of reinforcement, or mechanical anchor, or hook, or combination thereof, beyond point of zero stress in reinforcement. [Delete remainder of current definition]

General Zone - Region within which the concentrated prestressing force spreads out to a more linear stress distribution over the cross section of the member (Saint Venant Region)(Section 9.21.2.1).

Intermediate Anchorage - Anchorage not located at the end surface of a member or segment; usually in the form of embedded anchors, blisters, ribs, or recess pockets.

Local Zone - The volume of concrete surrounding and immediately ahead of the anchorage device, subjected to high local bearing stresses (Section 9.21.2.2).

Special Anchorage Device - Anchorage device whose adequacy must be proven experimentally in the standardized acceptance tests of Division II, Section 10.3.2.3.

9.14 LOAD FACTORS [add underlined to current Section 9.14]
The computed strength capacity shall not be less than the largest value from load factor design in Section 3.22. For the design of anchorage zones a load factor of 1.2 shall be applied to the maximum tendon jacking force.

9.21.1.3 For intermediate anchorages in addition to the length of Section 9.21.1.2 the anchorage zone shall be considered to also

For factory produced precast prestressed concrete members $\phi = 1.0$

For post-tensioned cast-in-place concrete members $\phi = 0.95$

For shear $\phi = 0.90$
For anchorage zones $\phi = 0.85$ for normal weight concrete and $\phi = 0.70$ for lightweight concrete.

9.21 POST-TENSIONED ANCHORAGE ZONES

9.21.1 Geometry of the Anchorage Zone

9.21.1.1 The anchorage zone is geometrically defined as the volume of concrete through which the concentrated prestressing force at the anchorage device spreads transversely to a linear stress distribution across the entire cross section.

9.21.1.2 For anchorage zones at the end of a member or segment, the transverse dimensions may be taken as the depth and width of the section. The longitudinal extent of the anchorage zone in the direction of the tendon (ahead of the anchorage) shall be taken as not less than the larger transverse dimension but not more than one and one-half times that dimension.

9.21.1.2 Design of general zones shall meet the requirements of Sections 9.14 and 9.21.3.

9.21.2 Local Zone
9.21.2.1 General Zone
9.21.2.1.1 The geometric extent of the general zone is identical to that of the overall anchorage zone as defined in Section 9.21.1 and includes the local zone.

9.21.2.2 Local Zone
9.21.2.2.1 The local zone is defined as the rectangular prism (or equivalent rectangular prism for circular or oval anchorages) of concrete surrounding and immediately ahead of the anchorage device and any integral confining reinforcement. The dimensions of the local zone are defined in Section 9.21.7.

9.21.2.2.2 Design of local zones shall meet the requirements of Sections 9.14 and 9.21.7 or shall be based on the results of experimental tests required in Section 9.21.7.3 and described in Section 10.3.2.3 of Division II. Anchorage devices based on the acceptance test of Division II, Section 10.3.2.3, are referred to as *special anchorage devices*.

9.21.2.3 Responsibilities

9.21.2.3.1 The engineer of record is responsible for the overall design and approval of working drawings for the general zone, including the specific location of the tendons and anchorage devices, general zone reinforcement, and the specific stressing sequence. The engineer of record is also responsible for the design of local zones based on Section 9.21.7.2 and for the approval of special anchorage devices used under the provisions of Section 9.21.7.3. All working drawings for the local zone must be approved by the engineer of record.

9.21.2.3.2 Anchorage device suppliers are responsible for furnishing anchorage devices which satisfy the anchor efficiency requirements of Division II, Section 10.3.2. In addition, if special anchorage devices are used, the anchor-device supplier is responsible for furnishing anchorage devices that satisfy the acceptance test requirements of Section 9.21.7.3 and of Division II, Section 10.3.2.3. This acceptance test and the anchor efficiency test shall be conducted by an independent testing agency acceptable to the engineer of record. The anchorage device supplier shall provide records of the acceptance test in conformance with Division II, Section 10.3.2.3.12 to the engineer of

record and to the constructor and shall specify auxiliary and confining reinforcement, minimum edge distance, minimum anchor spacing, and minimum concrete strength at time of stressing required for proper performance of the local zone.

9.21.2.3.3 The responsibilities of the contractor are specified in Division II, Section 10.4.

9.21.3 Design of the General Zone

9.21.3.1 Design Methods

The following methods may be used for the design of general zones:

- (1) Equilibrium based plasticity models (strut-and-tie models) (see Section 9.21.4)
- (2) Elastic stress analysis (finite element analysis or equivalent) (see Section 9.21.5)
- (3) Approximate methods for determining the compression and tension forces, where applicable (see Section 9.21.6).

Regardless of the design method used, all designs shall conform to the requirements of Section 9.21.3.4.

The effects of stressing sequence and three-dimensional effects shall be considered in the design. When these three dimensional effects appear significant, they may be analyzed using three-dimensional analysis procedures or may be approximated by considering two or more

planes. However, in these approximations the interaction of the planes' models must be considered, and the model loadings and results must be consistent.

9.21.3.2 Nominal Material Strengths

9.21.3.2.1 The nominal tensile strength of bonded reinforcement is limited to f_{sy} for non-prestressed reinforcement and to f_y^* for prestressed reinforcement. The nominal tensile strength of unbonded prestressed reinforcement is limited to $f_{se} + 15,000$ psi.

9.21.3.2.2 The effective nominal compressive strength of the concrete of the general zone, exclusive of confined concrete, is limited to $0.7f_c$. The tensile strength of the concrete shall be neglected.

9.21.3.2.3 The compressive strength of concrete at transfer of prestressing shall be specified on the construction drawings. If not otherwise specified, stress shall not be transferred to concrete until the compressive strength of the concrete as indicated by test cylinders, cured by methods identical with the curing of the member, is at least 4,000 psi.

These compressive stresses may be determined according to the strut-and-tie model procedures of Section 9.21.4, from an elastic stress analysis according to Section 9.21.5.2, or by the approximate method outlined in Section 9.21.6.2. These compressive stresses shall not exceed $0.7 \phi f_{ci}'$.

9.21.3.4 General Design Principles and Detailing Requirements

Good detailing and quality workmanship are essential for the satisfactory performance of anchorage zones. Sizes and details for anchorage zones should respect the need for tolerances on the bending, fabrication and placement of reinforcement, the size of aggregate and the need for placement and sound consolidation of the concrete.

9.21.3.4.1 Compressive stresses in the concrete ahead of basic anchorage devices shall meet the requirements of Section 9.21.7.2.

9.21.3.4.2 Compressive stresses in the concrete ahead of special anchorage devices shall be checked at a distance measured from the concrete bearing surface equal to the smaller of:

- (1) The depth to the end of the local confinement reinforcement.
- (2) The smaller lateral dimension of the anchorage device.

These compressive stresses may be determined according to the strut-and-tie model procedures of Section 9.21.4, from an elastic stress analysis according to Section 9.21.5.2, or by the approximate method outlined in Section 9.21.6.2. These compressive stresses shall not exceed $0.7 \phi f_{ci}'$.

9.21.3.4.3 Compressive stresses shall also be checked where geometry or loading discontinuities within or ahead of the anchorage zone may cause stress concentrations.

- 9.21.3.4** The bursting force is the tensile force in the anchorage zone acting ahead of the anchorage device and transverse to the tendon axis. The magnitude of the bursting force, T_{burst} , and its corresponding distance from the loaded surface, d_{burst} , can be determined using the strut-and-tie model procedures of Section 9.21.4, from an elastic stress analysis according to Section 9.21.5.3, or by the approximate method outlined in Section 9.21.6.3. Three-dimensional effects shall be considered for the determination of the bursting reinforcement requirements.
- 9.21.3.4.5** Resistance to bursting forces, $\phi A_s f_{sy}$ and/or $\phi A_g f_g$, shall be provided by non-prestressed or prestressed reinforcement, in the form of spirals, closed hoops, or well anchored transverse ties. This reinforcement is to be proportioned to resist the total factored bursting force. Arrangement and anchorage of bursting reinforcement shall satisfy the following:
- (1) Spacing of bursting reinforcement shall exceed neither 24 bar diameters nor 12 inches.
- (2) Spalling reinforcement between multiple anchorage devices shall effectively tie these anchorage devices together.
- 9.21.3.4.6** Edge tension forces are tensile forces in the anchorage zone acting parallel and close to the transverse edge and longitudinal edges of the member. The transverse edge is the surface loaded by the anchors. The tensile force along the transverse edge is referred to as *spalling force*. The tensile force along the longitudinal edge is referred to as *longitudinal edge tension force*.
- 9.21.3.4.7** Spalling forces are induced in concentrically loaded anchorage zones, eccentrically loaded anchorage zones, and anchorage zones for multiple anchors. Longitudinal edge tension forces are induced when the resultant of the anchorage forces considered causes eccentric loading of the anchorage zone. The edge tension forces can be determined from an elastic stress analysis, strut-and-tie models, or in accordance with the approximate methods of Section 9.21.6.4.
- 9.21.3.4.8** In no case shall the spalling force be taken as less than two percent of the total factored tendon force.
- 9.21.3.4.9** Resistance to edge tension forces, $\phi A_s f_{sy}$ and/or $\phi A_g f_g$, shall be provided in the form of non-prestressed or prestressed reinforcement located close to the longitudinal and transverse edge of the concrete. Arrangement and anchorage of the edge tension reinforcement shall satisfy the following:

(1) Bursting reinforcement shall extend over the full width of the member and must be anchored as close to the outer faces of the member as cover permits.

(2) Bursting reinforcement shall be distributed ahead of the loaded surface along both sides of the tendon throughout a distance of 2.5 d_{burst} for the plane considered, but not to exceed 1.5 times the corresponding lateral dimension of the section. The centroid of the bursting reinforcement shall coincide with the distance d_{burst} used for the design.

duced using Equation (9-32), if permanent compressive stresses are generated behind the anchor from other loads.

$$T_{ia} = 0.25P_s - f_{cb}A_{cb} \quad (9-32)$$

(1) Minimum spalling reinforcement satisfying Section 9.21.3.4.8 shall extend over the full width of the member.

(2) Spalling reinforcement between multiple anchorage devices shall effectively tie these anchorage devices together.

(3) Longitudinal edge tension reinforcement and spalling reinforcement for eccentric anchorage devices shall be continuous. The reinforcement shall extend along the tension face over the full length of the anchorage zone and shall extend along the loaded face from the longitudinal edge to the other side of the eccentric anchorage device or group of anchorage devices.

A_{cb} is the area of the continuing cross section within the extensions of the sides of the anchor plate or blister.

The area of the blister or rib shall not be taken as part of the cross section.

9.21.3.5 Intermediate Anchorage

9.21.3.5.1 Intermediate anchorages shall not be used in regions where significant tension is generated behind the anchor from other loads. Whenever practical, blisters shall be located in the corner between flange and webs, or shall be extended over the full flange width or web height to form a continuous rib. If isolated blisters must be used on a flange or web, local shear, bending and direct force effects shall be considered in the design.

9.21.3.5.2 Bonded reinforcement shall be provided to tie back at least 25 percent of the intermediate anchorage unfactored stressing force into the concrete section behind the anchor. Stresses in this bonded reinforcement are limited to a maximum of $0.6f_{sy}$ or 36 ksi. The amount of tie back reinforcement may be reduced using Equation (9-32), if permanent compressive stresses are generated behind the anchor from other loads.

9.21.3.5.3 Tie back reinforcement satisfying Section 9.21.3.5.2 shall be placed no further than one plate width from the tendon axis. It shall be fully anchored so that the yield strength can be developed at a distance of one plate width or half the length of the blister or rib ahead of the anchor as well as at the same distance behind the anchor. The centroid of this reinforcement shall coincide with the tendon axis, where possible. For blisters and ribs, the reinforcement shall be placed in the continuing section near that face of the flange or web from which the blister or rib is projecting.

9.21.3.5.4 Reinforcement shall be provided

throughout blisters or ribs as required for shear friction, corbel action, bursting forces, and

deviation forces due to tendon curvature. This reinforcement shall be in the form of ties or U-stirrups which encase the anchorage and tie it effectively into the adjacent web and flange. This reinforcement shall extend as far as possible into the flange or web and be developed by standard hooks bent around transverse bars or equivalent. Spacing shall not exceed the smallest of blister or rib height at anchor, blister width, or 6 inches.

9.21.3.5.5 Reinforcement shall be provided to resist local bending in blisters and ribs due to eccentricity of the tendon force and to resist lateral bending in ribs due to tendon deviation forces.

9.21.3.5.6 Reinforcement required by Sections 9.21.3.4.4 through 9.21.3.4.9 shall be provided to resist tensile forces due to transfer of the anchorage force from the blister or rib into the overall structure.

9.21.3.6 Diaphragms

9.21.3.6.1 For tendons anchored in diaphragms, concrete compressive stresses shall be limited within the diaphragm in accordance with Sections 9.21.3.4.1 through 9.21.3.4.3. Compressive stresses shall also be checked at the transition from the diaphragm to webs and flanges of the member.

9.21.3.6.2 Reinforcement shall be provided to ensure full transfer of diaphragm anchor loads into the flanges and webs of the girder. The more general methods of Section 9.21.4 or 9.21.5 shall be used to determine this reinforcement. Reinforcement shall also be provided to

tie back deviation forces due to tendon curvature.

9.21.3.7 Multiple Slab Anchorage

9.21.3.7.1 Minimum reinforcement meeting the requirements of Sections 9.21.3.7.2 through 9.21.3.7.4 shall be provided unless a more detailed analysis is made.

9.21.3.7.2 Reinforcement shall be provided for the bursting force in the direction of the thickness of the slab and normal to the tendon axis in accordance with Sections 9.21.3.4.4 and 9.21.3.4.5. This reinforcement shall be anchored close to the faces of the slab with standard hooks bent around horizontal bars, or equivalent. Minimum reinforcement is two #3 bars per anchor located at a distance equal to one-half the slab thickness ahead of the anchor.

9.21.3.7.3 Reinforcement in the plane of the slab and normal to the tendon axis shall be provided to resist edge tension forces, T_1 , between anchorages (Equation (9-33)) and bursting forces, T_2 , ahead of the anchorages (Equation (9-34)). Edge tension reinforcement shall be placed immediately ahead of the anchors and shall effectively tie adjacent anchors together. Bursting reinforcement shall be distributed over the length of the anchorage zones (see Section 9.21.1.4).

9.21.4 Reinforcement shall be provided to ensure full transfer of diaphragm anchor loads into the flanges and webs of the girder. The more general methods of Section 9.21.4 or 9.21.5 shall be used to determine this reinforcement. Reinforcement shall also be provided to

straight tension members (ties) that are connected at discrete points (nodes). Compression forces are carried by concrete compression struts and tension forces are carried by non-prestressed or prestressed reinforcement.

9.21.4.1.2 The selected strut-and-tie model shall follow a load path from the anchorages to the end of the anchorage zone. Other forces acting on the anchorage zone, such as reaction forces, tendon deviation forces, and applied loads, shall be considered in the selection of the strut-and-tie model. The forces at the end of the anchorage zone can be obtained from an axial-flexural beam analysis.

9.21.4.2 Nodes

Local zones which meet the provisions of Section 9.21.7 or Division II, Section 10.3.2.3 are considered as properly detailed, adequate nodes. The other nodes in the anchorage zone are adequate if the effective concrete stresses in the struts meet the requirements of Section 9.21.4.3 and the tension ties are properly detailed to develop the full yield strength of the reinforcement.

9.21.4.3 Struts

9.21.4.3.1 The effective concrete compressive strength for the general zone shall usually be limited to $0.7\phi f_{ci}'$. In areas where the concrete may be extensively cracked at ultimate due to other load effects, or if large plastic rotations are required, the effective compressive strength shall be limited to $0.6\phi f_{ci}'$.

9.21.4 Application of Strut-and-Tie Models to the Design of Anchorage Zones

9.21.4.1 General

9.21.4.1.1 The flow of forces in the anchorage zone may be approximated by a series of straight compression members (struts) and



9.21.4.3.2 In anchorage zones the critical section for compression struts is ordinarily located at the interface with the local zone node. If special anchorage devices are used, the critical section of the strut can be taken as that section whose extension intersects the axis of the tendon at a depth equal to the smaller of the depth of the local confinement reinforcement or the lateral dimension of the anchorage device.

9.21.4.3.3 For thin members with a ratio of member thickness to anchorage width of no more than three, the dimension of the strut in the direction of the thickness of the member can be approximated by assuming that the thickness of the compression strut varies linearly from the transverse lateral dimension of the anchor at the surface of the concrete to the total thickness of the section at a depth equal to the thickness of the section.

9.21.4.3.4 The compression stresses can be assumed as acting parallel to the axis of the strut and as uniformly distributed over its cross section.

9.21.4.4 Ties
9.21.4.4.1 Tension forces in the strut-and-tie model shall be assumed to be carried completely by non-prestressed or prestressed reinforcement. Tensile strength of the concrete shall be neglected.

9.21.4.4.2 Tension ties shall be properly detailed and shall extend beyond the nodes to develop the full tension tie force at the node. The reinforcement layout must closely follow

the directions of the ties in the strut-and-tie model.

9.21.5 Elastic Stress Analysis

9.21.5.1 Analyses based on assumed elastic material properties, equilibrium, and compatibility of strains are acceptable for analysis and design of anchorage zones.

9.21.5.2 If the compressive stresses in the concrete ahead of the anchorage device are determined from a linear-elastic stress analysis, local stress maxima may be averaged over an area equal to the bearing area of the anchorage device.

9.21.5.3 Location and magnitude of the bursting force may be obtained by integration of the corresponding tensile bursting stresses along the tendon path.

9.21.6 Approximate Methods

9.21.6.1 Limitations

In the absence of a more accurate analysis, concrete compressive stresses ahead of the anchorage device, location and magnitude of the bursting force, and edge tension forces may be estimated by Equations (9-35) through (9-38), provided that:

9.21.6.2 Compressive Stresses

$$\text{f}_{ca} = \kappa \frac{0.6P_u}{A_b} \frac{1}{1 + \ell_c \left(\frac{1}{b_{eff}} - \frac{1}{t} \right)} \quad (9-35)$$

$$\kappa = 1 + \left(2 - \frac{s}{a_{eff}} \right) \left(0.3 + \frac{n}{15} \right) \quad \text{for } s < 2a_{eff}$$

$$\kappa = 1 \quad \text{for } s \geq 2a_{eff}$$

$$P_u = \text{factored tendon load};$$

$$t = \text{thickness of the section};$$

$$s = \text{center-to-center spacing of multiple anchorages};$$

$$n = \text{number of anchorages in a row}.$$

(2) The member has no discontinuities within or ahead of the anchorage zone.

(3) The minimum edge distance of the anchorage in the main plane of the member is at least one and one-half times the corresponding lateral dimension, a , of the anchorage device.

(4) Only one anchorage device or one group of closely spaced anchorage devices is located in the anchorage zone. Anchorage devices can be treated as closely spaced if their center-to-center spacing does not exceed one and one-half times the width of the anchorage devices in the direction considered.

(5) The angle of inclination of the tendon with respect to the center line of the member is not larger than 20 degrees if the anchor force points toward the centroid of the section and for concentric anchors, and is not larger than 5 degrees if the anchor force points away from the centroid of the section.

9.21.6.2 Compressive Stresses

9.21.6.2.1 No additional check of concrete compressive stresses is necessary for basic anchorage devices satisfying Section 9.21.7.2.

9.21.6.2.2 The concrete compressive stresses ahead of special anchorage devices at the interface between local zone and general zone shall be approximated by Equations (9-35) and (9-36).

If a group of anchorages is closely spaced in two directions, the product of the correction factors, κ , for each direction is used in Equation (9-36).

9.21.6.2.3 Effective bearing area, A_b , in Equation (9-35) shall be taken as the larger of the anchor bearing plate area, A_{plate} , or the bearing area of the confined concrete in the local zone, A_{conf} , with the following limitations:

- (1) If A_{plate} controls, A_{plate} shall not be taken larger than $4/\pi A_{conf}$.
- (2) If A_{conf} controls, the maximum dimension of A_{conf} shall not be more than twice the maximum dimension of A_{plate} or three times the minimum dimension of A_{plate} . If any of these limits is violated the effective bearing area, A_b , shall be based on A_{plate} .

Deductions shall be made for the area of the duct in the determination of A_b .

9.21.6.3 Bursting Forces

Values for the magnitude of the bursting force, T_{burst} , and for its distance from the loaded surface, d_{burst} , shall be estimated by application of Equations (9-37) and (9-38) the specified stressing sequence shall be considered if more than one tendon is present.

$$T_{burst} = 0.25 \sum P_u \left(1 - \frac{a}{h} \right) + 0.5P_u \sin\alpha \quad (9-37)$$

$$d_{burst} = 0.5 (h - 2e) + 5e \sin\alpha \quad (9-38)$$

where ΣP_u is the sum of the total factored tendon loads for the stressing arrangement considered;

a is the lateral dimension of the anchorage device or group of devices in the direction considered;

e is the eccentricity (always taken as positive) of the anchorage device or group of devices with respect to the centroid of the cross section;

h is the lateral dimension of the cross section in the direction considered;

α is the angle of inclination of the resultant of the tendon forces with respect to the centerline of the member.

Edge Tension Forces

For multiple anchorages with a center-to-center spacing of less than 0.4 times the depth of the section, the spalling forces shall be given by Section 9.21.3.4.8. For larger spacings, the spalling forces shall be determined from a more detailed analysis, such as strut-and-tie models or other analytical procedures.

9.21.6.4.2 If the centroid of all tendons considered is located outside of the kern of the section both spalling forces and longitudinal edge tension forces are induced. The longitudinal

The manufacturer's recommendations for spacing and edge distance of anchorages shall be considered minimum values.

9.21.7.1.3 The length of the local zone along the tendon axis shall be taken as the greater of:

(1) The maximum width of the local zone.

(2) The length of the anchorage device confining reinforcement.

(3) For anchorage devices with multiple bearing surfaces, the distance from the loaded concrete surface to the bottom of each bearing surface plus the maximum dimension of that bearing surface.

In no case shall the length of the local zone be taken as greater than one and one-half times the width of the local zone.

9.21.7.1.4 For closely spaced anchorages an enlarged local zone enclosing all individual anchorages shall also be considered.

9.21.7.2 Bearing Strength

9.21.7.2.1 Anchorage devices may be either basic anchorage devices meeting the bearing compressive strength limits of Sections 9.21.7.2.2 through 9.21.7.2.4 or special anchorage devices meeting the requirements of Section 9.21.7.3.

- (1) Twice the edge distance specified by the anchorage device supplier.
- (2) The center-to-center spacing specified by the anchorage device supplier.

DIVISION II - CONSTRUCTION

9.21.7.2.2 The effective concrete bearing compressive strength f_b used for design shall not exceed that of Equations (9-39) or (9-40).

$$f_b \leq 0.7\phi f_{ci} \sqrt{A/A_g} \quad (9-39)$$

$$\text{but } f_b \leq 2.25 \phi f'_{ci} \quad (9-40)$$

where

f_b is the maximum factored tendon load, P_u , divided by the effective bearing area A_b ;
 A_b is the concrete compressive strength at stressing;

A is the maximum area of the portion of the supporting surface that is geometrically similar to the loaded area and concentric with it;

A_g is the gross area of the bearing plate if the requirements of Section 9.21.7.2.3 are met, or is the area calculated in accordance with Section 9.21.7.2.4;
 A_g is the effective net area of the bearing plate calculated as the area A_g minus the area of openings in the bearing plate.

Equations (9-39) and (9-40) are only valid if a general zone reinforcement satisfying Section 9.21.3.4 is provided and if the extent of the concrete along the tendon axis ahead of the anchorage device is at least twice the length of the local zone as defined in Section 9.21.7.1.3.

9.21.7.2.3 The full bearing plate area may be used for A_g and the calculation of A_b if the anchorage device is sufficiently rigid. To be considered sufficiently rigid, the slenderness of the bearing plate (n/t) must not exceed the value

given in Equation (9-41). The plate must also be checked to ensure that the plate material does not yield.

$$n/t \leq 0.08 \sqrt{\frac{3}{E_b f_b}} \quad (9-41)$$

where

n is the largest distance from the outer edge of the wedge plate to the outer edge of the bearing plate. For rectangular bearing plates this distance is measured parallel to the edges of the bearing plate. If the anchorage has no separate wedge plate, the size of the wedge plate shall be taken as the distance between the extreme wedge holes in the corresponding direction.

t is the average thickness of the bearing plate.

E_b is the modulus of elasticity of the bearing plate material.

9.21.7.2.4 For bearing plates that do not meet the stiffness requirements of Section 9.21.7.2.3, the effective gross bearing area, A_g , shall be taken as the area geometrically similar to the wedge plate (or to the outer perimeter of the wedge hole pattern for plates without separate wedge plate) with dimensions increased by assuming load spreading at a 45 degree angle. A larger effective bearing area may be calculated by assuming an effective area and checking the new f_b and n/t values for conformance with Sections 9.21.7.2.2 and 9.21.7.2.3.

other devices that do meet the requirements of Section 9.21.7.2 but which the engineer-of-record requires to have tested may be used provided that they have been tested by an independent testing agency acceptable to the engineer of record according to the procedures described in Division II, Section 10.3.2 (or equivalent) and meet the acceptance criteria specified in Division II, Section 10.3.2.3.10. For a series of similar special anchorages devices, tests are only required for representative samples unless tests for each capacity of the anchorages in the series are required by the engineer of record.

9.22 PRETENSIONED ANCHORAGE ZONES

9.22.1 Vertical stirrups resisting at least two percent of the total factored prestressing force, P_u , shall be placed within the distance $d/4$ of the end of the beam, the end stirrups to be as close to the end of the beam as practicable.

9.22.2 For at least the distance d from the end of the beam, nominal reinforcement shall be placed to enclose the prestressing steel in the bottom flange.

9.22.3 For box girders, transverse reinforcement shall be provided and anchored by extending the leg into the web of the girder.

9.22.4 Unless otherwise specified, stress shall not be transferred to concrete until the compressive strength of the concrete as indicated by test cylinders, cured by methods identical with the curing of the member, is at least 4,000 psi.

10.3 MATERIALS

10.3.1 **Prestressing Steel** [Split current Section 10.3.1 into two sections to reduce number of sub levels]

10.3.2 Post-Tensioning Anchages and Couplers [same as first paragraph in current Section 10.3.1.4 except for underlined]

All anchorages and couplers shall develop at least 95 percent of the actual ultimate strength of the prestressing steel, . . .

10.3.2.1 **Bonded Systems** [same as current Section 10.3.1.4.1]

10.3.2.2 **Unbonded Systems** [same as current Section 10.3.1.4.2]

10.3.2.3 **Special Anchorage Device Acceptance Test** [replaces current Sections 10.3.1.4.3, 10.3.1.4.4, and 10.3.1.4.5]

10.3.2.3.1 The test block shall be a rectangular prism. It shall contain those anchorage components which will also be embedded in the structure's concrete. Their arrangement has to comply with the practical application and the suppliers specifications. The test block shall contain an empty duct of size appropriate for the maximum tendon size which can be accommodated by the anchorage device.

10.3.2.3.2

The dimensions of the test block perpendicular to the tendon in each direction shall be the smaller of the minimum edge

9.21.7.3 Special Anchorage Devices

Special anchorage devices that do not meet the requirements of Section 9.21.7.2 as well as

distance or the minimum spacing specified by the anchorage device supplier, with the stipulation that the cover over any confining reinforcing steel or supplementary skin reinforcement be appropriate for the particular application and environment. The length of the block along the axis of the tendon shall be at least two times the larger of the cross-sectional dimensions.

10.3.2.3.3 The confining reinforcing steel in the local zone shall be the same as that specified by the anchorage device supplier for the particular system.

10.3.2.3.4 In addition to the anchorage device and its specified confining reinforcement steel, supplementary skin reinforcement may be provided throughout the specimen. This supplementary skin reinforcement shall be specified by the anchorage device supplier but shall not exceed a volumetric ratio of 0.01.

10.3.2.3.5 The concrete strength at the time of testing shall be not more than the minimum specified concrete strength at time of tensioning, f_c , or $0.85 f_c$.

10.3.2.3.6 Either of three test procedures is acceptable: cyclic loading described in Section 10.3.2.3.7, sustained loading described in Section 10.3.2.3.8, or monotonic loading described in Section 10.3.2.3.9. The loads specified for the tests are given in fractions of the ultimate load F_{pu} of the largest tendon that the anchorage device is designed to accommodate. The specimen shall be loaded in accordance with normal usage of the device in post-tensioning applications except that load can be applied directly to the wedge plate or equivalent area.

10.3.2.3.7 Cyclic Loading Test

10.3.2.3.9 Monotonic Loading Test

10.3.2.3.7.1 In a cyclic loading test, the load shall be increased to $0.8F_{pu}$. The load shall then be cycled between $0.1F_{pu}$ and $0.8F_{pu}$ until crack widths stabilize, but for not less than 10 cycles. Crack widths are considered stabilized if they do not change by more than 0.001 in. over the last three readings. Upon completion of the cyclic loading the specimen shall be preferably loaded to failure or, if limited by the capacity of the loading equipment, to at least $1.1F_{pu}$.

10.3.2.3.7.2 Crack widths and crack patterns shall be recorded at the initial load of $0.8F_{pu}$, at least at the last three consecutive peak loadings before termination of the cyclic loading, and at $0.9F_{pu}$. The maximum load shall also be reported.

10.3.2.3.8 Sustained Loading Test

10.3.2.3.8.1 In a sustained loading test, the load shall be increased to $0.8F_{pu}$ and held constant until crack widths stabilize but for not less than 48 hours. Crack widths are considered stabilized if they do not change by more than 0.001 in. over the last three readings. After sustained loading is completed, the specimen shall be preferably loaded to failure or, if limited by the capacity of the loading equipment, to at least $1.1F_{pu}$.

10.3.2.3.8.2 Crack widths and crack patterns shall be recorded at the initial load of $0.8F_{pu}$, at least three times at intervals of not less than four hours during the last twelve hours before termination of the sustained loading, and during loading to failure at $0.9F_{pu}$. The maximum load shall also be reported.

one of the three specimens fails to pass the test, a supplementary test of three additional specimens is allowed. The three additional test specimen results must meet all acceptance criteria of Section 10.3.2.3.10.

For a series of similar special anchorage devices, tests are only required for representative samples unless tests for each capacity of the anchorages in the series are required by the engineer-of-record.

10.3.2.3.12 Records of the anchorage device acceptance test shall include:

- | | |
|--|---|
| 10.3.2.3.9.1 In a monotonic loading test, the load shall be increased to $0.9F_{pu}$ and held constant for 1 hour. The specimen shall then be preferably loaded to failure or, if limited by the capacity of the loading equipment, to at least $1.2F_{pu}$. | (1) Dimensions of the test specimen. |
| 10.3.2.3.9.2 Crack widths and crack patterns shall be recorded at $0.9F_{pu}$ after the one hour period, and at $1.0F_{pu}$. The maximum load shall also be reported. | (2) Drawings and dimensions of the anchorage device, including all confining reinforcing steel. |
| 10.3.2.3.10 The strength of the anchorage zone must exceed: | (3) Amount and arrangement of supplementary skin reinforcement. |
| Specimens tested under cyclic or sustained loading | (4) Type and yield strength of reinforcing steel. |
| Specimens tested under monotonic loading | (5) Type and compressive strength at time of testing of concrete. |
| The maximum crack width criteria specified below must be met for moderately aggressive environments. For higher aggressivity environments the crack width criteria shall be reduced by at least 50 percent. | (6) Type of testing procedure and all measurements required in Sections 10.3.2.3.7 through 10.3.2.3.10 for each specimen. |

10.4.1 Placement of Ducts [same as current Section 10.4.1]

A test series shall consist

of three test specimens. Each one of the tested

specimens must meet the acceptance criteria. If

10.4.2 Placement of Prestressing Steel [same as current Section 10.4.2]

10.4.3 Placement of Anchorage Hardware [add to current Section 10.4]

The contractor is responsible for the proper placement of all materials according to the design documents of the engineer of record and the requirements stipulated by the anchorage device supplier. The Contractor shall exercise all due care and attention in the placement of anchorage hardware, reinforcement, concrete and consolidation of concrete in anchorage zones. Modifications to the local zone details verified under provisions of Section 9.21.7.3 in Division I and Section 10.3.2.3 in Division II shall be approved by both the engineer of record and the anchorage device supplier.

COMMENTARY

C.9.1.2 The factored tendon force P_n is the product of the load factor (1.2 from Section 9.14) and the maximum tendon force allowed. Under AASHTO Section 9.15.1 this is usually overstressing to 0.90 f_y^* which is permitted for short periods of time. ASTM Specifications A416-90 provides that minimum yield strength be 85% of specified minimum breaking strength for stress relieved strand and 90% for the widely used low relaxation strand. Thus, typically

$$\begin{aligned} P_u &= (L.F.) 0.90f_y * A_s^* \\ &= (1.2)(0.90)(0.90)\bar{f}_s' A_s^* \\ &= (1.2)(0.81)\bar{f}_s' A_s^* \\ &= 0.972 \bar{f}_s' A_s^* \end{aligned}$$

C.9.21 POST-TENSIONED ANCHORAGE ZONES

Article 9.21 applies to anchorage zones for post-tensioned tendons only. Provisions for anchorage zones in pretensioned concrete are included in Article 9.22.

C.9.21.1 Geometry of the Anchorage Zone

C.9.21.1.1 Within the anchorage zone the usual assumption of beam theory that plane sections remain plane is not valid.

C.9.21.1.2 The definitions of Section 9.21.1.2 through 9.21.1.4 are based on the Principle of Saint Venant and are illustrated in Figure 1.

C.9.21.1.3 For intermediate anchorages large tensile stresses exist locally behind the anchor. These tensile stresses are induced by incompatibility of deformations ahead of and behind the anchorage. The entire region must be considered (Figure 1c).

Figure 1c also clarifies the terminology used to address the regions around intermediate anchorages. Locations at the rear of the anchorage (the direction opposite to the pre-stressing force) are referred to as "behind the

The load factor of 1.2 applied to the maximum tendon jacking force results in a design load of about 96% of the nominal ultimate strength of the tendon. This compares well with the maximum attainable jacking force which is limited by the anchor efficiency factor.

C.9.14 LOAD FACTORS

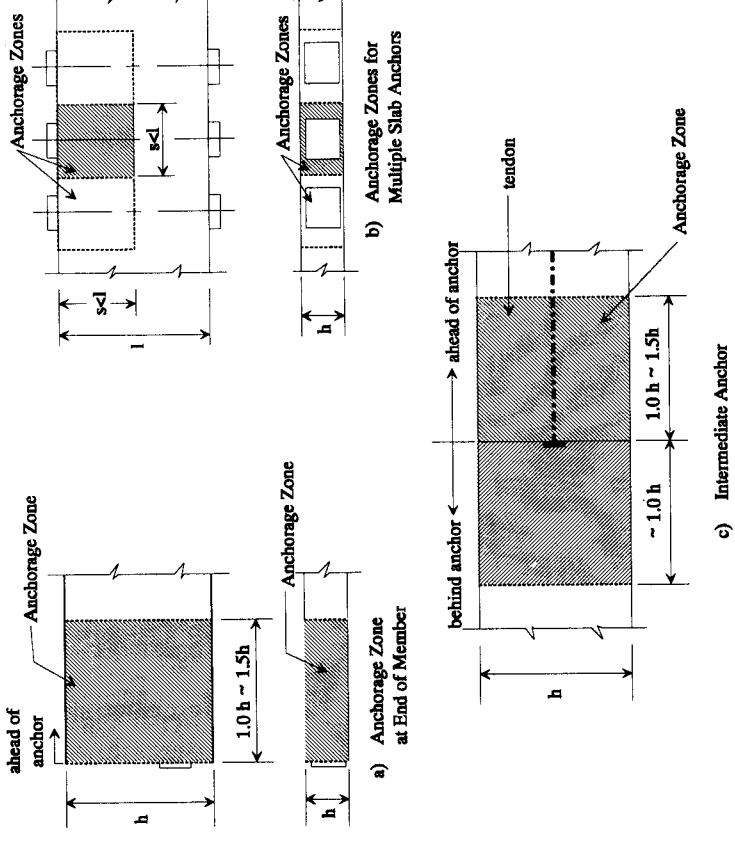


Figure 1 Geometry of the Anchorage Zone

However, for small anchorage zones, such as in slab anchorages, local zone effects (high bearing and confining stresses) and general zone effects (tensile stresses due to spreading of the tendon force) may occur in the same region.

C.9.21.2.1.2 The main considerations in general zone design are the determination of the reinforcement requirements for the tensile forces in the anchorage zone (such as bursting forces and spalling forces) and the check of the compressive stresses at the interface with the local zone.

C.9.21.2.2 Local Zone

C.9.21.2.2.1 The local zone must resist the very high local stresses introduced by the anchorage device and transfer them to the remainder of the anchorage zone. The behavior of the local zone is strongly influenced by the specific characteristics of the anchorage device and its confining reinforcement, and less influenced by the geometry and loading of the overall structure.

C.9.21.2.2.2 The main considerations in local zone design are the effects of the high bearing pressure and the adequacy of any confining reinforcement to increase the bearing strength. Anchorage devices either are basic anchorage devices which have to satisfy the bearing pressure limitations and stiffness requirements of Section 9.21.7 or are special anchorage devices which have to pass an acceptance test by an independent testing agency as described in Division II, Section 10.3.2.3.

C.9.21.2 General Zone and Local Zone

C.9.21.2.1 General Zone

C.9.21.2.1.1 In many cases the general zone and the local zone can be treated separately.

In segmental or similar sequential construction, the construction stage at time of stressing of the tendon should be used to determine whether an anchorage is an end anchor or an intermediate anchor.

C.9.21.2.1.4 For multiple slab anchorages the dimensions of the anchorage zone are determined by the anchorage spacing. For very widely spaced anchors the transverse dimension of the anchorage zone does not have to exceed the slab length in the direction of the tendon (Figure 1b). Anchorage zones for anchors on opposite sides of the slab may overlap.

C.9.21.2.1.5 Figure 2 illustrates the distinction between the local zone and the general zone. The region of very high compressive stresses immediately ahead of the anchorage device is the local zone. The region subjected to tensile stresses due to spreading of the concentrated tendon force into the structure is the general zone.

C.9.21.2.3 Responsibilities

C.9.21.2.3.1 The engineer of record has the responsibility for the location of individual tendons and anchorage devices. Should the plans show only total tendon force and eccentricity the engineer of record is responsible for approval of the specific tendon layout and anchorage arrangement submitted by the post-tensioning specialist or the contractor. The engineer of record is responsible for the proper design of general zone reinforcement required by the approved tendon layout and anchorage device arrangement.

If basic anchorage devices are used, the engineer of record is responsible for the design of the local zone in accordance with Section 9.21.7. If special anchorage devices are used, the anchorage device supplier assumes certain responsibilities as specified in Section 9.21.2.3.2. However, use of special anchorage devices does not relieve the engineer of record from the responsibility of approving the design and working drawings for the anchorage zone to ensure compliance with the anchorage device supplier's specifications.

C.9.21.2.3.2 The responsibility of demonstrating the adequacy of special anchorage devices and specifying the proper reinforcement of the local zone is assigned to the supplier of the anchorage device. The anchorage device supplier has to provide information on all requirements necessary for the satisfactory performance of the local zone to the engineer of record and to the contractor. The supplier is also responsible for furnishing the anchorage device proper. Necessary local zone

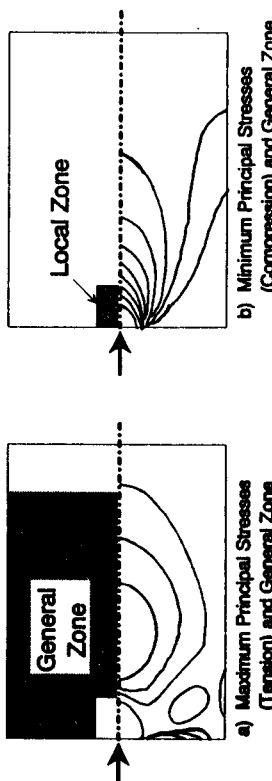


Figure 2 Local Zone and General Zone

confinement reinforcement has to be specified by the supplier. Contractual documents should make clear the responsibility of furnishing and the method of payment for the additional local zone reinforcement needed for special anchorage devices, above the indicated general zone plan quantity. Design of the general zone reinforcement is the responsibility of the engineer of record. Usually general zone reinforcement should not have to be furnished by the anchorage device supplier.

C.9.21.2.3.3 The constructor is responsible for the proper execution of the instructions of both the engineer of record and the anchorage device supplier.

C.9.21.3 Design of the General Zone

C.9.21.3.1 Design Methods

The list of design methods in Section 9.21.3.1 is not meant to preclude other recognized and verified procedures but includes some methods that have been found acceptable and useful for general zone design. In many anchorage applications where substantial or massive concrete regions surround the anchorages and where the members are essentially rectangular without substantial deviations in the force flow path (see Section C.9.21.6.1), the approximate procedures of Section 9.21.6 can generally be used. However, in the post-tensioning of thin sections, flanged sections, irregular sections, or when the tendons have appreciable curvature, the more general procedures of Section 9.21.4 and 9.21.5 will be required.

Different anchorage force arrangements have a significant effect on the general zone stresses. Therefore it is important to consider not only the final stage of a stressing sequence with all tendons stressed but also intermediate stages during construction.

The provision for three-dimensional effects was included to alert the designer to effects perpendicular to the main plane of the member, such as bursting forces in the thin direction of webs or slabs. In many cases these effects can be determined independently for each directions, but some applications require a fully three-dimensional analysis (for example diaphragms for the anchorage of external tendons).

C.9.21.3.2 Nominal Material Strengths

Since anchorage zone design is based on an infinite load approach some plastic concrete deformation is expected. The low value for the nominal concrete compressive strength for unconfined concrete reflects this possibility. For well confined concrete the effective compressive strength could be increased. The value for nominal tensile strength of bonded prestressed reinforcement is limited to the yield point of the prestressing steel since the more general AASHTO equations (9-17) and (9-17a) may not apply to these non-flexural applications. The value for unbonded prestressed reinforcement is based on the general AASHTO value of Section 9.17.4.

C.9.21.3.3 Use of Special Anchorage Devices

For the acceptance test of special anchorage devices, supplementary skin reinforcement in

addition to any required confining reinforcement is permitted (Division II, Section 10.3.2.3.4). Equivalent reinforcement should also be placed in the actual structure. Other general zone reinforcement in the corresponding portion of the anchorage zone may be counted towards this reinforcement requirement.

C.9.21.3.4 General Design Principles and Detailing Requirements

The provisions of this section include requirements that apply to all design methods, while Sections 9.21.4 through 9.21.6 address specific requirements for the various methods listed in Section 9.21.3.1.

C.9.21.3.4.1 With basic anchorage devices meeting the provisions of Section 9.21.7.2, concrete stresses are critical immediately ahead of the anchor plate.

C.9.21.3.4.2 With special anchorage devices, the interface between the confined concrete of the local zone and the usually unconfined concrete of the general zone is most critical. The provisions of Section 9.21.3.4.2 define the location where concrete stresses should be checked and apply the compressive stress limits of Section 9.21.3.2.2.

C.9.21.3.4.3 Stress concentrations may occur away from the critical regions defined in Sections 9.21.3.4.1 and 9.21.3.4.2 at locations of loading or geometry discontinuities. An example is the transition from a diaphragm to flanges and webs of a member.

C.9.21.3.4.8

The minimum spalling force for design is two percent of the total post-tensioning force. This value is smaller than the four percent proposed by Guyon (Reference 3), and reflects both analytical and experimental findings which show that Guyon's values for

C.9.21.3.4.4 Bursting forces are caused by lateral spreading of the concentrated prestressing forces. The emphasis on the three-dimensional nature of the spreading of the forces is important, because it was observed that out of major plane transverse reinforcement is often neglected in design. For example, in members with thin rectangular cross sections bursting forces not only exist in the major plane of the member, but also perpendicular to it.

C.9.21.3.4.5 The guidelines for the arrangement of the bursting reinforcement attempt to direct the designer towards reinforcement patterns which are relatively close to the elastic stress distribution. The experimental test results show that this leads to a satisfactory behavior under service loads by limiting the extent and opening of cracks, and at ultimate by limiting the required amount of redistribution of forces in the anchorage zone (Reference 4). A uniform distribution of the bursting reinforcement with its centroid at d_{burst} is acceptable (Figure 3).

C.9.21.3.4.6 Figure 4 illustrates the location of the edge tension forces. The term "spalling forces" to address the tensile forces along the transverse edge of the member is not really accurate since spalling tends to imply a compression type failure. It is used for historic reasons.

C.9.21.3.4.8

The minimum spalling force for design is two percent of the total post-tensioning force. This value is smaller than the four percent proposed by Guyon (Reference 3), and reflects both analytical and experimental findings which show that Guyon's values for

spalling forces are rather high and that spalling cracks are very rarely observed in experimental studies (References 1, 4).

C.9.21.3.4.9 Figure 5 illustrates the reinforcement requirements of Section 9.21.3.4.9.

C.9.21.3.5 Intermediate Anchorages

Intermediate anchorages are used for anchorage of tendons that do not extend over the full length of a member or segment. They are usually in the form of blisters, ribs, embedded anchors, or recess pockets. Local tensile stresses are generated behind intermediate anchorages due to compatibility requirements for deformations ahead of and behind the anchor. Arrangement of intermediate anchors in the junction of flange and web or in continuous ribs over the full slab width helps to reduce these stress concentrations.

Bonded reinforcement is required in the immediate vicinity of the anchorage to control cracking behind the anchor. In Equation (9-32) the beneficial effect of compression behind the anchor from other loads is considered. Should an intermediate anchorage be located in regions with moderate tension behind the anchor, additional reinforcement must be provided to carry these tensile forces. Figure 6 illustrates the definition of area A_{cb} for use in Equation (9-32).

Tie back reinforcement is also required where tendon curvature generates deviation forces. Problems have occurred in blisters where such tie back reinforcement was designed

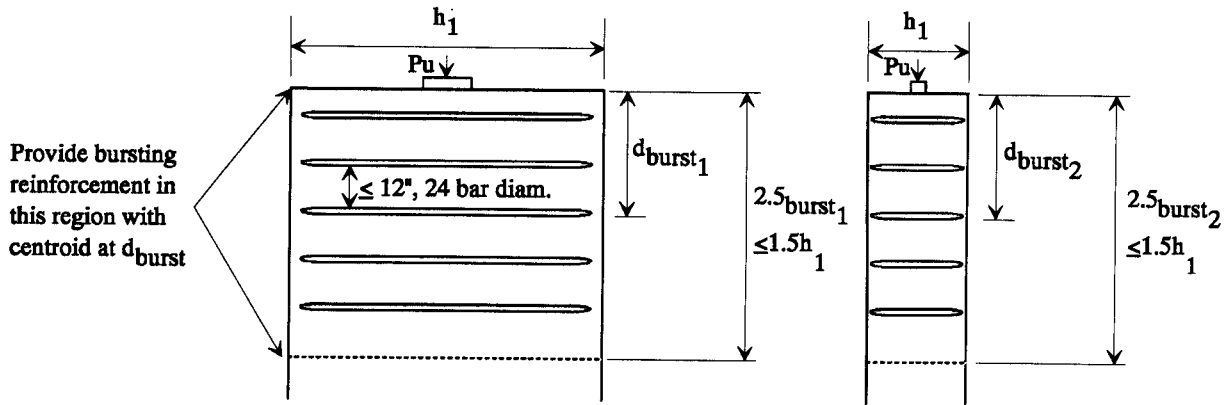


Figure 3 Bursting Reinforcement Arrangement

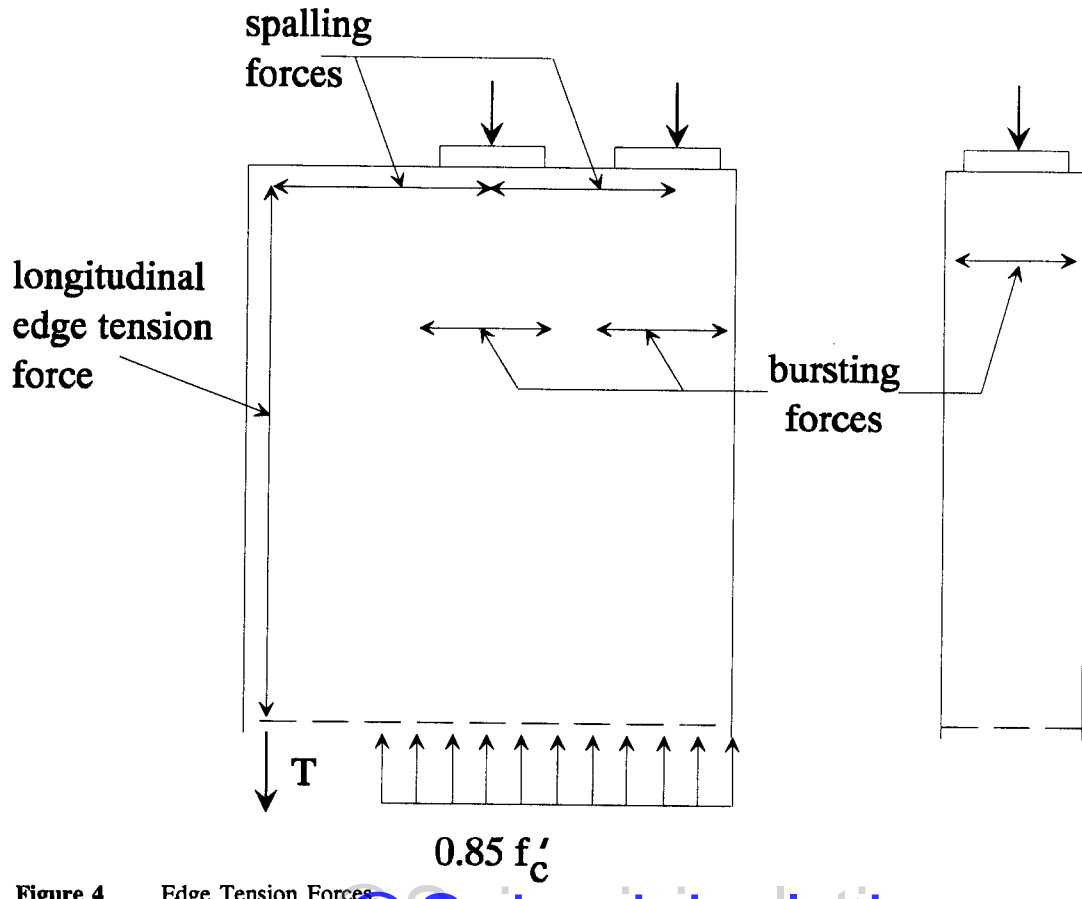
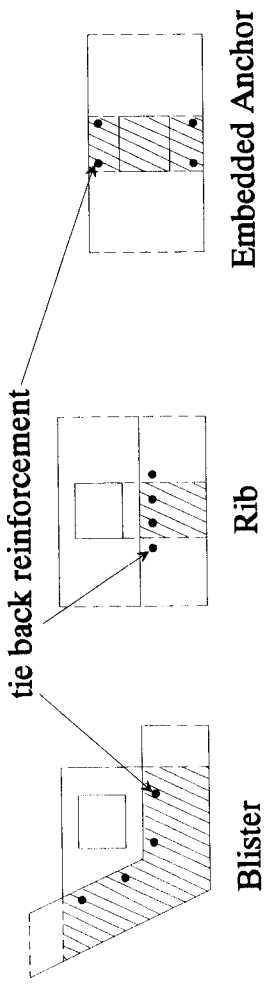
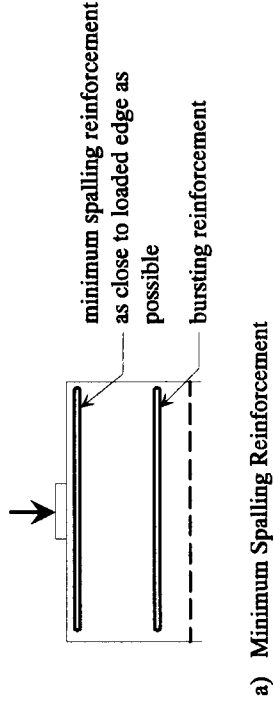


Figure 4 Edge Tension Forces



@Seismicisolation

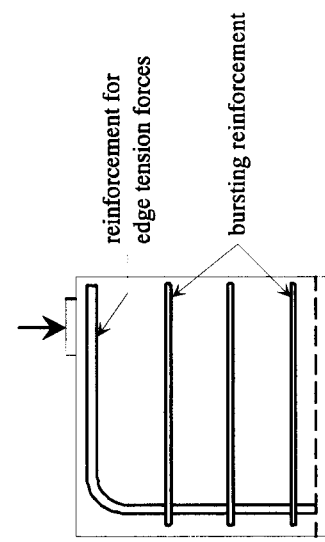
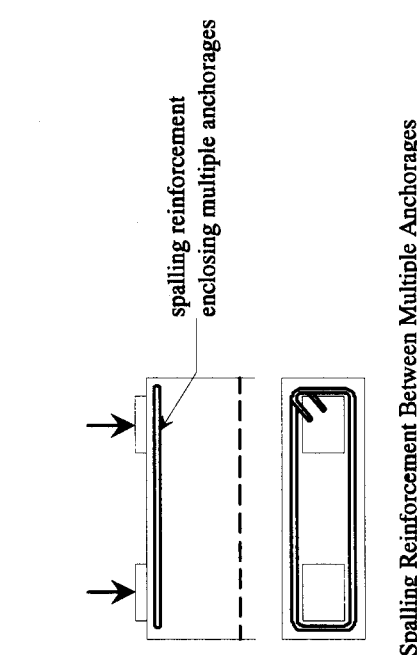


Figure 6 Area A_{cb} Behind Intermediate Anchorages

Embedded Anchor

Rib

Blister

a) Minimum Spalling Reinforcement

Embedded Anchor

Blister

a) Minimum Spalling Reinforcement

Rib

Blister

a) Minimum Spalling Reinforcement

Embedded Anchor

Blister

a) Minimum Spalling Reinforcement

Rib

Blister

a) Minimum Spalling Reinforcement

Embedded Anchor

Blister

a) Minimum Spalling Reinforcement

Rib

Blister

a) Minimum Spalling Reinforcement

Embedded Anchor

Blister

a) Minimum Spalling Reinforcement

Rib

Blister

a) Minimum Spalling Reinforcement

Embedded Anchor

Blister

a) Minimum Spalling Reinforcement

Rib

Blister

a) Minimum Spalling Reinforcement

Embedded Anchor

Blister

a) Minimum Spalling Reinforcement

Rib

Blister

a) Minimum Spalling Reinforcement

Embedded Anchor

Blister

a) Minimum Spalling Reinforcement

Rib

Blister

a) Minimum Spalling Reinforcement

Embedded Anchor

Blister

a) Minimum Spalling Reinforcement

Rib

Blister

a) Minimum Spalling Reinforcement

Embedded Anchor

Blister

a) Minimum Spalling Reinforcement

Rib

Blister

a) Minimum Spalling Reinforcement

Embedded Anchor

Blister

a) Minimum Spalling Reinforcement

Rib

Blister

a) Minimum Spalling Reinforcement

Embedded Anchor

Blister

a) Minimum Spalling Reinforcement

Rib

Blister

a) Minimum Spalling Reinforcement

Embedded Anchor

Blister

a) Minimum Spalling Reinforcement

Rib

Blister

a) Minimum Spalling Reinforcement

Embedded Anchor

Blister

a) Minimum Spalling Reinforcement

Rib

Blister

a) Minimum Spalling Reinforcement

Embedded Anchor

Blister

a) Minimum Spalling Reinforcement

Rib

Blister

a) Minimum Spalling Reinforcement

Embedded Anchor

Blister

a) Minimum Spalling Reinforcement

Rib

Blister

a) Minimum Spalling Reinforcement

Embedded Anchor

Blister

a) Minimum Spalling Reinforcement

Rib

Blister

a) Minimum Spalling Reinforcement

Embedded Anchor

Blister

a) Minimum Spalling Reinforcement

Rib

Blister

a) Minimum Spalling Reinforcement

Embedded Anchor

Blister

a) Minimum Spalling Reinforcement

Rib

Blister

a) Minimum Spalling Reinforcement

Embedded Anchor

Blister

a) Minimum Spalling Reinforcement

Rib

Blister

a) Minimum Spalling Reinforcement

Embedded Anchor

Blister

a) Minimum Spalling Reinforcement

Rib

Blister

a) Minimum Spalling Reinforcement

Embedded Anchor

Blister

a) Minimum Spalling Reinforcement

Rib

Blister

a) Minimum Spalling Reinforcement

Embedded Anchor

Blister

a) Minimum Spalling Reinforcement

Rib

Blister

a) Minimum Spalling Reinforcement

Embedded Anchor

Blister

a) Minimum Spalling Reinforcement

Rib

Blister

a) Minimum Spalling Reinforcement

Embedded Anchor

Blister

a) Minimum Spalling Reinforcement

Rib

Blister

a) Minimum Spalling Reinforcement

Embedded Anchor

Blister

a) Minimum Spalling Reinforcement

Rib

Blister

a) Minimum Spalling Reinforcement

Embedded Anchor

Blister

a) Minimum Spalling Reinforcement

Rib

Blister

a) Minimum Spalling Reinforcement

Embedded Anchor

Blister

a) Minimum Spalling Reinforcement

Rib

Blister

a) Minimum Spalling Reinforcement

Embedded Anchor

Blister

a) Minimum Spalling Reinforcement

Rib

Blister

a) Minimum Spalling Reinforcement

Embedded Anchor

Blister

a) Minimum Spalling Reinforcement

Rib

Blister

a) Minimum Spalling Reinforcement

Embedded Anchor

Blister

a) Minimum Spalling Reinforcement

Rib

Blister

a) Minimum Spalling Reinforcement

Embedded Anchor

Blister

a) Minimum Spalling Reinforcement

Rib

Blister

a) Minimum Spalling Reinforcement

Embedded Anchor

Blister

a) Minimum Spalling Reinforcement

Rib

Blister

a) Minimum Spalling Reinforcement

Embedded Anchor

Blister

a) Minimum Spalling Reinforcement

Rib

Blister

a) Minimum Spalling Reinforcement

Embedded Anchor

Blister

a) Minimum Spalling Reinforcement

Rib

Blister

a) Minimum Spalling Reinforcement

Embedded Anchor

Blister

a) Minimum Spalling Reinforcement

Rib

Blister

a) Minimum Spalling Reinforcement

Embedded Anchor

Blister

a) Minimum Spalling Reinforcement

Rib

Blister

a) Minimum Spalling Reinforcement

Embedded Anchor

Blister

a) Minimum Spalling Reinforcement

Rib

Blister

a) Minimum Spalling Reinforcement

Embedded Anchor

Blister

a) Minimum Spalling Reinforcement

Rib

Blister

a) Minimum Spalling Reinforcement

Embedded Anchor

Blister

a) Minimum Spalling Reinforcement

Rib

Blister

a) Minimum Spalling Reinforcement

Embedded Anchor

Blister

a) Minimum Spalling Reinforcement

Rib

Blister

a) Minimum Spalling Reinforcement

Embedded Anchor

Blister

a) Minimum Spalling Reinforcement

Rib

Blister

a) Minimum Spalling Reinforcement

Embedded Anchor

Blister

a) Minimum Spalling Reinforcement

Rib

Blister

a) Minimum Spalling Reinforcement

Embedded Anchor

Blister

a) Minimum Spalling Reinforcement

Rib

Blister

a) Minimum Spalling Reinforcement

Embedded Anchor

Blister

a) Minimum Spalling Reinforcement

Rib

Blister

a) Minimum Spalling Reinforcement

Embedded Anchor

Blister

a) Minimum Spalling Reinforcement

Rib

Blister

a) Minimum Spalling Reinforcement

Embedded Anchor

Blister

a) Minimum Spalling Reinforcement

Rib

Blister

a) Minimum Spalling Reinforcement

Embedded Anchor

Blister

a) Minimum Spalling Reinforcement

Rib

Blister

a) Minimum Spalling Reinforcement

Embedded Anchor

Blister

a) Minimum Spalling Reinforcement

Rib

Blister

a) Minimum Spalling Reinforcement

Embedded Anchor

Blister

a) Minimum Spalling Reinforcement

Rib

Blister

a) Minimum Spalling Reinforcement

Embedded Anchor

Blister

for a gradual tendon curvature but the tendons were actually kinked at the toe of the blister. These problems can be avoided by either ensuring the envisioned gradual tendon curvature is actually provided during construction or, more realistically, by providing additional tie back reinforcement to compensate for accidental kinking of the tendon.

C.9.21.3.6 Diaphragms

In diaphragms, compressive stresses may become critical not only immediately ahead of the anchorages, but also at the transition from the massive diaphragm to the relatively thin flanges and webs of the cross section.

Bursting reinforcement requirements in diaphragms may be significantly larger than for beams with a continuous rectangular section (Figure 11). In particular, the approximate equations of Section 9.21.6 or Guyon's symmetrical prism (Reference 3) should not be used to determine these reinforcement requirements.

C.9.21.3.7 Multiple Slab Anchorages

Edge tension forces and bursting forces in slabs with multiple anchors along an edge can be visualized as the tie forces existing in an inverted uniformly loaded continuous deep beam supported at the locations of the anchorages. Figure 7 illustrates the requirements of Section 9.21.3.7.

The bursting reinforcement in the thin direction of the slab is frequently omitted. This may be acceptable and approved by the engineer of record for large anchorage spacing if

indicated as satisfactory by well documented past experience or more detailed analysis, provided that anchorage failures would cause only local damage. For more closely spaced anchors the full bursting reinforcement as required in Section 9.21.3.7.2 should always be provided.

The bursting reinforcement in the plane of the slab can often be provided by slab reinforcement which is present for thermal, shrinkage or load distribution requirements. The engineer is always free to make a more detailed analysis as per 9.21.3.7.1

C.9.21.4 Application of Strut-and-Tie Models to the Design of Anchorage Zones

C.9.21.4.1 General

C.9.21.4.1.1 A lower bound of the ultimate load that a given concrete structure or member can carry can be obtained by application of the lower bound theorem of the theory of plasticity of structures. Models in which the actual flow of forces in a structure is approximated by a series of straight compression members (struts), and straight tension members (ties) which are connected at discrete points (nodes) are called strut-and-tie models. If sufficient ductility (rotation capacity) is present in the system, strut-and-tie models fulfill the conditions for the application of the above mentioned theorem, and the ultimate load predicted on the basis of a strut-and-tie model will be a conservative estimate of the actual ultimate load of the structure or member. Figure 8 shows the

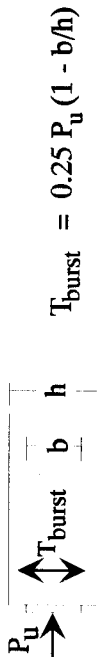
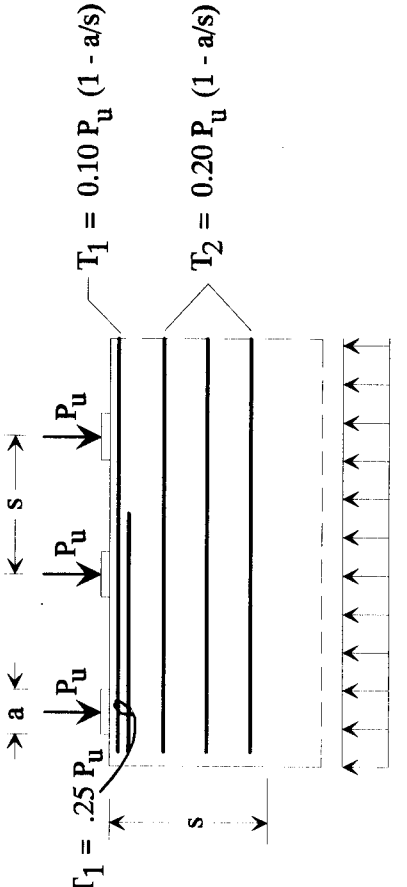


Figure 7 Reinforcement Requirements for Multiple Slab Anchorages

@Seismicisolation

linear elastic stress field and a corresponding strut-and-tie model for the case of an anchorage zone with two eccentric anchors (Reference 5).

C.9.21.4.1.2 Because of the limited ductility of concrete, strut-and-tie models not greatly different from the elastic solution should be selected. This procedure will limit the required stress redistributions in the anchorage zone, and will also ensure that crack control reinforcement is provided where cracks are most likely to occur. In Figure 9 strut-and-tie models for some typical load cases for anchorage zones are shown.



Figure 8 Stress Field and Strut-and-Tie Model (from Reference 4)

strut-and-tie model deviates considerably from the elastic stress distribution, large plastic deformations are required and the concrete strength should be reduced. The concrete strength should also be reduced if the concrete is cracked due to other load effects.

C.9.21.4.3.2 Ordinarily the geometry of the local zone node and thus of the interface between strut and local zone is determined by the size of the bearing plate and the selected strut-and-tie model, as indicated in Figure 10a. For special anchorage devices based on the acceptance test of Division II, Section 10.3.2.3, it is suggested (Reference 1) that stresses be checked at a larger distance from the node, assuming that the width of the strut increases with the distance from the local zone (Figure 10b).

C.9.21.4.3.3 The determination of the dimension of the strut in the direction of the thickness of the member is illustrated in 10c. For members with a ratio of member thickness to anchorage width of more than three, strut-and-tie models for each direction should be considered.

The local zone nodes for the development of a strut-and-tie model may be selected at a depth of $a/4$ ahead of the anchorage plate (Figure 10).

C.9.21.4.4 Ties

C.9.21.4.4.1 Because of the unreliable strength of concrete in direct tension, it is prudent to neglect it entirely.

C.9.21.4.3 Struts

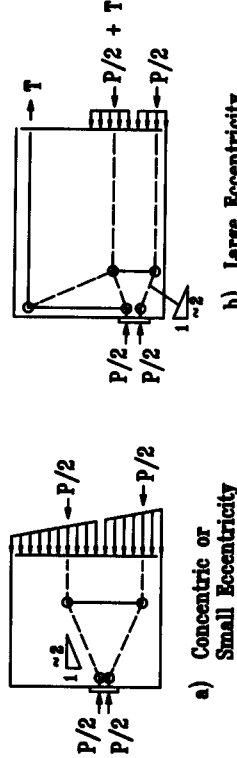
C.9.21.4.3.1 For strut-and-tie models oriented on the elastic stress distribution the nominal concrete strength specified in Section 9.21.3.2 is adequate. However, if the selected arrangements should be considered.

C.9.21.5 Elastic Stress Analysis

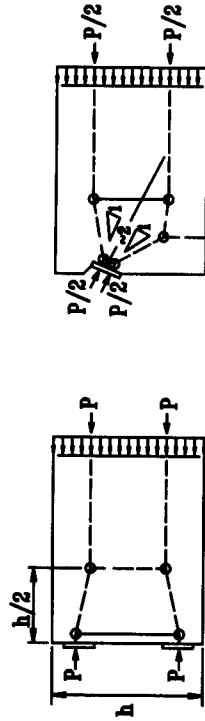
compares the bursting forces for a member with a continuous rectangular cross section and for a member with a non-continuous rectangular cross section.

(3) The approximate equations for the concrete compressive stresses are based on the assumption that the anchor force can spread in all directions. Requirement 3 ensures this assumption and is illustrated in Figure 12.

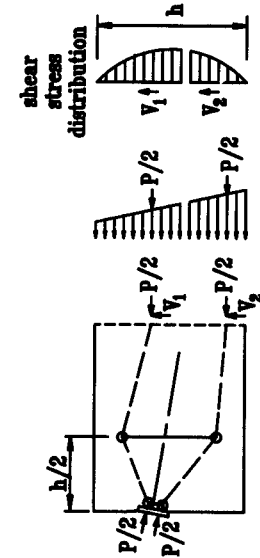
(4) The approximate equations for bursting forces are based on finite element analyses for a single anchor acting on a rectangular cross section. Equation (9-37) gives conservative results for the bursting reinforcement even if limitation (4) is violated and the anchors are not closely spaced, but the resultant of the bursting force is located closer to the anchor than indicated by Equation (9-38).



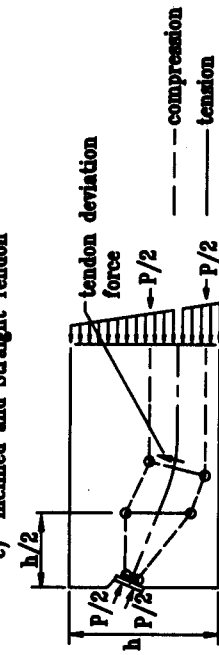
b) Large Eccentricity



c) Multiple Anchors
d) Eccentric Anchor and Support Reaction



e) Inclined and Straight Tendon



f) Inclined and Curved Tendon

C.9.21.6 Approximate Methods

C.9.21.6.1 Limitations

(1) The equations in this section are based on the analysis of members with a rectangular cross section and an anchorage zone at least as long as the largest dimension of that cross section. For cross sections that deviate significantly from a rectangular shape, for example I-girders with wide flanges, the approximate equations should not be used.

(2) Discontinuities, such as web openings, disturb the flow of forces and may cause higher compressive stresses, bursting forces, or edge tension forces in the anchorage zone. Figure 11

C.9.21.5.1 Although the development of cracks in the anchorage zone causes stress redistributions, elastic analysis of anchorage zone problems has been found acceptable and useful (Reference 1).

C.9.21.5.2 Results of a linear-elastic analysis can be adjusted by smoothing out local stress maxima to reflect the non-linear behavior of concrete at higher stresses.

C.9.21.5.3 This procedure gives a conservative estimate of the reinforcement required in the anchorage zone. A reinforcement arrangement deviating from the elastic stress distribution is acceptable (for example uniform distribution of bursting reinforcement), as long as the centroid of the bursting reinforcement coincides with the location of the bursting force.

C.9.21.6 Approximate Methods

Equations (9-35) and (9-36) are based on linear-elastic finite element analysis for a single concentric anchor and a rectangular cross section of the member. In a plane stress analysis, the compressive stresses at a distance equal to one plate width ahead of the anchor are not more than 60% of the bearing pressure (Reference 1). Equation (9-35) was modified to approximate dispersal of compressive stresses in the thin direction of the member (Figure 10c) and to account for the beneficial effect of a larger spiral.

For multiple anchorages spaced closer than $2a$, a correction factor κ is necessary. This factor is based on an assumed stress distribution

Figure 9 Typical Strut-and-Tie Models for Anchorage Zones

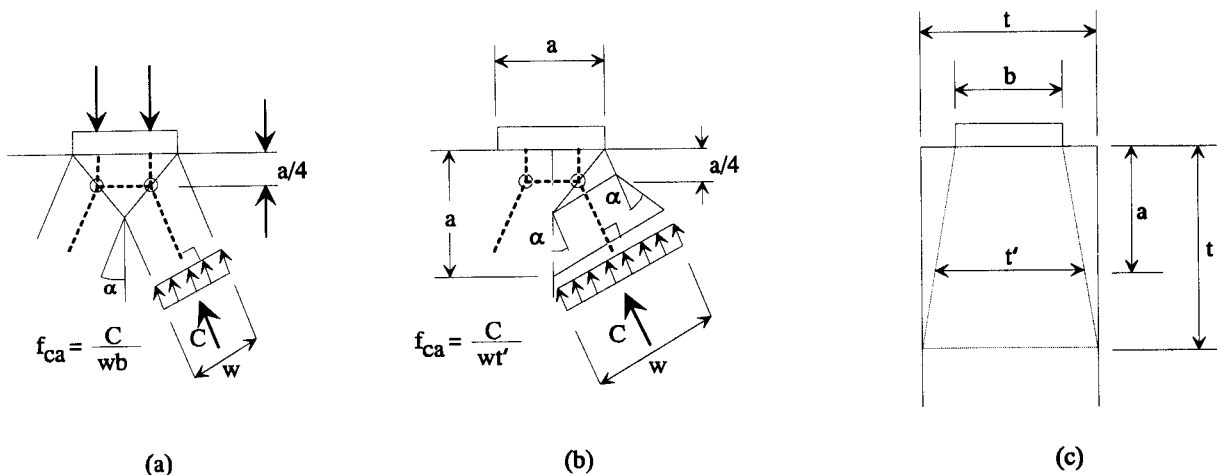


Figure 10 Critical Section for Compression Struts in Anchorage Zones

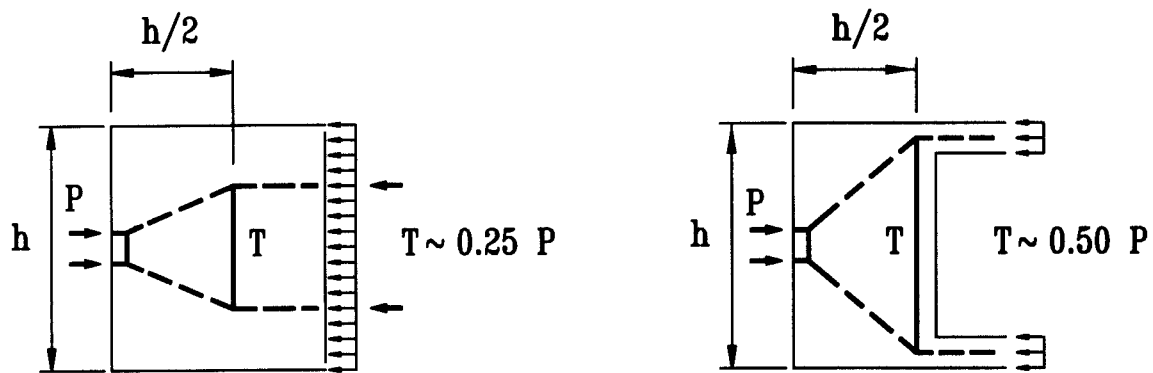


Figure 11 Effect of Discontinuity in Anchorage Zone

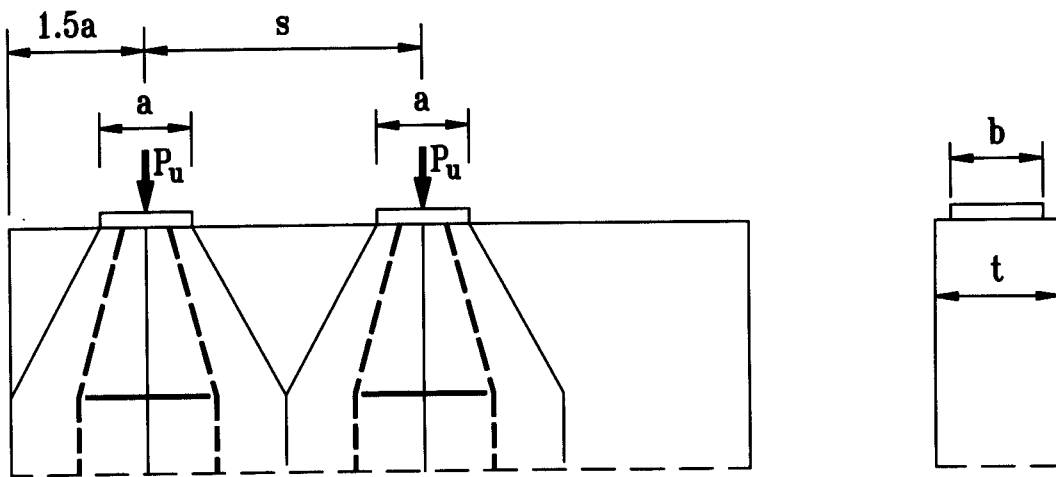


Figure 12 Notations for Equations (9-35) and (9-36)

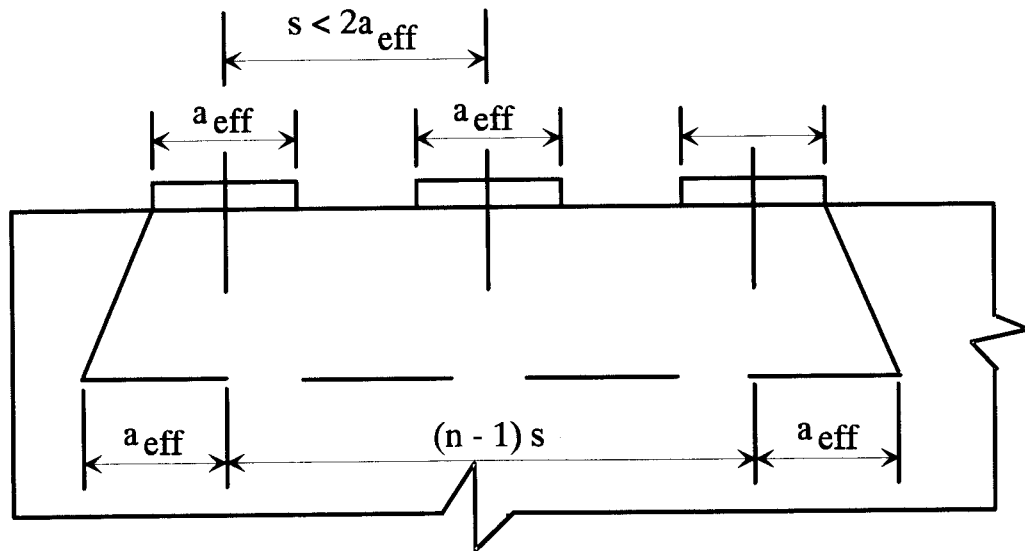


Figure 13 Closely Spaced Multiple Anchorages

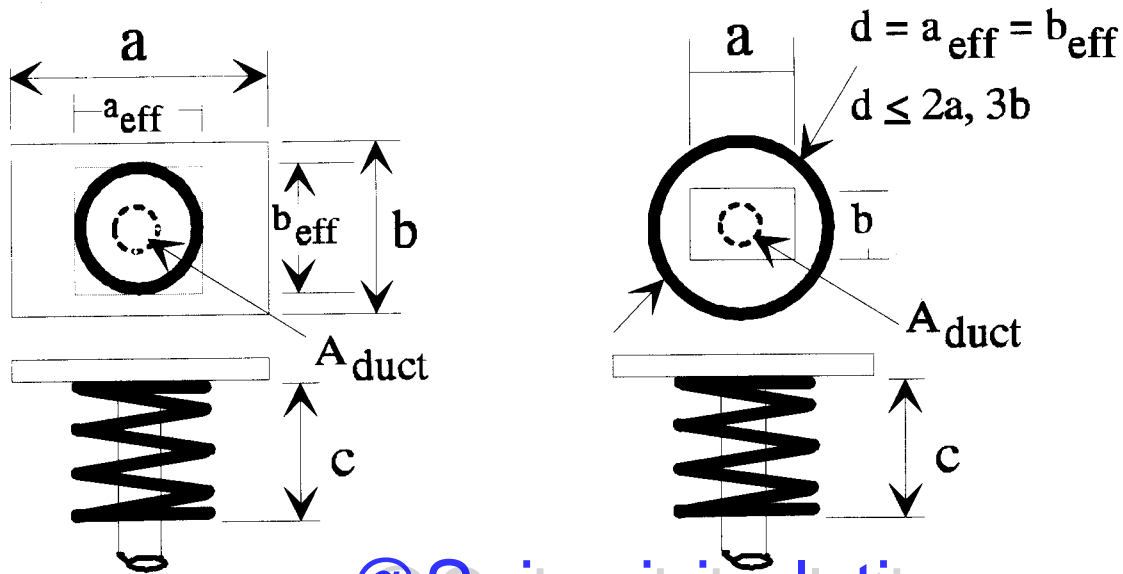
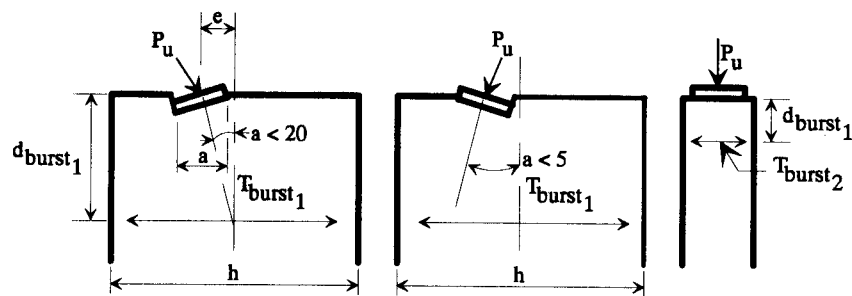
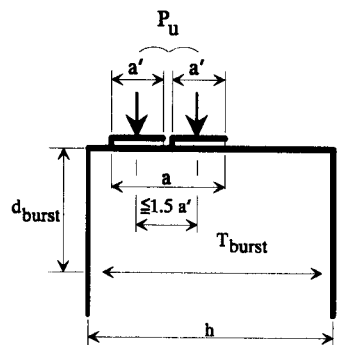


Figure 14 Effective Bearing Area in Equation (9-35)

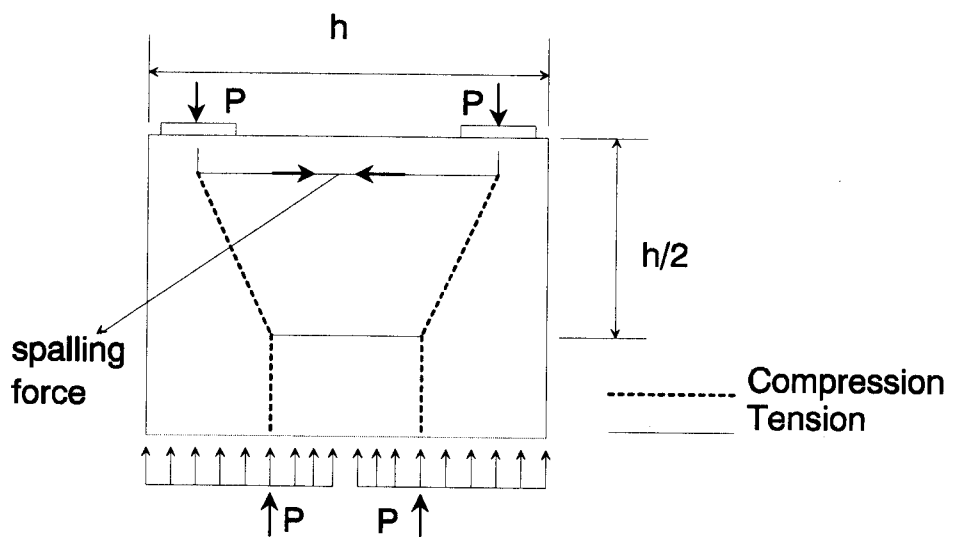
@Seismicisolation



a) Inclined Tendons



b) Closely Spacing Anchorage Devices

Figure 15 Notations in Equations (9-37) and (9-38)**Figure 16** Spalling Forces Between Multiple Anchorages.

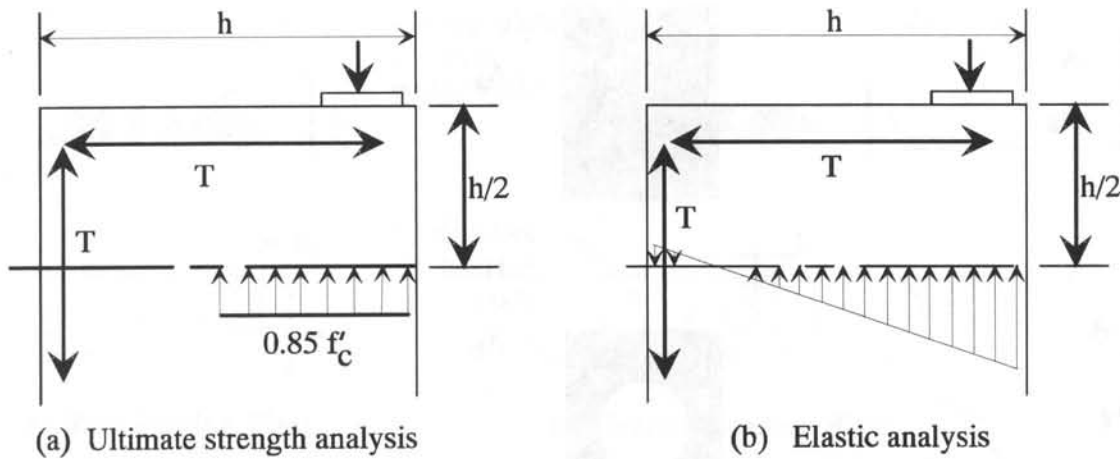


Figure 17 Determination of Edge Tension Forces for Eccentric Anchorages.

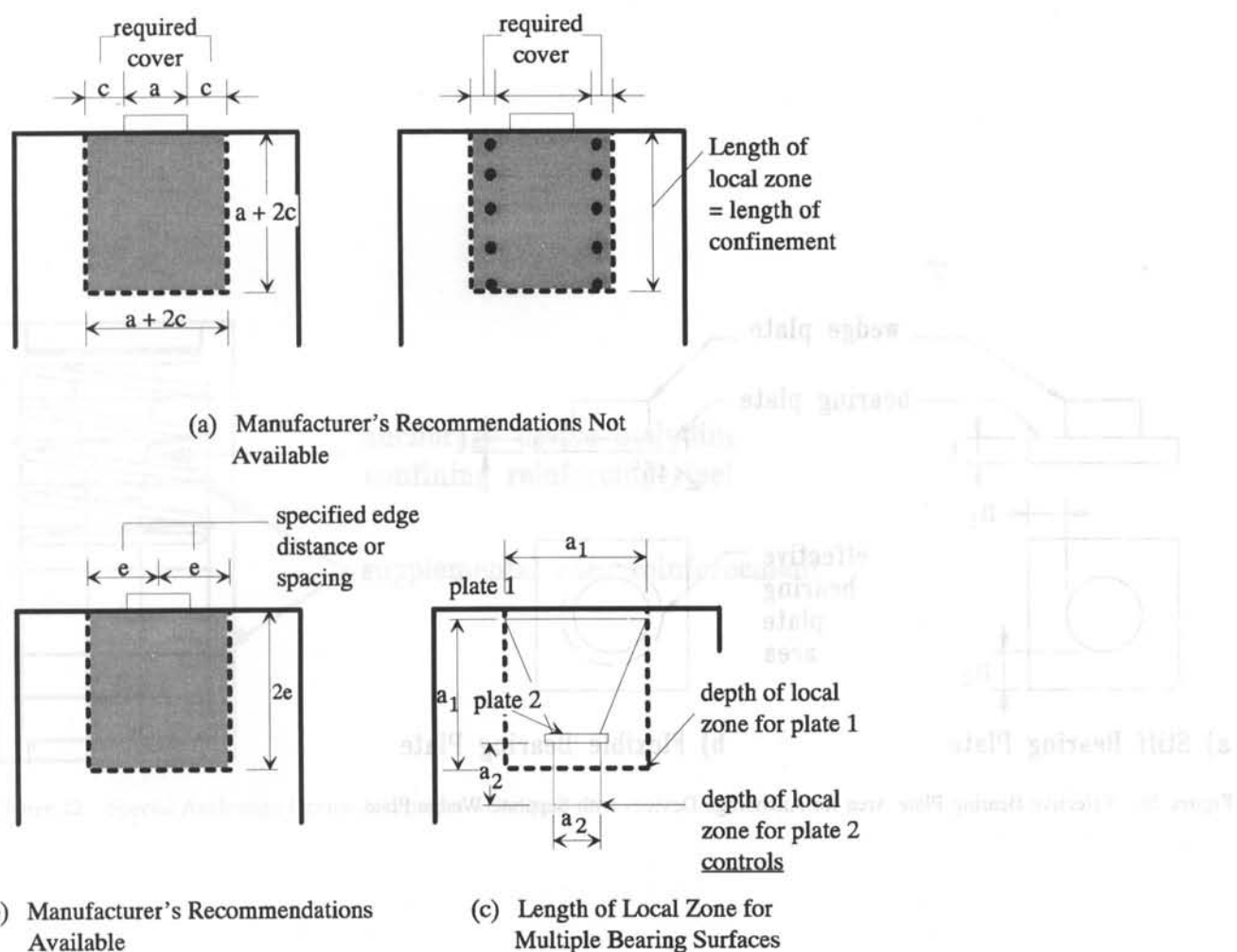


Figure 18

Geometry of Local Zone

@Seismicisolation

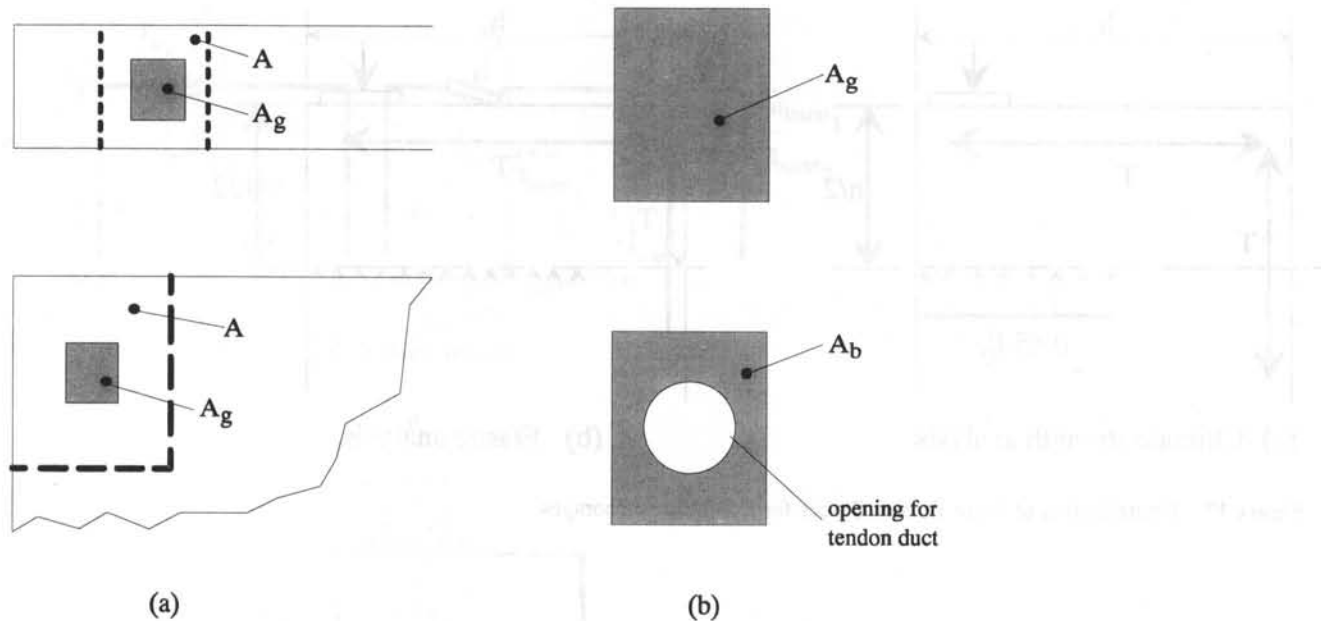


Figure 19 Area of Supporting Concrete Surface in Equation (9-39)

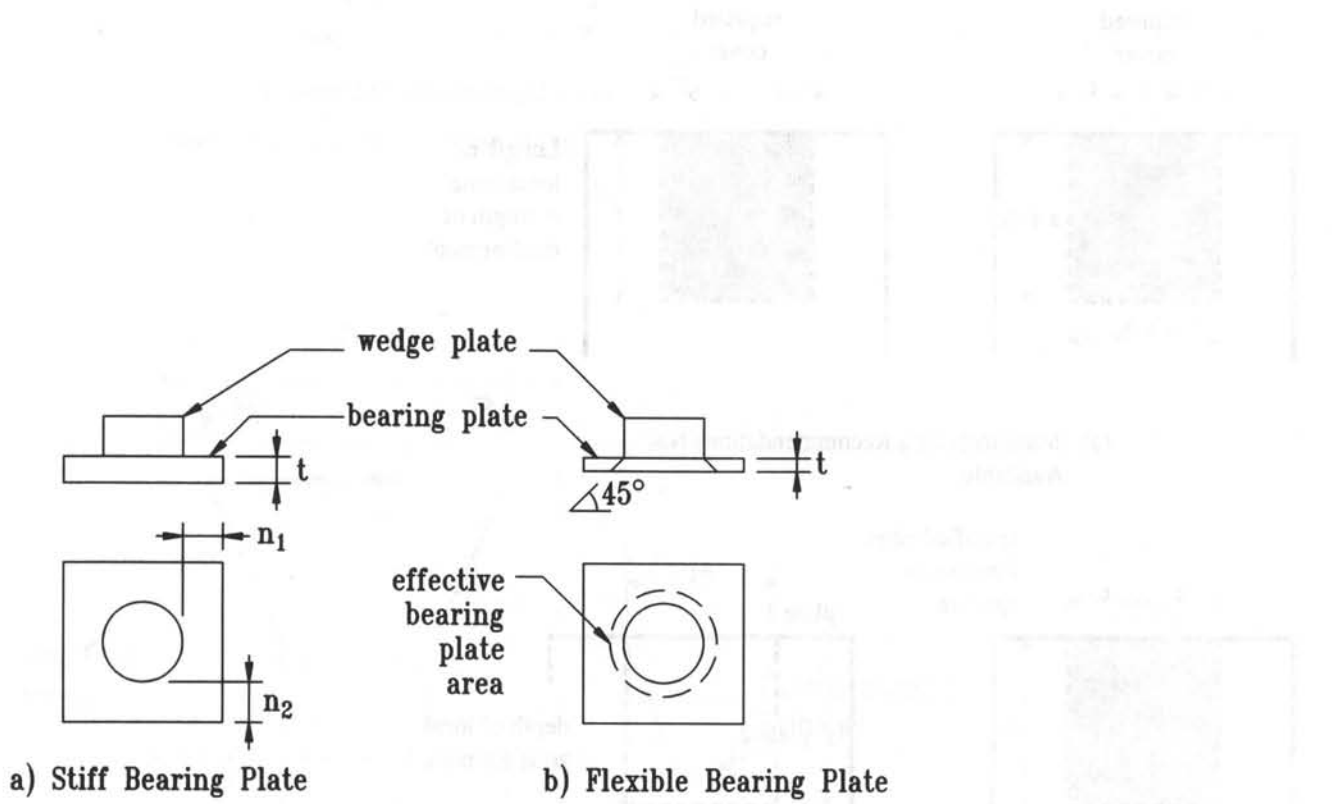


Figure 20 Effective Bearing Plate Area for Anchorage Devices with Separate Wedge Plate

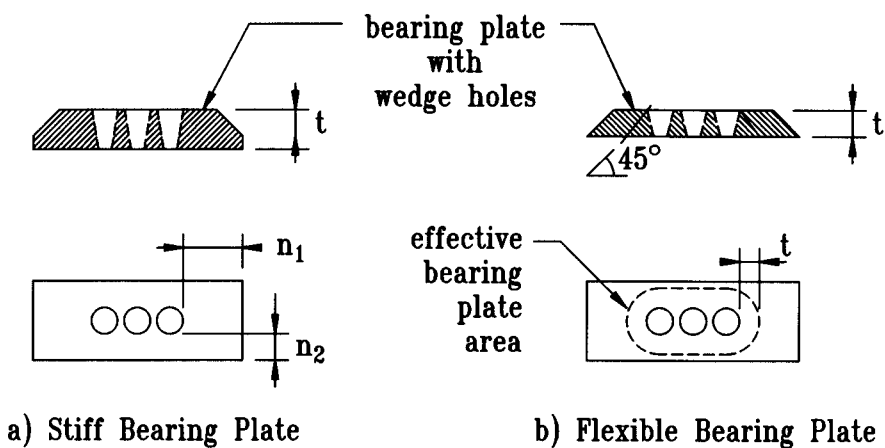


Figure 21 Effective Bearing Plate Area for Anchorage Devices Without Separate Wedge Plate

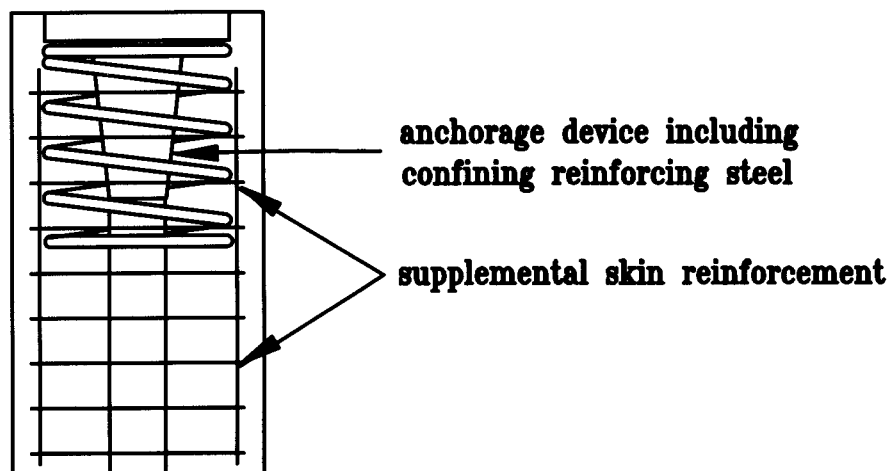


Figure 22 Special Anchorage Device Acceptance Test Specimen

than 5 percent. This can only be measured in reference to the actual strength of the particular prestressing steel used in the test.

C.10.3.2.3 Special Anchorage Device Acceptance Test

C.10.3.2.3.1 Figure 22 shows a local zone specimen with the local zone confining reinforcement in the upper portion of the specimen and the optional supplementary reinforcement of Section 10.3.2.3.4 over the full length of the specimen. However, an anchorage device supplier could also choose to eliminate such reinforcement in either or both portions of the block.

C.10.3.2.3.4 The supplemental reinforcement in the specimen is specified by the anchorage device supplier within the limits of Section 10.3.2.3.4. The same amount of reinforcement is also required in the actual structure, as stipulated in Section 9.21.3.3. However, other reinforcement in the corresponding portion of the structure (such as minimum reinforcement for creep and shrinkage or bursting reinforcement) may be counted towards this requirement. Since the confinement and supplementary reinforcement in the test specimens will generally be provided in orthogonal directions, similar reinforcement in the actual structure must be furnished to achieve an equivalent orthogonal action.

C.10.3.2.3.6 Long term loading has been found to be more critical for the behavior of the local zone than short term loading. A cyclic loading test gives comparable results to sustained loading tests, but is less time

consuming than the sustained loading test (Reference 6). A monotonic short term loading test procedure is also included in the provisions. Stricter acceptance criteria are necessary to make the short term loading test comparable to the other test methods.

aggressive environment is characterized by moist environments where deicing or sea salts may be present in mists, but where direct exposure to corrosive agents is prevented (Reference 6). This should include most bridge applications.

C.10.3.2.3.7 Loading in accordance with normal usage of the anchorage device in post-tensioning applications means loading through the wedge plate if available, or over an area formed by the perimeter of the wedge openings pattern. It is not required to load the specimen through the tendon.

C.10.3.2.3.8 The required minimum failure load of $1.1F_{pu}$ for cyclic and sustained loading tests reflects the incorporation of the maximum allowable stressing level of $0.8F_{pu}$ with a load factor of 1.2 and a ϕ -factor of 0.85. Alternatively, if limited by test equipment capacity, a minimum failure load of $0.95F_{pu}$ can be specified, provided the actual concrete strength of the specimen is reduced proportionately.

C.10.3.2.3.9 In the monotonic loading test the required minimum failure load is increased to $1.2F_{pu}$, reflecting comparative test experience with monotonic, sustained, and cyclic loading procedures. Alternatively, if limited by test equipment capacity, a minimum failure load of $1.0F_{pu}$ can be specified, provided the actual concrete strength of the specimen is reduced proportionately.

C.10.3.2.3.10 The crack width requirements of Section 10.3.2.3.10 are based on recommendations in Reference 9. A moderately

C.10.3.2.3.9 If representative samples out of a series of similar anchorage devices pass the acceptance test, the anchorage device supplier may elect not to test the other anchorage devices in the series. However, the responsibility for the proper performance of such untested anchorage devices remains with the supplier.

C.10.3.2.3.10 Records of the anchorage device acceptance test have to be provided by the anchorage device supplier to the engineer of record and to the constructor. These records must include all the necessary information for proper installation of the anchorage device including all confining and supplementary reinforcement.

C.10.4.3 Placement of Anchorage Hardware

Anchorage zones are very critical regions of a structure. Therefore construction should follow exactly the specifications by the engineer of record and the anchorage device supplier. Change of anchorage zone details have to be approved by the engineer of record and the anchorage device supplier.

THE TRANSPORTATION RESEARCH BOARD is a unit of the National Research Council, which serves the National Academy of Sciences and the National Academy of Engineering. It evolved in 1974 from the Highway Research Board which was established in 1920. The TRB incorporates all former HRB activities and also performs additional functions under a broader scope involving all modes of transportation and the interactions of transportation with society. The Board's purpose is to stimulate research concerning the nature and performance of transportation systems, to disseminate information that the research produces, and to encourage the application of appropriate research findings. The Board's program is carried out by more than 270 committees, task forces, and panels composed of more than 3,300 administrators, engineers, social scientists, attorneys, educators, and others concerned with transportation; they serve without compensation. The program is supported by state transportation and highway departments, the modal administrations of the U.S. Department of Transportation, the Association of American Railroads, the National Highway Traffic Safety Administration, and other organizations and individuals interested in the development of transportation.

The National Academy of Sciences is a private, nonprofit, self-perpetuating society of distinguished scholars engaged in scientific and engineering research, dedicated to the furtherance of science and technology and to their use for the general welfare. Upon the authority of the charter granted to it by the Congress in 1863, the Academy has a mandate that requires it to advise the federal government on scientific and technical matters. Dr. Bruce M. Alberts is president of the National Academy of Sciences.

The National Academy of Engineering was established in 1964, under the charter of the National Academy of Sciences, as a parallel organization of outstanding engineers. It is autonomous in its administration and in the selection of its members, sharing with the National Academy of Sciences the responsibility for advising the federal government. The National Academy of Engineering also sponsors engineering programs aimed at meeting national needs, encourages education and research and recognizes the superior achievements of engineers. Dr. Robert M. White is president of the National Academy of Engineering.

The Institute of Medicine was established in 1970 by the National Academy of Sciences to secure the services of eminent members of appropriate professions in the examination of policy matters pertaining to the health of the public. The Institute acts under the responsibility given to the National Academy of Sciences by its congressional charter to be an adviser to the federal government and, upon its own initiative, to identify issues of medical care, research, and education. Dr. Kenneth I. Shine is president of the Institute of Medicine.

The National Research Council was organized by the National Academy of Sciences in 1916 to associate the broad community of science and technology with the Academy's purpose of furthering knowledge and advising the federal government. Functioning in accordance with general policies determined by the Academy, the Council has become the principal operating agency of both the National Academy of Sciences and the National Academy of Engineering in providing services to the government, the public, and the scientific and engineering communities. The Council is administered jointly by both Academies and the Institute of Medicine. Dr. Bruce M. Alberts and Dr. Robert M. White are chairman and vice chairman, respectively, of the National Research Council.

Transportation Research Board
National Research Council
2101 Constitution Avenue, N.W.
Washington, D.C. 20418

ADDRESS CORRECTION REQUESTED

@Seismicisolation